ISBN 978-82-326-0846-1 (printed version)
ISBN 978-82-326-0847-8 (electronic version)
ISSN 1503-8181

Doctoral theses at NTNU, 2015:95

Omar Al-Saif

Slugging in Large Diameter Pipelines: Field Measurements, Experiments and Simulation

NTNU
Norwegian University of
Science and Technology
Faculty of Engineering
Science and Technology
Department of Energy and
Process Engineering

Doctoral theses at NTNU, 2015:95

Omar Al-Saif
Doctoral Thesis

NTNU – Trondheim
Norwegian University of
Science and Technology

NTNU – Trondheim
Norwegian University of
Science and Technology

NTNU

Omar Al-Saif

Slugging in Large Diameter Pipelines: Field Measurements, Experiments and Simulation

Thesis for the degree of Philosophiae Doctor

Trondheim, May 2015

Norwegian University of Science and Technology
Faculty of Engineering Science and Technology
Department of Energy and Process Engineering

NTNU – Trondheim
Norwegian University of
Science and Technology

NTNU
Norwegian University of Science and Technology

Thesis for the degree of Philosophiae Doctor

Faculty of Engineering Science and Technology
Department of Energy and Process Engineering

ISBN 978-82-326-0846-1 (printed version)
ISBN 978-82-326-0847-8 (electronic version)
ISSN 1503-8181

Doctoral theses at NTNU, 2015:95

Printed by Skipnes Kommunikasjon as

Slugging in Large Diameter Pipelines: Field Measurements, Experiments and Simulation

By:
Omar A. Al-Saif

Thesis submitted in partial fulfilment of the requirements for
the degree of Doctor Philosophiae

NTNU – Norwegian University of Science and Technology
Faculty of Engineering Science and Technology
Department of Energy and Process Engineering

Trondheim,
December 2014

Acknowledgement

I would like to express my deepest gratitude and appreciation for:

- Professor *Ole Jørgen Nydal*, for being my main supervisor and providing me with all of his kindness and support throughout my PhD experience at NTNU.
- Dr. *Mikal Espedal* at Saudi Aramco, for being my co-supervisor and all of the advice and help throughout my PhD endeavor at NTNU.
- The flow assurance team at Saudi Aramco, Satya Putra and Ahmed Harb, who made this work possible by providing me with all the support especially during the field measurement period at Saudi Aramco.
- The NTNU multiphase flow lab staff who provided me with all the support and help to conduct my experiments at the lab in a very short notice.
- Saudi Aramco management for providing me with this opportunity to pursuit my PhD at NTNU and allowing me to utilize the data obtained from field measurements in my PhD thesis.
- I would like also to thank my parents, my wife, Toqa, and my kids Zainab, Zahra, Ahmed and the little one, Hasan, who was born during my PhD work. For all your patience and support throughout these years, words are not enough to express my deepest gratitude but all I can say is *truly thanks*, from the bottom of my heart.

Finally, I would like to dedicate this work to my grandfather, Abu Malik, who passed away about three years ago while I was still pursuing my PhD. He was a very special person to me and to the whole family and I still deeply miss him.

Table of Contents

Table of Figures

Table of Tables

Nomenclature

Latin Letters	Description	Unit
A	Area	m^2
B	Build-up Factor	-
C_o	Coefficient for bubble velocity	-
D	Diameter	m
DF	Distribution Coefficient	-
Dia.	Diameter	m
D_{hg}	Hydraulic gas phase diameter	M
D_{hl}	Hydraulic liquid phase diameter	m
E_o	Eotvos number	-
F_r	Froude Number	-
g	Gravitational acceleration constant	m/s^2
H	Non-dimensional liquid holdup (area fraction)	-
h	Non-dimensional liquid height	-
L	Length	M
M	Secondary flux of photons	-
N	Primary flux of photons	-
P	Pressure	(bar) or (psi)
R	Gas constant	J/(Kg K)
Re	Reynolds number	-
S_f	Slug fraction	-
S_{gw}	Gas-wall perimeter	m
S_{lw}	Liquid-wall perimeter	m
S_i	Gas-liquid interfacial perimeter	m
t	Time	Seconds
T	Temperature	Kelvin
U	Velocity	m/sec
U	Detector output signal	-
U_o	Drift velocity of bubble in stagnant liquid	m/sec
U_b	Bubble front velocity	m/sec
U_f	Slug front velocity	m/sec
U_g	Gas velocity	m/sec
U_l	Liquid velocity	m/sec
U_{gs}	Gas velocity in slug	m/sec
U_{gb}	Gas velocity in bubble	m/sec
U_{ls}	Liquid velocity in slug	m/sec
U_{lb}	Liquid velocity in bubble	m/sec
U_{sg}	Superficial gas velocity	m/sec
U_{sl}	Superficial liquid velocity	m/sec
USW	Superficial water velocity	m/sec^3
USG	Superficial gas velocity	m/sec
V	Volume	m^3
x	Distance	m

Greek Letters	Description	Unit
α	Void fraction	-
β	Pipe inclination relative to horizontal	deg
ε	Pipe wall roughness	m
θ	Wetted half angle in pipe cross section	rad
λ	Friction factor	-
μ	Dynamic viscosity	Pa s
π	Pi constant = 3.14	-
ρ	Density	Kg/m^3
σ	Surface tension	N/m
τ	Shear stress	Pa
υ_s	Slug frequency	Hz

Subscripts	Description
acc	Acceleration
b	Bubble
film	Film
fric	Friction
g	Gas
h	Hydraulic
i	Gas-liquid interface
l	Liquid
lam	Laminar
m	Mixture
s	Superficial
s	Slug
w	Wall

1. EXECUTIVE SUMMARY

This work has been performed primarily utilizing field measurement holdup and pressure data provided by Saudi Aramco Oil Company. The holdup data was obtained using gamma measurement technique and simulated using two slug prediction models; slug capturing in LedaFlow and slug tracking in OLGA.

The work presents a unique set of large diameter, high pressure data which can be utilized to develop and/or improve multiphase flow simulation tools for industrial oil and gas applications. The data were presented to the OLGA Verification and Improvement Project (OVIP) as part of Saudi Aramco contribution to the improvement program.

Recent OVIP reports which were published by OLGA development team in the 3rd and 4th quarters of 2014 confirmed the author conclusion which indicates a significant over-prediction of the pipelines pressure drop when slug tracking is enabled in most of the cases. The OLGA development team explored this issue and reported a critical flaw in the slug tracking module which is currently being tackled by the team in order to resolve it in a timely manner. A temporary solution was implemented which improved the results as per the published reports, however a more thorough analysis is required before any final solution is implemented. The discovery of this major flaw in OLGA slug capturing module proves the importance of field measurement data in developing accurate multiphase flow simulation models.

LedaFlow on the other hand required the use of a fine mesh in order to obtain good results using the slug capturing module. In most of the cases, a fine mesh which was constructed using (10 * Diameter) was found to provide reasonable results. A finer mesh could have been used but that would require a significant increase in computational time, especially for long pipeline cases which sometimes exceeded (50) Km.

In addition to the simulation work, a detailed statistical analysis was carried out to extract the most important information from the holdup data. This mostly included information about the slugs lengths, tail and front velocities, amplitude and frequency. The data was obtained using a Matlab code which was customized specifically for each case.

The analyzed data consists of two main parts:

- The first part, Field-A, was obtained by Mikal Espedal in 1999 as part of a field measurement project. The work was focused on extremely high hilly terrain multiphase flow pipelines which were 16 inch and 20 inch in diameter. These pipelines were operated in a very high pressure mode, 30 to 60 bar. The high hilly terrain, 100 meter high hills, implies that the dominant slugging mechanism is terrain-slugging and as such accurate predictions of pressure drop and pressure cycles were expected from the simulation tools. However, the combination of terrain slugging with choked valves introduced a new phenomenon which provided an interesting and challenging simulation problem. The simulation work indicates a negative impact of the choke on most of the slugging cases.

  This is counter-intuitive and has not been addressed by any researcher in large diameter oil and gas pipelines prior to this work. Most of the earlier work on choke-slug interactions indicates a positive impact on slug reduction/elimination in offshore pipeline-riser systems. However, the present work indicates that with terrain-induced slugs, the slugging behavior is amplified and a careful investigation of the pipeline system is required before any installation of choked valves. The new phenomenon was

further confirmed by the experimental work carried out at NTNU multiphase flow lab. The lab experiments indicate that the additional force created by the choked valves does not help to overcome the compressibility force that exists in the pipeline system. As a result, slugs are still created in the pipeline system and they are amplified by the accumulation of liquid at the tight valve opening. This liquid accumulation compresses the gas upstream and causes a further pressurizing of the system, which eventually leads to larger pressure fluctuations.

In addition, OLGA simulation results indicated that, with exception of one pipeline, G2NT1, the non-slug tracking option provided the best results as expected in the cases were large terrain-induced slugs dominate the multiphase flow behavior. Utilizing the slug tracking option in OLGA did not improve the results and in some cases caused larger deviations from the field measurements. Slug tracking also was not able to correctly predict any of the small hydrodynamic slugs measured during holdup measurements.

On the other hand, LedaFlow simulation results provided similar results to OLGA as expected. Both multiphase flow codes utilize the same unit cell model to predict large terrain-induced slugs with possibly minor differences in the correlations used in each code. The non-slug capturing cases provided the best results with LedaFlow and the use of slug capturing module did not significantly improve the results as these pipelines where mostly exhibiting large terrain slugging. Slug capturing with relatively fine grid, (5) meters sections, was evaluated to simulate the small hydrodynamic slugs observed between the large slugs. However, LedaFlow could not correctly predict these hydrodynamics slugs using the utilized fine mesh.

In general OLGA and LedaFlow produced large deviations in average pressure drops which ranged between 15% and 25%, especially in the longer pipelines, G3ST1 pipeline (18) Km and G3ST2 pipeline (20) Km. On the other hand, the frequency and amplitude of slugs were better predicted by both multiphase flow transient codes. The deviations cannot be solely attributed to the multiphase flow simulation codes as uncertainties with field measurements exist and particularly the ones related to fluid flow rates, which were estimated based on historical well production data.

- The second part, field measurement of Field-B, C, D and E, was obtained by the author and members of the flow assurance team at Saudi Aramco in 2012, with the help of a gamma-licensed contractor, Tracerco Ltd., who carried out the physical gamma measurement based on the project requirements set by Saudi Aramco. The work covered variety of onshore and offshore pipelines with very large diameters that ranges from 24 inch to 42 inch. The analysis of the data was performed by the author and are presented in the present work. Although slugging was not experienced in most of these pipelines, a different set of challenges were encountered in each one of them as explained separately in each chapter. The hydrodynamic-slugs initiated differently by the simulation codes OLGA and LedaFlow, seem to have a significant impact on the pressure drop results obtained in each case and as such should be used with caution when simulating multiphase flow pipelines.

  OLGA simulation indicated an overall good agreement with pressure and holdup field measurements when slug tracking option was disabled. A significant over-prediction in pressure drop was observed in OLGA predictions when slug tracking option was enabled, as was also noticed by OLGA development team in their latest reports. However, there was an exception for this overall good agreement which was observed at Field-E TL-12. At TL-12 pipeline, the oil wells where connected to the trunkline over a long distance along the pipeline, which created a situation where the flow rates were considerably low at the start of the pipeline. The superficial gas and liquid velocities ranges from 0.15 m/sec and 0.14

m/sec at the beginning of the pipeline to 10 m/sec and 0.75 m/sec at the end of the pipeline, respectively. The OLGA pressure under-prediction in the non-slug tracking case was approximately (75) psi, which is equivalent to 20% error.

LedaFlow on the other hand showed a similar behavior to OLGA predictions without slug capturing. When slug capturing is enabled, then a fine grid is required to obtain accurate predictions. The slug capturing generally provided better results in terms of pressure drop and holdup if a fine grid is utilized. The one exception where LedaFlow did not perform very well was the same Field-E TL-12 remote header case where OLGA also did not perform very well. In that particular case, both options in LedaFlow, the slug capturing and non-slug capturing cases proved equally poor with pressure under-predictions of approximately (60) psi which is equivalent to approximately 16% error.

The large pressure discrepancy noted for Field-E TL-12 pipeline case could partially be attributed to the uncertainties with pipeline profile which is closely related to the static head pressure component known to be the dominant phenomena in low multiphase flow rates cases. However, a large pressure discrepancy was also noted about two years ago in a 36 inch pipeline which was operating in the same area. OLGA simulation at that time was carried out using an approximated pipeline profile and resulted in a pressure under-prediction of more than 100%. When using a more accurate pipeline profile, the pressure predictions where greatly improved but still showed significant under-prediction in pressure of approximately 35%. Therefore, there seems to be a general tendency for multiphase simulation packages to under-predict pressure drop in very low flow rates pipelines such as TL-12.

Finally, the work included a thorough analysis of the gamma measurement technique. It showed how a careful and deep understanding of the methodology is required in order to obtain accurate holdup results especially in a field measurement environment were uncertainties are normally higher than the controlled experimental laboratory environment. In particular, there was a focus on the gamma calibration techniques and the unavailability of calibration pipeline spools with the same wall thickness during the field measurements. This issue created a great challenge that had to be pursued carefully by correcting for the additional wall thickness in order to obtain the right mixture density.

2. INTRODUCTION

Slug flow is a transient phenomenon which occurs in many industrial applications such as fluid flow in multiphase oil and gas pipelines, liquid-vapor flow in nuclear power plants and buoyancy-driven fermentation equipment, A. Dukler & Fabre (1994). This phenomenon is largely described as being undesirable mode of operations due to its transient nature, which affects the downstream facilities operations, and causes higher pressure drop across the pipeline.

Slug flow is a very complex and transient multiphase flow regime where, unsteady sequence of large bubbles and liquid slugs occurs at a randomly fluctuating frequency in the pipe, (J. Fabre & Liné (1992); Woods & Hanratty (1999)). These liquid slugs can be made of pure liquid or could be aerated due to gas entrainment from the neighboring bubbles, (Nydal & Andreussi (1991); Andreussi, Bendiksen, et al. (1993); Bendiksen et al. (1996)).

There are two known mechanisms for the generation of slugs in horizontal and nearly horizontal pipes. These mechanisms are: (i) natural growth of hydrodynamic instabilities (Kelvin-Helmholtz) and (ii) liquid accumulation due to the local imbalance between pressure and gravitational forces mainly caused by pipeline undulations. These two mechanisms could potentially occur together in many industrial applications leading to a very complicated slug pattern, Issa & Kempf (2003). These slugs may grow, merge or decay based on the slug front and tail velocities (Taitel & Barnea (1990); Zheng et al. (1994)).

The prediction of phase velocities, hold-up, pressure drop, slug velocities, slug void fraction and other slug parameters is considered as a very difficult task. Thus, researchers have spent a lot of time and efforts to collect valuable lab and field data about this phenomenon and present various types of models that would reflect the correct physics of the slug flow problem.

The existing multiphase flow data available in the oil industry can be divided into three categories as described by Kristiansen (2004): (i) small scale, atmospheric air water experiments, (ii) medium and large scale experiments and (iii) large diameter field data. This research will include mainly collection and analysis of field data from various oil fields for large diameter pipelines, which are operated by Saudi Aramco in Saudi Arabia.

Various slug modeling approaches have been developed over years of research and investigation, which can be categorized into steady state and transient models.

The first attempt was made using the traditional unit cell model for fully developed steady state slug flow. In this model, a control volume approach is used where, both the gas bubble and liquid slug is analyzed in a steady state manner by selecting a moving frame reference travelling at the speed of the cell and applying mass and momentum balances over the control volume (Wallis (1969); A. E. Dukler & Hubbard (1975); Taitel & Barnea (1990)).

Transient models soon followed with two important contributions: (i) slug tracking models and (ii) slug capturing models. A hybrid model, NTNU SLUGGIT code, which possess features from both slug tracking and slug capturing models also exists and is currently being further developed by several PhD students at NTNU.

In slug tracking models slugs are generated and tracked individually so that the position of the tail and front of each slug is known along the pipe with time. OLGA (Bendiksen et al. (1991)) is a good example of a slug tracking model application where empirical correlations are used to model certain slug characteristics.

Similar slug tracking technique has been also proposed by Zheng et al. (1994), where a prediction of slug growth, generation and dissipation is monitored for each slug along the pipeline.

In slug capturing techniques, slug flow is predicted by a strict application of the two fluid model in a mechanistic way. This minimizes the use of empirical correlations and provides a natural transition from stratified to slug flow. As a result, slugs are created, grow, merge and decay naturally as a pure outcome of the numerical solution of the two fluid model, Issa & Woodburn (1998).

A hybrid model has recently been developed at NTNU which exhibit features of both slug tracking and slug capturing techniques. The new model, SLUGGIT, was initially developed by Nydal & Banerjee (1996) as a lagrangian slug tracking method with a moving grid. The method has grown since then with more detailed modeling especially on in the stratified region, bubble and liquid film below it, to become more rigorous and incorporate features from the slug capturing technique removing the necessity to include an empirical criterion for slug initiation.

The objective of this work is to collect, analyze and simulate field data from various large diameter pipelines at Saudi Aramco oil and gas fields that are known to be slugging. The data originates from two main sources: (i) an old set of data which was collected in 1991 and (ii) a new set of data which was recently collected by the author in late 2011 and early 2012. The holdup data was collected using a gamma measurement technique which enables accurate calculation of the holdup in the pipeline at very high frequency. This data was then analyzed thoroughly to obtain the relevant slug characteristics and associated pressure drop and phase velocities through careful post-processing techniques. Finally, these pipelines were simulated using various simulation techniques which enabled us to modify and tune those simulation packages and draw conclusions accordingly.

The project's specific objectives are:

- Analyze and simulate an old collection of pressure and holdup information which represents a unique set of data on a high pressure, (30 to 50) bars, highly undulating pipeline with variation in elevation that reaches more than 100 meters.
- Prepare, design and conduct accurate field pressure and gamma-holdup measurements at four (4) different geographical locations, both onshore and offshore pipelines, with a total of six (6) pipelines with various flow rates and boundary conditions. The pipeline diameters range from 24 inch to 42 inch with various crude oil properties and terrain characteristics.
- Conduct a thorough analysis of the collected data using various statistical techniques such as cross-correlations, in order to obtain various general flow characteristics and slug behavior. Such slug characteristics would include, slug length, frequency and slug tail and front velocities.
- Carry out various simulation experiments using different tools with various numerical schemes and bases such as slug tracking (OLGA) and slug capturing (LedaFlow).
- Conduct lab experiments on specific terrain-slugging phenomena if deemed required.

Holdup measurement which requires gamma measurement technique is often used in multiphase flow loops at research labs and universities. Several attempts have also been made to utilize this measurement technique in online oil and gas field applications. The results were encouraging such as the ones carried out at Prudhoe Bay field in Alaska in 1981, Brill et al. (1981). In Prudhoe Bay measurements a total of 29 multiphase flow tests were conducted on two pipelines, one 12 inch diameter and one 16 inch diameter. The pipelines were approximately (5) kilometres long, and the tests were conducted with various oil and gas flow rates and boundary conditions.

A more recent field measurement was conducted at the North Sea Heidrun offshore field which was carried out by Statoil in August 2000 and reported by Andreussi et al. (2011). The measurements were carried out on two wells in order to investigate the slugging behaviour experienced in that field. The pipeline diameters were only 10 inch with a total pipeline length of approximately (5) kilometres.

British Petroleum (BP) conducted new measurements on a 30 inch diameter, (11) kilometre long pipeline which was experiencing slugging behaviour. The pipeline had an almost flat pipeline profile and the holdup and pressure measurements collected from this pipeline were compared against OLGA simulation with various delay constants, Fan et al. (2013).

In general, the amount of field data available in literature is limited and does not cover very large diameter pipelines, which makes the information collected in this project very unique.

This page was intentionally left blank

3. LITERATURE REVIEW

This section will cover the literature review of five main subjects related to multiphase flow in pipelines and in particular to slug flow regime: (i) multiphase flow regimes flow maps, (ii) review of slug flow regime, (iii) stratified flow two-fluid model, (iv) slug flow unit cell model and (v) slug flow transient prediction models.

3.1. Multiphase Flow Regimes and Flow Maps

Multiphase flow is a common phenomenon that exists in many real life and industrial applications. It occurs when fluids at different states, such as liquid and gas, and properties, such as oil and water, co-exist together. Usually this phenomenon occurs during the transportation of these fluids from one location to another using a transportation scheme, such as oil and gas pipeline, heat exchangers tubes, micro or nano-channels in computer processers. The co-existence of these fluids normally takes many forms depending on flow conditions and fluid properties. These forms are technically referred to as flow multiphase flow regimes, which are subject to extensive research and investigation to evaluate its behavior and flow characteristics at various conditions.

Multiphase flow regimes in pipelines are normally categorized into two main categories: (i) separated flow and (ii) distributed flow. A third category can also be added, which is basically a combination of both types of flows and that is the intermittent flow. Flow regimes are also categorized based on the pipeline orientations, horizontal pipelines, Figure 3-1, and vertical pipelines, Figure 3-2.

In horizontal pipelines, the most common flow regime is the stratified flow regime especially with zero degree inclination or negative degree inclination pipelines. As you increase the gas flow rate, the interface becomes wavy and with even higher gas flow rates and sufficient liquid flow rates, a slug flow regime usually occurs, where a sequence of liquid slugs are followed by large gas bubbles. At extremely high gas flow rates, the liquid tend to wet the pipeline wall with gas going through the middle of the pipe in what is normally referred to as annular flow. On the other hand, with extremely high liquid flow rates a bubbly flow regime occurs where small dispersed bubbles exist throughout a liquid flow medium.

In vertical pipelines, the same fluid flow behavior occurs with similar flow regimes except for the stratified flow which does not exist in a vertical flow pipeline due to the gravitational force which prevents this kind of flow regime from occurring in vertical pipeline.

In order to predict the transition from one flow regime to another, a simple visual tool was created which is called the flow regime maps. These maps were created by several researchers over the last 60 years with the oldest being present by Baker (1954) for horizontal pipes. Later on, Mandhane et al. (1974) presented his valuable flow map where flow patterns were function of superficial liquid and gas velocities as shown in Figure 3-4. Another example of old but still very useful flow maps is the Taitel & Dukler (1976) flow map shown in Figure 3-5.

These two flow maps and many others which were developed over the years such as the one presented by D. Barnea (1987) provide a useful guideline in the predictions of flow regime transitions and comparisons with new flow transition mechanistic models.

Finally, most of these flow maps were developed using experimental small scale, atmospheric pressure lab data with pipe diameters in the range of ($D<100$ mm) and ($L/D<250$). Therefore, care should be applied when extrapolating the results to large diameter and high pressure systems, Kristiansen (2004).

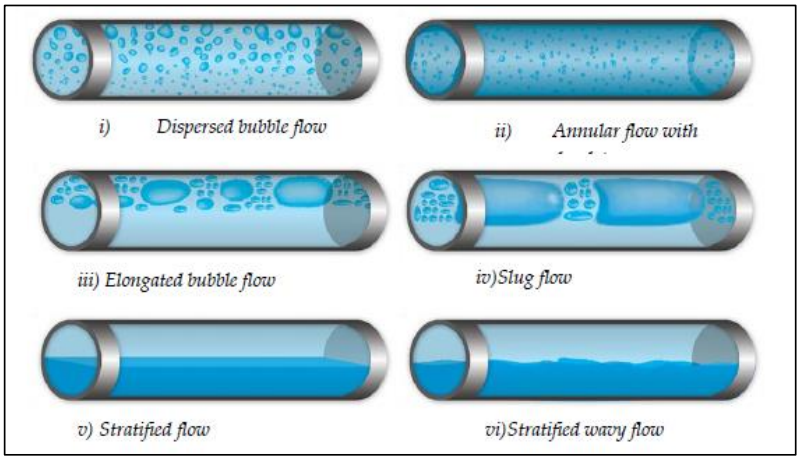

Figure 3-1: Gas-liquid flow regimes in horizontal pipes from Bratland (2010)

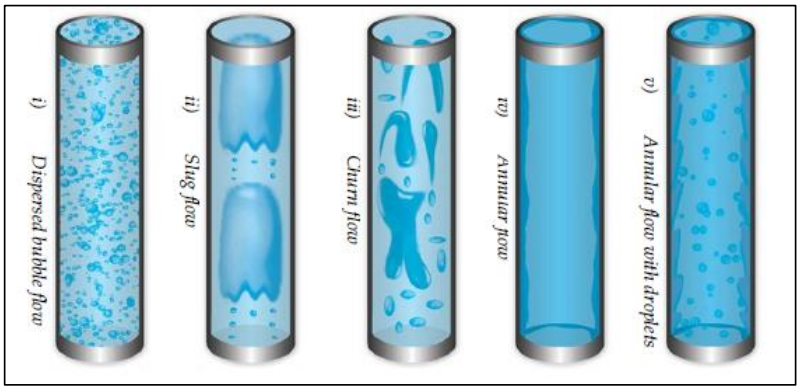

Figure 3-2: Gas-liquid flow regimes in vertical pipes from Bratland (2010)

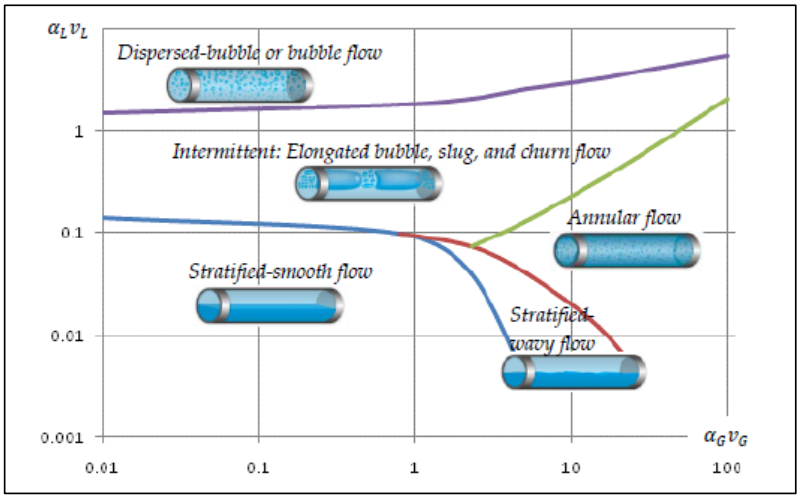

Figure 3-3: Example of steady state flow regime map for horizontal flow from Bratland (2010)

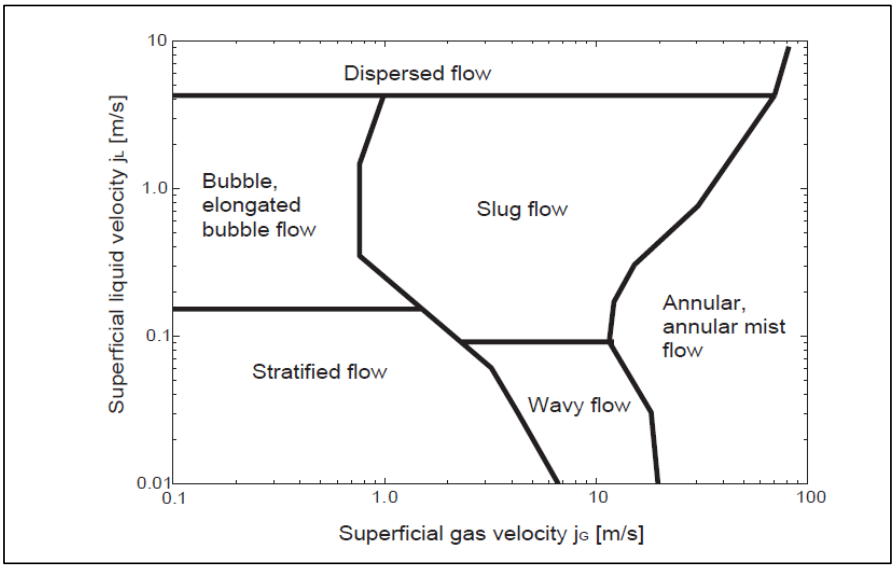

Figure 3-4: Flow pattern map proposed by Mandhane et al. (1974)

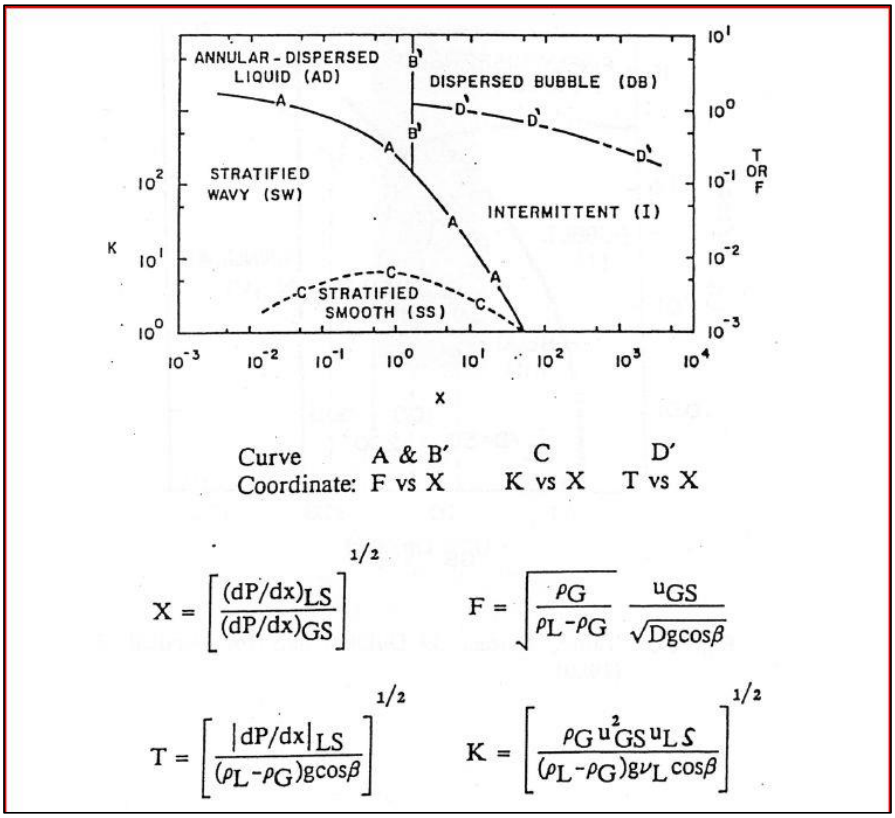

Figure 3-5: Flow pattern map proposed by Taitel & Dukler (1976)

3.2. Review of Slug Flow Regime

Slug flow is often defined as an intermittent flow regime characterized by a sequence of liquid slugs followed by large gas bubbles. It is considered as one of the most complex multiphase flow regimes, which is frequently encountered in many industrial applications. The complexity of the slug flow regime stems out of its unsteady and chaotic nature, which results in time and space fluctuation in flow parameters. Figure 3-6 shows the details of a slug flow unit where a large Taylor bubble is followed by a large aerated liquid slug with a front mixing section. The dynamics of such a slug flow unit that changes with time and space and the various flow variables which are affected by flow and fluid conditions makes it difficult for any steady state or transient models to accurately predict important flow parameters such as pressure drop, phase velocities and heat and mass transfer, Taitel & Barnea (1990) and Bendiksen et al. (1996).

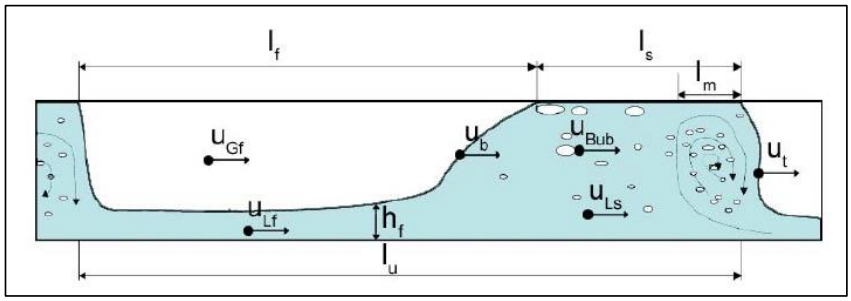

Figure 3-6: Details of a Slug Flow Unit from A. E. Dukler & Hubbard (1975)

Slugs can be divided into two main categories based on their initiation mechanism. Hydrodynamic slugs are initiated due to wave instabilities at the surface of the stratified flow. These instabilities grow until the liquid bridges the pipeline top surface to create a slug, which is normally short, less than 100-D. Terrain-induced slugs on the other hand are initiated due to changes in pipeline inclinations from negative to positive. The liquid usually accumulates at those low points causing a large pressure and flow disturbances in the pipeline system. A severe type of terrain-induced slugging is often encountered in offshore oil and gas base-riser system.

One of the earliest issues tackled by researchers related to slug flow regime was the transition criteria to slug flow from stratified flow regime. The work on this issue can be divided to two basic categories: (i) stability of stratified flow approach and (ii) stability of slug flow approach.

The stability of stratified flow transition criterion can be defined as the critical gas velocity needed to induce instabilities in the smooth stratified flow. This condition is achieved when the destabilizing variations of wave-induced pressures overcome the stabilizing restoring force of gravity. This transition criteria is based on the original work conducted by Milne-Thomson & Rott (1968) on Kelvin-Helmholtz (K-H) waves. There are two types of K-H analysis that have been investigated by researchers over the years, namely viscous and inviscid K-H analysis. The viscous Kelvin-Helmholtz (VKH) utilizes the two-fluid model and takes into account the shear stresses (Wallis (1969), Lin & Hanratty (1986), N Andritsos & Hanratty (1987). The inviscid K-H analysis, on the other hand neglects the shear stresses, (Taitel & Dukler (1976), Kordyban (1977), Mishima & Ishii (1980)), Dvora Barnea & Taitel (1993).

The Kelvin-Helmholtz criteria starts with the two-fluid model which is constituted by the conservation of mass and momentum equations which is linearized by various procedures such as the general approach presented by Dvora Barnea & Taitel (1989). Perturbing the liquid level and solving for the angular frequency and the steady state is considered unstable whenever the imaginary part of angular frequency is

negative. This approach provides a criterion for the transition from stratified smooth to stratified non-smooth flow, Kristiansen (2004). The Taitel & Dukler (1976) inviscid Kelvin-Helmholtz criteria as reported by Hurlburt & Hanratty (2002) can written as follows:

$$\rho_g\left(U_g - U_l\right)^2 = \left(1 - \frac{h_l}{D}\right)\frac{\rho_l g \alpha_g A}{dA_l/dh_l} \tag{3.1}$$

The slug stability criterion on the other hand, predicts slug flow when slugs can be sustained rather than initiated. This condition occurs when the slug front velocity exceeds the slug tail velocity, which is equal to the Taylor front bubble velocity. This criterion was first developed by Bendiksen & Espedal (1992) and further developed by Hurlburt & Hanratty (2002). The model applies simple mass balance over the slug-bubble border to reach the following condition, as shown in Figure 3-7:

$$U_b < U_f \quad ; \quad or \tag{3.2}$$

$$U_b < U_{gD}\left[\frac{\alpha_b - \alpha_s \frac{U_{gs}}{U_{gD}}}{\alpha_D - \alpha_s}\right] \tag{3.3}$$

where subscript (D) in equation (3.3) refers to the bubble section downstream of the slug body. A special case can be obtained from equation (3.3) when ($\alpha_s = 0$) as follows:

$$U_b < U_{gD} \tag{3.4}$$

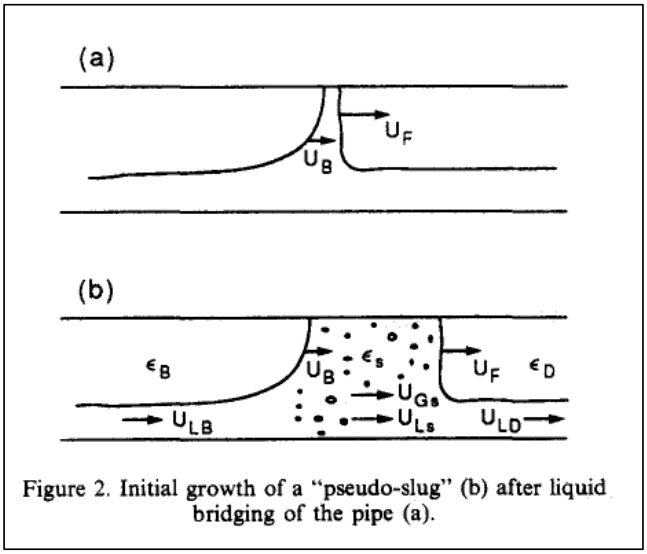

Figure 2. Initial growth of a "pseudo-slug" (b) after liquid bridging of the pipe (a).

Figure 3-7: Initial growth of a "pseudo-slug" (b) after liquid bridging of pipe from Bendiksen & Espedal (1992)

Hurlburt & Hanratty (2002) argued that the instability of the stratified flow is a necessary but not sufficient condition to sustain slug flow regime. Slug stability criteria must also be satisfied for slug flow to be sustained.

On the other hand, the prediction models for slug flow can be divided into two main categories: (i) steady state slug flow models and (ii) transient slug flow models. The most important example of steady state

models is unit cell model which assumes a fixed slug frequency and slug length that repeats itself in a train-like scheme. Whereas, transient slug flow models come into two broad methods, slug tracking methods and slug capturing methods. All of these steady state and transient models will be discussed in more details in the following sections.

3.3. Stratified Flow Two-Fluid Model

The two fluid model presented in this section consists of the mass and momentum equation for liquid and gas phases. The two-fluid model is based on the following assumptions: (i) isothermal conditions, (ii) no liquid entrainment, (iii) no gas entrainment and (iv) a flat gas-liquid surface, Kristiansen (2004).

Using exact geometrical relationships, shown in Figure 3-8, one can obtain an expression for the liquid holdup (H) in terms of the wetted half-angle as follows:

$$H = \frac{1}{\pi}(\theta - \frac{1}{2}\sin(2\theta)) \tag{3.5}$$

Biberg (1999) introduced an approximate expression for (θ) in terms of (H) within ±0.002 rad.

$$\theta = \pi H + \left(\frac{3\pi}{2}\right)^{\frac{1}{3}}\left[1 - 2H + H^{\frac{1}{3}} - (1-H)^{\frac{1}{3}}\right] \tag{3.6}$$

Defining the liquid height (h) as the non-dimensional vertical center-line fraction of liquid, (θ) can be related to (h) as follows:

$$\theta = \cos^{-1}(1 - 2h) \tag{3.7}$$

Similarly, (h) can be obtained in terms of (θ) as follows, Kristiansen (2004):

$$h = \frac{1}{2}(1 - cos\ \theta) \tag{3.8}$$

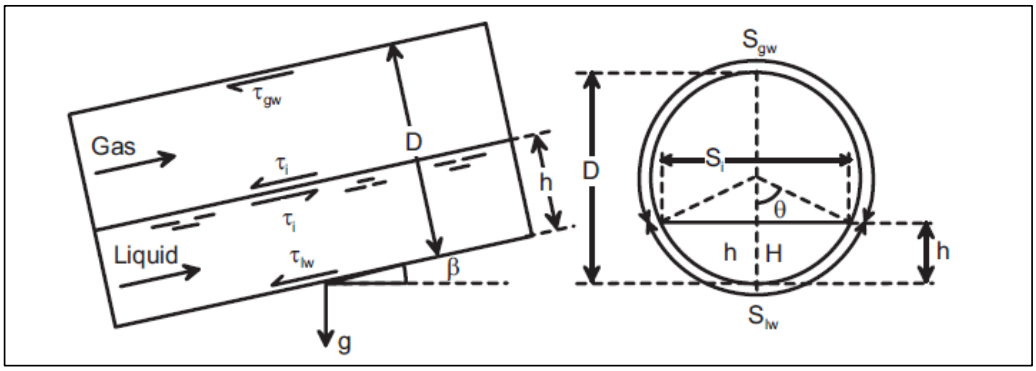

Figure 3-8: Ideal cross-section geometry for two-phase stratified flow from Kristiansen (2004)

3.3.1. Conservation of Mass

Conservation of mass is applied for each phase assuming no droplet/bubbles deposition or entrainment. The conservation of mass equations can be written as follows:

$$\frac{\partial}{\partial t}(H\rho_l) + \frac{1}{A}\frac{\partial}{\partial x}(H\rho_l U_l A) = 0 \tag{3.9}$$

$$\frac{\partial}{\partial t}(\alpha_g\rho_g) + \frac{1}{A}\frac{\partial}{\partial x}\left(\alpha_g\rho_g U_g A\right) = 0 \tag{3.10}$$

$$H + \alpha_g = 1 \tag{3.11}$$

3.3.2. Conservation of Momentum

Conservation of momentum is also applied to each phase as described in two phase flow literature such as Taitel & Dukler (1976) and Bendiksen et al. (1991). The full momentum equation with mass sources and convective and acceleration terms can be written as follows:

$$\frac{\partial}{\partial t}(\rho_k \cdot u_k) + \frac{\partial}{\partial x}\left(\rho_k\ u_k(u_k - u_b)\right) = -\frac{\partial p}{\partial x} + \frac{\partial \tau_k}{\partial x} - \rho_k\, g \cdot sin\beta + \dot{\rho}_k^s\, u_k^s \tag{3.12}$$

where (k) represents each phase independently. Making the assumptions of constant liquid holdup, equal pressures in both phases and neglecting acceleration and convective terms, Kristiansen (2004), one can obtain the simplified momentum equation:

$$-H\frac{\partial P}{\partial x} - \frac{S_{lw}}{A}\tau_{lw} + \frac{S_i}{A}\tau_i + H\rho_l \cdot gsin(\beta) = 0 \tag{3.13}$$

$$-\alpha_g\frac{\partial P}{\partial x} - \frac{S_{gw}}{A}\tau_{gw} - \frac{S_i}{A}\tau_i + \alpha_g\rho_g \cdot gsin(\beta) = 0 \tag{3.14}$$

The pressure equation can be obtained by adding equations (3.13) and (3.14) to eliminate the interfacial shear stress term as follows:

$$\frac{\partial P}{\partial x} = \frac{S_{lw}}{A}\tau_{lw} + \frac{S_{gw}}{A}\tau_{gw} + (H\rho_l + \alpha_g\rho_g) \cdot gsin(\beta) \tag{3.15}$$

In addition, the holdup equation can be obtained by subtracting equations (3.13) and (3.14) to eliminate the pressure gradient term as follows:

$$\frac{S_i}{A}\tau_i = -H\frac{S_{lw}}{A}\tau_{lw} + \alpha_g\frac{S_{gw}}{A}\tau_{gw} + (\rho_l - \rho_g) \cdot H\alpha_g gsin(\beta) \tag{3.16}$$

The gas, liquid and interfacial shear stress terms are calculated based on empirical correlations that determine the gas-wall, liquid-wall and interfacial friction factors as follows:

$$\tau_{lw} = \frac{\lambda_{lw}}{4}\frac{\rho_l U_l|U_l|}{2} \tag{3.17}$$

$$\tau_{lg} = \frac{\lambda_{lg}}{4}\frac{\rho_g U_g|U_g|}{2} \tag{3.18}$$

$$\tau_i = \frac{\lambda_i}{4}\frac{\rho_g(U_g - U_l)|U_g - U_l|}{2} \tag{3.19}$$

In order to calculate the friction factor terms (λ_k) is hydraulic diameters and Reynolds numbers need to be calculated as follows:

$$Re_l = \frac{\rho_l U_l D_{hl}}{\mu_l} \quad ; \quad Re_g = \frac{\rho_g U_g D_{hg}}{\mu_g} \tag{3.20}$$

$$D_{hl} = 4 \cdot \frac{A_l}{S_l} \quad ; \quad D_{hg} = 4 \cdot \frac{A_g}{S_g + S_i} \tag{3.21}$$

Liquid-wall and gas-wall friction factors are calculated based on the calculated Reynolds numbers as follows:

For Laminar Cases:

$$\lambda_{lw,laminar} = \frac{64}{Re_l} \quad ; \quad \lambda_{lg,laminar} = \frac{64}{Re_g} \tag{3.22}$$

For Turbulent Cases:

$$\lambda_{lw,turb} = \frac{1}{\left[-1.8 \cdot \log_{10}\left(\frac{6.9}{Re_l} + \left(\frac{\epsilon/D_{hl}}{3.7}\right)^{1.11}\right)\right]^2} \tag{3.23}$$

$$\lambda_{lg,turb} = \frac{1}{\left[-1.8 \cdot \log_{10}\left(\frac{6.9}{Re_l} + \left(\frac{\epsilon/D_{hg}}{3.7}\right)^{1.11}\right)\right]^2} \tag{3.24}$$

where (ϵ) is the pipe roughness in meters. The friction factors are calculated based on the respective Reynolds numbers and the maximum value is normally used for any Reynolds number value.

The interfacial friction factor remains to be calculated and based on the literature many empirical correlations are available for this term. The correlations take many forms and they vary from very simple relations in terms of gas friction factor to a very complicated modified roughness form which include many parameters such as velocity and liquid holdup. Espedal (1998) in his PhD thesis included a very detailed review of a wide range of interfacial friction factor correlations. A few of those correlations reported by Espedal (1998) will be discussed below, which represents the different forms of correlations.

Russell et al. (1974) proposed a very simple model where he assumed that the gas sees a slid boundary at the interface and as such he concluded that interfacial friction factor is equal to the gas friction factor:

$$\lambda_i = \lambda_g \tag{3.25}$$

Cheremisinoff & Davis (1979) proposed a model which was based on a model for small amplitude waves and the interfacial frication factor was stated as follows:

$$\lambda_i = 0.0142\left(\frac{U_g}{U_g - U_l}\right)^2 \tag{3.26}$$

Kawaji et al. (1987) proposed a model that better fitted his high pressure steam-water data. The proposed model utilizes the gas-wall friction factor which is based on Reynolds number calculated using the superficial gas velocity as follows:

$$\lambda_i = 3\lambda_{sg} \tag{3.27}$$

$$\lambda_{sg} = 0.1840 \cdot Re_{sg}^{0.2} \quad , \quad Re_{sg} = \frac{p_g U_{sg} D}{\mu_g}$$

Hidy & Plate (1966) utilized a different form of interfacial friction factor correlations, which is based on channel flow approach. The correlation, which was based on water waves, stated the following:

$$\lambda_i = 0.005336 \cdot \left(\frac{U_g^2}{(U_g - U_l)}\right) \tag{3.28}$$

Linehan (1968) in his PhD thesis developed a correlation which was based on the hydraulic diameter in a liquid channel. The correlation was based on the experimental data collected by Cohen & Hanratty (1968). The correlation was stated as follows:

$$\lambda_i = 0.0524 + 0.92 \cdot 10^{-5} \cdot Re_l^* \quad ; \quad Re_l^* = \frac{3}{8} Re_l \tag{3.29}$$

Kim et al. (1985) proposed a correlation which is based on the counter-current stratified flow in rectangular channels. The proposed correlation was very similar to Linehan (1968) correlation:

$$\lambda_i = 0.084 + 0.56 \cdot 10^{-5} \cdot Re_l^* \quad ; \quad Re_l^* = \frac{3}{8} Re_l \tag{3.30}$$

Hart et al. (1989) proposed a correlation based on their experimental results that showed a strong dependency on the superficial liquid phase Reynolds number, as follows:

$$\lambda_i = \lambda_l \cdot \left(\frac{Re_{sl}^{0.726}}{108}\right) \tag{3.31}$$

Andreussi & Persen (1987) proposed a more complex correlation which depends on the dimensionless film height and gas Froude number. The correlation for stratified wavy flow took the form of:

$$\lambda_i = \lambda_g \left[1 + 29.7\left(Fr_g - 0.36\right)^{0.67} \left(\frac{h_l}{D}\right)^{0.2}\right] \quad ; \quad for \quad Fr_g > 0.36 \tag{3.32}$$

and for stratified smooth flow:

$$\lambda_i = \lambda_g \quad ; \quad for \quad Fr_g < 0.36 \tag{3.33}$$

Nikolaos Andritsos (1986) proposed a correlation that was fitted to air-water stratified flow with large amplitude waves. The correlation stated that for gas superficial velocity higher than a critical transition value, ($U_{sg} > U_{sgt} = 5.0\ m/\text{sec}$), the correlation states the following:

$$\lambda_i = \lambda_g \left[1 + 15\sqrt{\left(\frac{h_l}{D}\right)} \left(\frac{U_{sg}}{U_{sgt}} - 1\right)\right] \quad ; \quad for \quad U_{sgt} > 5.0\ m/sec \tag{3.34}$$

and for stratified smooth flow with small amplitudes:

$$\lambda_i = \lambda_g \quad ; \quad for \quad for \quad U_{sgt} < 5.0\ m/sec \tag{3.35}$$

3.4. Slug Flow Unit Cell Model (UCM)

The slug flow steady state unit cell model was first presented by Wallis (1969) and since then it has established itself as the easiest and most reliable method for predicting the general characteristics of slug flow. A. E. Dukler and Hubbard (1975) later published his famous paper which properly formulated the unit cell model for all pipeline inclinations. The basic idea of the unit cell model is to assume an idealized slug flow model made of identical cells Jean Fabre (2002). The unit cell model is based on two basic assumptions:

- The existence of a steady state frame with a constant velocity at which slugs and bubbles pass through.
- A fully developed flow is assumed in this frame for all slugs and bubbles.

These assumptions are very important as they allow for the uncoupling of the phase fractions and pressure gradients from slug lengths as we will see later on when developing the models equations. Although the first assumption seem to be contradicting the usual observations made with slug flow regimes where slugs and bubbles have random distribution of lengths and velocities. Careful analysis of the velocities of slugs and bubbles indicates that they are narrowly distributed around their average values, as shown in Figure 3-9. The second assumption assumes that in each part of the unit cell, the flow is fully developed, which consequently means that the phase fractions and velocities are independent of the x-coordinate Jean Fabre (2002).

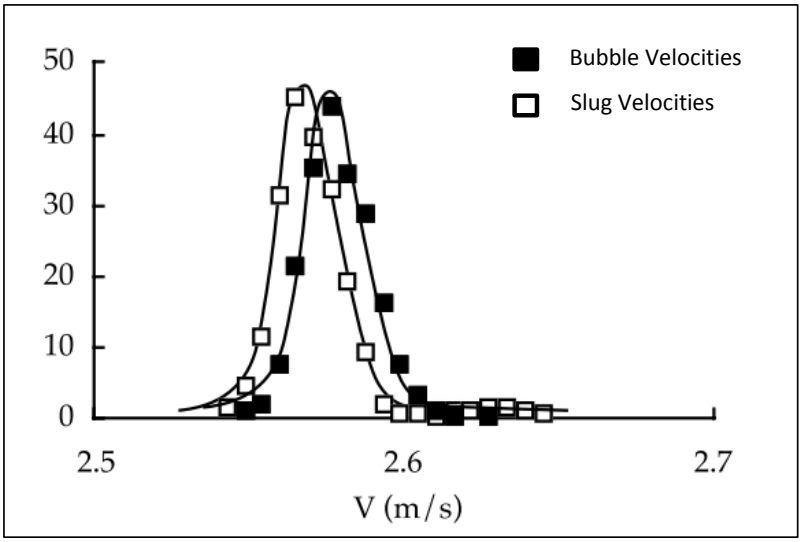

Figure 3-9: Probability density distribution of bubble and slug velocities from J. Fabre et al. (1993)

The slug unit cell shown in Figure 3-10 indicates (9) unknowns needed to complete the solution of the unit cell model. These (9) unknowns are described in Table 2-1:

Table 3-1: List of the (9) Unknowns in Unit Cell Model

Variable	Description	Comments
α_s	Void fraction in slug	Requires empirical correlations
H_b	Liquid fraction in bubble film, ($H_b = 1 - \alpha_b$)	Obtained using the holdup equation derived in the two-fluid model
U_{gs}	Gas velocity in slug	Requires empirical correlations
U_{gb}	Gas velocity in bubble	Obtained from gas velocity balance equations at the slug-bubble border
U_{ls}	Liquid velocity in slug	Obtained from the total volume balance
U_{lb}	Liquid velocity in bubble	Obtained from liquid velocity balance equations at the slug-bubble border
U_b	Bubble front velocity	Requires empirical correlations
S_f	Slug fraction	$S_f = \frac{L_s}{L_s + L_b}$
L_s	Slug length	Requires empirical correlations

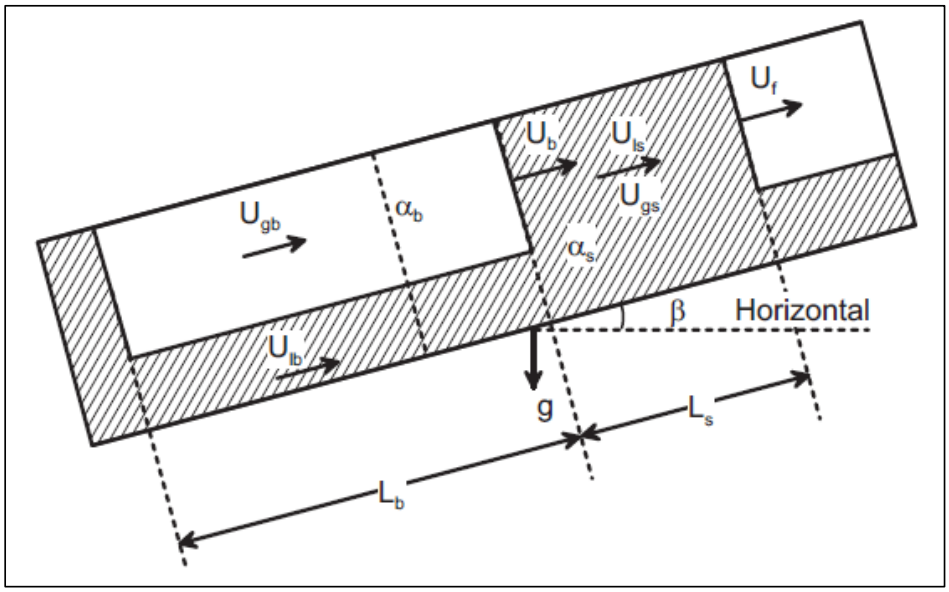

Figure 3-10: Gas-Liquid Slug Flow Unit Cell made of Total Slug length (L) divided into slug liquid body length (L_s) and long gas bubble length (L_b) – from Kristiansen (2004)

Four (4) closure laws in the form of empirical correlations are required to solve for the (9) unknowns. The accuracy of the model largely depends on these empirical correlations and the bases and flow conditions used to develop them. As shown in Figure 3-10, the unit cell model consists of a bubble followed by a liquid slug with an average slug void fraction (α_s). The slug section can be modeled as bubbly flow regime while

the bubble section can be modeled as a stratified gas-liquid flow regime. The large bubble in the bubble section is assumed to be free of droplets while the buoyancy force for the gas bubbles in the slug body is modelled by a drift flux model.

3.4.1. Formulation of the Unit Cell Model (UCM) Equations

The formulation depicted in this section will follow the one developed by Fuchs (1997) and was presented and elaborated by Kristiansen (2004) in his excellent review of unit cell model as part of his doctoral thesis literature review. We start by defining the mixture velocity as:

$$U_m = U_{sg} + U_{sl} \tag{3.36}$$

where ($U_{sg} = \alpha_g U_g$) and ($U_{sl} = \alpha_l U_l$) are the superficial gas and liquid velocities respectively. The mixture velocity is assumed to be constant in both of the slug and bubble sections. Therefore, the mixture velocity can also be written as:

$$U_m = \alpha_s U_{gs} + (1 - \alpha_s) U_{ls} \tag{3.37}$$

$$U_m = \alpha_b U_{gb} + (1 - \alpha_b) U_{lb} \tag{3.38}$$

The gas and liquid balances across the slug-bubble borders can be obtained as follows:

$$\alpha_b (U_b - U_{gb}) = \alpha_s (U_b - U_{gs}) \tag{3.39}$$

$$(1 - \alpha_b)(U_b - U_{lb}) = (1 - \alpha_s)(U_b - U_{ls}) \tag{3.40}$$

Equation (3.40) can be re-arranged to obtain an expression for (U_b):

$$U_b(\alpha_s - \alpha_b) = (1 - \alpha_b) U_{lb} - (1 - \alpha_s) U_{ls} \tag{3.41}$$

The total liquid volume balance can be written as follows:

$$U_{sl} = U_{ls}(1 - \alpha_s) S_f + U_{lb}(1 - \alpha_b)(1 - S_f) \tag{3.42}$$

Using the definition of slug fraction (S_f):

$$S_f = \frac{L_s}{L_s + L_b} \tag{3.43}$$

Re-arranging equation (3.42):

$$S_f = \frac{U_{sl} - U_{lb}(1 - \alpha_b)}{[U_{ls}(1 - \alpha_s) - U_{lb}(1 - \alpha_b)]} \tag{3.44}$$

Using equation (3.41):

$$S_f = \frac{U_{sl} - U_{lb}(1 - \alpha_b)}{[U_b(\alpha_b - \alpha_s)]} \tag{3.45}$$

3.4.2. Void Fraction in Slugs (α_s)

The void fraction in slugs is obtained from empirical correlations as stated before. Numerous correlations are available in literature and the oldest is the one developed by Gregory et al. (1978). The equation takes the form of a function mixture density as follows:

$$\alpha_s = 1 - \frac{1}{\left(\frac{U_m}{8.66}\right)^{1.39}} \tag{3.46}$$

The correlation was based on air-light oil mixtures in pipes with diameters of 25.8 mm and 51.2 mm. Malnes (1983) utilized the same set of data to define a new correlation which contains more physical properties, as follows:

$$\alpha_s = 1 - \frac{U_m}{C_{malnes} + U_m} \tag{3.47}$$

$$C_{malnes} = 83 \left(\frac{g\sigma}{\rho_l}\right)^{0.25} \tag{3.48}$$

Where (g) is gravity constant, (σ) is the surface tension and (ρ_l) is the liquid density.

More recently, researchers such as Abdul-Majeed (2000) utilized (435) slug void fraction points from various sources to develop a new correlation. Analyzing the large set of data indicated that the slug void fraction is very slightly affected by the surface tension and pipe diameter. Thus, he proposed a new correlation which is dependent on fluid viscosities, (μ_g, μ_l), and mixture density as reported in Rogero (2009):

$$\alpha_s = (1.009 - C_{Abd} U_m)(1 - sin\beta) \tag{3.49}$$

$$C_{Abd} = 0.006 + 1.3377 \frac{\mu_g}{\mu_l} \tag{3.50}$$

Gomez et al. (2000) also utilized a large set of data from other researchers with pipe diameters ranging from 5.1 to 20.3 cm and pressures ranging from 1.5 to 20 bar. The data also included various pipe inclination angles that ranged from 0 to 90 degrees. Similar to Abdul-Majeed conclusions, the data indicated a dependency on pipe angle in addition to Reynolds number and mixture velocity. The proposed correlation was as follows:

$$\alpha_s = 1 - 1.0^{-(0.45\beta_R + C Re_l)} \qquad 0 \le \beta_R \le \frac{\pi}{2} \tag{3.51}$$

Where, (β_R) is the pipe angle in radian and ($C = 2.48 \cdot 10^{-6}$) is a constant, while the Reynolds number is defined as reported by Kristiansen (2004) as follows:

$$\mathrm{Re}_l = \frac{\rho U_m D}{\mu_l} \tag{3.52}$$

3.4.3. Velocity of Gas Bubbles in Liquid Slug (U_{gs})

As stated earlier, the slug body is modelled as a bubbly flow in the unit cell model, see Figure 3-11.

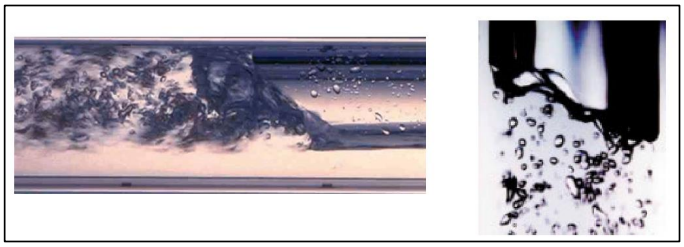

Figure 3-11: Photos of entrainment of gas bubbles in Vertical and Horizontal Slugs from Jean Fabre (2002)

This assumption requires the knowledge of the gas bubble velocity in the liquid slugs. Malnes (1983) proposed a gas-liquid slip relation that consists of a combination of liquid slug velocity and drift velocity as follows:

$$U_{gs} = S_D(U_{ls} + U_{0s}) \tag{3.53}$$

Where, (S_D) is the distribution factor defined as follows:

$$S_D = \frac{1 - \alpha_s}{DF - \alpha_s} \tag{3.54}$$

The distribution factor (DF=0.95) and vertical local drift velocity (U_{0s}) is defined as follows:

$$U_{0s} = 1.18\left[\frac{g\sigma_{gl}(\rho_l - \rho_g)}{\rho_l^2}\right]^{1/4}\sqrt{(1-\alpha_s)} \tag{3.55}$$

Bonizzi (2003) proposed a new approach by solving for the local balance between pressure and drag forces as follows:

$$U_{gs} = U_m - \sqrt{\frac{-4D_{Bub}(dp/dx)}{3C_D\rho_l}} \tag{3.56}$$

Where (C_D) is the drag coefficient defined by Tomiyama (1998) in terms of bubble Reynolds and Eötvös numbers:

$$C_D = \frac{C_{DT}}{\sqrt{\alpha_s}} \tag{3.57}$$

$$C_{DT} = \max\left[\frac{24}{\mathrm{Re}_{Bub}}\left(1 + 0.15Re_{Bub}^{0.687}\right), \frac{8}{3}\frac{E_o}{E_o + 4}\right] \tag{3.58}$$

$$Re_{Bub} = \frac{\rho_l D_{Bub}|U_m - U_{Bub}|}{\mu_l} \tag{3.59}$$

$$E_o = \frac{g(\rho_l - \rho_g)D_{Bub}^2}{\sigma} \tag{3.60}$$

3.4.4. Bubble Front Propagation Velocity (U_b)

The bubble front propagation velocity is probably considered the most important correlation used by the unit cell model. The fact that the slug moves with a higher velocity compared to the mixture velocity is a very well established fact that led to the investigation of the bubble front velocity. The slug velocity is believed to be constant for a fully developed slug flow. At this case, the shedding at the back of the slug body and the entrainment at the front is equal, and as such the slug velocity can be assumed to be equal to the bubble front velocity (U_b).

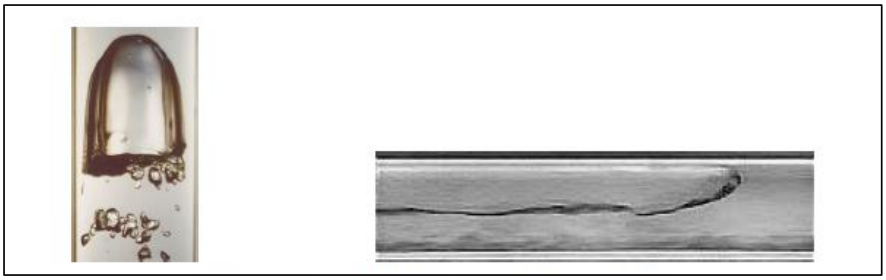

Figure 3-12: Long Bubbles Shape in vertical and horizontal tubes from Jean Fabre (2002)

The research in bubble front propagation velocity started with the work of Nicklin et al. (1962), who investigated the bubble velocity in vertical pipes. Nicklin et al. (1962) proposed a correlation which consists of a center line velocity and a rise velocity in stagnant liquid as follows:

$$U_b = C_0 U_m + C_\infty \sqrt{gD} \tag{3.61}$$

The value of (C_0) coefficient quickly reaches a steady state value of 1.2 as shown by the experiments carried out by Nicklin et al. (1962) shown in Figure 3-13.

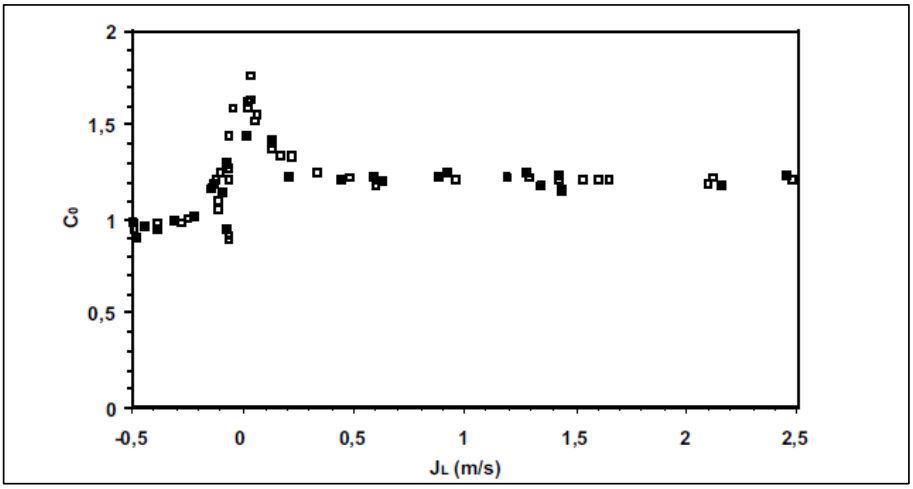

Figure 3-13: (C_0) Coefficient plotted from experiments of Nicklin et al. (1962) from Jean Fabre (2002)

Many other researchers worked on the horizontal case such as Gregory & Scott (1969), A. E. Dukler & Hubbard (1975) and Nydal et al. (1992). Bendiksen (1984) proposed his famous bubble front velocity correlation, which states the following:

$$U_b = C_0 U_m + U_0 \tag{3.62}$$

where U_m is the mixture velocity and C_0 reflects the effects of velocity distribution across the pipe with typical values of (1.05 to 1.2) for turbulent flow and (2.0) for laminar flow. (U_0), on the other hand, reflects the effect of drift velocity of the bubble on the total bubble velocity.

$$C_0 = \begin{cases} 1.05 + 0.15\cos^2(\varphi), & \mathrm{Fr} \le \mathrm{Fr_{lim}} \\ 1.2, & \mathrm{Fr} > \mathrm{Fr_{lim}} \end{cases} \tag{3.63}$$

$$U_0 = \begin{cases} -U_{0v}\cos(\varphi) + U_{0h}\sin(\varphi); & \mathrm{Fr} \le \mathrm{Fr_{lim}} \\ -U_{0v}\cos(\varphi); & \mathrm{Fr} > \mathrm{Fr_{lim}} \end{cases} \tag{3.64}$$

And

$$U_{0v} = 0.35\sqrt{gD\left(\frac{\rho_l - \rho_g}{\rho_l}\right)} \tag{3.65}$$

$$U_{0h} = 0.54\sqrt{gD\left(\frac{\rho_l - \rho_g}{\rho_l}\right)} \tag{3.66}$$

where φ is the pipe angle relative to gravity ($\varphi = \beta + 90^{\circ}$). The Froude number ($Fr$) is defined as follows:

$$\mathrm{Fr} = \frac{U_m}{\sqrt{gD\left(\frac{\rho_l - \rho_g}{\rho_l}\right)}} \tag{3.67}$$

The limiting Froude number for horizontal flows is $Fr_{lim} = 3.6$ as has been confirmed by Fuchs (1997) in the high pressure measurements at the large scale flow loop at SINTEF Multiphase Flow Laboratory.

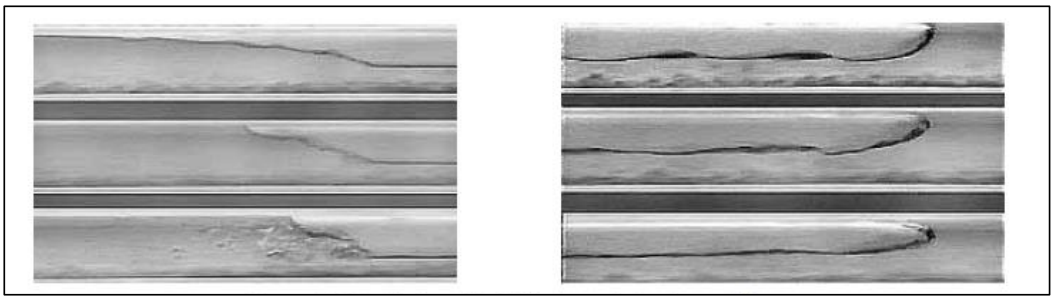

Figure 3-14: Bubble shape in horizontal flow when liquid velocity increases (top to bottom) from Jean Fabre (2002)

It is also worth noting that the shape of the long bubble is not fixed and it's a function of liquid velocity, shown in Figure 3-14. At low velocity, the shape of the bubble follows the Benjamin (1968) shape and the tip is located at the top of pipeline. With higher velocities the tip of the bubble gradually drifts towards the center the pipeline. The shift of the bubble nose from the top to the center is based on the balance between the gravitational force that pushes the nose to the top and inertia force which centers the bubble. This force balance is represented by the Froude number and this was this observation which resulted in Bendiksen (1984) correlation. The experiments carried out by Bendiksen (1984), shown in Figure 3-15 suggested a transition criteria at approximately (Fr = 3.5), Jean Fabre (2002).

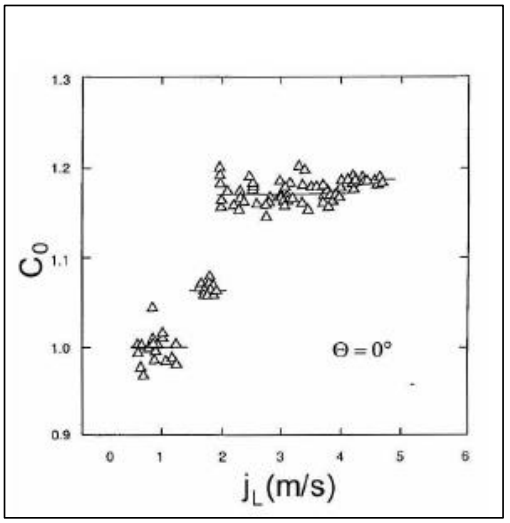

Figure 3-15: Experimental data by Bendiksen (1984) from Jean Fabre (2002)

3.4.5. Slug Length (L_s) – Slug Frequency (v_s)

Slug length (L_s) and slug frequency (v_s) are interchangeable terms which are related by the following definition of slug fraction (S_f):

$$S_f = \frac{L_s v_s}{U_b} \tag{3.68}$$

The mean slug length as reported by many researchers is thought to be of relatively constant length regardless of the superficial gas and liquid velocities. In general, ($L_s \approx 10D - 50D$) for horizontal cases and ($L_s \approx 10D - 15D$) for vertical cases as reported by A. E. Dukler & Hubbard (1975), Nicholson et al. (1978), Gregory et al. (1978) and Nydal et al. (1992). A summary of slug lengths in horizontal case is depicted in Table 3-2 from various researchers.

Table 3-2: Slug Lengths in Horizontal Pipes from Rogero (2009)

Slug Length	Experiment Fluids	Experiment Dia. (mm)	Researchers
12D – 30D	air-water	38.1	A. E. Dukler & Hubbard (1975)
30D	air-light oil	25.8, 51.2	Nicholson et al. (1978)
30D	air-light oil	25.8, 51.2	Gregory et al. (1978)
15D-20D	air-water	53	Nydal et al. (1992)
12D-16D	air-water	90	Nydal et al. (1992)

Brill et al. (1981) investigated a total of (29) two-phase flow tests which was conducted in two (3) miles long pipelines. The investigation suggests that the steady state liquid slug lengths follow the log-normal distribution. This finding was further confirmed by the work conducted by Nydal et al. (1992) in his 53mm and 90mm air-water experiments.

Slug lengths do not affect the slug average velocities and pressure drop in the unit cell model. However, slug lengths are also believed to affect the velocity profiles inside the slugs, as shown in Figure 3-16. The slug-liquid film mixing process was simulated by the researchers such as Taitel et al. (1980) and Dvora Barnea & Brauner (1985). This process indicates that maximum liquid velocity in short slugs are higher than those in long slugs which translate into higher long bubble velocity behind short slugs than long bubble velocity behind long slugs. It is believed that this mechanism that explains the merger of short slugs into larger ones, Taitel & Barnea (1990).

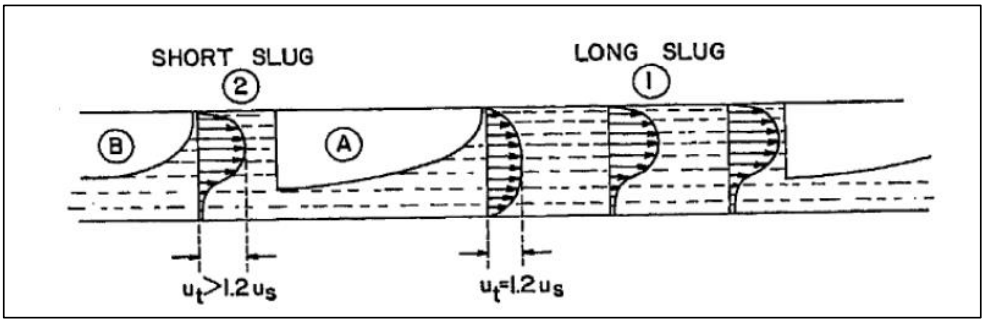

Figure 3-16: Velocity profiles in liquid slugs from Taitel & Barnea (1990)

Slug frequency on the other hand shows a wide range of correlations that are proposed in literature dating back to 1969 when Gregory & Scott (1969) proposed his correlation which states the following:

$$v_s = 0.0226\left[\frac{U_{sl}}{gD}\left(\frac{19.75}{U_m} + U_m\right)\right]^{1.2} \tag{3.69}$$

The data was based on the experiments conducted by Hubbard; (1965) in his PhD thesis. The experiments were conducted using carbon-dioxide – water fluid with a 19.1 mm tube.

Greskovich (1972) proposed a new correlation which was based on the same parameters as Gregory & Scott (1969) correlation. The new correlation was based on air-water data collected in a 1.5 inch and 1.25 inch tubes.

$$v_s = 0.0226\left[\frac{U_{sl}}{U_m}\left(\frac{19.75}{U_m} + \frac{U_m^2}{gD}\right)\right]^{1.2} \tag{3.70}$$

Taitel & Dukler (1977) developed a hydrodynamic model that related the frequency of slugs initiated at the pipe entrance. The slug initiation process shown in Figure 3-17 indicates the formation of small waves at the interface which grows to block the cross section of the pipeline. The level behind the newly formed slug drops considerably as liquid is swept into the slug body. The slug frequency is then defined as the time it takes for the liquid level to build up again for new slug to be initiated again, Al-Safran (2009).

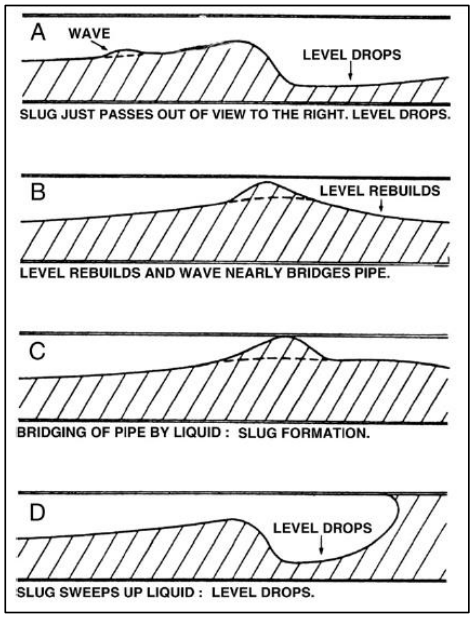

Figure 3-17: The process of slug formation from Taitel & Dukler (1977)

Zabaras (2000) proposed a new correlation which was also based on Gregory & Scott (1969) correlation but included a term which represented the dependency of the slug frequency on pipeline inclination angle. The data set used to tune the correlation included positive pipe angles ranging from (0 to 11) degrees relative to horizontal.

$$v_s = 0.0226\left[\frac{U_{sl}}{gD}\left(\frac{19.75}{U_m} + U_m\right)\right]^{1.2} + [0.836 + 2.75(sin\beta)^{0.25}] \quad ,(\beta)\ in\ degrees \tag{3.71}$$

More recent contributions included the work of Shea (2004) which developed a slug frequency correlation in terms of pipe length measured from pipeline inlet. Despite the fact that the correlation had no theoretical basis and is considered as pure curve fitting exercise, it had a reasonable agreement with a large set of data which was used to tune the correlation. This correlation was mainly developed for the prediction of the delay constant used in OLGA slug tracking module which was presented in OLGA 2000, Al-Safran (2009). The correlation was stated as follows:

$$v_s = \frac{0.47 \cdot U_{sl}^{0.75}}{D^{1.2} \cdot L_p^{0.55}} \tag{3.72}$$

Finally, a new correlation was proposed by Al-Safran (2009) which was validated using a large set of data from various researchers. The data was developed using TUFFP multiphase flow testing facility at Tulsa University which consists of 420 meters long and 5.08 mm diameter pipe. The fluids used in the experiments were compressed air with mineral oil with density of 890 Kg/m3. Al-Safran (2009) study objective was to investigate the slug frequency dependency on slug initiation mechanisms at the entrance of the pipe and on the flow development along the pipeline. The study findings indicate significant effect of slug initiation frequency on slug frequency while the study indicated minimal dependency on pipeline length. The correlation states the following:

$$\ln(v_s) = 0.8 + 1.53 \cdot \ln(U_l) + 0.27\left(\frac{U_s}{U_m}\right) - 34.1(D) \tag{3.73}$$

The data range for $(U_l, \frac{U_s}{U_m}, D)$ is (0.084 to 2.82) m/sec, (1.29 to 6.86) and (0.025 to 0.203) meters, respectively, Al-Safran (2009). (U_s) here, as per the author, refers to the slug velocity, which should be the same as the bubble front propagation velocity.

3.4.6. Pressure Drop across a Slug Unit

The pressure drop across a slug unit described in this section follows the work of Cook & Behnia (2000) which provides a comprehensive treatment of the pressure drop sources in a slug unit. The total pressure gradient in a slug unit consists of four terms: (i) hydrostatic pressure drop, (ii) frictional pressure drop, (iii) viscous pressure drop associated with eddy motion in mixing section and (iv) accelerated pressure drop due to gas expansion:

$$\frac{dp}{dx} = \left(\frac{dp}{dx}\right)_H + \left(\frac{dp}{dx}\right)_F + \left(\frac{dp}{dx}\right)_v + \left(\frac{dp}{dx}\right)_A \tag{3.74}$$

The hydrostatic pressure drop is an averaged density pressure drop as shown in following equation:

$$\left(\frac{dp}{dx}\right)_H = -[\rho_l H_l + \rho_g(1 - H_L)]g \cdot \sin(\beta) \tag{3.75}$$

The frictional pressure drop can be obtained using the following equation:

$$\left(\frac{dp}{dx}\right)_F = -\frac{\tau_s \pi D}{A}\frac{L_s}{L_u} - \frac{1}{L_u}\int_0^{L_f} \frac{\tau_L S_L + \tau_G S_G}{A} dx_f \tag{3.76}$$

Equation (3.76) consists of two terms that represents the frictional pressure drop in the slug body and bubble region respectively. In the film region, the normal liquid and gas shear stresses are calculated based on the two-fluid model. In the slug region, the shear stress (τ_s) term requires the consideration of gas entrainment. Most researchers base the slug body shear stress on mixture properties. However, this tends to under predict the pressure drop in wall friction as noted by Andreussi, Minervini, et al. (1993). Cook & Behnia (2000) accounted for the effects of dispersed gas bubbles by using Einstein (1906) equation for the effective viscosity:

$$\mu_{eff} = \mu_l(1 + 2.5\alpha_s) \tag{3.77}$$

Einstein (1906) equation is based on three important assumptions which are thought to be valid for the slug body case with low void fraction. These assumptions are as follows: (i) Bubbles can be assumed as rigid spheres, (ii) Spherical bubbles are evenly distributed and (iii) Void fraction is small.

For non-rigid bubble assumption, a modified effective viscosity developed by Taylor (1932) can be used as follows:

$$\mu_{eff} = \mu_l\left(1 + \frac{(2.5\mu_g + \mu_l)}{(\mu_g + \mu_L)}\alpha_s\right) \tag{3.78}$$

In addition, although the second assumption will not be valid for low velocities where bubbles normally accumulate in the top of the pipe, the holdup value in this case will be very low and therefore, the error associated with this assumption would also be very low. The wall shear stress in the slug body can thus be calculated using a mixture density and effective viscosity as follows:

$$\tau_s = f\rho_m \frac{U_m^2}{2} \tag{3.79}$$

$$Re_{eff} = \frac{\rho_m U_m D}{\mu_{eff}} \tag{3.80}$$

Where the friction factor (f) can be calculated using standard friction factor correlations such as Blasius for smooth cases and Colebrook-White for turbulent cases.

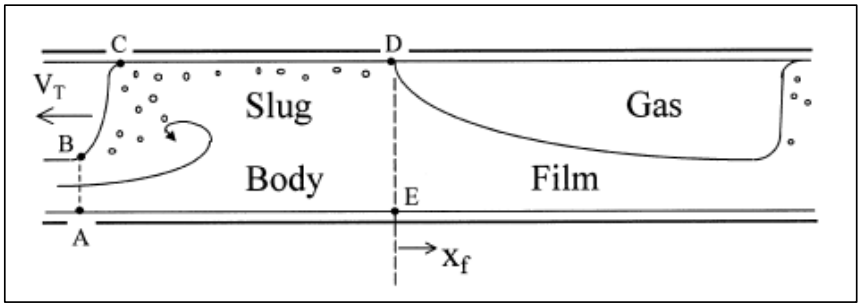

Figure 3-18: Slug Unit Representation from Cook & Behnia (2000)

The viscous pressure drop is calculated using the concept of sudden enlargement of single phase flow. The concept accounts for the pressure drop resulting from the shearing motion of the viscous fluid within the eddies which is usually accompanied by dissipation of mechanical energy, see Figure 3-18. The analogy is carried even further by assuming that the pressure drop is similar to the pressure loss through a diffuser, Cook & Behnia (2000). Thus, the viscous pressure drop can be estimated as follows:

$$\left(\frac{dp}{dx}\right)_v = \frac{K\rho_l}{2}\left(U_m - U_{fe}\right)^2 \tag{3.81}$$

Where, (K) represents the loss coefficient which is a function of the diffusion angle. Examination of the slug fronts angle at low and moderate rates, it was found that the angle is consistently around 20 degrees, see Figure 3-19. Using this assumption, one can obtain (K) value of approximately (0.3). (U_{fe}) is defined to be the liquid film prior to the entrance of the slug body.

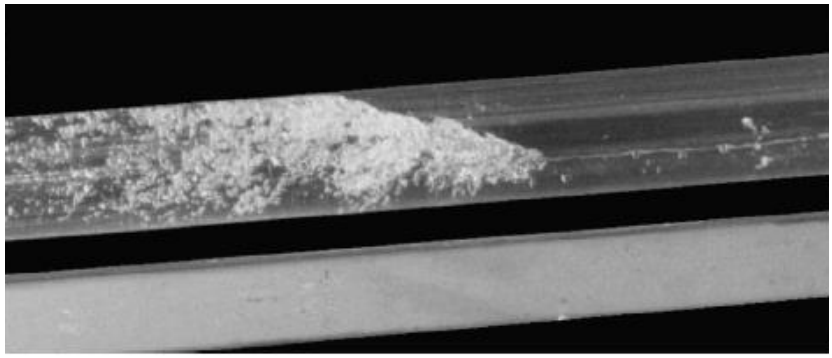

Figure 3-19: Typical Slug showing slope angle (~20 Degrees) from Cook & Behnia (2000)

The acceleration pressure drop is often neglected due to the assumption of incompressible fluid flow within the slug body. This however could lead to significant errors in pressure drop estimation and a proper treatment of the acceleration pressure drop is required. The evaluation considers the overall increase in momentum flux using average phase velocities. The resultant acceleration pressure drop is given by:

$$\left(\frac{dp}{dx}\right)_A = Z\frac{dp}{dx} \tag{3.82}$$

$$Z = \frac{1.2U_{ls}U_{gs}}{PU_b^2}\left[\frac{\rho_g U_{sg}^2}{(1-H_L)^2} - \frac{\rho_l U_{sl}^2}{(H)^2}\right] - \frac{U_{sg}^2}{RT(1-H_L)} \tag{3.83}$$

A detailed analysis can be obtained from Cook & Behnia (2000).

3.5. Slug Flow Transient Prediction Models

Transient slug flow models are normally utilized to predict the details of slug flow behavior in pipelines with complex geometry and variable boundary conditions. A number of multiphase transient models are available which include, TRAC, RELAP and CATHERE for nuclear reactors while OLGA, LedaFlow, MAST, SLUGGIT, TACITE and PLAC are available for oil and gas pipelines.

In general, these codes solve a one-dimensional mass, momentum and energy governing equations on fixed or moving grid in order to obtain the fluid flow parameters. The set of conservative equations are solved numerically for the various phases in space and time.

These transient codes falls into two main categories, namely: slug tracking and slug capturing schemes. The slug tracking scheme follows a Lagrangian model where individual slugs are tracked by tracking the position of their fronts and tail ends. This approach allows for coarse grid implementations and allows for robust simulation of long and complex pipeline geometries. The initiation mechanism in this approach is a challenging task as separate models has to be implemented to enable hydrodynamics slugs to be initiated at certain positions and time throughout the pipeline.

On the other hand, slug capturing uses an Eulerian formulation and strictly applies the two fluid model over the whole two fluid domain without any distinction between slug or non-slug region. The initiation mechanism in this approach follows the normal slug growth mechanisms discussed earlier in the IKH and VKH criteria. However, in order to insure a proper initiation of the hydrodynamic slugs in this approach and avoid diffusion of the slug front which is normally associated with Eulerian formulations, a fine grid is required, sometimes in the order of (1 D) or less, which makes the simulation of long pipelines a very difficult task, Bratland (2010). In oil and gas industry, the slug tracking models is best represented by OLGA, while LedaFlow represents the slug capturing scheme.

OLGA slug tracking scheme is a separate module that could be enabled or disabled based on user input. OLGA applies the standard two-fluid model and unit cell model when slug tracking is not enabled and in this case the model only accounts for terrain-induced slugs. Hydrodynamics slugs are only accounted for when slugs tracking is initiated. The mechanism for initiating hydrodynamics slugs, based on OLGA manual, applies the following rules:

- The flow regime is identified to be a slug flow regime at the boundary section.
- There is a required distance, default is 10 D, between the new slug and the downstream one.
- The time delay set by the user, which is known to be the delay constant (DC), is fulfilled.

When all of these conditions are fulfilled, then a new slug is formed with a minimum length to avoid instabilities in the numerical scheme. The delay constant is considered to be an important factor in the OLGA slug tracking scheme as it determines the initiating frequency of hydrodynamic slugs. OLGA recommends the use of a delay constant value of DC=150. This value however turns out to be useful for very limited cases. The initiation mechanism of hydrodynamic slugs in OLGA is considered a weak point in the model and the development team in OLGA is currently addressing this issue hoping to release a new mechanistic model for the initiation mechanism in the near future. The definition of delay constant as stated in OLGA manual is as follows:

$$\Delta t = DC \cdot \frac{D}{U_l} \tag{3.84}$$

LedaFlow on the other hand has recently adopted the slug capturing scheme in order to simulate the effect of hydrodynamic slugs. Similar to OLGA, LedaFlow has the option of enabling or disabling the slug capturing module. The module does not provide any recommendation of the required mesh size; however, the holdup results seem to vary considerably with various grid sizes. This was noted when simulating some of the field cases in this project. In addition, the computation time increase considerably with smaller and smaller grid sizes which makes the simulation of long pipelines for long simulation periods a cumbersome task for the flow assurance engineers.

SLUGGIT on the other hand applies a hybrid scheme with Eulerian formulation in the bubble region and a Lagrangian formulation on the slug region. The SLUGGIT code also uses a moving grid scheme to following the slug front and avoids any diffusion problem that might occur due to the Eulerian formulation.

3.6. Slug statistical analysis – Matlab Script

Slug statistical analysis was conducted using a Matlab script which was developed mainly for this project. The Matlab script originated from the one developed by professor Ole J. Nydal at NTNU and used by many master and PhD students at NTNU to analyze slugs, such as Kristiansen (2004), who provided a detailed analysis of the various statistical parameters used in the analysis tool. The original code was developed to handle slugs in laboratory conditions which normally have a clear slug shape with a specific slug initiation mechanism.

During this project, the code was modified considerably to adopt the field measurements slug data. The approach followed the schematic presented in Figure 3-20.

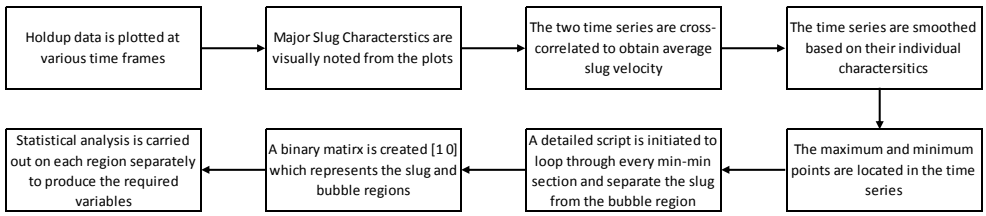

Figure 3-20: Slug Statistical Analysis Approach

This page was intentionally left blank

4. GAMMA MEASUREMENT TECHNIQUE & CALIBRATION

The liquid holdup in a multiphase pipeline is considered a key parameter in the investigation of multiphase hydraulics. The non-intrusive gamma radiation densitometry technique is commonly used in multiphase flow lab experiments and active nuclear and oil and gas applications. Accurate hold-up measurement in active multiphase flow pipelines is necessary to obtain valuable information in order to validate and tune multiphase flow simulation tools.

The configuration of gamma holdup measurement consists mainly of a gamma source, such as Ce 137 or Co 60, and a detector clamped on a pipeline spool that normally contains multiphase fluid, as shown in Figure 4-1. The source emits a beam of photons in a specific cone shape that get deflected by the presence of water, oil and gas in the pipeline and then finally being absorbed by the detector at the bottom of the pipeline spool. The data is then analyzed and interpreted based on calibrated information to obtain the relative density of the fluid that existed in the gamma beam path.

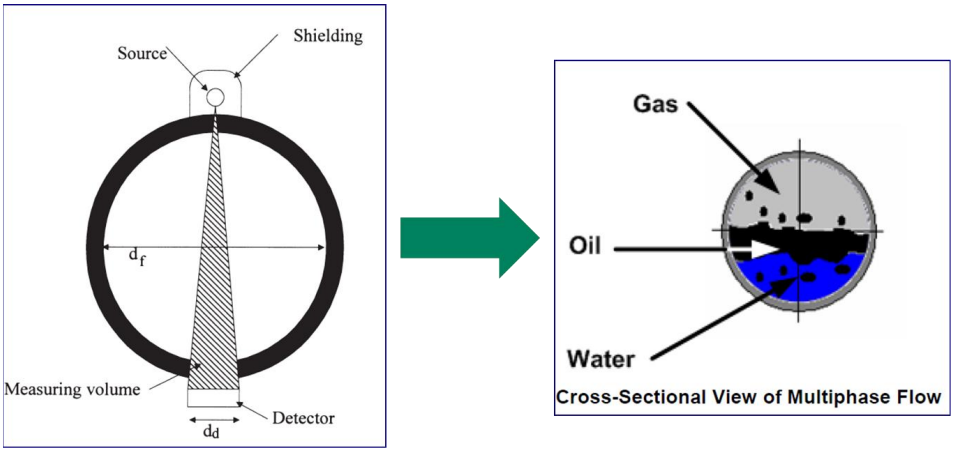

Figure 4-1: Gamma Holdup Measurement – Source-Detector Arrangement

Despite the relatively simple concept behind this technique, a careful application of the equipment arrangement and theory is required to obtain accurate and meaningful results. Errors posed by the surrounding environment, instruments, radiation scattering, pipeline geometry, fluid impurities all affect the results. These errors if not considered appropriately could lead to great deviation from the expected measurements.

In this section the theory of gamma radiation and its applications will be discussed thoroughly along with the calibration procedure utilized while conducting the recent holdup field measurements at Saudi Aramco oil and gas fields.

4.1. Gamma Holdup Measurements – Theoretical Background

The theory of gamma holdup measurements is based on the basic principle of the attenuation of gamma flux due the presence of various layers of matter in the path of the emitted photon. In other words, the intensity of photons that are emitted from a gamma source reduces exponentially when going through an

absorber. This exponential decay is governed by the photons interaction mechanisms which depend on various factors, such as the absorber density, gamma source intensity, gamma source angle etc.

The photons interaction mechanisms with the absorber has been described by Falcone et al. (2009) in Multiphase Flow Metering Handbook, as follows:

Photoelectric Effect: Gamma photon interacts with an atom and gives all of its energy, which causes the release of an electron from the atom inner orbit.

Pair Production Effect: Gamma photon creates a positron-electron pair and as a result, the photon is absorbed in this process.

Compton Effect: Gamma photon interacts with atomic electron, which causes a partial loss of photon's energy, as shown in Figure 4-2. Compton effect predominates the other interaction mechanisms and thus would be considered as the only interaction mechanism when modeling the linear mass attenuation coefficient for Saudi Aramco field measurements, see Figure 4-4 and Figure 4-5.

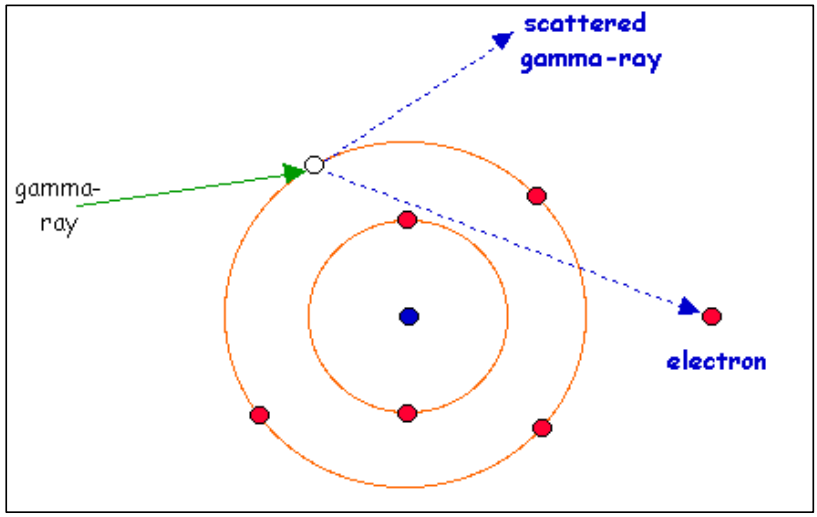

Figure 4-2: Illustration of Compton Effect from Maher (2006)

The photons which arrive at the detector can be divided into scattered (secondary) and un-scattered (primary) photons. The majority of these photons are of the primary, un-scattered type, but with some scattered photons also arriving at the detector. With detectors unable to distinguish between levels of energy, both types of photons will be recorded and as such careful calibration of the source-detector arrangement is required to compensate for those issues in order to obtain an accurate gamma holdup measurement. This is mainly due to the fact that linear attenuation coefficients for solid materials and fluids, which are available in literature, accounts only for primary (un-scattered) photons, Linga (1991).

The gamma attenuation coefficients for different isotopes through various materials are tabulated in literature. Examples are the attenuation coefficients forCobalt-60 (Co-60) shown in Table 4-1 and Figure 4-3.

Table 4-1: Attenuation Coefficients for Co-60

Gas component	Molar mass [g]	Attenuation coefficient [cm2/g]
CH_4	16.04	0.0710
$C_nH_{2n+2,}$ n=4	58.12	0.0666
CO_2	44.01	0.0569
H_2S	34.08	0.0603
air	28.97	0.0569

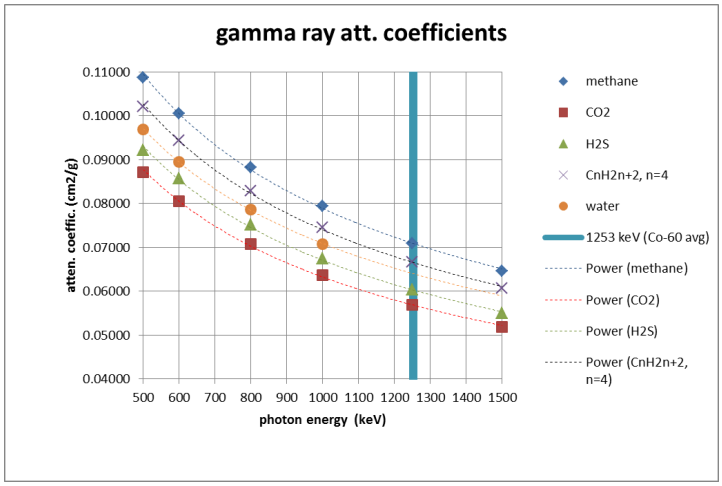

Figure 4-3: Attenuation coefficients for different materials with Co-60 Highlighted at (1253 KeV)

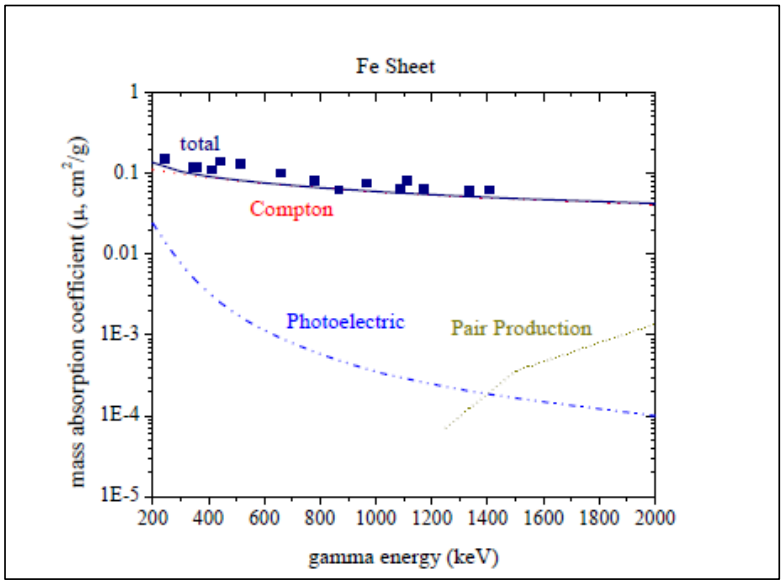

Figure 4-4: Gamma Attenuation in (Steel) with various Attenuation Effects from McAlister (2012)

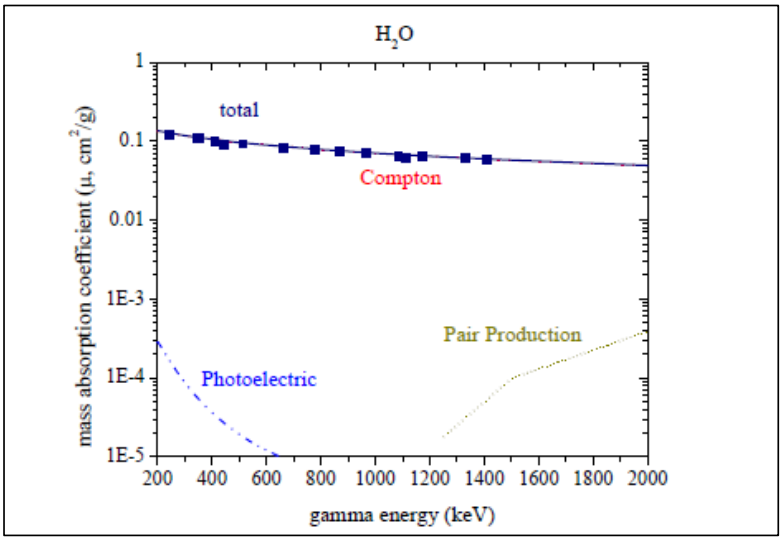

Figure 4-5: Gamma Attenuation in (Water) with various Attenuation Effects from McAlister (2012)

4.2. Gamma Holdup Measurements – Mathematical Modeling

Mathematical modeling of the gamma holdup measurements follows two approaches that stems from the basic gamma-attenuation equations. The first approach utilizes the mass attenuation coefficients and derives a build-up factor which is defined as the ratio between the detected photons and the flux of primary (un-scattered) photons that should arrive at the detector, as has been described in details by Linga (1997).

The second approach utilizes a more practical approach which is being applied by most industrial applications and is usually referred to as the half thickness approach. This approach makes use of the simple idea of what would be the thickness of the material that causes the original gamma flux to be reduced by a factor of two.

4.2.1. Mass Attenuation Coefficient Approach

As stated earlier, the approach start with the basic gamma-attenuation equation and follows a systematic mathematical modeling techniques with clear assumptions to arrive at the holdup prediction at the end. The derivation that will be described here follows Linga (1997) model, with slightly more insight into the assumptions made in that paper. A full derivation with more details is available in Appendix-B.

The two basic equations established by Evans (1955) and then further developed by Petrick and Swanson (1958), state that the general expression for the relation between the detector output signal, (U), and the detector photon flux $(N + M)$ is:

$$U = U_0 + U_1(N + M) \tag{4.1}$$

where, (U_0) and (U_1) are instrument constants and (N) and (M) are primary and secondary fluxes of photons. The primary flux of photons, (N), is given by:

$$N = N_0 \cdot e^{-\left\{\left(\mu_g \cdot \rho_g \cdot (1-H)\right)+\left(\mu_l \cdot \rho_l \cdot (H)\right)\right\} \cdot Z_0} \tag{4.2}$$

where, (g) and (*l*) stand for gas and liquid phases and (H) stands for liquid holdup. Density is denoted by (ρ) and (μ) represents the linear mass attenuation coefficient. The effective beam length in pipe is (Z_0) and (N_0) is the flux of primary photons if no attenuation occurs in the fluid.

Now, we introduce the build-up factor, (B) which describes the ratio between detected photons and the primary photons that should arrive at the detector, as follows:

$$B = \frac{N+M}{N} = 1 + \frac{M}{N} \tag{4.3}$$

Introducing the attenuation factor (K) as follows:

$$K = e^{-\left\{\left(\mu_g \cdot \rho_g \cdot (1-H)\right) + \left(\mu_l \cdot \rho_l \cdot (H)\right)\right\} \cdot Z_0} \tag{4.4}$$

One would be able to write equation (4.2) as follows:

$$N = N_0 \cdot K \tag{4.5}$$

We could also write equation (4.3) as follows:

$$N + M = N \cdot B \tag{4.6}$$

Combining equations (4.1) and (4.6), one can obtain:

$$U = U_0 + U_1 \cdot N_0 \cdot B \cdot e^{-\left\{\left(\mu_g \cdot \rho_g \cdot (1-H)\right) + \left(\mu_l \cdot \rho_l \cdot (H)\right)\right\} \cdot Z_0} \tag{4.7}$$

Utilizing the definition of the attenuation factor (K) and assuming a pipe full of gas only:

$$U_g = U_0 + U_1 \cdot N_0 \cdot B_g \cdot K_g \tag{4.8}$$

Utilizing the definition of the attenuation factor (K) and assuming a pipe full of liquid only:

$$U_l = U_0 + U_1 \cdot N_0 \cdot B_l \cdot K_l \tag{4.9}$$

Subtracting equations (4.8) and (4.9), one would obtain the instrument coefficients in equation (4.1) as follows:

$$U_1 \cdot N_0 = \frac{\frac{1}{B_g}(U_l - U_g)}{\frac{B_l}{B_g} \cdot K_l - K_g} \tag{4.10}$$

Now, if we substitute in equation (4.8), one would obtain the other instrument constant:

$$U_0 = \frac{\frac{B_l}{B_g} \cdot K_l \cdot U_g - K_g \cdot U_l}{\frac{B_l}{B_g} \cdot K_l - K_g} \tag{4.11}$$

Now, we define the attenuation ratio as follows:

$$R = \frac{K_g}{K_l} \tag{4.12}$$

We also define the gas and liquid attenuation factors, $(\mathrm{K_g})$ and $(\mathrm{K_l})$ and the void fraction (ε) as follows:

$$K_g = e^{-\{(\mu_g \cdot \rho_g)\} \cdot Z_0} \tag{4.13}$$

$$K_l = e^{-\{(\mu_l \cdot \rho_l)\} \cdot Z_0} \tag{4.14}$$

$$\varepsilon = (1 - H) \tag{4.15}$$

Now, we can express the attenuation factor as follows:

$$K = R^{\varepsilon} \cdot K_l = \left(\frac{K_g}{K_l}\right)^{\varepsilon} \cdot K_l = \left(K_g\right)^{\varepsilon} \cdot (K_l)^{1-\varepsilon} \tag{4.16}$$

Now by using equations (4.10), (4.11), (4.12) and (4.16) and then plugging back into equation (4.7), one would obtain the following expression for the detector output signal:

$$U = U_0 + U_1 \cdot N_0 \cdot B \cdot R^{\varepsilon} \cdot K_l \tag{4.17}$$

Replacing $(\mathrm{U_0})$, $(\mathrm{U_1 \cdot N_0})$ and $(\mathrm{K_l})$ and after some mathematical manipulation, one would obtain:

$$U \cdot \left[\frac{B_l}{B_g} - R\right] = \left[\frac{B_l}{B_g} - \frac{B}{B_g} R^{\varepsilon}\right] \cdot (U_g - U_l) + \left[\frac{B_l}{B_g} - R\right] \cdot U_l \tag{4.18}$$

This can be re-arranged to obtain the following expression for (U), as follows:

$$U = U_l + \frac{\left[\frac{B}{B_g} R^{\varepsilon} - \frac{B_l}{B_g}\right]}{\left[R - \frac{B_l}{B_g}\right]} \cdot (U_g - U_l) \tag{4.19}$$

Now we need an expression for (R), so we start manipulating equation (4.11) as follows:

$$U_0 \cdot \left(\frac{B_l}{B_g} \cdot K_l - K_g\right) = \frac{B_l}{B_g} \cdot K_l \cdot U_g - K_g \cdot U_l \tag{4.20}$$

Dividing by $(\mathrm{K_l})$ provides the following equation:

$$U_0 \cdot \left(\frac{B_l}{B_g} - R\right) = \frac{B_l}{B_g} \cdot U_g - R \cdot U_l \tag{4.21}$$

Now, we can solve for (R) as follows:

$$R = \frac{B_l}{B_g} \cdot \frac{(U_g - U_0)}{(U_l - U_0)} \tag{4.22}$$

Plugging (R) expression into equation (4.19), one would obtain the following:

$$U = U_l + \frac{\left[\frac{B}{B_g} R^{\varepsilon} - \frac{B_l}{B_g}\right]}{\left[\frac{B_l}{B_g} \cdot \frac{(U_g - U_0)}{(U_l - U_0)} - \frac{B_l}{B_g}\right]} \cdot (U_g - U_l) \tag{4.23}$$

After some mathematical manipulation, one can obtain a formula for the void fraction as follows:

$$\varepsilon = \frac{ln\left(\frac{B_l}{B} \cdot \frac{U - U_0}{U_l - U_0}\right)}{ln\left(\frac{B_l}{B_g} \cdot \frac{U_g - U_0}{U_l - U_0}\right)} \tag{4.24}$$

4.2.2. Half Thickness Approach

Similar to the mass attenuation coefficient approach, the half thickness approach starts with the basic exponential attenuation decay equation, which if written for one material with density (ρ), the equation will look like as follows:

$$U = U_0 \cdot e^{(-\mu * \rho * x)} \tag{4.25}$$

Taking the natural log of both sides of the equation we will get:

$$\ln\left(\frac{U}{U_0}\right) = -\mu * \rho * x \tag{4.26}$$

Now, assuming that we have a certain material, with density (ρ), and with specific thickness (x), that would attenuate half of the initial flux such that ($U_0 = \frac{1}{2}$ U). Therefore we could write the above equation as:

$$\ln(0.5) = -\mu * \rho * x \tag{4.27}$$

Defining the half thickness variable as ($T_{1/2} = \rho * x$) one could obtain:

$$\ln(0.5) = -\mu * T_{1/2} \tag{4.28}$$

Solving for the half thickness ($T_{1/2}$):

$$T_{1/2} = -\frac{0.69315}{\mu} \tag{4.29}$$

The half thickness value of a particular radiation absorbed by a particular medium and detector arrangement ($T_{1/2}$) has units of (gram/cm2) and has the following properties:

a. ($T_{1/2}$) is dependent on radiation energy, collimation, source, absorber and detector geometry.
b. ($T_{1/2}$) for high energy gamma radiation (e.g. Caesium-137 or Cobalt-60) is independent of the elemental composition of the absorber.
c. ($T_{1/2}$) is the amount of material (density and thickness) required to absorb half of the radiation transmitted by the source.

Generalizing the half thickness concept by assuming that the half thickness can be extrapolated such that if two half thicknesses are installed between the source and detector, then the radiation will be reduced with a factor of (0.5^2) and so on. So one can generalize this finding to come up with the following general equation for any (density-thickness) combination:

$$U = U_0 \cdot (0.5)^{\left(\frac{\rho * x}{T_{1/2}}\right)} \tag{4.30}$$

Taking the natural logarithm of the above equation:

$$ln\left(\frac{U}{U_0}\right) = \frac{\rho * x}{T_{1/2}} \cdot \ln(0.5) \tag{4.31}$$

Solving for the density, one could obtain the following equation:

$$\rho = \left[\frac{ln\left(\frac{U}{U_0}\right)}{\ln(0.5)}\right] \cdot \left(\frac{T_{1/2}}{x}\right) \tag{4.32}$$

Equation (4.32) solves for the mixture density of the material that lies between source and detector. Therefore, using the known densities of the individual layers of solid and fluid, one would be able to obtain the holdup in the multiphase pipeline.

4.2.3. Gamma Calibration Process

Before the startup of the recent Saudi Aramco field measurement campaign in 2012, a calibration of the gamma sources had to be carried out in order to insure the accuracy of the holdup measurements. The calibration process utilized three sets of pipeline spools, 42 inch, 30 inch and 24 inch, which matches the diameters of the pipelines in field measurements. The calibration was carried using tap water and air, where gamma measurements were conducted with full water and empty pipe cases for each pipeline size and for adequate time, approximately (20) minutes for each case, to obtain enough statistical data for accurate measurements. The empty pipeline, air, results were also compared against the field cases where liquid holdup were below 50% by taking gamma measurements in the (9-3), horizontal position. These horizontal field measurement results were also corrected for gas density in the pipeline in order to correctly compare and confirm the results against the empty, (air), calibration results.

Figure 4-6: Calibration Pipeline Spools – from right to left (One 42”, Two 30”, Two 24”)

The wall thickness of the calibration spools differed from the ones in active pipeline field measurements, as shown in

Table **4-2**. As a result, a special treatment of the calibration data had to be carried out to correct for the difference in wall thickness as will be discussed in the next section.

Table 4-2: Calibration Pipeline Thickness vs. Active Pipeline Thickness

	42 inch Pipe		30 inch Pipe		24 inch Pipe	
	Calibration Spool	Active Pipeline	Calibration Spool	Active Pipeline	Calibration Spool	Active Pipeline
Wall Thickness (mm)	22	25.4	32	13.767	15	12.7

4.2.4. Application of Half Thickness Approach to Saudi Aramco Field Measurements

Due to the simplicity and practicality of the half thickness approach, it was decided to utilize this approach for the conversion of detector signal to mixture density. This decision was made with a mutual agreement between the contractor who conducted the gamma measurements, and Saudi Aramco. The models used in this section were also developed by cooperation between the two parties, with more focus on the correction terms for difference in wall thickness. The equation that needs to be solved in order to find the mixture density is as follows:

$$\rho_{mixture} = \left[\frac{ln\left(\frac{U_{detected}}{U_{empty-corrected}}\right)}{\ln(0.5)}\right] \cdot \left(\frac{(T_{1/2})_{water}}{I.D.}\right) \tag{4.33}$$

Equation (4.33) has few parameters that need to be determined before it can be used to solve for the mixture density. The internal pipe diameter (I.D.) and the detected field measurement gamma signal ($U_{detected}$) are straight forward input parameters that do not require any further treatment. However, the other two parameters, which are the water half thickness value, $(T_{1/2})_{water}$, and corrected empty count rate, ($U_{empty-corrected}$) require special treatment, which is explained in the following section:

1. Water Half Thickness Value ($T_{1/2}$):

The half thickness value ($T_{1/2}$) for water, was obtained using the gamma calibration values carried out with water and air. Utilizing equation (4.30), the half thickness value for water can be obtained by first taking the natural logarithm:

$$ln\left(\frac{U}{U_0}\right) = \frac{\rho * x}{T_{1/2}} \cdot \ln(0.5) \tag{4.34}$$

Now we can solve for the half thickness value as follows:

$$T_{1/2} = \left[\frac{\ln(0.5)}{ln\left(\frac{U}{U_0}\right)}\right] \cdot (\rho \cdot x) \tag{4.35}$$

Substituting for ($\rho = \rho_{water}$) and ($x = Pipe\ Inner\ Dia.$). Also, using the calibration results for air and water as follows, $U = U_{water}$ and $U_0 = U_{air}$, one could obtain a value for $(T_{1/2})_{water}$.

$$(T_{1/2})_{water} = \left[\frac{\ln(0.5)}{ln\left(\frac{U_{water}}{U_{air}}\right)}\right] \cdot (\rho_{water} \cdot Pipe\ Inner\ Dia.) \tag{4.36}$$

The values for $(T_{1/2})_{water}$ was calculated for each pipeline diameter as shown in Table 4-3:

Table 4-3: Half Thickness Value for Water with various Pipeline Diameters

	42 inch Pipe	30 inch Pipe	24 inch Pipe
Half Thickness Value – (mm) of Water	174	177	148

2. Corrected Empty Count Rate ($U_{empty-corrected}$)

The pipeline empty count rate, air measurement, is an important factor in the calculation of mixture density. The normal procedure would be to obtain this parameter from the calibration pipe with empty pipe, assuming the calibration pipe and the active pipe both have the same pipeline thickness and material. During this field measurement campaign, a calibration pipe with the same pipeline thickness as the one in actual field could not be obtained and as such pipeline spools with different pipeline thickness had to be used.

In addition a correction procedure had to be developed and applied to correct for this parameter. The correction procedure starts with the same half thickness equation:

$$U = U_0 \cdot (0.5)^{(\frac{\rho * x}{T_{1/2}})} \tag{4.37}$$

Substituting for ($U = U_{air-corrected}$) and ($U_0 = U_{air-calibrated}$), one would obtain:

$$U_{air-corrected} = U_{air-calibrated} \cdot (0.5)^{(\frac{\rho * x}{T_{1/2}})} \tag{4.38}$$

Now, we correct for the difference in wall thickness by replacing the (density*distance) term with the steel density and wall thickness difference as follows:

$$(\rho * x) = \{2 * (W.T.Difference) * (\rho_{steel})\}$$

One would obtain a correction equation for empty count rate which could be used to calculate the mixture density in a multiphase flow pipeline:

$$U_{air-corrected} = U_{air-calibrated} \cdot (0.5)^{\left[\frac{\{2*(W.T.Difference)*(\rho_{steel})\}}{T_{1/2}}\right]} \tag{4.39}$$

The results obtained from equation (4.39) were compared against the available gas readings in active pipelines in (9-3) o'clock horizontal position and the comparison provided reasonable agreement with the correction procedure as shown in Table 4-4 with one exception in pipeline TL-13, where the wall thickness difference between the calibration pipe and the active pipeline was very large. In this particular case, the information from the vapor count was used in the mixture density equation.

Table 4-4: Comparison of Corrected Empty Count Rate vs. Vapor Count Rate from Online (9-3) Position

Pipeline	Pipeline size (inches)	Pipeline wall thickness (mm)	Calibration pipe wall thickness	Radioactive source	'Empty count' from Calibration after WT correction	'Vapor count' from online (9-3) o'clock orientation	Online 'Empty count' adjusted for gas density
TL-9	42	25.4	22	1	1361	1381	1419
				2	3392	3440	3486
TL-10				1	1361	Not obtained	-
				2	3392	Not obtained	-
TL-12	24	12.7	15	1	2842	2667	2750
				2	6059	5845	6026
TL-13	30	13.767	32	1	6443	4529	4812
				2	15838	11133	11828
TL-AB01	42	25.4	22	1	2708	2997	3128
				2	6081	6144	6413
G2-X1	30	27.7876	32	1	1168	1065	1111
				2	598	535	558
G2-M1	30	27.7876		1	1168	1065	1086
				2	598	535	545

4.2.5. A Different Correction Method

A different correct approach is investigated ins this section for the difference in wall thickness by utilizing a simple form of correction as follows:

$$Correction = \frac{\rho_{steel} * 2 * (W.T.Difference)}{ID} \tag{4.40}$$

This formula should be used with the original ($U_{air-calib}$) as (U_0) which results a certain mixture density that can be corrected using the above correction factor.

The above correction factor is obtained by starting with the basic equation:

$$U_1 = U_0 \cdot e^{(-\mu * \rho * x)} \tag{4.41}$$

If we assume an increase in the wall thickness from calibrated pipe (1) to measured pipe (2), then the increase in wall thickness will cause a decrease in measured counts from (U_1) to (U_2), as follows:

$$U_2 = U_1 \cdot e^{(-\mu * \rho_{steel} * t)} \tag{4.42}$$

Where (t) here represents the increase in wall thickness at the top and bottom. So, the measurements in the field with the thicker, or thinner pipe, will result the following gamma measurement:

$$U_2 = U_0 \cdot e^{(-\mu * \rho * x)} \tag{4.43}$$

Hence, we can solve for corrected mixture density as follows:

$$-\rho = \frac{1}{\mu * x} \cdot ln\left(\frac{U_2}{U_0}\right) \tag{4.44}$$

$$-\rho = \frac{1}{\mu * x} \cdot ln\left(\frac{U_1 \cdot e^{(-\mu * \rho_{steel} * t)}}{U_0}\right) \tag{4.45}$$

$$-\rho = \frac{1}{\mu * x} \cdot \left[ln\left(\frac{U}{U_0}\right) + ln\left(e^{(-\mu * \rho_{steel} * t)}\right)\right] \tag{4.46}$$

$$-\rho = \left[\frac{1}{\mu * x} \cdot ln\left(\frac{U}{U_0}\right)\right] - \left[\frac{1}{\mu * x} \cdot \mu * \rho_{steel} * t\right] \tag{4.47}$$

$$\rho = -\left[\frac{1}{\mu * x} \cdot ln\left(\frac{U_1}{U_0}\right)\right] + \left[\frac{\rho_{steel} * t}{x}\right] \tag{4.48}$$

The first term in the last equation is the mixture density if the wall thickness had stayed the same as the calibrated pipe. The second term is the correction factor that can be used to correct for the increase or decrease in wall thickness in the measured pipe.

A comparison was made between the two correction approaches and the difference between the two results was less than (3%).

This page was intentionally left blank

5. FIELD-A – HOLDUP & PRESSURE MEASUREMENTS

Field-A measurement was conducted on May and June of 1999 with an objective to investigate the severe terrain slugs encountered in an onshore hilly terrain oilfield and calibrate the transient multiphase flow simulator, OLGA, which was used for the design and troubleshooting of this oilfield.

In this oilfield, multiphase crude oil is being transported from well sites at low and flat locations, called Sabkhahs, to three Gas Oil Separation Plants (GOSP) passing through a hilly terrain with very large sand dunes that rise up to 200 meters above sea level, as shown on Figure 5-1 and Figure 5-2.

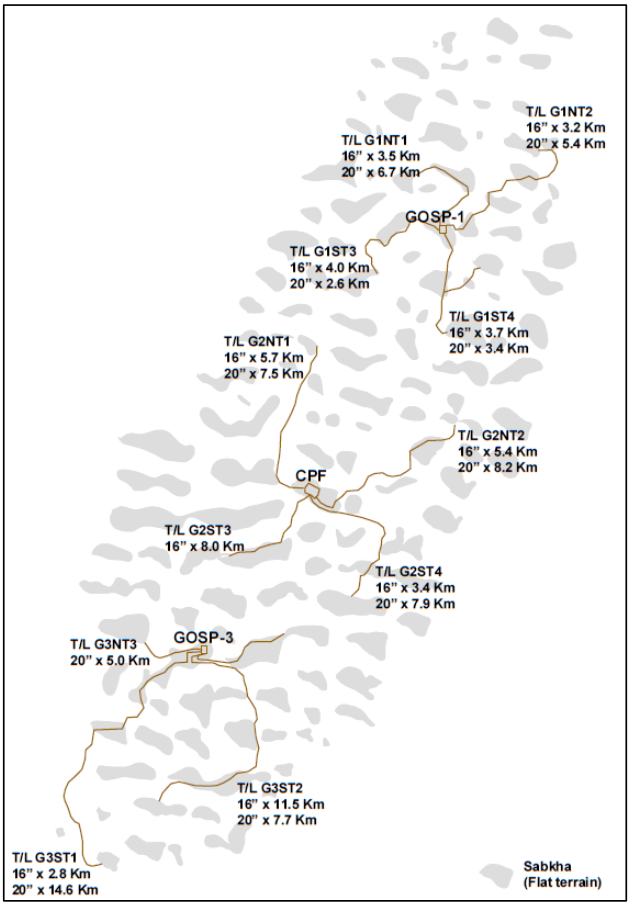

Figure 5-1: Oilfield Pipeline Network – 1999, Alvarez & Al-Awwami (1999)

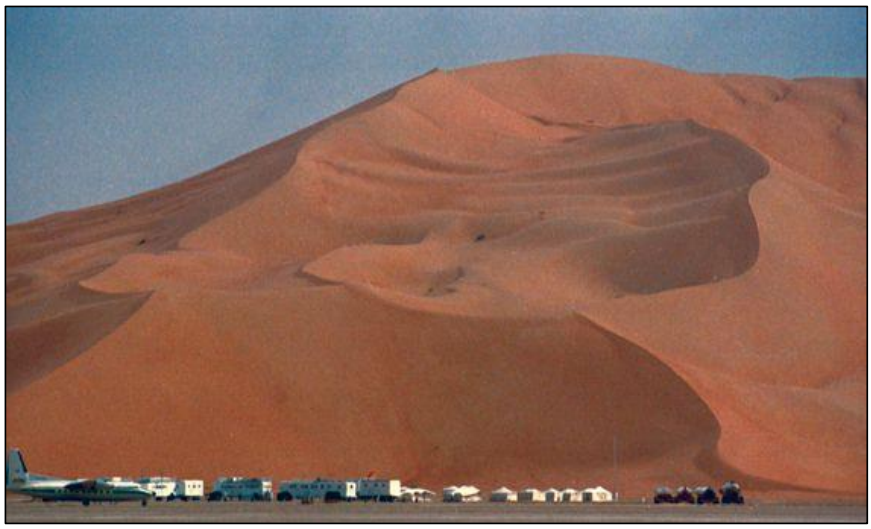

Figure 5-2: Oilfield Sand Dunes

At the time of the measurement, several steady state codes were used to investigate the pressure drop across those multiphase pipelines. The steady state codes provided inconsistent and inaccurate results when compared to field data. The transient multiphase simulation code used at the time of the measurement, OLGA v3.4, also produced pressure drop results which were generally under predictive, Alvarez & Al-Awwami (1999).

Therefore, more investigation was required to understand the reasons behind these deviations in pressure drop predictions. Consequently, liquid holdup measurements were carried out on 6 oil pipelines, 16 and 20 inch in diameter, using two Gamma Densitometers both located upstream and / or downstream of a slug valve. The field measurement campaign had another objective which was to investigate the detailed terrain slugging behavior and the effect of the slug control valves installed upstream of the GOSP separators on slug and pressure fluctuations.

The measurements were carried out by Scandpower AS, Norway in cooperation with personnel from Saudi Aramco and SINTEF, Norway. As expected, the pipelines behaved as classical terrain induced slugging pipeline systems with large pressure and holdup oscillations as reported by Mikal Espedal, who conducted the gamma field measurement, in his Scandpower report Espedal (1999). The report described the overall behavior of the measured pipelines and all the related field measurements obtained during the campaign such as pressures and temperatures at various pipeline locations. However, Espedal made no attempt to thoroughly analyze the data and compare it against the available transient simulation models such as OLGA as that was not part of the measurement project. However, Espedal reported some of the slugs' statistical parameters such as slug length and velocities for some of the cases.

In May 2004, Scandpower AS, Norway issued two internal reports comparing the field measurement data against their latest transient simulation models at that time, OLGA 2000-v4.12 and OLGA 2000-v.4.05.

Saudi Aramco 1999 Data Comparison Report – Part-1 investigated the field measurements from two pipelines and compared them against OLGA transient models. The investigation was carried using the slug tracking module with various delay constants and boundary conditions to reflect the uncertainties revolving around the field measurement data. The results showed general tendency to under predict the

oscillation by 10% to 30% for both pipelines. The pressure drop showed a similar behavior of under prediction that ranged from 10% to 20%, Rasmussen (2004).

Saudi Aramco 1999 Data Comparison Report – Part-2 investigated the field measurements from the remaining four pipelines and compared them against OLGA transient models. The investigation was similarly carried out using the slug tracking module with various delay constants and boundary conditions to reflect the uncertainties revolving around the field measurement data. The results showed general tendency for under prediction of the oscillation period by 5% to 20% for all four pipelines. The pressure drop however showed greater discrepancies with under predictions that ranged from 5% to 70%, Al-Taweel (2004).

The analysis presented in Alvarez & Al-Awwami (1999) paper and the Scandpower reports were not thorough enough and did not reflect all the slug information that is available in the oil field measurement data. In addition, the new multiphase transient simulation tools that are currently available provide a good opportunity to re-examine the data using those tools.

Thus, a re-examination of the 1999 field measurement data will be carried out in this section. The analysis will attempt to obtain all the relevant statistical slug data such as slug frequency, slug front and tail velocity, slug length and slug body and the stratified film holdup. In addition, a detailed simulation will be carried out to reproduce and compare the field measurement data using various multiphase transient simulation techniques, mainly slug tracking and slug capturing. Finally, an attempt will be made to re-investigate the optimum choke settings for slug valves based on predictions provided by the latest available transient multiphase codes. All the basic information related to pipelines geometry and size in addition to the pressure and flow rates data was obtained from Espedal (1999) report.

Measurement Location:

As described by Espedal in his report, Espedal (1999), the measurements were carried out on several pipelines at various locations. The current analysis will be carried out on (5) of these pipelines as shown in Table 5-1.

Table 5-1: 1999 Field Measurement – Pipelines and Measurement Locations Details

Pipeline Name	Distance between meters (m)	Approx. pipeline inclination (degrees)	Location of Gammas relative to slug valve	Approx. distance to slug valve	Approx. distance to GOSP fence	Approx. pipe W/T (inch/mm)
G2NT1	36.95	0	Downstream	16 m	250 m	0.787 / 20
G2NT2	55.7	+ 0.08	Downstream	2 km	400 m	0.787 / 20
G3ST1	54.1	+ 0.16	Upstream	450 m	3.2 km	0.63 / 16
	46.0	- 0.08	Downstream	2.1 km	650 m	0.787 / 20
G3ST2	51.6	- 3.92	Upstream	100 m	1.4 km	0.63 / 16
	53.3	+ 0.07	Downstream	800 m	500 m	0.787 / 20
G1ST3	23.3	+ 4.56	Uphill, upstream	800 m	2 km	0.63 / 16
	38.9	- 8.52	Downhill, upstream	250 m	1.5 km	0.63 / 16

The selection of the gamma location was based on the project's main objective to measure the slug sizes and velocities as it arrives at the GOSP facilities. Thus all the gammas were mounted at various locations a short distance upstream the GOSP facilities. The project's other objective was to examine the effect of slug valve installation on the slug characteristics and consequently the gammas where installed upstream and downstream the slug valves as deemed feasible at the time of the measurement.

The gamma meters were installed at a total of 9 different locations on the 6 selected pipelines. At the measurement location, the pipeline had different inclination angles and pipeline wall thicknesses as shown on Table 5-1.

Gamma Measurement and Calibration:

The gamma sources which were used in the 1999 field measurement utilized Cs 137 with a strength of 37 GBq. A detector is installed on the opposite side of the pipeline as shown on Figure 5-3, to detect the photons which pass through the pipe's wall and fluid.

The detected photon is then converted to average mixture density through carefully developed mathematical models. The gamma models are then converted to holdup by the utilizing the already known liquid and gas densities.

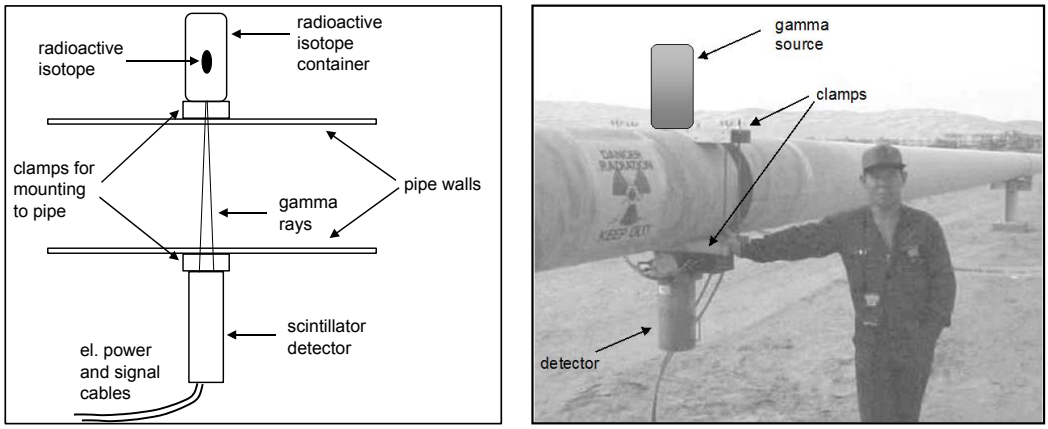

Figure 5-3: Gamma Measurement Principle of Operation & Pipe Mounting

Calibration of the gamma densitometers was conducted prior to the measurement campaign using calibration spools that were specifically made by Saudi Aramco workshops. The calibration spools were 1 to 1.5 m long spool pipes which had dead oil in them with a known density, 795 kg/m3 (API 46.5) at atmospheric pressure and a temperature of 40 – 50 °C (104 – 122 °F).

Each gamma densitometer was calibrated with the calibration pipe being empty and filled with dead oil and the counting rate was measured at both conditions. The equation used for oil levels between empty and full pipe had earlier been tested against partly filled pipes in connection with large scale laboratory experiments at SINTEF in Norway Espedal (1999).

Fluid and PVT

The composition of the Arab Extra Light (AXL) produced oil at the oil field is generally characterized by high GOR. The GOR at the time of the field measurement in 1999 was estimated at 860 scf/stb and API at 60°F is 40. The phase envelope of AXL crude oil is shown in Figure 5-4, which indicates that the pipeline system is clearly in the two phase region.

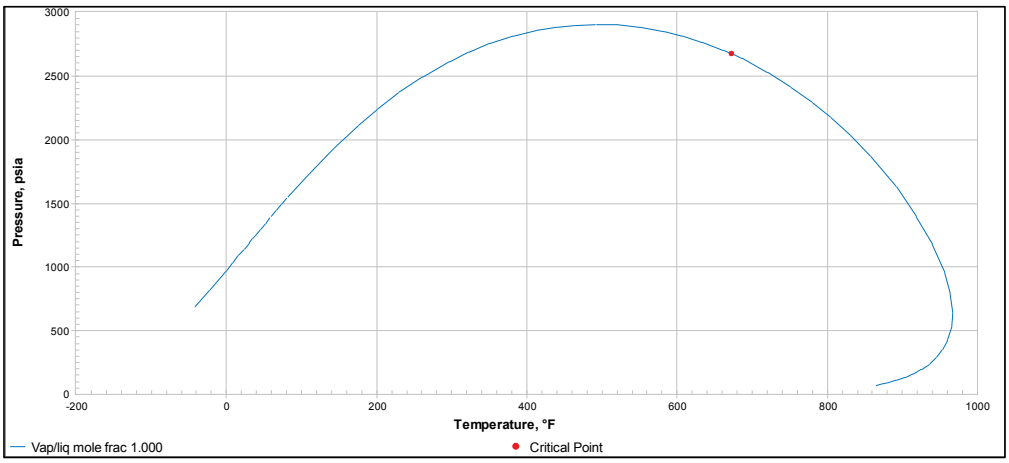

Figure 5-4: Phase Envelope of AXL

The gas and liquid densities variations with pressure are shown in Figure 5-5 and Figure 5-6. These figures were plot for the AXL fluid using OLGA at a temperature of 100°F. The oil and gas viscosity was also plot at the same temperature which shows the variation with pressure from 0 to 800 psig as shown in Figure 5-7 and Figure 5-8. The surface tension is also plotted for the entire pressure range in Figure 5-9.

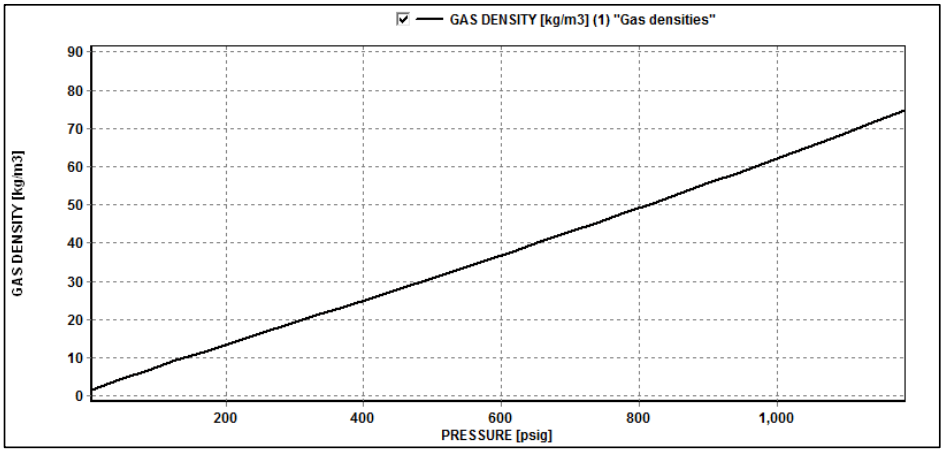

Figure 5-5: Gas Density (Kg/m3) – Temperature @ (100°F)

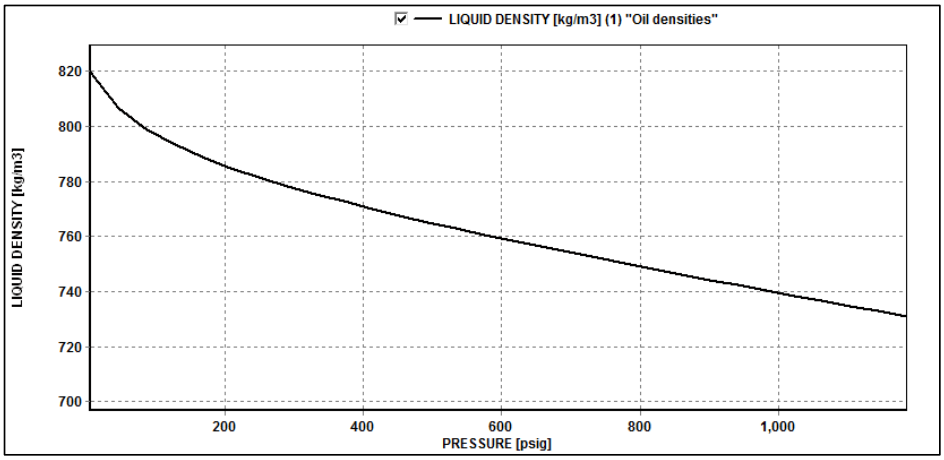

Figure 5-6: Oil Density (Kg/m3) – Temperature @ (100°F)

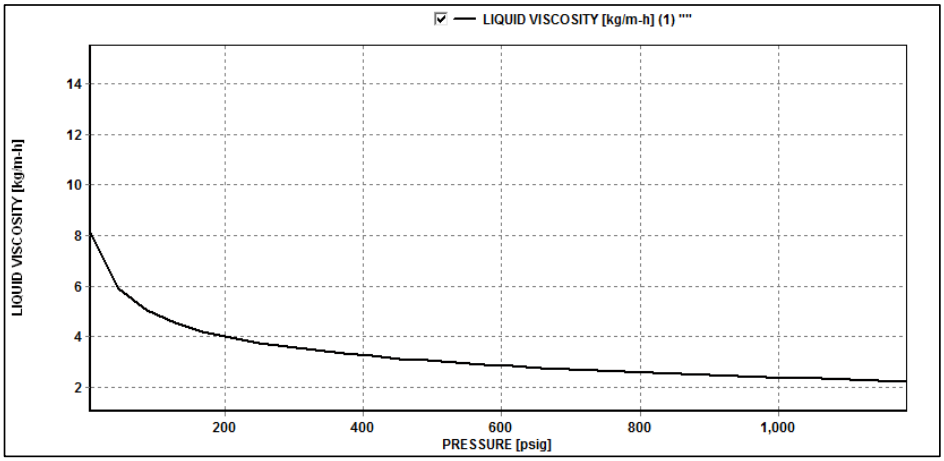

Figure 5-7: Oil Viscosity (Kg/m-h) – Temperature @ (100°F)

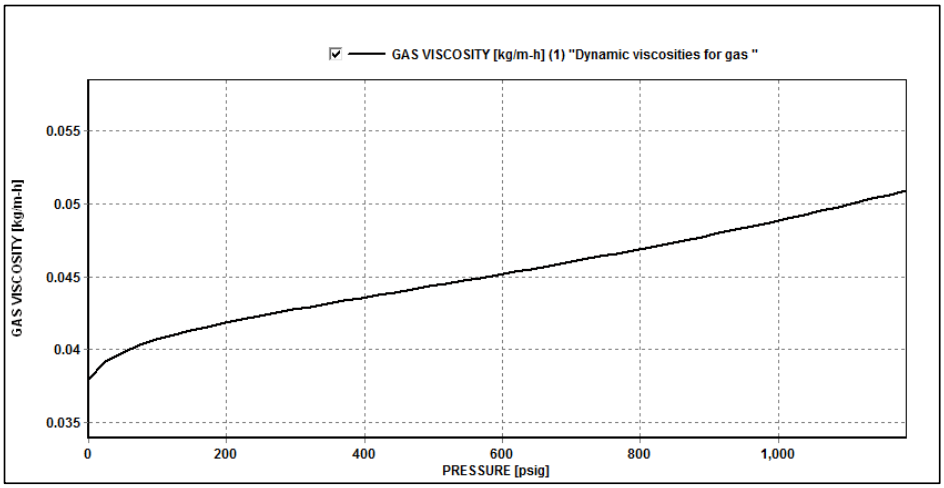

Figure 5-8: Gas Viscosity (Kg/m-h) – Temperature @ (100°F)

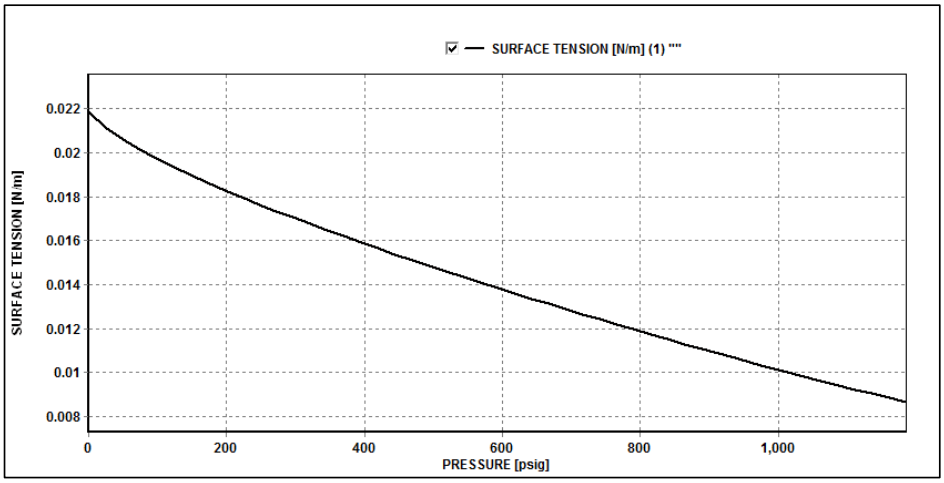

Figure 5-9: Gas-Oil Surface Tension (N/m) – Temperature @ (100°F)

5.1. G2NT1 Pipeline Results:

G2NT1 measurements were conducted on May 27, 1999. The measurements were conducted downstream of the slug valve installed at the end of the pipeline upstream of GOSP-2.

5.1.1. Pipeline Profile Details

The total pipeline length is approximately 13 Km and starts from Sabkhah 38 (S-38) to GOSP-2 going through Sabkhah 46 (S-46) and Sabkhah 56 (S-56). The pipeline has two different diameters 16 inch and 20 inch as shown on Figure 5-10.

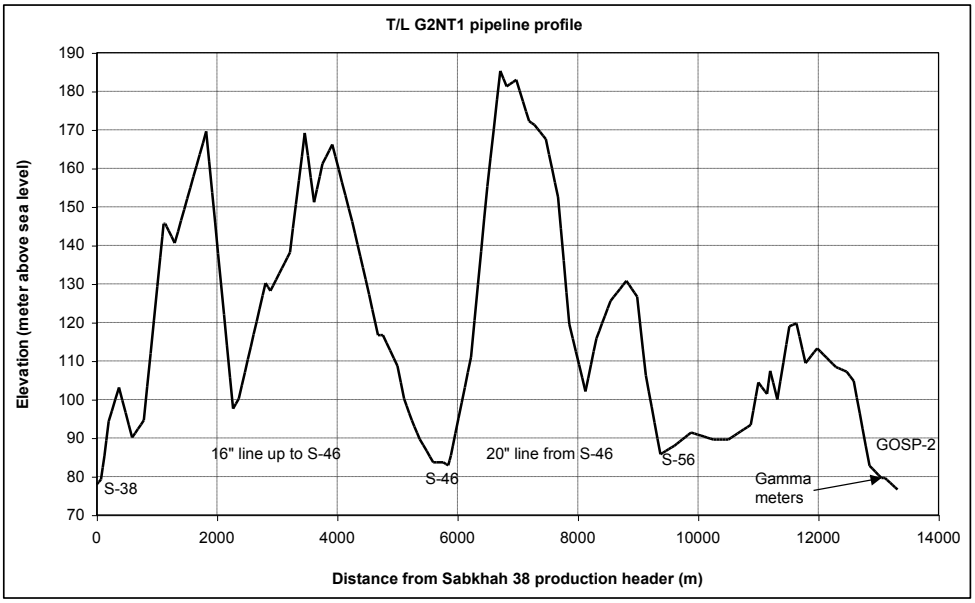

Figure 5-10: G2NT1 pipeline profile - slug valve and gamma densitometer locations

The measurements were made at a normal production rate of 64,000 BBL/Day at standard conditions. The flow rates were based on forecasts made by the production engineers and no flow rate measurements were carried out at the time of the experiments. The flow rates from each Sabkhah were estimated as follows:

Sabkhah	Volumetric Flow Rate (BBL/Day) @ std. cond.
S-38	16,000
S-46	24,000
S-56	24,000
Total	**64,000**

The superficial gas and liquid velocities ranged from (0.3 to 4.1) m/sec for gas and (0.3 to 2.0) m/sec for liquid, based on OLGA predictions.

The distance between the gamma meters was set at 36.95 m, while the pipeline inclination angle was measured at 0 degrees. The distance of the gammas to the upstream slug valve was measured at approximately 16 m. In addition the distance to GOSP-2 was approximately 250 m, as shown in Figure 5-11. The pipeline wall thickness was measured using ultra sonic measurement device at 0.787 inch (20 mm). The GOSP-2 pressure was set at 400 psig during the measurement period.

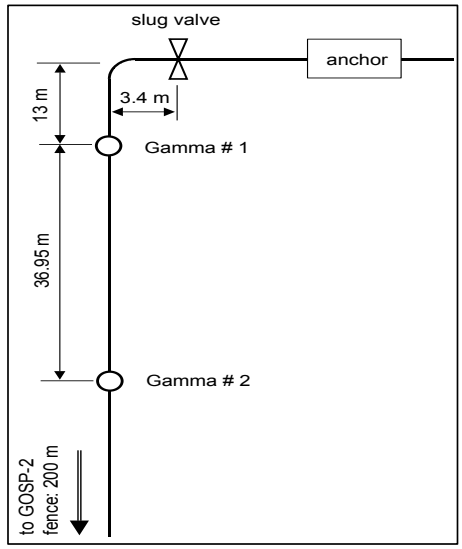

Figure 5-11: Gammas Location with respect to Slug Valve and GOSP-2

5.1.2. Production Header Time Series:

The pressure log at Sabkhah 38 (S-38) showed a clear cyclic behavior with pressure fluctuating by approximately 70 psi between 870 psig and 940 psig with a 20 minutes period as shown in Figure 5-12.

The pressure log from Sabkhah 46 (S-46) showed a similar behavior with pressure fluctuations of 30 psi between 690 psig and 720 psig as shown in Figure 5-13. The figure also shows the pressure readings from nearby connected wells which confirm the cyclic behavior. The slugging period was similar to the S-38 pressure period with approximately 20 minutes cycle.

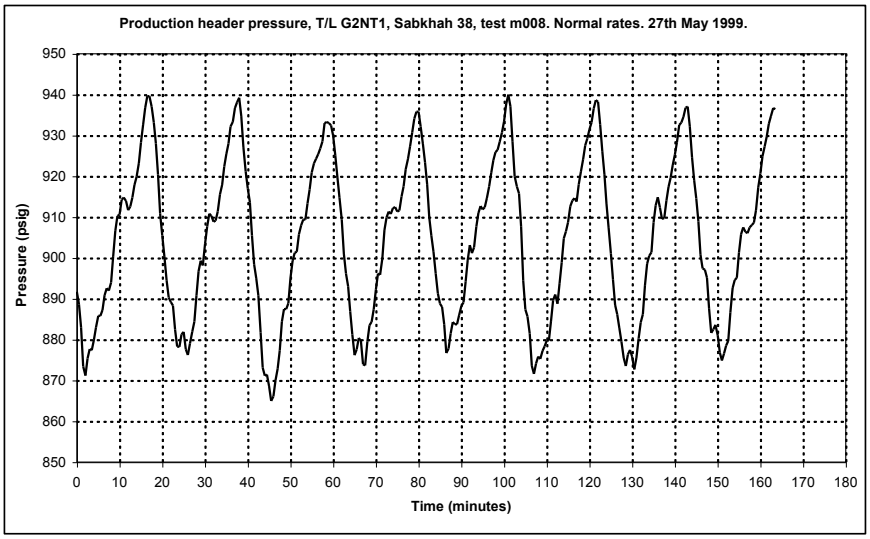

Figure 5-12: G2NT1 Production header pressure at S-38, May 27, 1999

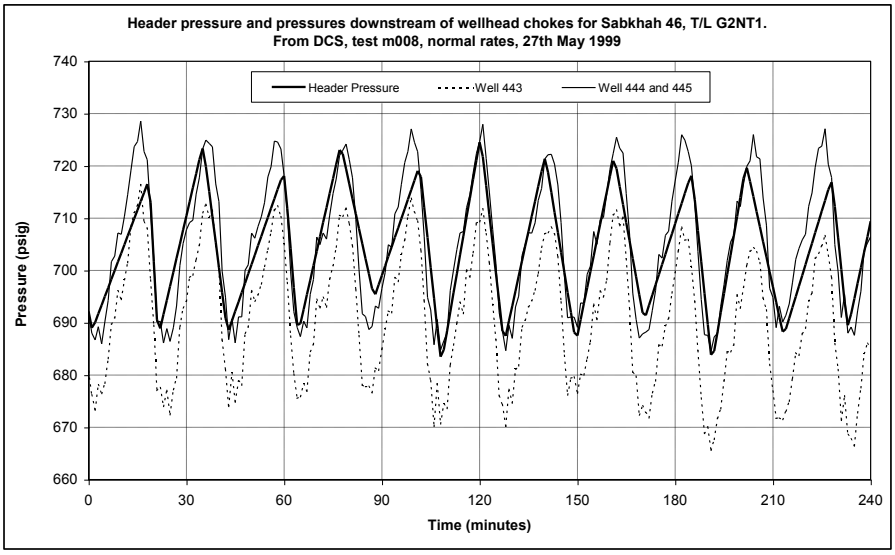

Figure 5-13: G2NT1 Production header pressure at S-46, May 27, 1999

5.1.3. Slug Valve Pressure Drop:

The pressure drop across the slug valve was not logged during the measurement tests due to the malfunction of the manometers at the slug valve location. However, observation of close by manometers showed average differential pressure of approximately (140) psi, which is extremely high.

5.1.4. Analysis of Holdup Time Series:

Analyzing the holdup time series in Figure 5-14, one observes that there are 5 minute periods with 6 – 8 slugs of equal size, followed by two longer slugs with higher holdup. These two high holdup slugs are almost combined into one very long slug. The two patterns are shown better in Figure 5-15. In this figure

the holdup for both gamma meters are shown. In figures Figure 5-16 and Figure 5-17 further details of the slugs are shown.

One also observes that the gamma meter furthest downstream (gamma-2) always indicates a higher holdup than the upstream one (gamma-1). The reason for this behavior could be related to the fact that the gamma meters are located very close to the slug valve and the slug valve opening is estimated to be only a few percent open (pressure differential of around 140 psi), thus flashing the gas out of the liquid phase. The gas comes fast out of the liquid phase, and moves faster than the liquid further downstream. Thus one notices lower liquid holdup at gamma-1 than gamma-2.

The average liquid film in the bubble section at Gamma-1 location was approximately 0.05 and at gamma-2 location was approximately 0.15. On the other hand the slug peaks at location of gamma-1 were 0.65 for the short slugs and 0.73 for the long slugs, while at location of Gamma-2 the peaks of short slugs were 0.7 for the short slugs and 0.83 for the long ones.

The long slug cycle is in line with the 20 minutes cycle noticed in the production header pressure time traces. This indicates that the short slugs are in fact hydrodynamic slugs with very little impact on the overall pressure behavior of the pipeline system.

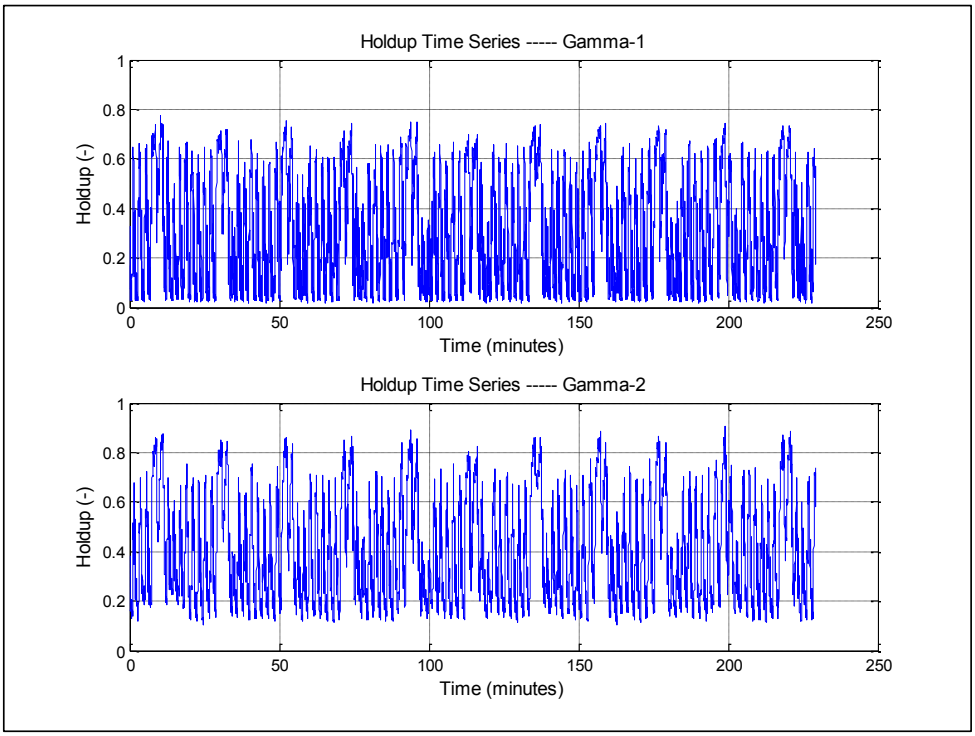

Figure 5-14: G2NT1 Holdup time series, (Gamma-1 & 2) – (Separate)

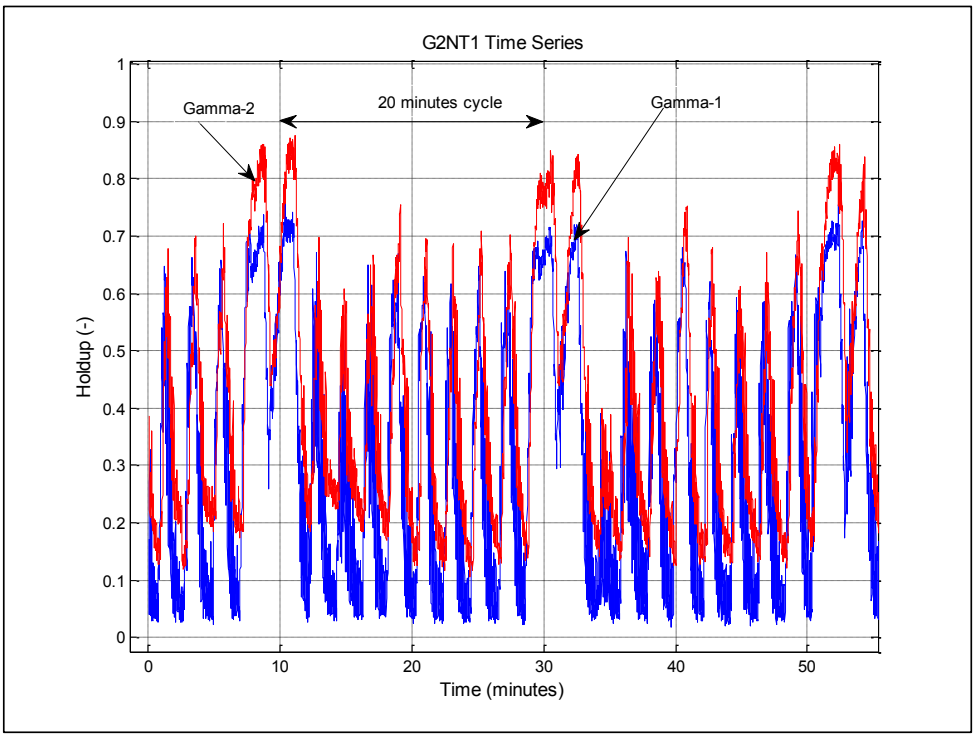

Figure 5-15: G2NT1 Holdup time series, (Gamma-1 & 2)

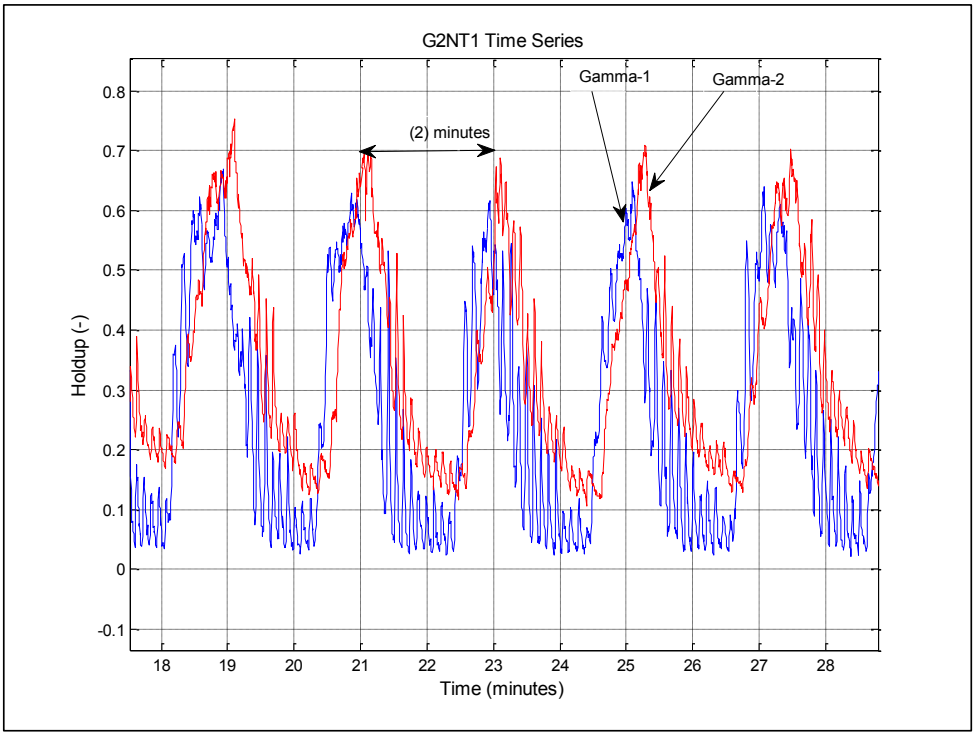

Figure 5-16: G2NT1 Holdup time series, Extract of the liquid holdup time series, short slugs

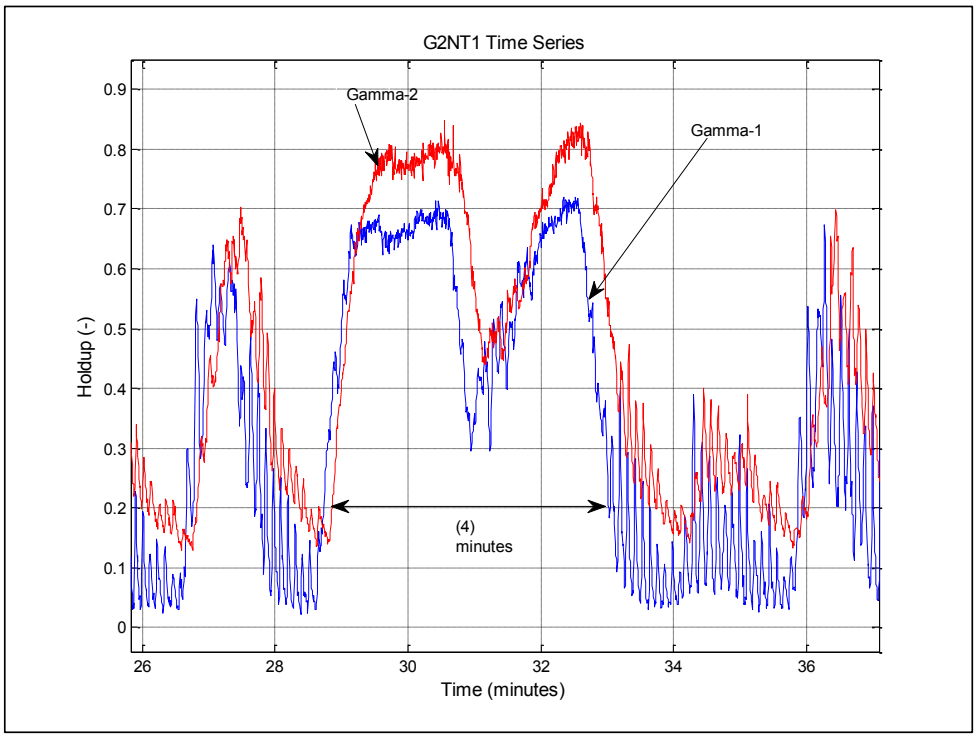

Figure 5-17: G2NT1 Holdup time series, Extract of the liquid holdup time series, Long slugs

Cross correlation was carried out using the two time series at gamma-1 and gamma-2 locations. The analysis showed a time lag delay of 15.2 seconds as shown in Figure 5-18. This results in a velocity of 2.43 m/sec.

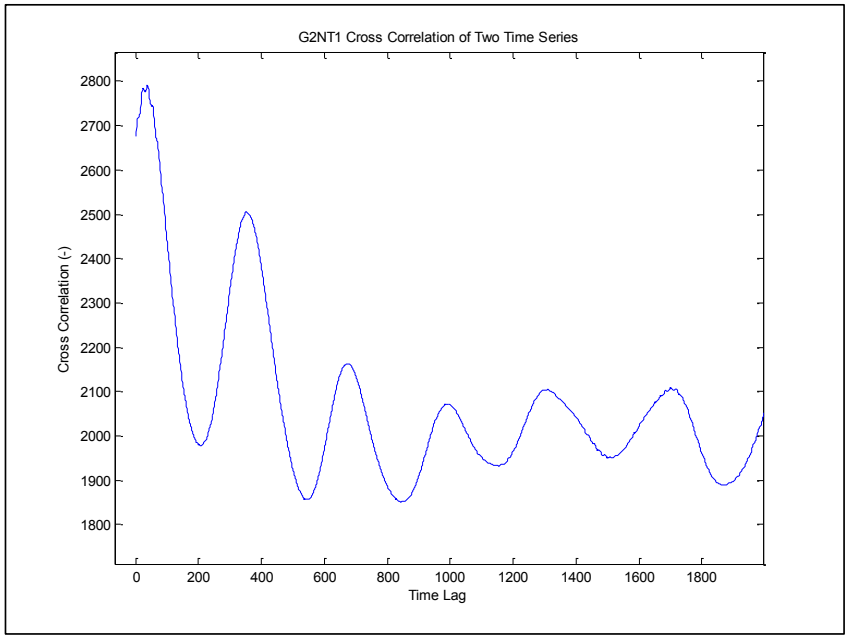

Figure 5-18: Cross correlation of holdup time series, G2NT1 Pipeline

Slugs were defined using the location of the minimum points in the holdup time traces. Once those minimum points are located then slug boxes are created to define the periods at which the holdup is high enough to create a slug as shown in figures Figure 5-19 and Figure 5-20. The remaining length is considered to be the bubble length. Using this approach, one can determine all the statistical parameters associated with the slugs such as slug length, front and tail velocities and slug frequencies.

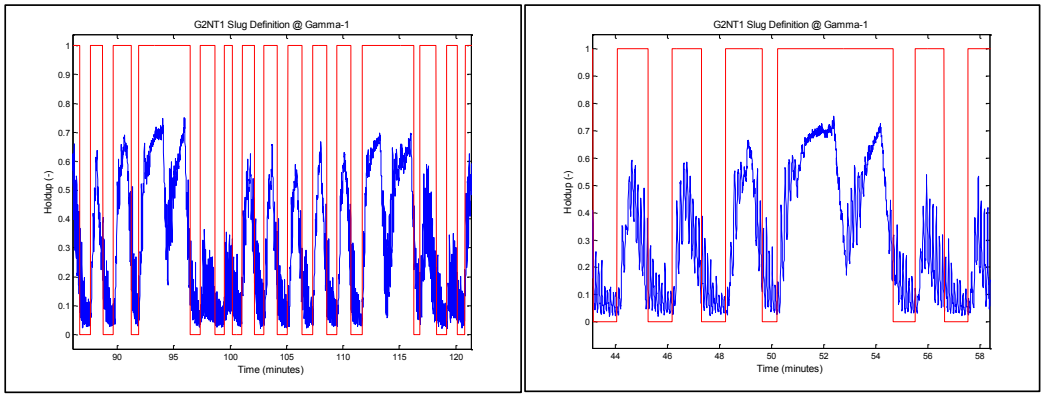

(a) (b)

Figure 5-19: Slug Definition at Gamma-1, Location G2NT1 Pipeline – (a) (35 Minutes) – (b) (12 Minutes)

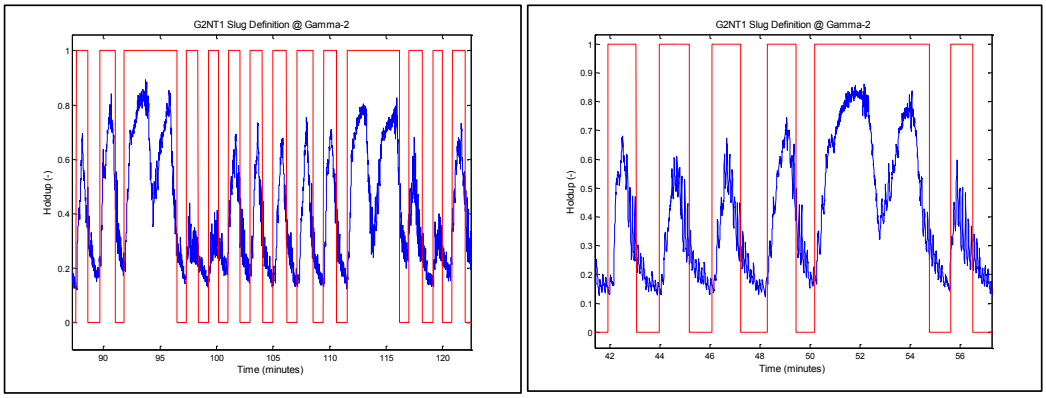

(a) (b)

Figure 5-20: Slug Definition at Gamma-2 Location, G2NT1 Pipeline – (a) (35 Minutes) – (b) (12 Minutes)

In Figure 5-21 the slug period distribution is shown. Most slugs appear to be within 2 to 2 ½ minutes interval. The set of two large slugs appears approximately every 20 minutes. The total number of slugs which were detected over the measurement period of 3 hours and 45 minutes was 80 slugs which give an average slug frequency of a slug every 2.8 minutes.

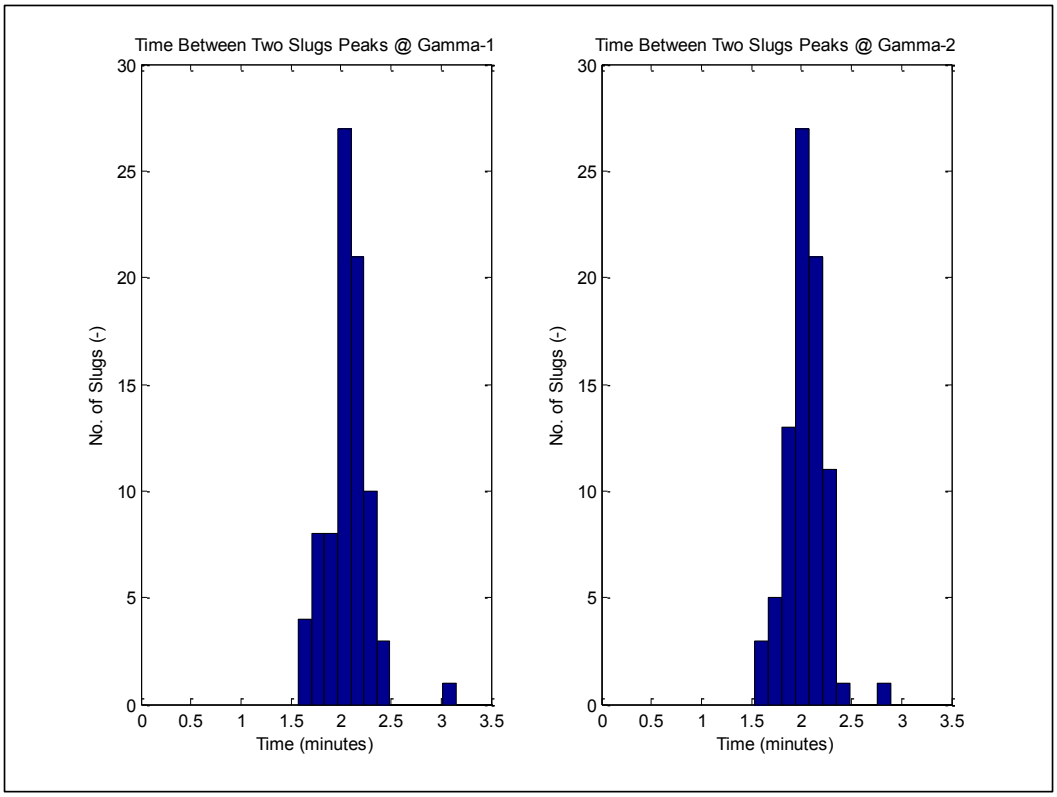

Figure 5-21: G2NT1, Distribution of Time between two slug peaks, (Gamma 1 & 2)

Distribution of slug length is shown in Figure 5-22. The bulk of short slugs had lengths of approximately 200 meters. However, the long slugs, which consist of two slugs coming together in 20 minutes cycles, were almost 800 meter in length as shown in the figure.

Distribution of slug length in number of diameters is also shown in Figure 5-23. The diameter used in calculating the slug length in this figure was the inner diameter at the gamma location of (0.47945) meters.

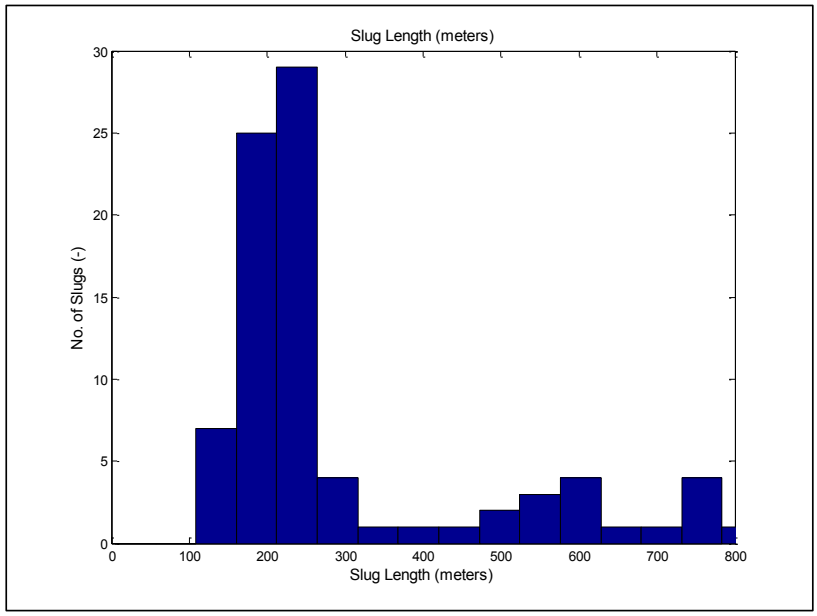

Figure 5-22: G2NT1 Slug Length (m) Distribution

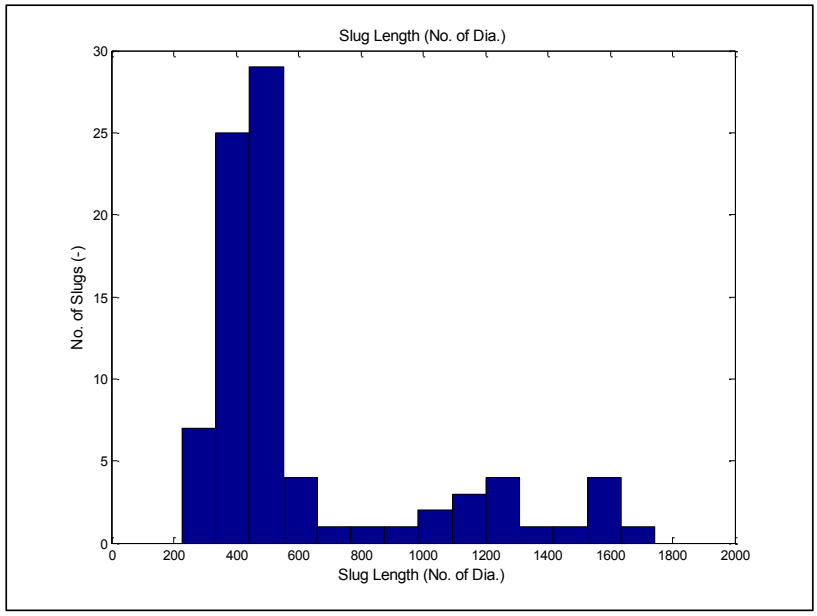

Figure 5-23: G2NT1 Slug Length (No. of Dia.) Distribution

The distribution of the averaged slug front and tail velocities is shown in Figure 5-24. The distribution indicates slightly higher velocities of 2.5 to 3.0 m/sec compared to the calculated average velocity using the cross correlation time shift which gave a velocity of 2.43 m/sec.

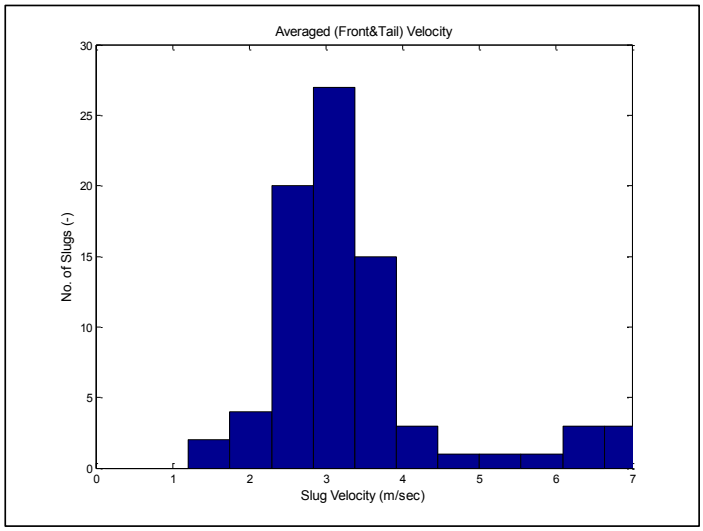

Figure 5-24: G2NT1 Averaged Slug Front & Tail Velocities

Comparing the slug front velocity against the tail velocity shows a general trend of higher tail velocities as shown in Figure 5-25. The average tail velocity was 3.35 m/sec while the average front velocity was 2.34 m/sec. This indicates a decay of the slugs between the two gamma meter locations. This also corresponds well to the increase in the slug holdup measured by the downstream gamma meter as more liquid is moving into the slug body and more gas comes out of the slugs, and travels in the slug bubble section between the slugs. Therefore, slugs at (gamma # 2) location are less aerated and have a higher holdup value.

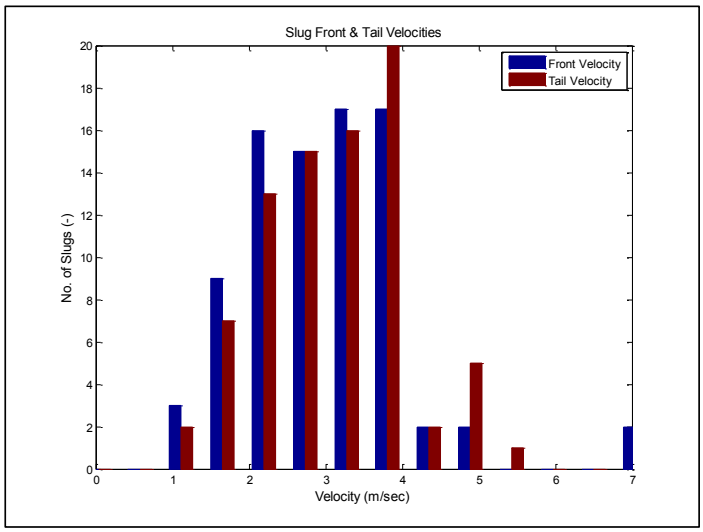

Figure 5-25: G2NT1 Slug Front & Tail Velocities

5.1.5. G2NT1 Pipeline Simulations

Extensive simulation work was carried out using various slug prediction techniques namely: slug tracking, OLGA and slug capturing, LedaFlow.

All holdup and pressure comparisons will be conducted against the results obtained at the gamma measurement location at the end of the pipeline for holdup comparison and at S-38 header at the beginning of the pipeline for pressure comparison, as shown in Figure 5-26.

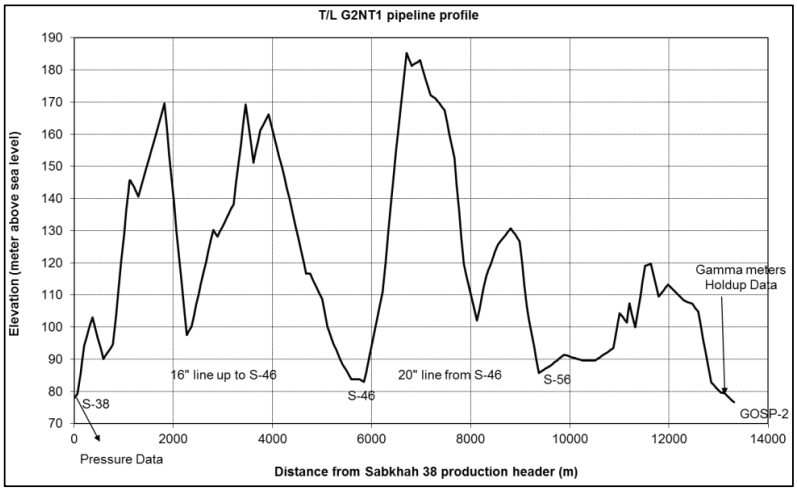

Figure 5-26: G2NT1 - Holdup and Pressure measurement locations for simulation comparison

5.1.6. G2NT1 Pipeline OLGA Simulations

OLGA is a commercial multiphase flow transient simulation package that has been widely used in the oil and gas industry. OLGA utilizes a slug tracking technique over a fixed grid to predict hydrodynamic slugs in multiphase oil and gas pipelines. It is also capable of predicting terrain slugs utilizing its default two-fluid model and the unit-cell model approach.

The simulation was carried out using OLGA 7.2, for a total simulation time of (600) minutes to allow the results to overcome the initial conditions effect and reach a steady state solution. The observation made from the results shows that after approximately (450) minutes the solution starts to reach steady state solution for the 2nd order scheme while it reaches the steady state solution much earlier for the 1st order scheme.

The simulation work was carried out with various options to fully test the capabilities of the OLGA simulation package to predict the terrain slugging phenomenon. The results are presented below in comparison with the measured pressure and holdup time series.

The parameters which were varied during the simulation were:

- Temperature Calculations (No temperature calculations vs. Simple heat transfer U-value approach)
- Slug Tracking (No Slug Tracking vs. Slug Tracking with various delay constants)
- Grid Size (Coarse grid vs. Fine grid (5 meters))
- Mass Equation Solution Scheme (1st Order vs. 2nd Order)

G2NT1 OLGA Simulations – (Heat Transfer vs. No Heat Transfer)

The first set of OLGA simulations was carried out to test the impact of temperature calculations on OLGA simulations. Therefore, OLGA simulations were set with adiabatic assumption, i.e. no heat transfer from the surroundings. In addition, the inlet and outlet temperature conditions where assume to be the same in order to neglect any temperature calculations. The results where compared against a set of simulations where a simplified heat transfer U-value = 0.35 (BTU / ft2*H*F) was used.

The results as shown on Figure 5-27 indicate minimum impact of enabling or disabling temperature calculations on the pressure results when utilizing normal 1st order solution scheme for the mass equations.

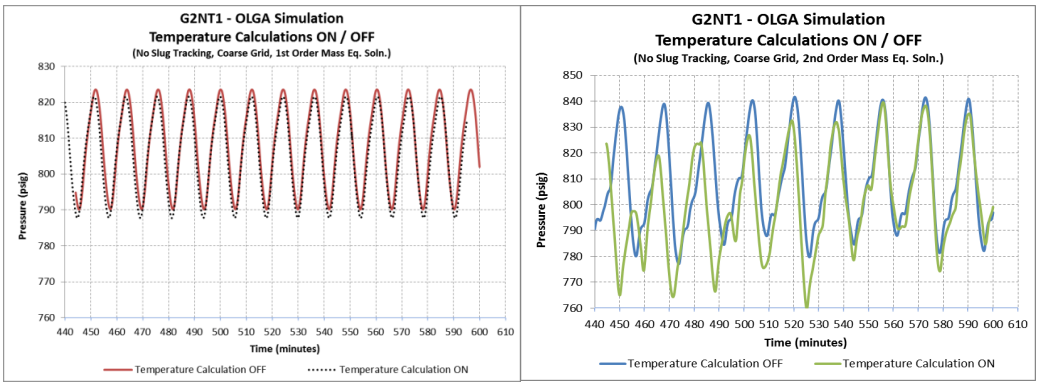

(a) (b)

Figure 5-27: G2NT1 OLGA Pressure Results – Tempe. Calculations (ON/OFF) – (No slug tracking, Coarse Grid) (a) 1st Order Mass Eq. Solution – (b) 2nd Order Mass Eq. Solution

When a 2nd order mass equation solution scheme is used the heat transfer impact can also be considered negligible as we can see clearly at the end of the plot in Figure 5-27 as we move away from the initial conditions zone into a more steady state solution. The pressure plot also indicates that with temperature calculations enabled, it takes more time to reach a steady state solution. The holdup results also indicate similar behavior as shown on Figure 5-28. The holdup with and without temperature calculations perfectly matches each other for the 1st order mass equation solution scheme. On the other hand, it almost matches each other towards the end of the simulation for the 2nd order mass equation solution scheme.

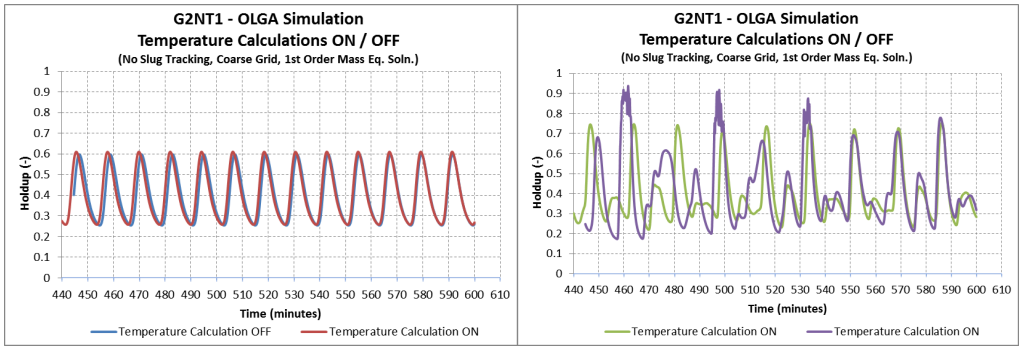

(a) (b)

Figure 5-28: G2NT1 OLGA Holdup Results – Tempe. Calculations (ON/OFF) – (No slug tracking, Coarse Grid) (a) 1st Order Mass Eq. Solution – (b) 2nd Order Mass Eq. Solution

Using the above holdup and pressure results from OLGA simulation, it was decided to ignore the temperature calculations for the remaining set of simulations for this pipeline and all similar pipelines in the 1999 terrain slugging cases.

G2NT1 OLGA Simulations – (Slug Tracking vs. No Slug Tracking)

OLGA Simulations were also carried out with and without slug tracking module. The results were plotted for various Delay Constants (DCs), which significantly impact the initiation of slugs in OLGA. The delay constants were used to simulate very slow to very fast slug initiation scenarios and note the impact on the pressure and holdup results.

The delay constant is defined in OLGA as the number of diameters a slug must travel before the slug model tries to initiate a new slug at the same boundary, thus defining the time between two consecutive slug initiations. It is mainly associated with hydrodynamic slugging phenomenon as terrain slugs are naturally predicted by the default OLGA two-fluid and unit cell model. In principle, the delay constant should not play an important role in predicting the large slugs with 20 minutes cycles, which determines the pressure cycle in the pipeline system as it should only impact the ability of OLGA to predict the small hydrodynamic slugs that occur downstream the slug valve with a frequency of approximately 2 minutes cycles.

However, due to the interactions between the two phenomena, even the results of the large scale terrain slugging phenomenon are impacted by the choice of simulation parameters for hydrodynamic slugs such as the delay constant.

Using the OLGA definition of the delay constant, one can derive the idle time between slug initiations that OLGA utilizes with each delay constant. The formula for calculating the idle time as described by OLGA is as follows:

$$\Delta t = DC \cdot \frac{D}{U_l}$$

where, (DC) is delay constant, (D) is internal diameter in meters measured at (0.47945) meters at the measurement location and (U_l) is the average liquid velocity set at 2.43 m/sec obtained from the cross correlation of the two gamma meters signals.

Table 5-2: Idle time between slug initiations for various delay constants

Idle time between Slug Initiation (DT) (sec)	Ul (m/sec)	Inner Dia (m)	DC
9.87	2.43	0.47945	50
29.60	2.43	0.47945	150
98.65	2.43	0.47945	500
157.84	2.43	0.47945	800

OLGA simulations were carried out with various delay constants ranging from 50 to 800. The pressure results are shown on figures Figure 5-29and Figure 5-30. Analysis of the pressure plots shows that with no slug tracking the pressure cycles are fixed at 12 minutes. When slug tracking module is enabled, and with various delay constants the cycle begins to change slightly as the delay constant is reduced from 800 to 50.

The plots show a pressure cycle that ranges between 17 to 21 minutes for delay constant 50 case. On the other hand, as we increase the delay constant to 150, 500 and 800, the pressure cycles decreases with less fluctuations between the pressure peaks.

When compared against the pressure traces obtained from the field measurements, the case with lowest delay constant of 50 is shown to be the closest in terms of pressure cycle and magnitude to the field measurement. So, although a delay constant of 50 which gives a very short idle time between slugs and very frequent slug initiation may seem to be inappropriate for a clearly terrain slugging case, it actually produces the best results when it comes to pressure magnitude and oscillation.

The results for the case with no slug tracking produce a very stable and repetitive slug behavior with pressure oscillation of exactly 12 minutes for each cycle. The pressure magnitudes predicted by OLGA using the default two-fluid model and the slug unit-cell model seem to be far away from the field measurements.

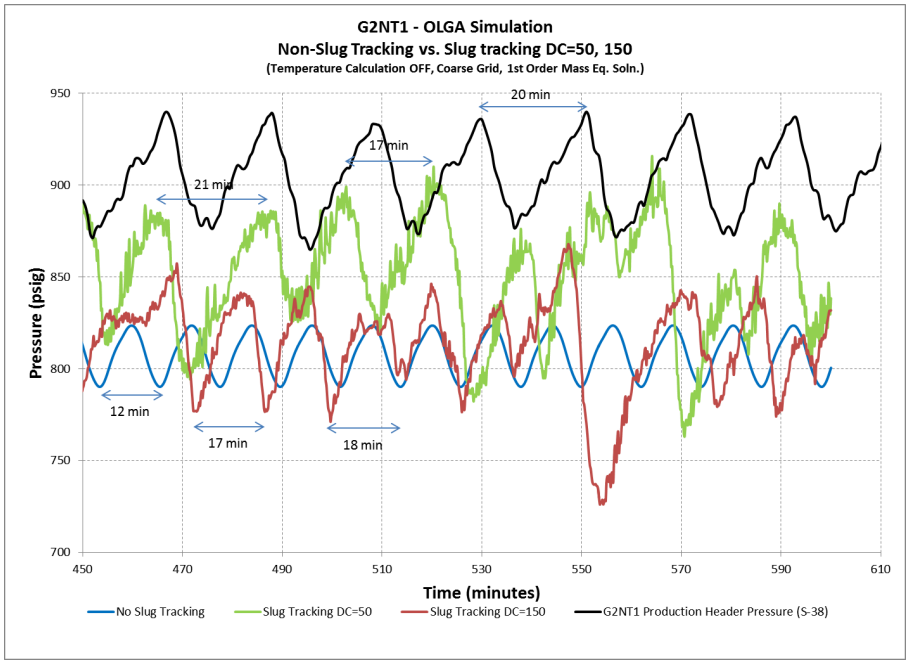

Figure 5-29: G2NT1 OLGA Pressure Results – Slug Tracking DC=50, 150 – (Temp. Calculation OFF, Coarse Grid, 1st Order Mass Eq. Solution)

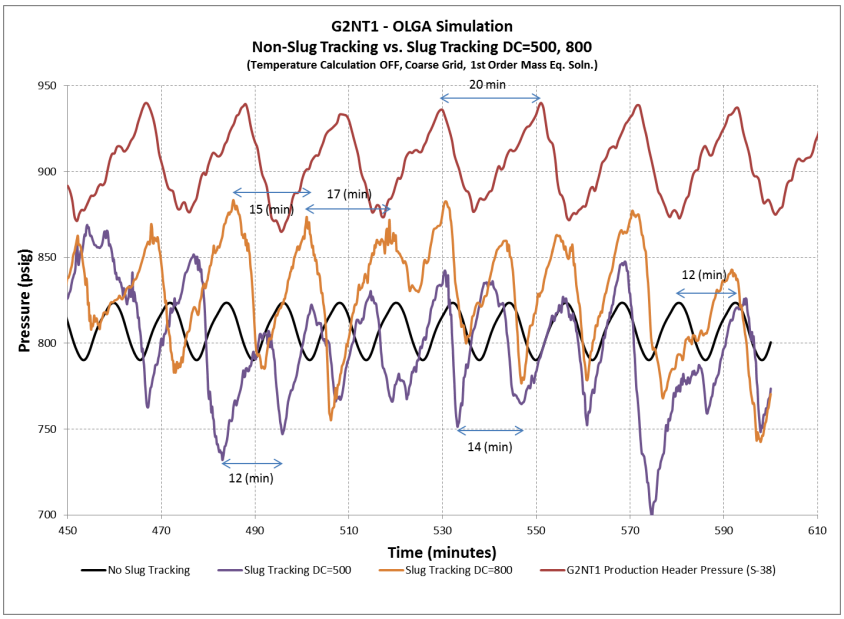

Figure 5-30: G2NT1 OLGA Pressure Results – Slug Tracking DC=500, 800 – (Temp. Calculation OFF, Coarse Grid, 1st Order Mass Eq. Solution)

Comparing the slug tracking holdup results versus field measurements produces less satisfactory results as OLGA were not able to predict the hydrodynamic slug behavior correctly as shown in figures Figure 5-31 and Figure 5-32. The holdup peak values seem in good agreement with the measured holdup as it ranges between 0.8 and 0.7 while liquid height film was a bit higher than the measured as it ranges between 0.2 and 0.3.

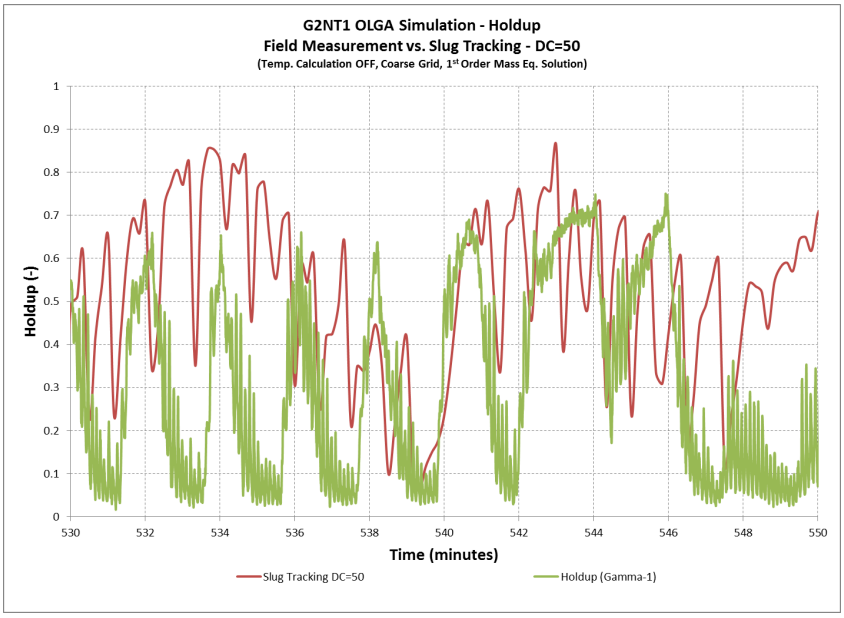

Figure 5-31: G2NT1 OLGA Holdup Results – Slug Tracking DC=50 – (Temp. Calculation OFF, Coarse Grid, 1st Order Mass Eq. Solution) – (20 minutes span)

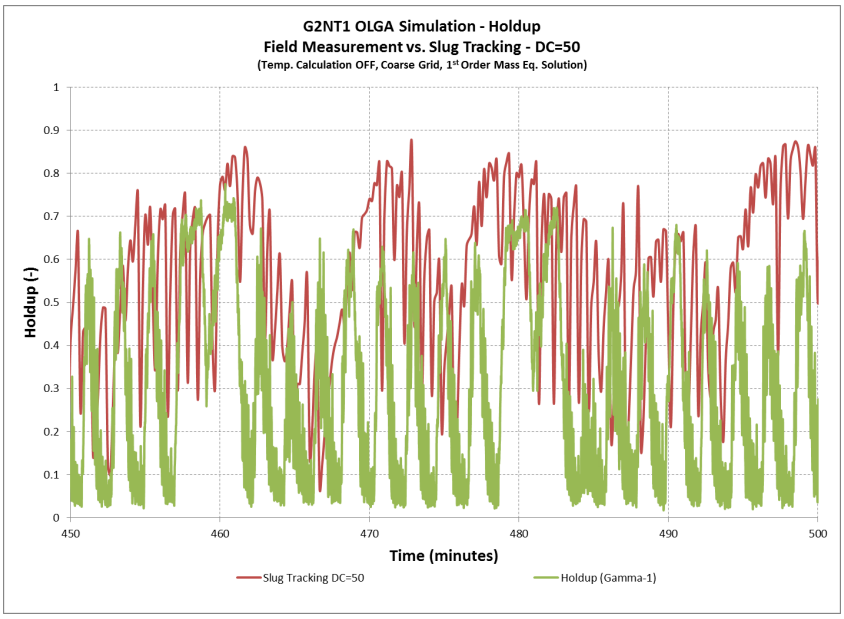

Figure 5-32: G2NT1 OLGA Holdup Results – Slug Tracking DC=50 – (Temp. Calculation OFF, Coarse Grid, 1st Order Mass Eq. Solution) – (50 minutes span)

G2NT1 OLGA Simulations – (Coarse Grid vs. Fine Grid)

Most of the OLGA simulations were carried out a fairly coarse grid as shown in Figure 5-33 and Figure 5-34.

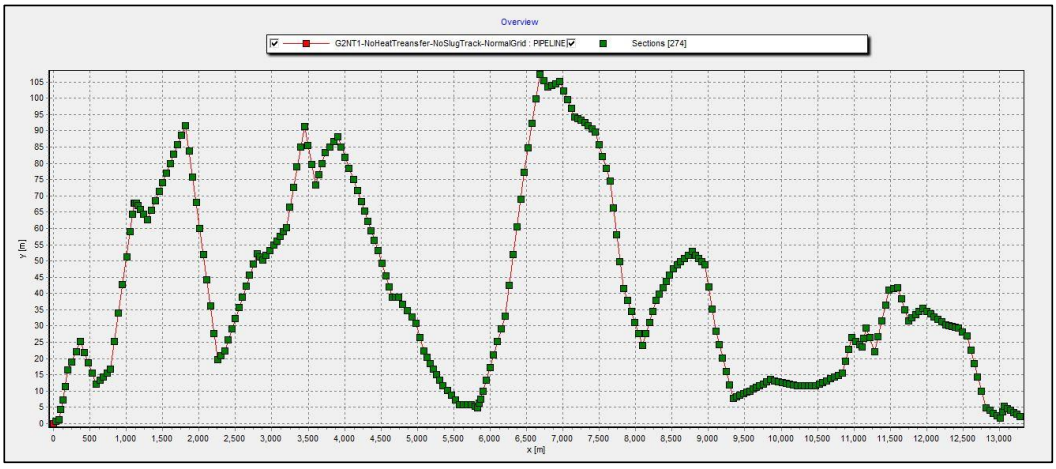

Figure 5-33: OLGA pipeline sections – default gridding option (coarse grid)

The section length ratio, which gives the ratio between two adjoining sections, is shown in Figure 5-34. The section ratio ranges between approximately 0.6 and 1.8, with an average section length of (48.6) meters per section. A histogram of section lengths is shown in Figure 5-35 which shows that most of the sections are 40 and 60 meters in length.

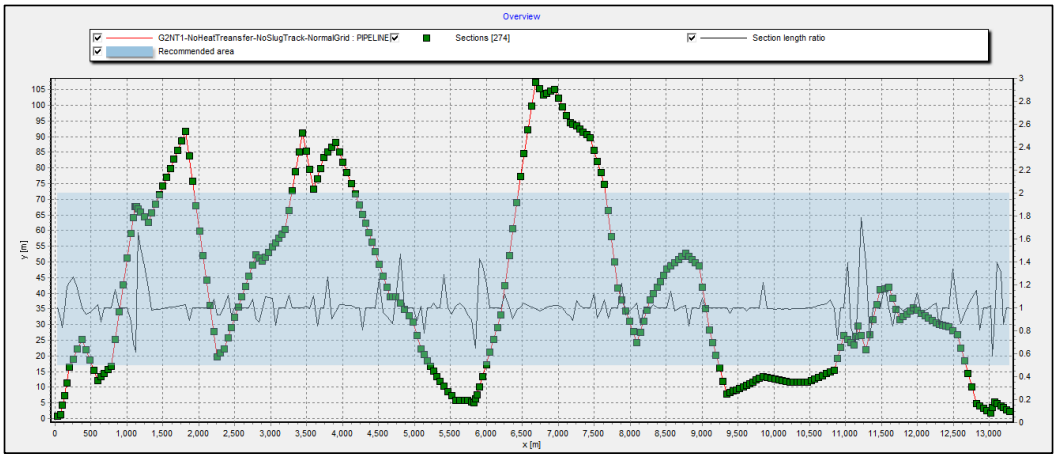

Figure 5-34: G2NT1 Coarse Grid Section Length Ratio

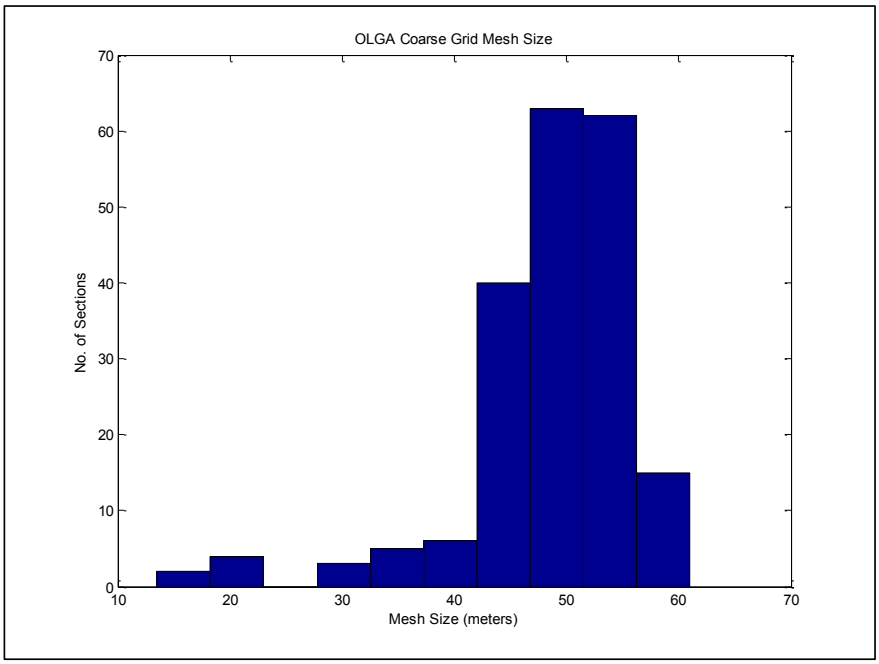

Figure 5-35: G2NT1 – Histogram of Coarse Grid Section Sizes in meters

In addition, a fine grid option was tested to investigate the impact of fine gridding on OLGA slug predictions. Therefore, a constant section of (5) meters was selected which is approximately (10.4 * Internal diameter of the pipeline) at the measurement location, shown in Figure 5-36.

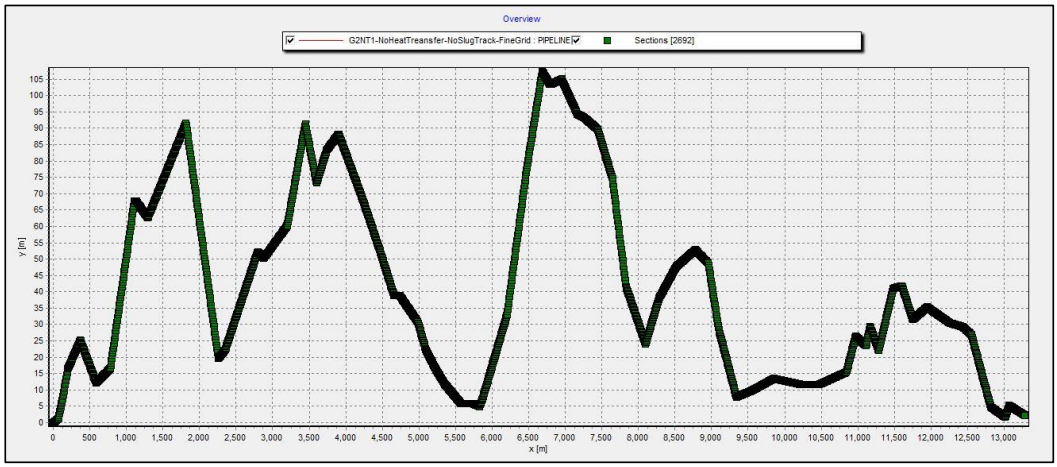

Figure 5-36: OLGA pipeline sections – (5 meter) Fixed Section Length (fine grid)

OLGA simulations were run with and without slug tracking and results are shown in figures Figure 5-37 and Figure 5-38. The results show minor impact of choosing a fine grid over a coarse grid with and without slug tracking.

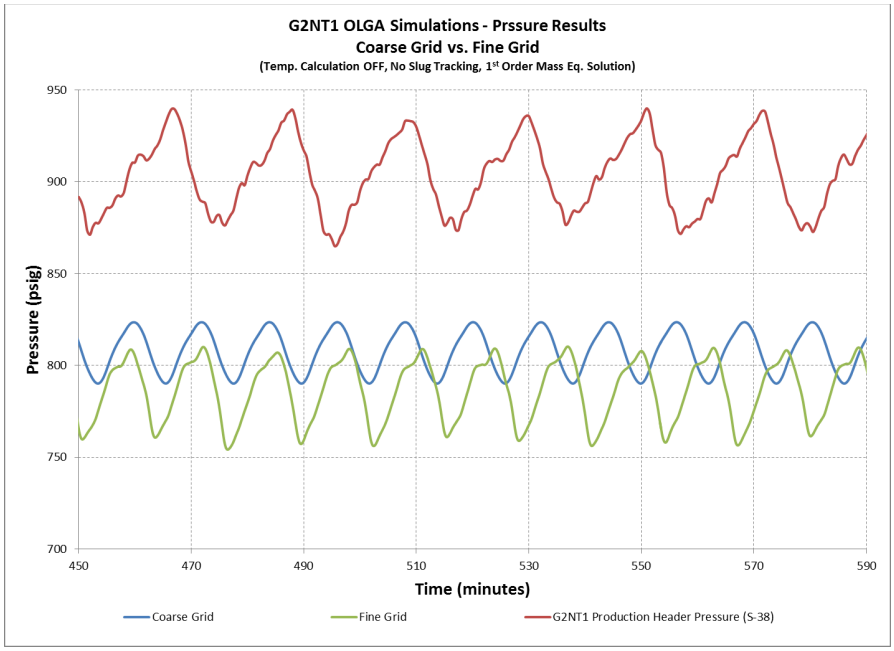

Figure 5-37: G2NT1 OLGA Pressure Results – Coarse vs. Fine Grid – (Temp. Calculation OFF, No Slug Tracking, 1st Order Mass Eq. Solution)

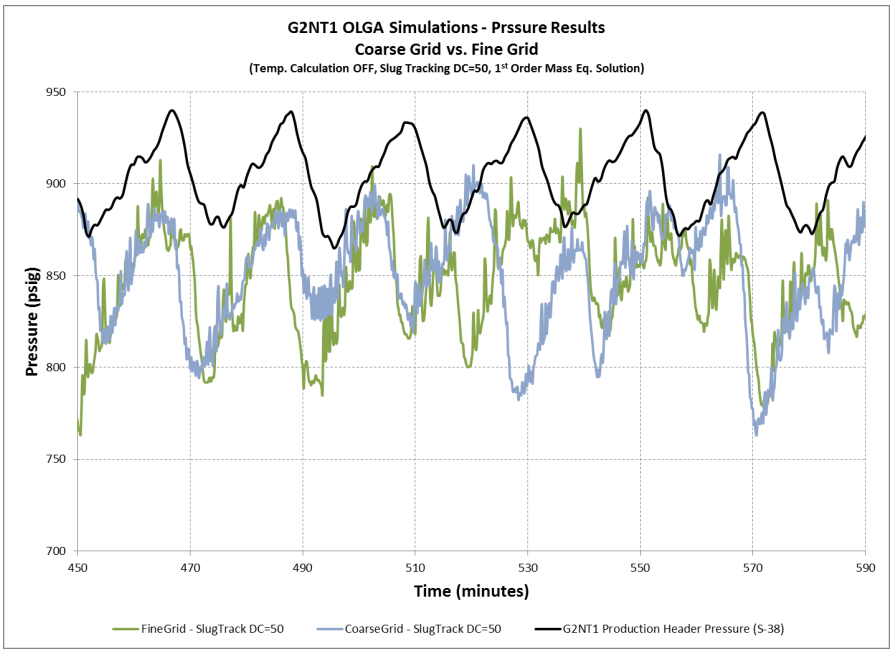

Figure 5-38: G2NT1 OLGA Pressure Results – Coarse vs. Fine Grid – (Temp. Calculation OFF, Slug Tracking DC=50, 1st Order Mass Eq. Solution)

G2NT1 OLGA Simulations – (1st Order vs. 2nd Order Mass Equation Solution Schemes)

Recently a new scheme was implemented in OLGA where the option of selecting a 2nd order scheme to solve the mass equations has been implemented in OLGA version 7.0. The default solution scheme for the mass equation is the 1st order upwind implicit scheme.

The main reason behind implementing the 2nd order scheme is to reduce numerical diffusion and therefore track the slug fronts more accurately. This method utilizes a combination of different numerical schemes in order to obtain a stable numerical approach which satisfies the Total Variation Diminishing (TVD) condition.

The pressure results, shown on Figure 5-39, shows better agreement with the field measurement results in terms of the pressure cycle as we obtain a cycle of (17) minutes compared to (20) minutes in the field measurement. The magnitude is still lagging approximately (100) psi between a measured peak of (940) psig compared to a simulated peak of (840) psig. In addition, the simulated pressure amplitude at (60) psi shows very good agreement with the field measurement pressure fluctuations at (70) psi. The holdup results, shown on Figure 5-40, also shows an improved agreement in terms of cyclic behavior, (17) minutes compared to (20) minutes, and magnitude of the holdup peak at (0.7) for both field measurements and simulation. The discrepancy in liquid film height is higher as it is approximately 0.25 for the OLGA simulation compared to 0.15 at Gamma-1 location.

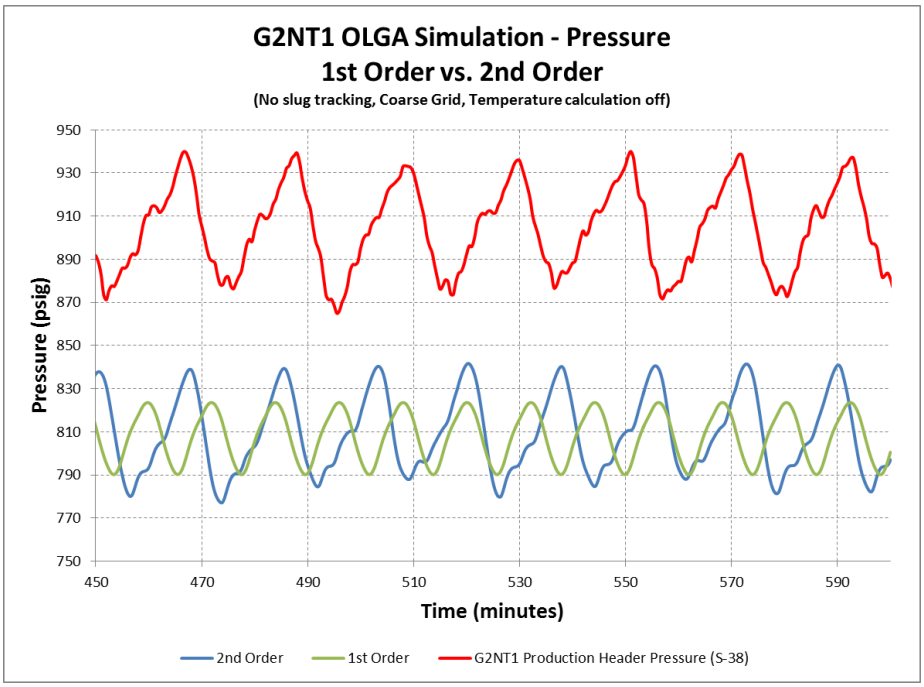

Figure 5-39: G2NT1 OLGA Pressure Results – 1st Order vs. 2nd Order – (Temp. Calculation OFF, No Slug Tracking, Coarse Grid)

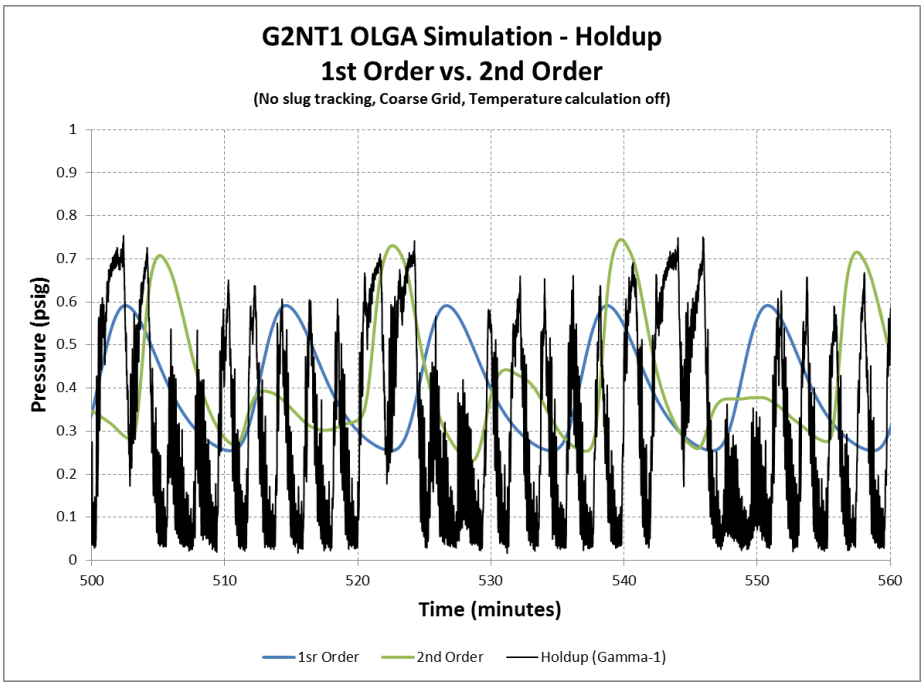

Figure 5-40: G2NT1 OLGA Holdup Results – 1st Order vs. 2nd Order – (Temp. Calculation OFF, No Slug Tracking, Coarse Grid)

5.1.7. G2NT1 Pipeline LedaFlow Simulations

LedaFlow is a fairly new commercial multiphase flow transient simulation package that has been developed by the leading SINTEF research center in Norway and is currently being commercialized by Kongsberg Oil & Gas Technologies AS, Norway. The development work started in 2001 in collaboration between Total, ConocoPhilips and SINTEF and the first commercial version was released in 2011.

LedaFlow utilizes a slug capturing scheme over a fine grid to predict hydrodynamic slugs in multiphase oil and gas pipelines. The slug capturing numerical scheme strictly applies the two-fluid model to predict perturbations at the fluid interface and as such allows for an automatic growth or decay of waves to slugs and vice versa.

The simulation was carried out using LedaFlow version (1.4.242.619), for a total simulation time of (600) minutes to allow the results to overcome the initial conditions effect and reach a steady state solution.

The observation made from the pressure results shows that after approximately (300) minutes the solution starts to reach steady state solution for the high order numerical scheme while it reaches the steady state solution much earlier for the normal order numerical scheme, as shown in figures Figure 5-41.

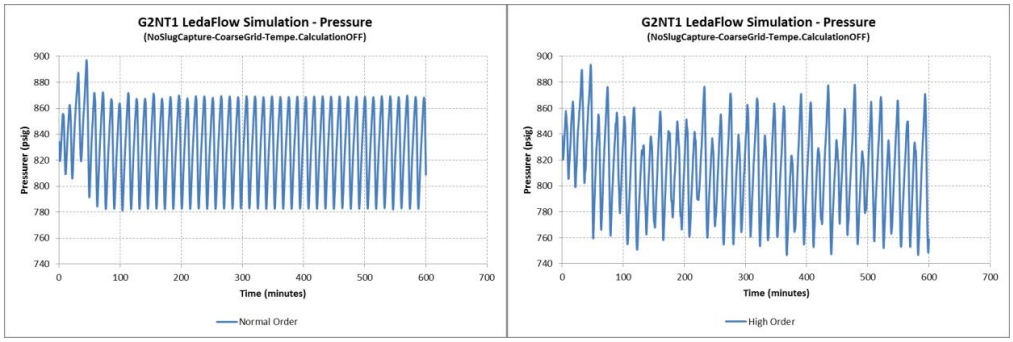

(a) (b)

Figure 5-41: G2NT1 LedaFlow Pressure Results – (No slug capturing, Coarse Grid) – (a) 1st Order Mass Eq. Solution – (b) 2nd Order Mass Eq. Solution

Similar to the OLGA simulations, LedaFlow was tested with various options to fully investigate its capabilities to predict the terrain slugging phenomenon. The results are presented below in comparison with the measured pressure and holdup time series.

The parameters which were varied during the simulation were:

- Temperature Calculations (No temperature calculations vs. Simple heat transfer U-value approach)
- Different Numerical Schemes (Normal Order vs. High Order)
- Slug Capturing (No Slug Capturing vs. Slug Capturing)
- Grid Size (Coarse grid vs. Fine grid (5 meters))

G2NT1 LedaFlow Simulations – (Heat Transfer vs. No Heat Transfer)

The first set of LedaFlow simulations was carried out to test the impact of temperature calculations on LedaFlow simulations. The temperature calculations were disabled for a group of simulations and the re results were compared against a set of simulations where a simplified heat transfer U-value = 0.35 (BTU / ft2*H*F) was used.

The results as shown on Figure 5-42 indicate minimum impact of enabling or disabling temperature calculations on the pressure results when utilizing normal and high order numerical schemes.

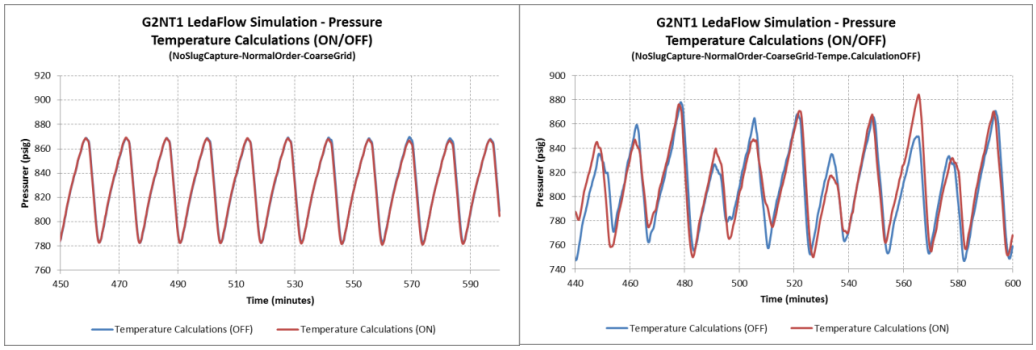

(a) (b)

Figure 5-42: G2NT1 LedaFlow Pressure Results – Temp. Calculations (ON/OFF) – (No slug capturing, Coarse Grid) - (a) Normal Order – (b) High Order

Similar to OLGA and based on the above pressure results; it was decided to ignore the temperature calculations for the remaining set of LedaFlow simulations for this pipeline and all similar pipelines in the 1999 terrain slugging cases.

G2NT1 LedaFlow Simulations – (Normal Order vs. High Order)

The effect of simulating G2NT1 pipeline with normal and high order numerical schemes was investigated. The results show minor impact on the pressure oscillation frequency as shown on Figure 5-43. The pressure magnitude however seems to be alternating with high order while it's very stable with the normal order option. When comparing it against S-38 pressure measurements, both give wrong predictions in terms of frequency as they give a frequency of approximately 13 minutes as opposed to 20 minutes in the pressure measurement. The magnitude is also off by approximately (60) psi when comparing the peaks of the simulated results against the peaks of measured production header pressure.

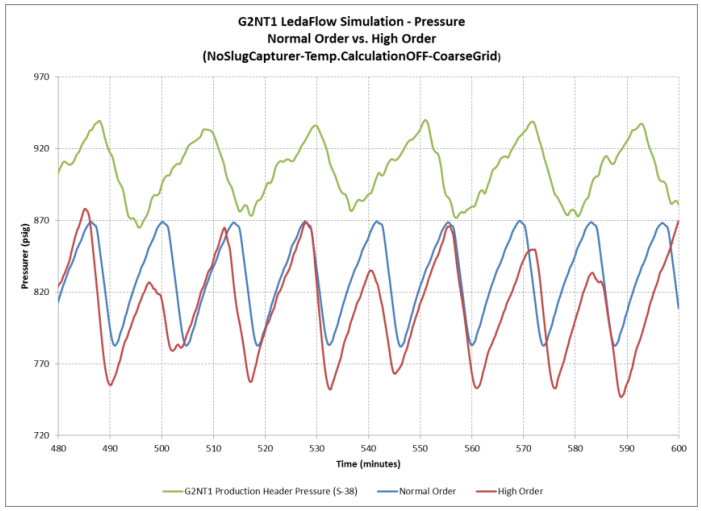

Figure 5-43: G2NT1 LedaFlow Pressure Results – Normal Order vs. High Order – (Coarse Grid, No Slug Capturing, Temp. Calc. OFF) – S-38 Pressure Measurement Comparisons

The holdup results show some deviation with the measured holdup. The prediction of hydrodynamic slugs, as expected, was not possible without the use of slug capturing module. However, it seems that the high order numerical scheme seems to provide a better prediction of the holdup cycle for the large slugs with frequencies that varies between (12) to (20) minutes. On the other hand, the normal order numerical scheme shows a fixed time interval of (13) minutes per cycle which reflect the pressure cycle shown at the pipe entrance. The holdup magnitude shows a better agreement for the normal order with holdup values of peaks at (0.8) which is very close to the measured value of approximately (0.85). However, the magnitude of the holdup peaks for the high order case shows values close to (1.0) as shown on Figure 5-44.

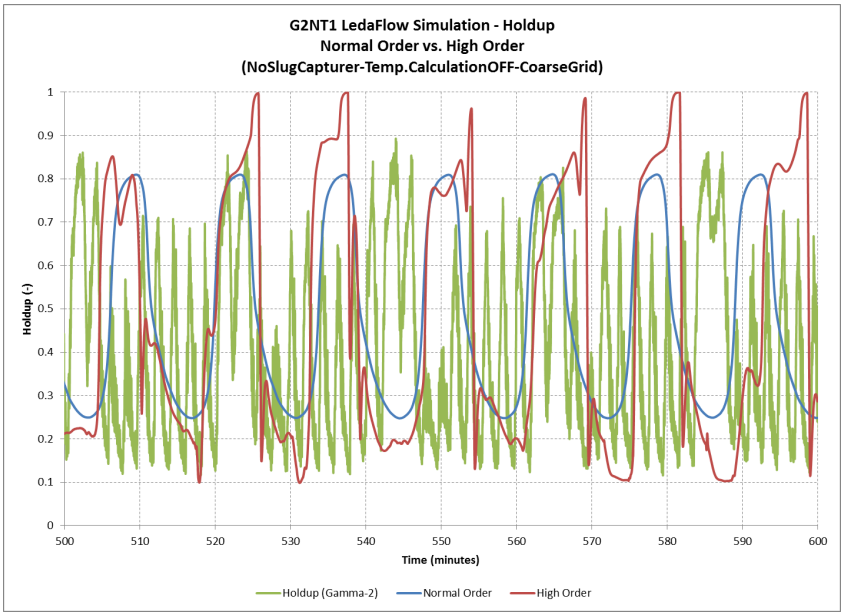

Figure 5-44: G2NT1 LedaFlow Holdup Results – Normal Order vs. High Order – (Coarse Grid, No Slug Capturing, Temp. Calc. OFF) – Gamma-2 Holdup Measurement Comparisons

G2NT1 LedaFlow Simulations – (Slug Capturing vs. No Slug Capturing) and (Coarse Grid vs. Fine Grid)

The unique ability of LedaFlow to predict slugs using its slug capturing technique was tested using its recently released beta slug capturing module. The slug capturing module heavily relies on the grid definition so the finer the grid the better it should be able to predict the small hydrodynamics slugs in multiphase flow system. However, terrain slugs generally do not require fine grids to be predicted and as such slug capturing may not be required to predict those large slugs. In LedaFlow, enabling the slug capturing automatically enables the high order scheme therefore all comparisons with non-slug capturing scheme would be with high order cases only.

Due to the significant impact of the grid size on slug capturing, simulation was carried out using both coarse and fine grids. The coarse grid was imported from OLGA automatic gridding option while the fine grid was implemented using a fixed (5 meters) grid similar to the fine grid utilized in OLGA simulation.

Using a coarse grid and utilizing a slug capturing module one can notice very little impact on the pressure results as shown in Figure 5-45. The holdup results on the other hand show minor deviations in slugging frequency and behavior as we can see small fluctuations between the large slugs, which we did not see

without slug capturing. These fluctuations cause the frequency of slugging to increase slightly as shown on panel (b) in Figure 5-45.

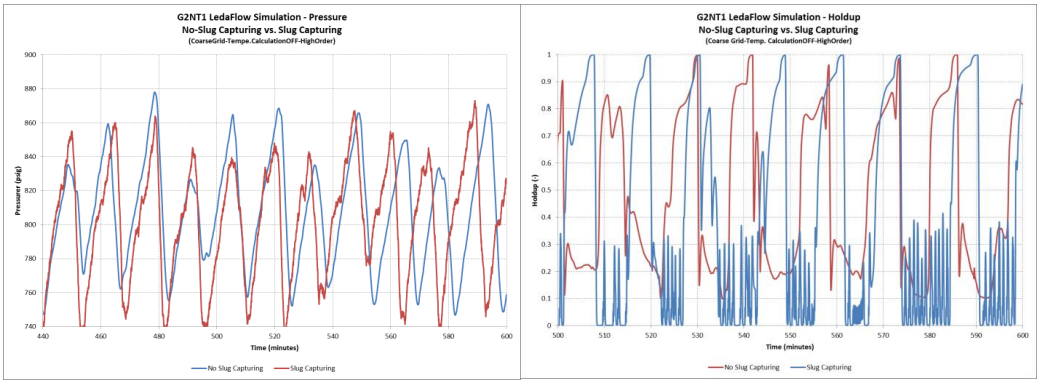

(a) (b)

Figure 5-45: G2NT1 LedaFlow Results – No Slug Capture vs. Slug Capture – (CoarseGrid, Temp. Calc. OFF) (a) Pressure Results – (b) Holdup Results

On the other hand, utilizing a fine grid with slug capturing causes a significant deviation in both pressure and holdup results. The pressure results shown on panel (a) in Figure 5-46 indicate a similar pressure frequency between the slug capture and no-slug capture cases. However, the pressure peaks shows approximately (40) psi difference between the no-slug capture case and slug capture case.

The holdup results show even more differences as the fine grid with slug capturing shows very frequent slug initiation, less than one minute between two slugs, while the fine grid case without slug capturing shows very low holdup, with holdup average equal to 0.2, with almost no slugs being captured, as shown in Figure 5-46.

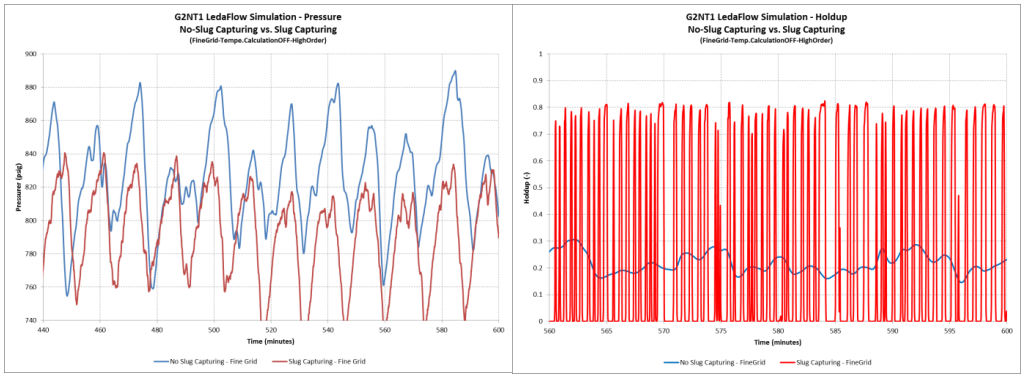

(a) (b)

Figure 5-46: G2NT1 LedaFlow Results – No Slug Capture vs. Slug Capture – (FineGrid, Temp. Calc. OFF) (a) Pressure Results – (b) Holdup Results

When comparing (S-38) pressure measurements against LedaFlow pressure simulation results with coarse grid with and without slug capturing, one could notice that the pressure cycles are approximately at (15) minutes compared to (20) minutes for the measured pressure, as shown on Figure 5-47. The pressure fluctuation is more than (100) psi for the simulation results while it's around (70) psi for the measured

pressure at S-38. In addition, the deviation in pressure magnitude between the measured and simulated pressure for the coarse grid cases is approximately (70) psi.

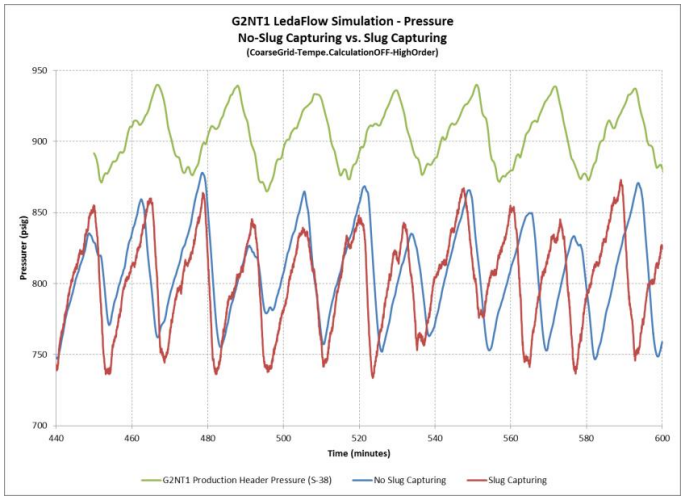

Figure 5-47: G2NT1 LedaFlow Pressure Results – No Slug Capture vs. Slug Capture – (Coarse Grid, Temp. Calc. OFF) – S-38 Pressure Measurement Comparison

On the other hand, when comparing the pressure measurements against LedaFlow pressure simulation results with fine grid with and without slug tracking, one could notice that the pressure cycles are still around (15) minutes, although the no-slug capturing case seems to indicate slightly higher frequencies, as shown on Figure 5-48. The pressure fluctuation is more than (100) psi for the simulation slug capturing results while it's around (80) psi for the slug capturing case. In addition, the pressure magnitude in the no-slug capturing case shows a better agreement with measured pressure than the slug capturing case. The fine grid, slug capturing, pressure simulation results indicate a peak pressure of almost (880) psig compared to (940) psig for the measured simulation. On the other hand, the fine grid, no-slug capturing, pressure simulation results indicate a peak pressure of almost (830) psig.

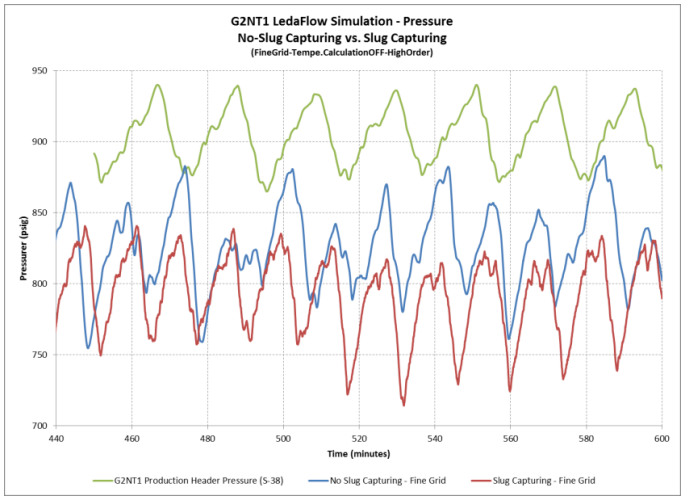

Figure 5-48: G2NT1 LedaFlow Pressure Results – No Slug Capture vs. Slug Capture – (Fine Grid, Temp. Calc. OFF) – S-38 Pressure Measurement Comparison

On the other hand, the coarse grid holdup simulation results, when compared against holdup measurements, show a reasonable qualitative agreement especially the slug capturing case as it predicts small hydrodynamic slugs between two large slugs. However, the holdup magnitude and frequencies deviate from the measured ones as the large slug frequency is still at approximately (15) minutes compared to (20) minutes for the measure pressure.

The fine grid cases holdup simulation results however provide deviated results from the measured holdup indicating inaccurate predictions by LedaFlow with and without slug capturing for the fine grid pipeline as shown in Figure 5-50. The slug capturing case show slugs with very high frequency, less than one minute, throughout the simulation period, while the non-slug capturing case shows very low slightly undulating holdup with an average of 0.2. Both predictions disagree with the holdup measurements made at the pipeline location downstream of the slug valve at gamma-1 and gamma-2.

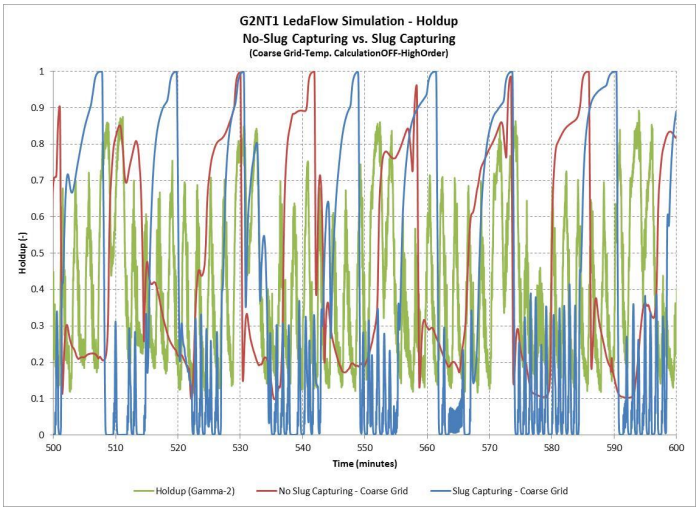

Figure 5-49: G2NT1 LedaFlow Holdup Results – No Slug Capture vs. Slug Capture – (Coarse Grid, Temp. Calc. OFF) – Gamma-2 Holdup Comparison

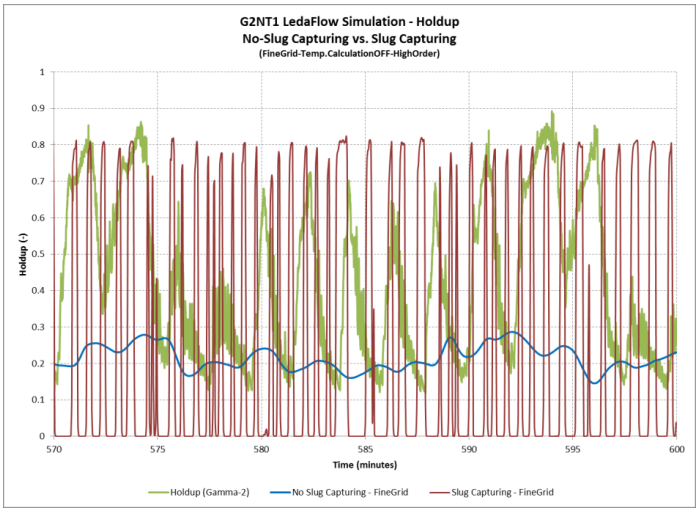

Figure 5-50: G2NT1 LedaFlow Holdup Results – No Slug Capture vs. Slug Capture – (Fine Grid, Temp. Calc. OFF) – Gamma-2 Holdup Comparison

5.1.8. G2NT1 OLGA and LedaFlow Simulation Conclusions

- OLGA simulation with slug tracking and a delay constant (DC=50) provides the best OLGA holdup and pressure results. This could be a pure coincident as OLGA development team and other results indicate that the slug tracking option tends to over predict the pressure drop in pipelines.
- Utilizing a fine grid had a minimum impact on OLGA results.
- Utilizing a 2nd order mass equation solution scheme provided good OLGA results.
- Using LedaFlow, the best results were obtained using a non-slug capturing case.
- Utilizing a fine grid or a high order options had a minimum impact on LedaFlow results.

5.1.9. G2NT1 Pipeline Slug Valve Optimization Study

A quick evaluation of the optimum choke settings that would have provided the best results for this particular pipeline was conducted using both OLGA and LedaFlow simulation packages. The study utilized a fine grid with non-slug tracking/capturing scheme along with various choke fixed slug valve settings. Each valve setting, shown in Table 5-3, was simulated for two hours before moving to the next setting and the study reported the pipeline inlet pressure as shown in Figure 5-51 and Figure 5-52 for OLGA and LedaFlow results.

OLGA and LedaFlow results show contradicting results in this case. OLGA indicates that with less choked valve, the flow will slug more suggesting that new slugs are created due to the less choked valve. LedaFlow on the other hand suggest that with less choked valve, the flow will experience less slugging and pressure fluctuation will almost diminish. This indicates that the existence of the choked valve is causing the system to slug. These results indicate a new phenomenon where slugs start to decrease in amplitude and gradually disappear with less choking of the slug valve. This is contradictive to the expected behavior of severe slugging in pipelines. This behavior is believed to be generated by the accumulation of liquid at the valve opening which causes gas blockage and thus creating more perturbations in pipeline system.

A set of lab experiments were planned and carried out at NTNU multiphase lab to study this phenomenon further and verify the multiphase flow simulation results.

Table 5-3: G2NT1 Pipeline Choke Opening Settings

	OLGA & LedaFlow Choke Opening (%)	**Simulation Time (hrs) Start - Finish**
1.	5 %	0 – 2
2.	5 %	2 – 4
3.	8 %	4 – 6
4.	10 %	6 – 8
5.	20 %	8 – 10
6.	40 %	10 – 12
7.	80 %	12 – 14
8.	100 %	14 – 16

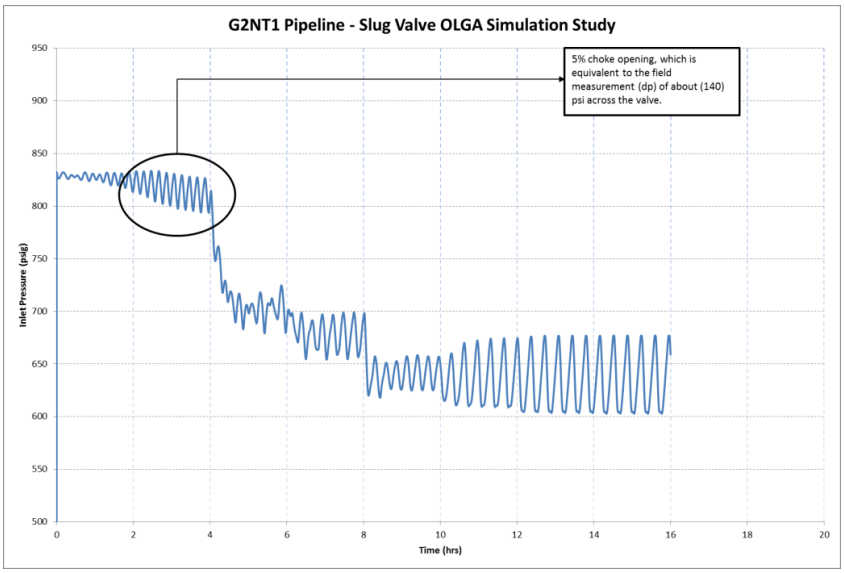

Figure 5-51: G2NT1 Pipeline – Slug Valve OLGA Simulation Study – (Coarse Grid, 1st Order, No-SlugTracking)

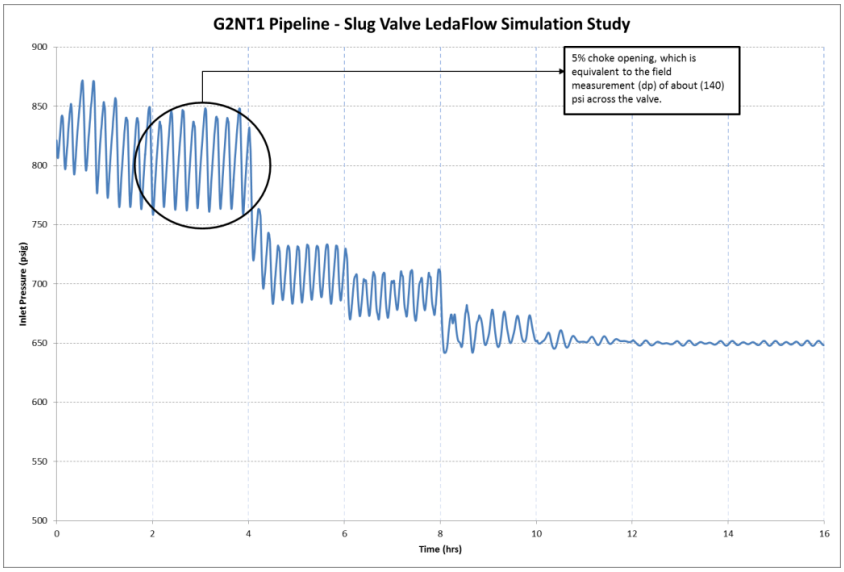

Figure 5-52: G2NT1 Pipeline – Slug Valve LedaFlow Simulation Study – (Coarse Grid, Normal Order, No-SlugCapturing)

5.2. G1ST3 Pipeline Results

G1ST3 measurements were conducted over three days: on June 8, 1999 upstream the slug valve on the uphill side and on June 7 and 9, 1999 also upstream of the slug valve but on the downhill side.

The measurements on the downhill section were repeated on two days, June 7 and 9, due to the unplanned slight increase in production rates from some of the connected oil wells approximately 1 hour before the measurement on June 7, 1999. That slight increase production did not impact the overall results as will be shown in holdup and pressure analysis.

5.2.1. Pipeline Profile Details

The total pipeline length is approximately 6.6 Km and starts from Sabkhah 27 (S-27) to GOSP-1, which is located at Sabkhah 20 (S-20) going through Sabkhah 19 (S-19). The pipeline has two (2) very high hills with heights that are approximately 40 to 60 meters. The pipeline has two different diameters 16 inch and 20 inch as shown on Figure 5-53.

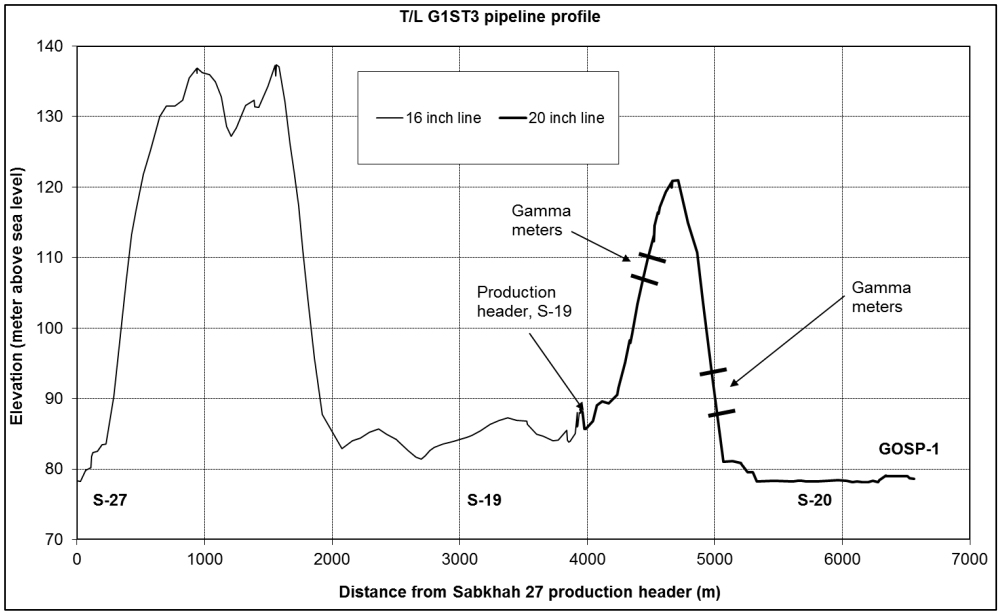

Figure 5-53: G1ST3 pipeline profile - slug valve and gamma densitometer locations

The measurement was made close to the slug valve which is installed at the end of the pipeline upstream of GOSP-3. The measurements were made at a production rate of 46,500 BBL/Day at standard conditions. The flow rates were based on forecasts made by the production engineers and no flow rate measurements were carried out at the time of the experiments. The flow rates from each Sabkhah were estimated as follows:

Table 5-4: G1ST3 Production Flow Rates

Sabkhah	Volumetric Flow Rate (BBL/Day) @ std. cond.
S-27	18,800
S-19	27,700
Total	**46,500**

The superficial gas and liquid velocities ranged from (1.0 to 2.7) m/sec for gas and (0.4 to 0.9) m/sec for liquid, based on OLGA predictions.

For the downhill measurements, on June 8, 1999, the distance between the gamma meters was set at 38.9 m, while the inclination angle was measured at (– 8.52) degrees. The distance of the gammas to the downstream slug valve was measured at approximately 250 m. In addition the distance to GOSP-1 was approximately 1.5 Km. The pipeline wall thickness was measured using ultra sonic measurement device at 0.63 inch (16 mm). The GOSP-1 pressure was set at 400 psig during the measurement period.

On the other hand, during the two uphill measurements, on June7 and 9, 1999, the distance between the gamma meters was set at 23.3 m, while the inclination angle was measured at (+ 4.56) degrees. The distance of the gammas to the downstream slug valve was measured at approximately 800 m. In addition the distance to GOSP-1 was approximately 2 Km. The pipeline wall thickness was measured using ultra sonic measurement device at 0.63 inch (16 mm). The GOSP-1 pressure was set at 400 psig during the measurement period.

5.2.2. Production Header Time Series:

The pressure logs at the producing Sabkhahs were not available from the DCS system due to a malfunction in the system. Therefore, a separate standalone pressure logging device was installed at Sabkhah 27 (S-27). The (S-27) pressure logs were obtained for only one day, June 7, 1999. During the remaining two days of measurement, no pressure recordings were obtained for S-27 due to a malfunctioning of the pressure logging device and therefore only manual readings were obtained for various wells connected to the pipeline system.

Sabkhah 27 pressure log on June 7, 1999, downhill measurement, shown on Figure 5-54, indicates an approximately 8 minutes pressure cycles. The short periods exhibits pressure oscillations of 10 psi with pressures fluctuating between 510 psig and 530 psig.

The manual readings obtained from S-19 and S-27 on June 8 and 9, 1999, shown in Figure 5-55 and Figure 5-56, indicate similar behavior with 10 psi pressure cycles occurring approximately every 8 minutes.

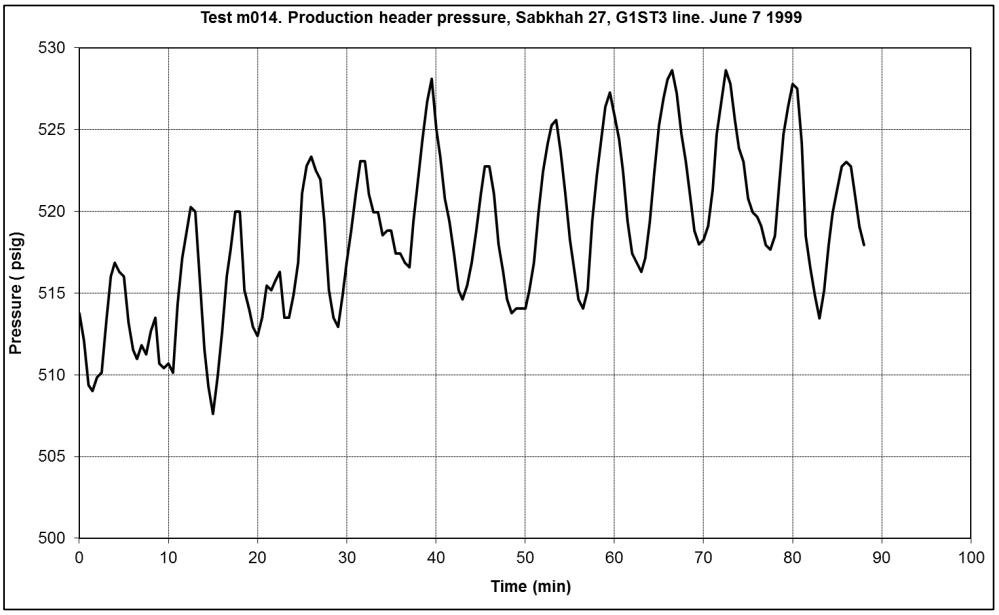

Figure 5-54: G1ST3 Production header pressure at S-27, June 7, 1999 (Downhill Measurement)

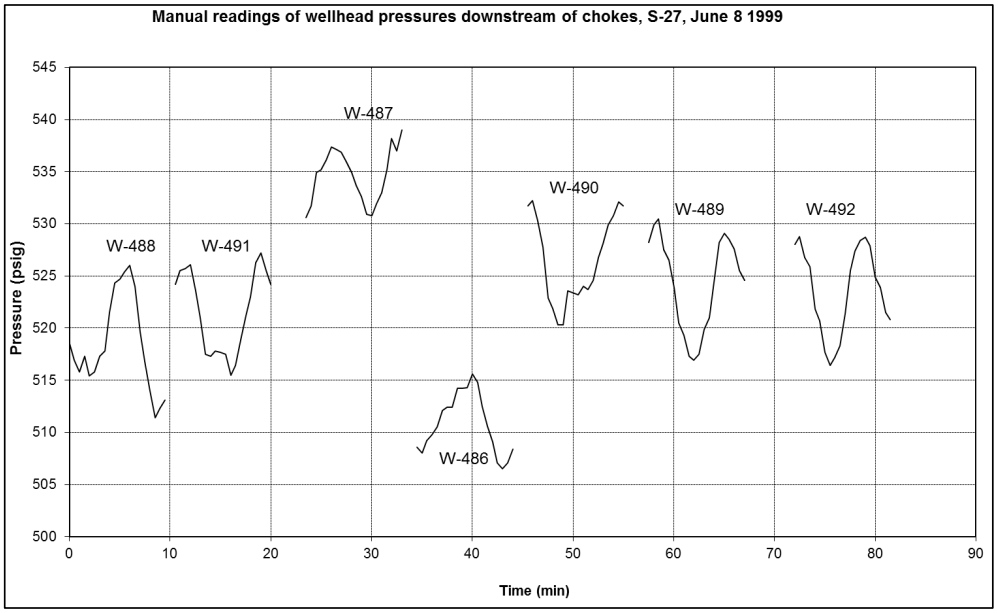

Figure 5-55: G1ST3 Manual readings of WH pressure at S-27, June 8, 1999 (Downhill Measurement)

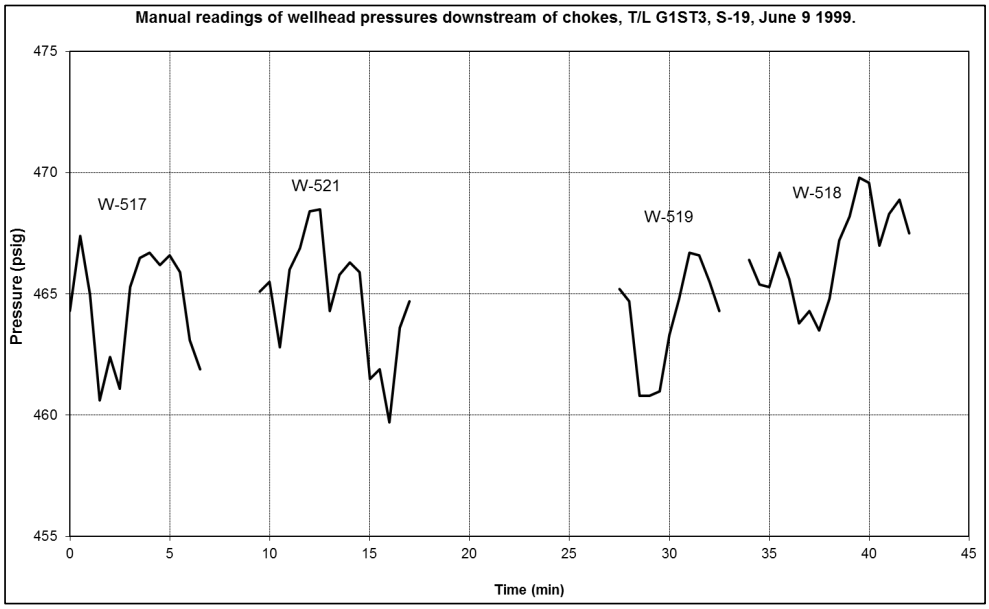

Figure 5-56: G1ST3 Manual readings of WH pressure at S-19, June 9, 1999 (Uphill Measurement)

5.2.3. Slug Valve Pressure Drop:

The slug valve at G1ST3 pipeline was installed about 1.2 km from GOSP-1. The pipeline was sloped down prior to the slug valve, but with a 100 to 150 meter long horizontal section before the upturned (U-Shape), on which the slug valve is mounted.

The pressure drop across the slug valve was logged during the measurement tests using Foxboro absolute pressure transmitters, which were installed in the same positions of the pressure manometers across the slug valve. The tabs of the manometers were installed approximately (1) meter upstream and downstream of the slug valve. The pressure signals were sampled at 2 Hz over a period of 90 minutes.

The pressure log upstream and downstream the slug valve is shown in Figure 5-57 for the downhill case. The figure depicts a pressure fluctuation of approximately 15 psi over a period of 8 minutes. The upstream pressure varies between 420 to 435 psig while the downstream pressure varies between 395 and 415 psig. One can also notice that the peak values in the upstream pressure log coincide with minimum values on the downstream side.

The differential pressure across the valve varies between 12 and 40 psi with an average value of 25 psi as shown in Figure 5-58.

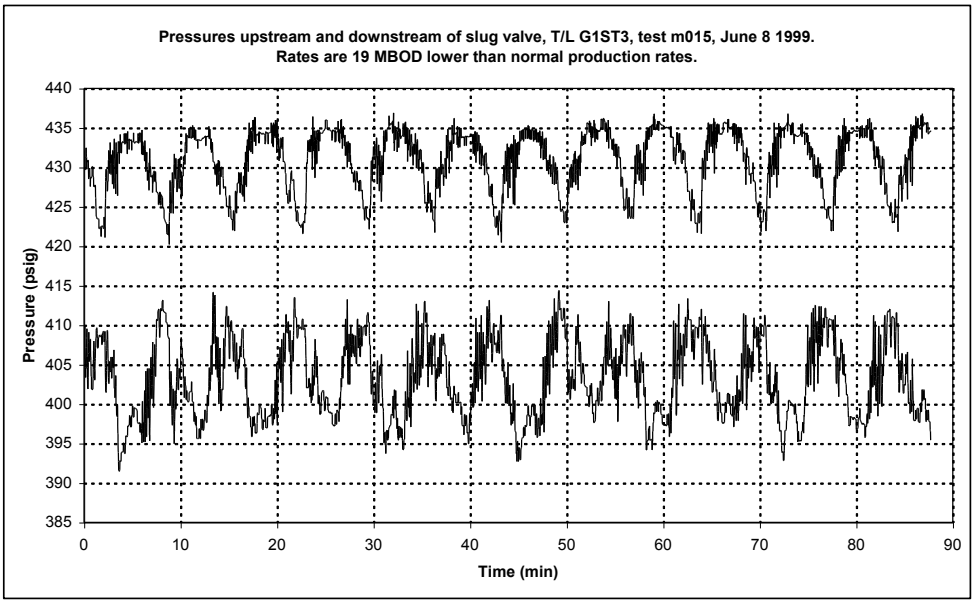

Figure 5-57: G1ST3 Pressure upstream and downstream of slug valve, Downhill, June 8, 1999

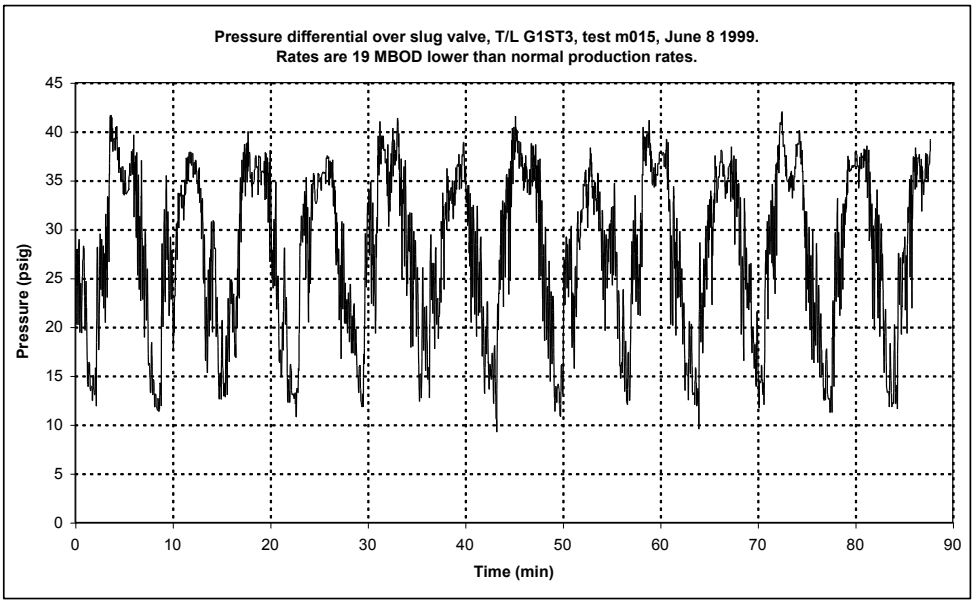

Figure 5-58: G1ST3 Pressure differential across slug valve, Downhill, June 8, 1999

5.2.4. Analysis of Holdup Time Series – Uphill:

The G1ST3 pipeline uphill measurements were conducted at the location shown in Figure 5-59. The 30 minutes liquid holdup time series depicted in Figure 5-60 shows two slug behaviors. One with short slugs which lasts for approximately 2 to 3 minutes, with the very dense zone, and one with long slugs which lasts for approximately 5 to 6 minutes with sparse zone as shown in Figure 5-61.

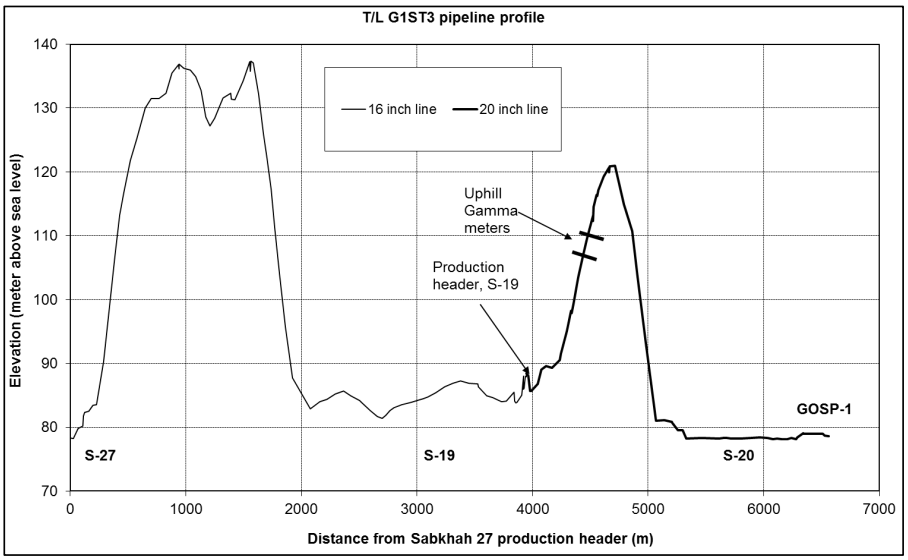

Figure 5-59: G1ST3 Pipeline – Uphill Gamma measurement location

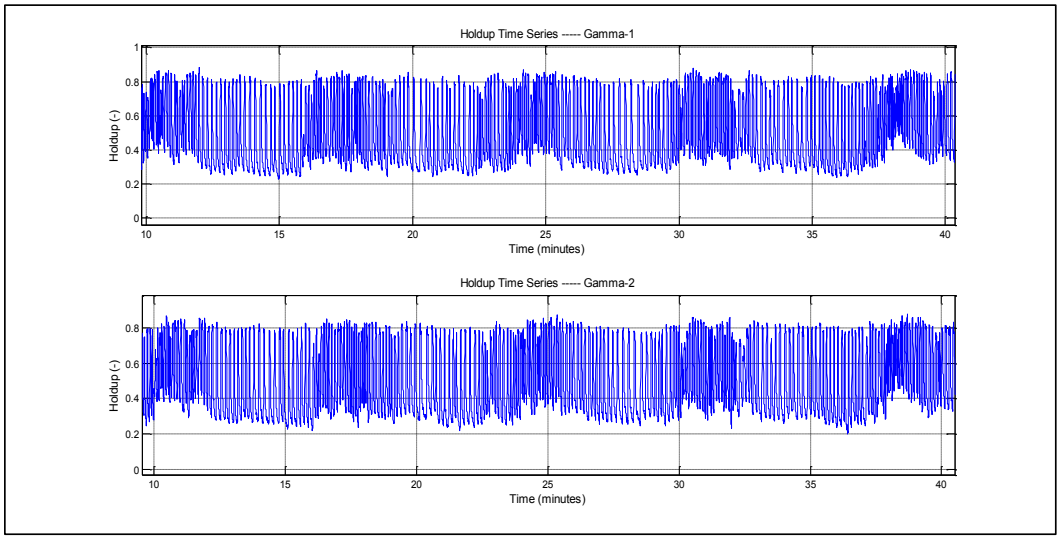

Figure 5-60: G1ST3 Holdup time series, Uphill, June 9, 1999, (30 minutes)

The slug body holdup in both the short and long slug periods were approximately 0.8 while the liquid film had a higher value for the short slugs of (0.4 to 0.5) and (0.25 to 0.3) for the long slugs as shown in Figure 5-63 and Figure 5-65.

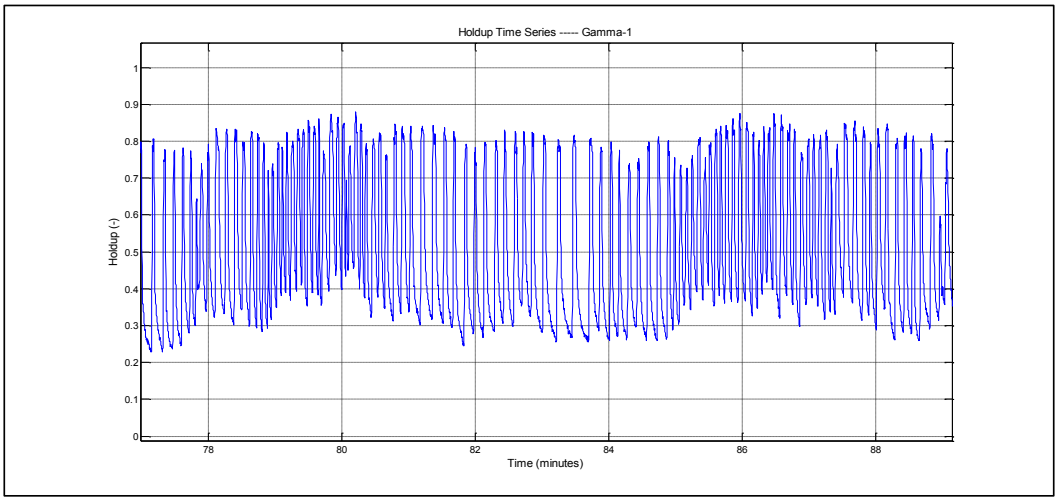

Figure 5-61: G1ST3 Holdup time series, Uphill, June 9, 1999, (10 minutes)

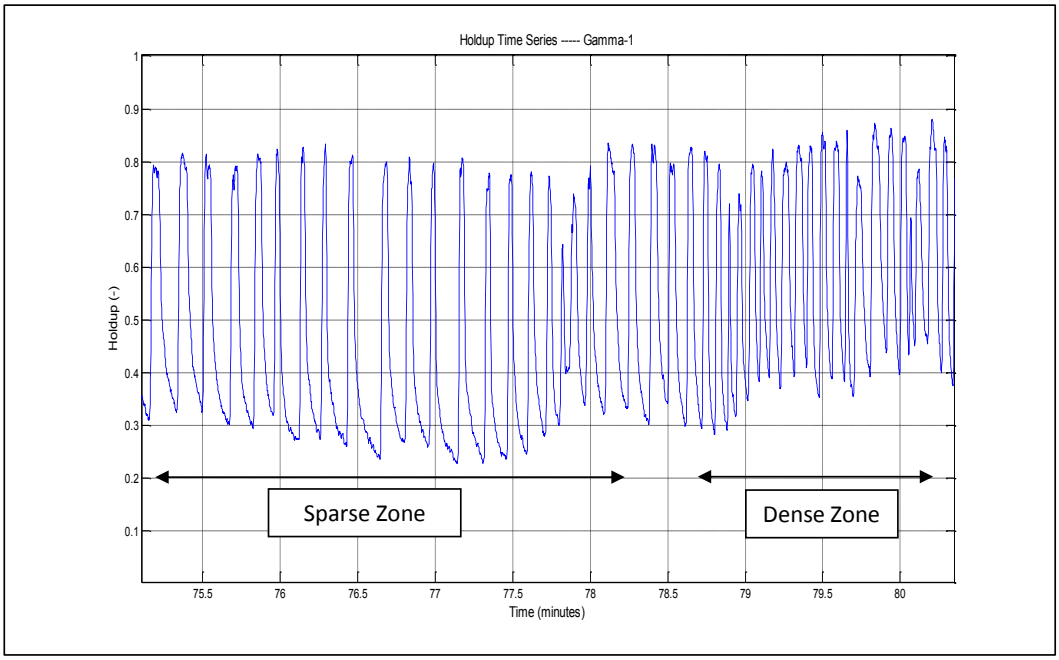

Figure 5-62: G1ST3 Holdup time series, June 9, 1999, (Uphill)-(1 minute)-(Dense & Sparse zone)

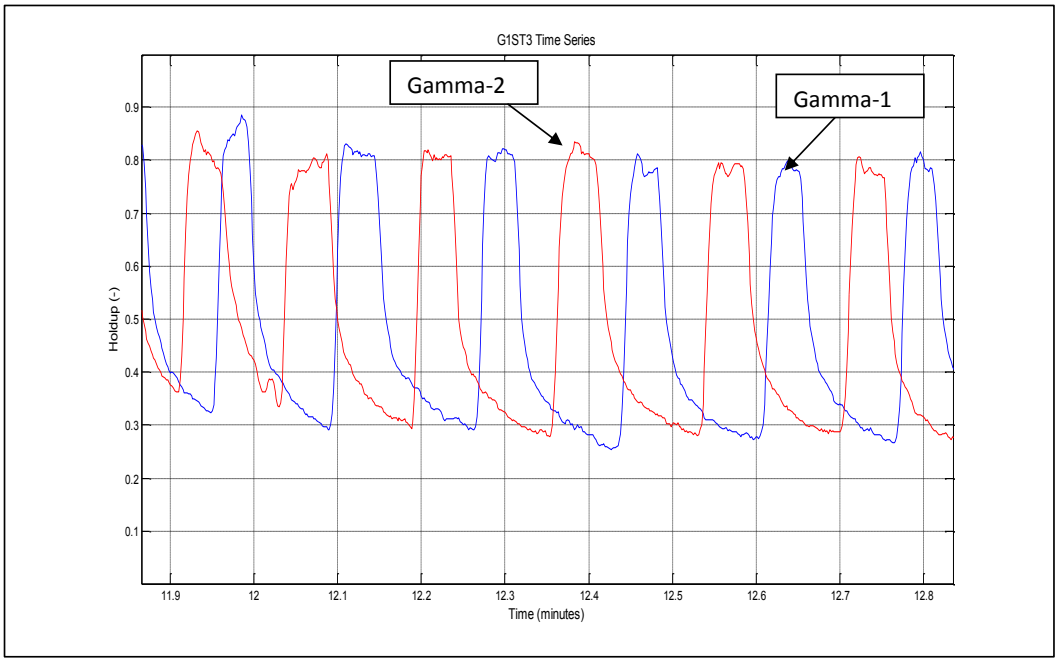

Figure 5-63: G1ST3 Holdup time series, June 9, 1999, (Uphill)-(1 minute)-(Long Slugs)

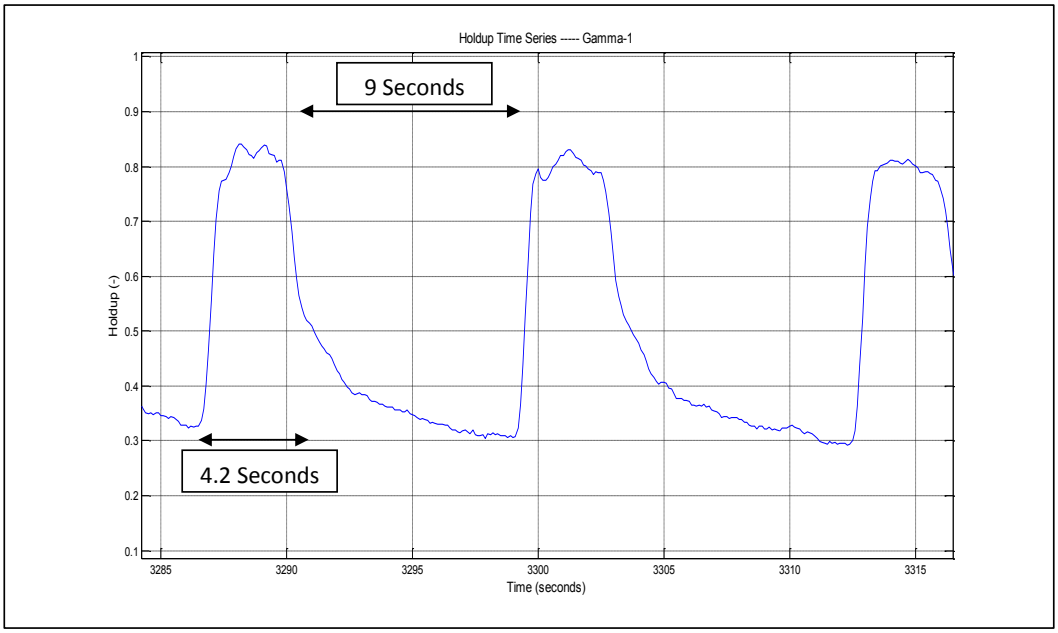

Figure 5-64: G1ST3 Holdup time series, June 9, 1999, (Uphill)-(Long Slugs)

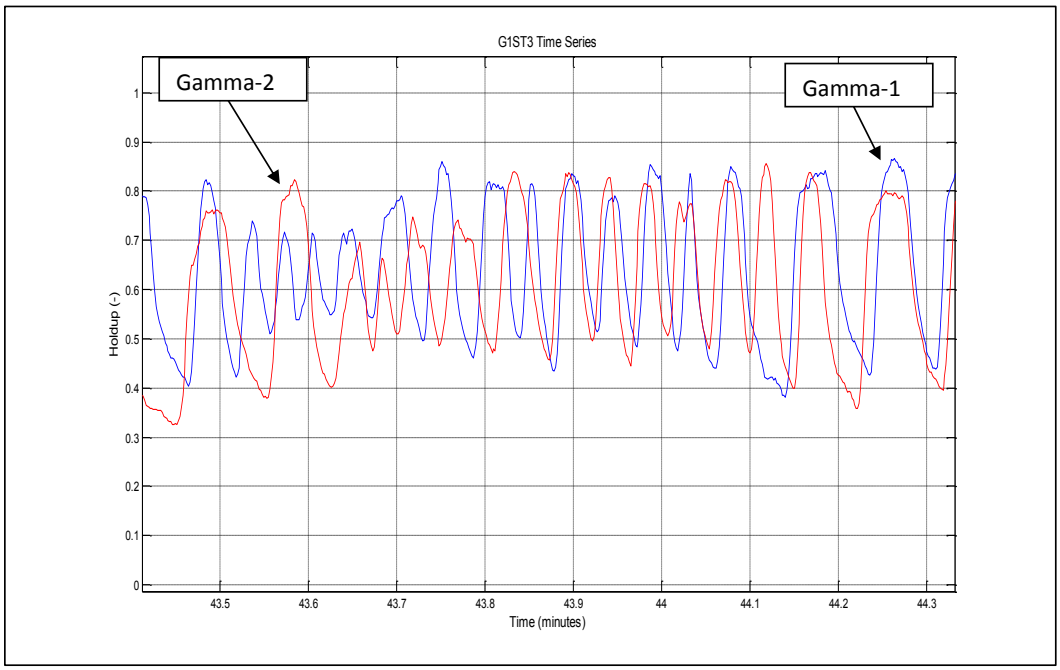

Figure 5-65: G1ST3 Holdup time series, June 9, 1999, (Uphill)-(1 minute)-(Short Slugs)

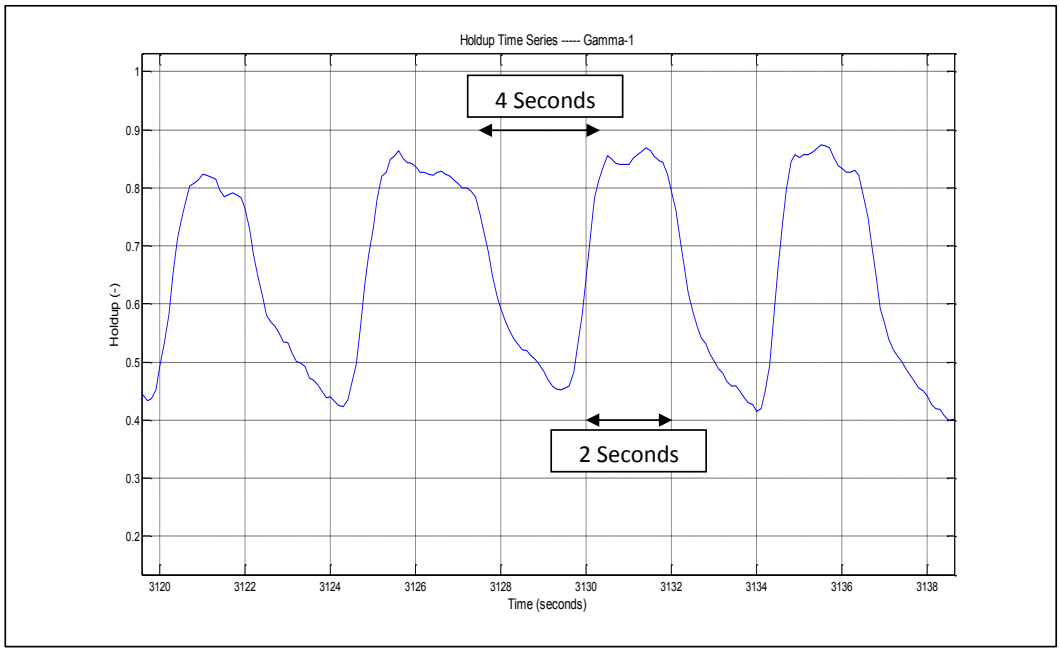

Figure 5-66: G1ST3 Holdup time series, June 9, 1999, (Uphill)-(Short Slugs)

Cross correlating the two gammas, one obtains a time lag of approximately 5.6 seconds using the full time series, as shown in Figure 5-67. Using the gamma distance of 23.3 meters one would obtain an average slug velocity of 4.16 m/sec.

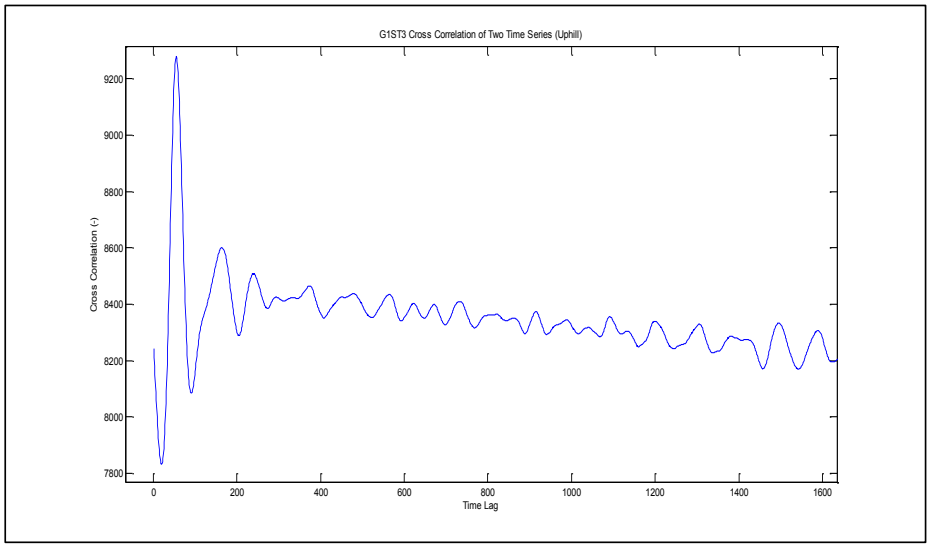

Figure 5-67: G1ST3 Cross Correlation of Two Gammas, June 9, 1999, (Uphill)

Slugs were defined by first defining the minimum and maximum points of the original time traces. Later, slugs were extracted by defining a customized holdup with respect to the maximum point, usually 80% to 85% of the maximum holdup as shown in Figure 5-68 and Figure 5-69. The remaining length of the slug unit is defined as a bubble section. Using this technique, one could obtain all the statistical parameters associated with the slugs and bubble sections, such as slug and bubble lengths, slug front and tail velocities, and slug frequencies.

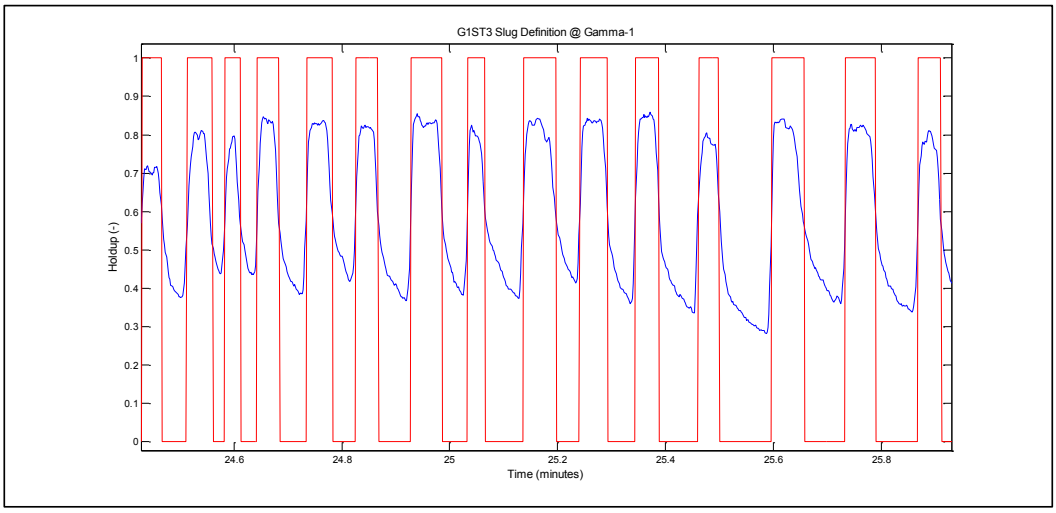

Figure 5-68: Slug Definition at Gamma-1 Location - G1ST3 Pipeline

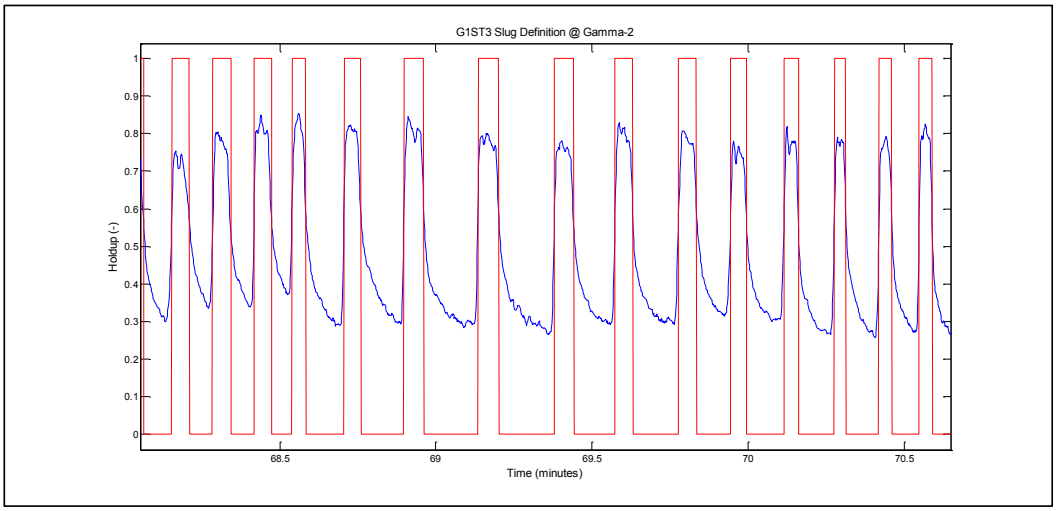

Figure 5-69: Slug Definition at Gamma-2 Location - G1ST3 Pipeline

As shown in Figure 5-70, slug period distribution is concentrated between (4) seconds, for short slugs and (10) seconds for long slugs. Most of the slugs appear to be within the (6 to 8) seconds period. The total number of slugs calculated for the whole period of 109 minutes was 872 slugs, which gives an average slug frequency of a slug every (7.5) seconds.

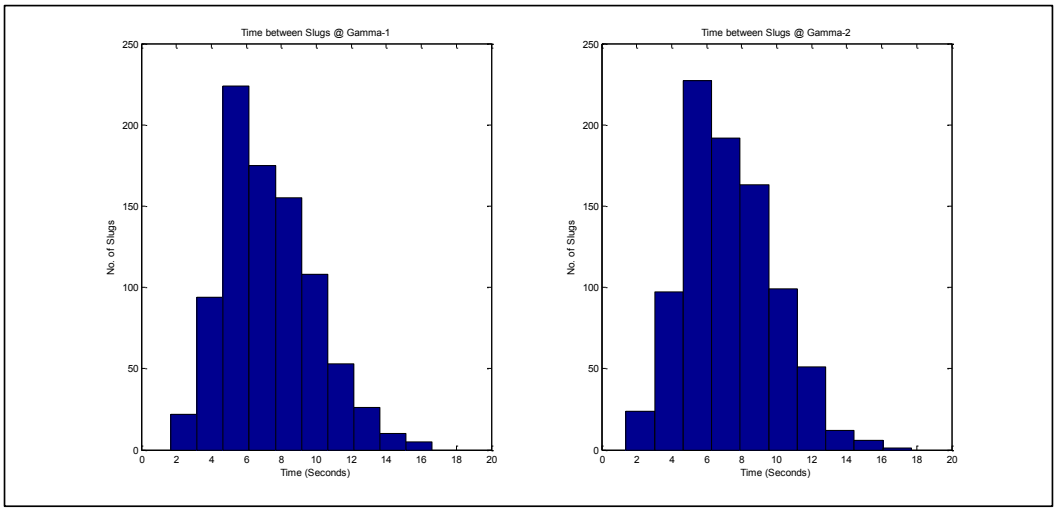

Figure 5-70: G1ST3 – Distribution of Slug Frequency (time between two peaks) (seconds)

Slug length distribution in meters is shown in Figure 5-71. The figure indicates slug lengths ranging mostly in between 7 and 15 meters based on the average slug and tail velocities. The distribution of slug length in number of diameters is also shown in Figure 5-72 which indicates similar results of (15 Dia.) to (30 Dia.) based on the inner diameter used in the calculation of (0.485) meters.

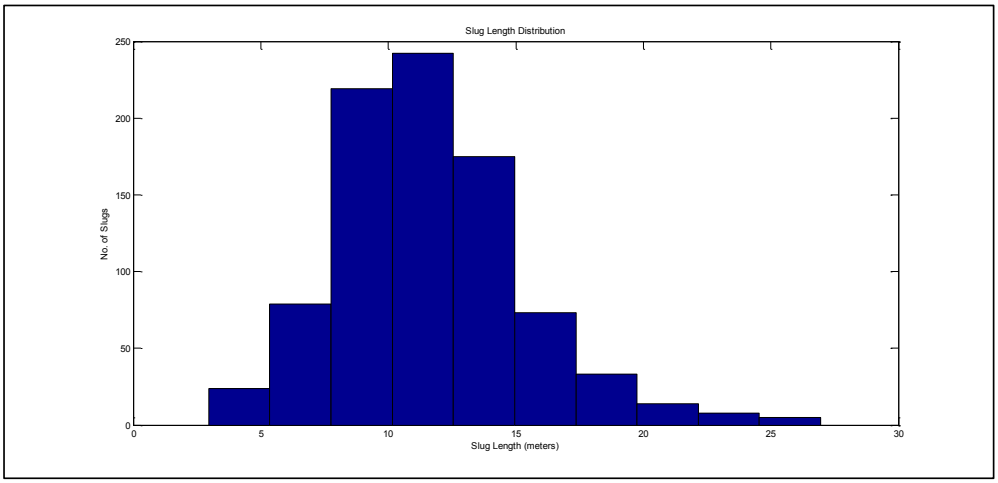

Figure 5-71: G1ST3 – Slug Length Distribution (meters)

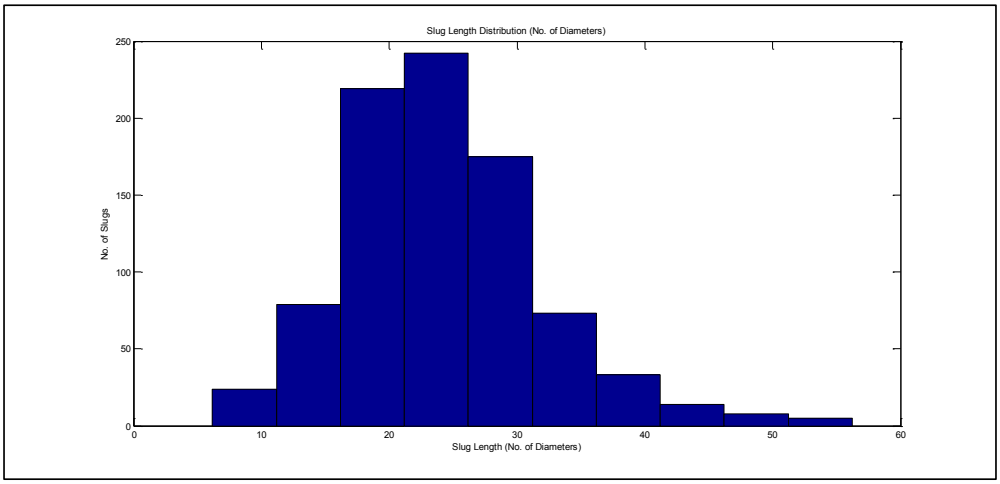

Figure 5-72: G1ST3 – Slug Length Distribution (No. of Diameters)

The distribution of the average slug front and tail velocities are shown in Figure 5-73. The distribution indicates a velocity that ranges between 3.5 m/sec and 5.5 m/sec. The mean of the averaged slug front and tail velocities is calculated at 4.457 m/sec compared to 4.161 m/sec calculated using the cross correlation time shift.

The comparison between slug front and tail velocities indicates a slightly higher front velocity of 4.51 m/sec compared to a tail velocity of 4.4 m/sec as shown in Figure 5-74. This also indicates growing of slugs between the two gamma locations.

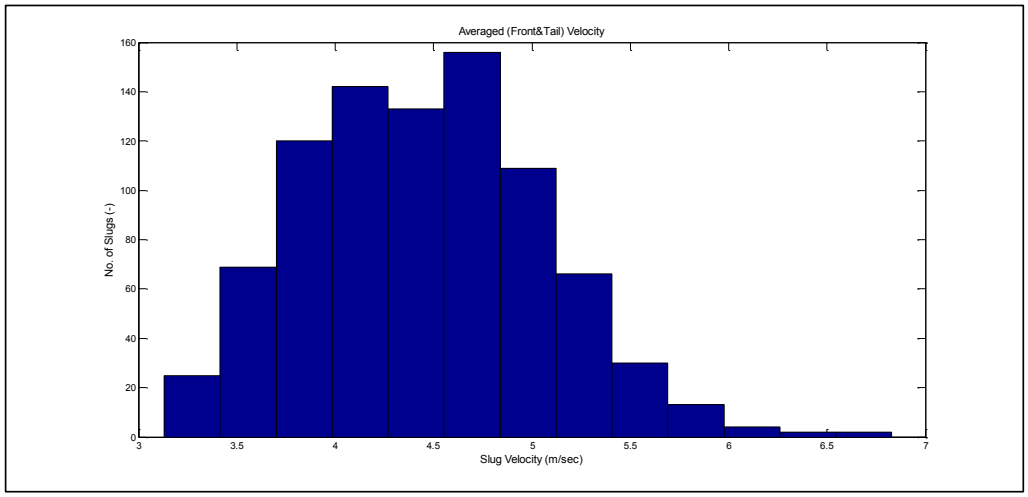

Figure 5-73: G1ST3 – Average Slug (Front & Tail) Velocities

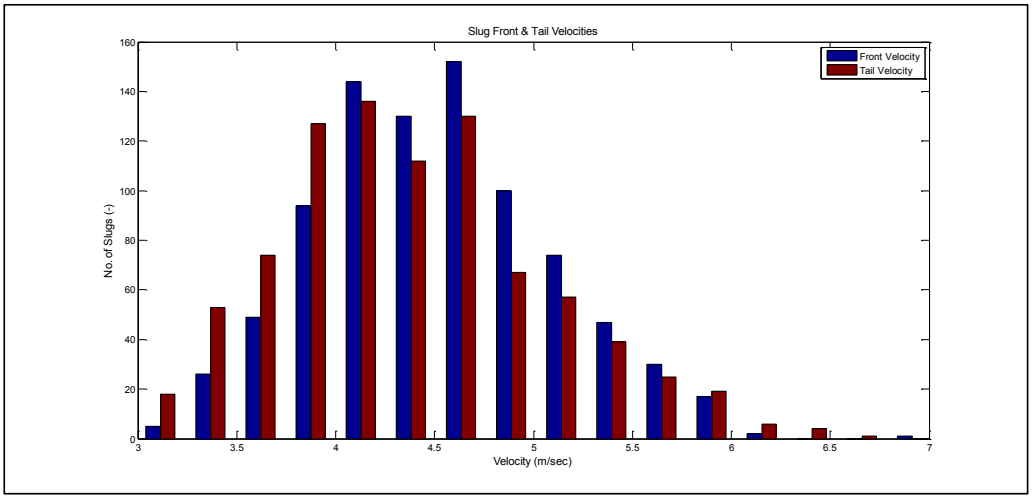

Figure 5-74: G1ST3 –Slugs Front & Tail Velocities

5.2.5. Analysis of Holdup Time Series – Downhill:

Gamma measurement was conducted for G1ST3 pipeline at downhill position as shown in Figure 5-75. The downhill measurement was carried out upstream of the slug valve and the distance between the two gammas was (38.9) meters with a pipe inclinations angle of (- 8.52). The distance measured to the gamma valves was (250) meters and approximately (1.5) Km to the GOSP.

he G1ST3 pipeline holdup time series for downhill measurement is depicted in Figure 5-76. The gamma measurements indicate an expected wavy stratified flow behavior with an average holdup of approximately (0.12) at both gamma locations.

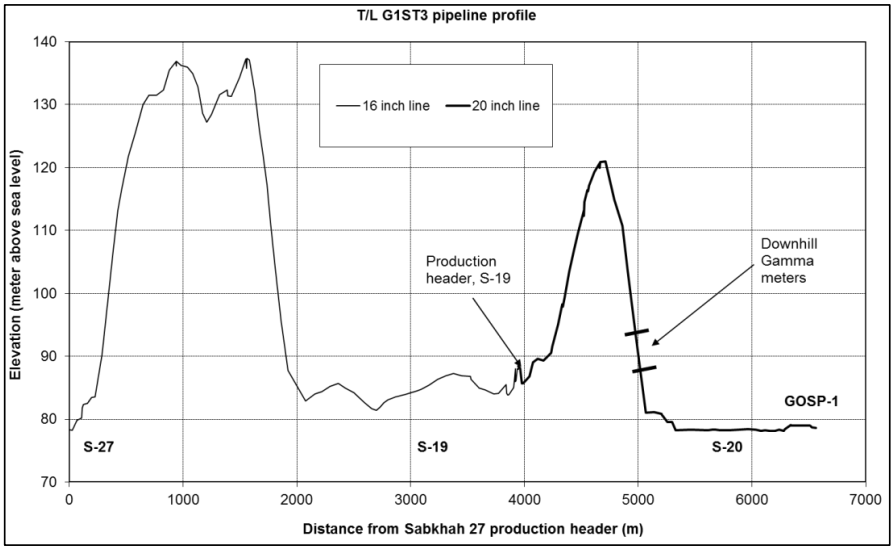

Figure 5-75: G1ST3 – Downhill Gamma Measurement Location

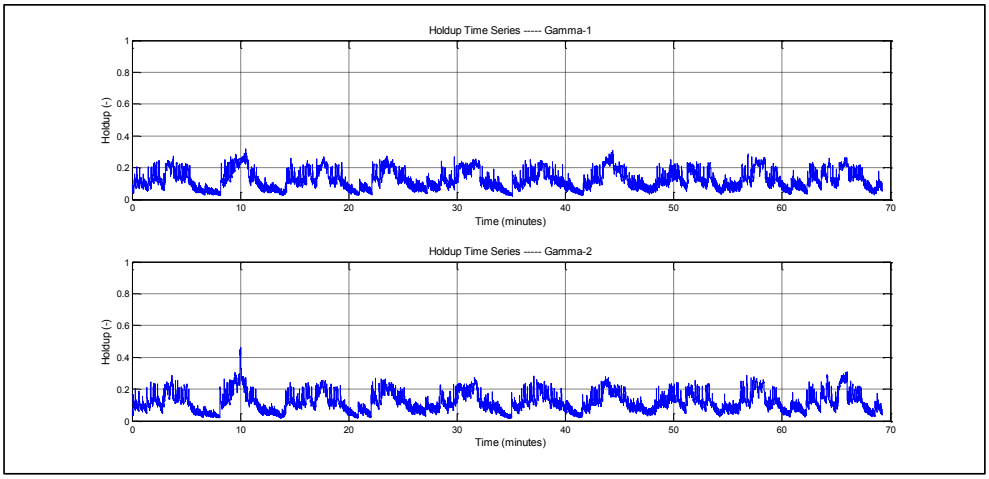

Figure 5-76: G1ST3 – Holdup Time Series – Downhill Measurement – (70 min)

The macro wavy structure shown in Figure 5-77, shows a clear cyclic behavior with a frequency of approximately (8) minutes which matches the earlier noted (8) minutes pressure cycles.

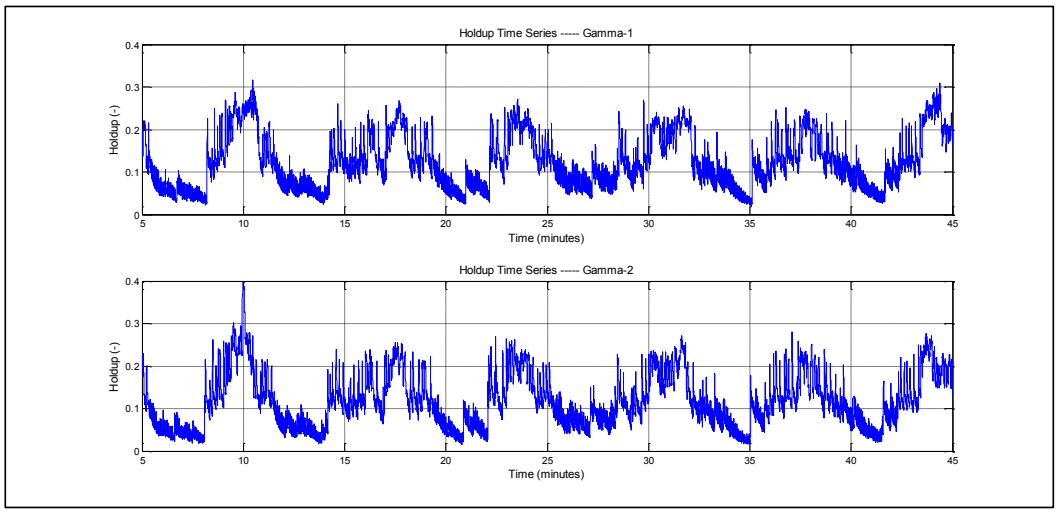

Figure 5-77: G1ST3 – Holdup Time Series – Downhill Measurement – (40 min)

5.2.6. G1ST3 Pipeline Simulation

Extensive simulation work was conducted using OLGA and LedaFlow. The results of the simulation were compared against the field data measurements in terms of holdup and pressure at gamma measurement locations and at the pipeline inlet.

5.2.7. G1ST3 Pipeline OLGA Simulations

OLGA simulation was carried out with various options to fully test the simulation package capabilities to predict slugging phenomena in the subject pipeline. In view of the results obtained from the previous pipeline, G2NT1, the parameters which were varied for G1ST3 pipeline are as follows:

- Slug tracking (No slug tracking vs. slug tracking with various delay constants)
- Grid size (Coarse grid vs. Fine grid)

As stated earlier in the G2NT1 pipeline simulation section, the heat transfer parameter will not be evaluated any more as it was found that had very little impact on the simulation results. Therefore, in all of the above simulation parameters, an adiabatic heat transfer conditions will be assumed for all simulation cases. In addition, the simulations will be utilizing 2nd order mass equation scheme only as it seems to provide better results than the 1st order scheme.

G1ST3 Pipeline OLGA Simulation – (Slug Tracking vs. No Slug Tracking)

OLGA Simulations were carried out with and without slug tracking module. The results were plotted for various Delay Constants (DCs), which significantly impact the initiation of slugs in OLGA.

Using an average liquid velocity of (4.16) m/sec obtained from the cross correlation of the two gamma meters at the uphill pipeline section, one can estimate the idle time between slug initiations as follows:

Table 5-5: G1ST3 – Idle time between slug initiations for various delay constants

Idle time between Slug Initiation (DT) (sec)	Ul (m/sec)	Inner Dia (m)	DC
5.76	4.16	0.47945	50
17.29	4.16	0.47945	150
57.63	4.16	0.47945	500
92.20	4.16	0.47945	800

OLGA simulations were carried out with various delay constants ranging from 50 to 800. The results are shown on figures Figure 5-78, Figure 5-79 and Figure 5-80. Analysis of the pressure plots shows that with no slug tracking the pressure cycles are fixed at (5) minutes with very stable and repetitive slug behavior. When slug tracking module is enabled, and with various delay constants, the cycle changes to approximately (8 to 10) minutes, which matches the field measurement pressure cycles.

When compared against the pressure traces obtained from the field measurements, the case with the delay constant of 150 seems to be the closest in terms of pressure cycle and magnitude to the field measurement. However, with respect to pressure fluctuation amplitude, the cases with slug tracking shows high fluctuations with approximately (30 – 40) psi, while the case with no slug tracking shows a more accurate fluctuations of (10) psi similar to the field measurement case.

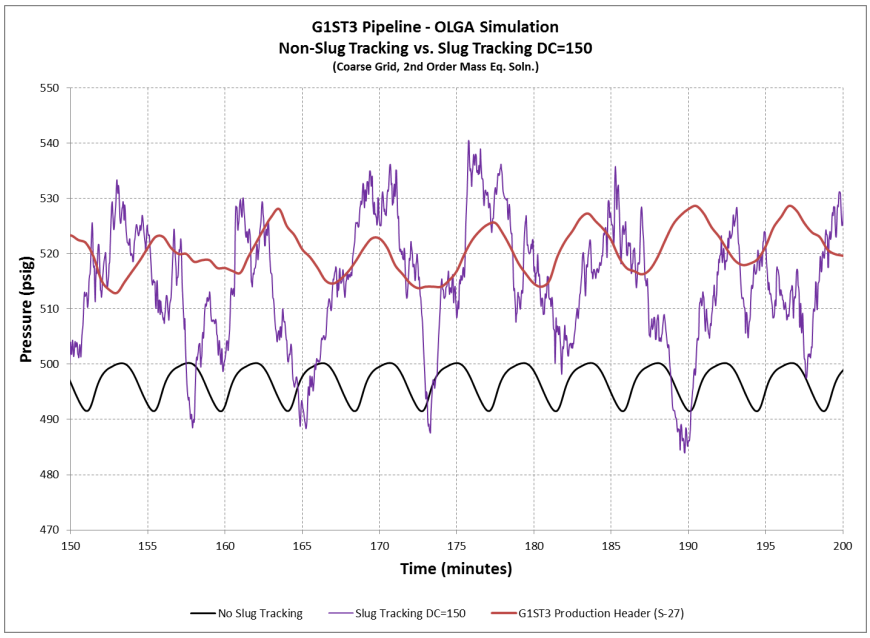

Figure 5-78: G1ST3 OLGA Pressure Results – Slug Tracking (DC=150) vs. No-Slug Tracking Simulations

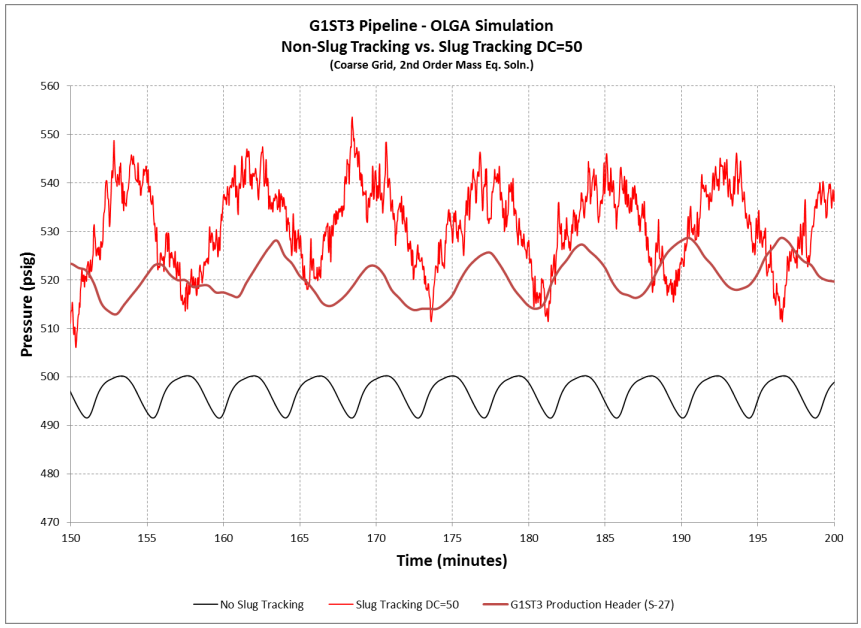

Figure 5-79: G1ST3 OLGA Pressure Results – Slug Tracking (DC=50) vs. No-Slug Tracking Simulations

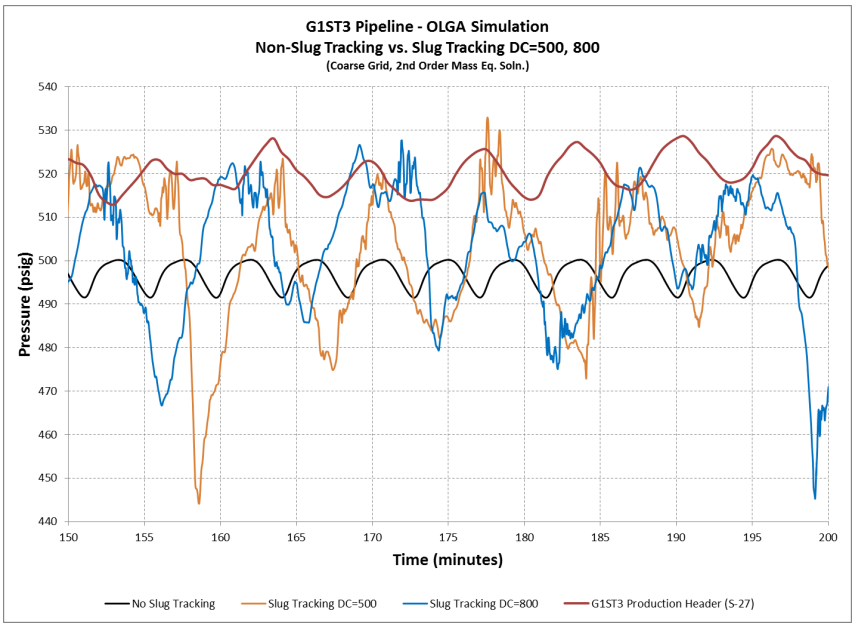

Figure 5-80: G1ST3 OLGA Pressure Results – Slug Tracking (DC=500, 800) vs. No-Slug Tracking Simulations

The comparison of holdup calculations against uphill holdup measurements, as expected, proved to be more challenging for OLGA code. Starting by comparing the results of the non-slug tracking case against uphill field measurements as shown in Figure 5-81, one can notice the large difference between the two in terms of fluctuations amplitude and frequency. The frequency in this case was fixed at (5) minutes, similar to the pressure oscillation frequency for the same case. Of course, OLGA, with slug tracking disabled, does not attempt to make any predictions for the small hydrodynamic slugs observed in the uphill field measurements. This however, does not justify the failure in predicting the amplitude of the holdup fluctuations, which was only around (0.1) for OLGA results compared to about (0.5) for uphill field measurements.

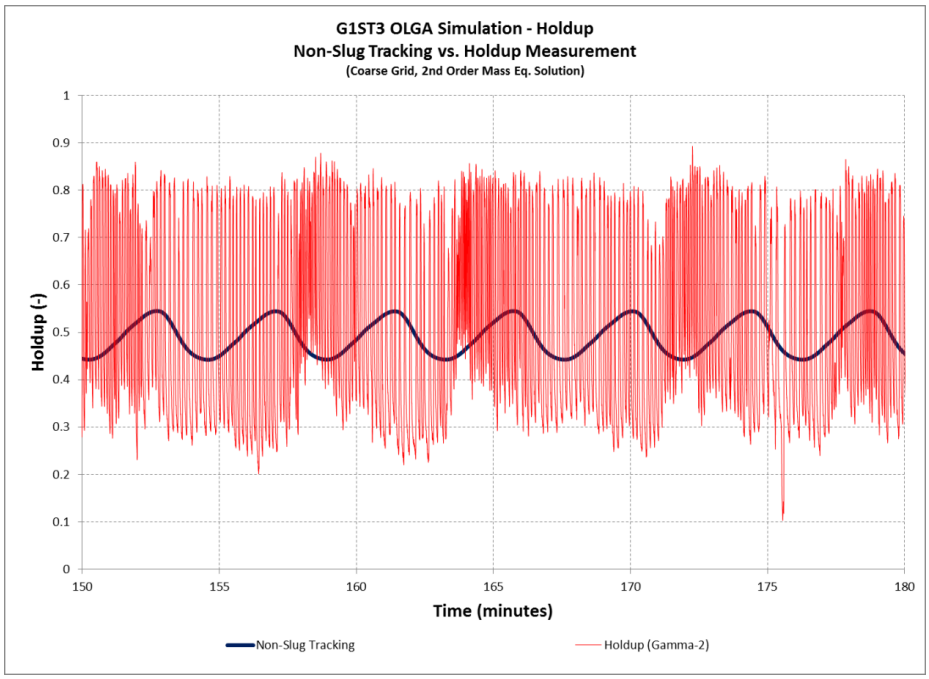

Figure 5-81: G1ST3 Uphill OLGA Holdup Results – Non-Slug Tracking vs. Holdup Measurements

With slug tracking enabled, the holdup results are greatly improved and best case that matches the uphill field measurement as shown in the pressure results so far, is the slug tracking with a delay constant of (150), see Figure 5-82. The figure shows clusters of small slugs separated by a period of approximately (5 to 6) minutes, which greatly matches the uphill field measurements, except for the frequency of the small hydrodynamic slugs and the existence of small hydrodynamic slugs in between those clusters. The amplitude of the OLGA holdup fluctuations, (0.7), is also slightly higher than the uphill field measurement, (0.5).

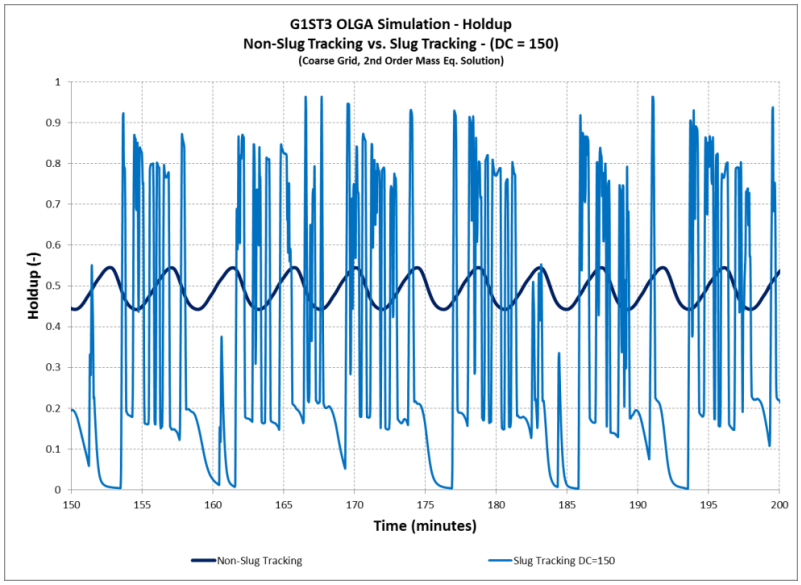

Figure 5-82: G1ST3 Uphill OLGA Holdup Results – Non-Slug Tracking vs. Slug Tracking (DC=150)

Using a delay constant of (50) causes more slug initiations and as such more hydrodynamic slugs are created as shown in Figure 5-83, while using larger delay constants, 500 and 800, causes less slug initiations as shown in Figure 5-84.

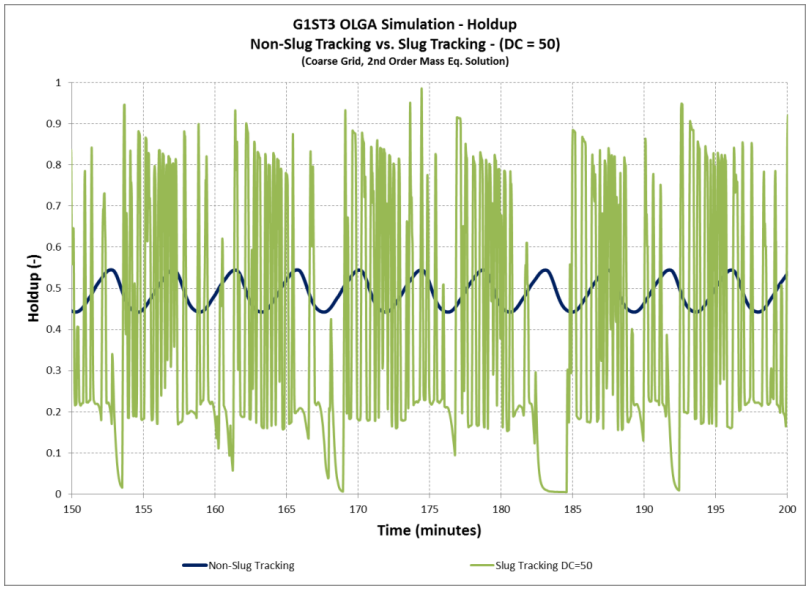

Figure 5-83: G1ST3 Uphill OLGA Holdup Results – Non-Slug Tracking vs. Slug Tracking (DC=50)

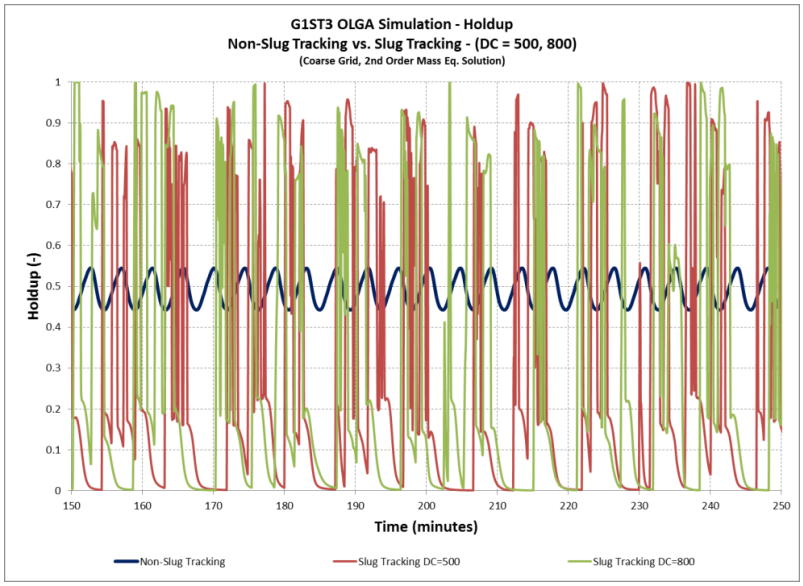

Figure 5-84: G1ST3 Uphill OLGA Holdup Results – Non-Slug Tracking vs. Slug Tracking (DC=500, 800)

The downhill holdup measurements, which showed a stratified-wavy flow regime, were also simulated. OLGA results are shown in Figure 5-85, for the case without slug tracking versus downhill holdup

measurements. The results indicate a much higher holdup values with an average of (0.5) compared to an average value of (0.12) in downhill field measurements.

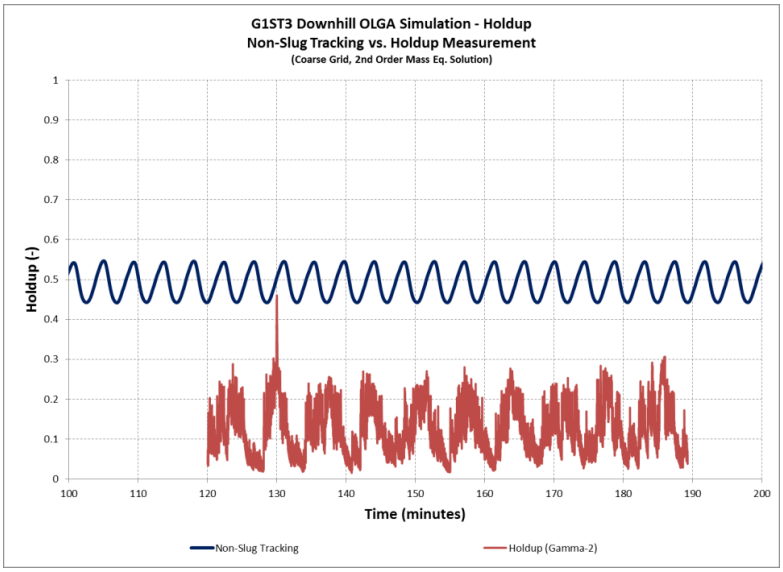

Figure 5-85: G1ST3 Downhill OLGA Holdup Results – Non-Slug Tracking vs. Holdup Measurement

Using slug tracking with delay constants of (50) and (150), the holdup values were considerably lower and compared better with the downhill field measurements. The frequency also matches well with the wavy-stratified flow frequency.

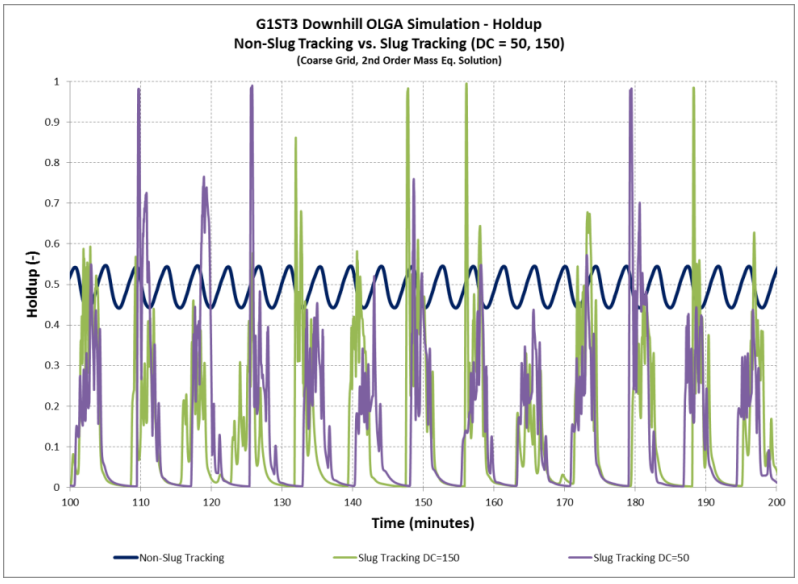

Figure 5-86: G1ST3 Downhill OLGA Holdup Results – Non-Slug Tracking vs. Slug Tracking (DC=50, 150)

G1ST3 Pipeline OLGA Simulation – (Coarse Grid vs. Fine Grid)

The OLGA simulations that were conducted so far utilized a relatively coarse grid as shown in Figure 5-87. The figure shows the section length ratio, which varies between 0.6 and 2.0.

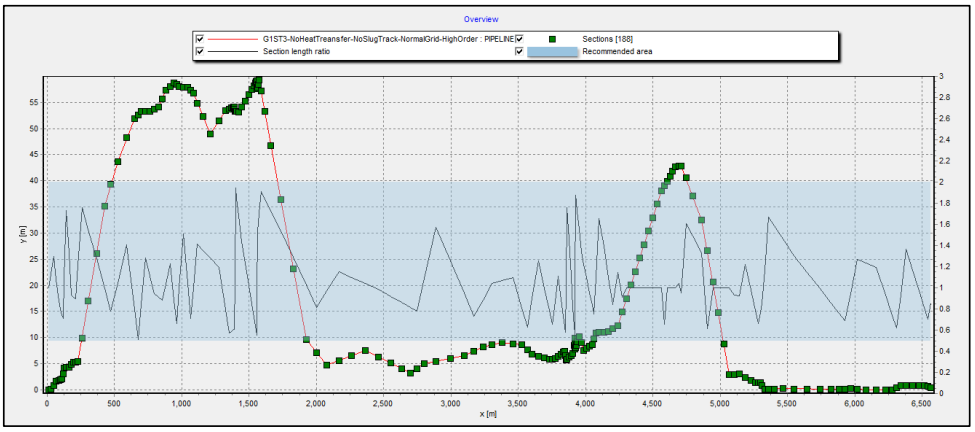

Figure 5-87: G1ST3 Pipeline OLGA Coarse Grid

A fine grid option was also evaluated to investigate the impact of small pipe sections on slug predictions in OLGA. A constant section length was selected at (5) meters which is equivalent to approximately (10.4 * Internal diameter) of the pipeline at the holdup measurement location.

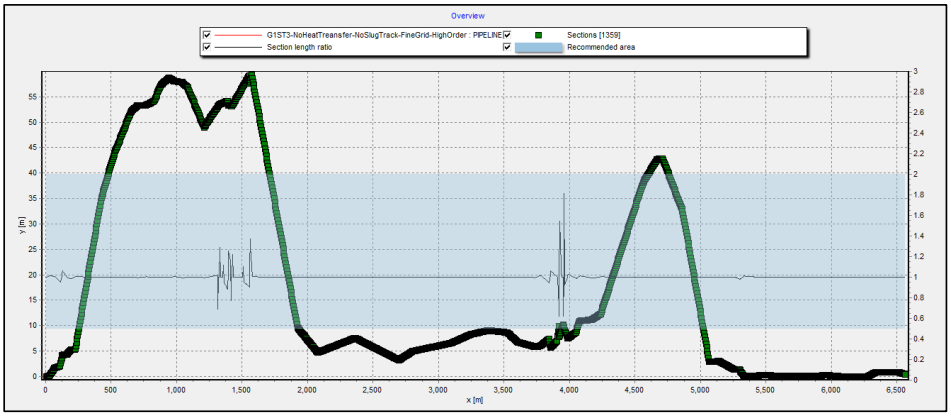

Figure 5-88: G1ST3 Pipeline OLGA Fine Grid (5 meter)

The pressure results indicate improved results in terms of frequency but not in amplitude. The fine grid case shows a frequency of approximately (8) minutes which matches the measured pressure frequency. The amplitude is slightly over predicted with a value of (20) psi versus (10) psi for field measurement.

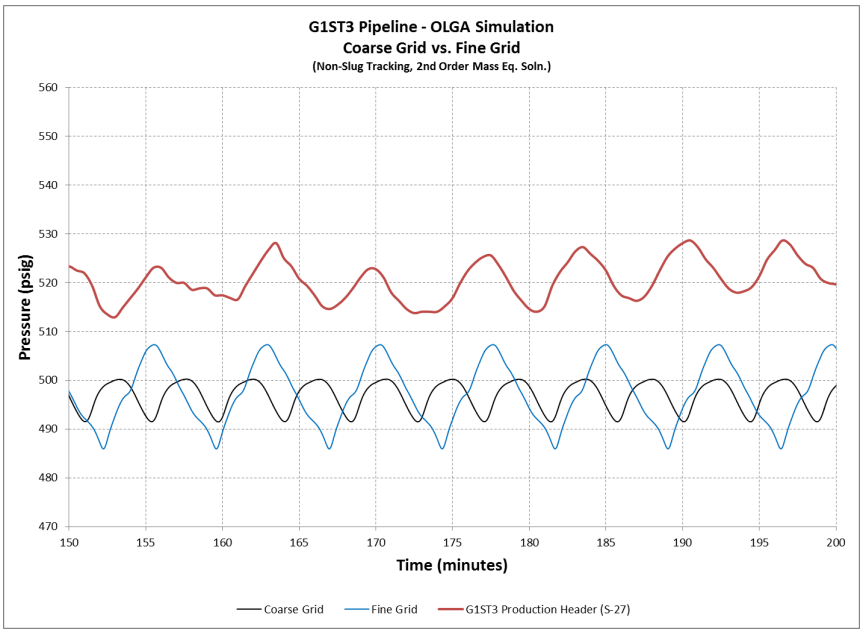

Figure 5-89: G1ST3 Pipeline OLGA Pressure Results: Coarse Grid vs. Fine Grid

The holdup results for the uphill position also shows an improvement in terms of frequency and amplitude. The frequency between the two large slugs is (8) minutes while the amplitude of fluctuation is about (0.4) compared to around (0.1) for coarse grid.

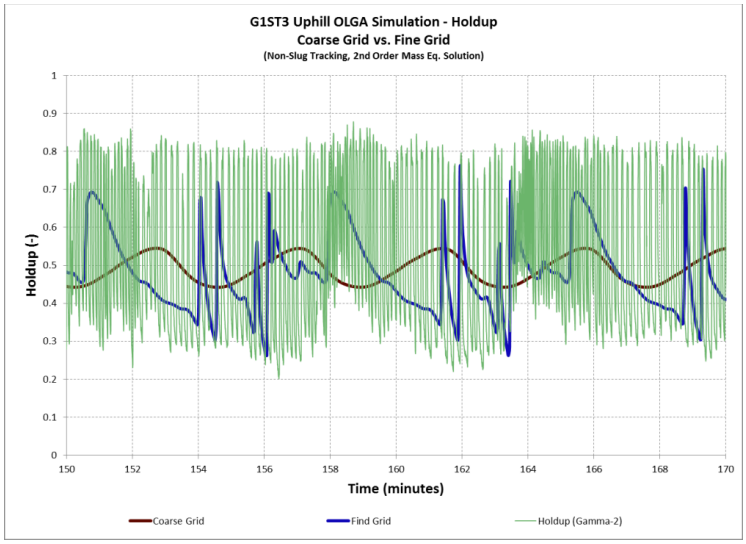

Figure 5-90: G1ST3 Uphill Pipeline OLGA Holdup Results: Coarse Grid vs. Fine Grid

The holdup results for the fine grid case on the downhill position provides a perfect match with field measurements in terms of both frequency and amplitude.

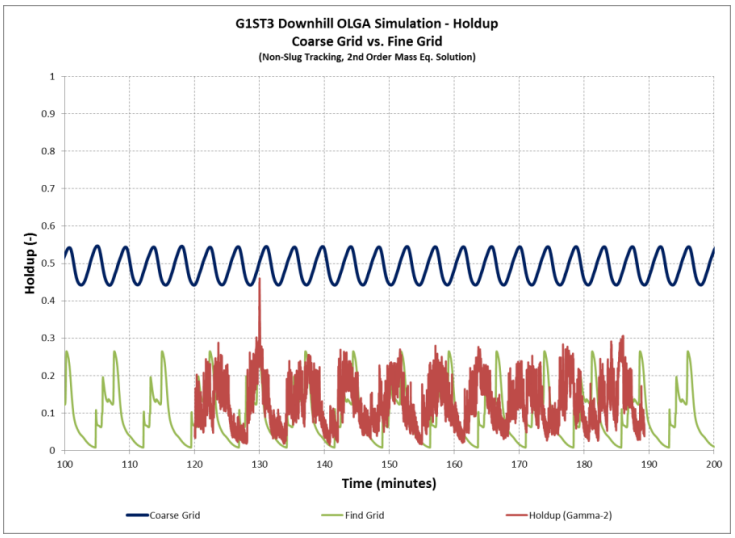

Figure 5-91: G1ST3 Downhill Pipeline OLGA Holdup Results: Coarse Grid vs. Fine Grid

5.2.8. G1ST3 Pipeline LedaFlow Simulations

Similar to OLGA simulations, LedaFlow simulations were carried out with various options to fully test the simulation package and the parameters which were varied for G1ST3 pipeline LedaFlow simulations are as follows:

- Slug capturing (No slug capturing vs. slug capturing)
- Grid size (Coarse grid vs. Fine grid (5) meter) – shown on Figure 5-92

Also, similar to OLGA simulations, heat transfer was not considered for all simulation cases. Finally, a high order scheme was considered for all simulation cases.

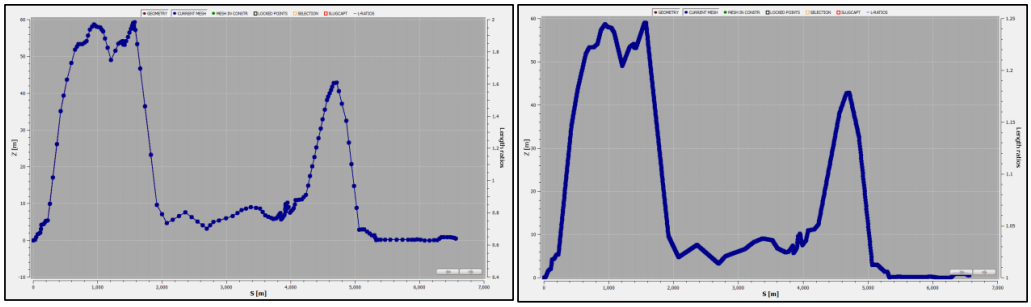

Figure 5-92: G1ST3 LedaFlow Coarse Grid (left) and Fine Grid (right) Sections

G1ST3 LedaFlow Simulation – (Slug Capturing vs. No Slug Capturing) + (Coarse Grid vs. Fine Grid)

LedaFlow simulations were carried out with and without slug capturing module. The pressure results shown on Figure 5-93 indicates a reasonable frequency agreement for both options, but with over-prediction of the slug amplitude as it indicates a pressure swing of approximately (35) psi compared to around (10) psi for field measurement. These results were obtained using a coarse grid similar to the one used in OLGA simulations.

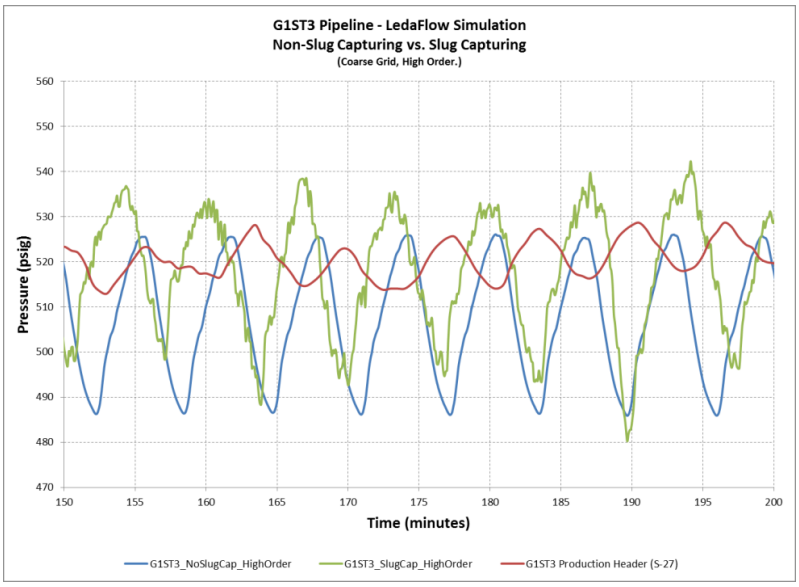

Figure 5-93: G1ST3 LedaFlow Pressure Results – Slug Capturing vs. Non-Slug Capturing Simulations (Coarse Grid)

Using a fine grid of (5) meters per section, a considerable improvement is achieved especially in amplitude as the pressure swing is reduced from (35) psi to (20) psi.

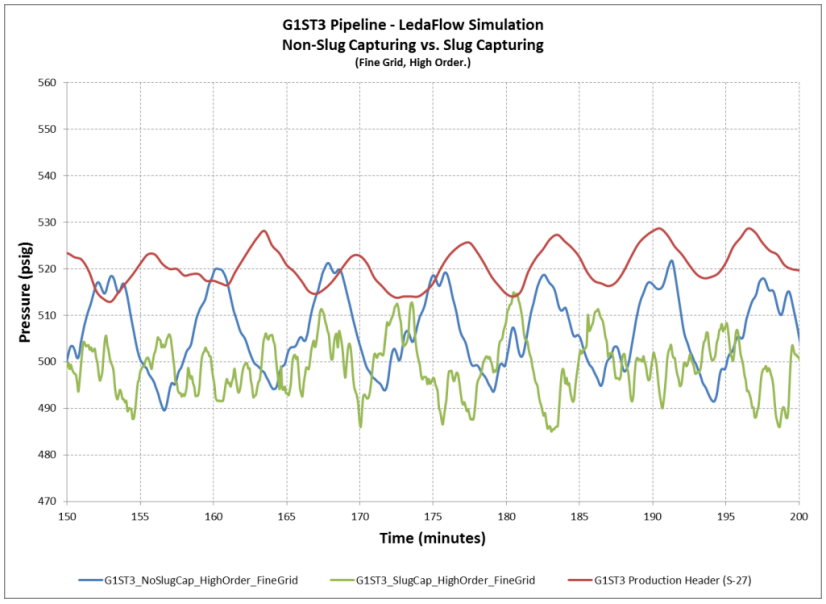

Figure 5-94: G1ST3 LedaFlow Pressure Results – Slug Capturing vs. Non-Slug Capturing Simulations (Fine Grid)

The uphill gamma LedaFlow simulation results, with coarse grid, indicate good agreement in terms of frequency for both options. However the non-slug capturing case provides better results in terms of holdup amplitude than the slug capturing case as sown in Figure 5-95.

Using a fine grid with (5) meter sections greatly improve the amplitude results with the slug capturing case. However, none of the cases were able to correctly predict the frequency of the small hydrodynamic slugs, as shown in Figure 5-96.

On the other hand, the downhill LedaFlow simulation results, with coarse grid, gave wrong predictions for both slug capturing and non-slug capturing cases, as shown in Figure 5-97. Using a fine grid, the results are greatly improved as the holdup mostly fluctuates between 0.03 and 0.25 for both cases, with a higher frequency for the slug capturing case, see Figure 5-98.

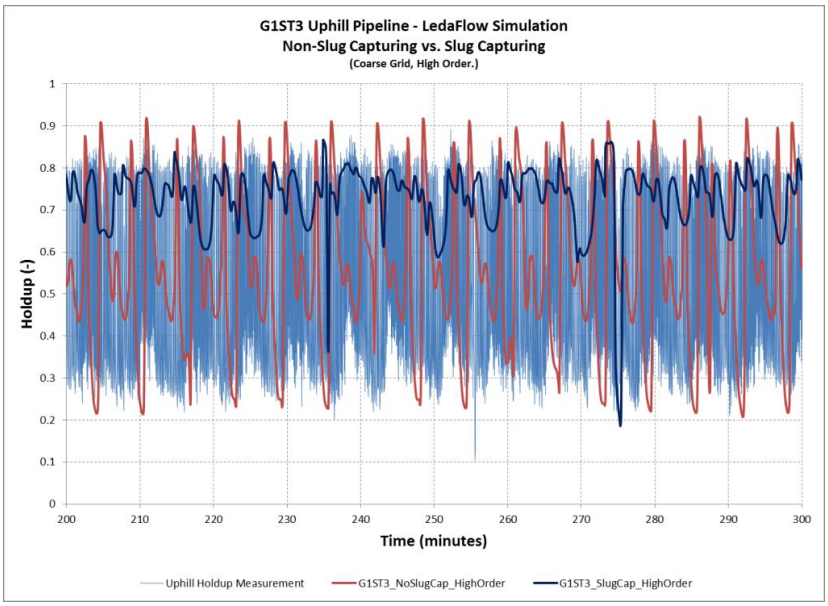

Figure 5-95: G1ST3 Uphill LedaFlow Holdup – Slug Capturing vs. Non-Slug Capturing Simulations (Coarse Grid)

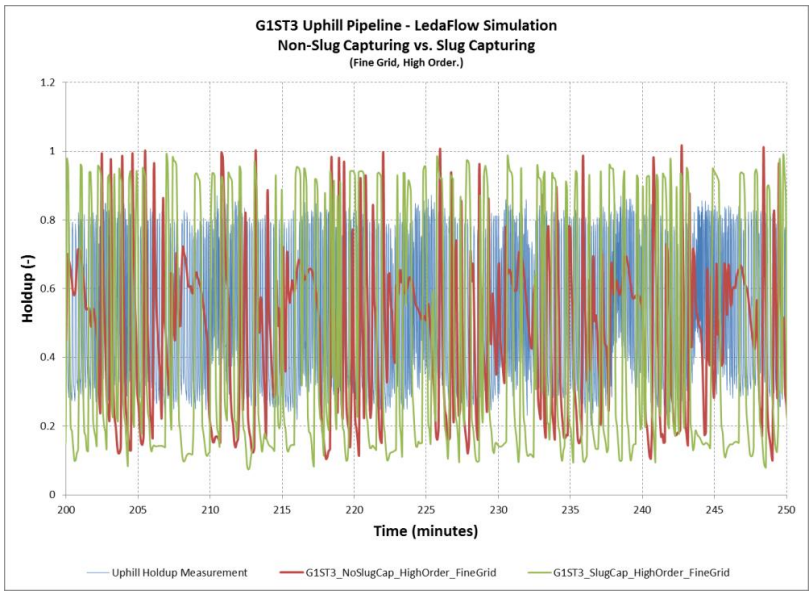

Figure 5-96: G1ST3 Uphill LedaFlow Holdup – Slug Capturing vs. Non-Slug Capturing Simulations (Fine Grid)

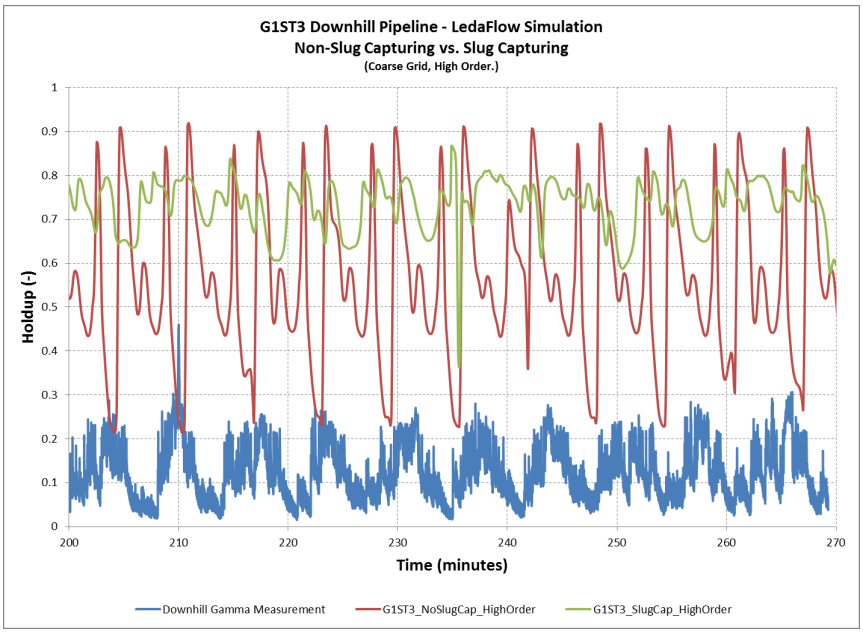

Figure 5-97: G1ST3 Downhill LedaFlow Holdup – Slug Capturing vs. Non-Slug Capturing Simulations (Coarse Grid)

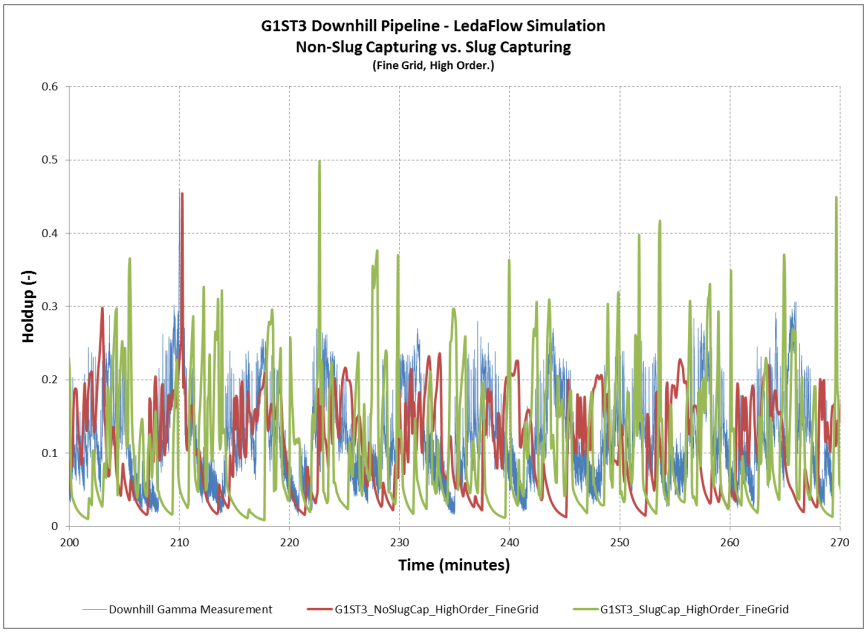

Figure 5-98: G1ST3 Downhill LedaFlow Holdup – Slug Capturing vs. Non-Slug Capturing Simulations (Fine Grid)

5.2.9. G1ST3 OLGA and LedaFlow Simulation Conclusions

- OLGA with non-slug tracking and a fine grid provided the best OLGA results in terms of pressure and holdup.
- Utilizing the slug tracking options in OLGA with various delay constants, one could not obtain the correct behavior of hydrodynamic slugs as obtained in the field measurements.
- LedaFlow holdup and pressure predictions were greatly improved using a fine grid with (5) meter sections. This applies to both the frequency and amplitude of the terrain induced slugs.
- Enabling or disabling the slug capturing module in LedaFlow had little impact on the pressure predictions. The holdup predictions showed higher frequency but without being able to match the small hydrodynamic slugs noticed in field measurements.

5.2.10. G1ST3 Pipeline Slug Valve Optimization Study

A quick evaluation of the optimum choke settings that would have provided the best results for this particular pipeline was conducted using both OLGA and LedaFlow simulation packages. The study utilized a fine grid with non-slug tracking/capturing scheme along with various choke fixed manual settings. Each valve setting, shown in Table **5-6**, was simulated for two hours before moving to the next setting and the study reported the pipeline inlet pressure as shown in Figure 5-99 and Figure 5-100 for OLGA and LedaFlow results.

These results indicate a new phenomenon where slugs start to decrease in amplitude and gradually disappear with less choking of the slug valve. This is contradictive to the expected behavior of severe slugging in pipelines. This behavior is believed to be generated by the accumulation of liquid at the valve opening which causes gas blockage and thus creating more perturbations in pipeline system.

A set of lab experiments were planned and carried out at NTNU multiphase lab to study this phenomenon further and verify the multiphase flow simulation results.

Table 5-6: G1ST3 Pipeline Choke Opening Settings

	OLGA & LedaFlow Choke Opening (%)	**Simulation Time (hrs) Start - Finish**
1.	4 %	0 – 2
2.	8 %	2 – 4
3.	10 %	4 – 6
4.	12 %	6 – 8
5.	15 %	8 – 10
6.	20 %	10 – 12
7.	40 %	12 – 14
8.	60 %	14 – 16
9.	80 %	16 – 18
10.	100 %	18 – 20

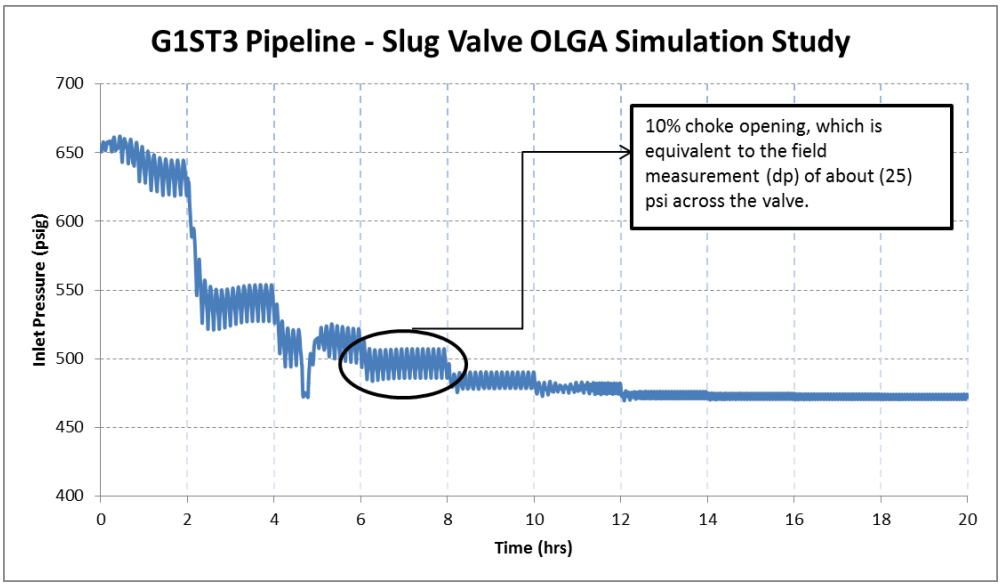

Figure 5-99: G1ST3 Pipeline – Slug Valve OLGA Simulation Study – (Fine Grid, 2nd Order, No-SlugTracking)

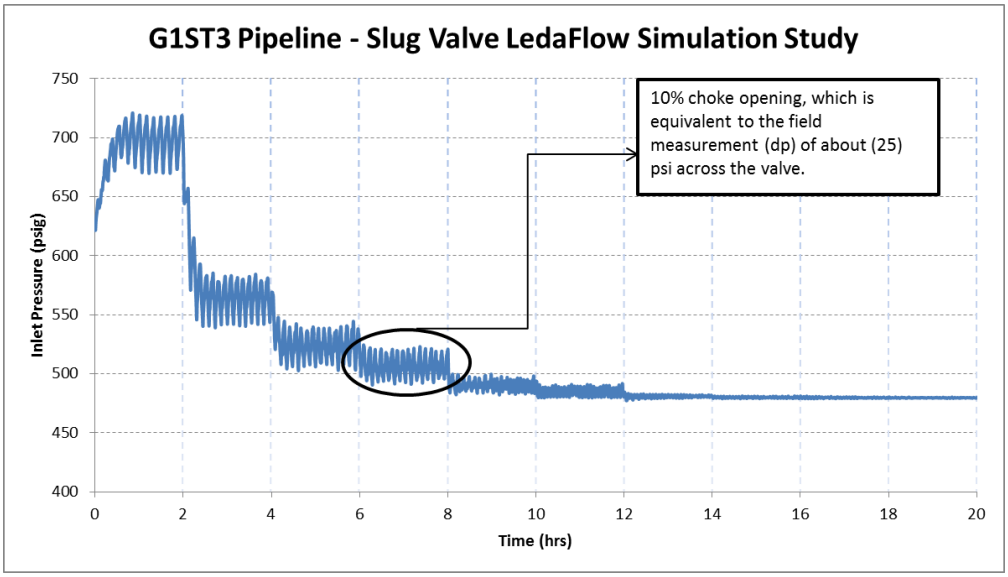

Figure 5-100: G1ST3 Pipeline – Slug Valve LedaFlow Simulation Study – (Fine Grid, High Order, No-SlugCapturing)

5.3. G2NT2 Pipeline Results

G2NT2 measurements were conducted over two days May 23, 1999 and May 24, 1999. The measurement was made downstream the slug valve which is installed at the end of the pipeline upstream of GOSP-2. The measurements were made at two different flow rates: a normal flow rate of 56,000 BBL/Day, and a reduced flow rate of 37,700 BBL/Day.

5.3.1. Pipeline Profile Details

The total pipeline length is approximately 14 Km and starts from Sabkhah 41 (S-41) to GOSP-2 going through Sabkhah 50 (S-50) and Sabkhah 54 (S-54). The pipeline has two different diameters 16 inch and 20 inch as shown on Figure 5-101.

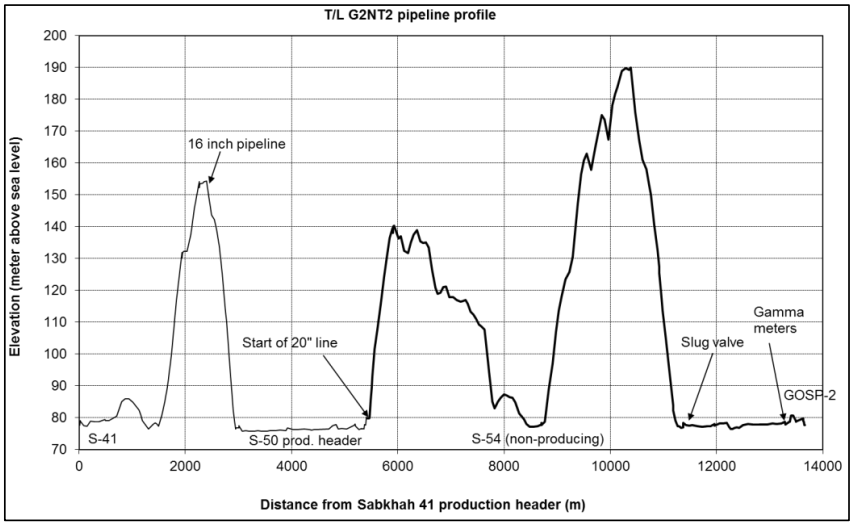

Figure 5-101: G2NT2 pipeline profile - slug valve and gamma densitometer locations

The distance between the gamma meters was set at 55.7 m, while the pipeline inclination angle was measured at +0.08 degrees. The distance of the gammas to the upstream slug valve was measured at approximately 2.0 Km. In addition the distance from the gamma meters to GOSP-2 was approximately measured at 400 m. The pipeline wall thickness was measured using ultra sonic measurement device at 0.787 inch (20 mm). The GOSP-2 pressure was set at 400 psig during the measurement period.

The flow rates were based on forecasts made by the production engineers and no flow rate measurements were carried out at the time of the experiments. The flow rates from each Sabkhah were estimated as follows:

Sabkhah	Volumetric Flow Rate (BBL/Day) @ std. cond.
S-41	1,000
S-50	55,000
S-54	0
Total	**56,000**

The superficial gas and liquid velocities for normal flow rates ranged from (0.2 to 3.5) m/sec for gas and (0.2 to 1.8) m/sec for liquid, based on OLGA predictions.

5.3.2. Production Header Time Series

The DCS signal and a separate logging of production header pressure at S-41 showed a very stable pressure signal at 550 psig. This is mainly due to the very low flow rate from this production header, approximately 1,000 BBL/Day during the two measurement tests.

However, the header pressure signal for (S-50) showed slightly higher fluctuations of approximately (10) psi between (534) and (544) psig with a period of (7 to 8) minutes as shown in Figure 5-102. Unfortunately the pressure signal at (S-50) was not available during the normal flow rate measurement day, May 23, 1999. Therefore, only the pressure during reduced flow rate measurement period, May 24, 1999, is reported.

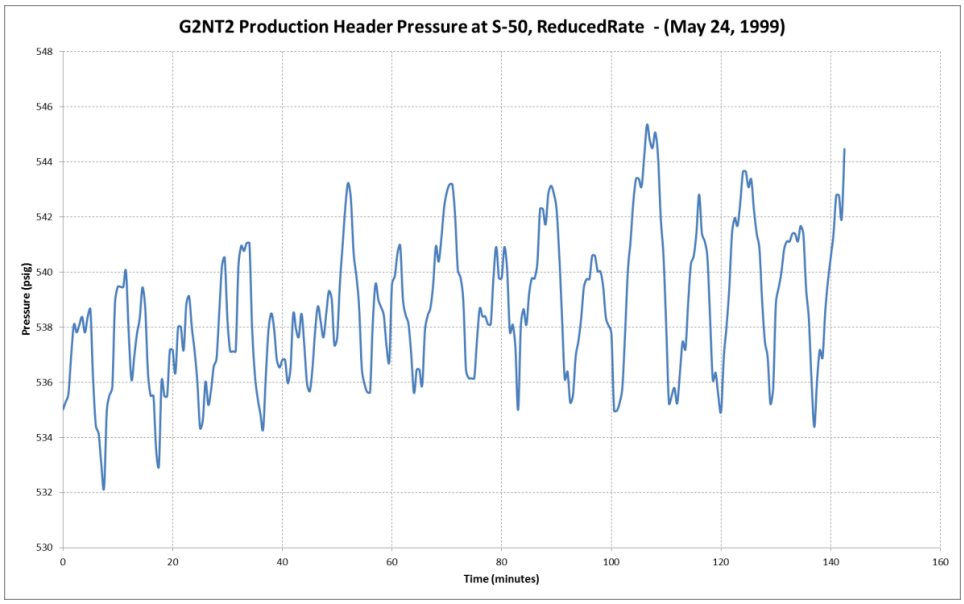

Figure 5-102: G2NT2 Production header pressure at S-50, 35% reduced rate, May 24, 1999

5.3.3. Slug Valve Pressure Drop

The pressure drop across the slug valve was not logged during the measurement tests. However, observation of the two manometers close to the slug valve showed average differential pressure of approximately (40 to 50) psi.

5.3.4. Analysis of Holdup Time Series – Normal Flow Rate

Analysis of the holdup time series for the normal flow rate measurement shows short slugs with large roll waves in between, as shown on figures Figure **5-103**, Figure **5-104**, and Figure **5-105**. One also notices that Gamma-2 shows typically 10% higher holdup than Gamma-1, which is mainly due to the down-sloping of gamma-1 position at (– 0.24) degrees, and up-sloping of gamma-2 position at (+ 0.4) degrees. This is in agreement with the inclination dependency of wavy flow. The average liquid film holdup for Gamma-1 position is approximately (0.25) while it was approximately (0.4) for Gamma-2 position.

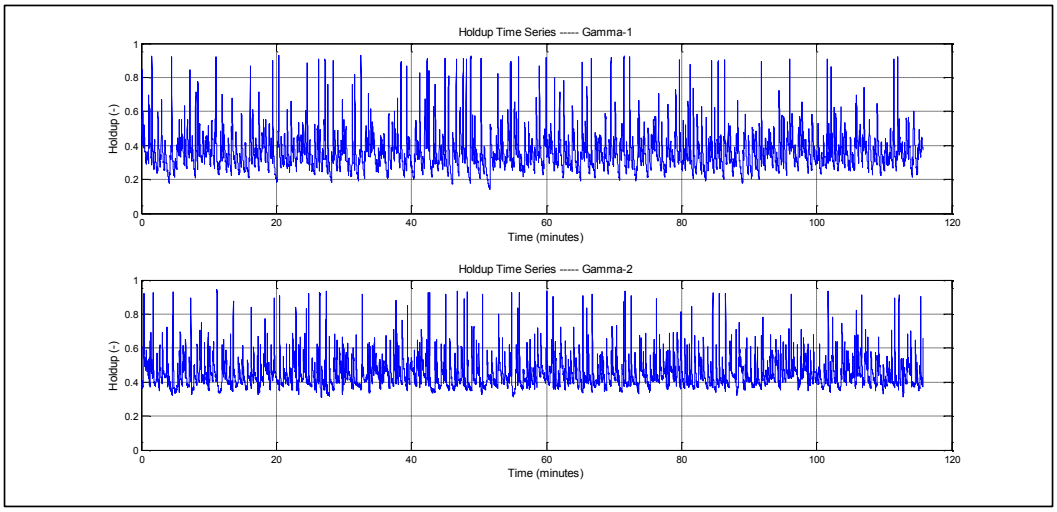

Figure 5-103: G2NT2 Holdup time series, Normal rate, May 23, 1999, (120 minutes)-(Gamma-1&2)

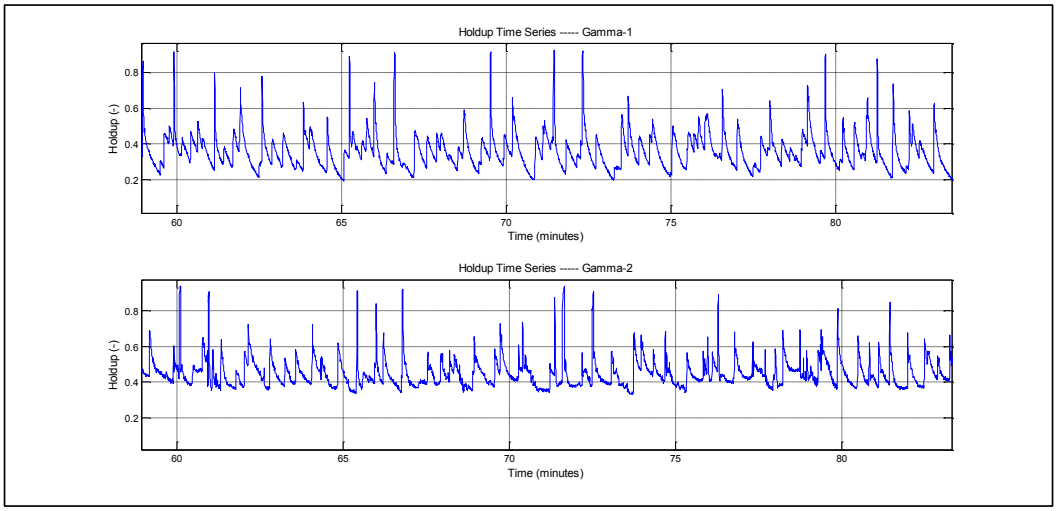

Figure 5-104: G2NT2 Holdup time series, Normal rate, May 23, 1999, (20 minutes)-(Gamma-1&2)

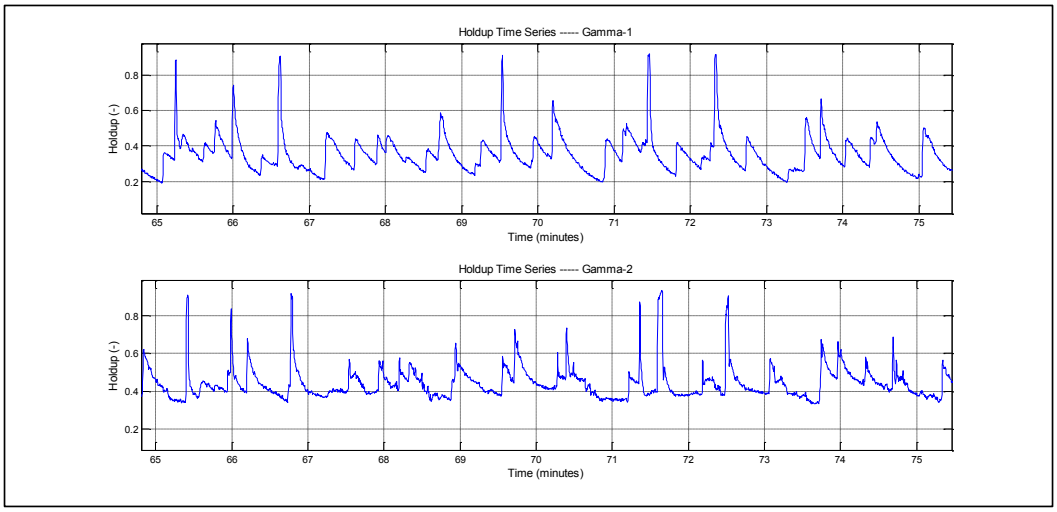

Figure 5-105: G2NT2 Holdup time series, Normal rate, May 23, 1999, (10 minutes)-(Gamma-1&2)

Cross correlation of the two time series provides a clear time lag delay of 10.8 seconds as shown in Figure **5-106**. Using the distance between the two gammas one can obtain the average slug velocity which turns out to be (5.15) m/sec.

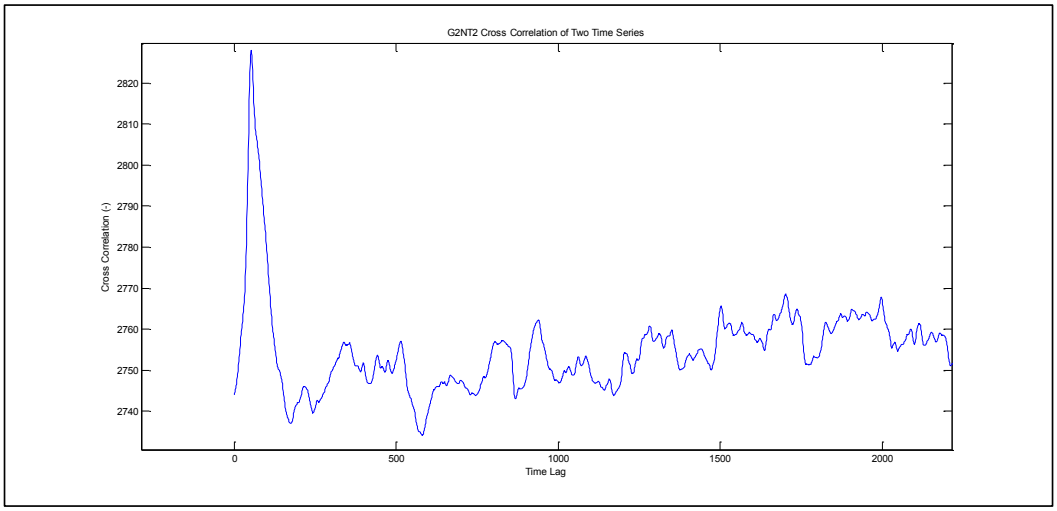

Figure 5-106: Cross Correlation of holdup time series – G2NT2 Pipeline – Normal rate

Using a holdup criterion of (0.7) to distinguish between slugs and large roll waves, a total of (45) slugs were detected in both time series, which provides a slug frequency of approximately a slug every (2.6) minutes. The small number of slugs detected does not provide good bases for statistical analysis. Nevertheless, statistical analysis was carried out and the results are shown in Figure **5-107**, Figure **5-108** and Figure **5-109**, for slug frequency and length.

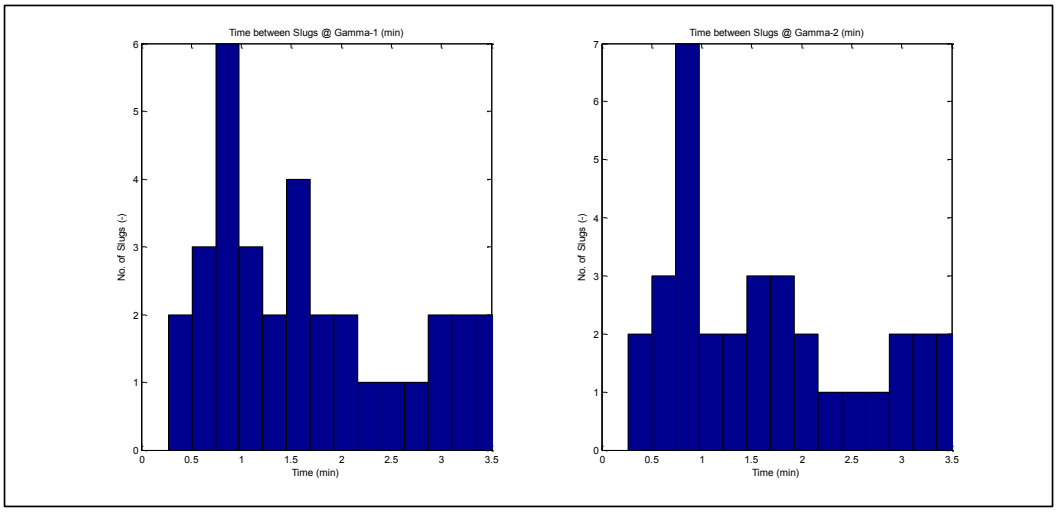

Figure 5-107: G2NT2 Slug Frequency Distribution (minutes) – Normal rate

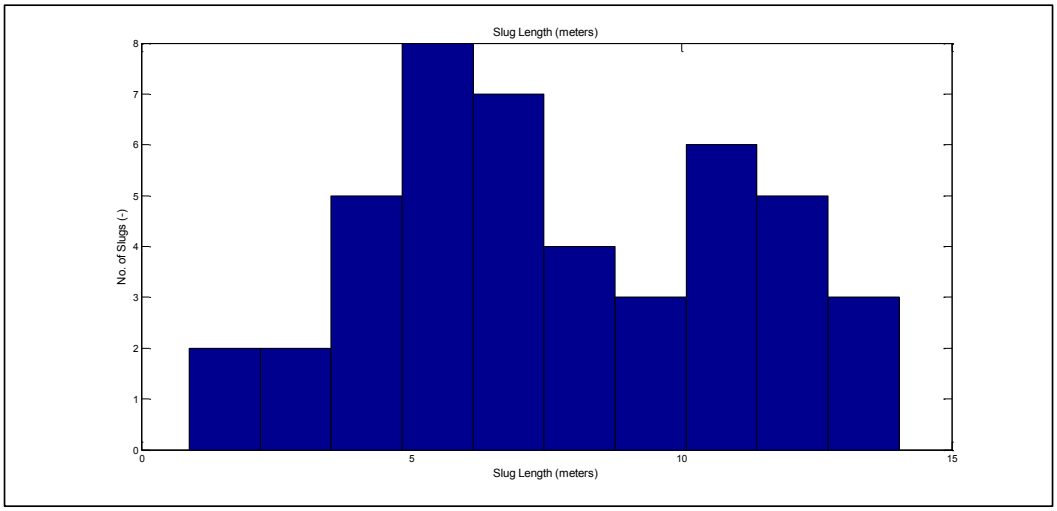

Figure 5-108: G2NT2 Slug Length Distribution (meters) – Normal rate

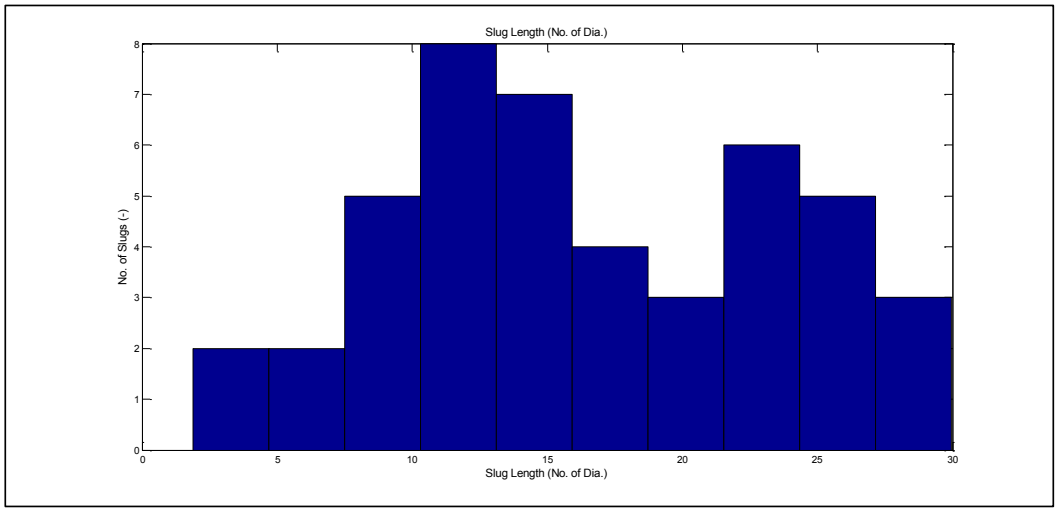

Figure 5-109: G2NT2 Slug Length Distribution (No. of Dia.) – Normal rate

Slug velocities were also created, as shown in Figure **5-110** and Figure **5-111**, and they confirm very well with the slug velocity obtained from the cross correlation calculations at 5.15 m/sec. The average slug front velocity was calculated at 5.28 m/sec compared to an average slug tail velocity of 5.57 m/sec, which suggests a decaying slug behavior.

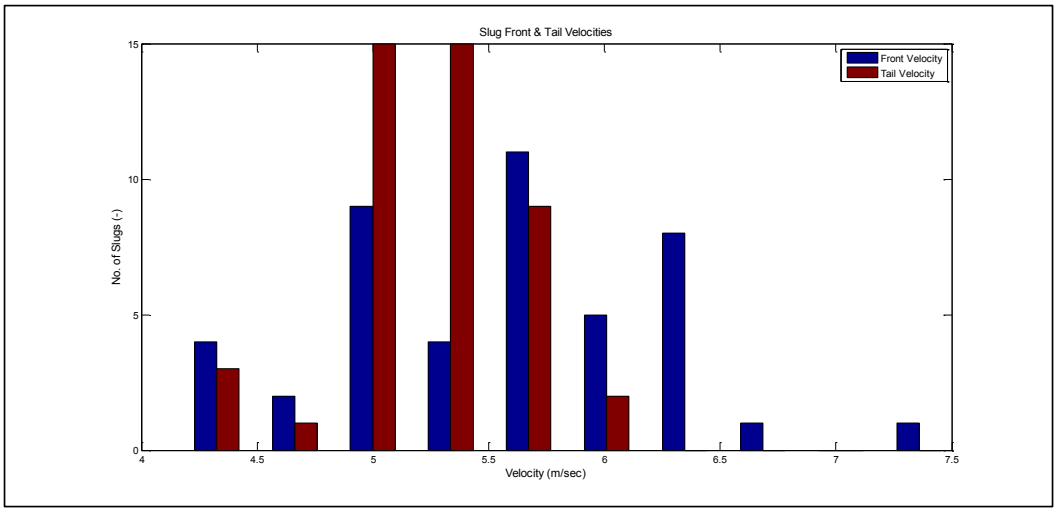

Figure 5-110: G2NT2 Front & Tail Velocities Distribution (m/sec) – Normal rate

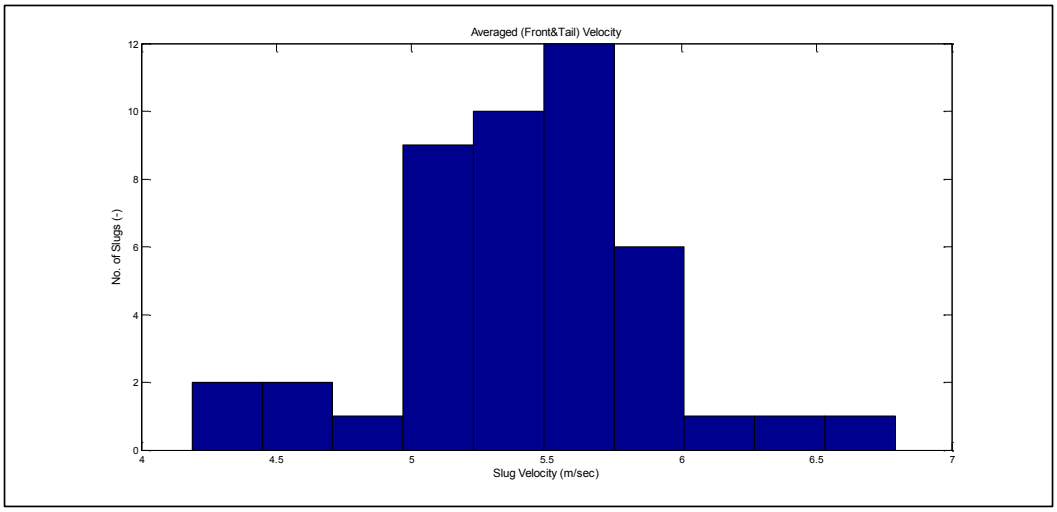

Figure 5-111: G2NT2 Average Front & Tail Velocity Distribution (m/sec) – Normal rate

The slugs observed in general, were very short and intermittent. These slugs are most likely a result of breaking up of larger slugs that have been created upstream of the slug valve.

5.3.5. Analysis of Holdup Time Series – Reduced Rate

With reduced flow rate, the flow behavior became generally more stable with fewer peaks as it seems that slugs are disappearing and instead only large roll waves exist. The holdup at Gamma-1 position fluctuates mostly between (0.2) and (0.6), while on Gamma-2 position, the holdup fluctuates mostly between (0.4) and (0.8) as shown on Figure **5-112**, Figure **5-113** and Figure **5-114**.

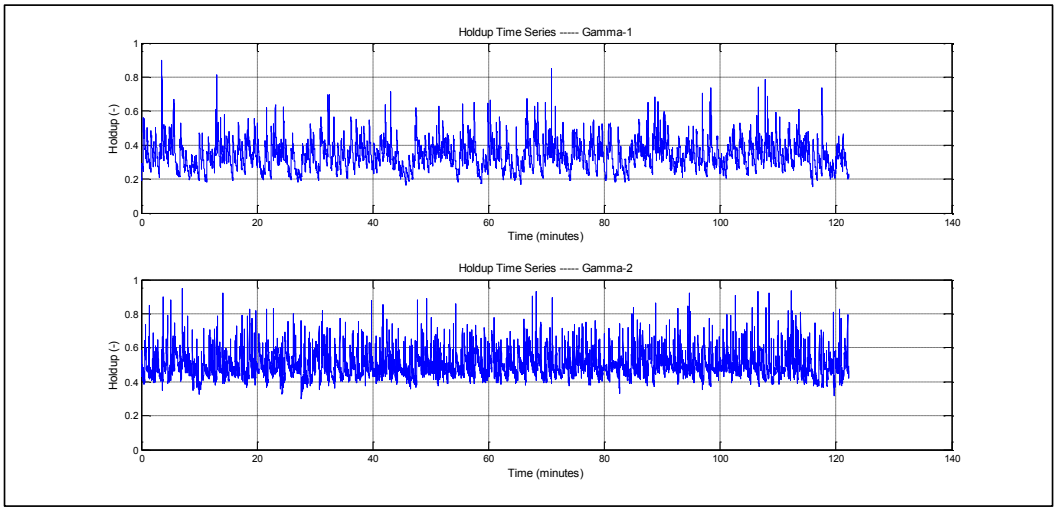

Figure 5-112: G2NT2 Holdup time series, Reduced rate, May 24, 1999, (120 minutes)-(Gamma-1&2)

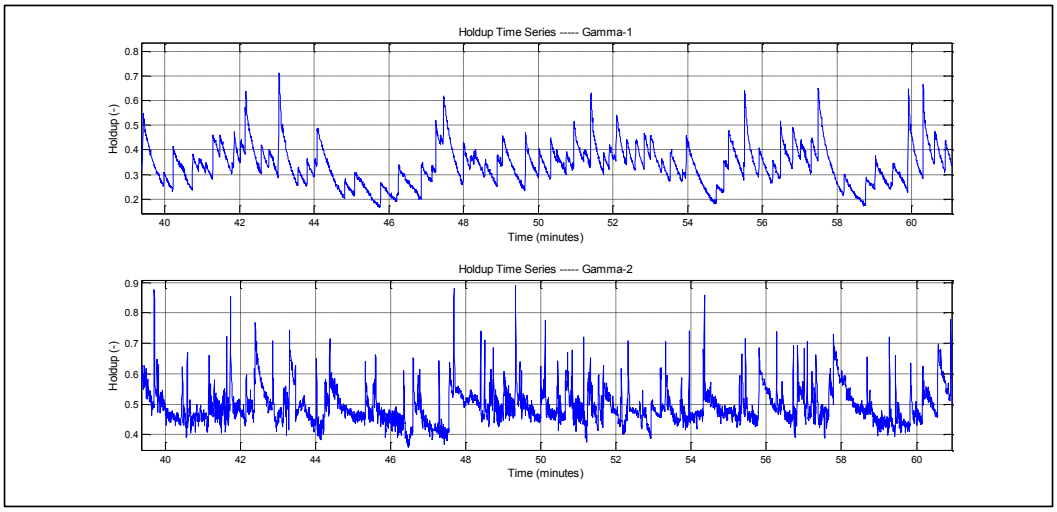

Figure 5-113: G2NT2 Holdup time series, Reduced rate, May 24, 1999, (20 minutes)-(Gamma-1&2)

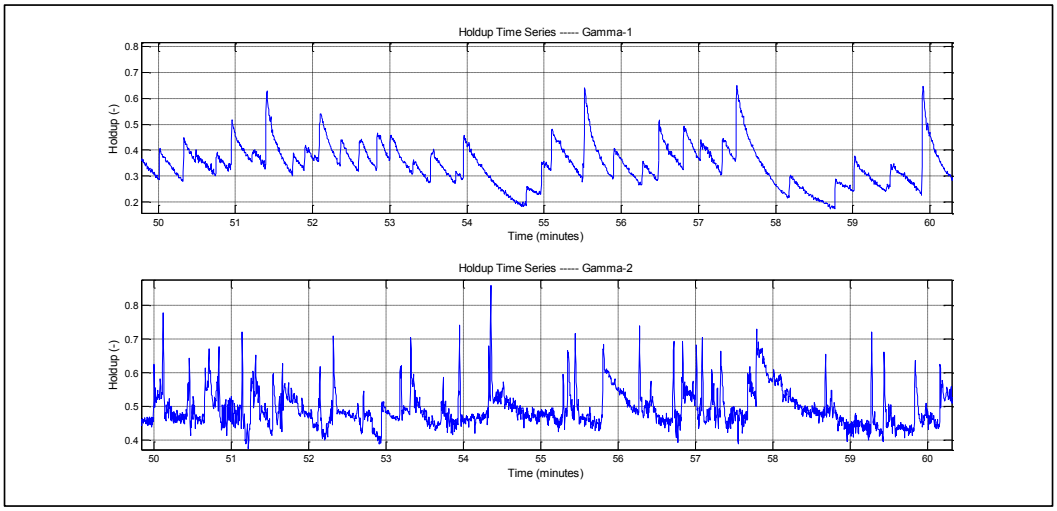

Figure 5-114: G2NT2 Holdup time series, Reduced rate, May 24, 1999, (10 minutes)-(Gamma-1&2)

The large macro-structure fluctuations, (7 to 8) minutes pressure cycles, that were visible in the pressure log obtained during the reduced flow rate measurements are not visible in the holdup measurements. Only small micro fluctuations in the order of one minute or less are visible in these holdup measurements.

5.3.6. G2NT2 Pipeline Simulation

Extensive simulation work was conducted using OLGA and LedaFlow. The simulation pressure results were compared against the reduced flow rate field measurements, while the holdup results were compared against the normal flow rate field measurements. The location of the holdup gamma measurements were downstream of the slug valve at the end of the pipeline and the available pressure measurements were at (S-50) production header, which is about (4,000) meter from the inlet of the pipeline.

5.3.7. G2NT2 Pipeline OLGA Simulations

OLGA simulation was carried out with various options to fully test the simulation package capabilities to predict slugging phenomena in the subject pipeline. Using 2nd order scheme for mass equations and an adiabatic heat transfer option, the other simulation parameters which were varied for G2NT2 pipeline are as follows:

- Slug tracking (No slug tracking vs. slug tracking with various delay constants)
- Grid size (Coarse grid vs. Fine grid)

G2NT2 Pipeline OLGA Simulation – (Slug Tracking vs. No Slug Tracking)

OLGA Simulations were carried out with and without slug tracking module. The results were plotted for various Delay Constants (DCs), which significantly impact the initiation of slugs in OLGA code.

Using an average slug velocity of (5.15) m/sec obtained from the cross correlation of the two gamma meters at the uphill pipeline section, one can estimate the idle time between slug initiations as follows:

Table 5-7: G2NT2 – Idle time between slug initiations for various delay constants

Idle time between Slug Initiation (DT) (sec)	Ul (m/sec)	Inner Dia. (m)	DC
4.54	5.15	0.468	50
13.63	5.15	0.468	150
45.44	5.15	0.468	500
72.69	5.15	0.468	800

OLGA simulations were carried out with various delay constants ranging from 50 to 800. The holdup results for the normal production case are shown on figures Figure 5-115, Figure 5-116, Figure 5-117 and Figure 5-118. Analysis of the holdup figures shows that with no slug tracking the holdup cycles are fixed at approximately (8) minutes with very stable and repetitive slug behavior, which agrees well with pressure frequency noted for the reduced flow rate case. The holdup fluctuates between (0.35) and (0.75), which also agrees well with the holdup amplitude for field measurements as shown in Figure 5-115.

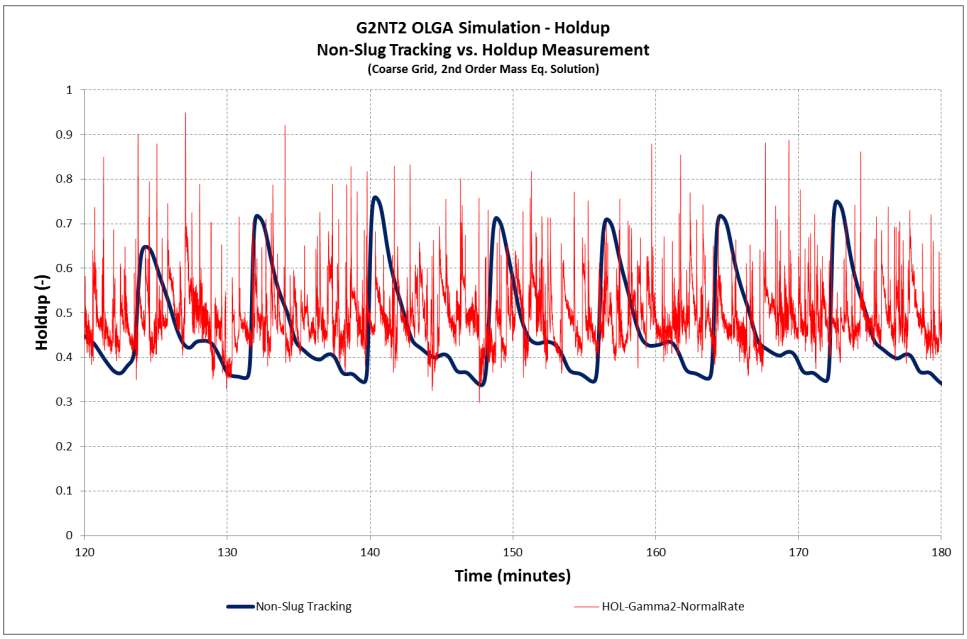

Figure 5-115: G2NT2 OLGA Holdup Simulation – Non-Slug Tracking vs. Holdup Measurement (Normal Rate)

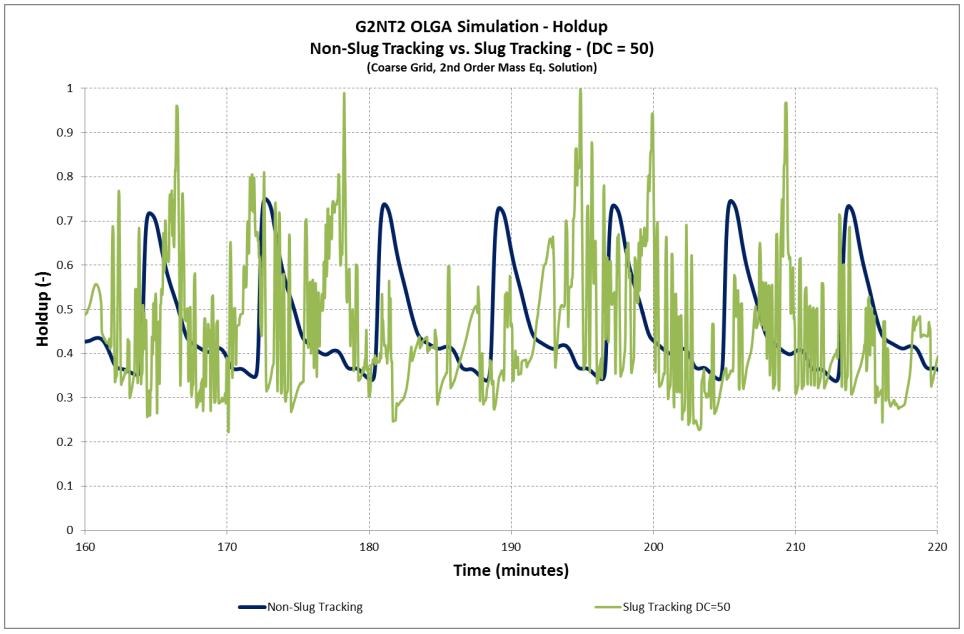

Figure 5-116: G2NT2 OLGA Holdup Simulation – Non-Slug Tracking vs. Slug Tracking (DC=50)

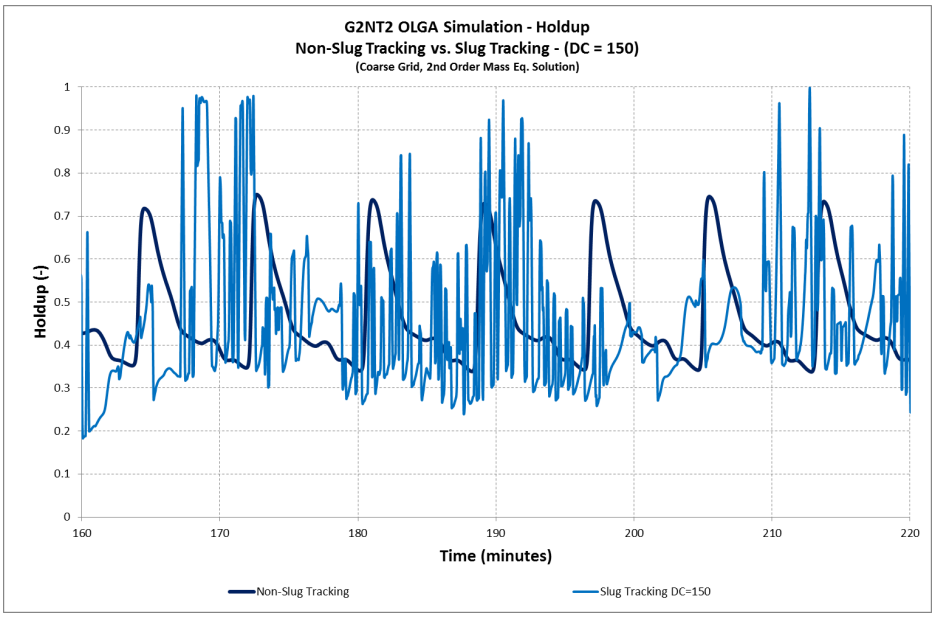

Figure 5-117: G2NT2 OLGA Holdup Simulation – Non-Slug Tracking vs. Slug Tracking (DC=150)

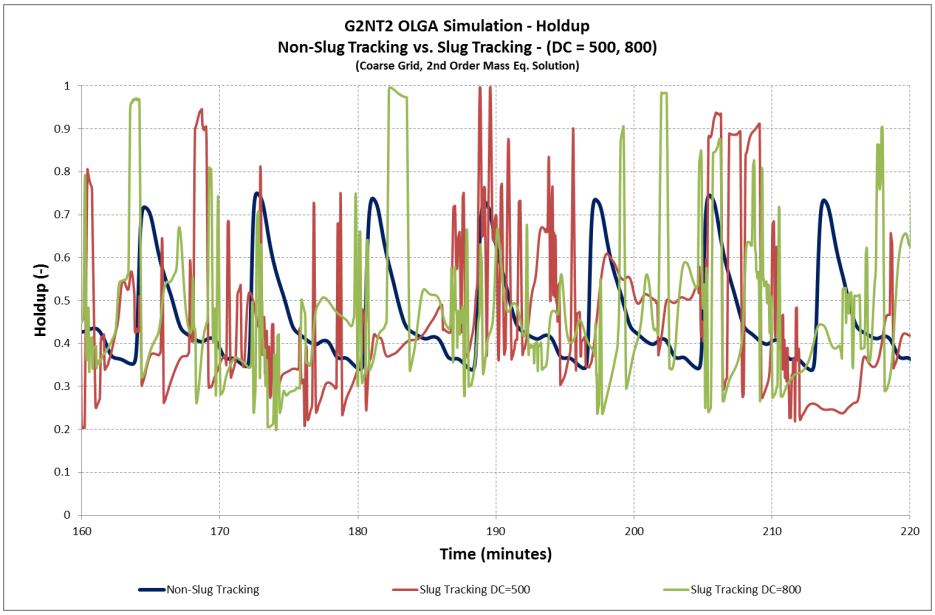

Figure 5-118: G2NT2 OLGA Holdup Simulation – Non-Slug Tracking vs. Slug Tracking (DC=500, 800)

When slug tracking module is enabled, OLGA shows hydrodynamic slugs with various frequencies depending on the slug's delay constant used in that particular case. However, none of the cases shown here seem to correctly predict the field measurement frequency as shown in Figure 5-116, Figure 5-117 and Figure 5-118. The amplitude of the holdup fluctuations seem to be higher than those with no slug tracking as holdup reaches almost (1.0).

Comparing field pressure measurements and OLGA simulation pressure results at reduced production rate of (37.7 MBD), one could notice a very good agreement in terms of pressure frequency and amplitude with the case of non-slug tracking, as shown in Figure 5-119.

The simulation frequency was approximately (9) minutes, with amplitudes ranging from (10) to (15) psi. This compares very well with the field measurements observations which had slightly lower amplitudes of (5) to (10) psi.

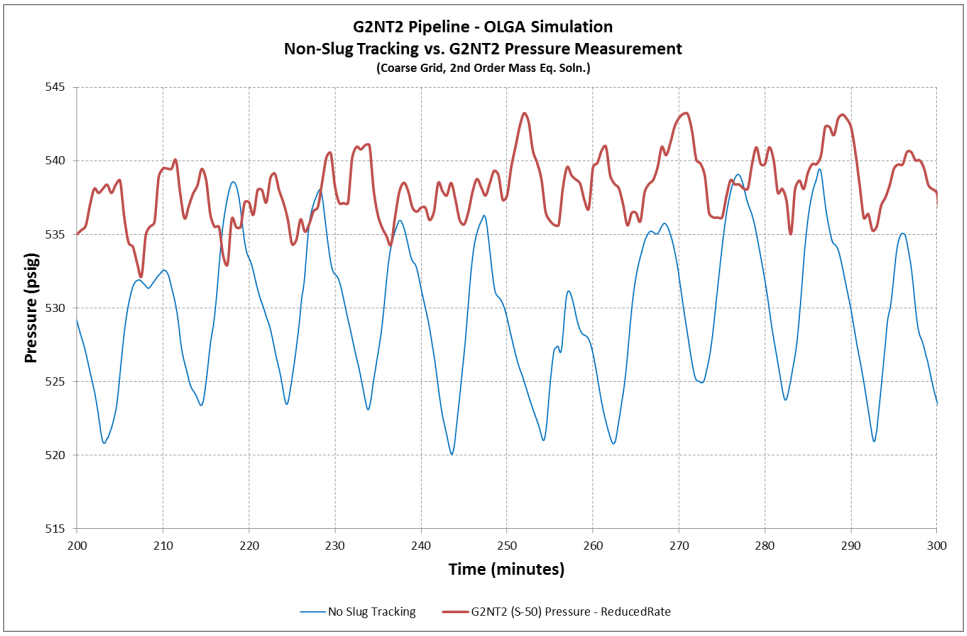

Figure 5-119: G2NT2 OLGA Pressure Results – Non-Slug Tracking vs. Pressure Measurement (Reduced Rate)

OLGA simulations with slug tracking with various delay constants show very large frequencies that range between (20) and (40) minutes. The slug amplitudes were also large, (50) psi, compared to the field measurements, (10) psi, as shown in Figure 5-120, Figure 5-121, Figure 5-122.

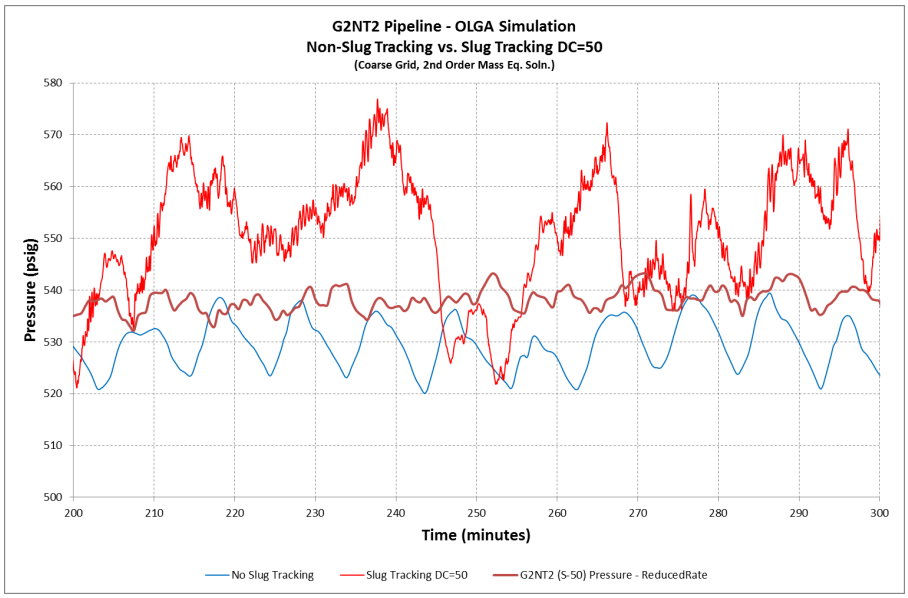

Figure 5-120: G2NT2 OLGA Pressure Results – Non-Slug Tracking vs. Slug Tracking (DC=50)

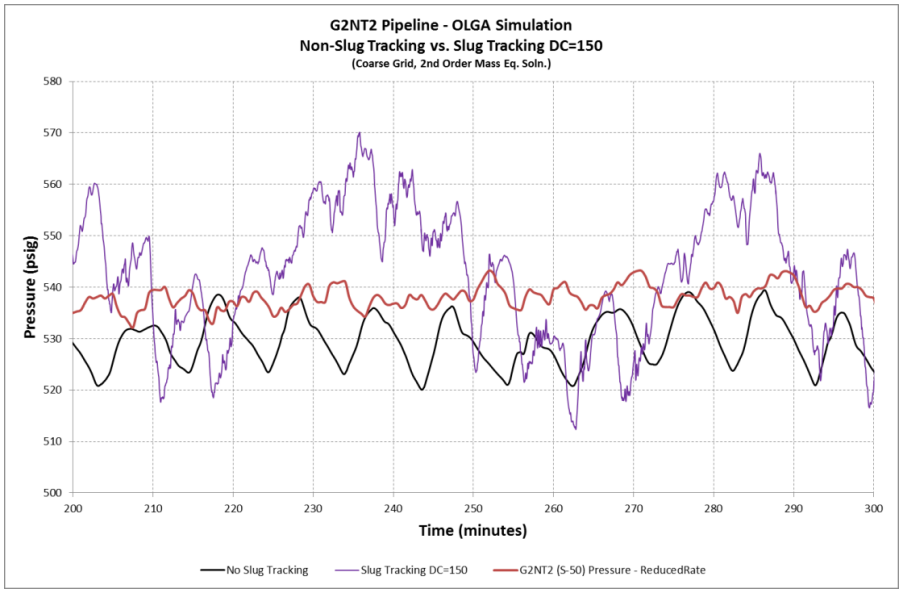

Figure 5-121: G2NT2 OLGA Pressure Results – Non-Slug Tracking vs. Slug Tracking (DC=150)

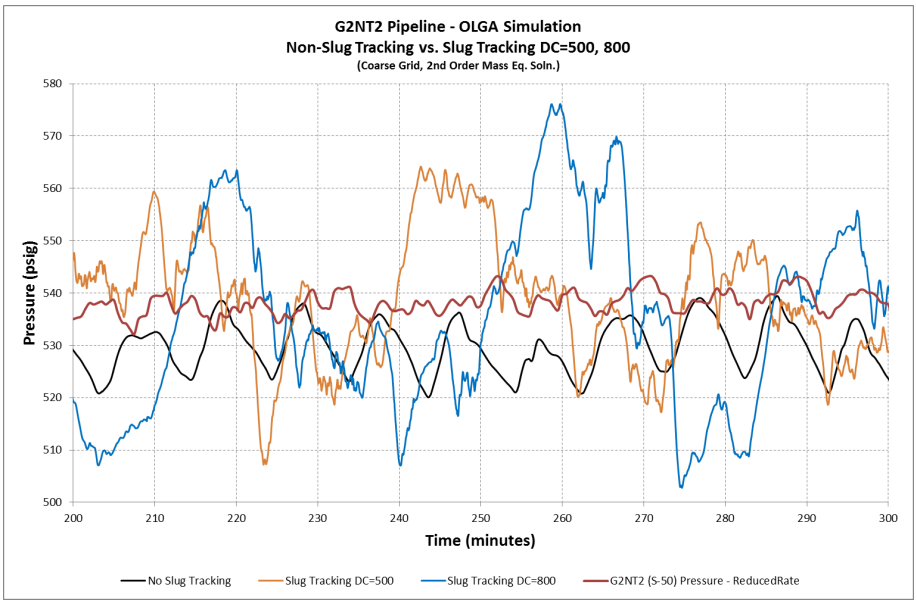

Figure 5-122: G2NT2 OLGA Pressure Results – Non-Slug Tracking vs. Slug Tracking (DC=500, 800)

G2NT2 Pipeline OLGA Simulation – (Coarse Grid vs. Fine Grid)

The previous G2NT2 pipeline OLGA simulations were conducted using a relatively coarse grid with an average pipe section of approximately (50) meters, as shown in Figure 5-123. In order to explore the impact of utilizing a fine grid on OLGA simulations, a fine grid case was simulated using a fixed (5) meters per section as shown in Figure 5-124.

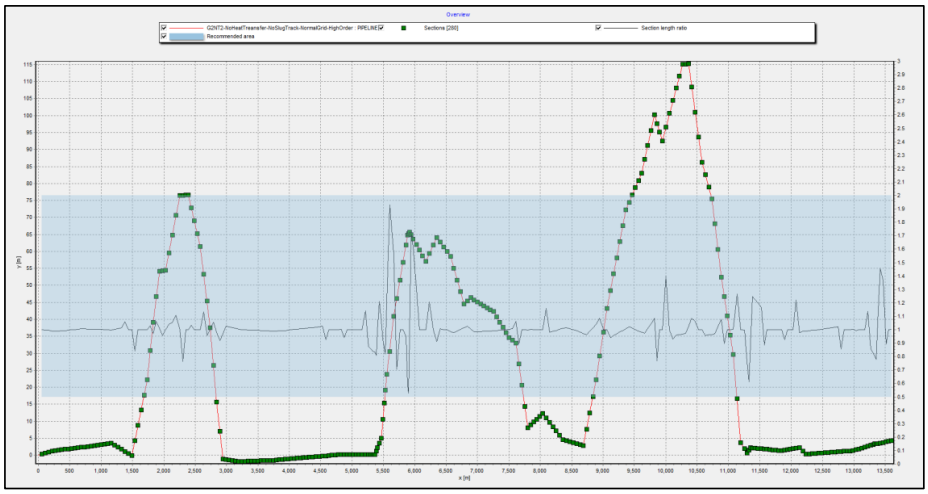

Figure 5-123: G2NT2 Pipeline Sections – OLGA Grid Options (Coarse Grid)

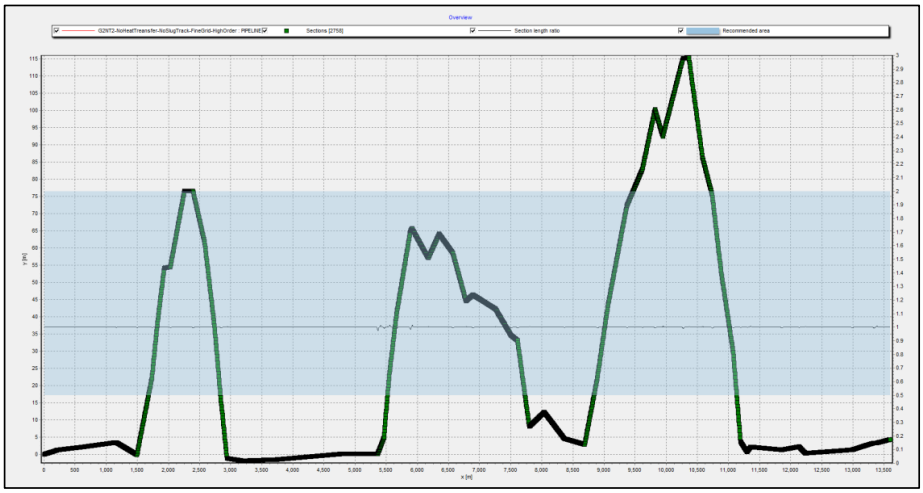

Figure 5-124: G2NT2 Pipeline Sections – (Fine Grid (5 meter))

The holdup results depicted in Figure 5-125 shows a slight difference between the coarse and fine grid cases, where the fine grid case shows a higher holdup amplitudes but with similar frequency to the case with the coarse grid.

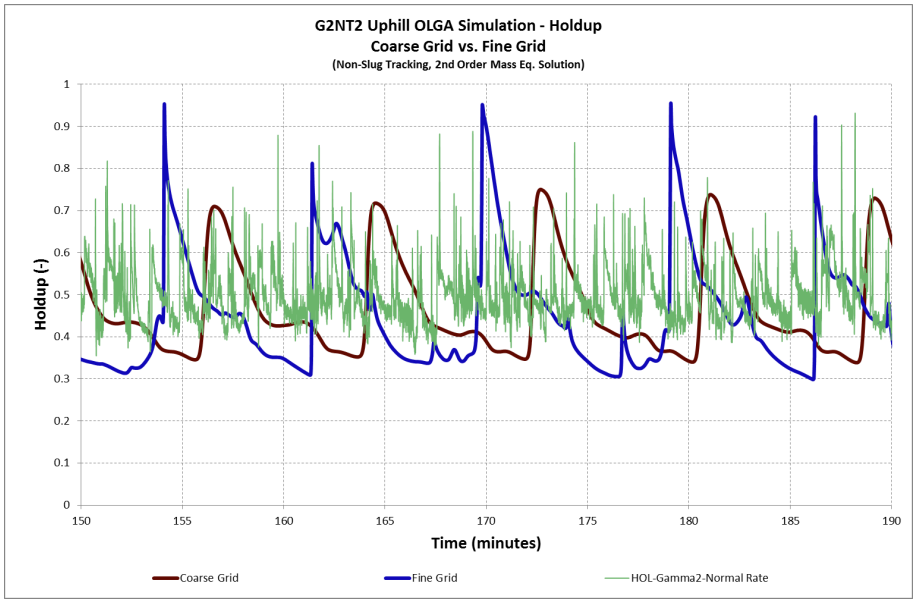

Figure 5-125: G2NT2 OLGA Holdup Simulation – Coarse Grid vs. Fine Grid (Normal Rate)

On the other hand, the pressure results shown in Figure 5-126, shows the fine grid case pressure average slightly below the field measurement pressure. However, both the frequency and amplitude of the fine grid case show a better agreement with the field measurements than the coarse grid case.

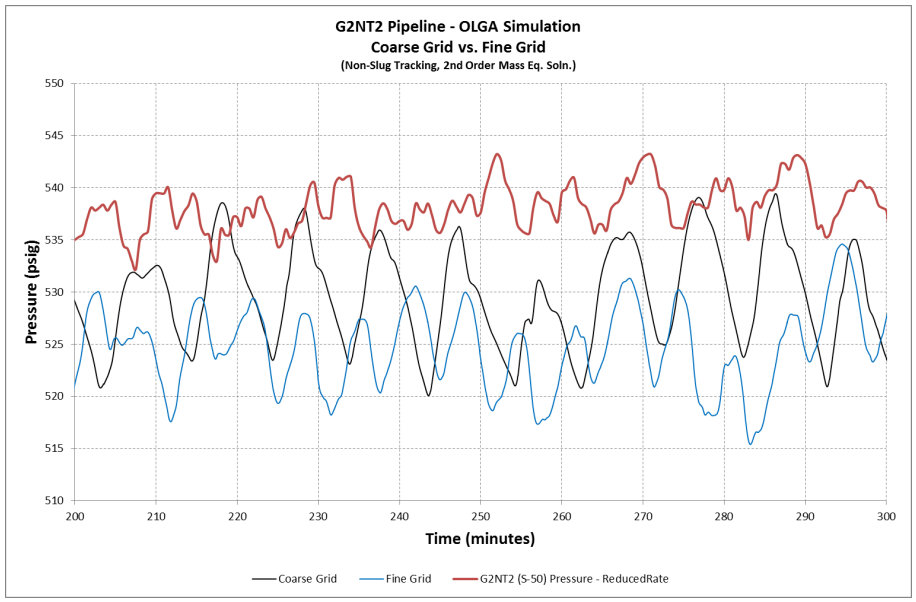

Figure 5-126: G2NT2 OLGA Pressure Simulation – Coarse Grid vs. Fine Grid (Reduced Rate)

5.3.8. G2NT2 Pipeline LedaFlow Simulations

Similar to OLGA simulations, LedaFlow simulations were carried out with various options to fully test the simulation package. The pressure results were compared against the reduced flow rate field measurements while the holdup was compared against the normal flow rate field measurements case. The parameters which were varied for G2NT2 pipeline LedaFlow simulations were as follows:

- Slug capturing (No slug capturing vs. slug capturing)
- Grid size (Coarse grid vs. Fine grid (5) meter) – shown on Figure 5-127

Also, similar to OLGA simulations, heat transfer was not considered for all simulation cases. Finally, a high order scheme was considered for all simulation cases.

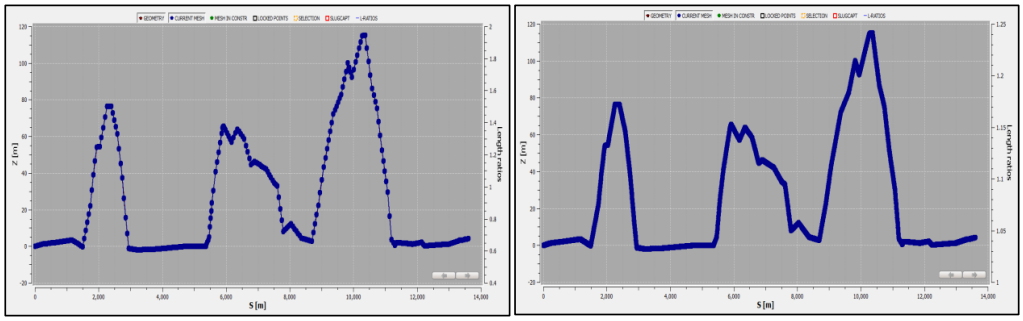

Figure 5-127: G2NT2 LedaFlow Coarse Grid (left) and Fine Grid (right) Sections

G2NT2 LedaFlow Simulation – (Slug Capturing vs. No Slug Capturing) + (Coarse Grid vs. Fine Grid)

LedaFlow simulations were carried out with and without slug capturing module. The pressure results shown on Figure 5-128 indicates a reasonable frequency agreement for the case with no slug capturing, but with over-prediction of the slug amplitude as it indicates a pressure swing of approximately (35) psi compared to around (7) psi for field measurement. The case also shows two large fluctuations separated by a small one but with the same frequency. However, the slug-capturing case, shows a higher pressure amplitude of (40) psi with even larger frequency of (10) minutes. The small fluctuations that were present in the non-slug capturing case seem to have been merged with nearby large one which creates the larger pressure amplitudes and frequencies.

These results were obtained using a coarse grid similar to the one used in OLGA simulations.

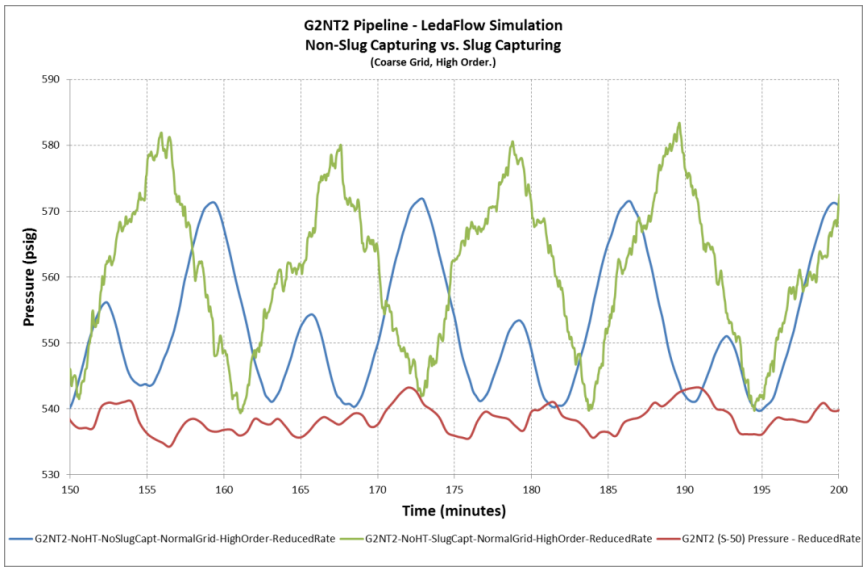

Figure 5-128: G2NT2 LedaFlow Pressure Results – Slug Capturing vs. Non-Slug Capturing Simulations (Coarse Grid)

Using a fine grid of (5) meters per section, the results were not improved in terms of frequency or amplitude for both cases. The only notable difference was the disappearance of the small fluctuations from the non-slug capturing case as shown in Figure 5-129.

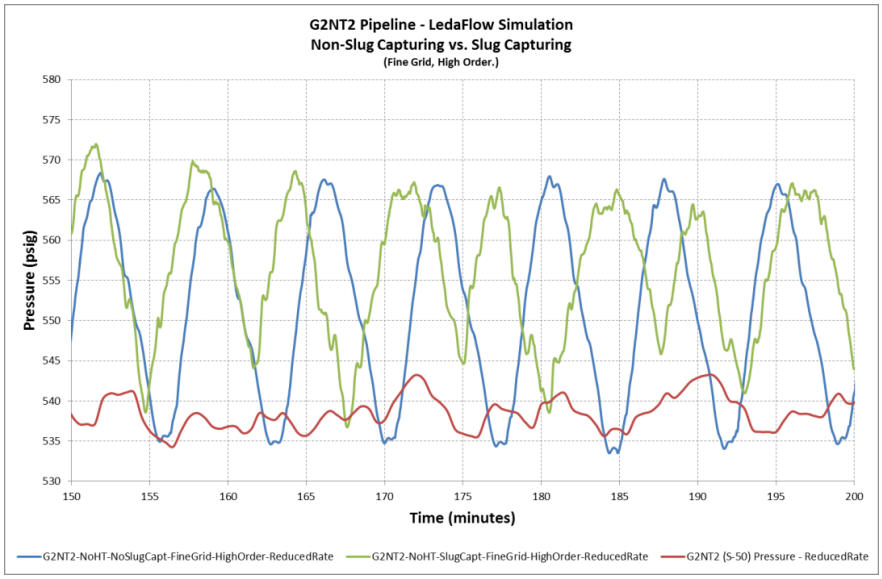

Figure 5-129: G2NT2 LedaFlow Pressure Results – Slug Capturing vs. Non-Slug Capturing Simulations (Fine Grid)

The LedaFlow holdup simulation results, with coarse grid, indicate good agreement in terms of amplitude for the cases with and without slug capturing. However the shape of the slugs in the slug capturing case was different as it had a higher holdup over most of the slug period. The frequency was still the same as it reflected the pressure fluctuations of approximately (8) minutes, as shown in Figure 5-130.

Using a fine grid with (5) meter sections the results were mostly similar to those of the coarse grid cases except for few more small hydrodynamic slugs, as shown in Figure 5-131.

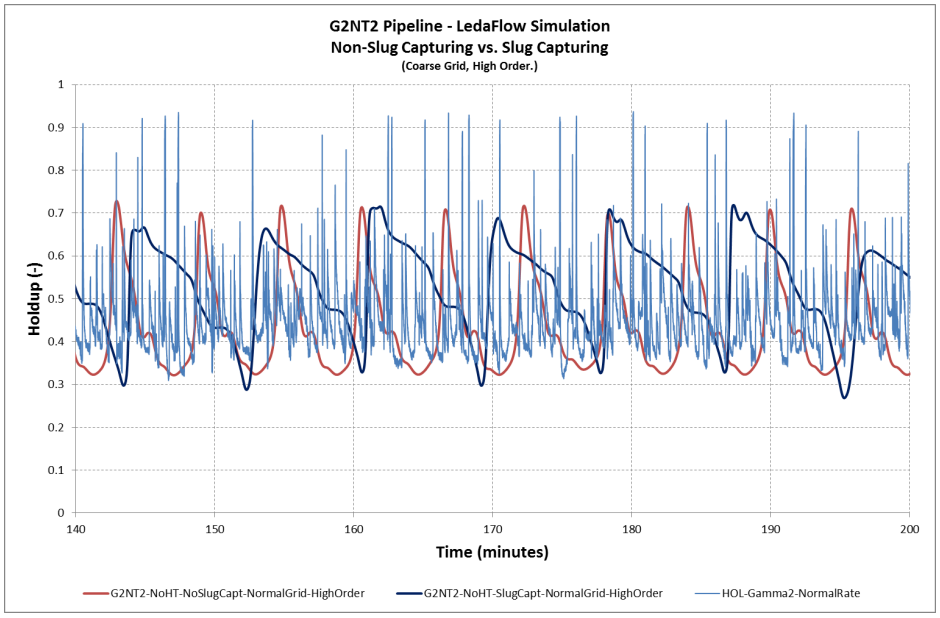

Figure 5-130: G2NT2 LedaFlow Holdup – Slug Capturing vs. Non-Slug Capturing Simulations (Coarse Grid)

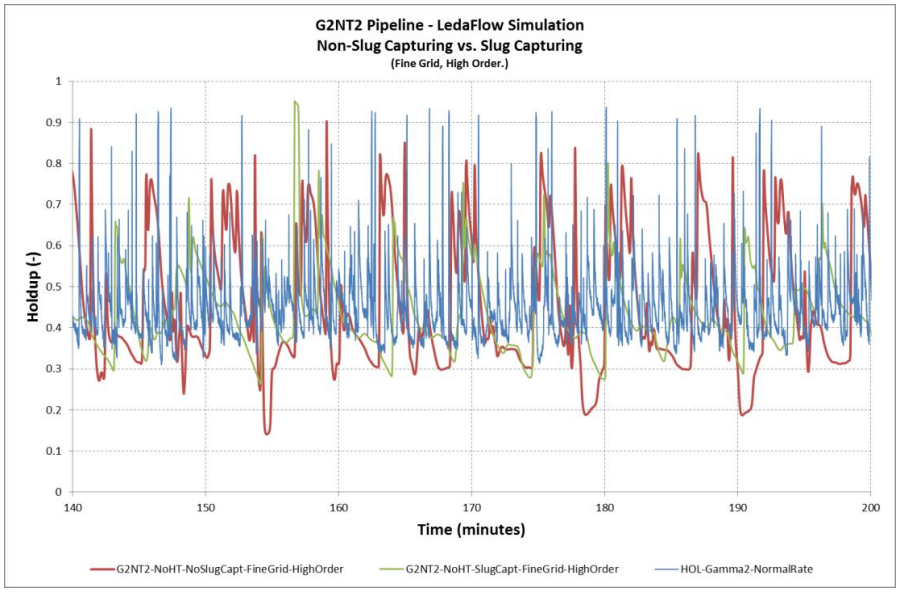

Figure 5-131: G2NT2 LedaFlow Holdup – Slug Capturing vs. Non-Slug Capturing Simulations (Fine Grid)

5.3.9. G2NT2 OLGA and LedaFlow Simulation Conclusions

- OLGA with no-slug tracking provided the best OLGA results.
- Utilizing a fine grid provided a slight improvement of the results in OLGA.
- LedaFlow did not provide satisfactory results.
- Utilizing a fine grid or enabling the slug capturing module did not help in improving the results in LedaFlow.

5.3.10. G2NT2 Pipeline – Slug Valve Analysis

A quick evaluation of the optimum choke settings that would have provided the best results for this particular pipeline was conducted using both OLGA and LedaFlow simulation packages. The study utilized a coarse grid, normal flow and non-slug tracking / non-slug capturing OLGA and LedaFlow cases a long with various choke fixed manual settings. Each valve setting, shown in Table **5-8**, was simulated for two hours before moving to the next setting and the study reported the pipeline inlet pressure as shown in Figure 5-132 and Figure 5-133 for OLGA and LedaFlow results.

These results further confirm the phenomenon that was observed earlier at G1ST3 pipeline where slugs start to decrease in amplitude and gradually disappear with less choking of the slug valve.

The phenomenon which will be further analyzed in the lab experiments section indicates a behavior where small waves or slugs accumulate at the valve tight opening that causes the upstream gas to be compressed which in turn results in higher pressure oscillation in the pipeline system.

Table 5-8: G2NT2 Pipeline Choke Opening Settings

	OLGA Choke Opening (%)	LedaFlow Choke Opening (%)	Simulation Time (hrs) Start - Finish
1.	3 %	4 %	0 – 2
2.	5 %	4 %	2 – 4
3.	6.6 %	5 %	4 – 6
4.	8 %	8 %	6 – 8
5.	10 %	10 %	8 – 10
6.	20 %	20 %	10 – 12
7.	40 %	40 %	12 – 14
8.	60 %	60 %	14 – 16
9.	80 %	80 %	16 – 18
10.	100 %	100 %	18 – 20

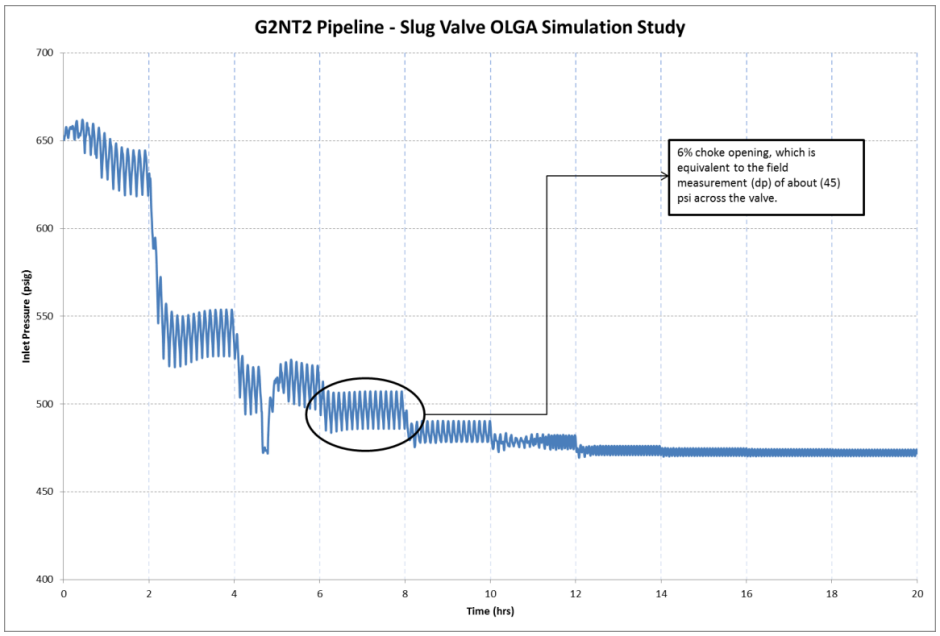

Figure 5-132: G2NT2 Pipeline – Slug Valve OLGA Simulation Study – (Coarse Grid, 2nd Order, No-SlugTracking)

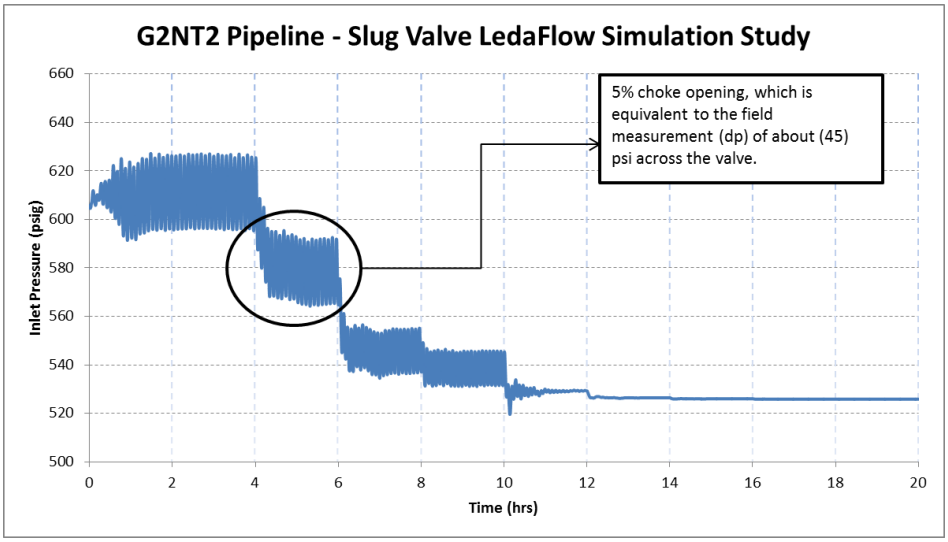

Figure 5-133: G2NT2 Pipeline – Slug Valve LedaFlow Simulation Study – (Coarse Grid, High Order, No-SlugCapturing)

5.4. G3ST1 Pipeline Results

G3ST1 measurements were conducted over two days on June 3, 1999, upstream of the slug valve and on June 5, 1999, downstream of the slug valve.

5.4.1. Pipeline Profile Details

The total pipeline length is approximately 18 Km and starts from Sabkhah 98 (S-98) to GOSP-3 going through Sabkhah 94 (S-94), Sabkhah 91 (S-91), Sabkhah 85 (S-85), Sabkhah 81 (S-81) and Sabkhah 80 (S-80). The pipeline has four (4) very high hills with heights that are approximately 80 to 100 meters. It also has one small hill that is 30 meter high. The pipeline has two different diameters 16 inch and 20 inch as shown on Figure 5-134.

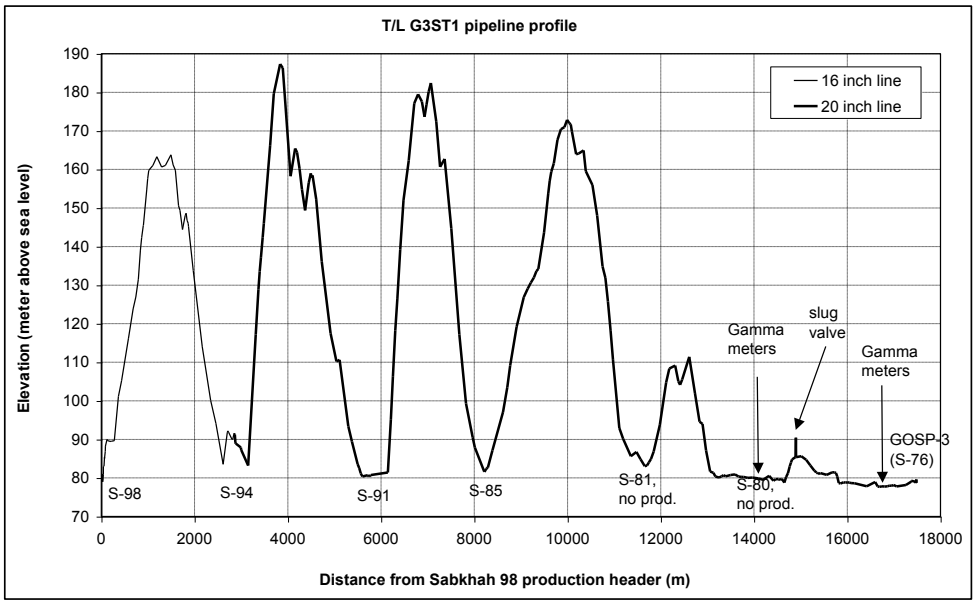

Figure 5-134: G3ST1 pipeline profile - slug valve and gamma densitometer locations

For the upstream measurement, the distance between the gamma meters was set at 54.1 m, while the pipeline inclination angle was measured at +0.16 degrees. The distance of the gammas to the downstream slug valve was measured at approximately 450 meters. In addition the distance from the gamma meters to GOSP-2 was approximately measured at 3.2 Km. The pipeline wall thickness was measured using ultra sonic measurement device at 0.63 inch (16 mm).

On the other hand, during the downstream measurement, the distance between the gamma meters was set at 46.0 m, while the pipeline inclination angle was measured at -0.06 degrees. The distance of the gammas to the upstream slug valve was measured at approximately 2.1 Km. In addition the distance from the gamma meters to GOSP-2 was approximately measured at 650 meters. The pipeline wall thickness was measured using ultra sonic measurement device at 0.787 inch (20 mm). The GOSP-2 pressure was set at 400 psig during the measurement period.

The measurements were made at a normal production rate of 76,400 BBL/Day at standard conditions. The flow rates were based on forecasts made by the production engineers and no flow rate measurements were carried out at the time of the experiments. The flow rates from each Sabkhah were estimated as follows:

Sabkhah	Flow Rate (BBL/Day) @ std. cond.
S-98	4,700
S-94	35,500
S-91	17,300
S-85	18,900
S-81	No Production
S-80	No Production
Total	**76,400**

The superficial gas and liquid velocities ranged from (0.6 to 4.1) m/sec for gas and (0.3 to 2.5) m/sec for liquid, based on OLGA predictions.

5.4.2. Production Header Time Series

The pressure logs at the producing Sabkhahs were not available from the DCS system due to a malfunction in the system. Therefore, a separate standalone pressure logging device was installed at (S-98) and (S-91). The (S-91) pressure log was obtained on June 4, 1999 on non-measurement period, while (S-98) pressure logs were taken on June 3, 1999 and June 5, 1999 during the upstream and downstream measurement periods.

The Sabkhah 98 pressure log indicates an approximately 20 minutes pressure cycles. One also observes that the pressure sinks deeper every two or three cycles which indicates an overlaying 40 to 60 minutes cycle with higher amplitudes. The pressure generally oscillates between 770 psig and 825 psig with a pressure fluctuation of 55 psig. This behavior was observed during the two days of measurements at (S-98) as shown on Figure 5-135 and Figure 5-136. Sabkhah 91 pressure log indicates a similar behavior with a cycle of approximately 20 minutes as shown on Figure 5-137. Unfortunately the pressure at S-91 was logged for a short period only and therefore no information could be obtained regarding the overlaying longer period oscillations from this location.

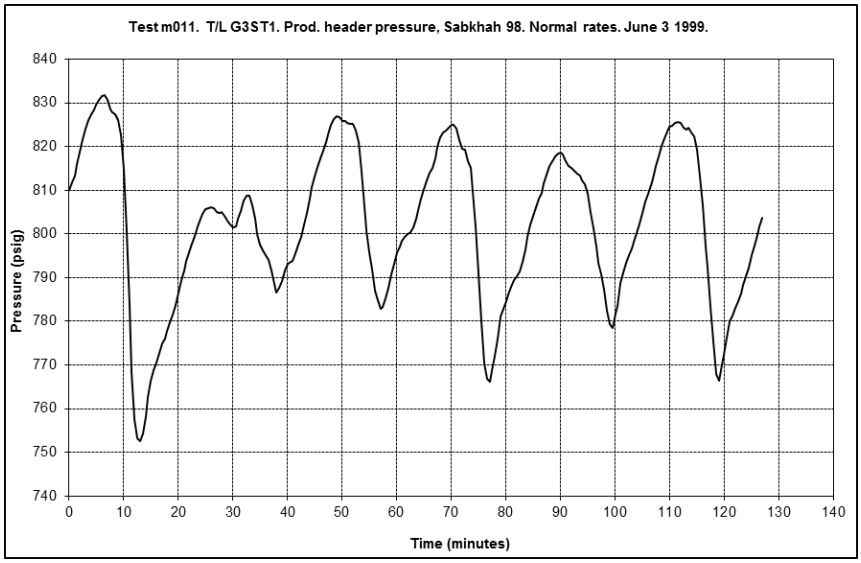

Figure 5-135: G3ST1 Production header pressure at S-98, Normal rate, June 3, 1999, (Upstream SV)

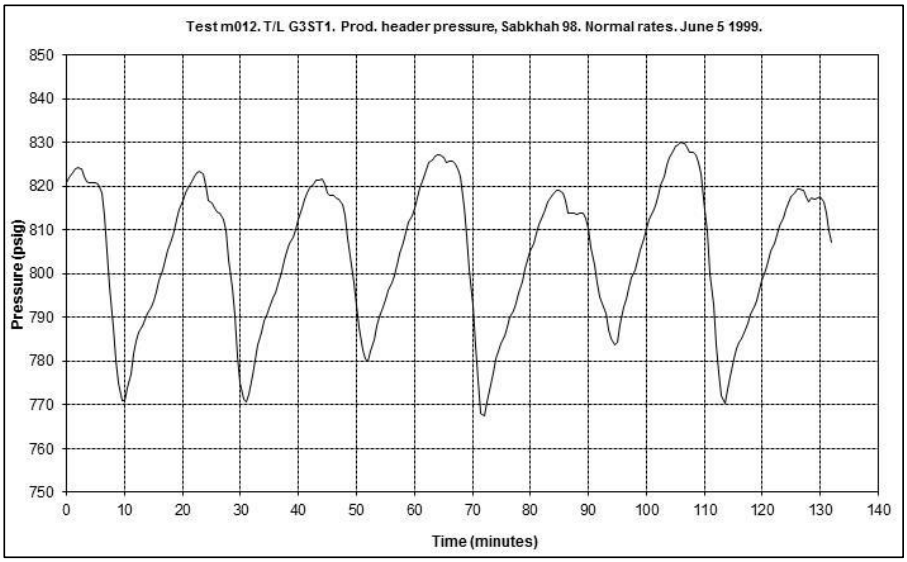

Figure 5-136: G3ST1 Production header pressure at S-98, Normal rate, June 5, 1999, (Downstream SV)

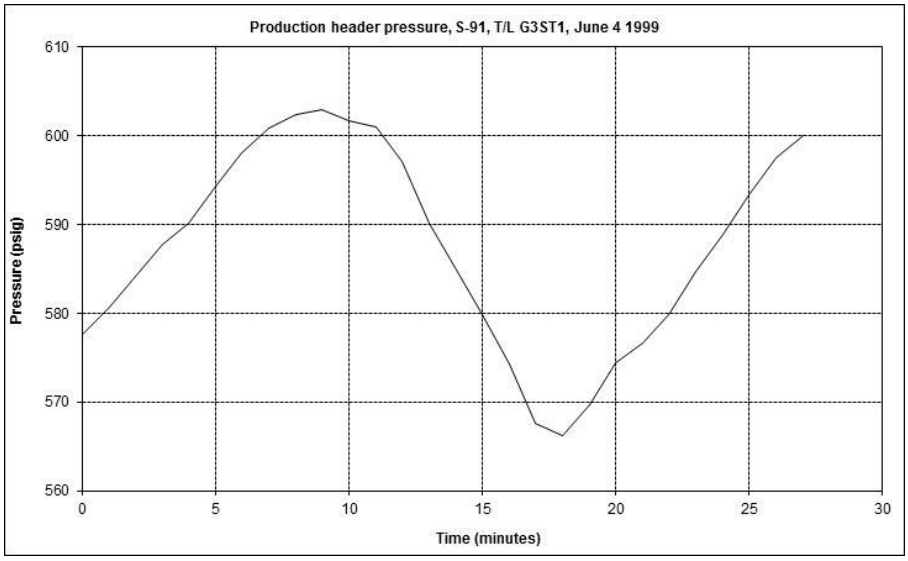

Figure 5-137: G3ST1 Production header pressure at S-91, Normal rate, June 4, 1999,

5.4.3. Slug Valve Pressure Drop

The pressure drop across the slug valve was logged during the measurement tests using Foxboro absolute pressure transmitters, which were installed in the same positions of the pressure manometers across the slug valve. The tabs of the manometers were installed approximately (1) meter upstream and downstream of the slug valve as shown in Figure 5-138. The pressure signals were sampled at 2 Hz over a period of 130 minutes.

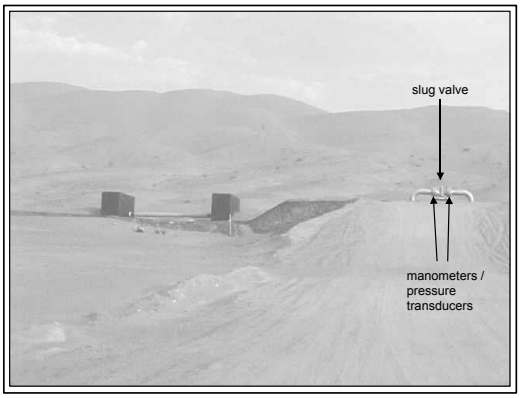

Figure 5-138: Arrangement of the slug valve, T/L G3ST1

The pressure measurements shown in Figure 5-139, shows a pressure cycle of approximately 30 psi every 15 to 20 minutes. The upstream pressure varies between 430 to 460 psig while the downstream pressure varies between 400 and 430 psig. The differential pressure across the valve varies between 10 and 40 psi with an average value of 25 psi as shown in Figure 5-140.

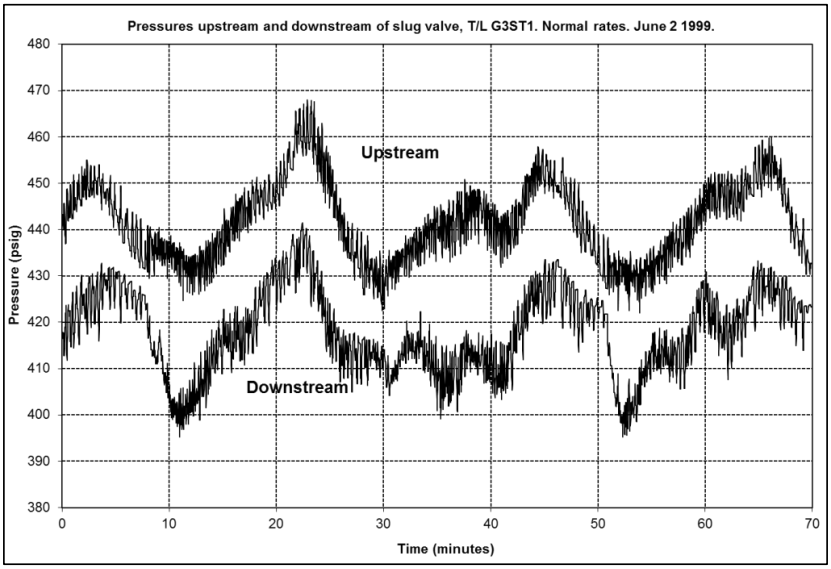

Figure 5-139: G3ST1 Pressure upstream and downstream of slug valve, Normal rate, June 2, 1999

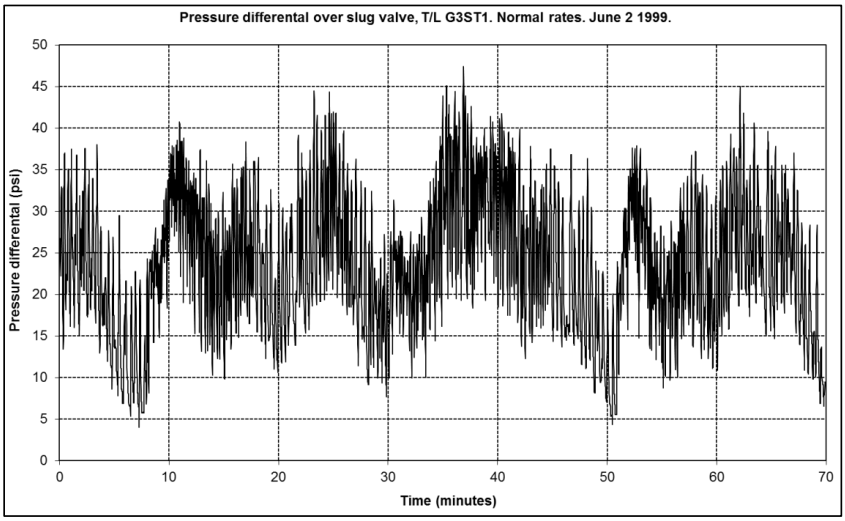

Figure 5-140: G3ST1 Pressure differential across slug valve, Normal rate, June 2, 1999

5.4.4. Analysis of Holdup Time Series – Upstream Slug Valve

Analyzing the holdup time series upstream the slug valve shown in figures Figure 5-141 and Figure 5-142, one observes a clear slugging pattern that repeats itself every 20 minutes. This is in line with the pressure logging at (S-98) that showed a 20 minutes periodic behavior. The peak of the slugs reaches a holdup of approximately (0.90) at both gamma locations. On the other hand, the liquid film holdup for Gamma-1 was approximately at (0.2), while the liquid file holdup at Gamma-2 was slightly higher at approximately (0.3). Examining the details of each slug cycle shown in Figure 5-143, one could notice a small group of hydrodynamic slugs at the front of the slug cycle for approximately (5) minutes followed by a wavy flow that extends for the remaining (15) minutes.

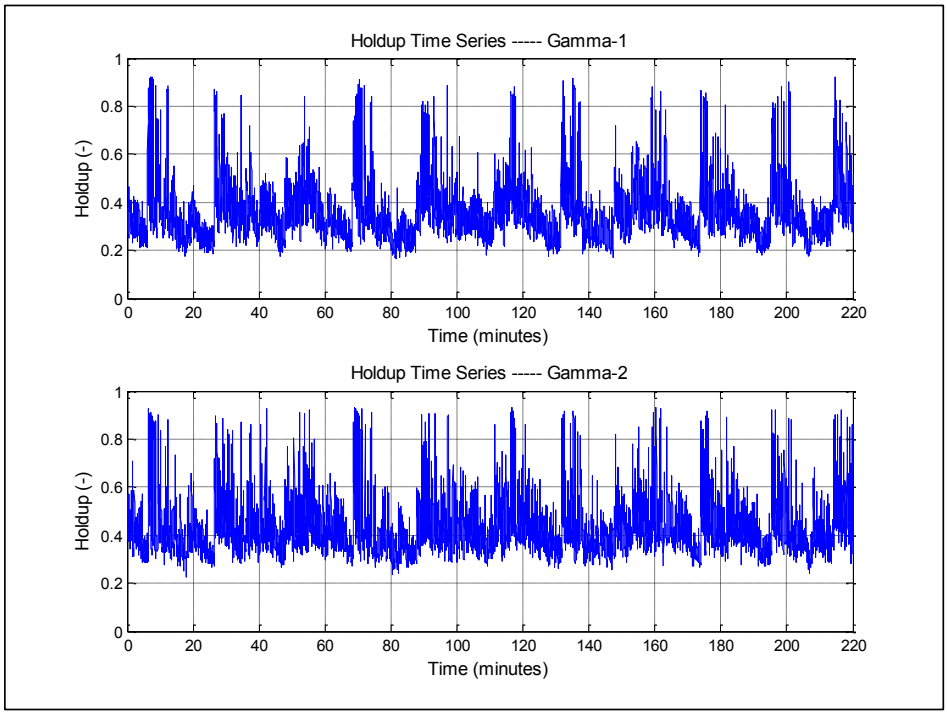

Figure 5-141: G3ST1 Holdup time series, Upstream Slug Valve, (220 minutes)-(Gamma-1&2)

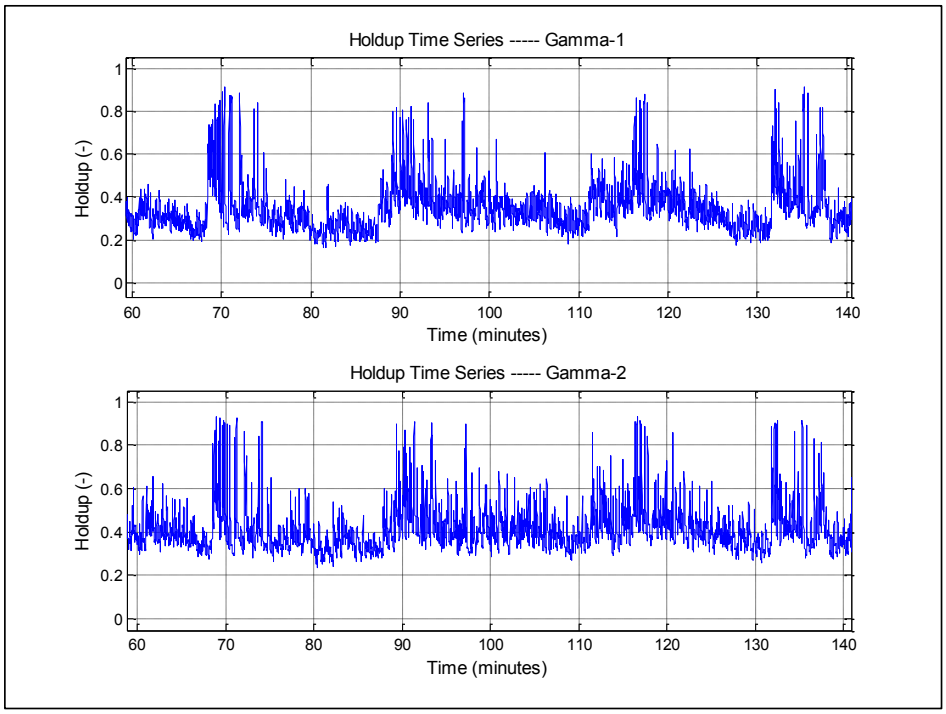

Figure 5-142: G3ST1 Holdup time series, Upstream Slug Valve, (80 minutes)-(Gamma-1&2)

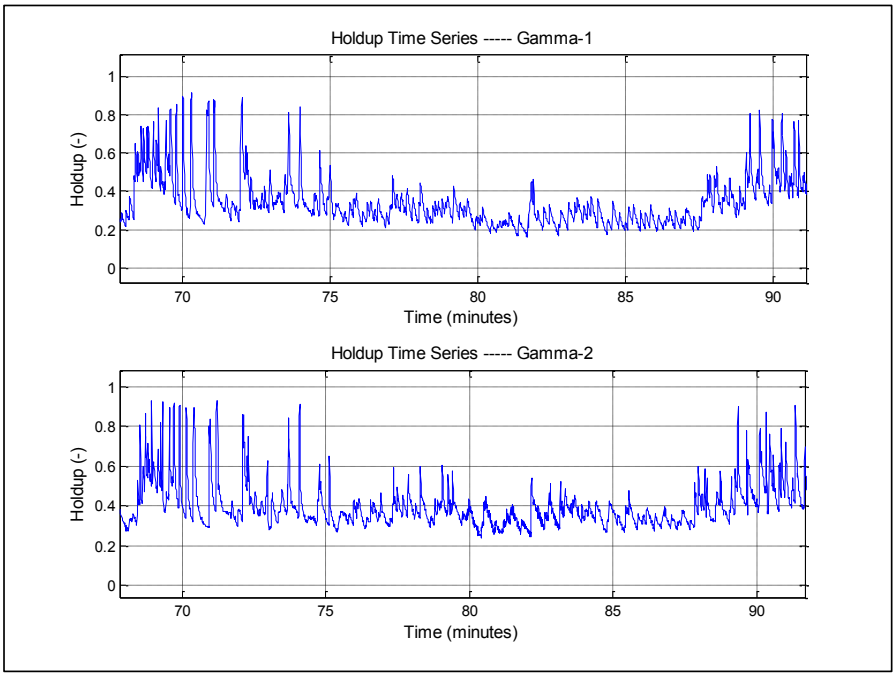

Figure 5-143: G3ST1 Holdup time series, Upstream Slug Valve, (20 minutes)-(Gamma-1&2)

Cross correlating the time series gives a time delay of 8.5 seconds, as shown in Figure 5-144. Using the distance between the gammas of (54.1) meters and the time delay, one would obtain the average slug velocity at (6.36) m/sec.

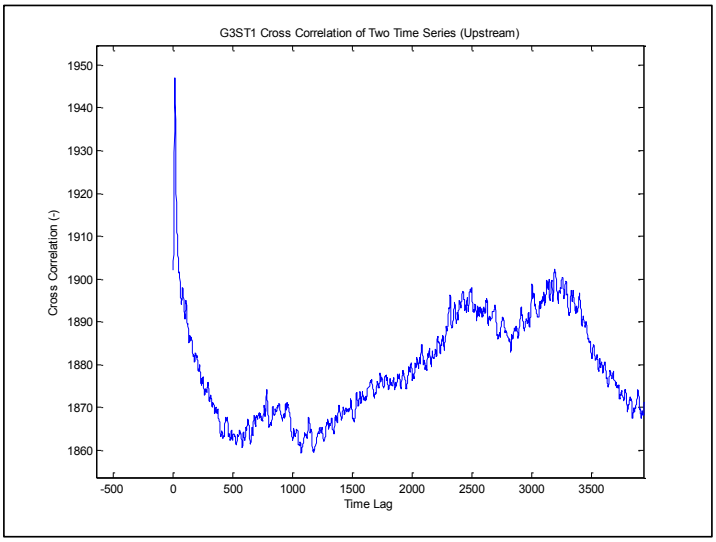

Figure 5-144: G3ST1 Cross Correlation of Two Gammas – Upstream Slug Valve

Despite the low number of slugs detected, statistical analysis was carried out using the available data to extract information related to slugs' length, velocity and frequency. The time between slugs shown in Figure 5-145, indicates a slug frequency of (20) minutes as expected. On the other hand, the slug length

shown on Figure 5-146, indicated long slugs which ranges between 500 to 6000 meters. The distribution of the average front and tail velocities is shown in Figure 5-147, indicates an average velocity that ranges between 2 and 7 m/sec.

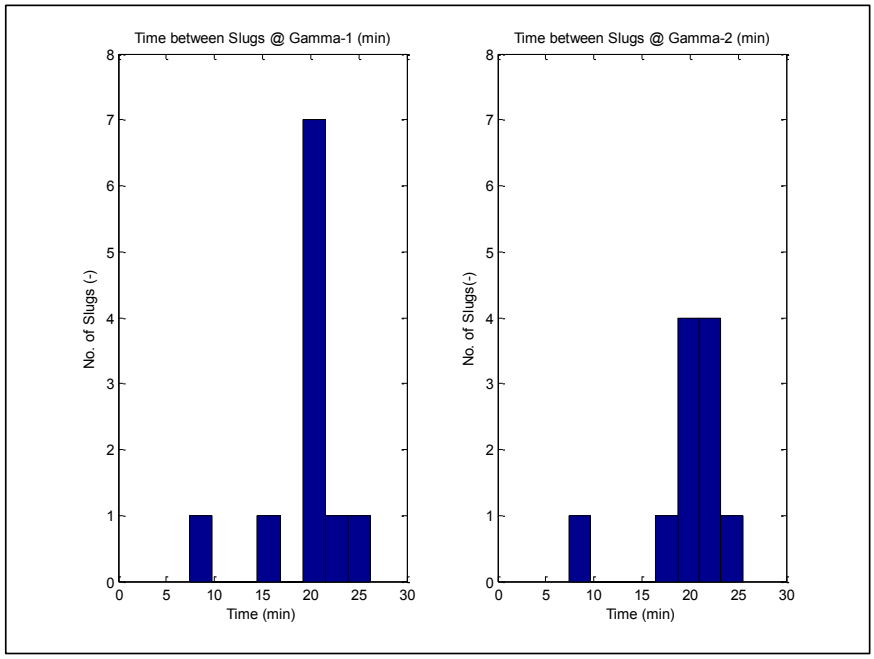

Figure 5-145: G3ST1 Slug Frequency Distribution (minutes) – Upstream Slug Valve

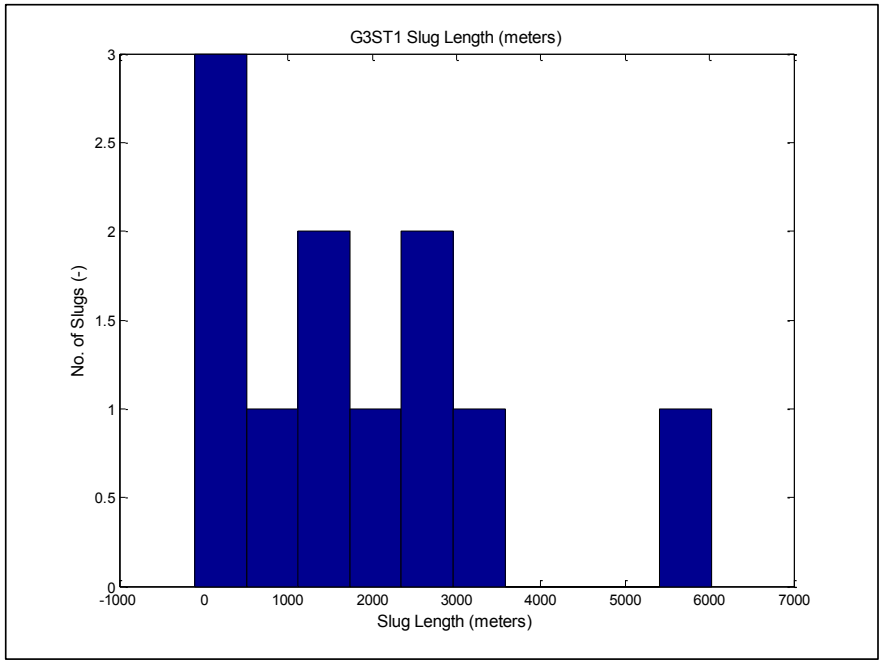

Figure 5-146: G3ST1 Slug Length Distribution (meters) – Upstream Slug Valve

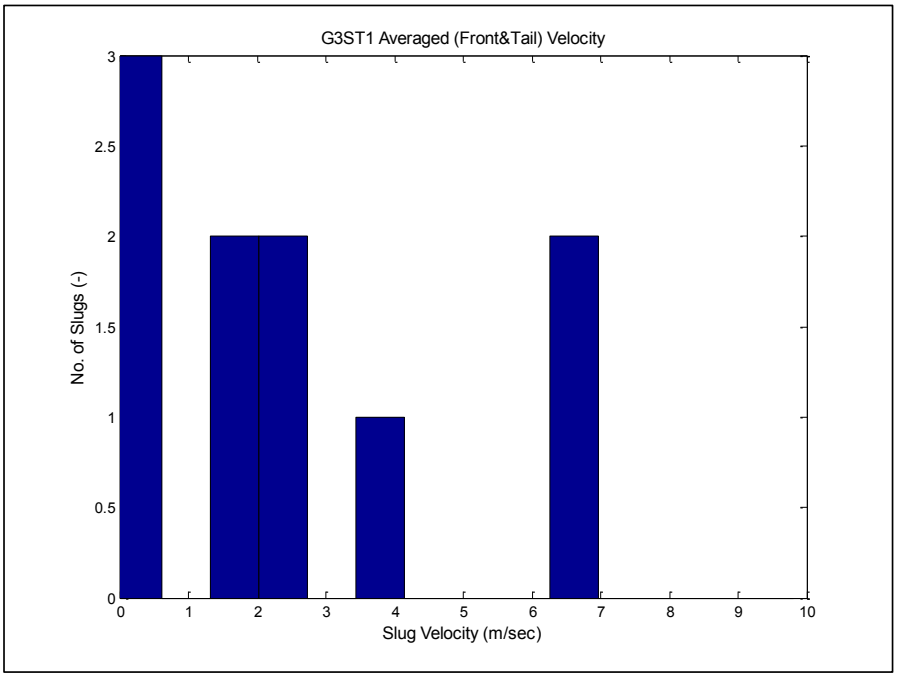

Figure 5-147: G3ST1 Average Front & Tail Velocity Distribution (m/sec) – Upstream Slug Valve

5.4.5. Analysis of Holdup Time Series – Downstream Slug Valve

Analyzing the holdup time series downstream of the slug valve in figures Figure 5-148 and Figure 5-149, one observes a similar behavior to the one shown in the upstream section with clear slugging pattern that repeats itself every 20 minutes. This is in line with the pressure logging at (S-98) that showed a 20 minutes periodic behavior. The peak of the slugs reaches a holdup of approximately (0.90) at both gamma locations. On the other hand, the liquid film holdup at both Gamma-1 and Gamma-2 was approximately at (0.2). Examining the details of each slug cycle shown in Figure 5-150, one could notice a small group of hydrodynamic slugs at the front of the slug cycle for approximately (5) minutes followed by a wavy flow that extends for the remaining (15) minutes.

The visual inspection of the time series shows great similarities with the ones observed upstream of the slug valve, which indicates that the slug valve did not have any significant impact on the slug characteristics.

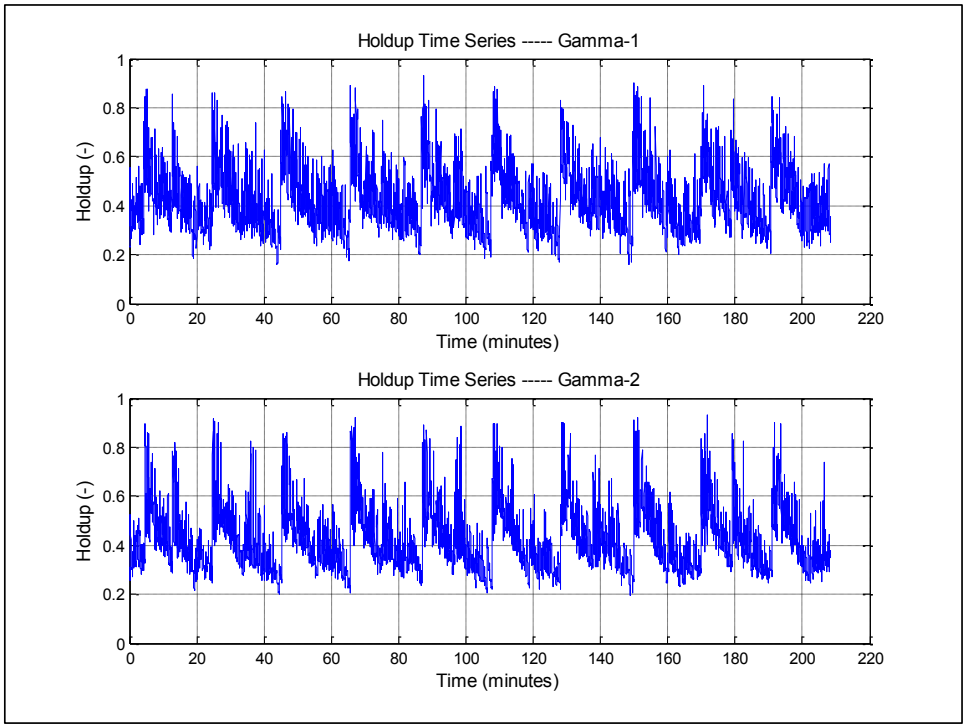

Figure 5-148: G3ST1 Holdup time series, Downstream Slug Valve, (220 minutes)-(Gamma-1&2)

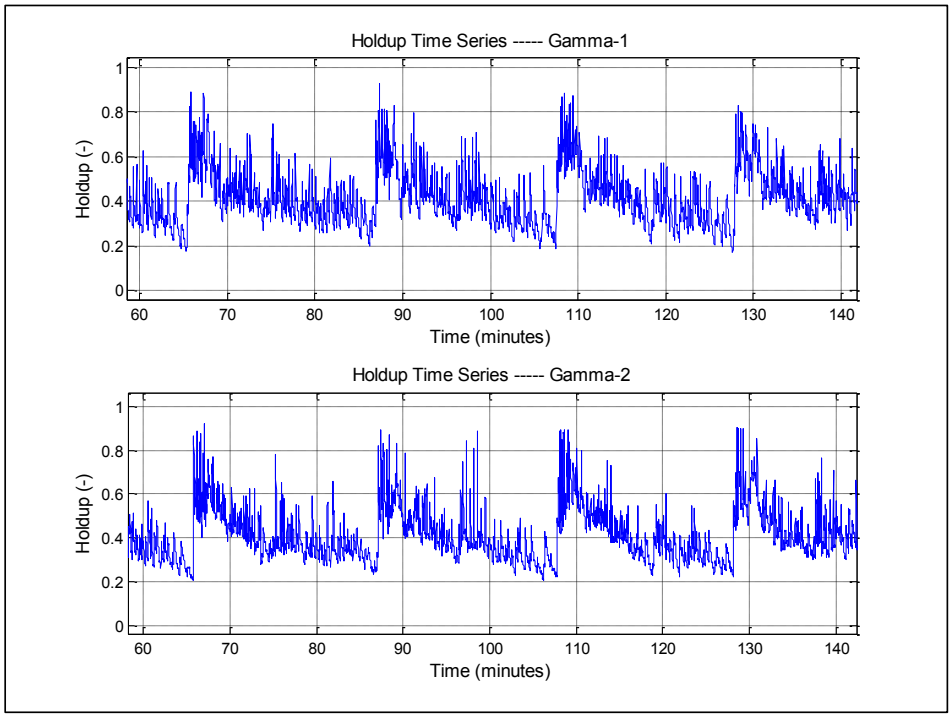

Figure 5-149: G3ST1 Holdup time series, Downstream Slug Valve, (80 minutes)-(Gamma-1&2)

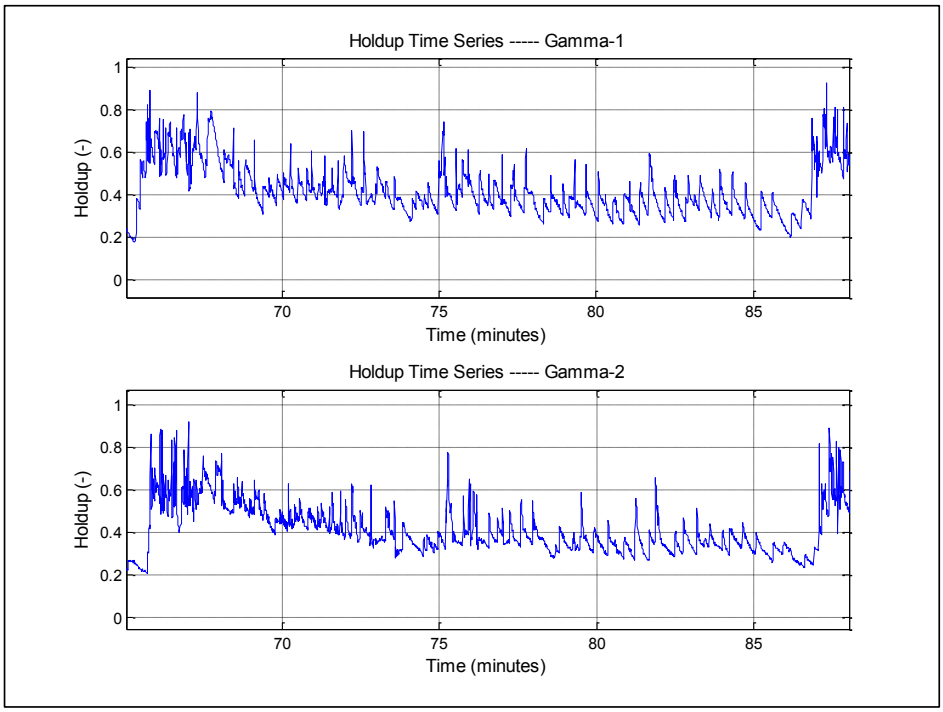

Figure 5-150: G3ST1 Holdup time series, Downstream Slug Valve, (20 minutes)-(Gamma-1&2)

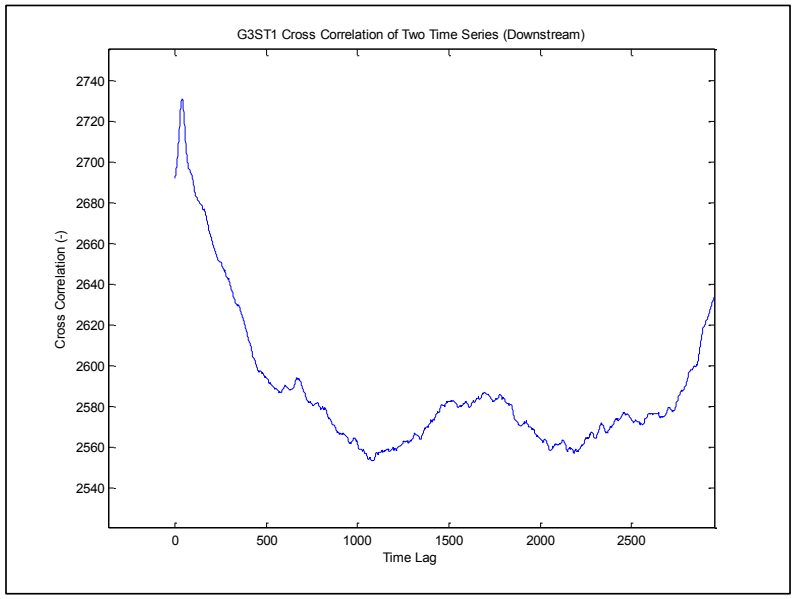

Figure 5-151: G3ST1 Cross Correlation of Two Gammas – Downstream Slug Valve

Cross correlating the time series gives a time delay of 16.8 seconds, as shown in Figure 5-151. Using the distance between the gammas of (46) meters and the time delay, one would obtain the average slug velocity at (2.74) m/sec. This indicates a much lower velocity compared to the one calculated upstream of the slug valve at (6.36) m/sec. The slowdown of the slugs could be attributed to the existence of the slug valve which slightly decrease the flow rate. In addition, the long straight section after the slug valve, approximately one (1) Km further slows down the slugs compared to the upstream position which was situated immediately at the end of a steep hill.

5.4.6. G3ST1 Pipeline Simulation

Extensive simulation work was conducted using OLGA and LedaFlow. The simulation pressure results were compared against pressure field measurements recorded on June 5, 1999, while the holdup results were compared against upstream and downstream slug valve field measurements.

5.4.7. G3ST1 Pipeline OLGA Simulations

OLGA simulation was carried out with various options to fully test the simulation package capabilities to predict slugging phenomena in the subject pipeline. Using 2nd order scheme for mass equations and an adiabatic heat transfer option, the other simulation parameters which were varied for G3ST1 pipeline are as follows:

- Slug tracking (No slug tracking vs. slug tracking with various delay constants)
- Grid size (Coarse grid vs. Fine grid)

G3ST1 Pipeline OLGA Simulation – (Slug Tracking vs. No Slug Tracking)

OLGA Simulations were carried out with and without slug tracking module. The results were plotted for various Delay Constants (DCs), which significantly impact the initiation of slugs in OLGA code.

Using an average liquid velocity of (6.36) m/sec obtained from the cross correlation of the two gamma meters upstream the slug valve, one can estimate the idle time between slug initiations as follows:

Table 5-9: G3ST1 – Idle time between slug initiations for various delay constants

Idle time between Slug Initiation (DT) (sec)	Ul (m/sec)	Inner Dia. (m)	DC
3.68	6.36	0.468	50
11.04	6.36	0.468	150
36.8	6.36	0.468	500
58.9	6.36	0.468	800

OLGA simulations were carried out with delay constants ranging from 50 to 800. The holdup results for the upstream position are shown on figures Figure 5-152, Figure 5-153, Figure 5-154 and Figure 5-155. Analysis of the holdup figures shows that with no slug tracking, the holdup cycles are fixed at (14) minutes with very stable and repetitive slug behavior, which is slightly shorter than the slugging frequency that was observed at the field measurements of approximately (20) minutes. The holdup fluctuates between (0.30) and (0.82), which agrees well with the holdup amplitude for field measurements as shown in Figure 5-115.

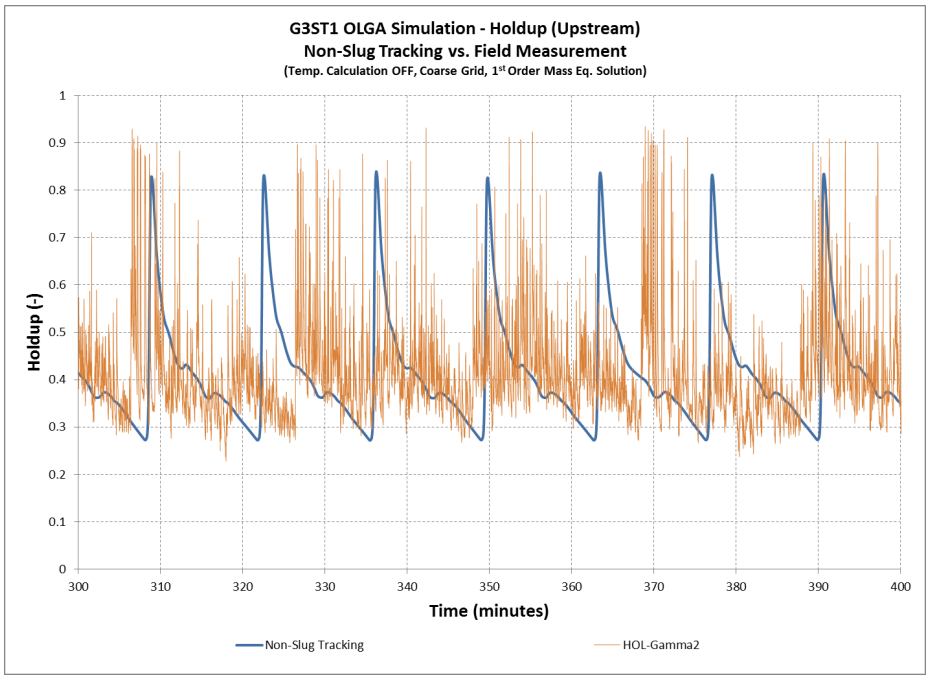

Figure 5-152: G3ST1 OLGA Holdup Simulation – Non-Slug Tracking vs. Holdup Measurement (Upstream)

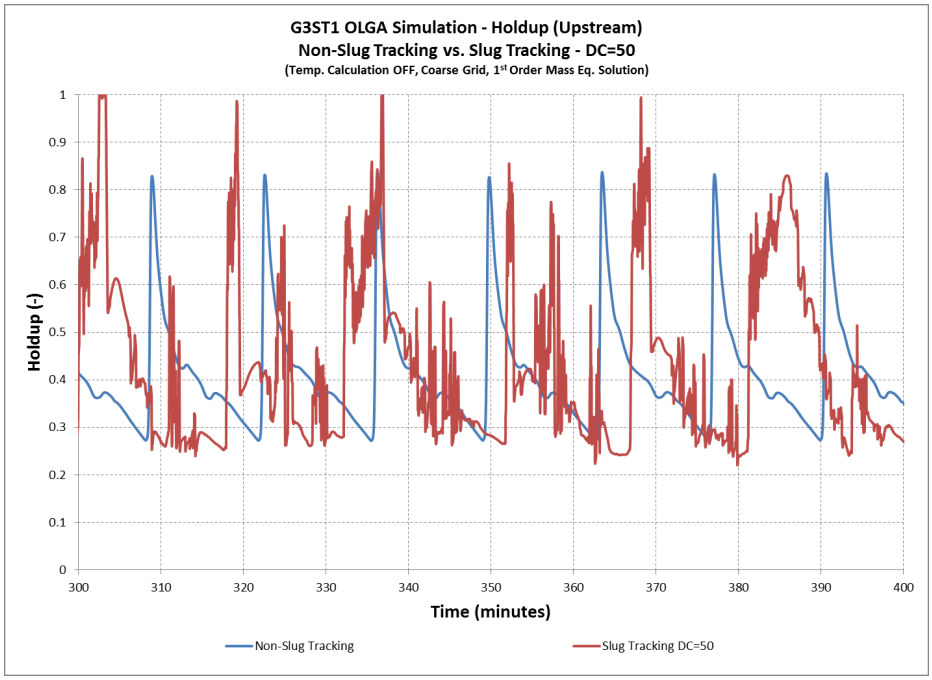

Figure 5-153: G3ST1 OLGA Holdup Simulation – Non-Slug Tracking vs. Slug Tracking (DC=50) – (Upstream)

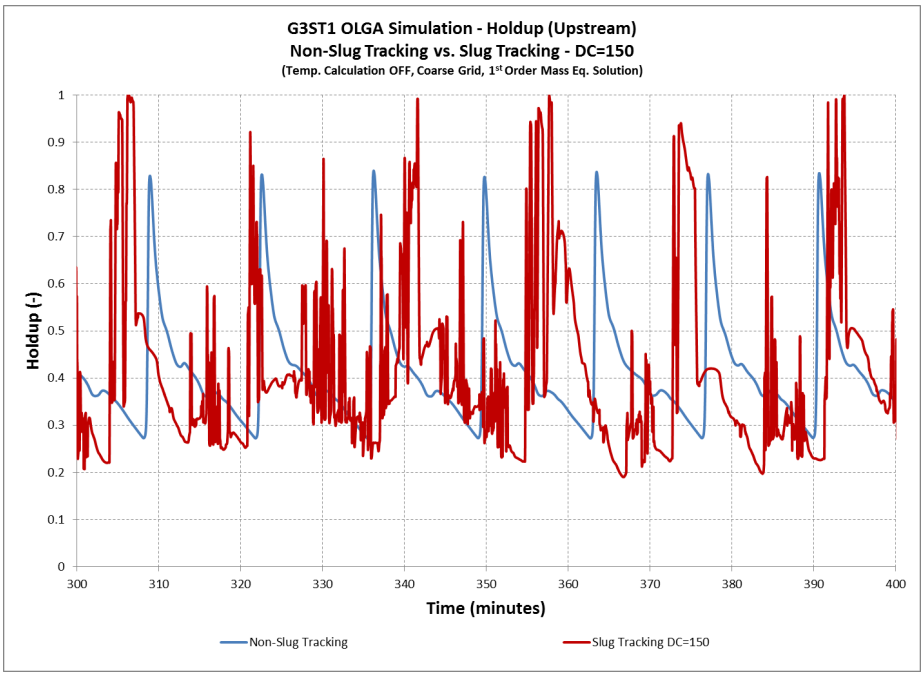

Figure 5-154: G3ST1 OLGA Holdup Simulation – Non-Slug Tracking vs. Slug Tracking (DC=150) – (Upstream)

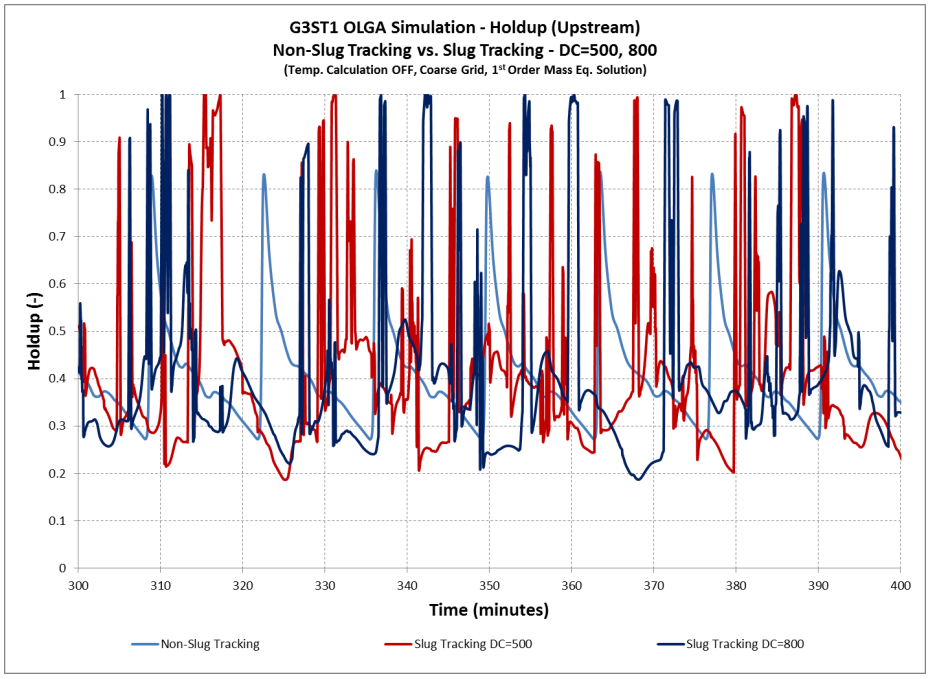

Figure 5-155: G3ST1 OLGA Holdup Simulation – Non-Slug Tracking vs. Slug Tracking (DC=500, 800) – (Upstream)

When slug tracking module is enabled, OLGA creates few hydrodynamic slugs between the large terrain slugs but with the same long frequency. However, the amplitude of the holdup fluctuations seem to be higher than those with no slug tracking as holdup reaches almost (1.0) as shown in Figure 5-153, Figure 5-154 and Figure 5-155.

The downstream holdup OLGA simulation results shows similar behavior and accuracy level to the ones noted upstream of the slug valve, see figures Figure 5-156, Figure 5-157 and Figure 5-158.

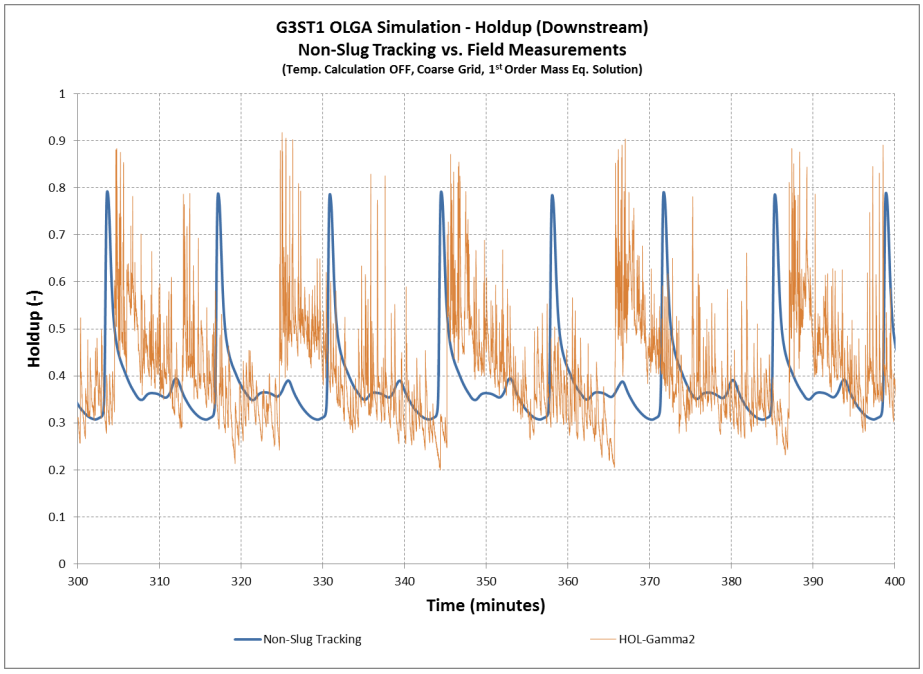

Figure 5-156: G3ST1 OLGA Holdup Simulation – Non-Slug Tracking vs. Holdup Measurement (Downstream)

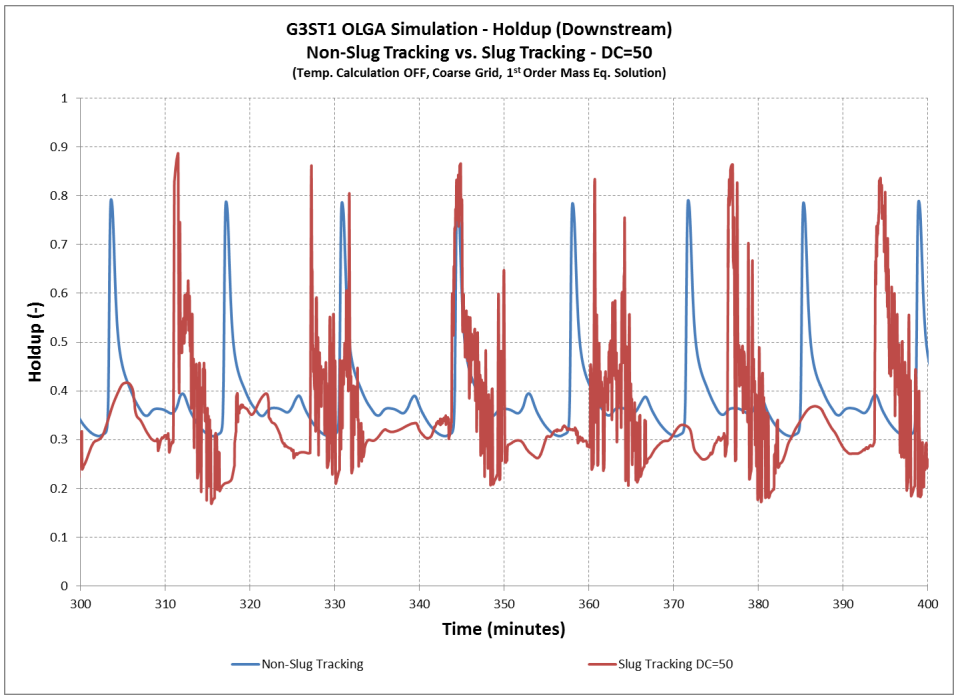

Figure 5-157: G3ST1 OLGA Holdup Simulation – Non-Slug Tracking vs. Slug Tracking (DC=50) – (Downstream)

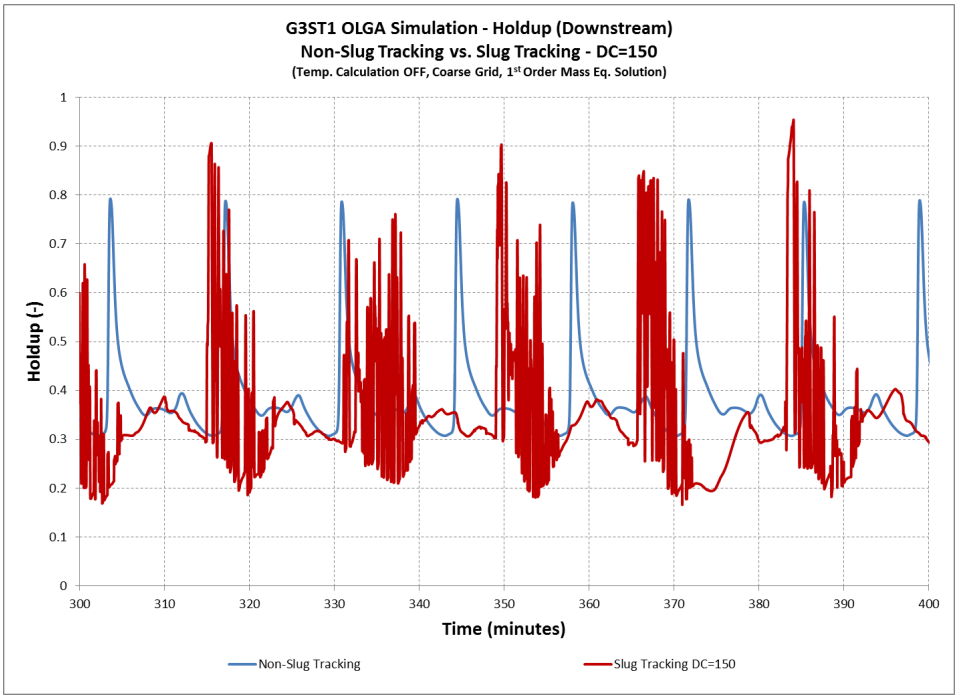

Figure 5-158: G3ST1 OLGA Holdup Simulation – Non-Slug Tracking vs. Slug Tracking (DC=150) – (Downstream)

Comparing field pressure measurements at (S-98) on June 5, 1999 versus OLGA simulation pressure results, one could notice a good agreement in terms of pressure amplitude at approximately (50) psi with the case of non-slug tracking, as shown in Figure 5-159. However, the frequency of the pressure oscillations was 14 minutes compared to the 20 minutes noticed in field measurements. Also, the average OLGA pressure prediction at (700) psig was considerably lower than the field measurement at (800) psig.

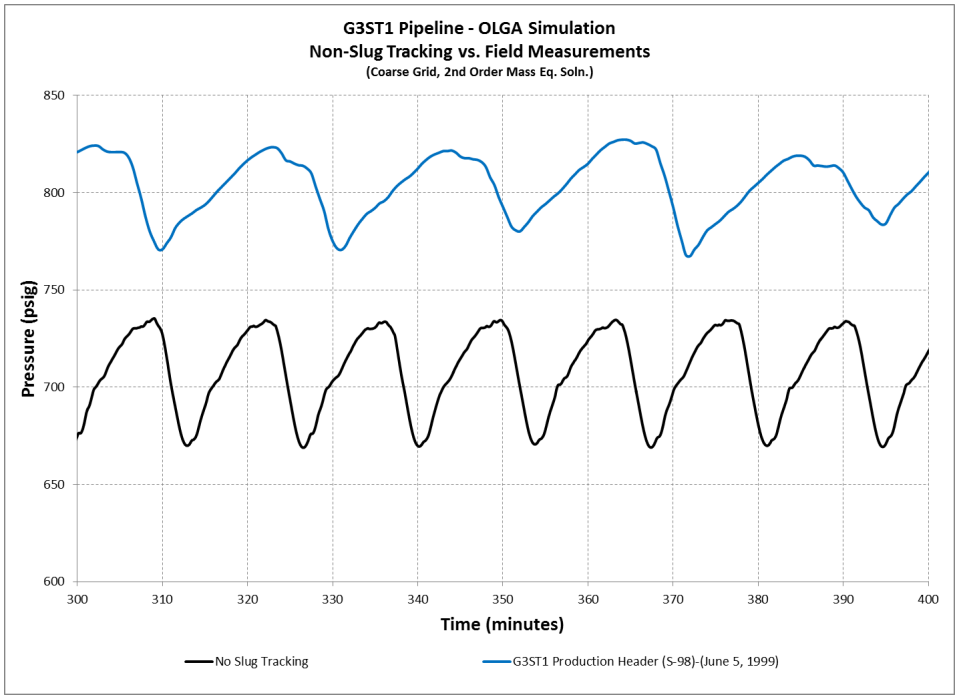

Figure 5-159: G3ST1 OLGA Pressure Results – Non-Slug Tracking vs. Pressure Measurements

OLGA simulations with slug tracking using various delay constants showed same slug frequency at (14) minutes. However, the slug amplitudes were higher, (120) psi, compared to the field measurements, (50) psi, as shown in Figure 5-160, Figure 5-161 and Figure 5-162.

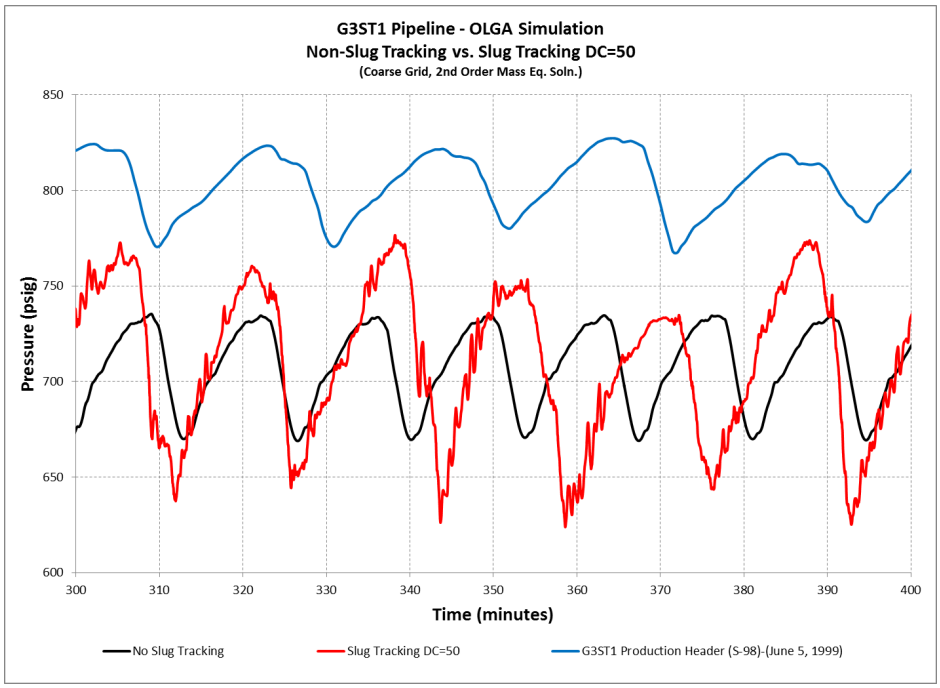

Figure 5-160: G3ST1 OLGA Pressure Results – Non-Slug Tracking vs. Slug Tracking (DC=50)

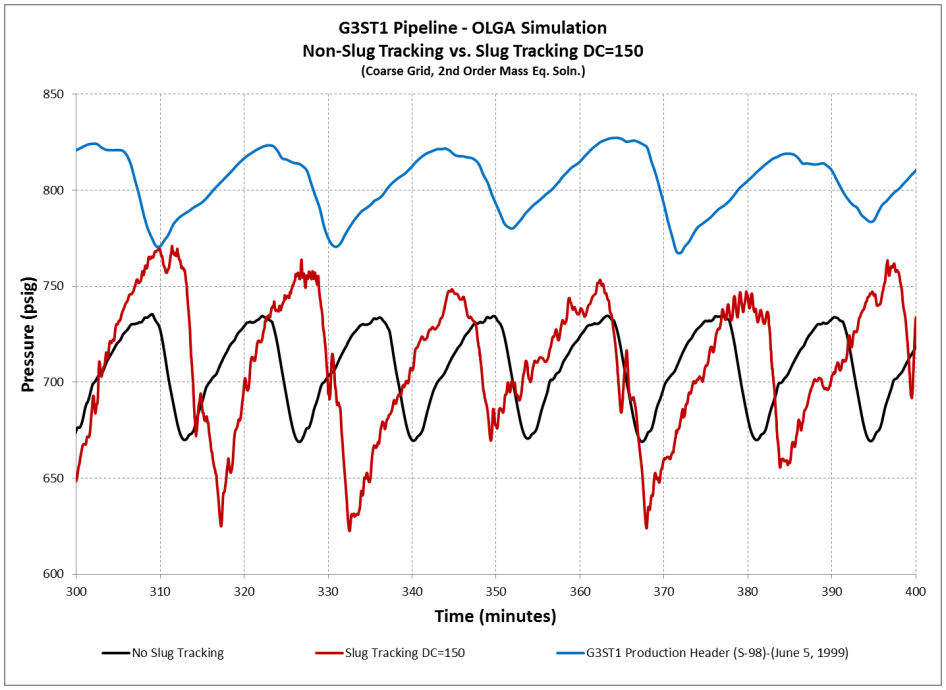

Figure 5-161: G3ST1 OLGA Pressure Results – Non-Slug Tracking vs. Slug Tracking (DC=150)

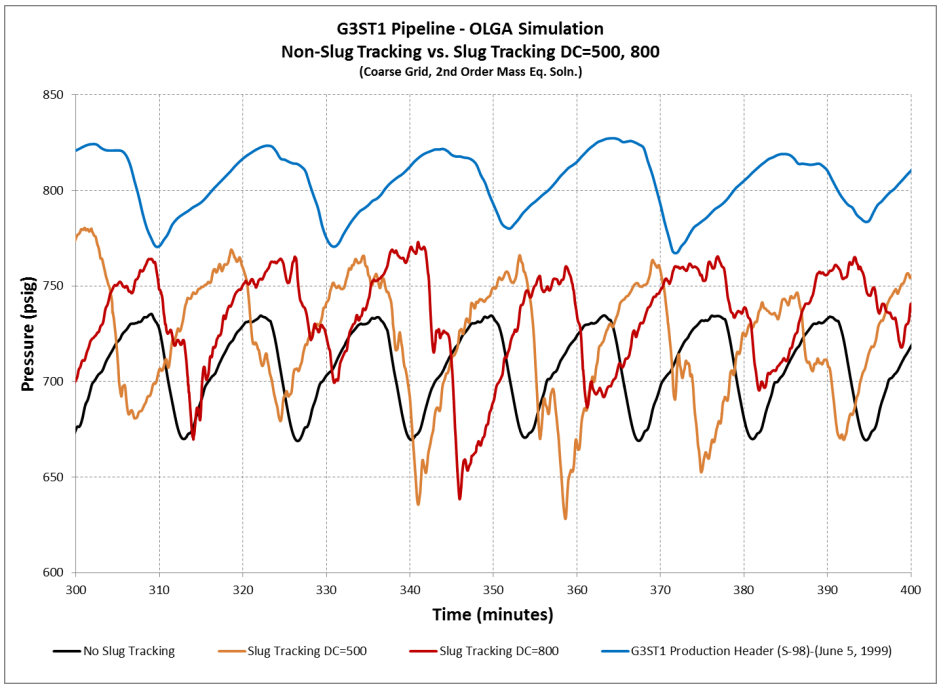

Figure 5-162: G3ST1 OLGA Pressure Results – Non-Slug Tracking vs. Slug Tracking (DC=500, 800)

G3ST1 Pipeline OLGA Simulation – (Coarse Grid vs. Fine Grid)

The previous G3ST1 pipeline OLGA simulations were conducted using a relatively coarse grid with an average pipe section of approximately (50) meters, as shown in Figure 5-163. In order to explore the impact of utilizing a fine grid on OLGA simulations, a fine grid case was simulated using a fixed (5) meters per section as shown in Figure 5-164.

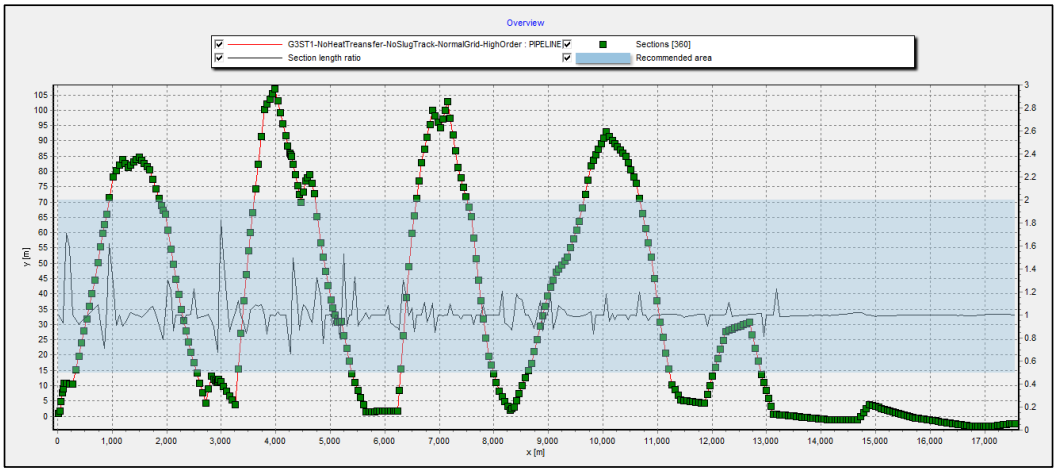

Figure 5-163: G3ST1 Pipeline Sections – OLGA Grid Options (Coarse Grid)

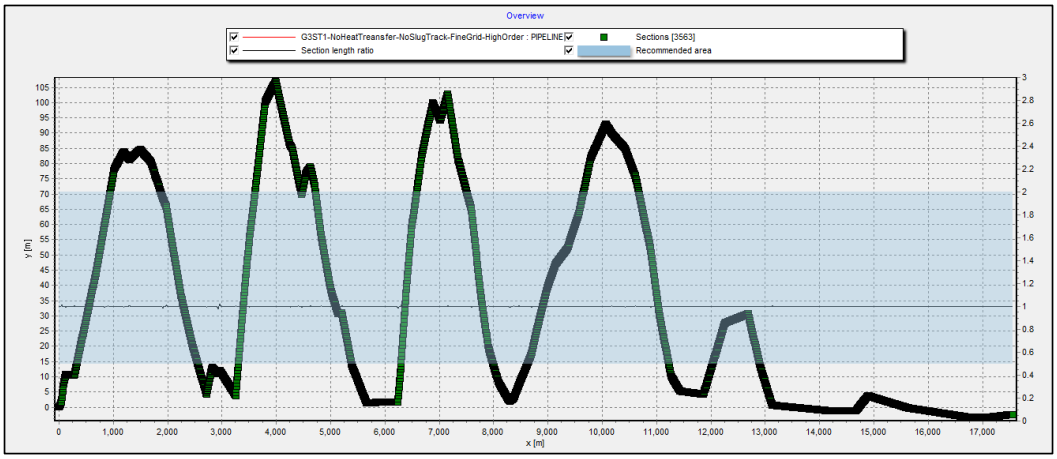

Figure 5-164: G3ST1 Pipeline Sections – (Fine Grid (5 meter))

The upstream and downstream holdup results depicted in Figure 5-165 and Figure 5-166 show a very small difference between the coarse and fine grid cases, where the fine grid case shows higher holdup amplitudes but with similar frequency to the case with the coarse grid.

The pressure results shown in Figure 5-167 indicate similar results for both fine grid and coarse grid cases.

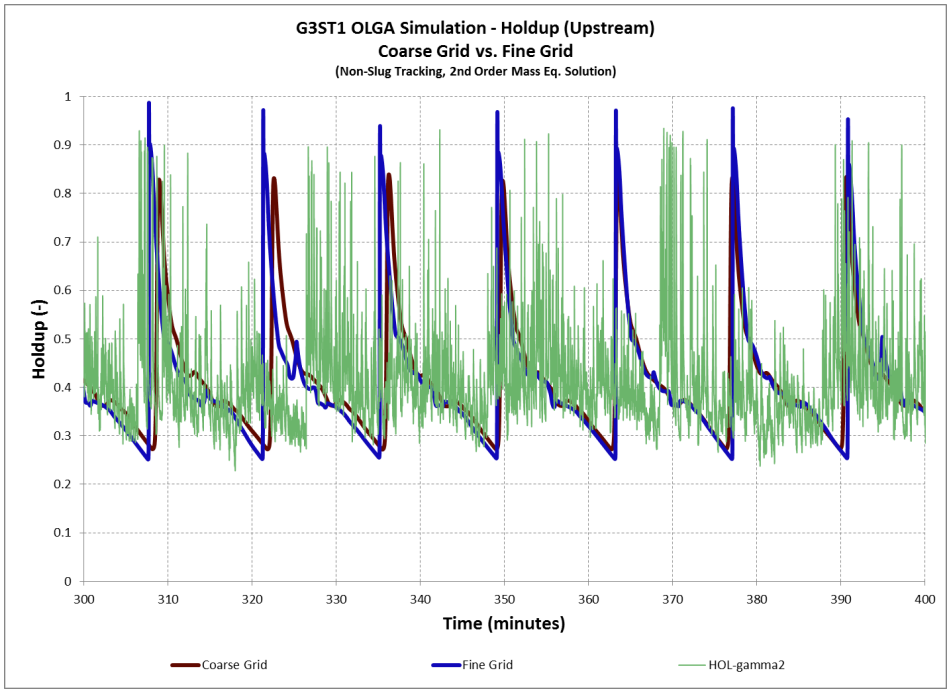

Figure 5-165: G3ST1 OLGA Holdup Simulation – Coarse Grid vs. Fine Grid (Upstream)

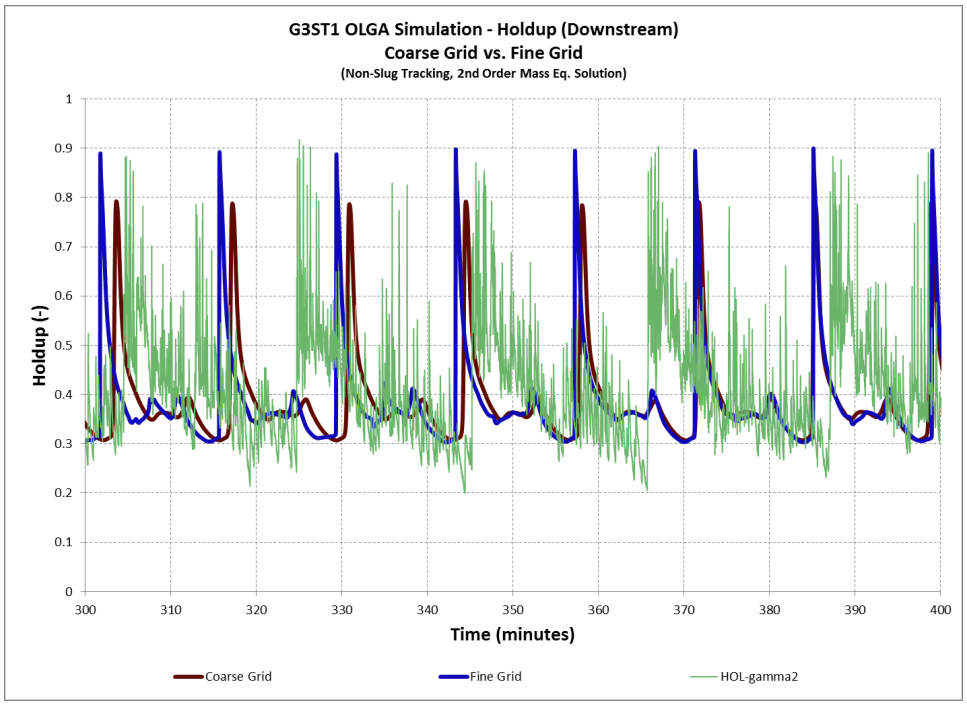

Figure 5-166: G3ST1 OLGA Holdup Simulation – Coarse Grid vs. Fine Grid (Downstream)

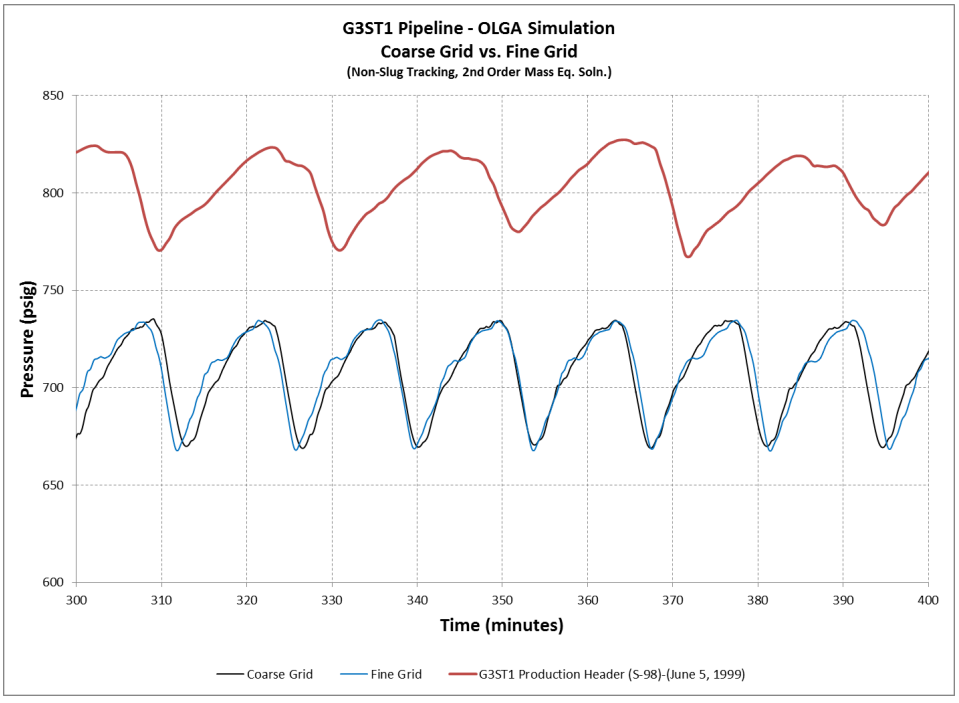

Figure 5-167: G3ST1 OLGA Pressure Simulation – Coarse Grid vs. Fine Grid (June 5, 1999)

5.4.8. G3ST1 Pipeline LedaFlow Simulations

Similar to OLGA simulations, LedaFlow simulations were carried out with various options to fully test the simulation package and the parameters which were varied for G3ST1 pipeline LedaFlow simulations are as follows:

- Slug capturing (No slug capturing vs. slug capturing)
- Grid size (Coarse grid vs. Fine grid (5) meter) – shown on Figure 5-168

Also, similar to OLGA simulations, heat transfer was not considered for all simulation cases. Finally, a high order scheme was considered for all simulation cases.

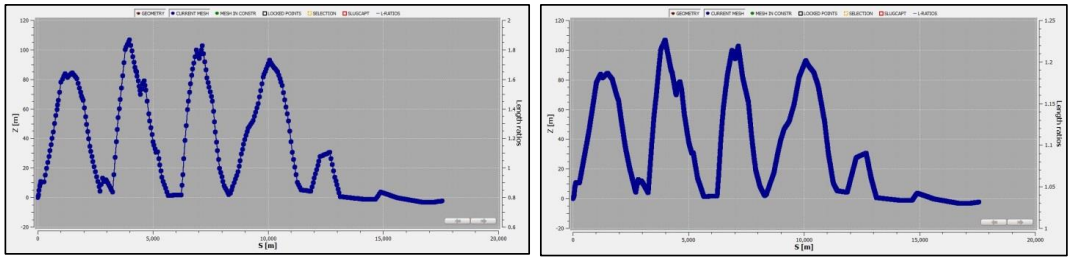

Figure 5-168: G3ST1 LedaFlow Coarse Grid (left) and Fine Grid (right)

G3ST1 LedaFlow Simulation – (Slug Capturing vs. No Slug Capturing) + (Coarse Grid vs. Fine Grid)

LedaFlow simulations were carried out with and without slug capturing module. The pressure results without slug capturing shown on Figure 5-169 and Figure 5-170 indicates a frequency of approximately (15) minutes compared to (20) minutes in field measurements. The amplitude of the pressure oscillations is in a good agreement with the field measurements at approximately (50) psi. However, when slug capturing is enabled, the amplitude of the pressure oscillations seem to reduce to approximately (30) psi. Using a fine grid of (5) meters per section indicates a minimal impact on the pressure results.

The upstream and downstream holdup results shown in Figure 5-171, Figure 5-172, Figure 5-173 and Figure 5-174 indicate a similar frequency as the pressure frequency of (15) minutes. The holdup amplitude shows to be slightly lower than the field measurement for the coarse grid cases, while the fine grid cases show higher amplitudes with small hydrodynamic slugs in between large terrain slugs.

The impact of slug capturing on holdup results is lower holdup amplitude with high peaks that occur approximately every (60 to 80) minutes.

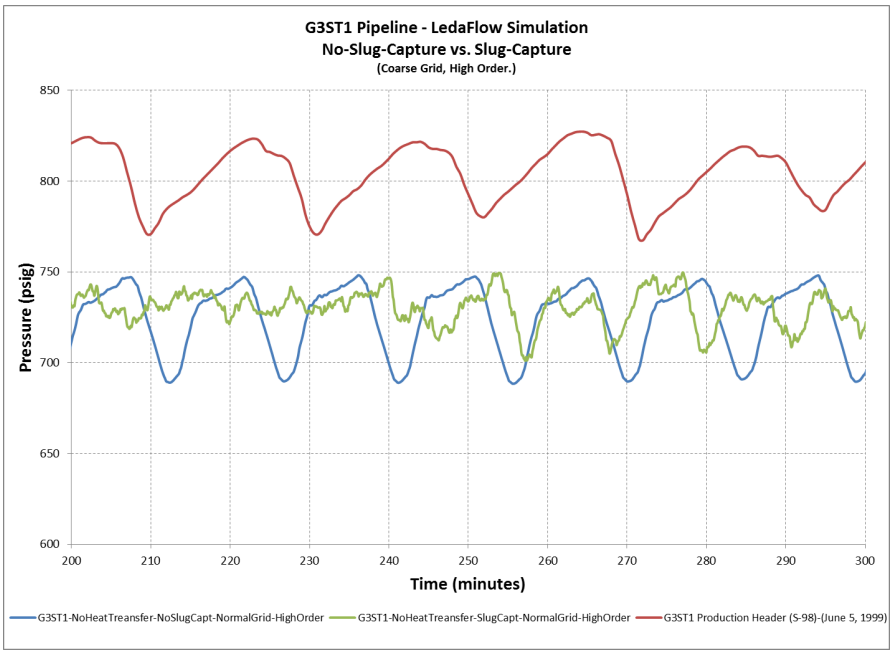

Figure 5-169: G3ST1 LedaFlow Pressure Results – Slug Capturing vs. Non-Slug Capturing Simulation (Coarse Grid)

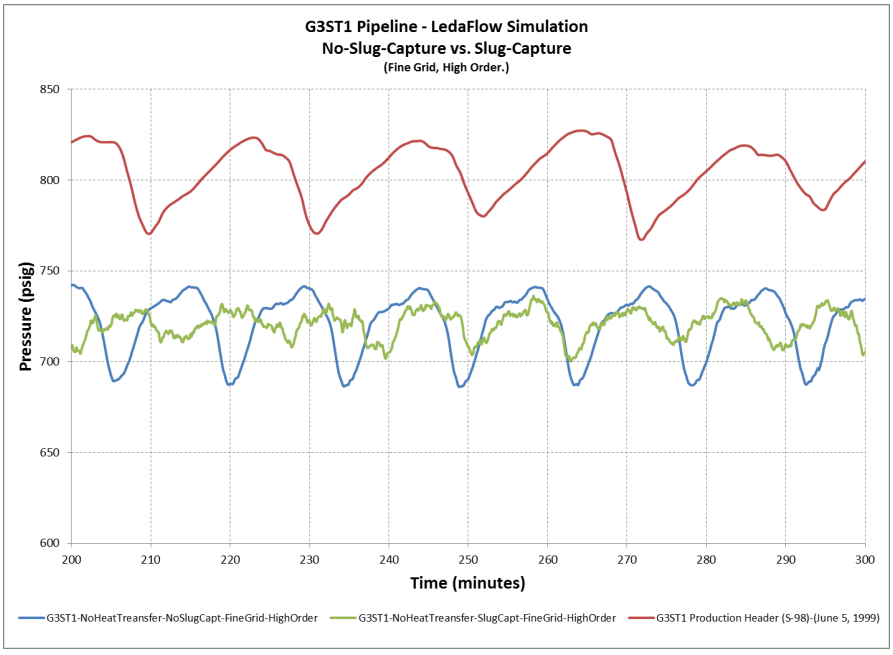

Figure 5-170: G3ST1 LedaFlow Pressure Results – Slug Capturing vs. Non-Slug Capturing Simulation (Fine Grid)

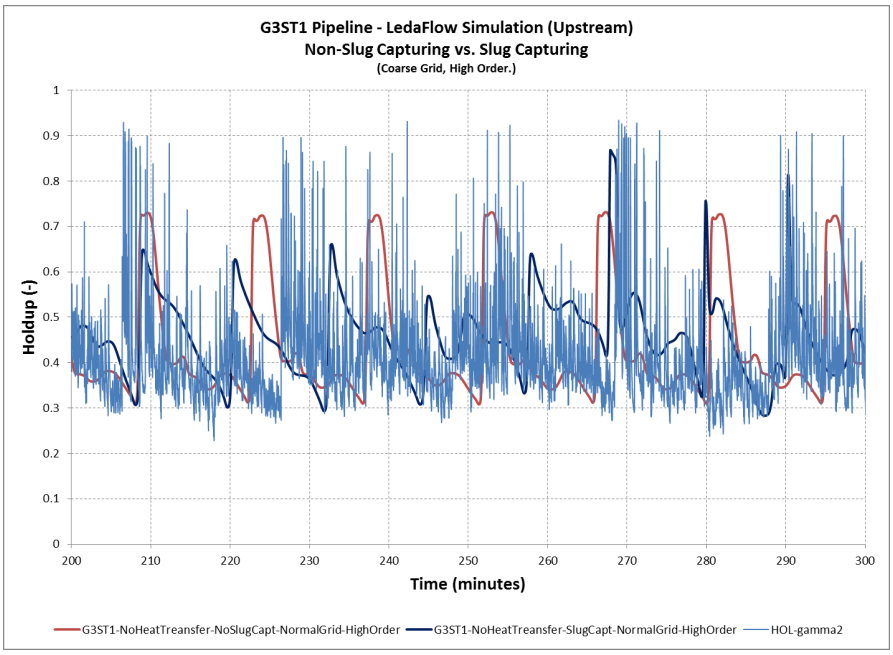

Figure 5-171: G3ST1 LedaFlow Holdup – Slug Capturing vs. Non-Slug Capturing Simulation (Coarse Grid) (Upstream)

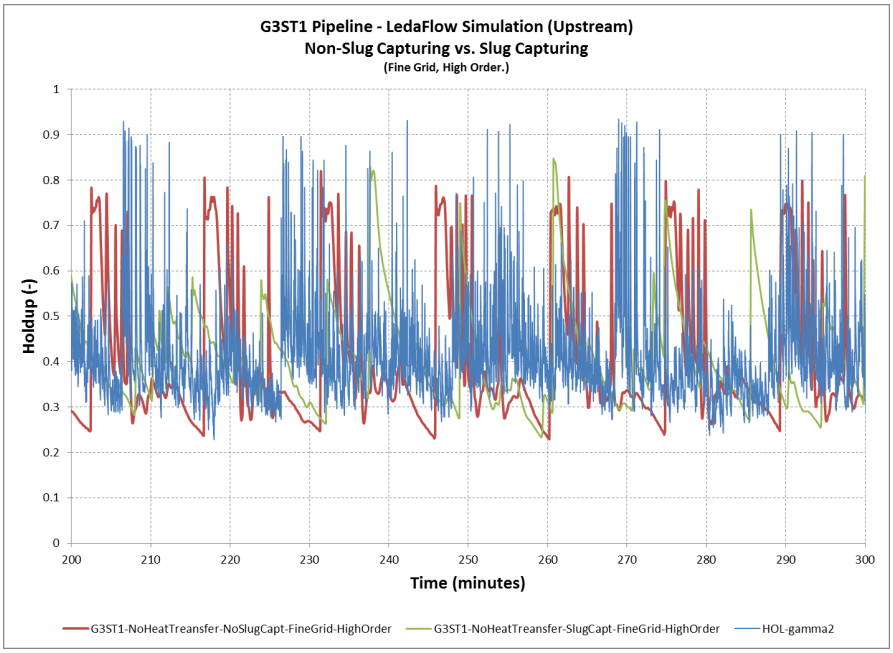

Figure 5-172: G3ST1 LedaFlow Holdup – Slug Capturing vs. Non-Slug Capturing Simulation (Fine Grid) (Upstream)

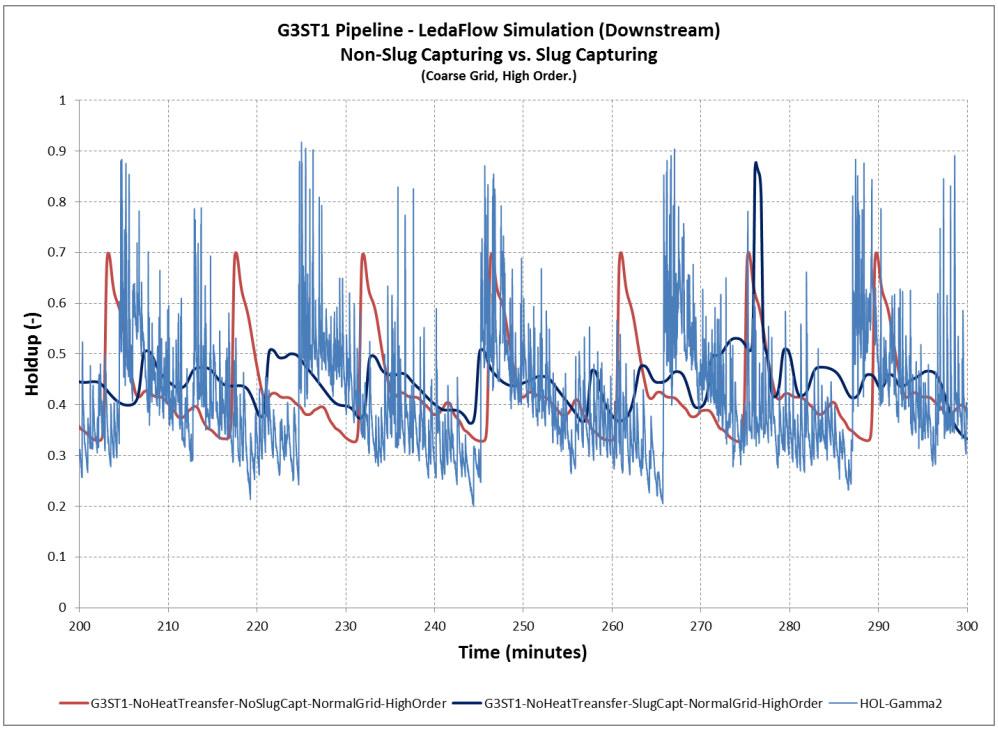

Figure 5-173: G3ST1 LedaFlow Holdup – Slug Capturing vs. Non-Slug Capturing Simulation (Coarse Grid) (Downstream)

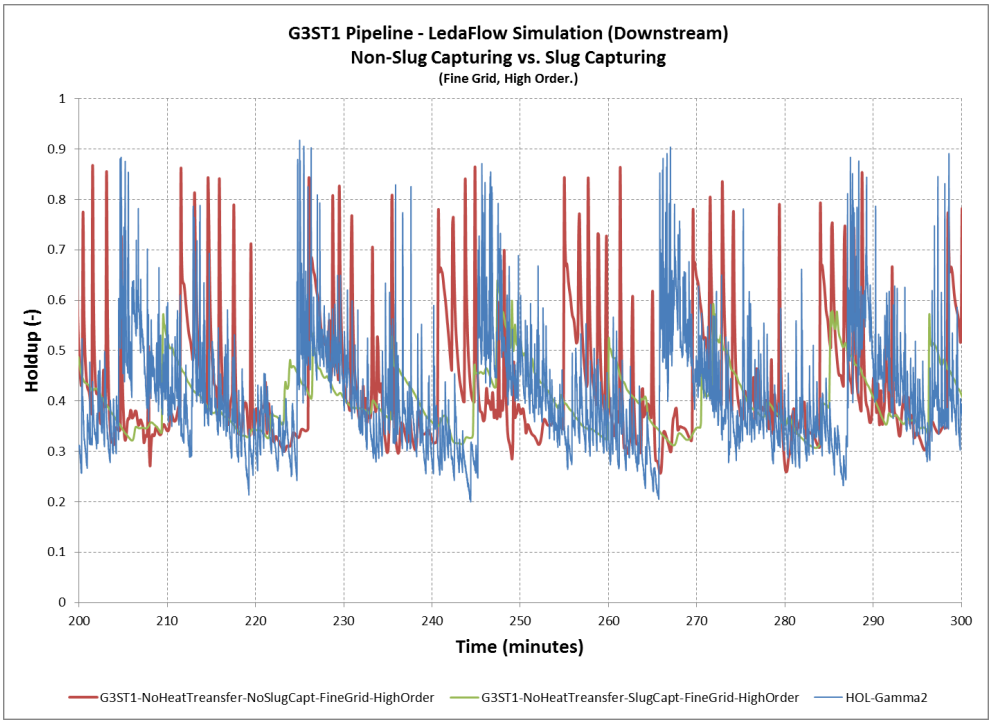

Figure 5-174: G3ST1 LedaFlow Holdup – Slug Capturing vs. Non-Slug Capturing Simulation (Fine Grid) (Downstream)

5.4.9. G3ST1 OLGA and LedaFlow Simulation Conclusions

- OLGA with no-slug tracking provided the best OLGA results. The frequency was slightly less than the one observed in the field measurements; (14) minutes vs. (20) minutes.
- Utilizing a fine grid did not improve the results.
- LedaFlow with non-slug capturing provided the best LedaFlow results with similar frequency as OLGA (15) minutes.
- LedaFlow holdup and pressure predictions were not improved using the fine grid option.
- Enabling the slug capturing module in LedaFlow had a negative impact on the slug amplitude.

5.4.10. G3ST1 Pipeline Slug Valve Optimization Study

A quick evaluation of the optimum choke settings that would have provided the best results for this particular pipeline was conducted using both OLGA and LedaFlow simulation packages. The study utilized a normal grid case without slug capturing / tracking options, along with various choke fixed manual settings. Each valve setting, shown in Table **5-10**, was simulated for two hours before moving to the next setting and the study reported the pipeline inlet pressure as shown in Figure 5-175 and Figure 5-176 for OLGA and LedaFlow results.

These results indicate a slugging behavior at all valve opening levels. The level of slugging oscillations appears to increase with less choke opening as it increases from (50) psi at choke opening of 10% to (75) psi at a choke opening of 5%. However, the slugs did not disappear from the pipeline system, when the valve was fully open as it happened in the other pipelines.

This behavior shows a behavior that was confirmed through lab experiments which indicates that slugs that are not eliminated by additional choke pressure drop are normally amplified by the liquid accumulation at the tight valve opening which compresses the gas upstream and causes a higher pressure oscillation in the pipeline system.

Table 5-10: G3ST1 Pipeline Choke Opening Settings

	OLGA Choke Opening (%)	LedaFlow Choke Opening (%)	Simulation Time (hrs) Start – Finish
1.	5 %	5 %	0 – 2
2.	5 %	5 %	2 – 4
3.	8 %	10 %	4 – 6
4.	10 %	10 %	6 – 8
5.	20 %	20 %	8 – 10
6.	40 %	30 %	10 – 12
7.	80 %	40 %	12 – 14
8.	100 %	60 %	14 – 16
9.		80 %	16 – 18
10.		100 %	18 – 20

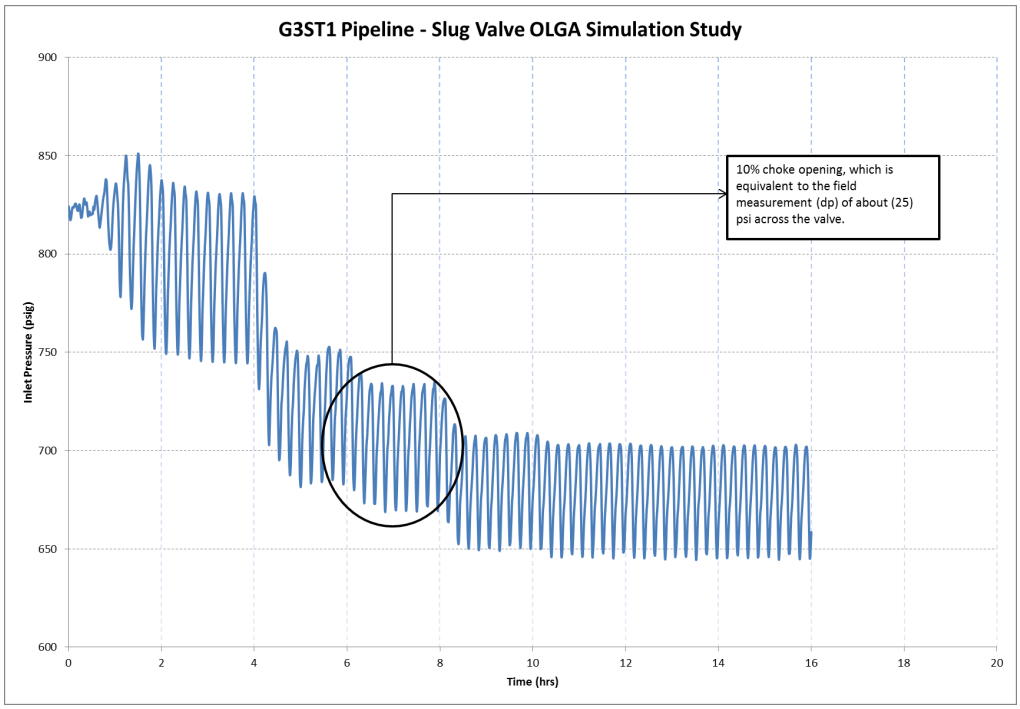

Figure 5-175: G3ST1 Pipeline – Slug Valve OLGA Simulation Study – (Coarse Grid, 2nd Order, No-SlugTracking)

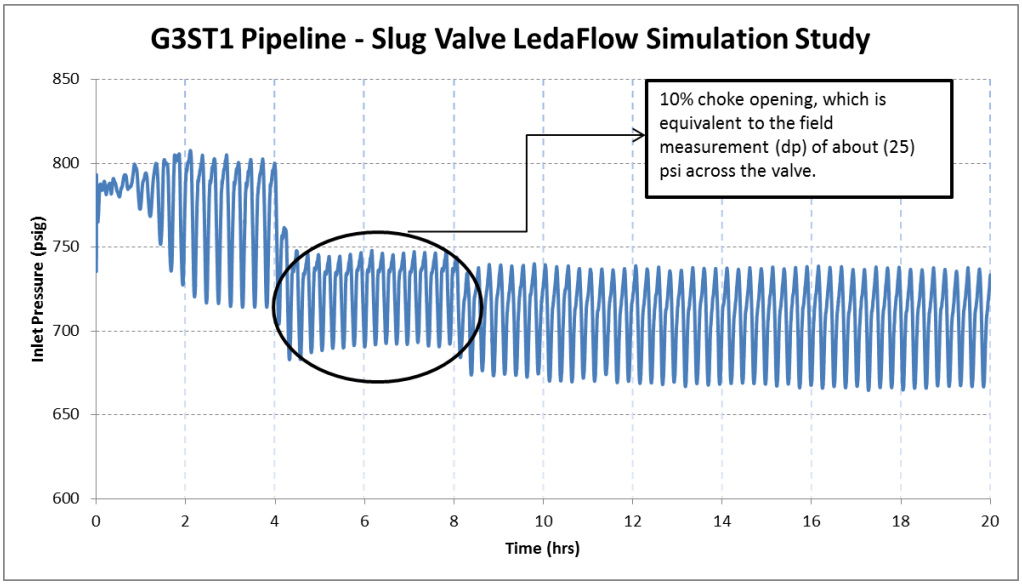

Figure 5-176: G3ST1 Pipeline – Slug Valve LedaFlow Simulation Study – (Coarse Grid, High Order, No-SlugCapturing)

5.5. G3ST2 Pipeline Results

G3ST2 measurements were conducted over three days: on May 29, 1999 downstream the slug valve at normal valve opening, on May 30, 1999 downstream the slug valve at restricted valve opening and on June 6, 1999 upstream the slug valve at normal valve opening.

5.5.1. Pipeline Profile Details

The total pipeline length is approximately 19 Km and starts from Sabkhah 95 (S-95) to GOSP-3 going through Sabkhah 92 (S-92), Sabkhah 88 (S-88), Sabkhah 84 (S-84), Sabkhah 77 (S-77). The pipeline has four (4) very high hills with heights that are approximately 60 to 100 meters. The pipeline has two different diameters 16 inch and 20 inch as shown on Figure 5-177.

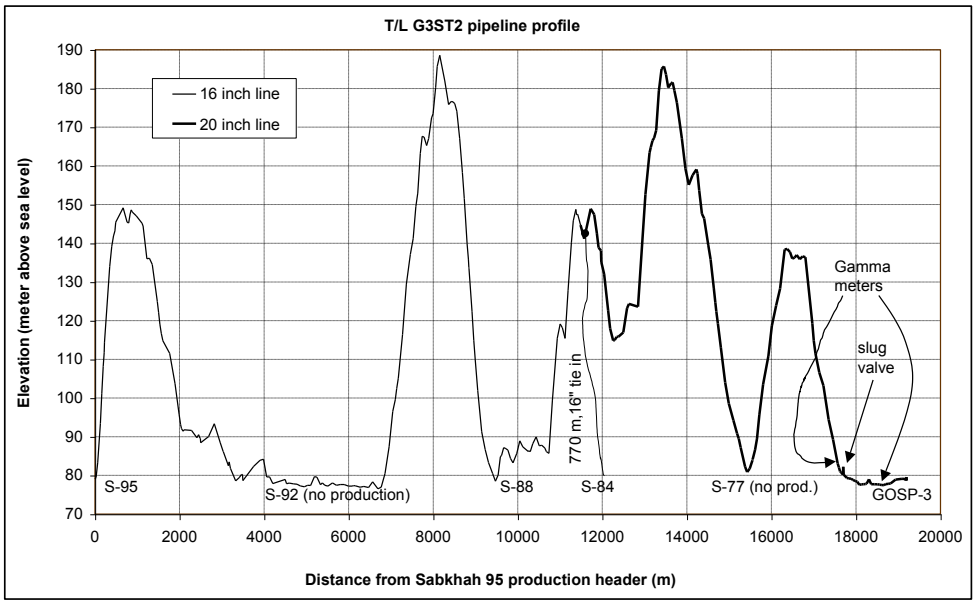

Figure 5-177: G3ST2 pipeline profile – slug valve and gamma densitometer locations

The measurement was made close to the slug valve which is installed at the end of the pipeline upstream of GOSP-3. The measurements were made at a normal production rate of 48,100 BBL/Day at standard conditions The flow rates were based on forecasts made by the production engineers and no flow rate measurements were carried out at the time of the experiments. The flow rates from each Sabkhah were estimated as follows:

Sabkhah	Flow Rate (BBL/Day) @ std. cond.
S-95	5,600
S-92	No Production
S-88	29,000
S-84	13,500
S-77	No Production
Total	**48,100**

The superficial gas and liquid velocities ranged from (0.2 to 1.5) m/sec for gas and (0.1 to 1.4) m/sec for liquid, based on OLGA predictions.

During the upstream measurement, on June 6, 1999, the distance between the gamma meters was set at 51.6 m, while the inclination angle was measured at (– 3.92) degrees. The distance of the gammas to the downstream slug valve was measured at approximately 100 m as shown in Figure 5-178. In addition the distance to GOSP-3 was approximately 1.4 Km. The pipeline wall thickness was measured using ultra sonic measurement device at 0.63 inch (16 mm). The GOSP-3 pressure was set at 400 psig during the measurement period.

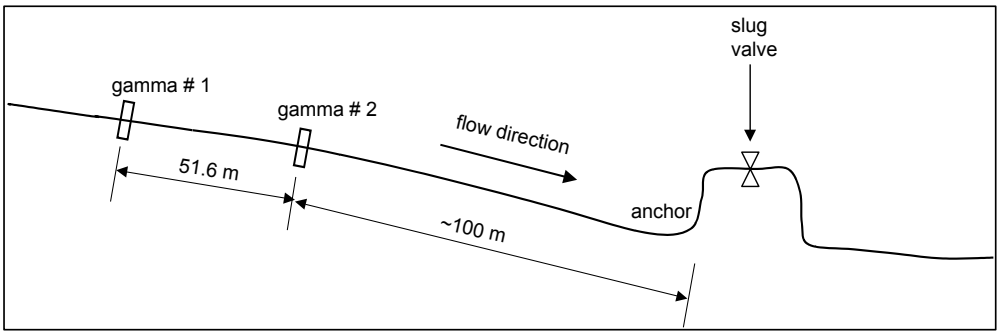

Figure 5-178: G3ST2 pipeline – Location of gammas with respect to Slug Valve (Upstream SV

On the other hand, during the two downstream of slug valve measurements, the distance between the gamma meters was set at 53.3 m, while the inclination angle was measured at (+ 0.07) degrees. The distance of the gammas to the upstream slug valve was measured at approximately 800 m. In addition the distance to GOSP-3 was approximately 500 m. The pipeline wall thickness was measured using ultra sonic measurement device at 0.787 inch (20 mm). The GOSP-3 pressure was set at 400 psig during the measurement period.

5.5.2. Production Header Time Series

The pressure logs at the producing Sabkhahs were not available from the DCS system due to a malfunction in the system. Therefore, a separate standalone pressure logging device was installed at (S-95). The (S-95) pressure logs were obtained on the three measurement days May, 29, May 30 and June 6, 1999.

Sabkhah 95 pressure log on May 29, 1999, normal opening downstream measurement, shown on Figure 5-179, indicates an approximately 10 to 15 minutes pressure cycles. One can also observes a overlaying longer cycles with a period of 50 to 60 minutes with higher pressure swings. The short periods exhibits pressure oscillations of 10 to 20 psi, while for the long periods the pressure oscillations were in the order of 30 psi. The pressure generally oscillates between 805 psig and 835 psig with a pressure swing of 30 psi.

Sabkhah 95 pressure log on May 30, 1999, restricted opening downstream measurement, shown on Figure 5-180, also indicates a similar behavior with 10 to 15 minutes pressure cycles. Unfortunately the logging period was not long enough to capture the longer period cycle as we can only notice the beginning of this cycle at the start of the pressure log. The short periods exhibits pressure oscillations of 15 to 20 psi. The pressure generally oscillates between 845 psig and 880 psig with a pressure oscillation of 35 psi. The higher pressure values is attributed to the higher pressure drop across the slug valve which was further restricted in this measurement period.

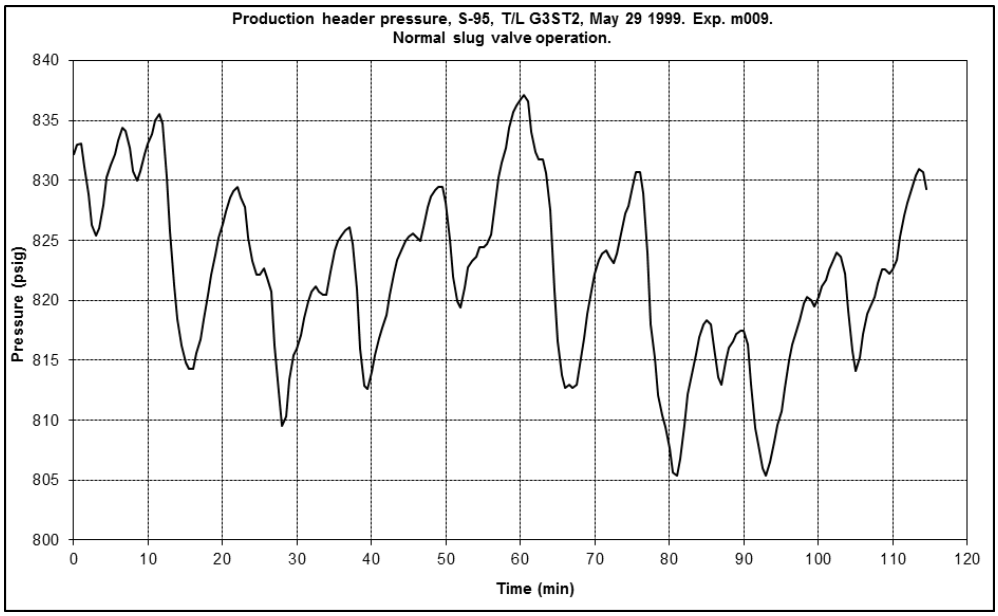

Figure 5-179: G3ST2 Production header pressure at S-95, Normal Opening, May 29, 1999, (Downstream SV)

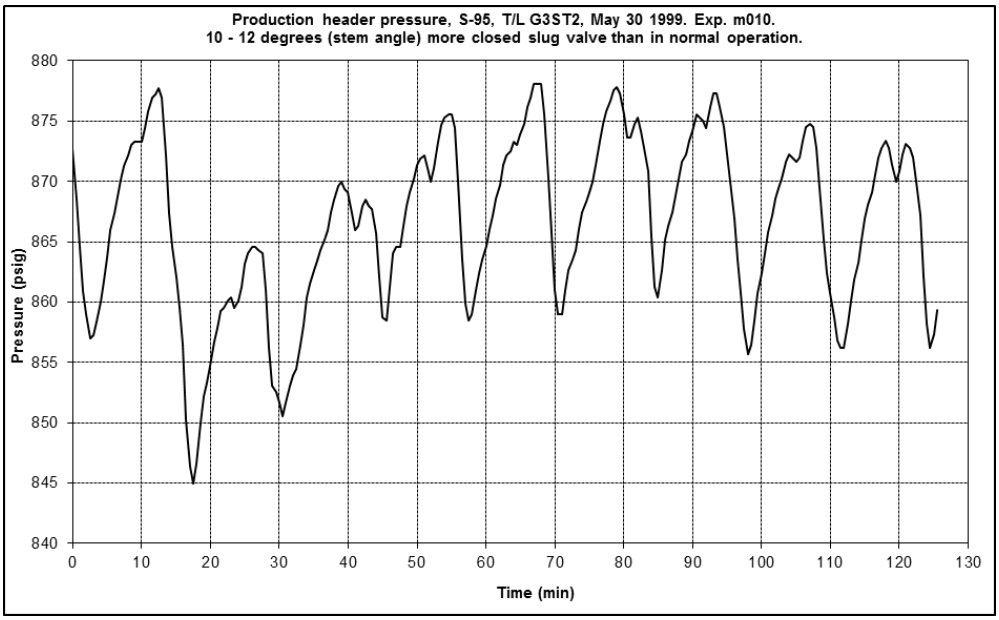

Figure 5-180: G3ST2 Production header pressure at S-95, Restricted Opening, May 30, 1999, (Downstream SV)

Sabkhah 95 pressure log on June 6, 1999, normal opening upstream measurement, shown on Figure 5-181, also indicates a similar cyclic behavior but this time with shorter time periods 5 to 10 minutes. The pressure oscillations were in the order of 10 to 15 psi. The pressure generally oscillates between 815 psig and 855 psig with a pressure swing of 40 psi. A larger pressure oscillation cycle might have been captured if the logging period was slightly longer as we could see in the very low pressure value logged at 810 psig at the beginning of the logging period.

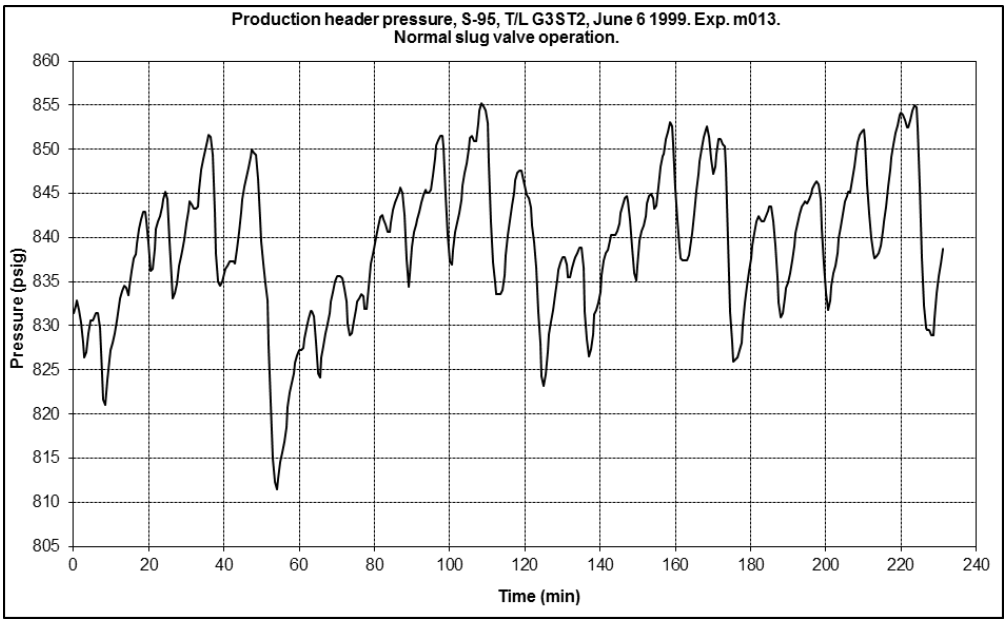

Figure 5-181: G3ST2 Production header pressure at S-95, Normal Opening, June 6, 1999, (Upstream SV)

5.5.3. Slug Valve Pressure Drop

The slug valve at G3ST2 pipeline was installed about 1.3 km from GOSP-3. The pipeline was sloped down to the slug valve, which causes a large accumulation of liquid upstream the slug valve.

The pressure drop across the slug valve was logged during the measurement tests using Foxboro absolute pressure transmitters, which were installed in the same positions of the pressure manometers across the slug valve. The taps of the manometers were installed approximately (1) meter upstream and downstream of the slug valve. The pressure signals were sampled at 2 Hz over a period of 70 minutes.

The normal slug valve opening case results are shown in Figure 5-182, which shows a pressure cycle of approximately 50 psi every 10 to 12 minutes. The downstream pressure varies between 390 to 430 psig while the upstream pressure varies between 440 and 490 psig. One can also notice that the peak values in the upstream pressure log coincide with minimum values on the downstream side.

This behavior is explained by the fact that the slug valve was very restricted even at normal slug valve conditions. Therefore, liquid accumulates upstream the slug valve very fast and then it is gradually drained through the small valve opening. This takes relatively long time to occur and in the meantime the liquid downstream the valve is drained all the way to the GOSP separators. Therefore one can notice the pressure downstream the slug valve being almost at GOSP-3 pressure levels of 400 psig during this period. Afterwards a new cycle is started with the upstream liquid being drained again through the small valve opening.

The differential pressure across the valve varies between 20 and 100 psi with an average value of 60 psi as shown in Figure 5-183.

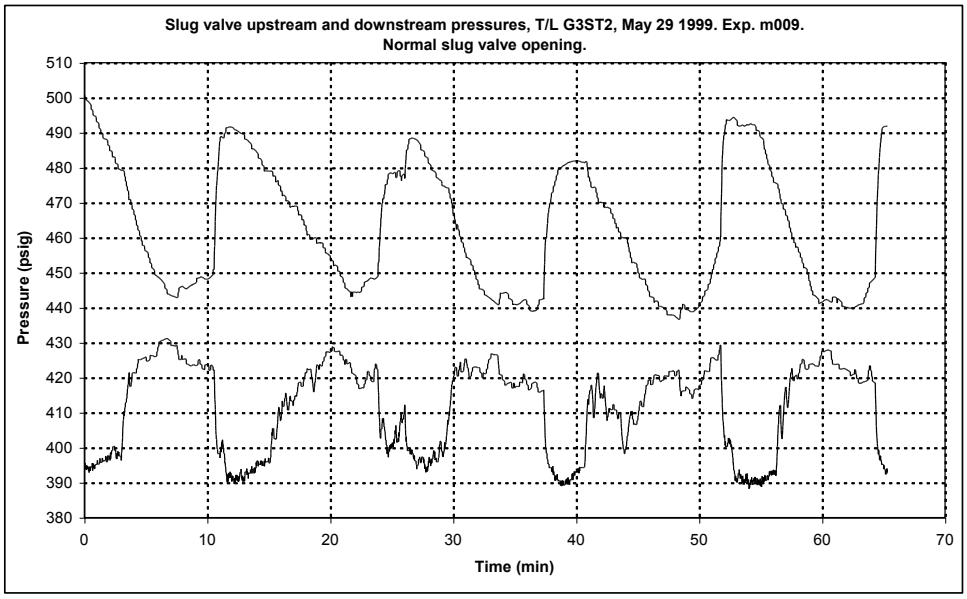

Figure 5-182: G3ST2 Pressure upstream and downstream of slug valve, Normal Opening, May 29, 1999

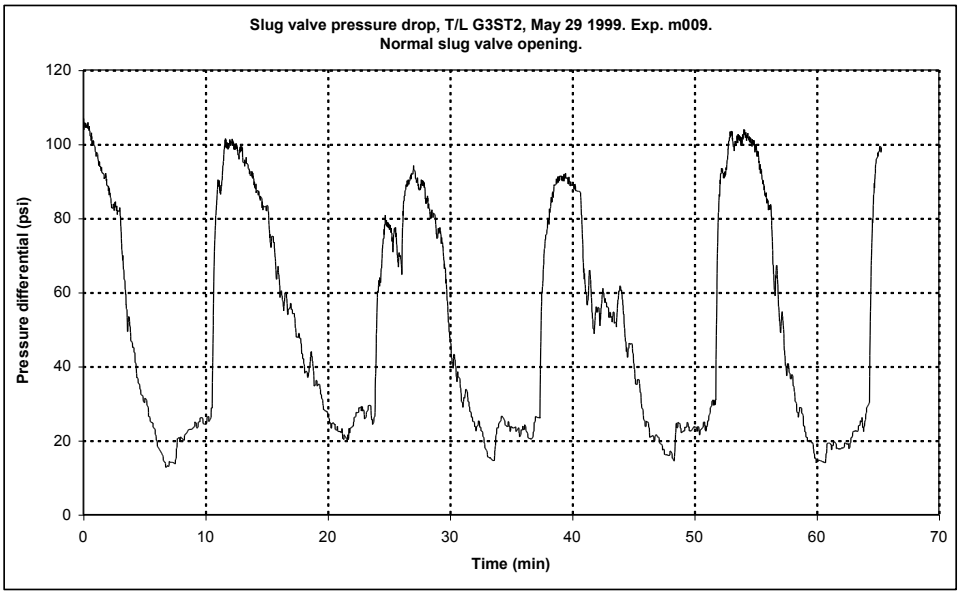

Figure 5-183: G3ST2 Pressure differential across slug valve, Normal Opening, May 29, 1999

The restricted slug valve opening case results are shown in Figure 5-184, which shows a similar pressure cycle of approximately 50 to 60 psi every 10 to 12 minutes. The upstream pressure varies between 470 to 550 psig while the downstream pressure varies between 390 and 440 psig. Again, one notices that the peak values in the upstream pressure log coincide with minimum values on the downstream side.

This behavior, which is similar to the behavior noticed in the normal slug valve opening case, is explained in the same manner as the previous case except for the fact the pressure oscillations are slightly higher with

higher pressure drop across the slug valve. The differential pressure across the valve varies between 40 and 160 psi with an average value of 100 psi as shown in Figure 5-185.

Finally, one can conclude from the sudden sharp increase and drop in the pressure upstream and downstream the slug valve that a slug flow regime exists at both sides despite the extreme slug valve restriction.

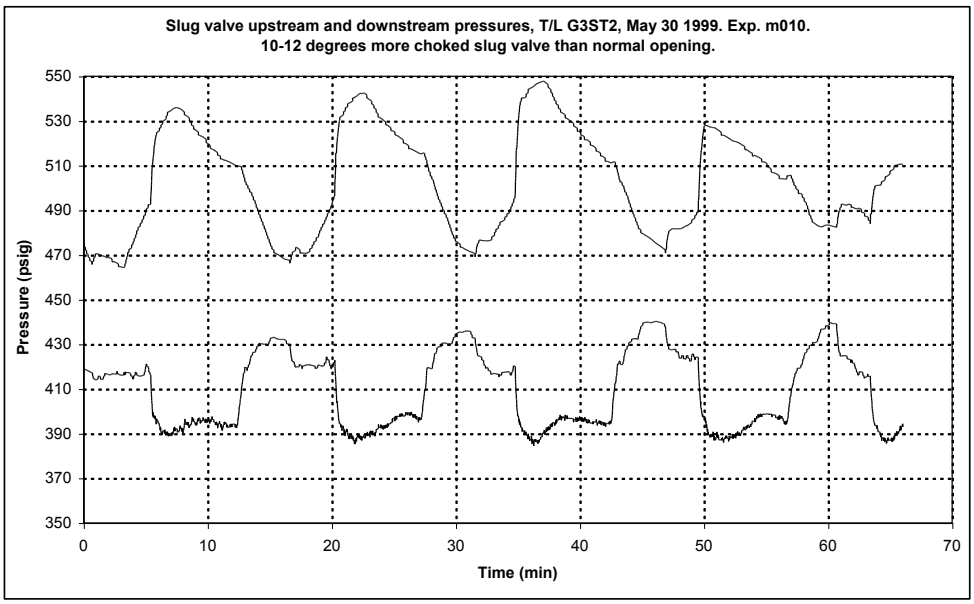

Figure 5-184: G3ST2 Pressure upstream and downstream of slug valve, Rest. Opening, May 30, 1999

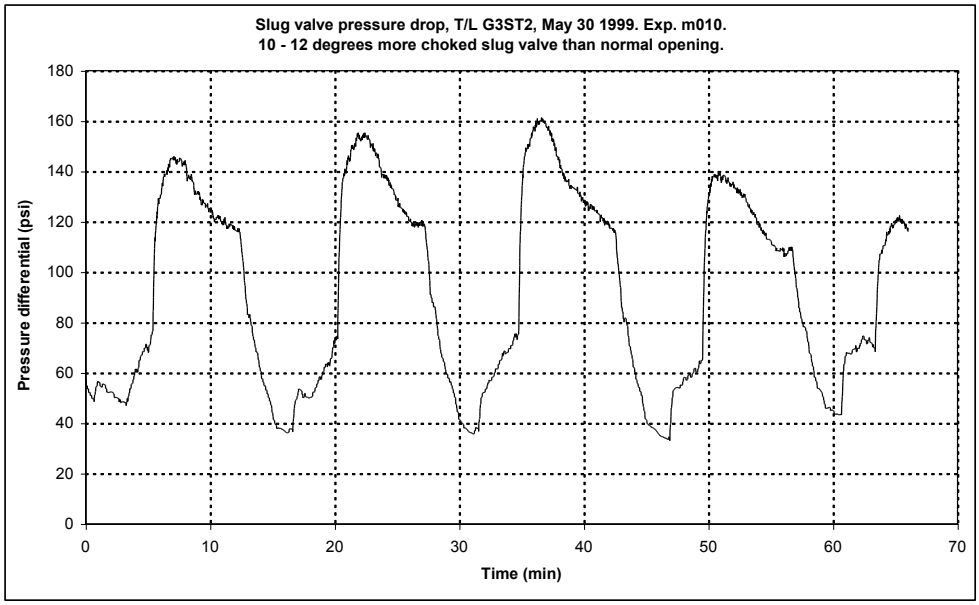

Figure 5-185: G3ST2 Pressure differential across slug valve, Rest. Opening, May 30, 1999

5.5.4. Analysis of Holdup Time Series – Upstream Slug Valve – Normal Valve Opening

Analyzing the holdup time series upstream of the slug valve in Figure 5-186 one could notice the small number of slugs, approximately (9) slugs, at each gamma position. This was expected as the position of the gammas were in a negatively sloped area, (- 3.92) degrees, which causes an expected stratified flow regime. The small number of slugs is possibly due to the existence of the nearby slug valve which was positioned (100) meters downstream of Gamma-2.

One could also notice a constant film holdup of approximately 10% with slugs and waves on top of it. The waves peaks ranges between 35% and 40%, while the slugs peaks were at 80%, as shown in Figure 5-187 and Figure 5-188. The slug body shows mostly to consist of two peaks, which indicate the breakage of one large slug into two slugs due to the downhill stratified effect. The slugs and waves showed a fixed frequency of (10 – 12) minutes.

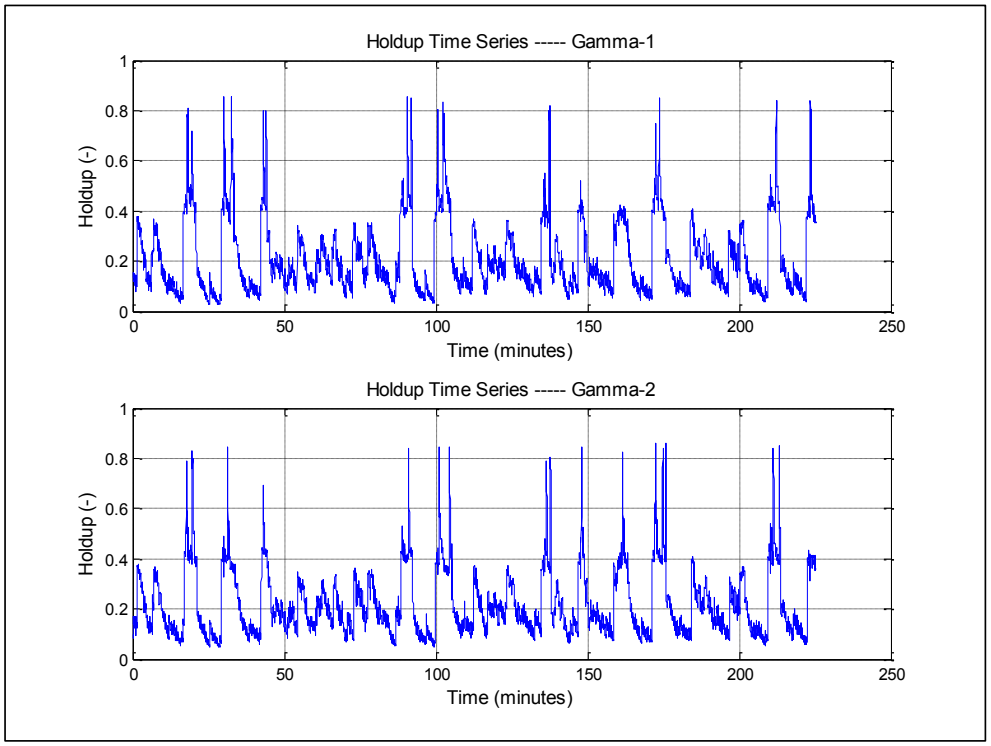

Figure 5-186: G3ST2 Holdup time series, Upstream Slug Valve, Normal Opening, (220 minutes)-(Gamma-1&2)

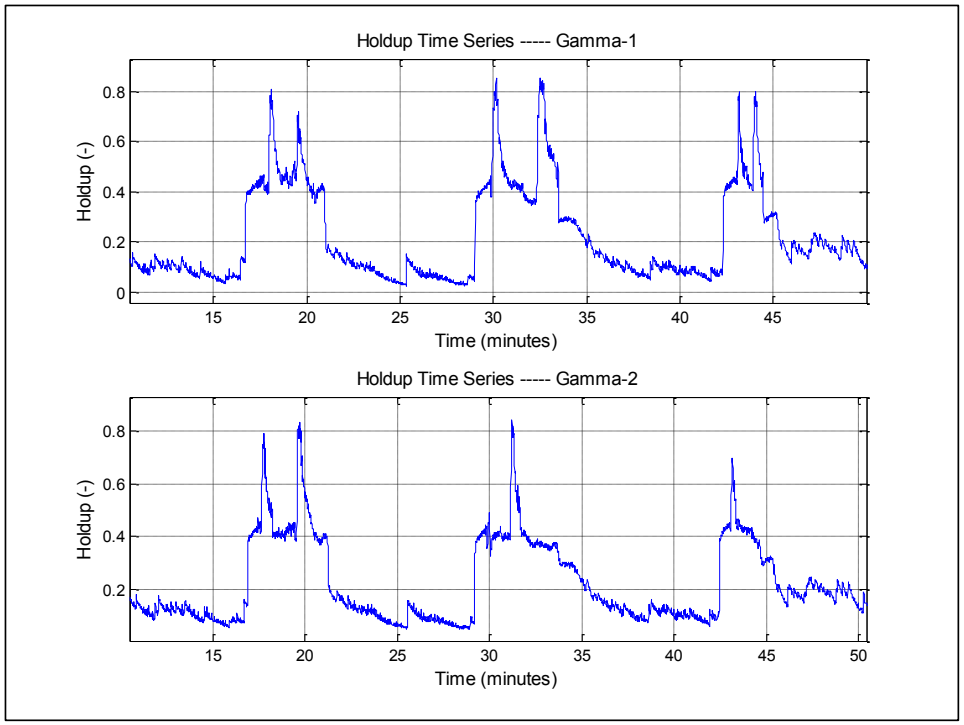

Figure 5-187: G3ST2 Holdup time series, Upstream Slug Valve, Normal Opening, (Slugs)-(Gamma-1&2)

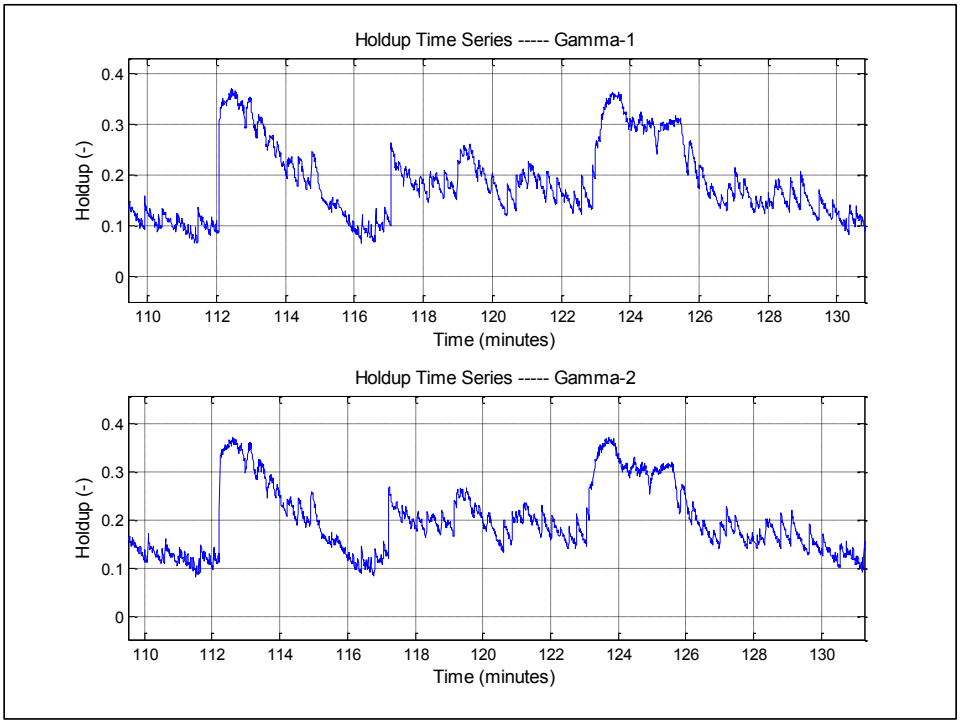

Figure 5-188: G3ST2 Holdup time series, Upstream Slug Valve, Normal Opening, (Waves)-(Gamma-1&2)

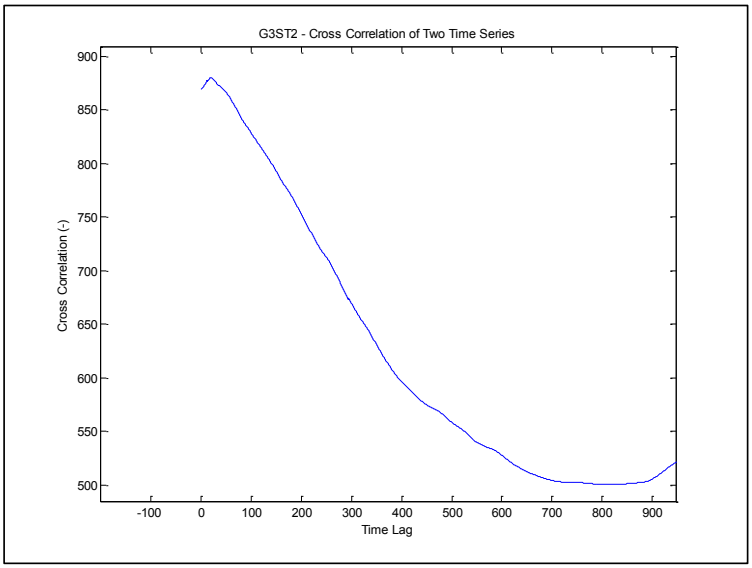

Figure 5-189: G3ST2 Cross Correlation of Two Gammas – Upstream Slug Valve, Normal Opening

Cross correlation of the time series, as shown in Figure 5-189, shows a time lag (10.5) seconds which translates into a velocity of (4.91) m/sec using the distance between the gammas which was set at (54.1) meters.

Due to the very low number of slugs present in this time series, no further statistical analysis was carried out for this case.

5.5.5. Analysis of Holdup Time Series – Downstream Slug Valve – Normal Valve Opening

Analyzing the holdup time series in figures Figure 5-190, Figure 5-191, Figure 5-192, Figure 5-200 and Figure 5-193 indicates a pattern of repetitive cycles of large terrain slugs. The holdup time series at Gamma-1 shows a constant liquid film of (0.15) while at Gamma-2 the liquid film was slightly higher at (0.25). The reason behind this difference is attributed to the slight downward inclination at Gamma-1 position, (– 0.24) degrees, whereas at Gamma-2 location, in inclination was slightly upward, (+ 0.38) degrees.

The slug peaks were at (0.95) at both gamma locations. The slug body which extends over (2 – 3) minutes consists of many small hydrodynamic slugs. The bubble body consists of many small waves that extends over (8 – 11) minutes.

A total of (19) large terrain slugs were observed in a (251) minutes period, which gives a frequency of a slug every (13.2) minutes. This is in agreement with the pressure oscillation frequency noted downstream of the slug valve. Examining the slug frequency distribution shown in Figure 5-195 one also can note that most of the slug frequency is concentrated around (11 – 15) minutes.

Cross correlating the two time series provides a time lag of (10) seconds, as shown in Figure 5-194, which translates into a velocity of (5.33) m/sec using the distance between the gammas which was measured at (53.3) meters.

Slug length calculations were carried out using the slug body time and the average slug velocity calculated based on the cross correlation information. This was made due to the low number of slugs which prevents

from obtaining a good statistical analysis of the slugs front and tail velocities. The results shown in Figure 5-196 and Figure 5-197 indicates very large slugs with lengths in the order of (2,000) meters or (4,000 * Pipeline Dia.).

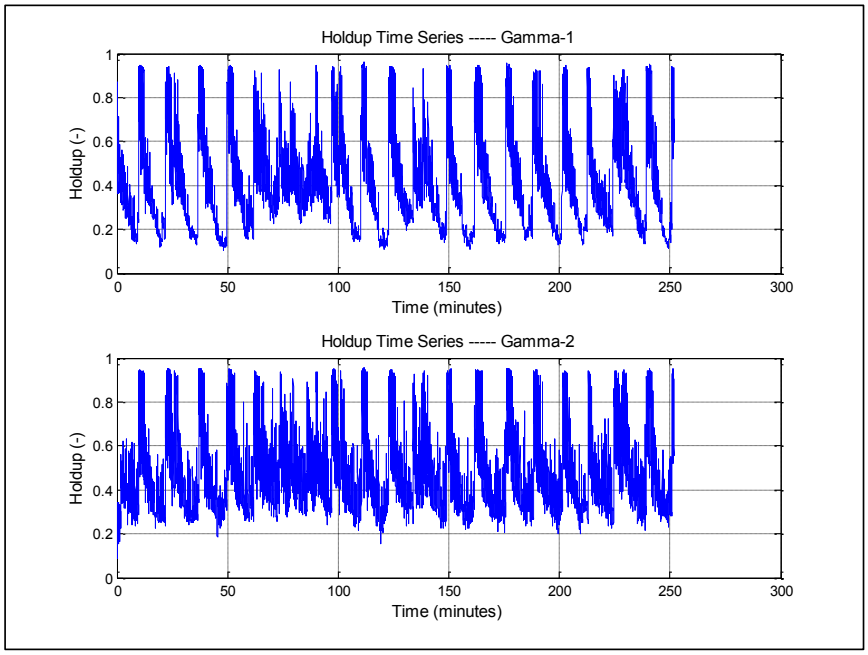

Figure 5-190: G3ST2 Holdup time series, Downstream Slug Valve, Normal Opening, (250 minutes)-(Gamma-1&2)

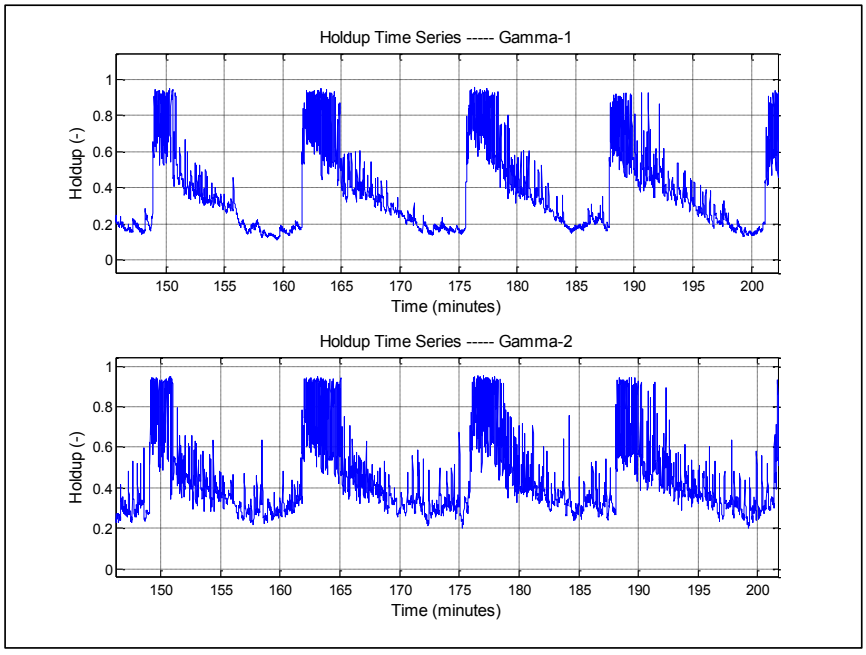

Figure 5-191: G3ST2 Holdup time series, Downstream Slug Valve, Normal Opening, (50 minutes)-(Gamma-1&2)

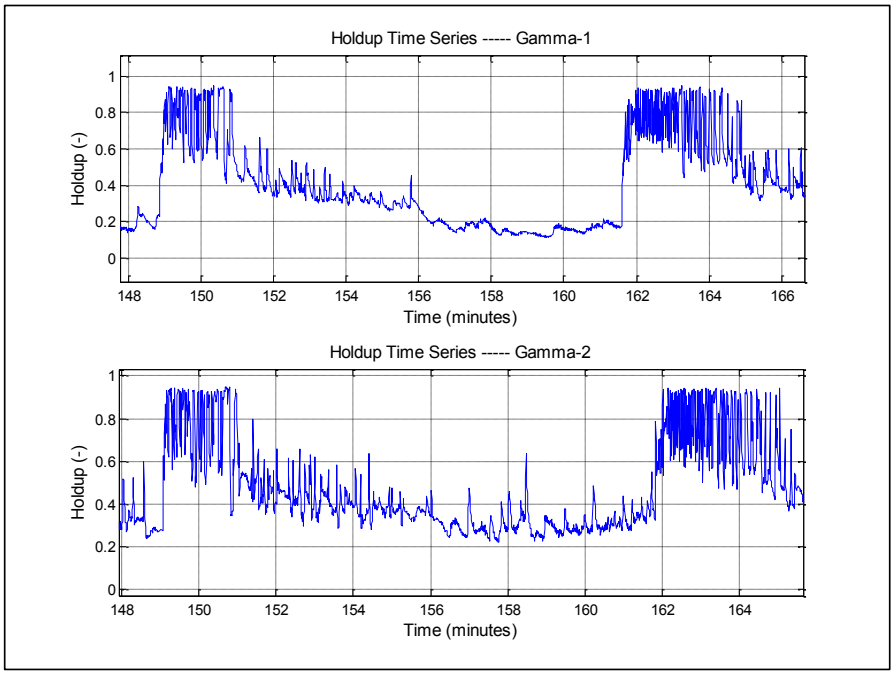

Figure 5-192: G3ST2 Holdup time series, Downstream Slug Valve, Normal Opening, (20 minutes)-(Gamma-1&2)

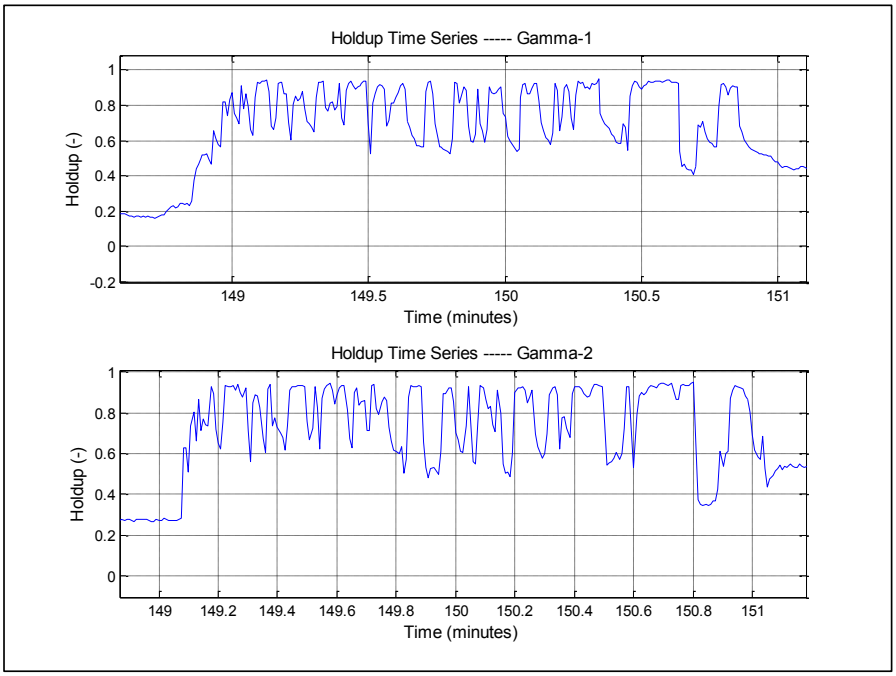

Figure 5-193: G3ST2 Holdup time series, Downstream Slug Valve, Normal Opening, (2 minutes)-(Gamma-1&2)

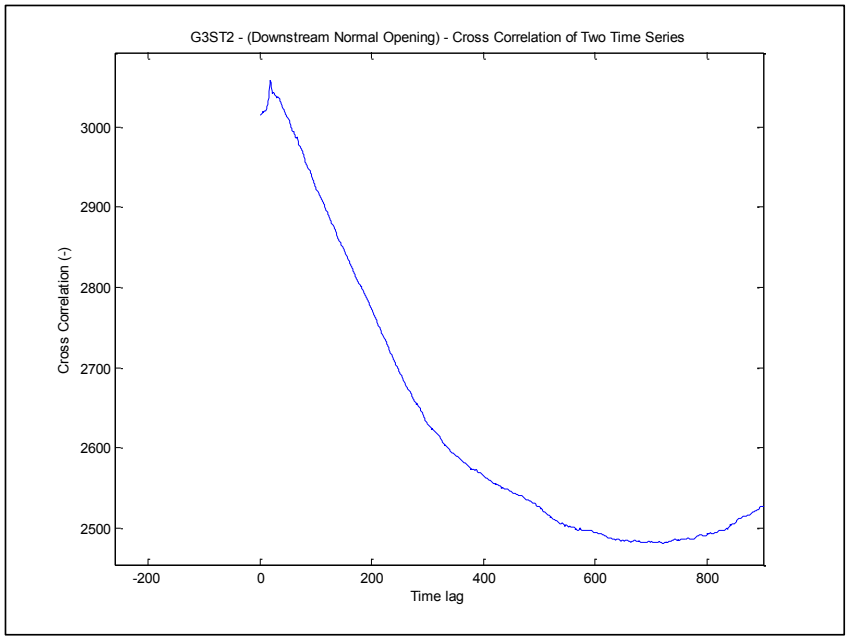

Figure 5-194: G3ST2 Cross Correlation of Two Gammas – Downstream Slug Valve, Normal Opening

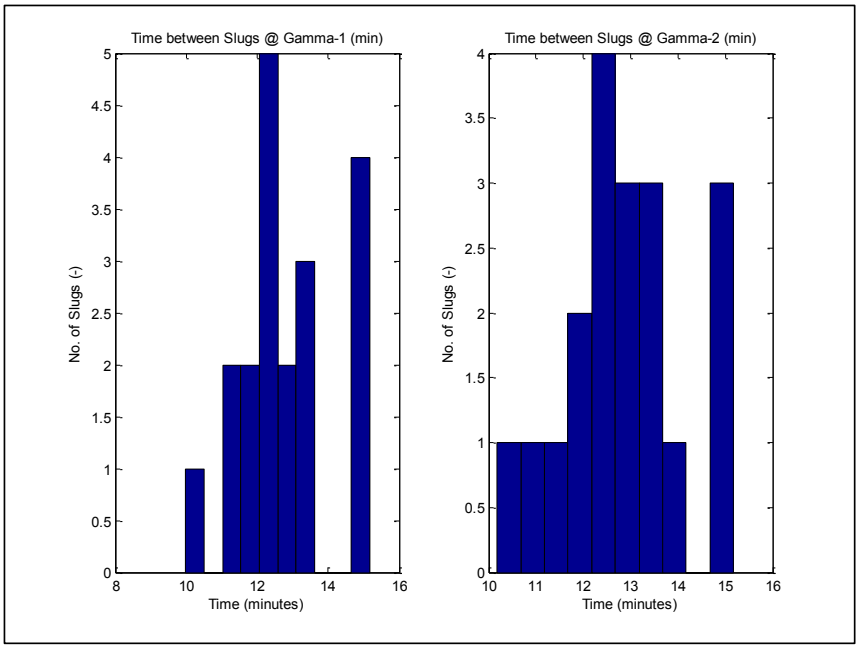

Figure 5-195: G3ST2 Distribution of Slug Frequency – Downstream Slug Valve, Normal Opening

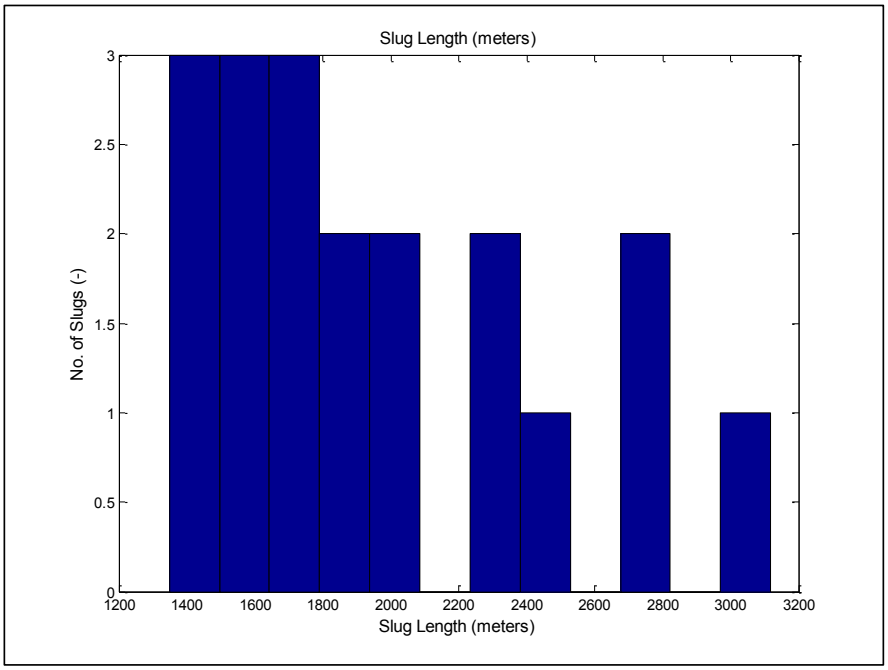

Figure 5-196: G3ST2 Distribution of Slug Length (m) – Downstream Slug Valve, Normal Opening

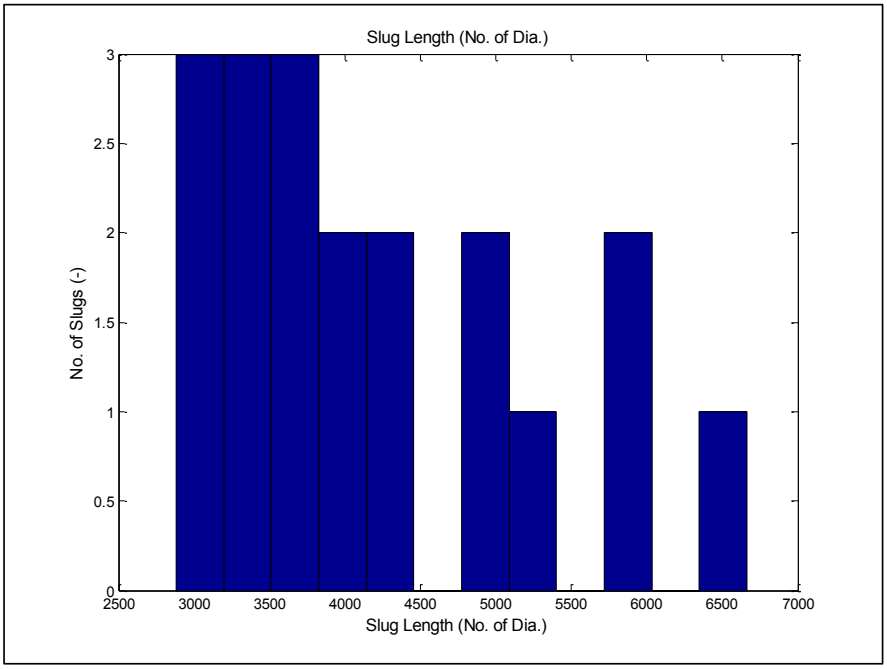

Figure 5-197: G3ST2 Distribution of Slug Length (No. of Dia.) – Downstream Slug Valve, Normal Opening

5.5.6. Analysis of Holdup Time Series – Downstream Slug Valve – Restricted Valve Opening

Analyzing the holdup time series in figures Figure 5-198, Figure 5-199, Figure 5-200 and Figure 5-201 indicates a pattern of repetitive cycles of large terrain slugs. The holdup time series at Gamma-1 shows a constant liquid film of (0.10) while at Gamma-2 the liquid film was slightly higher at (0.15). The reason behind this difference is attributed to the slight downward inclination at Gamma-1 position, (– 0.24) degrees, whereas at Gamma-2 location, in inclination was slightly upward, (+ 0.38) degrees.

The slug peaks were at (0.95) at both gamma locations. The slug body which extends over (3 – 4) minutes consists of many small hydrodynamic slugs. The bubble body consists of many small waves that extends over (9 – 10) minutes.

A total of (17) large terrain slugs were observed in a (223) minutes period, which gives a frequency of a slug every (13.1) minutes. This is also in agreement with the pressure oscillation frequency noted downstream of the slug valve. Examining the slug frequency distribution shown in Figure 5-203 one also can note that most of the slug frequency is concentrated around (11 – 15) minutes.

Cross correlating the two time series provides a time lag of (9.5) seconds, as shown in Figure 5-202, which translates into a velocity of (5.61) m/sec using the distance between the gammas which was measured at (53.3) meters.

Slug length calculations were carried out using the slug body time and the average slug velocity calculated based on the cross correlation information. This was made due to the low number of slugs which prevents from obtaining a good statistical analysis of the slugs front and tail velocities. The results shown in Figure 5-204 and Figure 5-205 indicates very large slugs with lengths in the order of (2,000) meters or (4,000 * Pipeline Dia.).

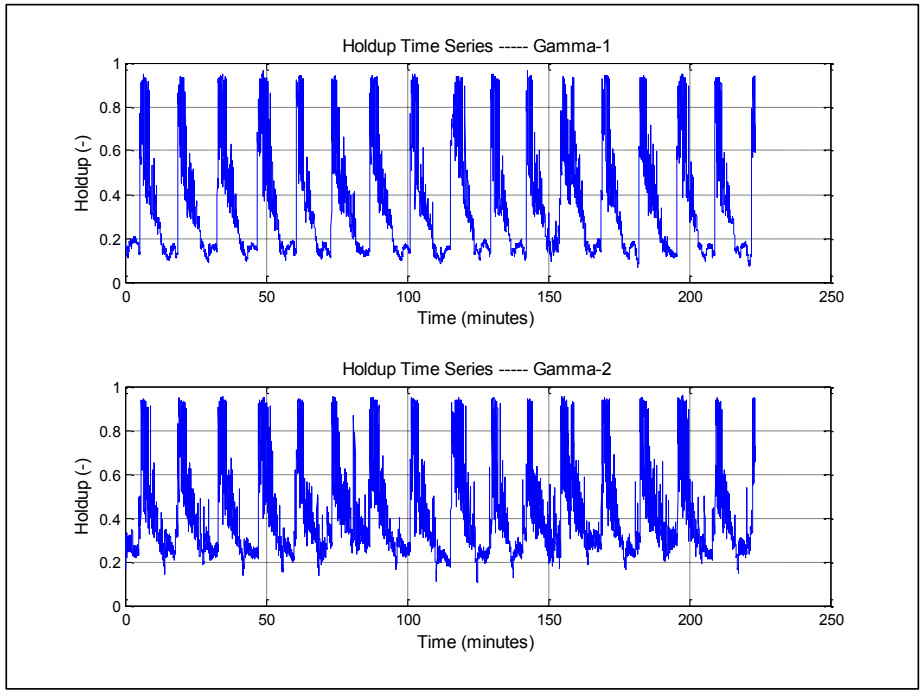

Figure 5-198: G3ST2 Holdup time series, Downstream Slug Valve, Restricted Opening, (250 minutes)-(Gamma-1&2)

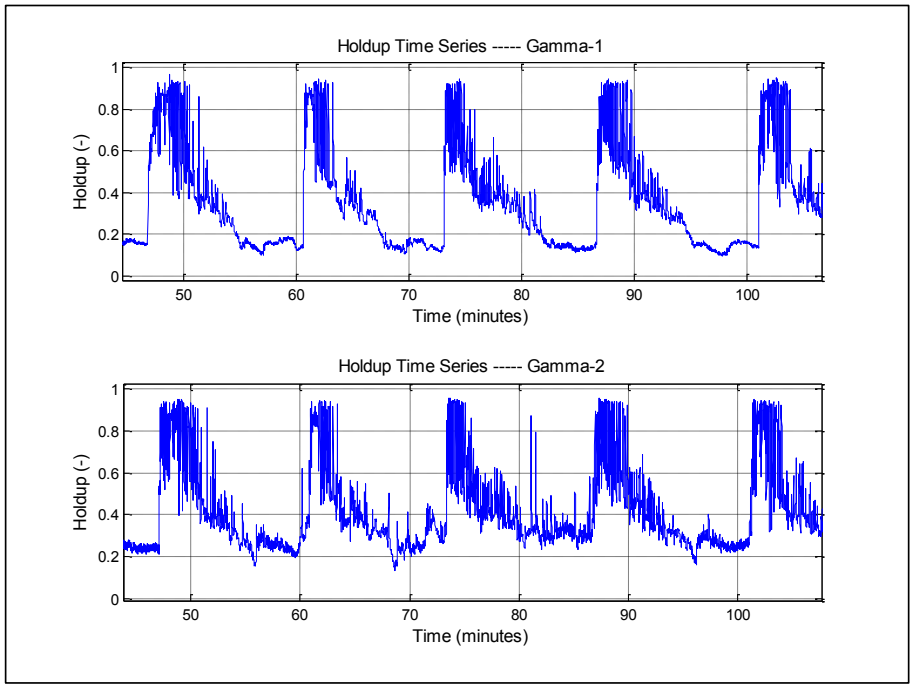

Figure 5-199: G3ST2 Holdup time series, Downstream Slug Valve, Restricted Opening, (60 minutes)-(Gamma-1&2)

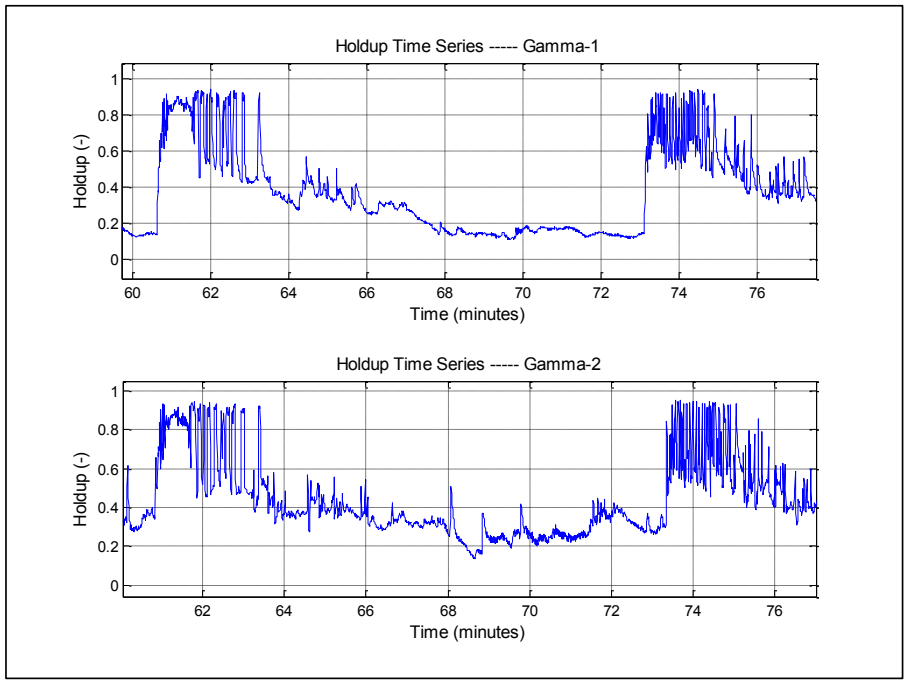

Figure 5-200: G3ST2 Holdup time series, Downstream Slug Valve, Restricted Opening, (15 minutes)-(Gamma-1&2)

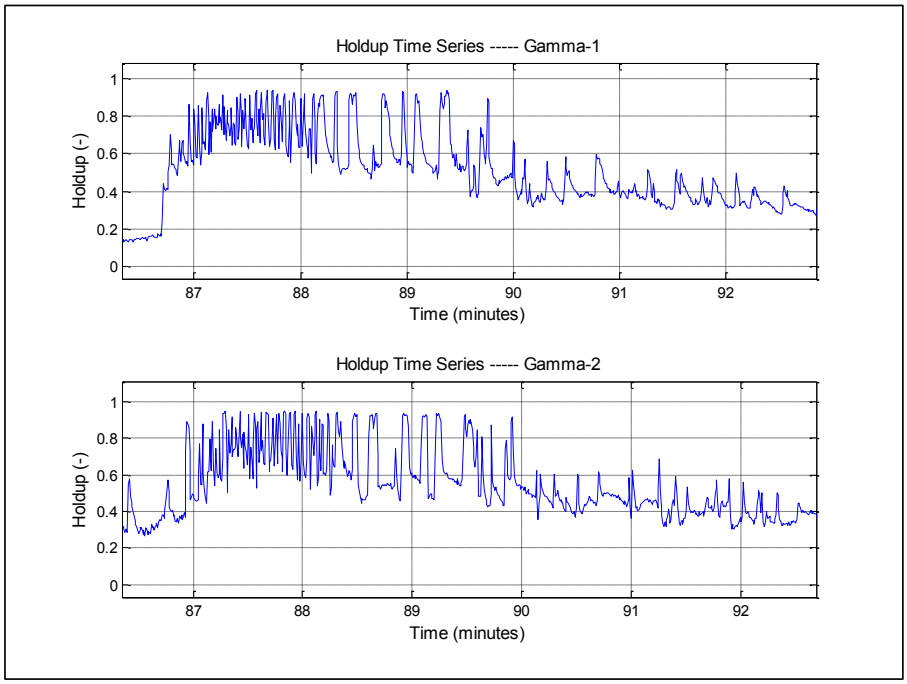

Figure 5-201: G3ST2 Holdup time series, Downstream Slug Valve, Restricted Opening, (5 minutes)-(Gamma-1&2)

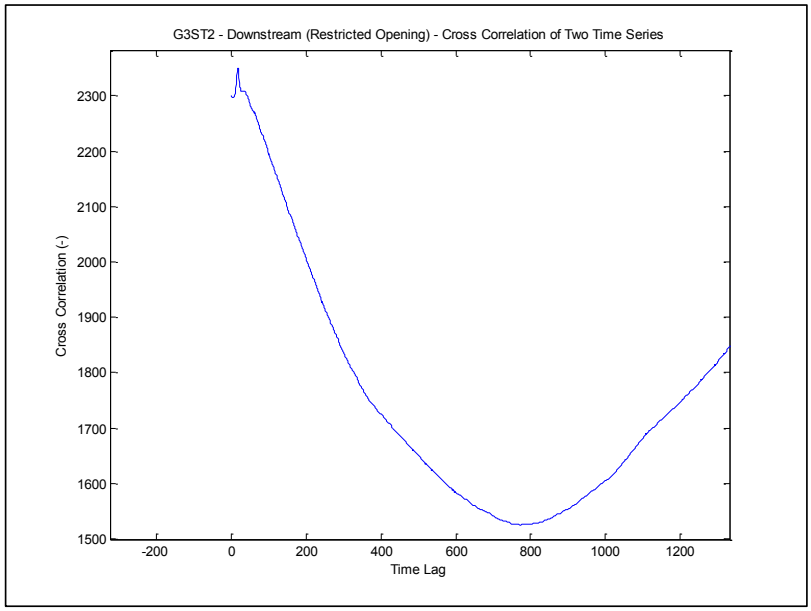

Figure 5-202: G3ST2 Cross Correlation of Two Gammas – Downstream Slug Valve, Restricted Opening

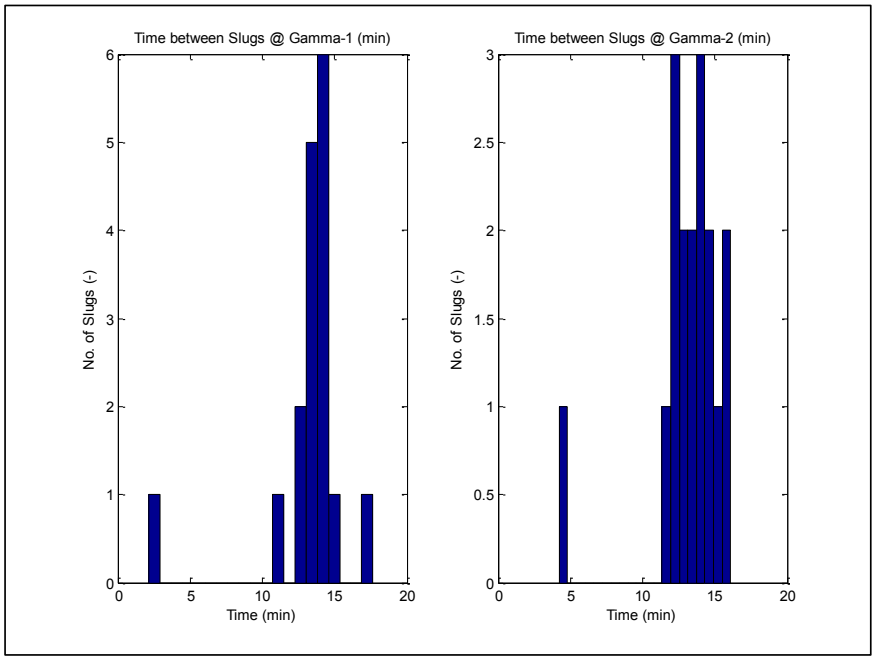

Figure 5-203: G3ST2 Distribution of Slug Frequency – Downstream Slug Valve, Restricted Opening

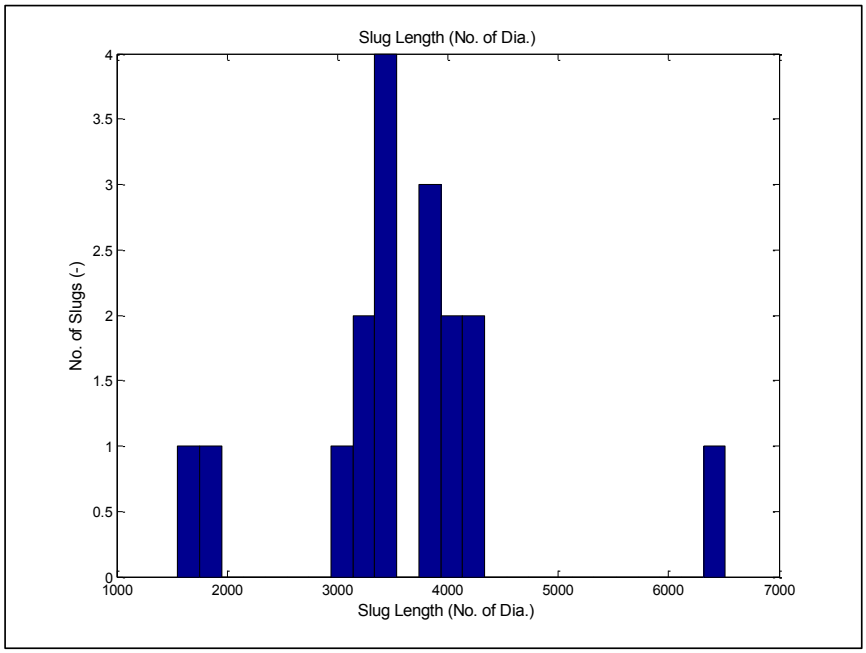

Figure 5-204: G3ST2 Distribution of Slug Length (No. of Dia.) – Downstream Slug Valve, Restricted Opening

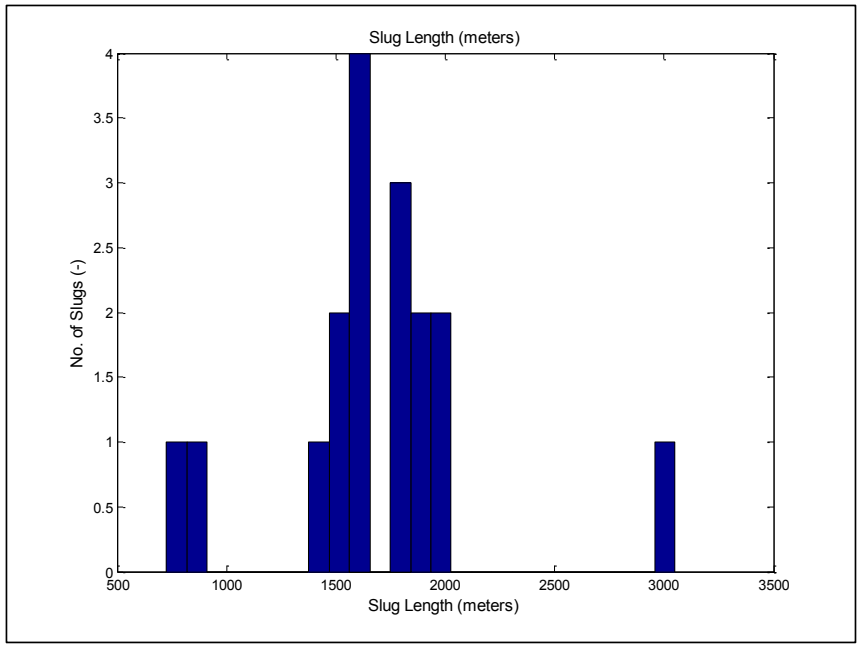

Figure 5-205: G3ST2 Distribution of Slug Length (meters) – Downstream Slug Valve, Restricted Opening

5.5.7. G3ST2 Pipeline Simulation – Slug Valve Normal Opening

Extensive simulation work was conducted using OLGA and LedaFlow. The simulation pressure results were compared against the reduced flow rate field measurements, while the holdup results were compared against the normal flow rate field measurements. The gamma measurements were both upstream and downstream of the slug valve at the end of the pipeline and the available pressure measurements were at (S-95) production header, at the inlet of the pipeline.

5.5.8. G3ST2 Pipeline OLGA Simulations

OLGA simulation was carried out with various options to fully test the simulation package capabilities to predict slugging phenomena in the subject pipeline. Using 2nd order scheme for mass equations and an adiabatic heat transfer option, the other simulation parameters which were varied for G3ST2 pipeline are as follows:

- Slug tracking (No slug tracking vs. slug tracking with various delay constants)
- Grid size (Coarse grid vs. Fine grid)

G3ST2 Pipeline OLGA Simulation – (Slug Tracking vs. No Slug Tracking)

OLGA Simulations were carried out with and without slug tracking module. The results were plotted for various Delay Constants (DCs), which significantly impact the initiation of slugs in OLGA code.

Using an average liquid velocity of (5.61) m/sec obtained from the cross correlation of the two time series, one can estimate the idle time between slug initiations as follows:

Table 5-11: G3ST2 – Idle time between slug initiations for various delay constants

Idle time between Slug Initiation (DT) (sec)	Ul (m/sec)	Inner Dia. (m)	DC
4.17	5.61	0.468	50
12.51	5.61	0.468	150
41.71	5.61	0.468	500
66.74	5.61	0.468	800

OLGA simulations were carried out with various delay constants ranging from 50 to 800. The holdup results for the upstream position are shown on figures, Figure 5-207, Figure 5-208 and Figure 5-209. Analysis of the holdup figures shows that with no slug tracking the holdup cycles are fixed at approximately (12) minutes with very stable and repetitive slug behavior, which agrees well with pressure frequency noted for the reduced flow rate case. The holdup fluctuates between (0.0) and (0.75) in few cycles and then fluctuates between (0.0) and (0.5) in another group of cycles, which also agrees well with the holdup amplitude for field measurements as shown in Figure 5-206.

With slug tracking enabled, the holdup predictions are still similar to non-slug tracking ones except for few small waves that appear in between the large slugs. These small waves tend to disappear with higher delay constants as can be seen with DC=500 and DC=800 cases.

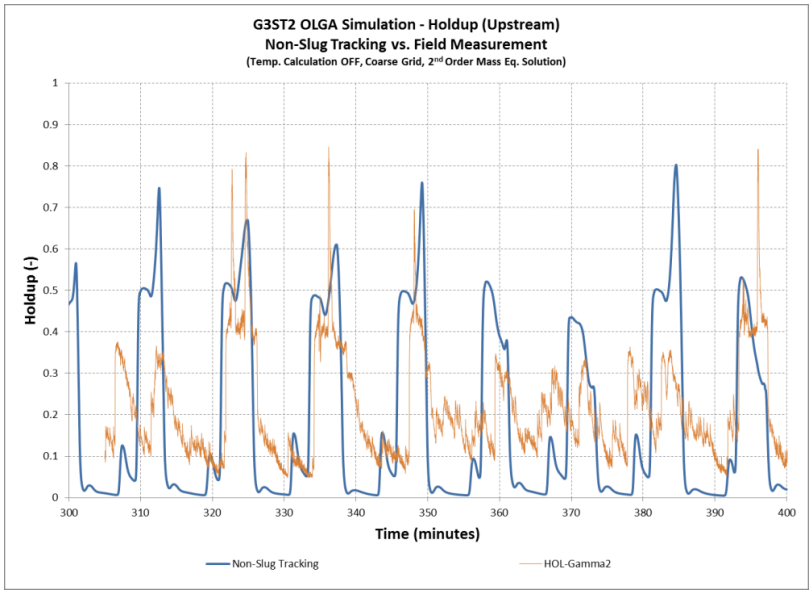

Figure 5-206: G3ST2 OLGA Holdup Simulation – Non-Slug Tracking vs. Holdup Measurement (Upstream)

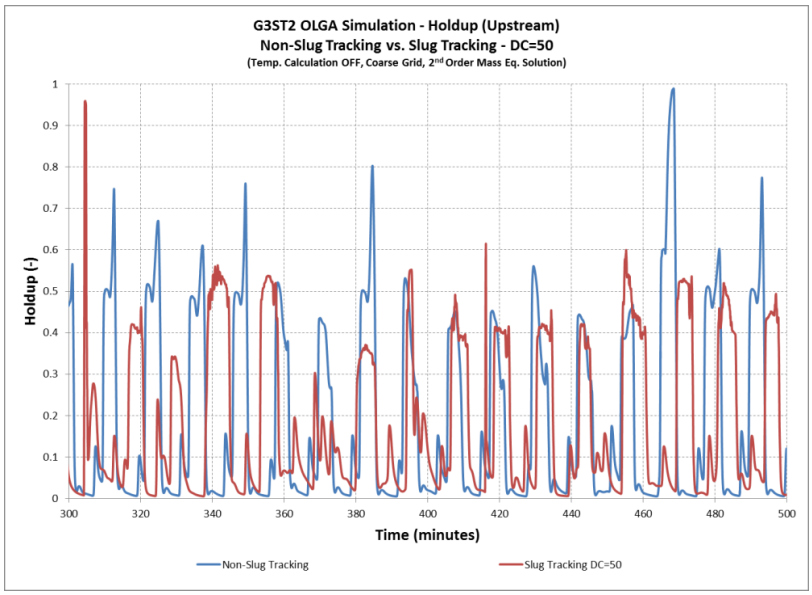

Figure 5-207: G3ST2 OLGA Holdup Simulation – Non-Slug Tracking vs. Slug Tracking (DC=50) – (Upstream)

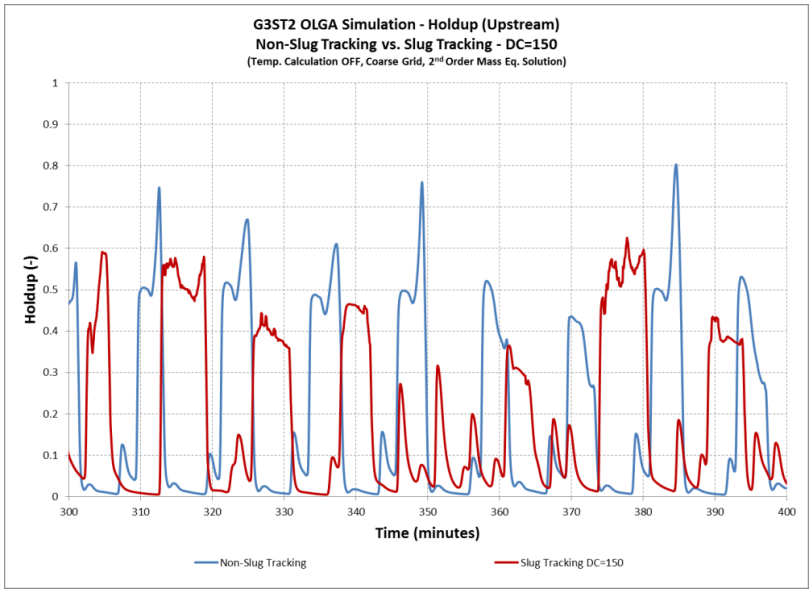

Figure 5-208: G3ST2 OLGA Holdup Simulation – Non-Slug Tracking vs. Slug Tracking (DC=150) – (Upstream)

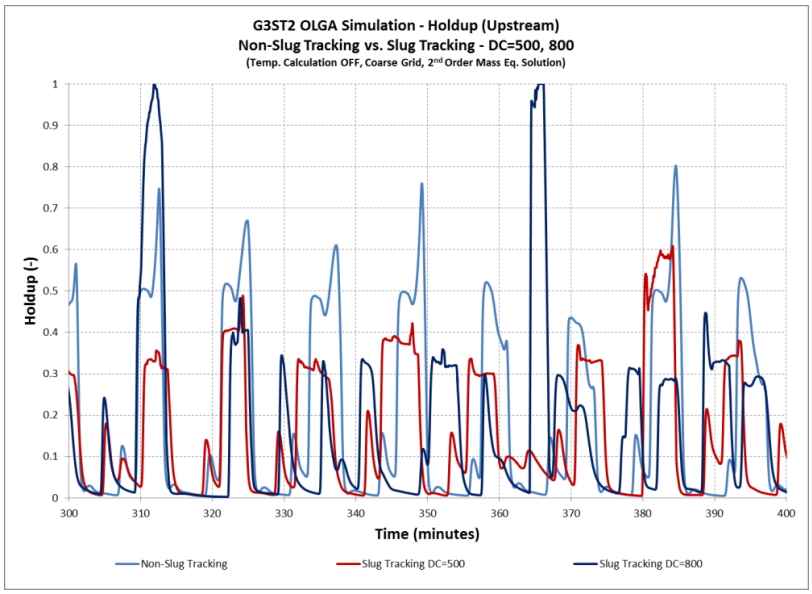

Figure 5-209: G3ST2 OLGA Holdup Simulation – Non-Slug Tracking vs. Slug Tracking (DC=500, 800) – (Upstream)

For the downstream position, the simulation also provided accurate predictions for the holdup with and without slug tracking. Only the liquid film was slightly lower than the holdup measurements as can be seen in Figure 5-210, Figure 5-211, Figure 5-212 and Figure 5-213.

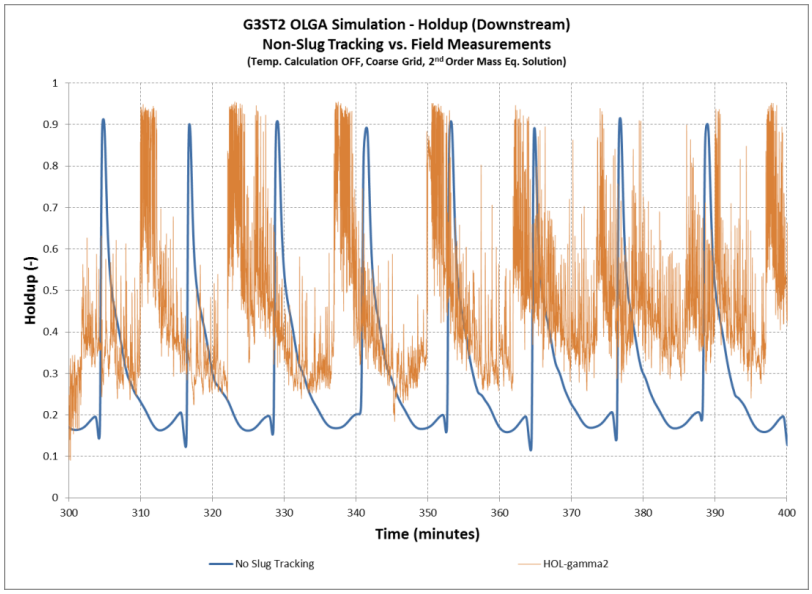

Figure 5-210: G3ST2 OLGA Holdup Simulation – Non-Slug Tracking vs. Holdup Measurement – (Downstream)

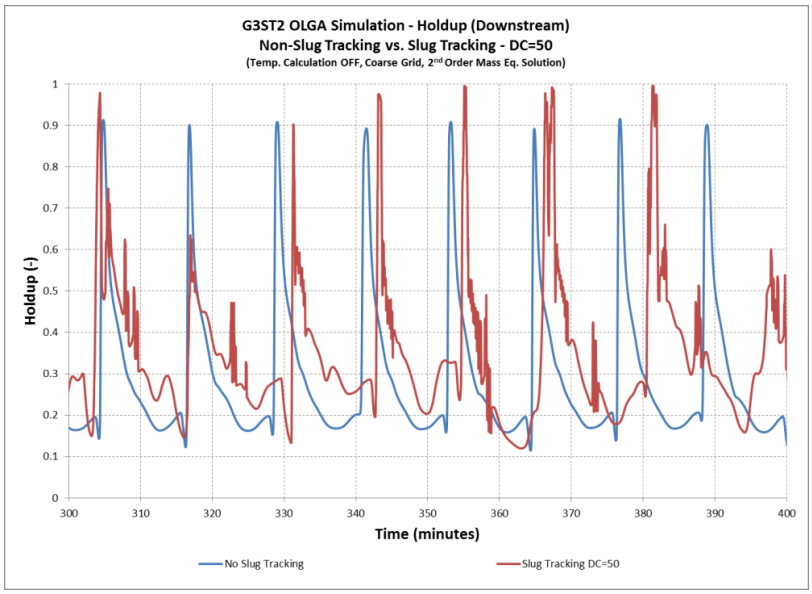

Figure 5-211: G3ST2 OLGA Holdup Simulation – Non-Slug Tracking vs. Slug Tracking (DC=50) – (Downstream)

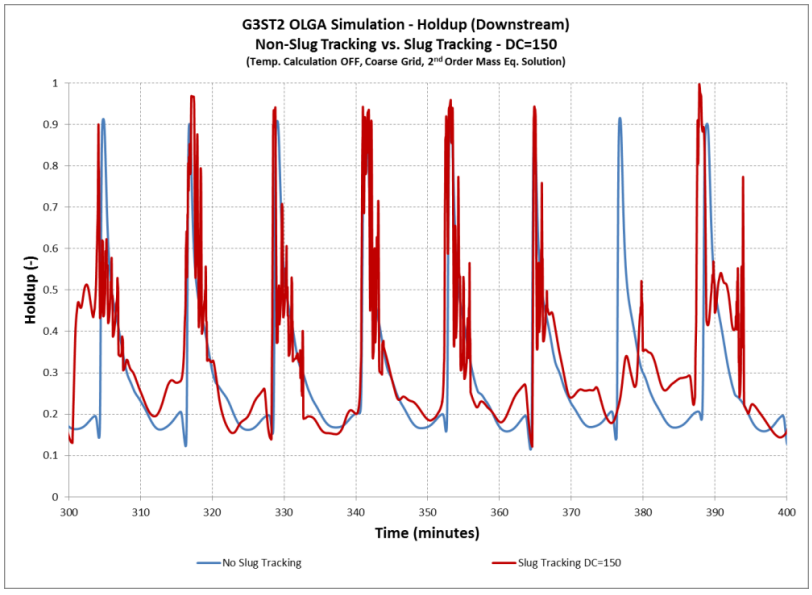

Figure 5-212: G3ST2 OLGA Holdup Simulation – Non-Slug Tracking vs. Slug Tracking (DC=150) – (Downstream)

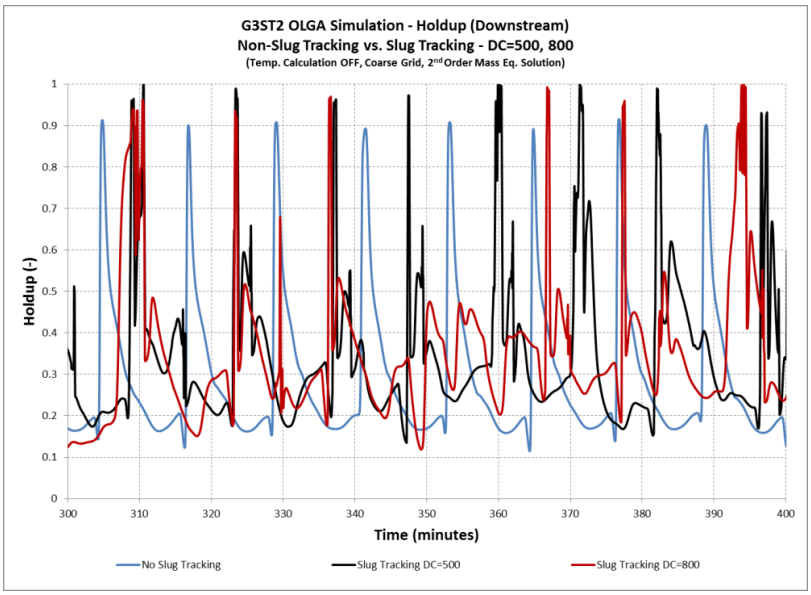

Figure 5-213: G3ST2 OLGA Holdup Simulation – Non-Slug Tracking vs. Slug Tracking (DC=500, 800) – (Downstream)

Analyzing the pressure results without slug tracking, versus pressure measurements, depicted on Figure 5-214, shows under prediction of total pressure drop by approximately (100) psi. This is a significant deviation in pressure predictions especially if you consider the percentage of the (100) psi out of the total pressure drop in the pipeline which is (440) psi, which comes to be around 22%. Using the slug tracking option in OLGA, the pressure predictions slightly improves, especially with the high frequency slug initiation case, DC=50, where the pressure deviation decreases from (100) psi to about (50) psi as shown in Figure 5-215.

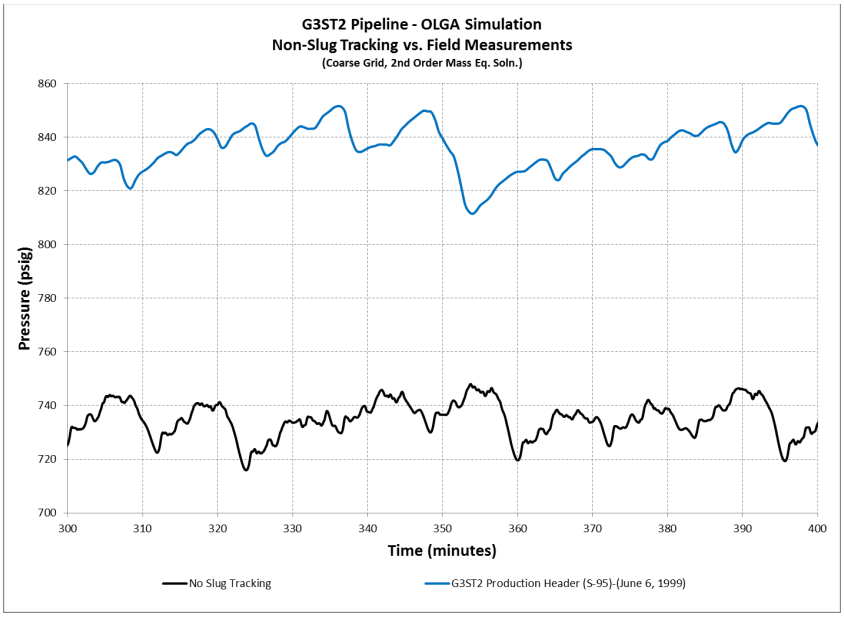

Figure 5-214: G3ST2 OLGA Pressure Results – Non-Slug Tracking vs. Pressure Measurements

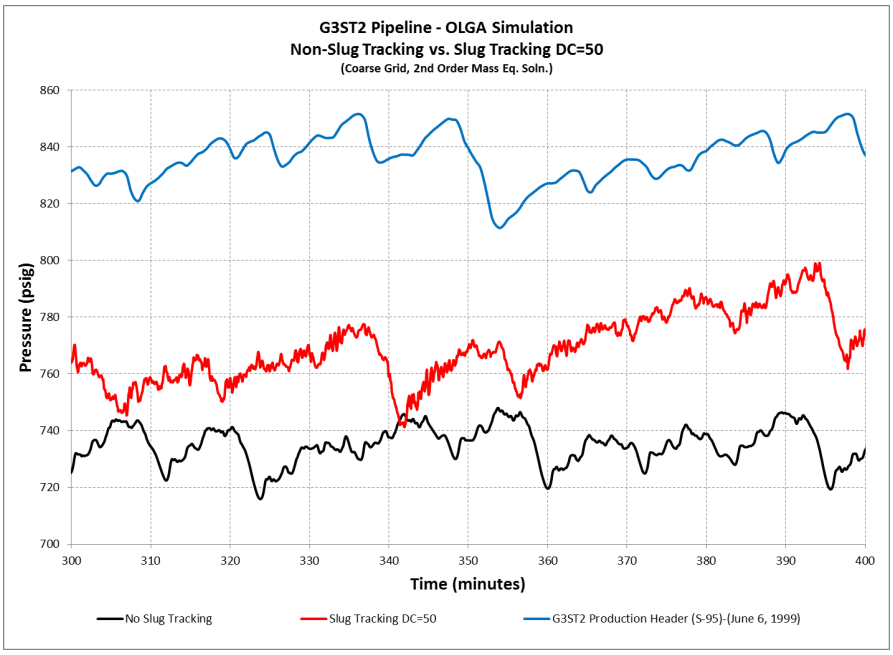

Figure 5-215: G3ST2 OLGA Pressure Results – Non-Slug Tracking vs. Slug Tracking (DC=50)

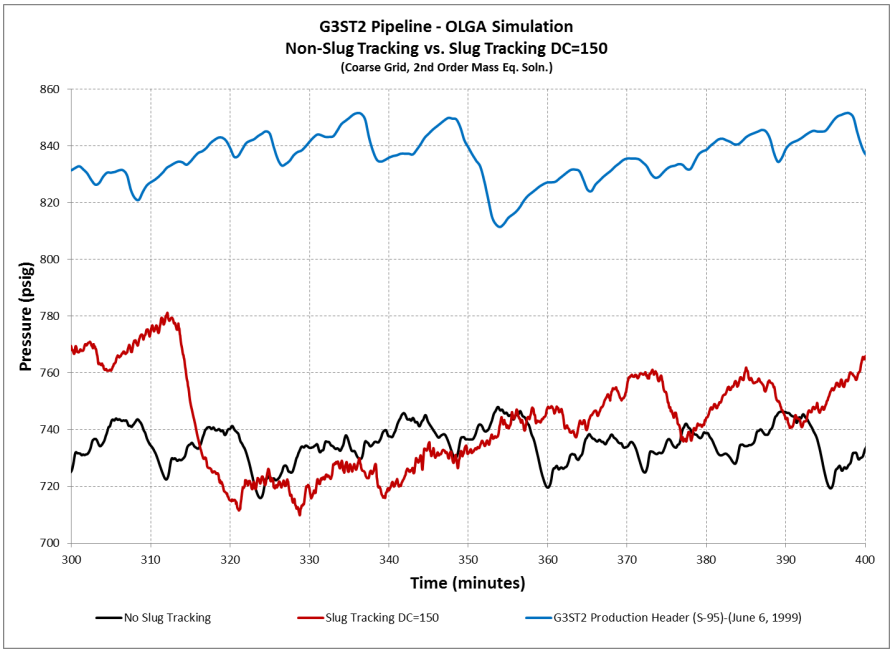

Figure 5-216: G3ST2 OLGA Pressure Results – Non-Slug Tracking vs. Slug Tracking (DC=150)

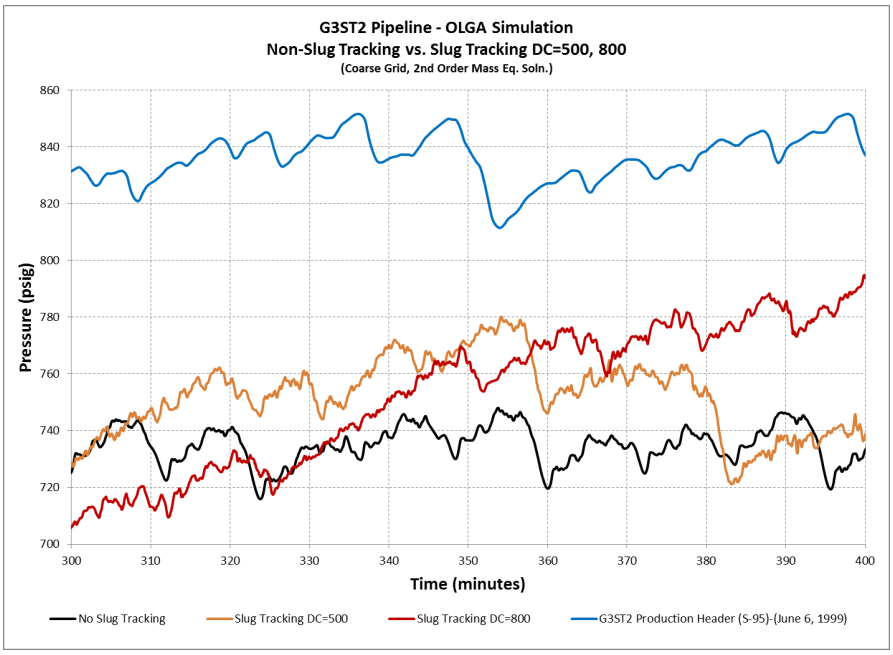

Figure 5-217: G3ST2 OLGA Pressure Results – Non-Slug Tracking vs. Slug Tracking (DC=500, 800)

G3ST2 Pipeline OLGA Simulation – (Coarse Grid vs. Fine Grid)

The previous G3ST2 pipeline OLGA simulations were conducted using a relatively coarse grid with an average pipe section of approximately (45) meters, as shown in Figure 5-218. In order to explore the impact of utilizing a fine grid on OLGA simulations, a fine grid case was simulated using a fixed (5) meters per section as shown in Figure 5-219.

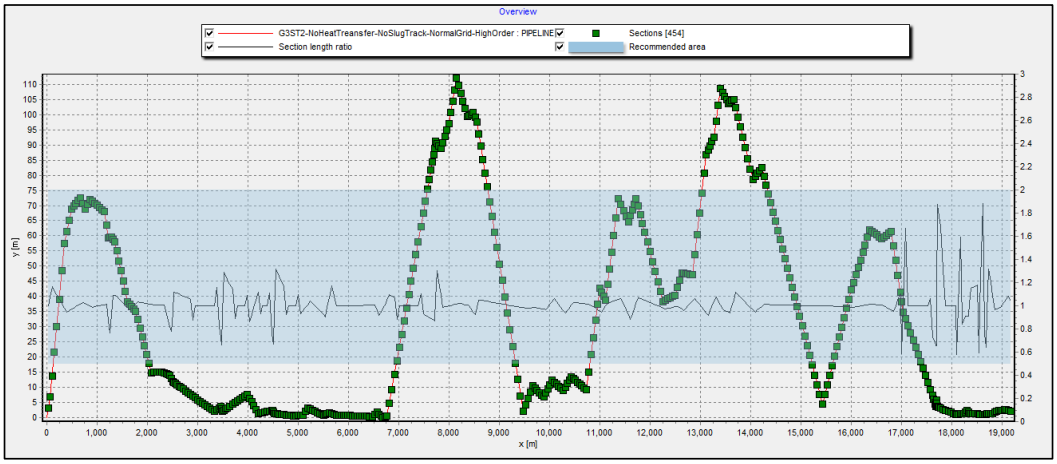

Figure 5-218: G3ST2 Pipeline Sections – OLGA Grid Options (Coarse Grid)

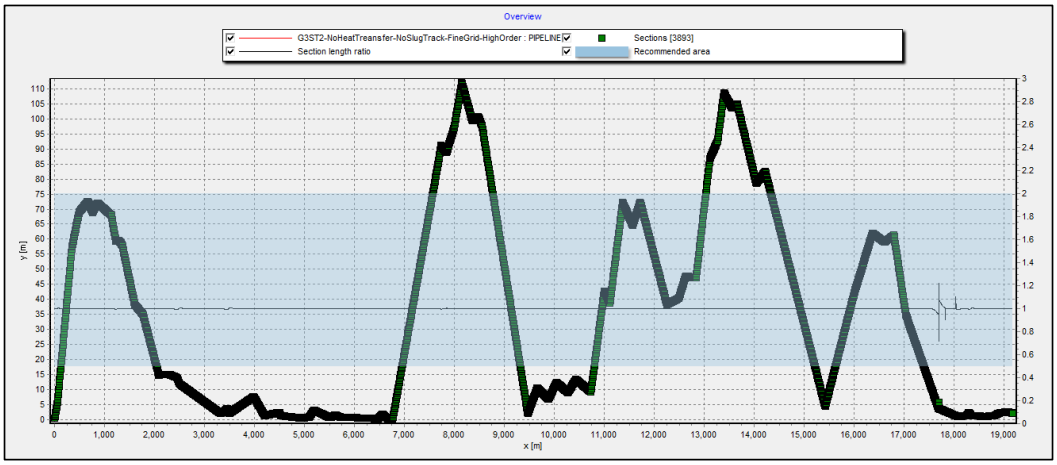

Figure 5-219: G3ST2 Pipeline Sections – (Fine Grid (5 meter))

The upstream and downstream holdup results depicted in Figure 5-220 and Figure 5-221 show a very small difference between the coarse and fine grid cases, where the fine grid case shows higher holdup amplitudes but with similar frequency to the case with the coarse grid. The pressure results indicate similar behavior where the two cases, coarse and fine grids, provide very similar results, as shown in Figure 5-222.

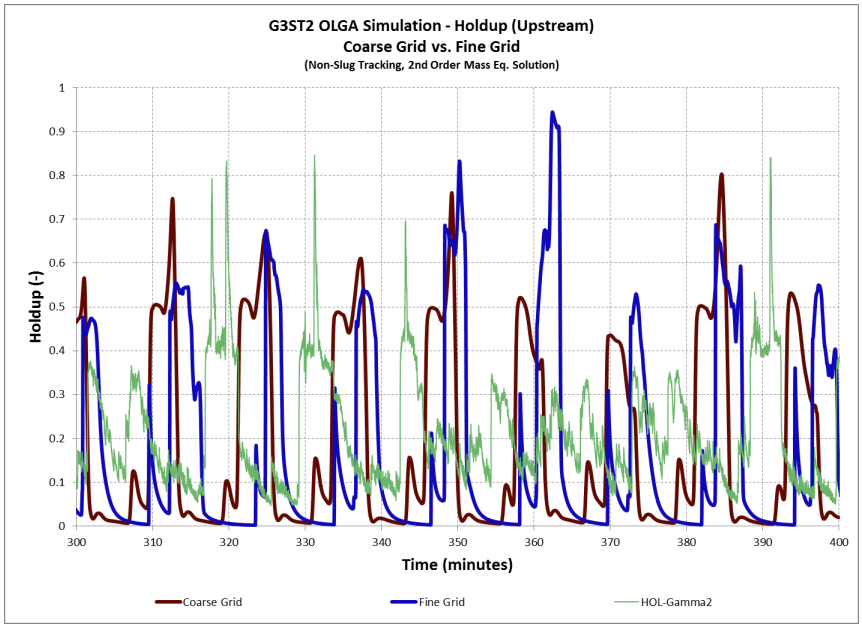

Figure 5-220: G3ST2 OLGA Holdup Simulation – Coarse Grid vs. Fine Grid (Upstream)

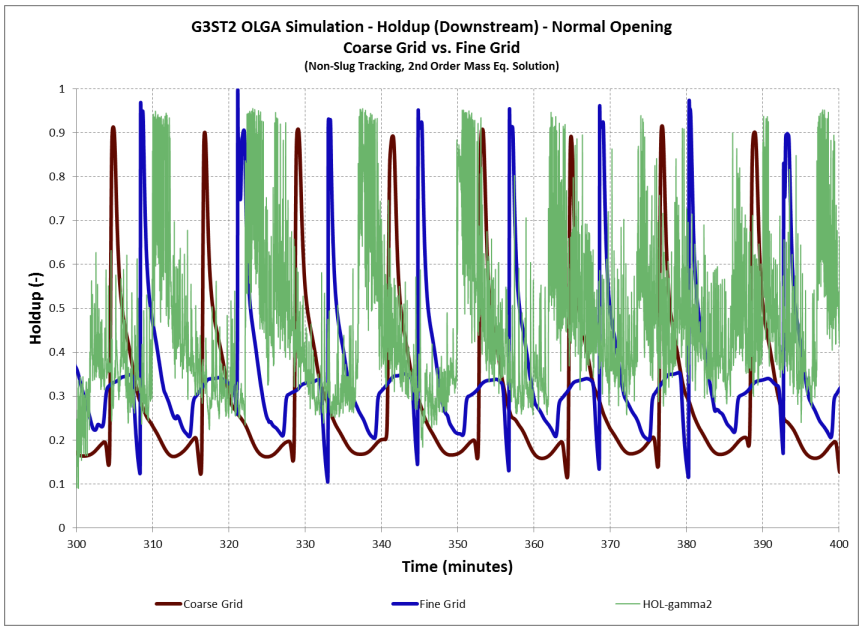

Figure 5-221: G3ST2 OLGA Holdup Simulation – Coarse Grid vs. Fine Grid (Downstream)

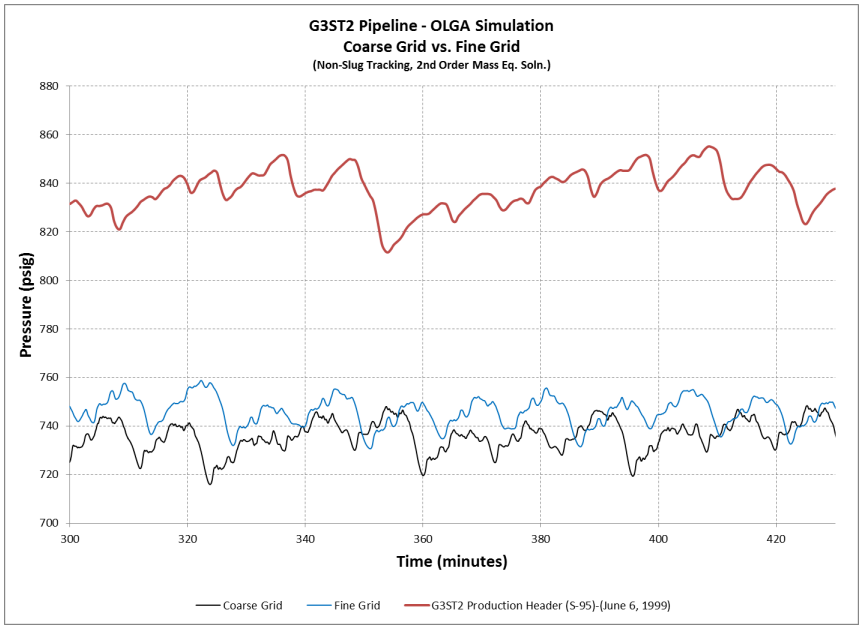

Figure 5-222: G3ST2 OLGA Pressure Simulation – Coarse Grid vs. Fine Grid (Downstream)

5.5.9. G3ST2 Pipeline LedaFlow Simulations

Similar to OLGA simulations, LedaFlow simulations were carried out with various options to fully test the simulation package and the parameters which were varied for G3ST2 pipeline LedaFlow simulations are as follows:

- Slug capturing (No slug capturing vs. slug capturing)
- Grid size (Coarse grid vs. Fine grid (5) meter) – shown on Figure **5-223**

Also, similar to OLGA simulations, heat transfer was not considered for all simulation cases. Finally, a high order scheme was considered for all simulation cases.

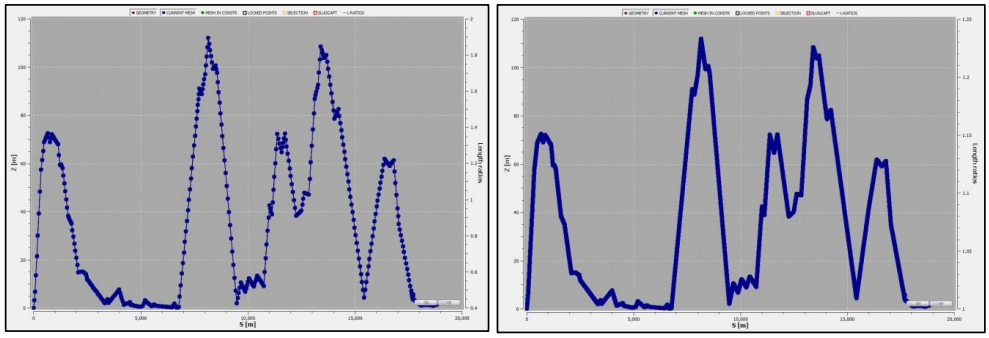

Figure 5-223: G3ST2 LedaFlow Coarse Grid (left) and Fine Grid (right)

G3ST2 LedaFlow Simulation – (Slug Capturing vs. No Slug Capturing) + (Coarse Grid vs. Fine Grid)

LedaFlow simulations were carried out with and without slug capturing module. The pressure results without slug capturing shown on Figure **5-224** and Figure **5-225** indicates a frequency of approximately (15) minutes compared to (15) minutes in field measurements. The amplitude of the pressure oscillations is in a good agreement with the field measurements at approximately (30) psi. However, when slug capturing is enabled, the amplitude of the pressure oscillations seem to reduce to approximately (20) psi. Using a fine grid of (5) meters per section indicates a minimal impact on the pressure results.

The upstream and downstream holdup results shown in Figure **5-226**, Figure **5-227**, Figure **5-228** and Figure **5-229** indicate a similar frequency as the pressure frequency of (15) minutes. The holdup amplitude shows to be very similar to the field measurement for the coarse and fine grid cases, with overall good agreements.

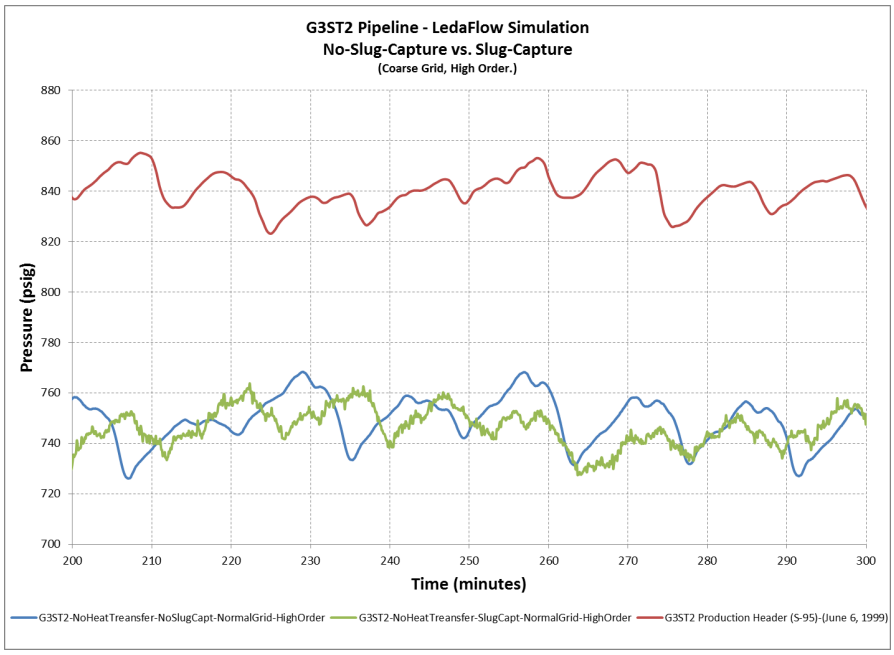

Figure 5-224: G3ST2 LedaFlow Pressure Results – Slug Capturing vs. Non-Slug Capturing Simulation (Coarse Grid)

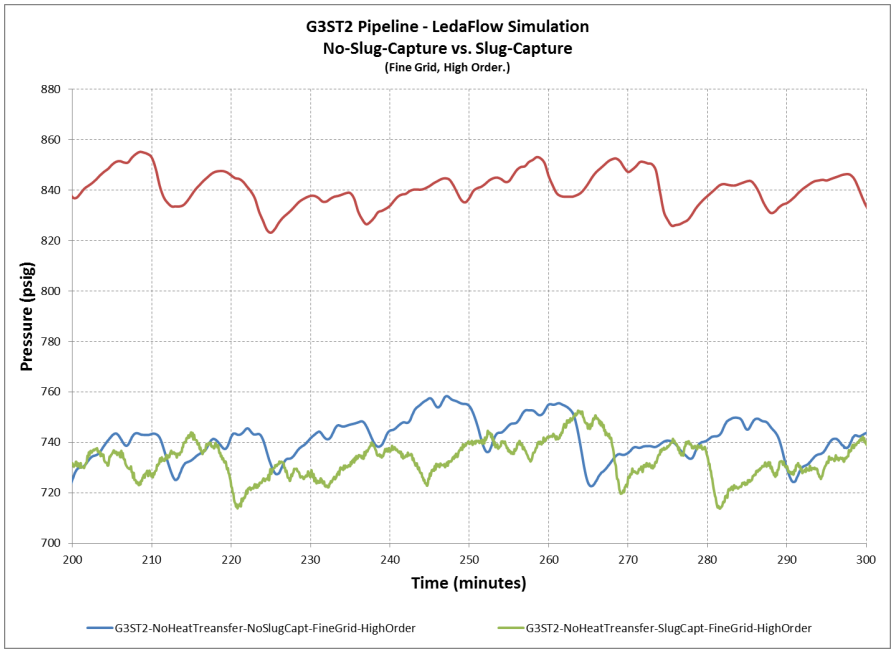

Figure 5-225: G3ST2 LedaFlow Pressure Results – Slug Capturing vs. Non-Slug Capturing Simulation (Fine Grid)

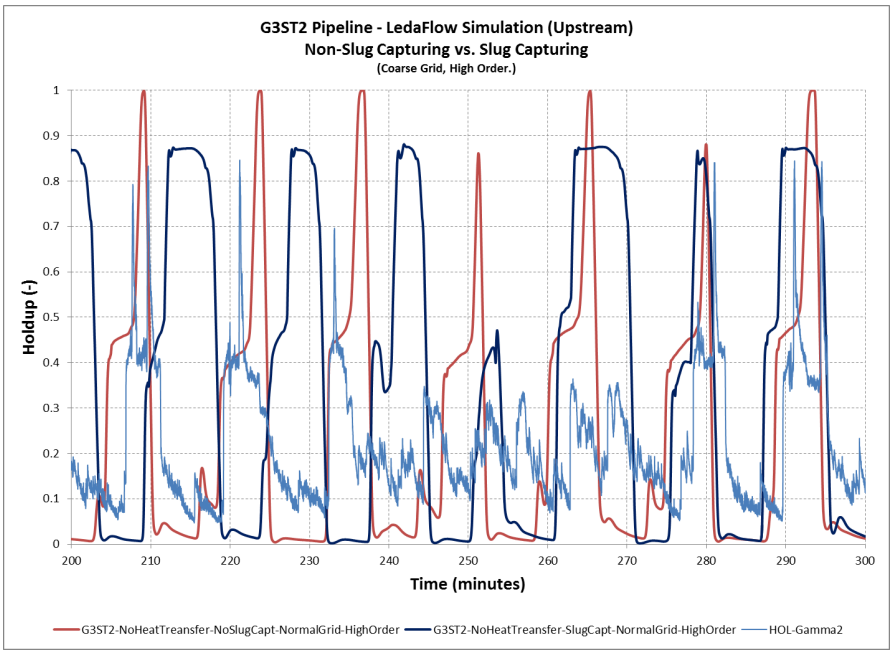

Figure 5-226: G3ST2 LedaFlow Holdup – Slug Capturing vs. Non-Slug Capturing Simulation (Coarse Grid) (Upstream)

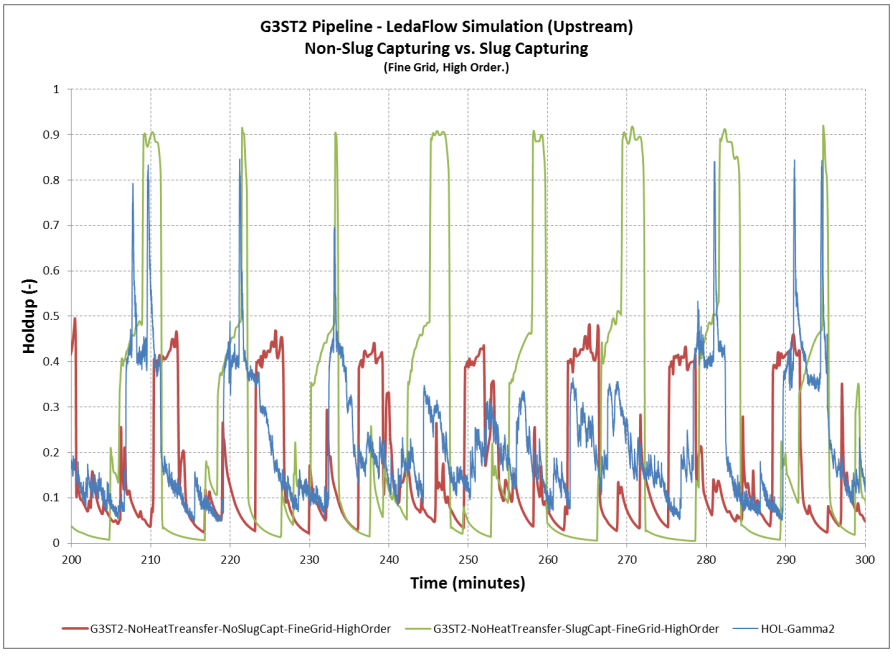

Figure 5-227: G3ST2 LedaFlow Holdup – Slug Capturing vs. Non-Slug Capturing Simulation (Fine Grid) (Upstream)

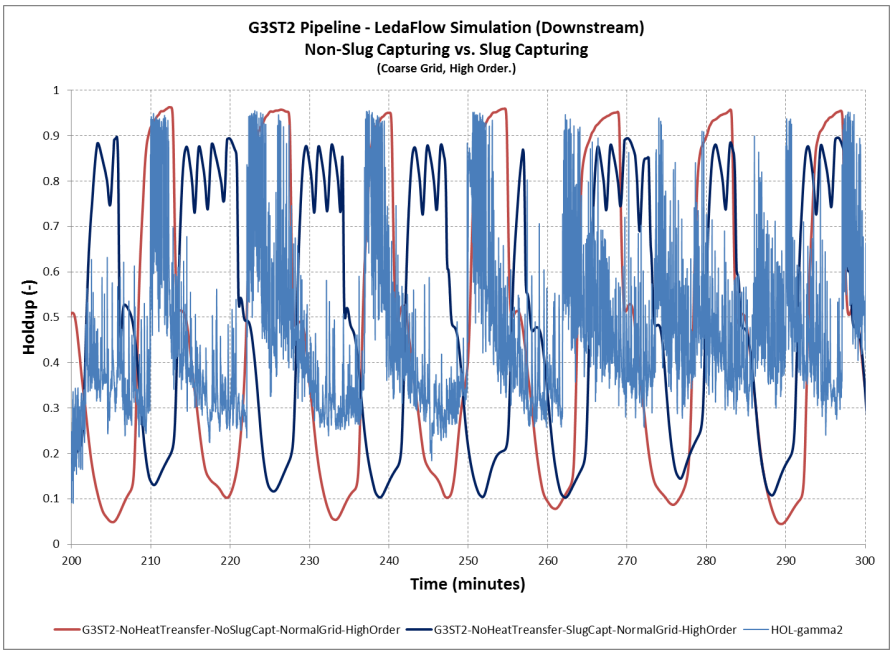

Figure 5-228: G3ST2 LedaFlow Holdup – Slug Capturing vs. Non-Slug Capturing Simulation (Coarse Grid) (Downstream)

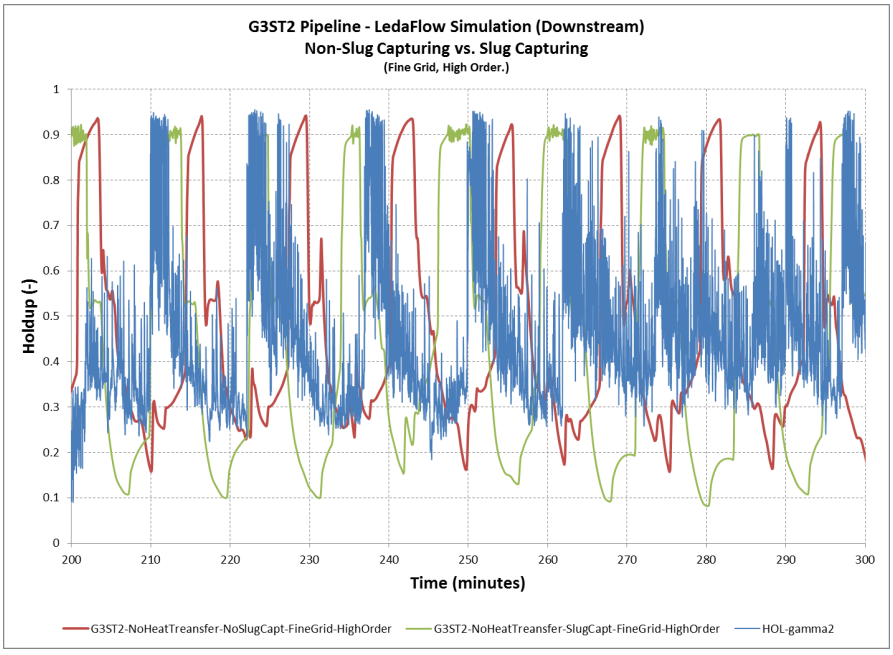

Figure 5-229: G3ST2 LedaFlow Holdup – Slug Capturing vs. Non-Slug Capturing Simulation (Coarse Grid) (Downstream)

5.5.10. G3ST2 OLGA and LedaFlow Simulation Conclusions

- The best OLGA holdup results were obtained using non-slug tracking case.
- OLGA pressure results were slightly improved using a slug tracking option with a delay constant of DC=50. This could be related to the over prediction behavior reported in OLGA slug tracking module.
- Utilizing a fine grid had a minimum impact on OLGA results.
- A non-slug capturing case provided the best LedaFlow results.
- Utilizing a fine grid or slug capturing module did not improve the results.

5.5.11. G3ST2 Pipeline Slug Valve Optimization Study

A quick evaluation of the optimum choke settings that would have provided the best results for this particular pipeline was conducted using both OLGA and LedaFlow simulation packages. The study utilized a normal grid case without slug capturing / tracking options, along with various choke fixed manual settings. Each valve setting, shown in Table 5-12, was simulated for two hours before moving to the next setting and the study reported the pipeline inlet pressure as shown in Figure 5-230 and Figure 5-231 for OLGA and LedaFlow results.

These results indicate a slugging behavior at all valve opening levels. The level of slugging oscillations increased with less choking of the valve. This was due to a new slug cycle that was created by the liquid accumulating at the uphill section downstream of (S-92). The liquid accumulating in this section was behaving as a stratified flow with the pipe almost full of liquid, and with the additional pressure from the valve acting to overcome the compressible gas force upstream this section. When the valve is fully open, the compressibility of the gas overcome the static head of the liquid which initiates a new slugging cycle which was not present when the valve was choked.

This behavior presents a new insight into the valve-slug interaction in a highly terrain profile and shows the complexity of the phenomenon in such pipeline systems.

Table 5-12: G3ST2 Pipeline Choke Opening Settings

	OLGA Choke Opening (%)	LedaFlow Choke Opening (%)	Simulation Time (hrs) Start – Finish
1.	2 %	3 %	0 – 2
2.	2 %	3 %	2 – 4
3.	3.5 %	3.5 %	4 – 6
4.	3.5 %	3.5 %	6 – 8
5.	10 %	5%	8 – 10
6.	20 %	10 %	10 – 12
7.	40 %	20 %	12 – 14
8.	80 %	40 %	14 – 16
9.	100 %	60 %	16 – 18
10.		100 %	18 – 20

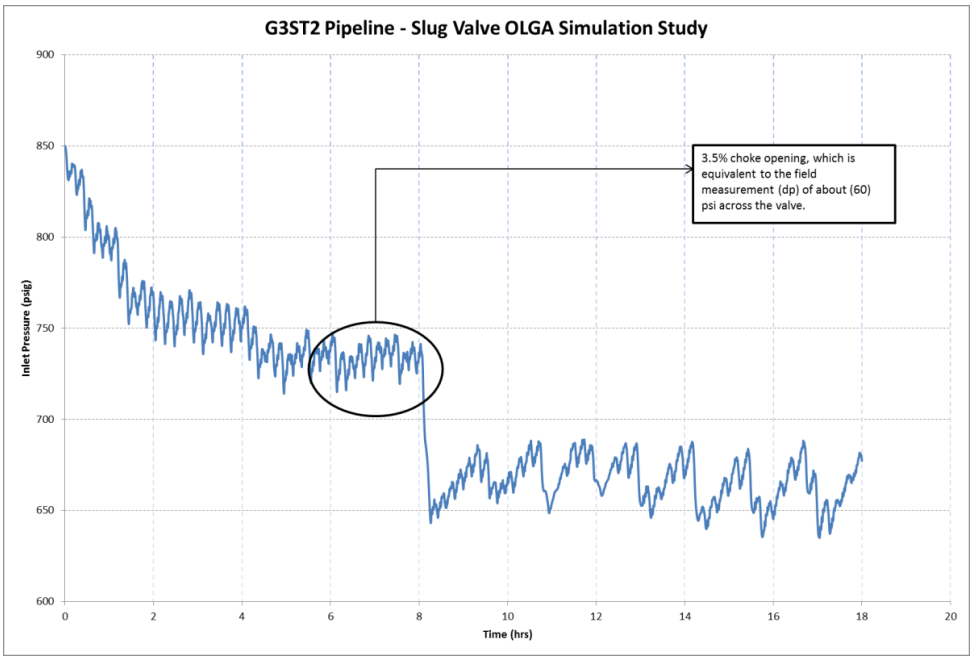

Figure 5-230: G3ST2 Pipeline – Slug Valve OLGA Simulation Study – (Coarse Grid, 2nd Order, No-SlugTracking)

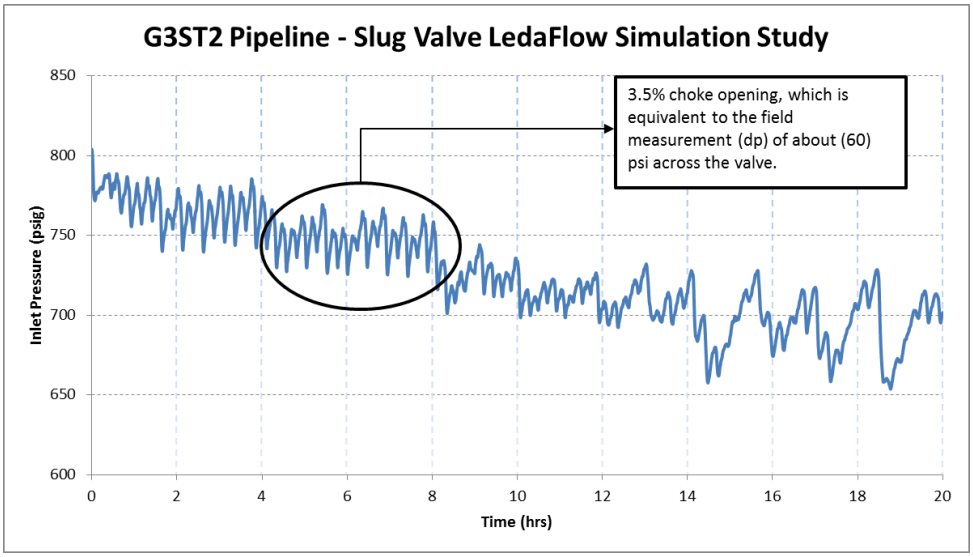

Figure 5-231: G3ST1 Pipeline – Slug Valve LedaFlow Simulation Study – (Coarse Grid, High Order, No-SlugCapturing)

This page was intentionally left blank

6. FIELD-B – HOLDUP & PRESSURE MEASUREMENTS

Field-B holdup and pressure measurements were carried out over two days on February 2nd and 3rd, 2013. They were carried out on a horizontal section near the Gas Oil and Separation Plant (GOSP) fence on two 30 inch diameter pipelines, labeled as G2M1 and G2X1, shown in Figure 6-1. The measurements were conducted using the gamma radiation densitometer technique.

Figure 6-1: Photos of Field-B Field Measurement (G2M1 & G2X1) Pipelines

The motivation behind this measurement was the several failures experienced at the high and low pressure separators at Field-B GOSP facilities. These failures were suspected to be due to the high pressure forces created by hydrodynamic slugs on the separators internals, which were designed for a much lower force rating. These failures occurred after approximately three years of operations, see Figure 6-2. Therefore, a gamma densitometer field measurement was planned to confirm the high slug velocities predicted by OLGA on these pipelines.

Figure 6-2: Damage to Field-B GOSP Low Pressure Separator

6.6. Field-B Description

At Field-B, oil is collected from various well sites to a scraper manifold area where the two main trunklines, G2M1 and G2X1, start and then ultimately end at GOSP-2 facilities.

The two grades of crude oil which are are bing produced, Aarab Medium (AM) and Arab Extra Light (AXL), are sent to GOSP-2 where the two grades are mixed as shown in the simplified process flow diagram in Figure 6-3. The figure shows how the AXL flow is being separated at the High Pressure Production Trap (HPPT) and then mixed with AM directed towards the Low Pressure Production Trap (LPPT).

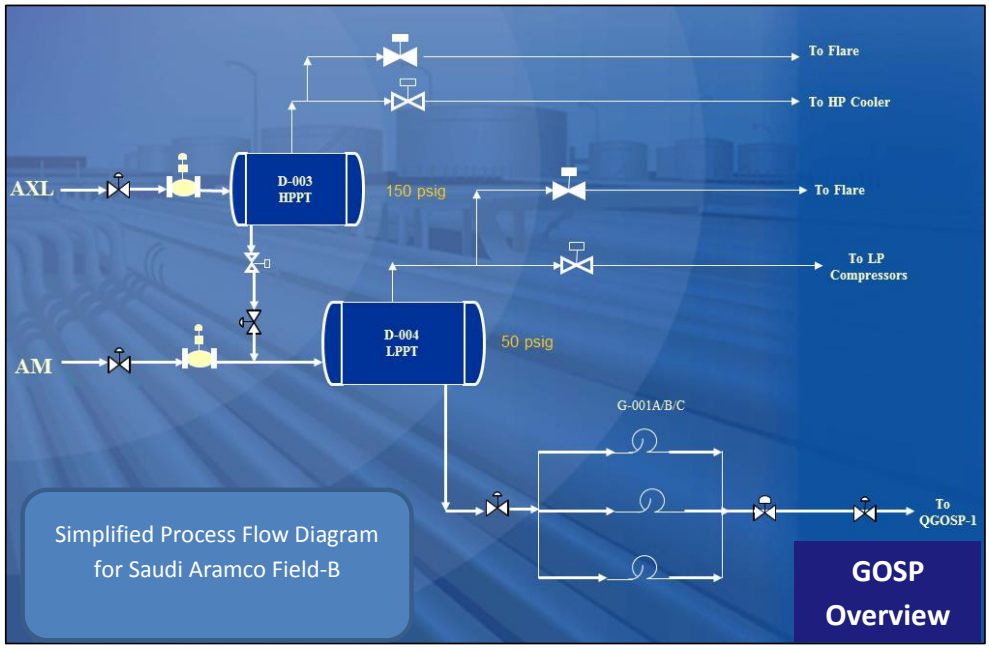

Figure 6-3: Simplified Process Flow Diagram of GOSP-2

6.7. Flow Rates

During field measurements, the G2M1 pipeline AM oil production was estimated at a flow rate of 46,000 BBL/Day at standard flow conditions and average water cut of 2.2%. On the other hand, the G2X1 pipeline AXL oil production was estimated at a flow rate of 37,000 BBL/Day at standard flow conditions and average water cut of 21%. These production figures are estimated based on individual wells historical production data obtained by the field production team. The G2M1 superficial liquid and gas velocities as calculated by OLGA were (0.26) m/sec and (1.2 to 1.8) m/sec respectively. On the other hand, the G2X1 superficial liquid and gas velocities as calculated by OLGA were (0.24) m/sec and (1.75) m/sec respectively.

Flow rates were also confirmed through the measurement of the total flow rate out of the GOSP. During the field measurement, the total flow rate out of the GOSP was reported at 102,000 BBL/Day at a pressure of approximately 130 psig. This flow rate includes both oil and water. Adding both the AXL and AM flow rates from the wells along with their water cut provide a total flow rate of 94,000 BBL/Day at standard conditions and 103,000 BBL/Day at GOSP outlet conditions. This provides assurance on the accuracy of the flow rates provided for the two pipelines.

6.8. Pipeline Details

G2X1 and G2M1 pipelines, both have an outside diameter of 30 inch with a wall thickness of 1.094 inch. The pipeline extends for approximately 10.5 Km from a scraping manifold area to the GOSP facilities. The terrain can be described as being moderately undulating with an overall downward slope as shown in Figure 6-4.

The pipeline goes under a major highway in the first kilometer and hence one can notice the pipeline going three meters underground before going up again and following the area terrain. In the third kilometer the pipeline goes above ground and thus one can notice the sudden increase of about five meters.

The area where the field measurement was carried out was a flat area upstream of the GOSP fence.

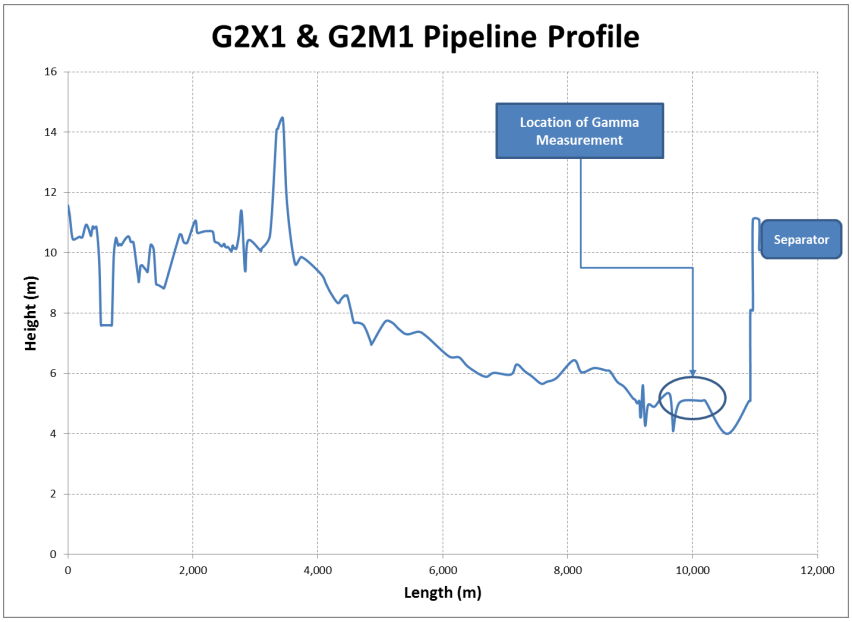

Figure 6-4: Pipeline Profile for Field-B pipelines G2X1 & G2M1

6.9. Inlet and Outlet Pressure

The GOSP separator pressure was set at 45 psig for (LPPT) and at 145 psig for the HPPT. The pressure control valves on the separator forces the pressure to fluctuate between (40 and 50) psig for the LPPT separator and between (140 and 150) psig for the HPPT separator as shown on Figure 6-5 and Figure 6-6.

The pipelines flow rates were controlled through flow control valves which were installed approximately 200 meters upstream of the separator. The pressure upstream of the flow control valves is shown in Figure 6-7 and Figure 6-8, with an average pressure of approximately (105) psig and (238) psig for G2M1 and G2X1 respectively, during the field measurement period, February 2nd and 3rd 2013. This implies a pressure drop across the valve of approximately (60) psig and (93) psig for G2M1 and G2X1 respectively.

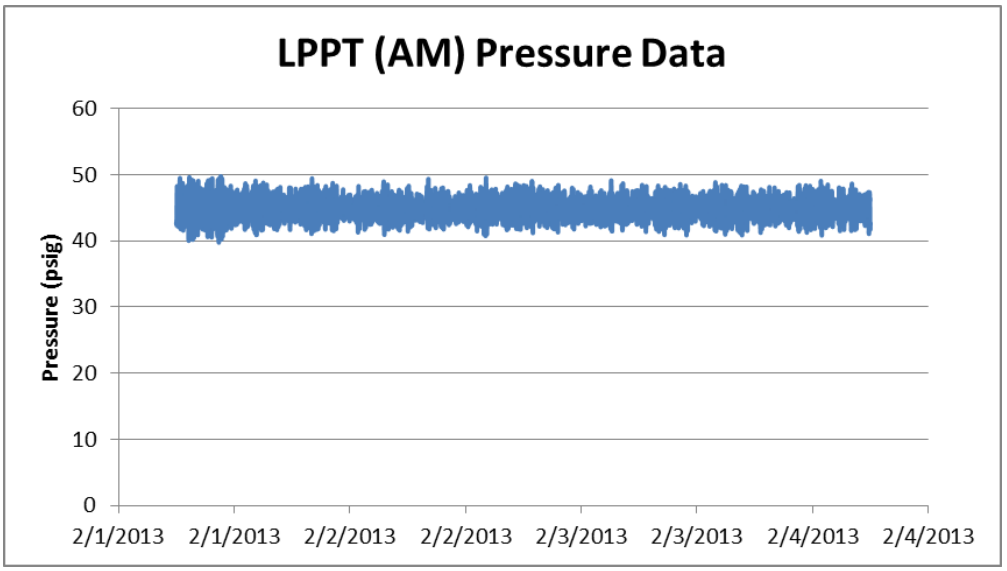

Figure 6-5: LPPT AM Pressure Reading during Field Measurement

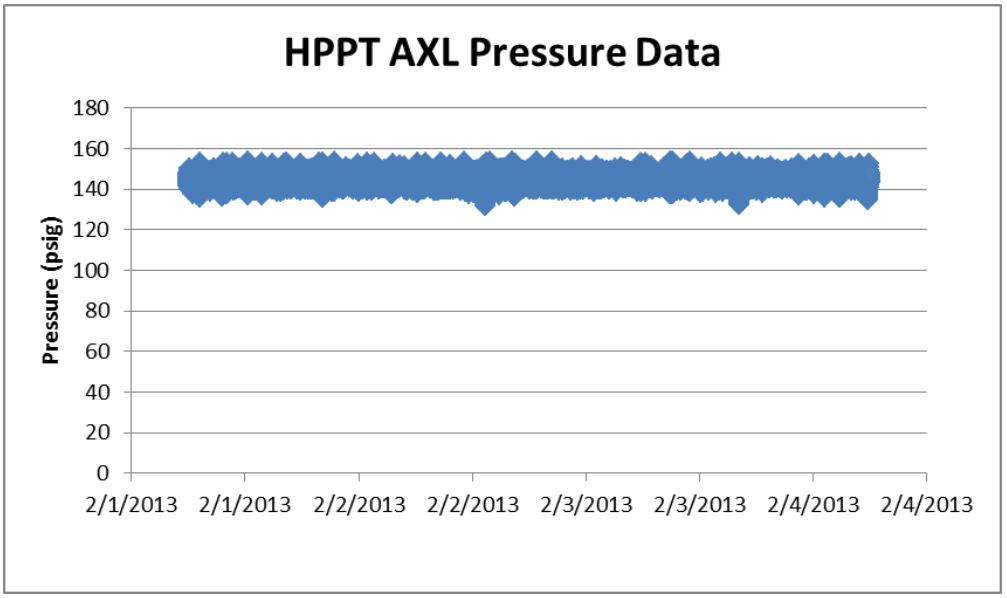

Figure 6-6: HPPT AXL Pressure Reading during Field Measurement

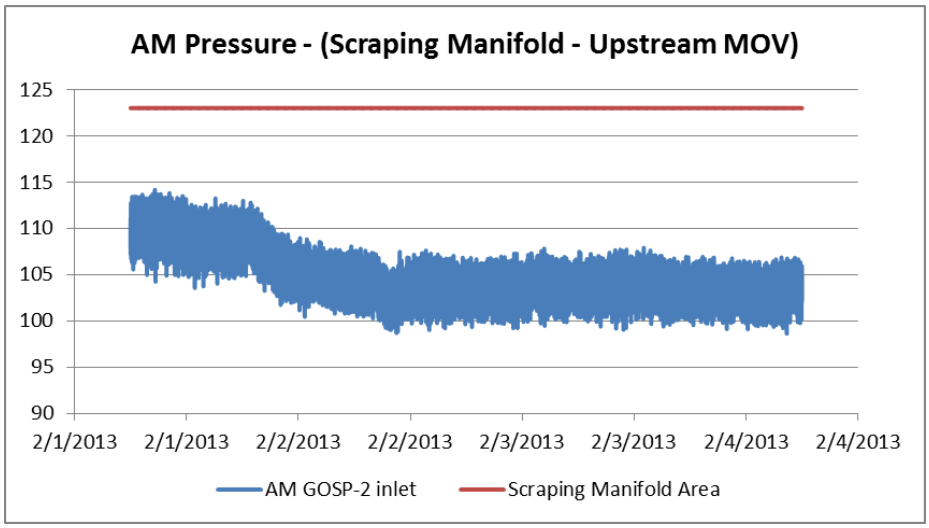

Figure 6-7: Pressure Readings at Scraper Manifold Area – G2M1

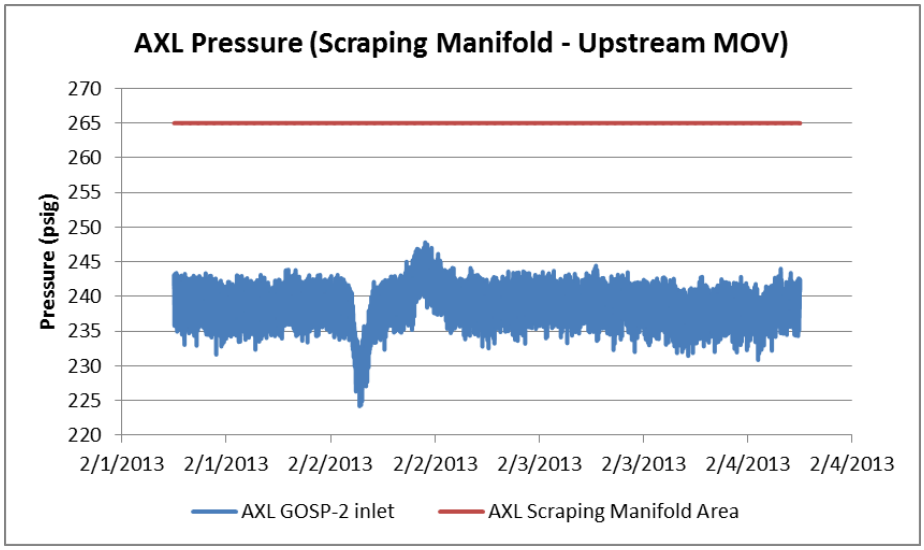

Figure 6-8: Pressure Readings at Scraper Manifold Area – G2X1

The pressure at the scraping manifold area at the inlet of the pipeline was not measured during the field measurement period on February 2nd and 3rd 2013. However, on Feb 20, the pressure measurement was taken at the scraping manifold area and the pressure was reported to be 106 psig. The flow rate at February 20 was confirmed to be the same as the one on February 2nd and 3rd. However, the pressure drop of just one psi appears to be extremely low and as such more investigation was carried out.

Examination of pressure data from wells connected to trunklines G2M1 at the scraping manifold area, on February 2nd and February 3rd 2013, indicates a pressure reading of 123 psig. Those wells are connected to the inlet of the 30 inch G2M1 trunkline with a 60 meter 20 inch pipeline which provides minimal pressure drop. Thus, one could safely assume that the pressure readings at those wells are of the same magnitude as the one at the inlet of G2M1 trunkline.

In addition, field operations were requested to obtain the pressures at the pipelines inlet and outlet locations on June 24, 2013. The results show a similar pressure drop across the 10.5 kilometer trunkline of approximately 10 to 20 psi.

A summary of all the pressure readings and associated flow rates at different dates are presented in Table 6-1.

Table 6-1: G2M1 Pressure & Flow Rates

Date	Press. @ Scraper Manifold Area (psig)	Press. Upstream of Choke Valve (MOV-102) (psig)	Pressure @ LPPT (psig)	Estimated Flow Rate (MBD)
Feb 2-3, 2013	123*	105	45	46
Feb 20, 2013	106	N/A	45	46
June 24, 2013	130	120	45	55

*Pressure obtained from the nearby wells at scraping manifold area.

Similarly, G2X1 pressure at the scraping manifold area at the inlet of the pipeline was never measured during the field measurement period on February 2nd and 3rd 2013. However, on Feb 20, the measurement was taken at the scraping manifold area and the pressure was reported to be 283 psig. The flow rate at February 20 was confirmed to be the same as the one on February 2nd and 3rd.

Examination of pressure data from wells connected to trunkline G2X1 at site P-23, the scraping manifold area, on February 2nd and 3rd 2013 indicate pressures of approximately 265 psig. Those wells are connected to the inlet of the 30 inch G2X1 trunkline with a 60 meter 20 inch pipeline which provides minimum pressure drop. Thus, one could safely assume that the pressure readings at those wells are of the same magnitude as the one at the inlet of G2X1 trunkline.

In addition, field operation was requested to obtain the pressures at the three locations on June 24, 2013. The results show a similar pressure drop across the 10.5 kilometer trunkline of approximately 20 to 40 psi. A summary of all the pressure readings and associated flow rates at different dates are presented in Table 6-2.

Table 6-2: G2X1 Pressure & Flow Rates

Date	Press. @ Scraper Manifold Area (psig)	Press. Upstream of Choke Valve (MOV-101) (psig)	Pressure @ HPPT (psig)	Estimated Flow Rate (MBD)
Feb 2-3, 2013	265*	240	145	37
Feb 20, 2013	283	240	145	37
June 24, 2013	215	205	145	42

*Pressure obtained from the nearby wells at scraping manifold area.

6.10. Field-B Fluid Properties

Field-B contains two types of oil and gas fluids. One can be characterized as Arab Medium (AM) crude oil and the other one can be characterized as Arab Extra Light (AXL). The two fluids are then mixed at the GOSP to create a new crude oil grade characterized as Arab Light (AL).

The fluid average properties which include the GOR, Gas MW and API are depicted in Table 6-3.

Table 6-3: Field-B AM and AXL Fluid Properties

Fluid Property	AM	AXL
API @ 60 F	25.8	35.4
Gas MW	0.36844	0.062079
GOR	330 SCF/STB	1195 SCF/STB

The phase envelopes of (AM) and (AXL) crude oil are shown in Figure 6-9 and Figure 6-10, which indicates that we are clearly in the two phase region.

The gas and liquid densities variations with pressure are shown in Figure 6-11, Figure 6-12, Figure 6-13 and Figure 6-14. These figures were plot for the (AM) and (AXL) fluid using OLGA at a temperature of 120°F. The oil viscosity was also plot at the same temperature which shows the variation with pressure from 0 to 500 psig as shown in Figure 6-15 and Figure 6-16 for (AM) and (AXL) respectively.

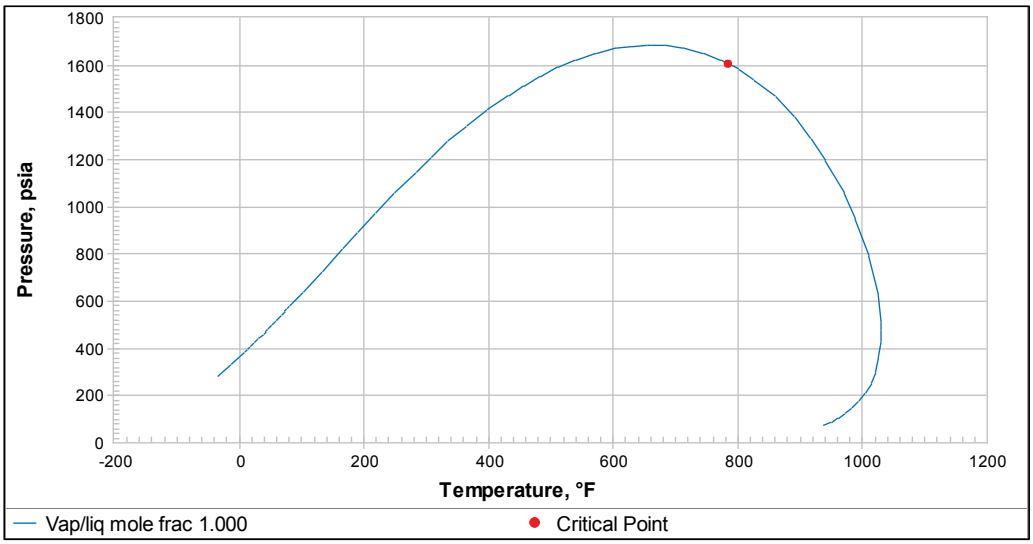

Figure 6-9: Phase Envelope of Field-B (AM) Crude Oil

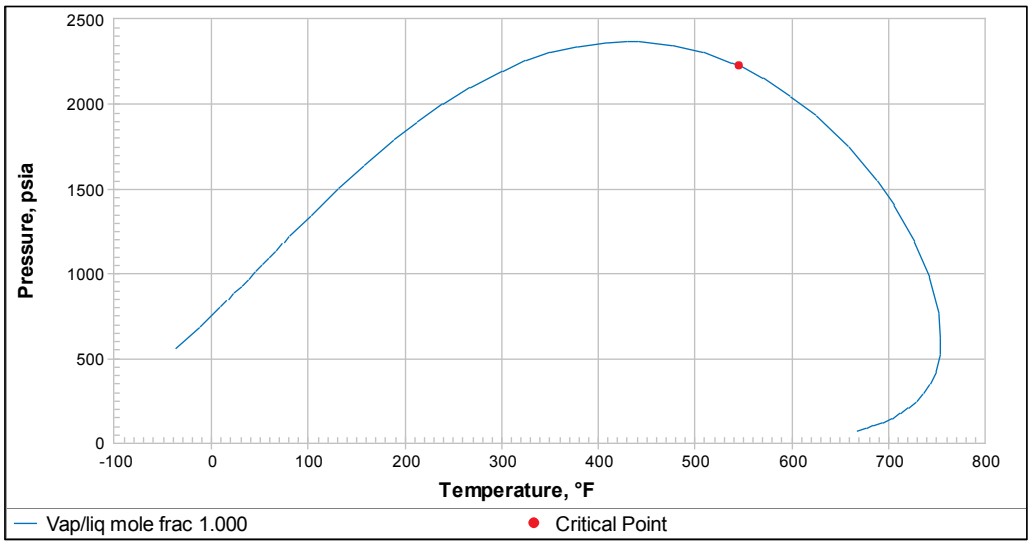

Figure 6-10: Phase Envelope of Field-B (AXL) Crude Oil

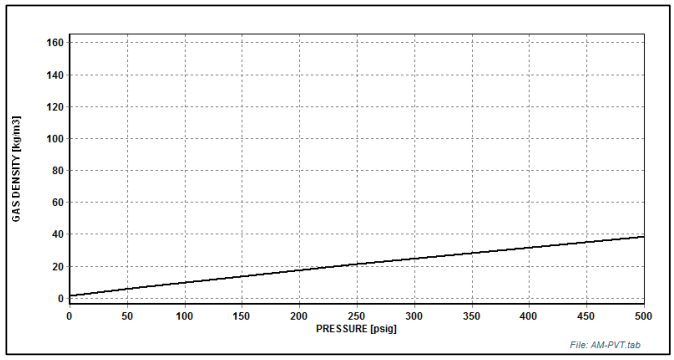

Figure 6-11: (AM) Gas Density (Kg/m3) – Temperature @ (120°F)

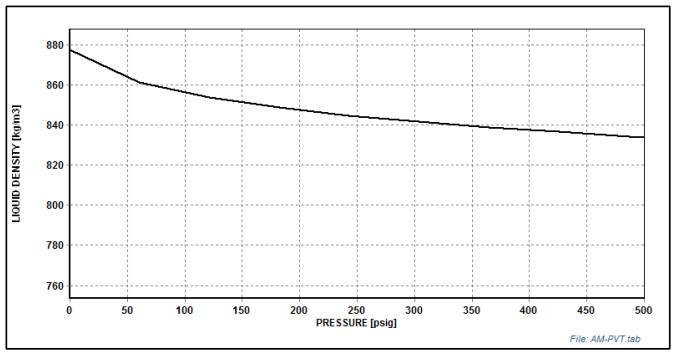

Figure 6-12: (AM) Oil Density (Kg/m3) – Temperature @ (120°F)

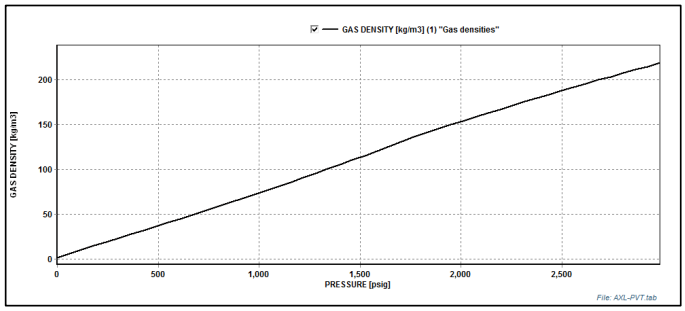

Figure 6-13: (AXL) Gas Density (Kg/m3) – Temperature @ (120°F)

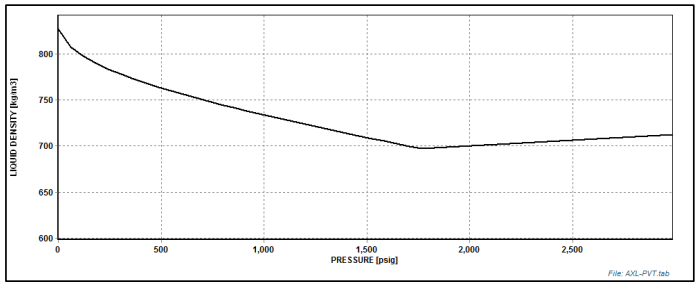

Figure 6-14: (AXL) Oil Density (Kg/m3) – Temperature @ (120°F)

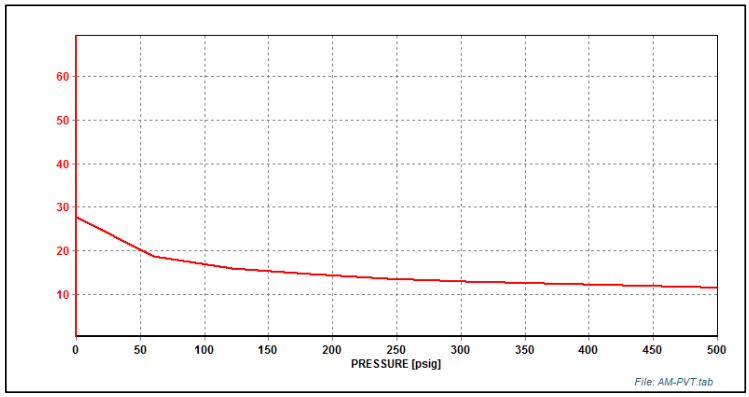

Figure 6-15: (AM) Oil Viscosity (Kg/m-h) – Temperature @ (120°F)

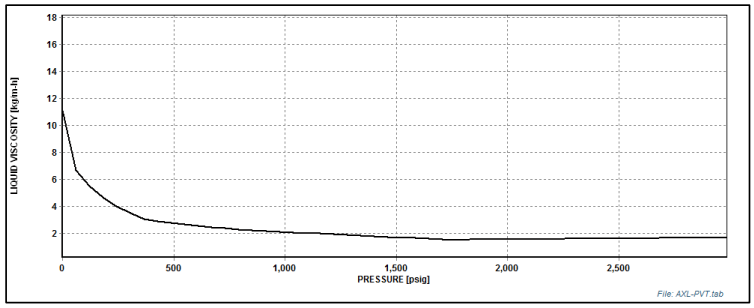

Figure 6-16: (AXL) Oil Viscosity (Kg/m-h) – Temperature @ (120°F)

6.11. Gamma Calibration

The calibration of the gamma meters was carried out prior to the field measurement using a 30 inch pipeline spool. The wall thickness of this calibration spool was 1.26 inch compared to 1.094 inch. This provided a challenge for the field measurement team to correct for the difference in wall thickness. A detailed analysis was carried out to achieve this by correcting for the additional steel density encountered in the calibration spool. This analysis was further compared with the information collected from the field measurement at various angle positions as will be discussed in details in gamma calibration chapter.

6.12. Field-B – Holdup Field Measurements

The field measurement was carried out on February 2nd and February 3rd 2013. The two gammas where located approximately 1.0 Km upstream of the LPPT separator. The estimated pressure and temperature of the AM fluid at the measurement location were 105 psig and 120°F respectively.

The measurement was carried out using two gamma sources, Cobalt 60. The distance between the two gammas was (27.4) m and the pipe inclination was measured at zero degrees at both locations.

The measurement was made with different angles ranging from 90 (vertical) to 45 degrees around the pipe. However, the focus of the measurement was more on the 90 degree position which provides a direct representation of the holdup in the pipeline.

6.12.1. Field-B Holdup Measurements – G2M1

The holdup data was also calculated based on the following oil, gas and water densities and average water cut. The local water cut is expected to be similar to the average water cut as the area of the measurement was observed to be completely flat.

Table 6-4: G2M1 Holdup Calculation Parameters

Holdup Calculation Parameters		
Oil Density	0.8600	gr/cc
Gas Density	0.0066	gr/cc
Water Density	1.0176	gr/cc
Water-cut (%)	2.2%	
Liquid Density	0.8635	gr/cc

The holdup time series depicted in Figure 6-17, Figure 6-18, Figure 6-19 and Figure 6-20 show the holdup data for various time durations in order to obtain as much details as possible from the time series. As one can clearly observe, there is a clear micro cyclic behavior in the system.

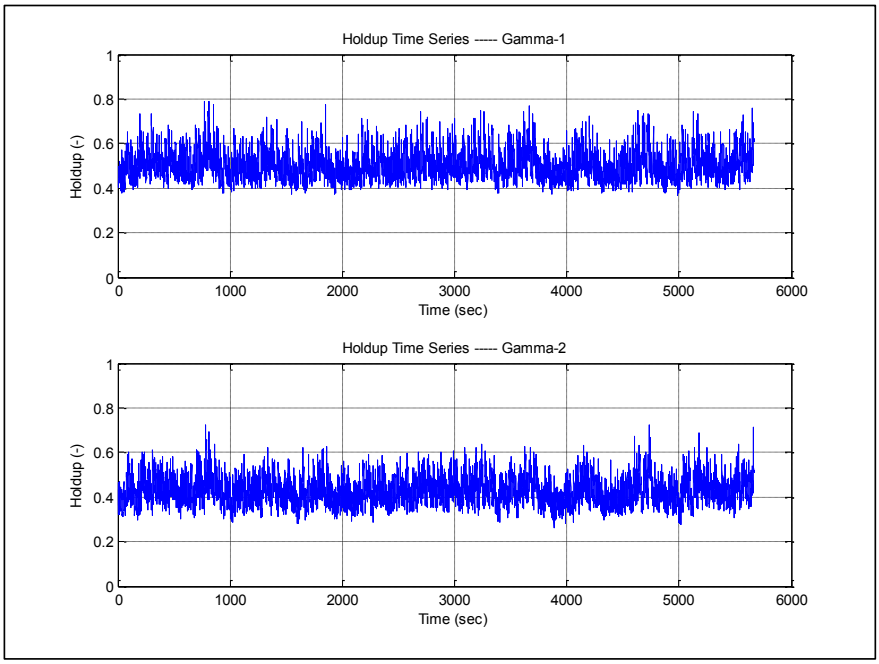

Figure 6-17: Holdup Time Series for G2M1 in Vertical Position – (Gamma 1 & 2) – (95 min)

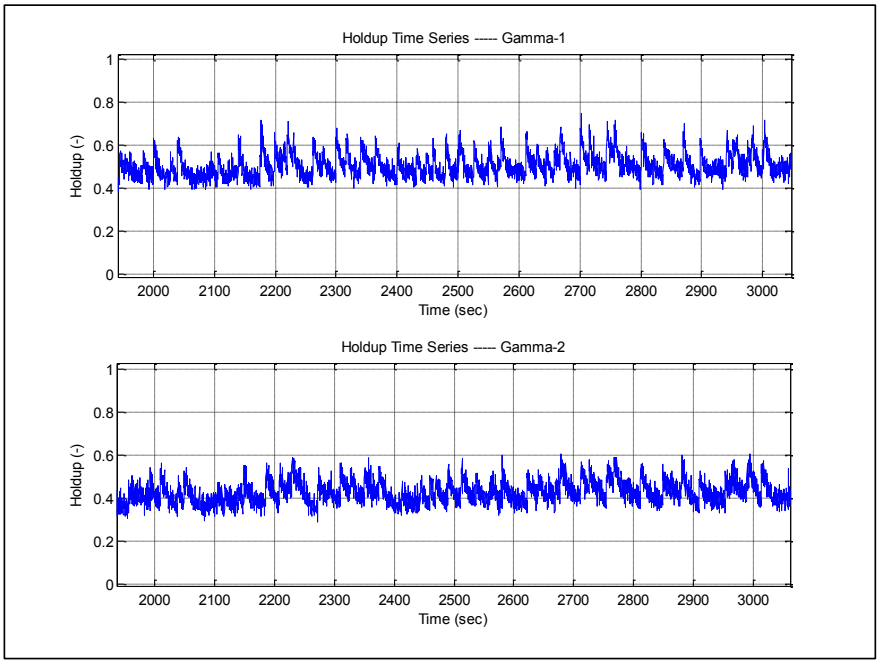

Figure 6-18: Holdup Time Series for G2M1 in Vertical Position – (Gamma 1 & 2) – (16 min)

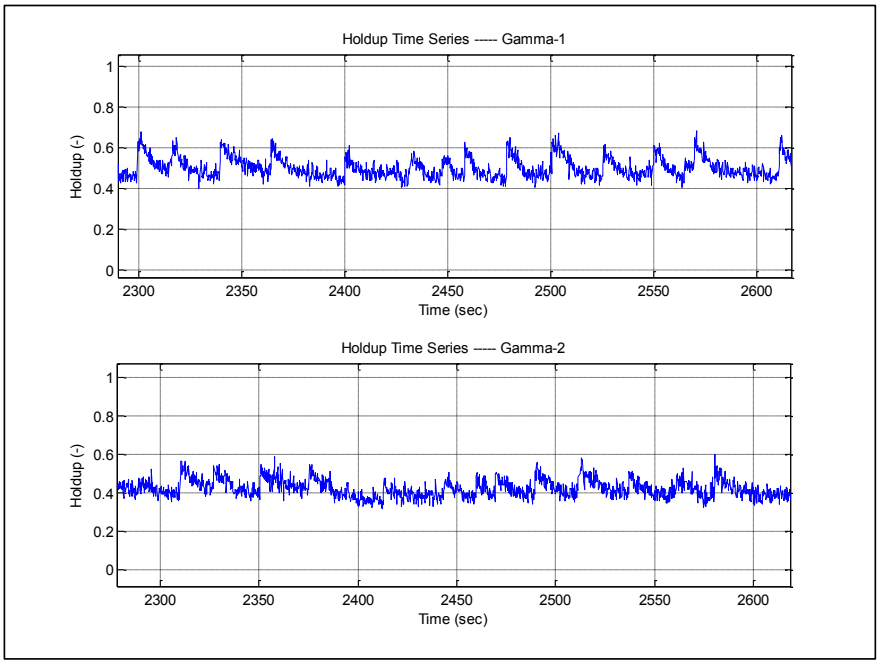

Figure 6-19: Holdup Time Series for G2M1 in Vertical Position – (Gamma 1 & 2) – (300 sec)

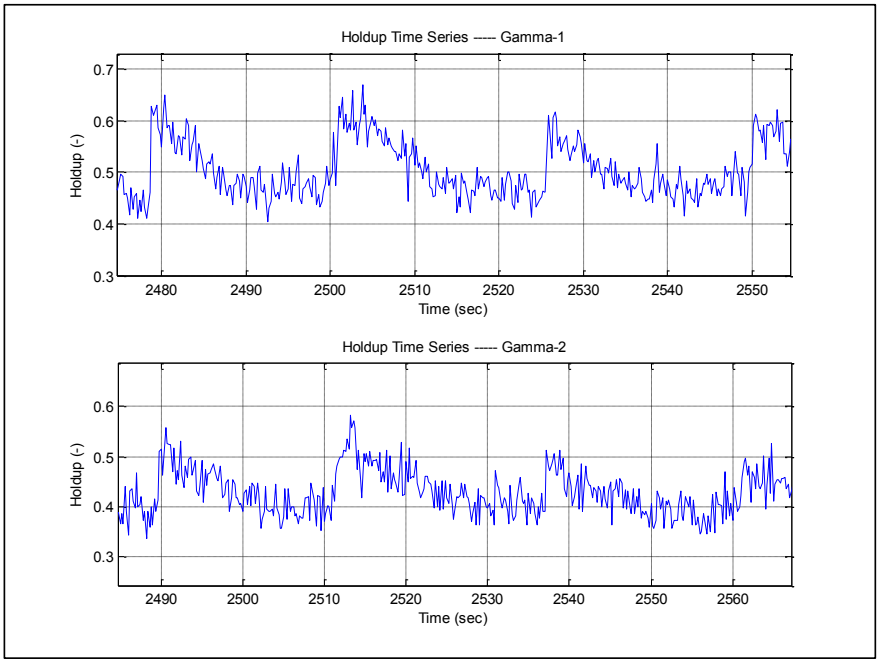

Figure 6-20: Holdup Time Series for G2M1 in Vertical Position – (Gamma 1 & 2) – (80 sec)

A careful look at the holdup in the two positions, one can notice that the holdup at position-1 has a higher average holdup of approximately 0.51 while the average holdup on position-2 was 0.43. The main reason behind this difference is the downward inclined pipe downstream of the gamma source at position-2, which pulls the liquid towards the downstream direction and as such, reduces the holdup upstream.

Cross-correlating the two gamma series, shown in Figure 6-21 one can observe a maximum frequency of 57 points, with each point representing a time step of 0.2 seconds, which gives a total time shift of 11.4 second. Using the already measured distance between the two gammas of 27.4 meter, one can calculate the velocity of the slugs/waves which turns out to be 2.4 m/sec.

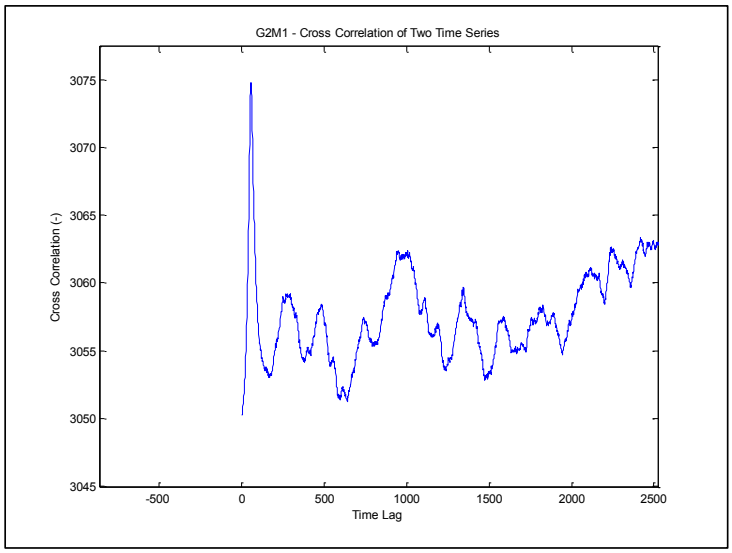

Figure 6-21: G2M1 Cross-Correlation of the Holdup Data – (Gamma 1 & 2)

By finding and examining the peaks of the time series, one can obtain detailed information about the wave frequency as shown in Figure 6-20. A MATLAB code was developed to find all the peaks in the holdup time series and then obtain all the associated statistics accordingly.

A close examination of the holdup at Gamma position-1, one can obtain a wave frequency that ranges mostly between 10 and 40 seconds, as shown on Figure 6-22. Examining the whole time series, for the full duration, one can observe a total of approximately 210 clear peaks which translates into an average frequency of 27 seconds which is in line of the visual observation made with the short duration.

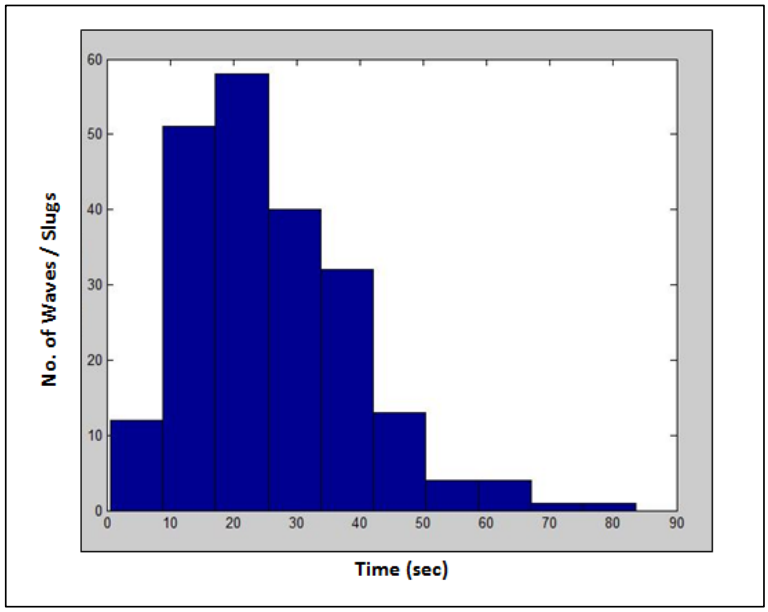

Figure 6-22: G2M1 Histogram of Wave Frequency at Gamma Position-1 (Time Between Peaks)

A similar behavior can be observed at Gamma-2 position. The frequency ranges between 10 to 40 seconds and the total number of clear peaks is estimated at 200 which give an average frequency of approximately 27.5 seconds. The reason behind the lower number of waves noticed at gamma-2 is the possible diminishing of some of the waves due to the overall lower holdup.

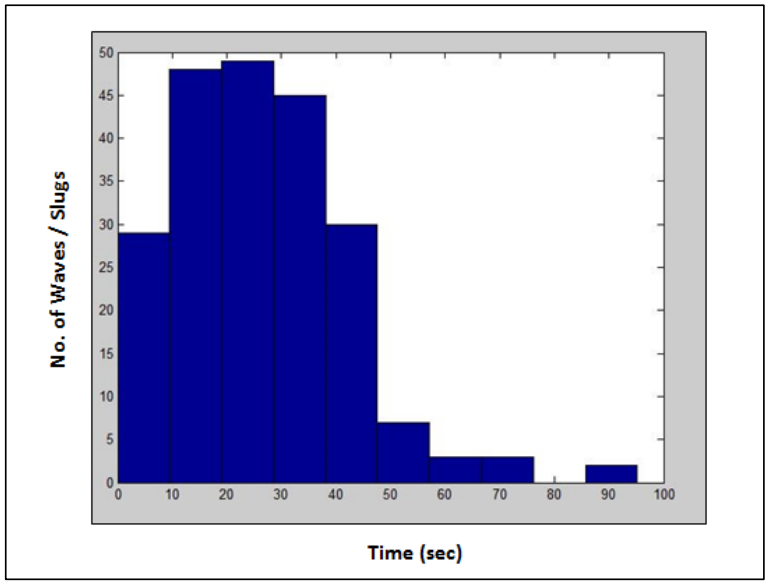

Figure 6-23: Histogram of Wave Frequency at Gamma Position-2 (Time Between Peaks)

One can also obtain the average wave length by utilizing the wave velocity calculated earlier at 2.4 m/sec, assuming that the average wave length, peak to peak, is 27.5 seconds. This would result in an average wave length of approximately 66 meters at both locations.

In addition, the average holdup of the peaks at gamma position-1 was calculated at 0.65 while at gamma position-2 it is calculated at 0.56. The average of the minimum points was also calculated at 0.42 at gamma position-1 while it was calculated at 0.35 at gamma position-2. The minimum points represent the continuous liquid film below the waves while the peaks represent the tip of the waves.

6.12.2. Field-B Holdup Measurements – G2X1

The holdup data was also calculated based on the following oil, gas and water densities and average water cut. The local water cut is expected to be similar to the average water cut as the area of the measurement was observed to be completely flat.

Table 6-5: G2X1 Holdup Calculation Parameters

Holdup Calculation Parameters		
Oil Density	0.7850	gr/cc
Gas Density	0.0144	gr/cc
Water Density	1.0176	gr/cc
Water-cut (%)	21.5%	
Liquid Density	0.8350	gr/cc

The holdup time series depicted in Figure 6-24, Figure 6-25, Figure 6-26 and Figure 6-27 show the holdup data for various time durations in order to obtain as much details as possible from the time series.

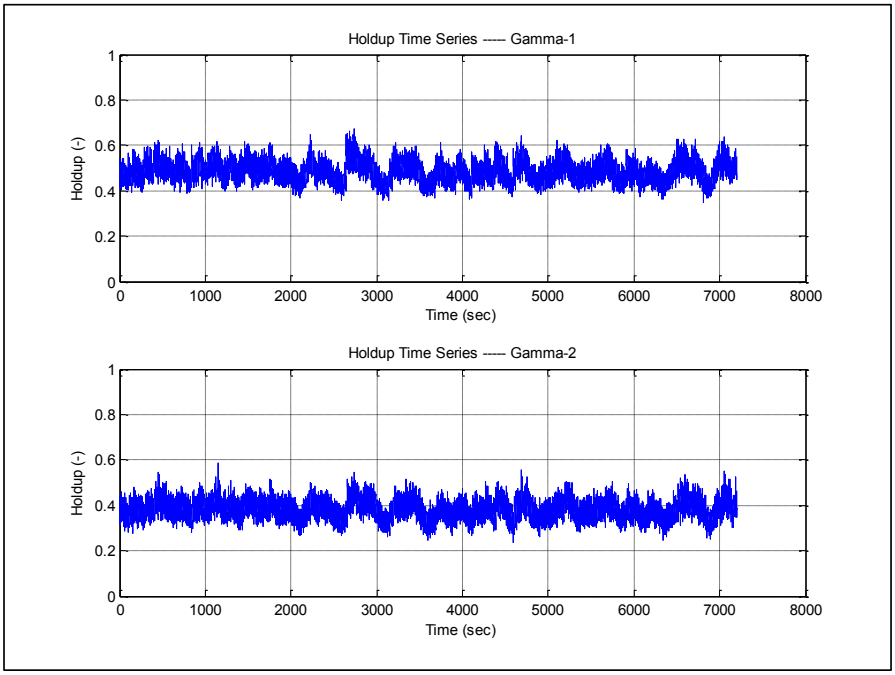

Figure 6-24: G2X1 Holdup Time Series in Vertical Position – (Gamma 1 & 2) – (120 min)

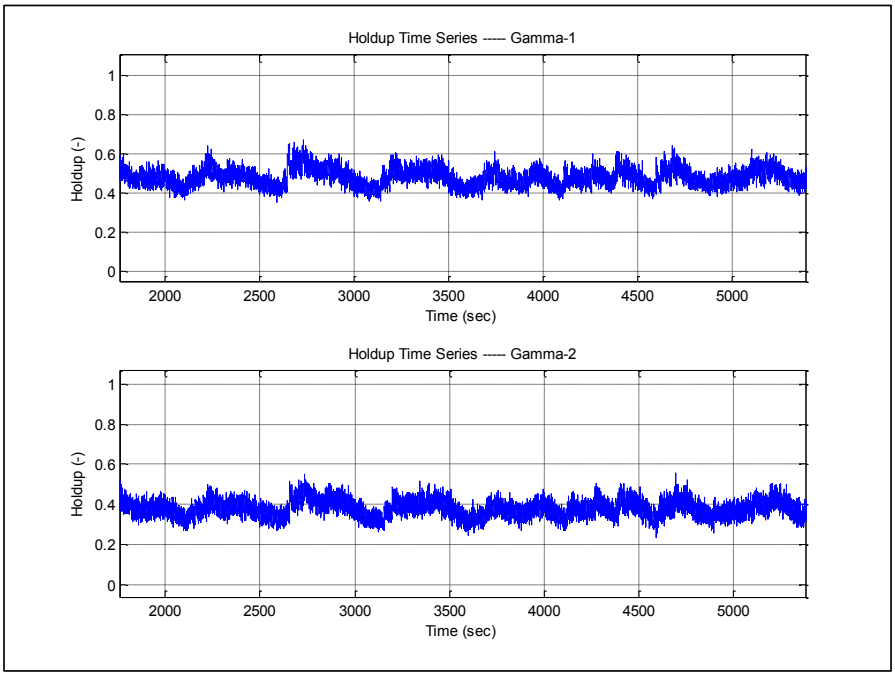

Figure 6-25: G2X1 Holdup Time Series in Vertical Position – (Gamma 1 & 2) – (60 min)

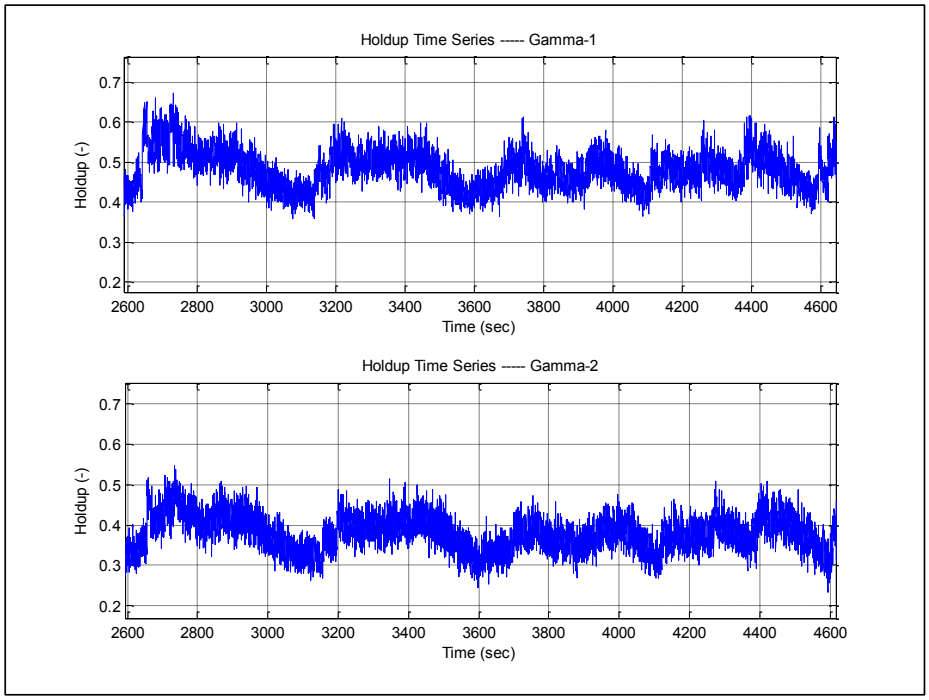

Figure 6-26: G2X1 Holdup Time Series in Vertical Position – (Gamma 1 & 2) – (35 min)

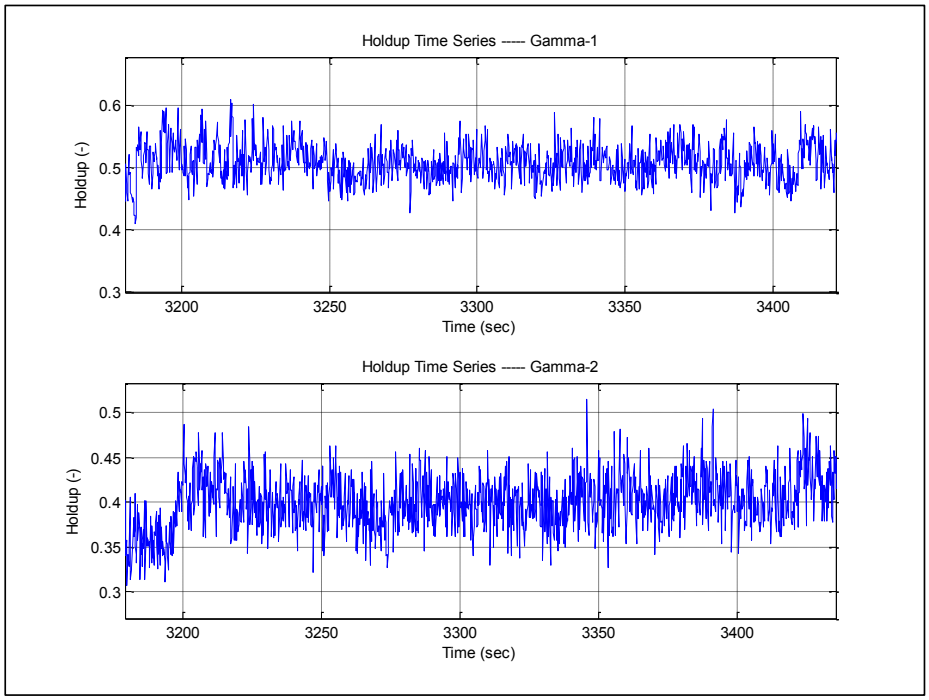

Figure 6-27: G2X1 Holdup Time Series in Vertical Position – (Gamma 1 & 2) – (300 sec)

A careful look at the holdup in the two positions, one can notice that the holdup at position-1 has a higher average holdup of approximately 0.484 while the average holdup on position-2 was 0.381. The main reason behind this difference is the downward inclined pipe downstream of the gamma source at position-2, which pulls the liquid towards the downstream locations and as such, reduces the holdup upstream.

Cross-correlating the two gamma series, shown in Figure 6-28, one can observe a maximum frequency of 66 points, with each point representing a time step of 0.2 seconds, which gives a total time shift of 13.2 seconds. Using the already measured distance between the two gammas of 27.4 meter, one can calculate the velocity of the waves which turns out to be 2.07 m/sec.

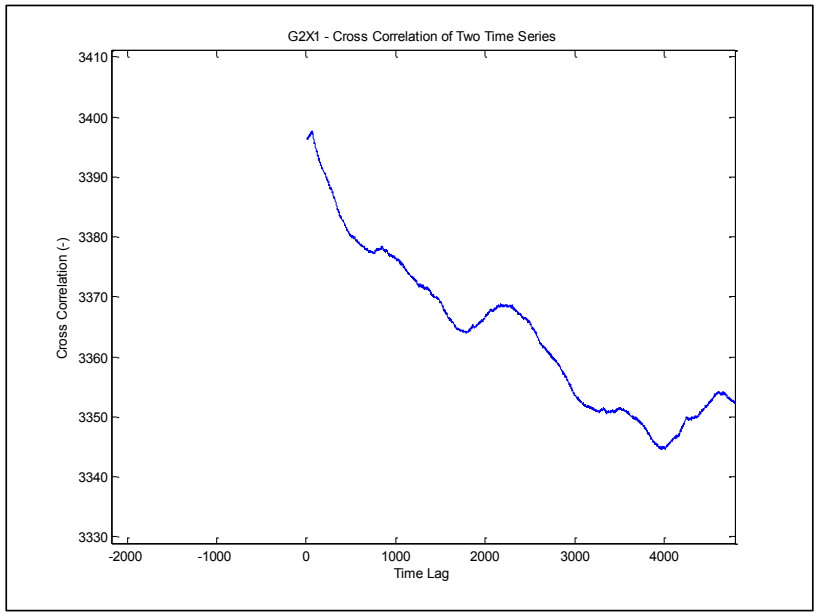

Figure 6-28: G2X1 – Cross-Correlation of the Holdup Data – (Gamma 1 & 2)

By finding and examining the peaks of the time series, one can obtain detailed information about the wave frequency as shown clearly in Figure 6-26. A MATLAB code was developed to find all the peaks in the holdup time series and then obtain all the associated statistics accordingly.

A close examination of the holdup at Gamma position-1, one can obtain a wave frequency that ranges mostly between 200 and 600 seconds, as shown in Figure 6-29. Examining the whole time series, for the full duration, one can observe a total of approximately 23 peaks which translates into an average wave frequency of 5.22 minutes.

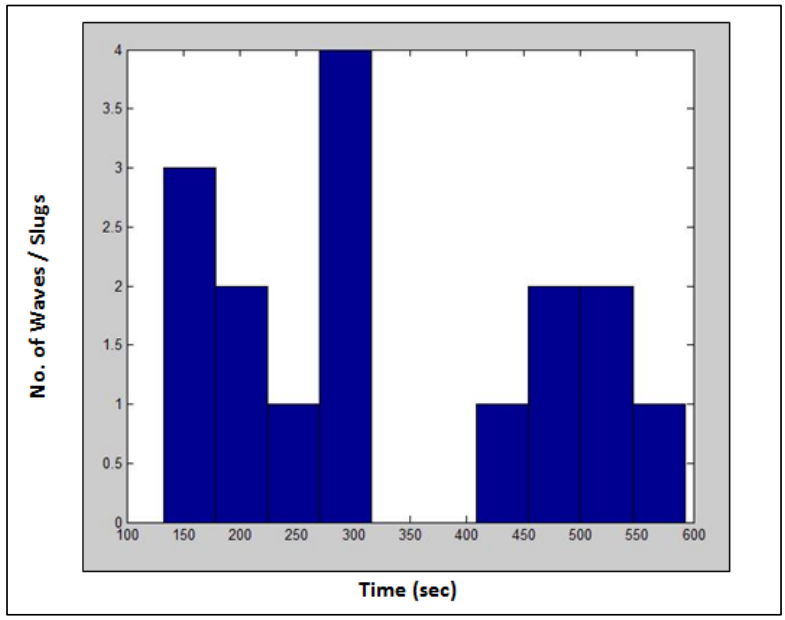

Figure 6-29: G2X1 - Histogram of Wave Frequency at Gamma Position-1 (Time Between Peaks)

A similar behavior can be observed at Gamma-2 position. The frequency ranges between 200 to 600 seconds and the total number of peaks is estimated at 23 which give an average frequency of approximately 5.22 minutes.

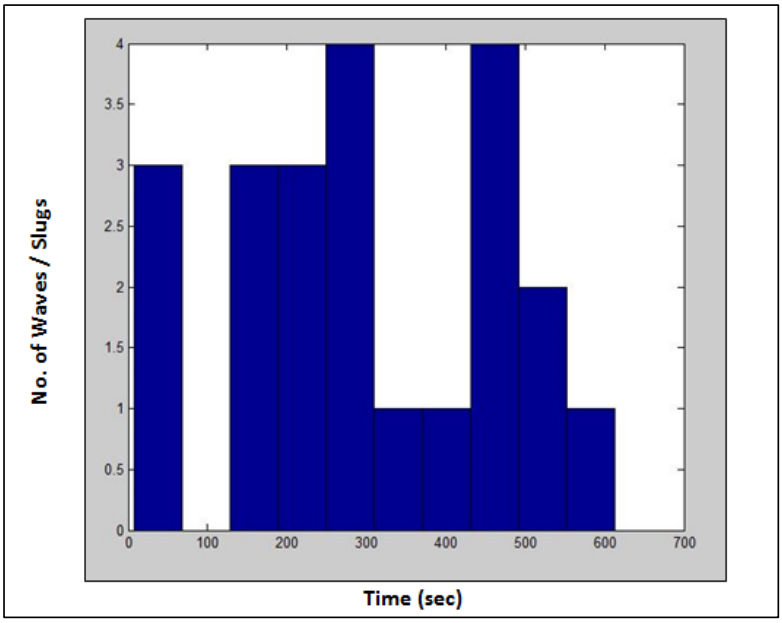

Figure 6-30: G2X1 - Histogram of Wave Frequency at Gamma Position-2 (Time between Peaks)

One can also obtain the average wave length by utilizing the wave velocity calculated earlier at 2.0757 m/sec, assuming that the average wave length, peak to peak, is 5.22 minutes. This would result in an average wave length of approximately 659 meters.

In addition, the average holdup of the peaks at gamma position-1 was calculated at 0.617 while at gamma position-2 it is calculated at 0.515. The average of the minimum points was also calculated at 0.382 at gamma position-1 while it was calculated at 0.280 at gamma position-2. The minimum points represent the continuous liquid film below the waves while the peaks represent the tip of the waves.

6.13. G2M1 and G2X1 Pipelines OLGA Simulation

Detailed simulation analysis was carried out using OLGA-7.2 for G2M1 and G2X1 pipelines. The simulation results were generally in a good agreement with the pressure and holdup results. The simulation was carried out with a relatively coarse grid, (23) meter average section length, specified heat transfer coefficient of 0.35 Btu/(hr-ft2°F) and first order mass equation solver. The comparison was carried out against the pipelines inlet pressure and the holdup measurements at the end of the pipeline.

The pressure comparison for G2M1 pipeline shown in Figure 6-31 indicates OLGA pressure predictions with and without slug tracking. The pressure predictions without slug tracking show pressure fluctuations of (4) psi at a low frequency. The pressure predictions with slug tracking show a slightly higher pressure drop at an average of (126) psig with a higher fluctuation frequency.

G2X1 pipeline OLGA pressure predictions shown in Figure 6-32 indicates slight under prediction when compared against average pressure reading. The slug tracking case shows pressure fluctuations of approximately (8) psi, while the non-slug tracking case shows fixed pressure prediction at (250) psig.

OLGA holdup predictions for both pipelines showed a good overall agreement with the measured values. However, the few peaks, slugs, predicted by the slug-tracking cases were not observed in the holdup measurements. In addition, the small hydrodynamic slugs/waves observed in the holdup measurements for both pipelines were not predicted by the slug tracking code in OLGA.

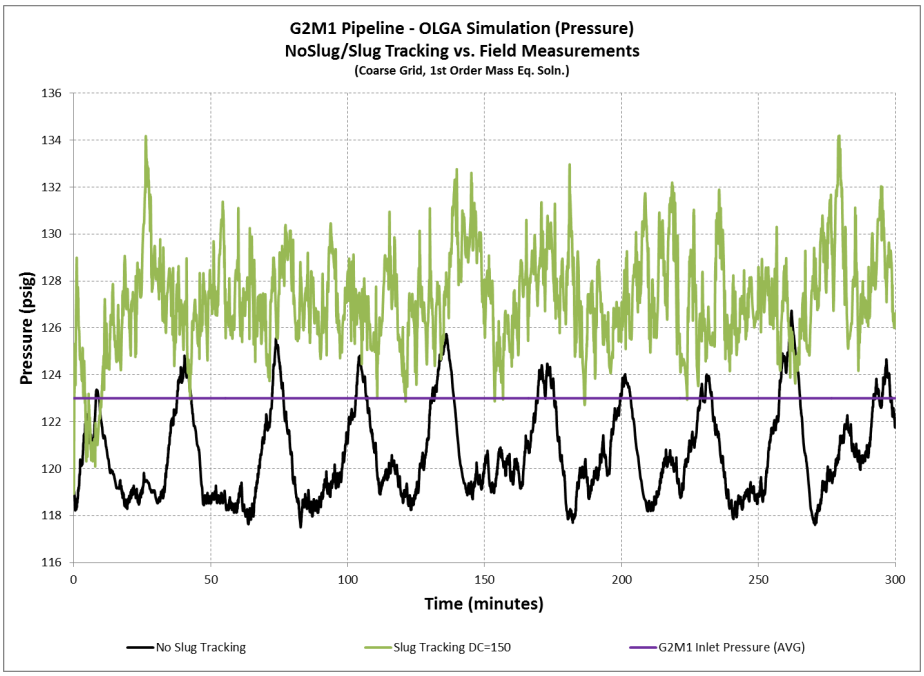

Figure 6-31: G2M1 Pipeline – OLGA Simulation Results (Pressure) – (Pipe Inlet)

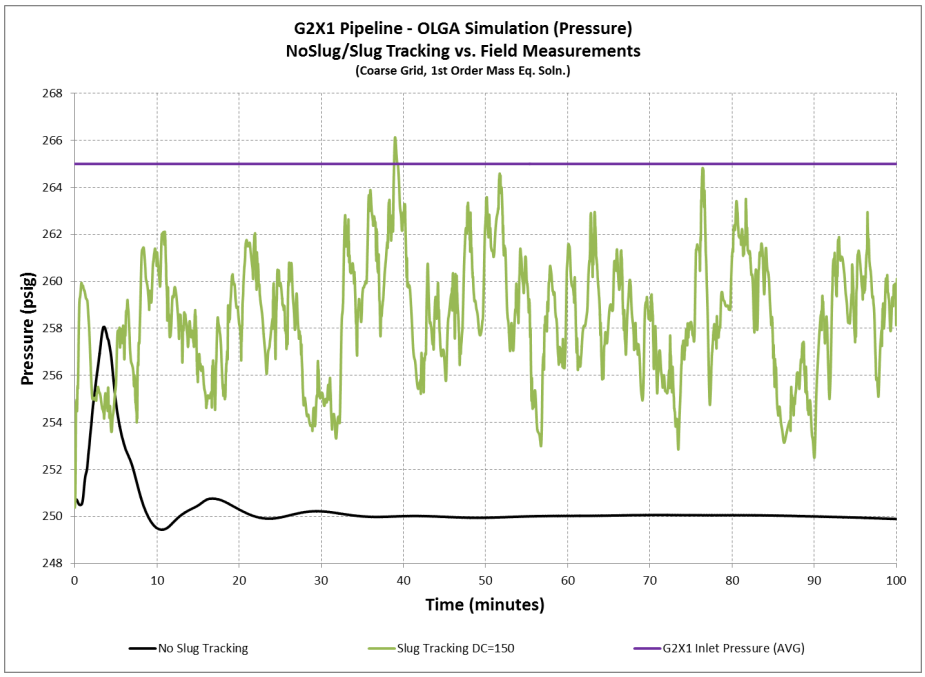

Figure 6-32: G2X1 Pipeline – OLGA Simulation Results (Pressure) – (Pipe Inlet)

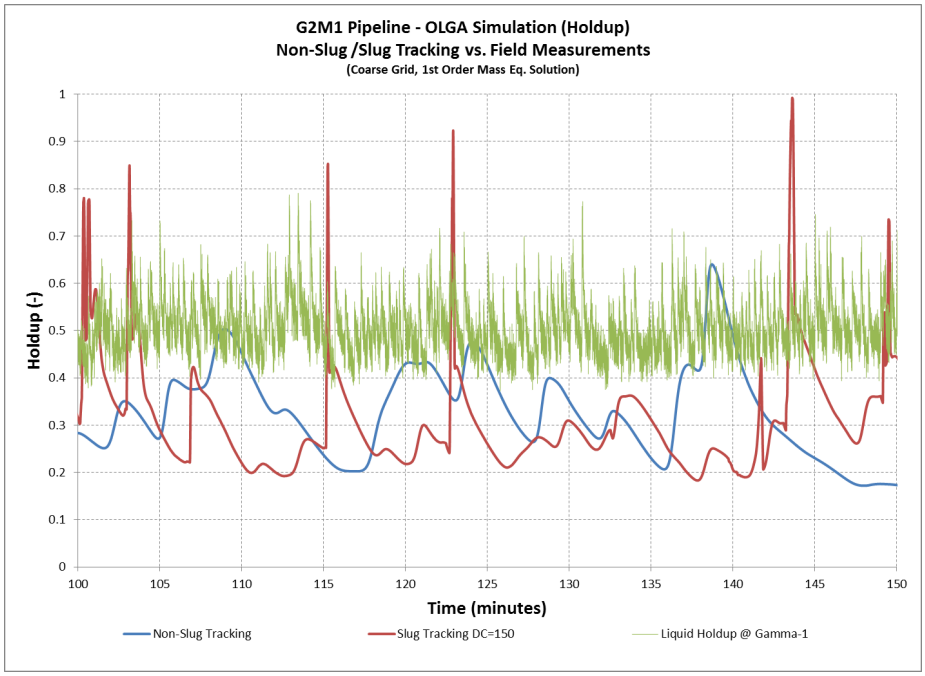

Figure 6-33: G2M1 Pipeline – OLGA Simulation Results (Holdup)

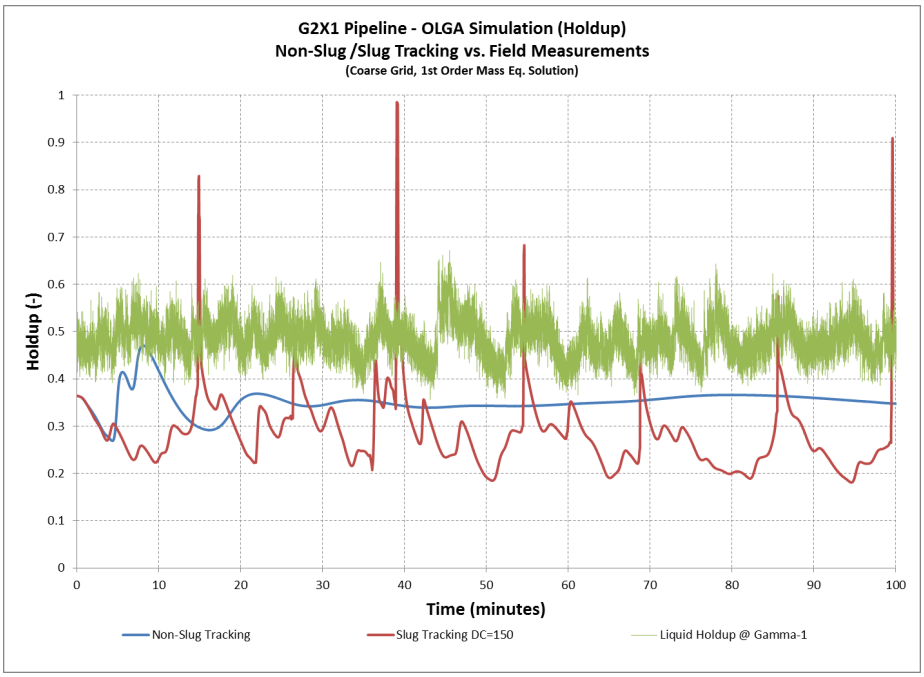

Figure 6-34: G2X1 Pipeline – OLGA Simulation Results (Holdup)

6.14. G2M1 and G2X1 Pipelines LedaFlow Simulation

Detailed simulation analysis was carried out using LedaFlow version (1.4.242.619), for G2M1 and G2X1 pipelines. The simulation results were generally in a good agreement with the pressure and holdup results. The simulation was carried out with a coarse grid, (23) meter average section length, specified heat transfer coefficient of 0.35 Btu/(hr-ft2°F) and first order mass equation solver. The comparison was carried out against the pipelines inlet pressure and the holdup measurements at the end of the pipeline.

The pressure comparison for G2M1 pipeline shown in Figure 6-35 indicates OLGA pressure predictions with and without slug capturing. The pressure predictions without slug capturing show a fixed pressure value of approximately (118) psig. The pressure predictions with slug capturing show a slightly higher pressure drop at an average of (120) psig with a fluctuation of (2) psi.

G2X1 pipeline LedaFlow pressure predictions shown in Figure 6-36 indicates slight under prediction when compared against average pressure reading. The slug capturing case shows a slightly higher pressure prediction at (254) psig, while the non-slug capturing case shows fixed pressure prediction at (250) psig.

LedaFlow holdup predictions for both pipelines showed a good overall agreement with the measured values, as shown in Figure 6-37 and Figure 6-38. However, the small hydrodynamic slugs/waves observed in the holdup measurements for both pipelines were not predicted by the slug capturing code in LedaFlow.

The pressure results shown in Figure 6-39 and Figure 6-40 indicates a reasonable improvement in pressure predictions by using a fine grid of (10*D). This was anticipated as the slug capturing scheme normally requires a fine grid in order to correctly predict the little hydrodynamic slugs created in the multiphase flow system.

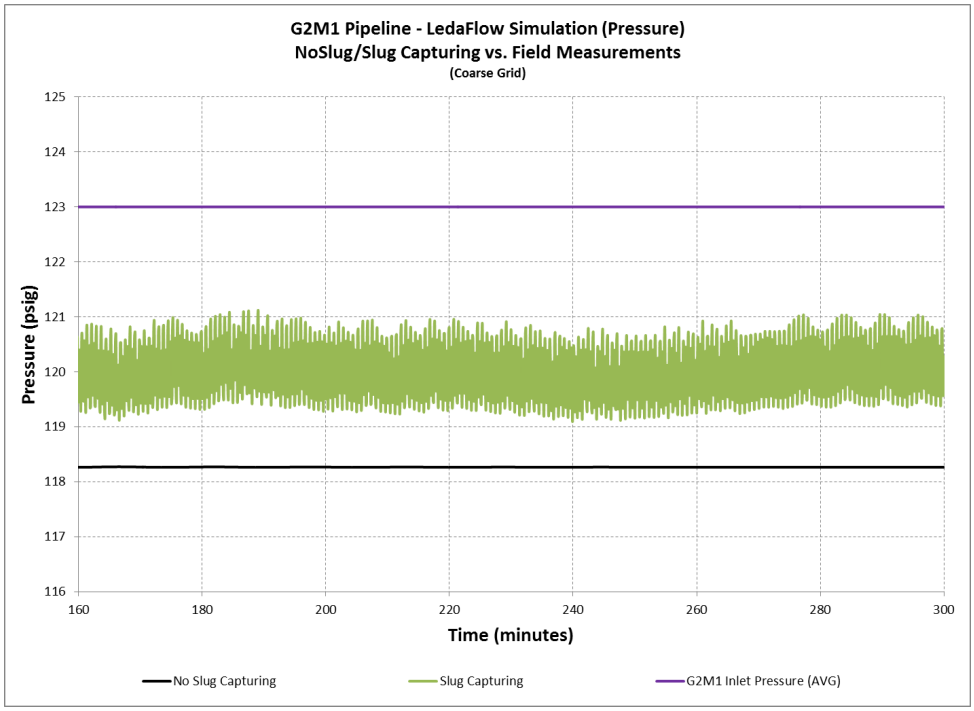

Figure 6-35: G2M1 Pipeline – LedaFlow Simulation Results (Pressure)

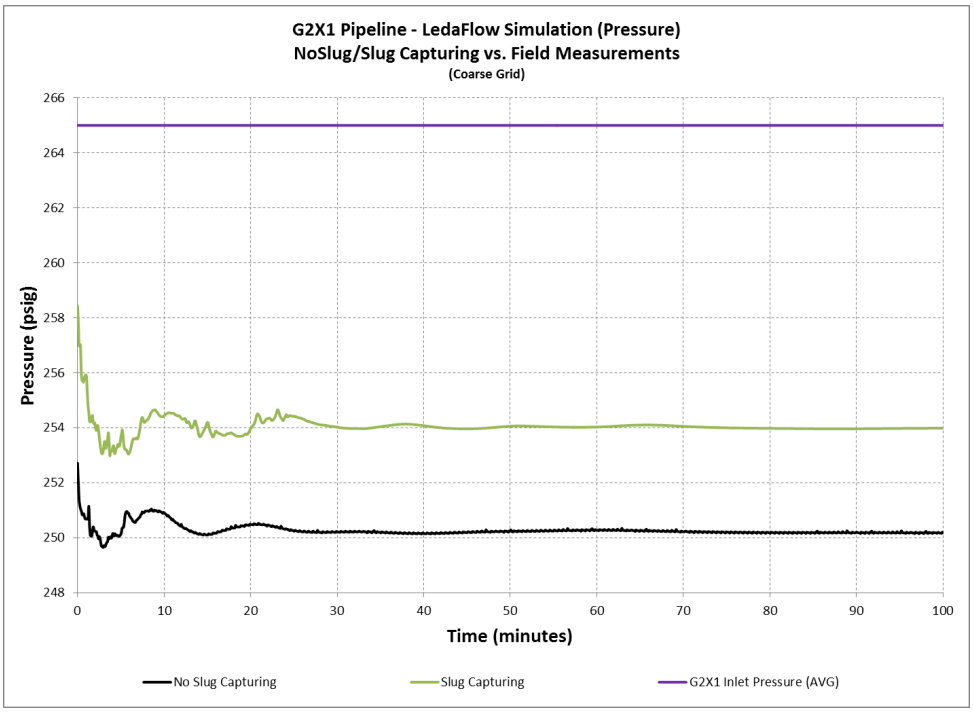

Figure 6-36: G2X1 Pipeline – LedaFlow Simulation Results (Pressure)

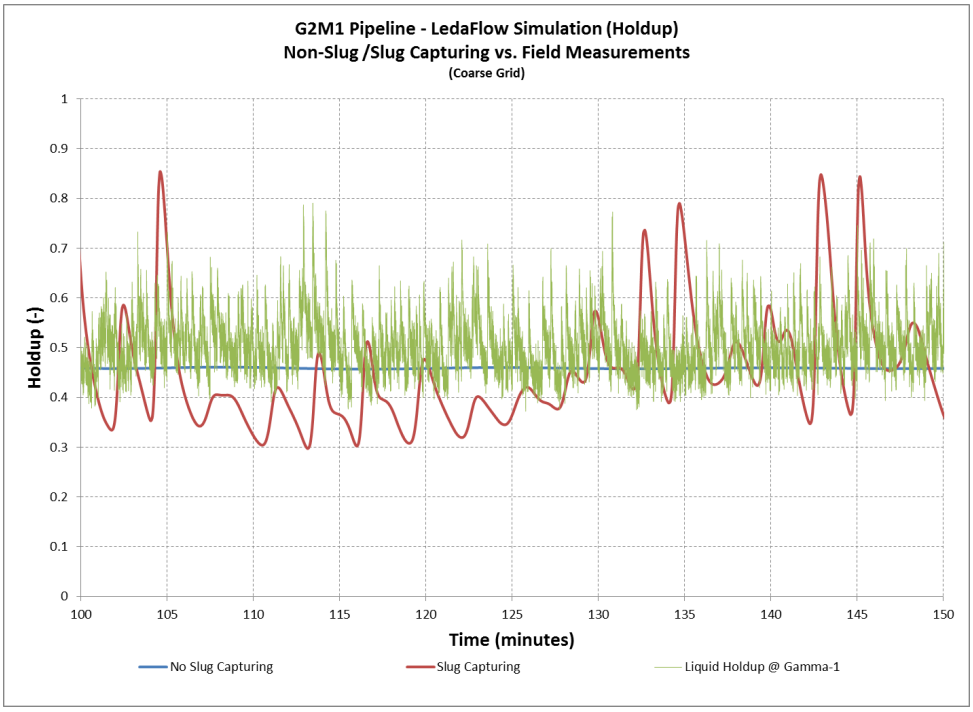

Figure 6-37: G2M1 Pipeline – LedaFlow Simulation Results (Holdup)

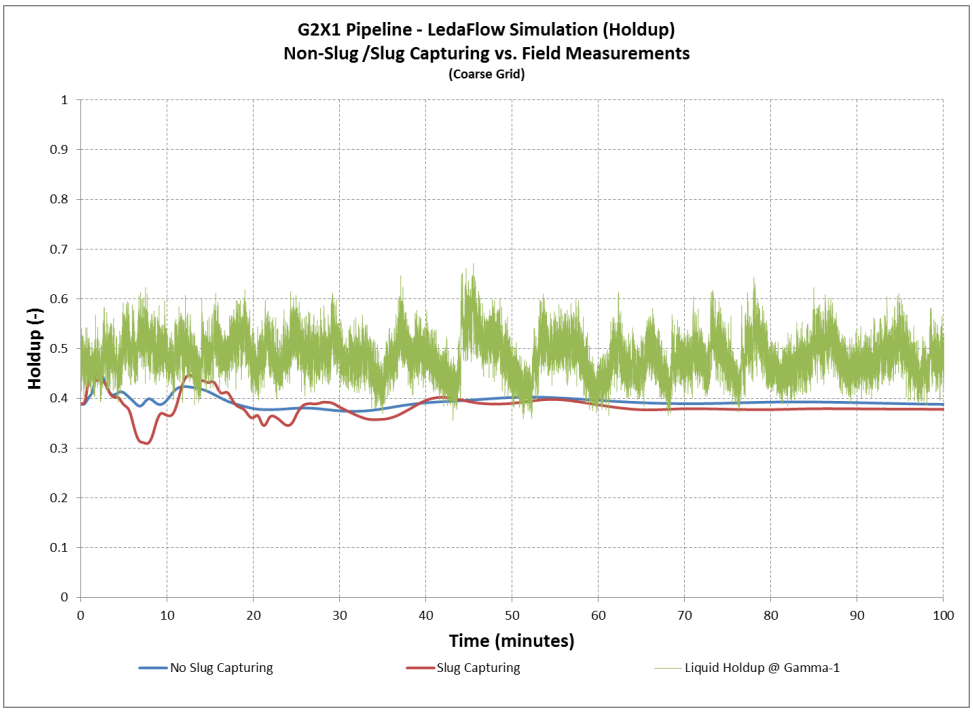

Figure 6-38: G2X1 Pipeline – LedaFlow Simulation Results (Holdup)

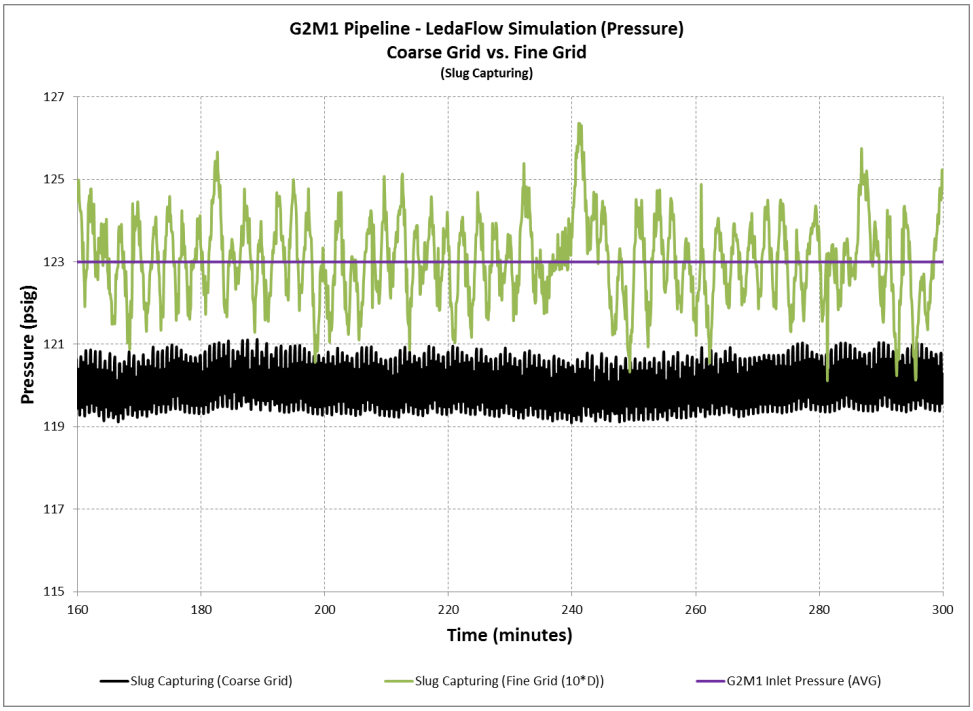

Figure 6-39: G2M1 Pipeline – LedaFlow Simulation Results (Pressure) – (Fine Grid)

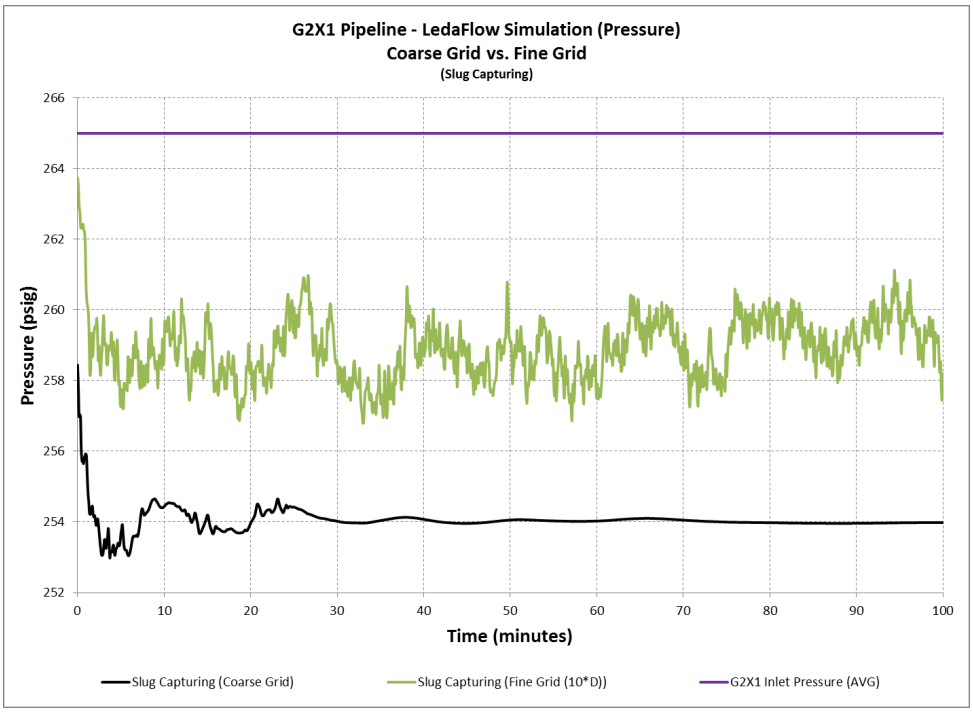

Figure 6-40: G2X1 Pipeline – LedaFlow Simulation Results (Pressure) – (Fine Grid)

6.15. Field-B Repetitive HPPT and LPPT Failures

The existing Field-B GOSP HPPT and LPPT vessels internals (multi-vane inlet device, anti-wave baffles and foam breaker), shown in Figure 6-41, experienced multiple failures since the startup of Field-B field in August 2004. HPPT internals were found damaged during a normal shutdown in December 2007. LPPT internals were also observed damaged in July 2008 when shutdown was taken after abnormal metallic sounds were reported by Operations earlier on May 14, 2008.

Both of the HPPT and LPPT vessels were originally fitted with an inlet device of Multi-Vane-Inlet type (MVI). The MVI is normally suitable for low to medium momentum forces up to 2 kilo-Newton only.

Figure 6-41: Multi-Vane Inlet Type at Field-B GOSP

The investigation team who worked on this issue at the time of failures carried out transient multiphase hydraulic analysis using OLGA which showed hydrodynamic slugs of velocities ranging from 10 to 50 ft/sec, which creates hydrodynamic slug forces ranging from 3 to 83 kilo-Newton.

$$Slug\ Force = (Density * Area * Velocity^2)$$

Based on these findings, the team concluded that the reason for these failures are the hydrodynamic slugs created by the flow and therefore a new vessel internals were recommended with higher force ratings to counter these slugs. However, this theory did not address three important issues that could lead to a different conclusion. The first one is the fact that there is a flow control valve with considerable pressure drop, 30 to 60 psi depending on the flow rate, upstream of the HPPT and LPPT vessels. The second one is the sudden increase in flow rate from 140,000 BBL/Day to 180,000 BBL/Day prior to the failure. The third issue is the fact that with this very low force rating of 2 kilo-Newton, the vessels internals should have failed long time ago. So this theory does not explain the survival of the vessels for more than three years of operations. In addition transient multiphase simulation of the two pipelines using OLGA, without slug tracking, does not indicate any slugging behavior. It's only with slug tracking option that OLGA creates those artificial slugs that the team used to base their theory on.

On the other hand, the field measurement findings confirm the unavailability of large slugging behavior in the pipeline. In addition, any small hydrodynamic slugs that might have occurred with the higher flow rates during the time of the failure in 2007 and 2008, would have been dampened by the flow control valve

upstream of the separator vessels. Therefore, a new scenario is thought to be the root cause for these failures. The scenario assumes a human error which causes a fast opening of the flow control valve to increase the flow rate. This scenario will create a very large slug with very high velocity that could easily destroy the vessels internals. Unfortunately, no records of the control valve opening could be found from the time of the incident. However, we have recordings of a large step in flow rate from 140,000 BBL/Day to 180,000 BBL/Day occurring over one day period on April 30, 2008. This could potentially be the reason behind the failure that was first noticed on May 14, 2008, as shown on Figure 6-42.

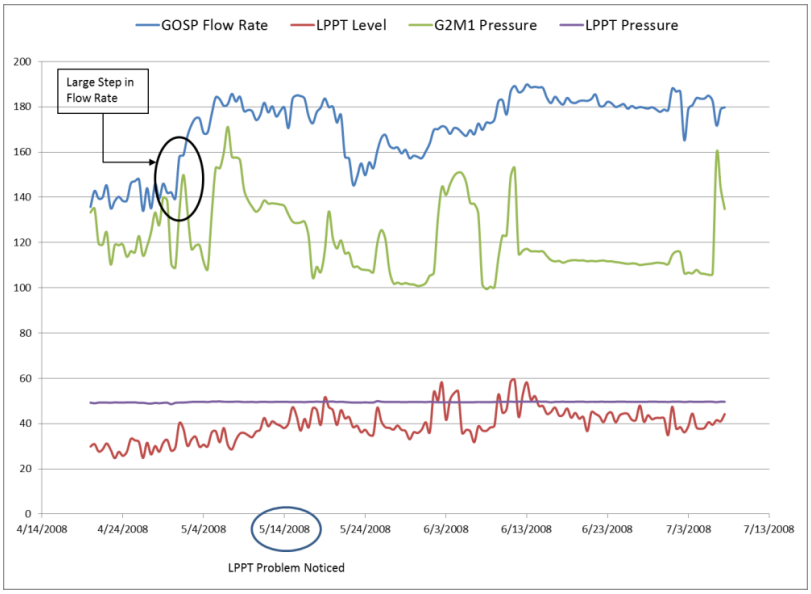

Figure 6-42: GOSP Flow rate, G2M1 Pressure, LPPT Level & LPPT Pressure During LPPT Failure

Multiphase transient simulation has also been conducted using OLGA to reproduce the above scenario and it has been confirmed the existence of the large slug with very high velocity in the order of 50 ft/sec that is more than capable of destroying the vessels internals.

Therefore, in view of the new findings, it's strongly believed that the root cause of the numerous failures of the low and high pressure traps is the fast opening of the flow control valve upstream of those separators. This causes the whole pipeline system to depressurize and as a result causes the gas to expand and create a large slug with a very high velocity which could end up destroying the separators internals.

This page was intentionally left blank

7. FIELD-C – HOLDUP & PRESSURE MEASUREMENTS

Field-C holdup and pressure measurements were carried out over three days, November 13, 14 and 17 2012. They were carried out on a horizontal section near the onshore Gas Oil and Separation Plant (GOSP) fence on two 42 inch diameter offshore pipelines, shown in Figure 7-1. The measurement was carried out using two gamma sources and detectors applied at various angles on the onshore side of the pipeline.

Figure 7-1: TL-10 Pipeline (42 inch)

The field measurements were carried out on TL-09 on November 13, 2012 at lower oil flow rate which was approximated at 330,000 BBL/Day. These flow rates were reduced and allowed to stabilize two days before any pressure or holdup measurements were carried out. On November 14, 2012, the field measurements were carried out on another 42 inch pipeline, TL-10, which runs in a different pipeline profile with slightly different fluid characteristics. The estimated oil flow rate at TL-10 was relatively low at 120,000 BBL/Day. Finally, a new set of measurements were carried on TL-09 at a higher oil flow rate, 375,000 BBL/Day. The new flow rate was started two days earlier, on November 15, 2012, to allow for the stabilization of the system before taking any field measurements.

The motivation behind this measurement was the over-prediction made by OLGA with slug tracking of the slug sizes which were estimated to be between 5,000 to 8,000 BBL, which translates to 1,000 m to 1,500 m in slug length for generally high oil flow rates; 500,000 BBL/Day. This prediction was not in accordance with the observation made by the field operators in terms of noticed pressure or flow rate fluctuations at the separators. To further confirm this, field measurement was planned and carried out to make an accurate measurement of the slug sizes on the onshore part of the pipeline very close to the separators.

7.1. Field-C Description

At the offshore side of Field-C, the oil is collected from various offshore production platforms into a main offshore Tie-in Platform (TP). The main TP is then connected to an onshore crude oil processing facilities through large diameter multiphase pipelines. For the concerned trunklines, TL-09 and TL-10, TP-17 and TP-18 are used to collect the crude oil from the satellite platforms and then deliver it to onshore processing facilities through 42 inch diameter multiphase pipelines.

7.2. Flow Rates

Three different flow rates were reported at the two measured trunklines as has been highlighted earlier. The details of these flow rates estimation and measurements are explained below:

7.2.1. TL-09 Low Flow Rate on November 13, 2012

On November 11 2012, the flow rate in TL-09 was decreased by approximately 50,000 BBL/Day from the normal production rate. On November 13, 2012, the measurements were started on TL-09 after insuring that the flow rate has been stabilized over the last two days. The new flow rate was supposed to be in the order of 325,000 BBL/Day.

Due to a malfunction of some of the control devices associated to the receiving separator, a reliable outflow rate could not be obtained directly from the flow meters data at the separator, as the range fluctuates extensively between 50,000 and 900,000 BBL/Day, see Figure 7-2. However, averaging the whole data range gives a reasonable prediction of the flow rate, 329,359 BBL/Day, which is in line with the flow rate estimation made through the individual well oil flow rate table, 333,485 BBL/Day. The simulation cases will be using an average oil flow rate of 330,000 BBL/Day.

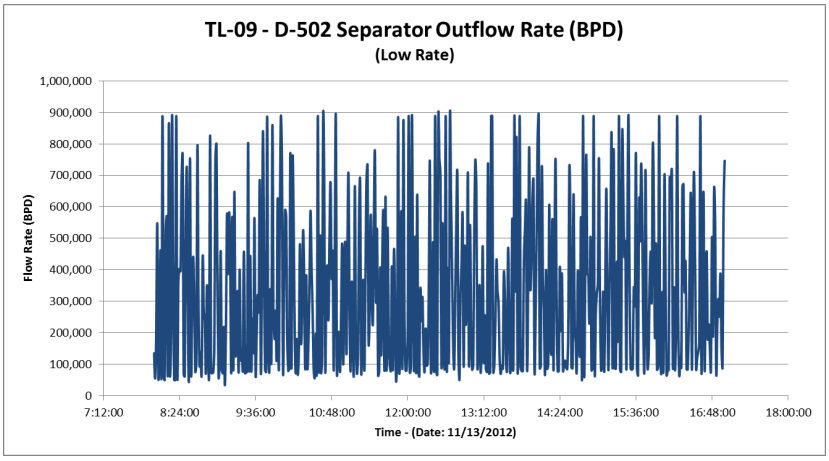

Figure 7-2: TL-09 Separator Outflow Rate (BBL/Day) – Low Flow Rate

The offshore production is shown in Table 7-1 for each offshore platform. The estimated offshore water flow rates gives an average water cut of 16.2%.

The superficial liquid and gas velocities as estimated by OLGA were (0.92) m/sec for liquid and (1.08 to 4.37) m/sec for gas.

Table 7-1: Platform Production – TL-09 (Date: 11/13/2012)

Platform	Oil Prod. Rate (BBL/Day)	Water Flow Rate (BBL/Day)
PF-1	14,060	1,913
PF-2	13,120	652
PF-3	12,572	973
PF-4	29,495	6,620
PF-5	23,182	7,044
PF-6	24,069	9,886
PF-7	31,350	2,164
PF-8	76,464	12,261
PF-9	50,231	21,236
PF-10	31,255	925
PF-11	27,687	1,012
Total	**333,485**	**64,686 - (16.2%)**

7.2.2. TL-10 Normal Flow Rate on November 14, 2012

TL-10 flow rates were not altered and holdup and pressure measurements were carried out at the pipelines normal flow rate conditions.

Due to a malfunction of some of the control devices associated to the receiving separator, a reliable outflow rate could not be obtained directly from the flow meters data at the separator as the range fluctuates mostly between 40,000 and 170,000 BBL/Day, see Figure 7-3. However, averaging the whole data range gives a reasonable prediction of the flow rate, 110,750 BBL/Day, which is in line with the flow rate estimation made through the individual platform rate table, 125,540 BBL/Day. The simulation cases will be using an average oil flow rate of 120,000 BBL/Day.

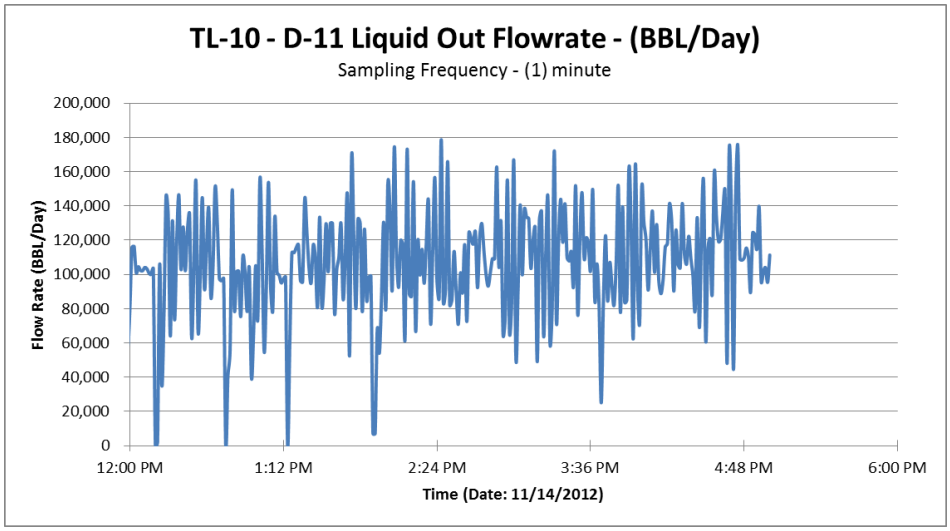

Figure 7-3: TL-10 Separator Outflow Rate (BBL/Day) – Normal Flow Rate

The offshore production is shown in Table 7-2 per offshore platform. The estimated offshore water flow rates gives an average water cut of 1.43%.

The superficial liquid and gas velocities as estimated by OLGA were (0.29) m/sec for liquid and (0.6 to 1.02) m/sec for gas.

Table 7-2: Platform Production – TL-09 (Date: 11/14/2012)

Platform	Oil Prod. Rate (BBL/Day)	Water Flow Rate (BBL/Day)
PF- 1	0	0
PF- 2	47,140	377
PF- 3	47,400	0
PF- 4	31,000	1,443
Total	**125,540**	**1,820 - (1.43%)**

7.2.3. TL-09 Normal Flow Rate on November 17, 2012

On November 15 2012, the flow rate in TL-09 was increased from the lower rate which was implemented on November 13, 2012. On November 17, 2012, the measurements were started on TL-09 after insuring that the flow rate has been stabilized over the last two days. The new flow rate was supposed to be approximately 50,000 BBL/Day higher than the lower rate.

Due to a malfunction of some of the control devices associated to the receiving separator, a reliable outflow rate could not be obtained directly from the flow meters data at the separator, as the range fluctuates extensively between 50,000 and 900,000 BBL/Day, see Figure 7-4. However, averaging the whole data range gives a reasonable prediction of the flow rate, 378,417 BBL/Day, which is in line with the flow rate estimation made through the individual well flow rate table, 373,535 BBL/Day. The simulation cases will be using an average oil flow rate of 375,000 BBL/Day.

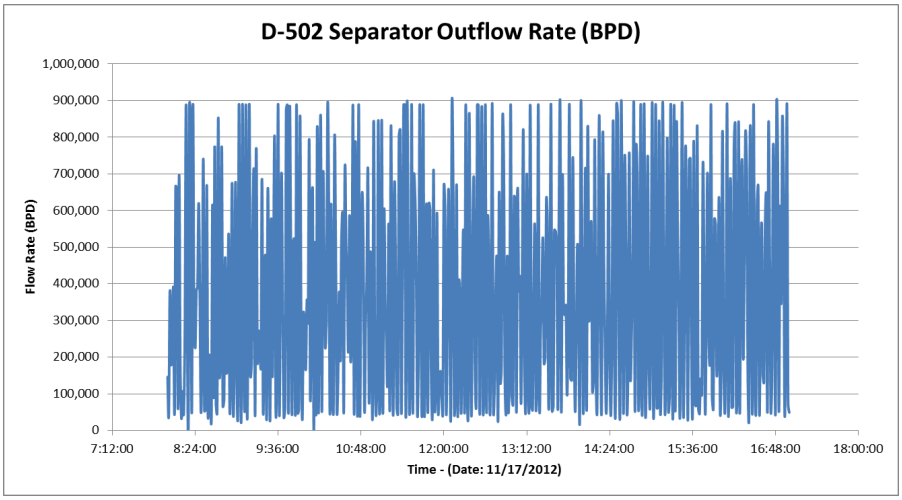

Figure 7-4: TL-09 Separator Outflow Rate (BBL/Day) – Normal Flow Rate

The offshore production is shown in Table 7-3 per offshore platform. The estimated offshore water flow rates gives an average water cut of 16.2%.

The superficial liquid and gas velocities as estimated by OLGA were (1.05) m/sec for liquid and (1.04 to 4.72) m/sec for gas.

Table 7-3: Platform Production – TL-09 (Date: 11/17/2012)

Platform	Oil Prod. Rate (BBL/Day)	Water Flow Rate (BBL/Day)
PF-1	14,060	1,913
PF-2	13,120	652
PF-3	12,572	973
PF-4	29,495	6,620
PF-5	23,182	7,044
PF-6	24,069	9,886
PF-7	31,350	2,164
PF-8	76,464	12,261
PF-9	50,231	21,236
PF-10	31,255	925
PF-11	27,687	1,012
Total	**373,535**	**64,686 - (14.8%)**

7.3. Pipeline Details

TL-09 and TL-10 pipelines, both have an outside diameter of 42 inch with a wall thickness of 1.0 inch. The two pipelines extends for approximately 50 Km from the offshore tie-in platforms, TP-17 and TP-18, to the onshore GOSP facilities. The terrain can be described as being highly undulating with an overall upward slope as shown in Figure 7-5 and Figure 7-6. The area where the holdup field measurements were carried out was an above ground area where a sectionalizing valve is installed at the beach side.

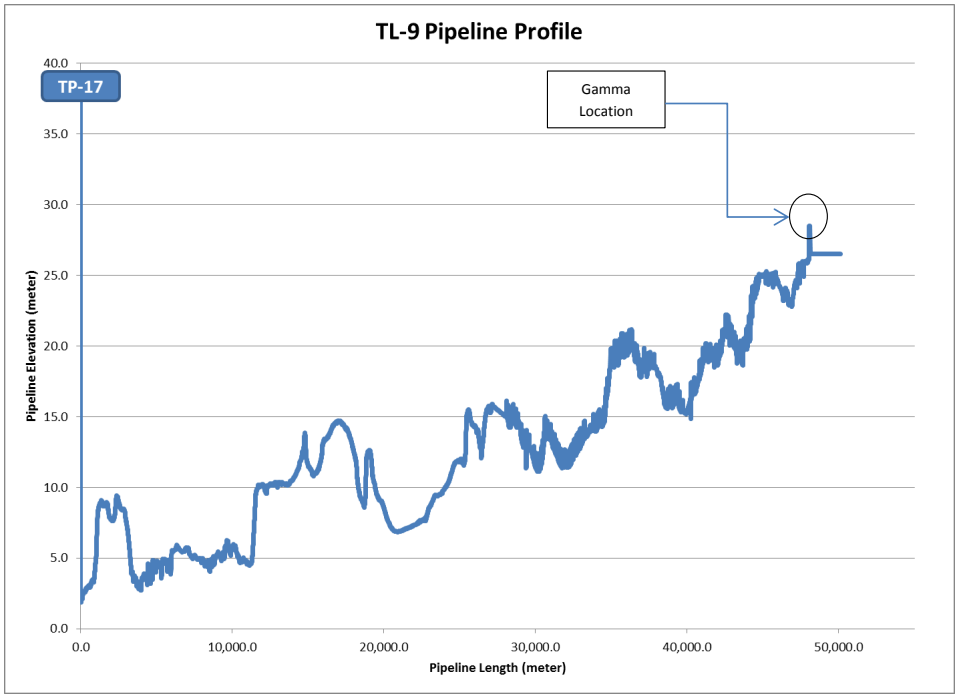

Figure 7-5: TL-09 Pipeline Profile

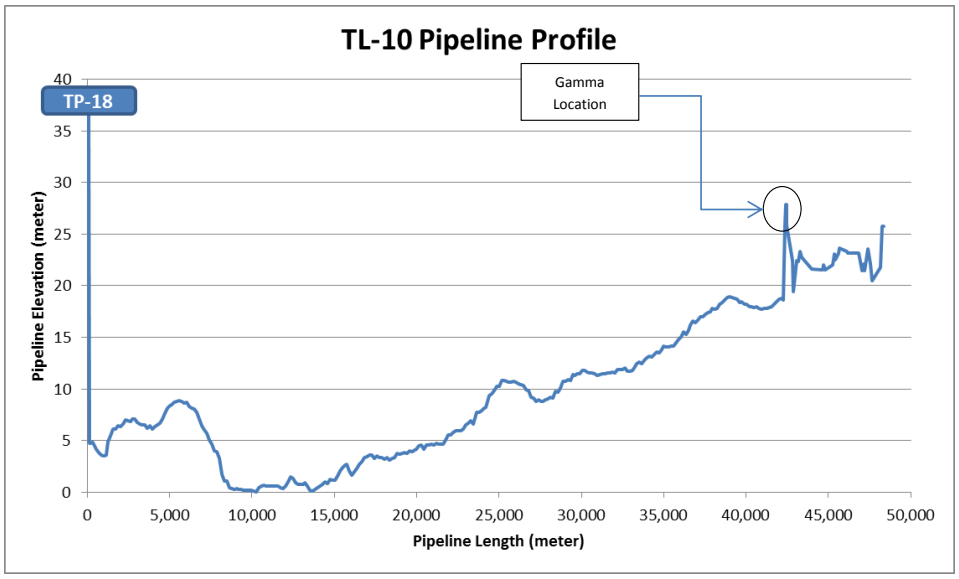

Figure 7-6: TL-10 Pipeline Profile

7.4. Inlet and Outlet Pressure

Obtaining the correct the inlet and outlet pressure for TL-09 and TL-10 pipelines was a challenging process, especially for TL-09, as the data was not readily available from the control system and many assumptions had to be made in order to make the best out of the available data.

7.4.1. TL-09 Inlet and Outlet Pressure – Low Flow Rate & Normal Flow Rate

The GOSP separator pressure was set at 50 psig. The header pressure upstream of the separator was recorded at an average of 57 psig at both flow rates as shown on Figure 7-7 and Figure 7-8. The sampling frequency at the GOSP was (1) minute.

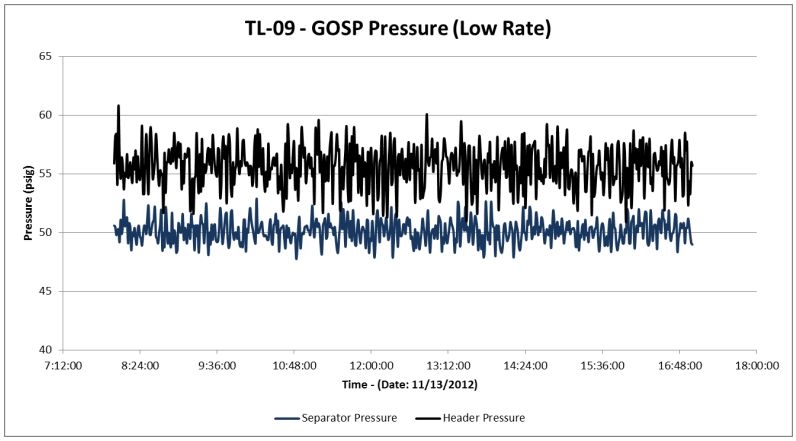

Figure 7-7: TL-09 GOSP Pressure Readings – Low Rate

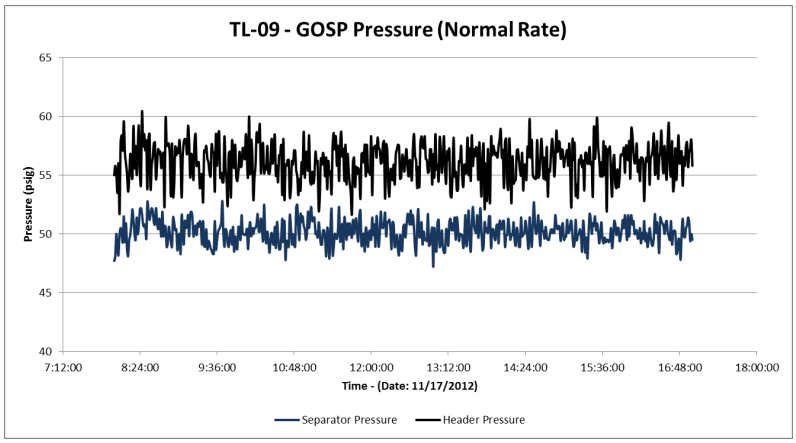

Figure 7-8: TL-09 GOSP Pressure Readings – Normal Rate

At the measurement location, the pressure was not recorded during the measurement period on November 13, 2012. On November 17, 2012, the pressure was recorded at 80 psig.

Pressure at TP-17 was not available due to malfunctioning of certain DCS systems, so pressure at a nearby TP-19 was obtained. The pressure drop between TP-19 and TP-17 was calculated using OLGA and verified through the pressure drop obtained from the pressure drop across similar offshore pipelines within the same area.

The pressure drop between PF-950-959 and TP-19 was measured at 36 psi over 18.25 inch and 3.75 Km. This produces a 9.6 psi/Km for that particular pipeline, with a flow rate of 40 MBD at standard conditions. The pipeline between TP-19 and TP-17 is a 33 inch, 1.6 Km pipeline with an estimated flow rate of 99 MBD at standard conditions. When simulated using OLGA, it provides a pressure drop of approximately 13 psi which provides 8.125 psi/Km, which is similar to what was observed with PF-950-959 and TP-19 pressure drop. Therefore, the pressure at TP-17 was estimated by deducting 13 psi from the recorded TP-19 pressure.

The pressure at the main offshore tie-in platform TP-19 at the inlet of the pipeline was recorded with a sampling frequency of (1) minute. The pressure log obtained from the SCADA system was fixed at 233 psig on November 13, 2012 as shown on Figure 7-9. This is most probably due to a malfunction of the system as the pressure is not expected to be static at a fixed number. However, the pressure is expected to be reasonably close to the reported pressure of 233 psig at TP-19. In addition, Figure 7-11 shows the pressure from a close by offshore platform which is directly connected to TP-17. The pressure shows fluctuations (10) psi around an average of (230) psig which is very close to the earlier estimated pressure of (233) psig.

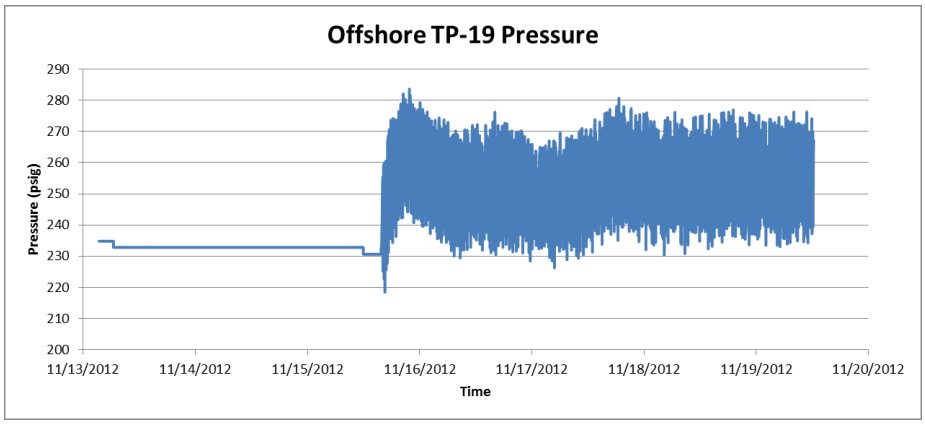

Figure 7-9: TP-19 Pressure Readings – Low Flow Rate

When reducing the pressure of TP-19 by 13 psi, one obtains the pressure at TP-17 at 220 psig on November 13, 2012, as shown on Figure 7-10.

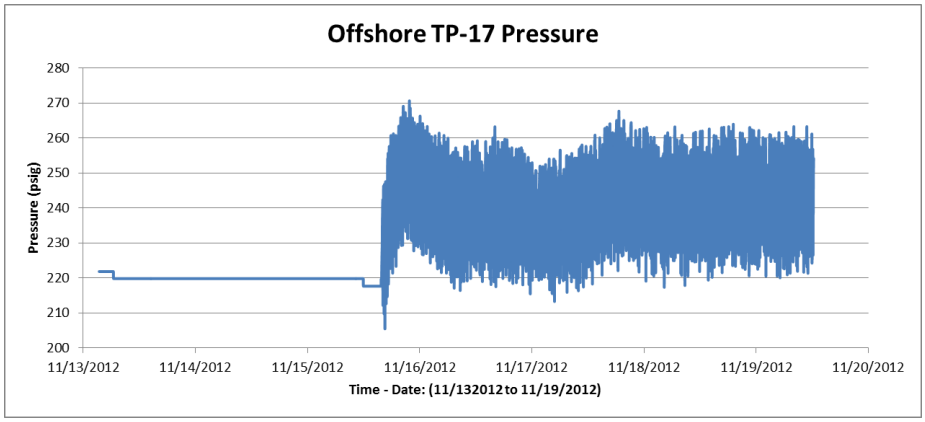

Figure 7-10: TP-17 Pressure Calculations – Low Flow Rate

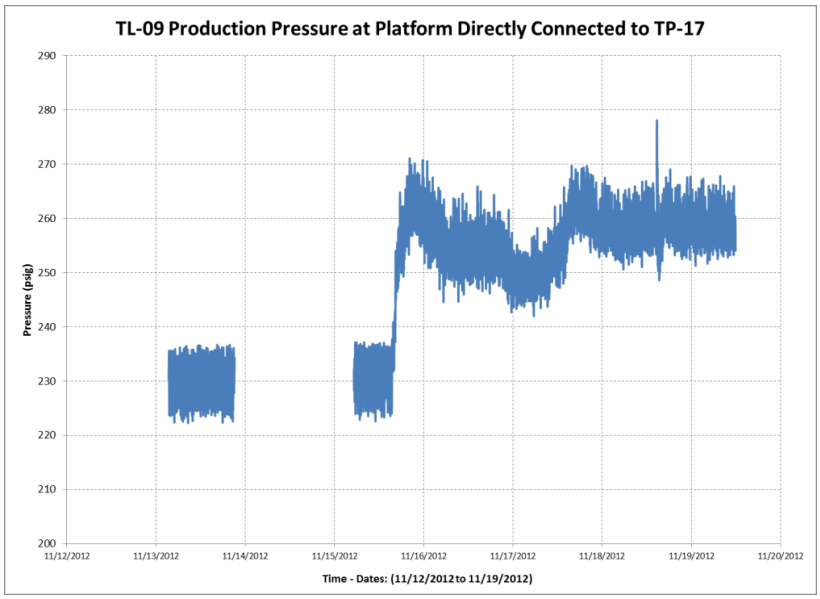

Figure 7-11: Pressure at an offshore platform directly connected to TP-17

Despite the suspected malfunctioning of the SCADA system and the loss of the data during the measurement period on November 13, 2012, the simulation will be utilizing pressure reported by the system, which was fixed at 220 psig as it seems to be a reasonable estimation of the pressure at that location.

On November 17, 2012, the pressure data was available on TP-19 and hence on TP-17. Taking a closer look at the pressure data on TP-17, depicted in Figure 7-12, shows a clear pressure fluctuation of approximately 35 psig, with a frequency that ranges from 10 to 20 minutes. This could be a sign of slugging behavior which will be investigated later when analyzing the holdup data.

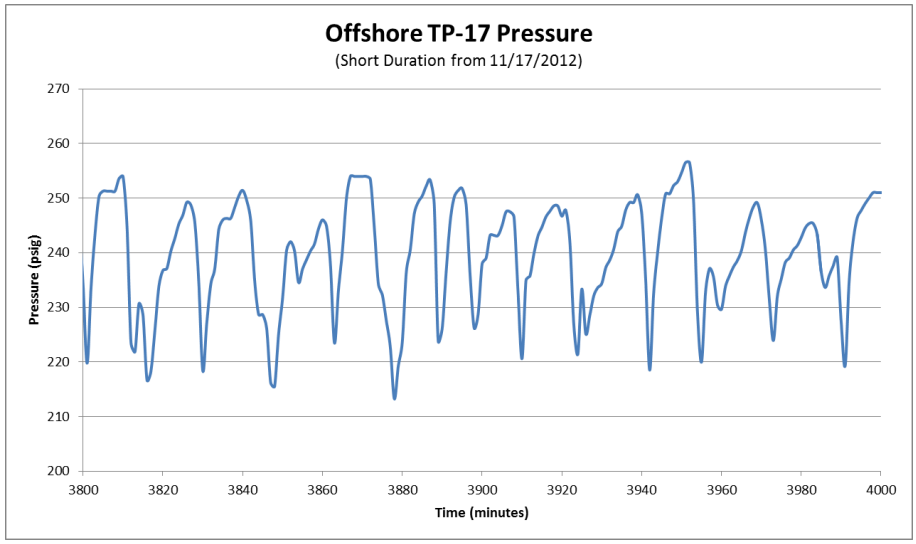

Figure 7-12: TP-17 Pressure Calculations (200 Minutes) – Normal Flow Rate

7.4.2. TL-10 Inlet and Outlet Pressure – Normal Flow Rate

The GOSP separator pressure was set at 50 psig. The header pressure upstream of the separator was recorded at an average of 57 psig as shown on Figure 7-13. The sampling frequency at the GOSP was (1) minute.

At the measurement location, the pressure was recorded during the measurement period and the pressure was fluctuating between 81 and 84 psig on November 14, 2012. The offshore platform (TP-18) pressure was fluctuating between (124 and 128) psig as shown in Figure 7-14.

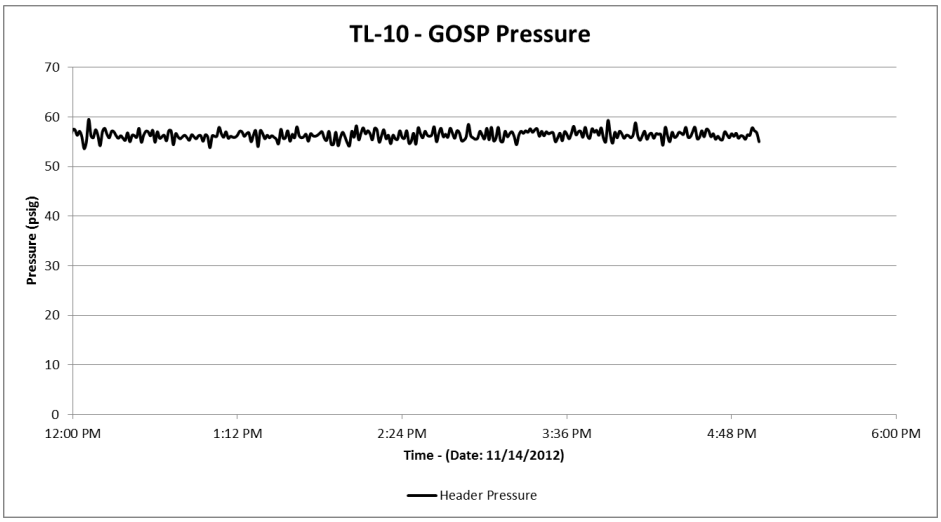

Figure 7-13: TL-10 GOSP Pressure Readings

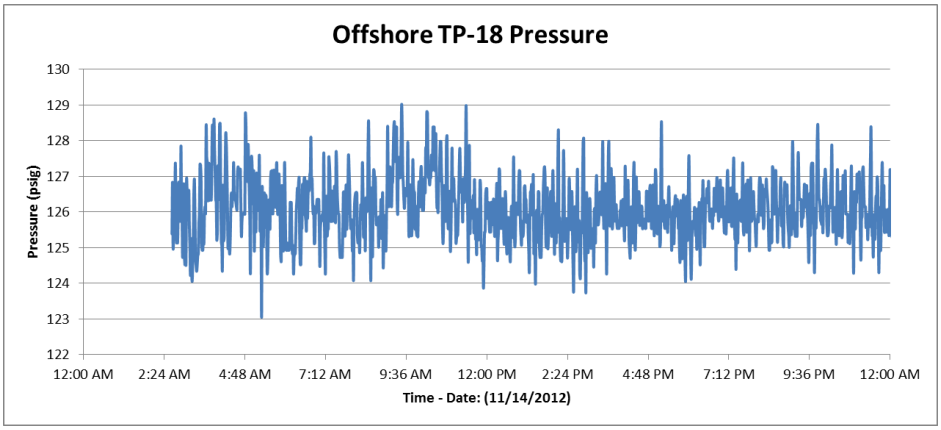

Figure 7-14: TL-10 TP-18 Pressure Readings

7.5. Field-C Fluid Properties

Field-C contains two types of oil and gas fluids. One can be characterized as Arab Medium (AM) crude oil and the other can be characterized by Arab Heavy (AH) crude oil. The gas-oil ration (GOR) of the two fluids are 250 scf/stb and 160 scf/stb respectively. The API of the two fluids at 60°F are 25.3 and 22.7 respectively.

The phase envelopes of TL-09 (AM) and TL-10 (AH) crude oil are shown in Figure 7-15 and Figure 7-16, which indicates that the pipeline system is clearly in the two phase region.

The gas and liquid densities variations with pressure for both fluids are shown in Figure 7-17, Figure 7-18, Figure 7-20 and Figure 7-21. These figures were plotted for the (AM) and (AH) fluids using OLGA at a temperature of 100°F. The oil viscosity was also plot at the same temperature which shows the variation with pressure from 0 to 800 psig as shown in Figure 7-19 and Figure 7-22.

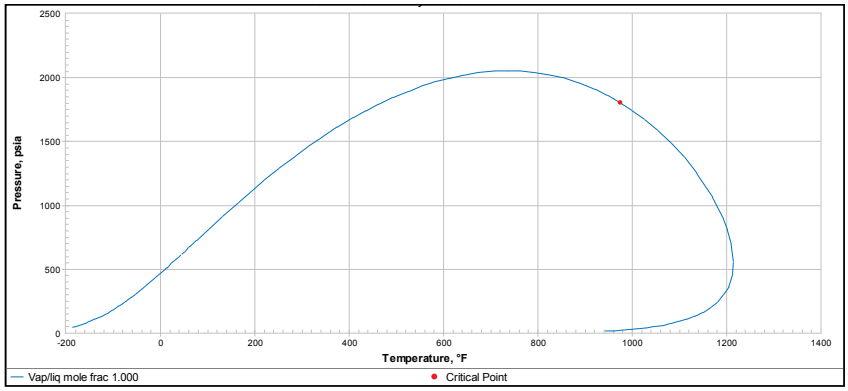

Figure 7-15: Phase Envelope of TL-09 (AM) Crude Oil

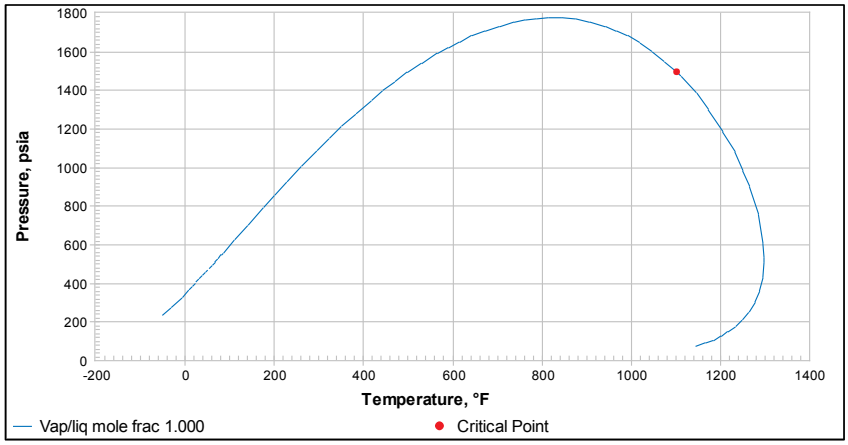

Figure 7-16: Phase Envelope of TL-10 (AH) Crude Oil

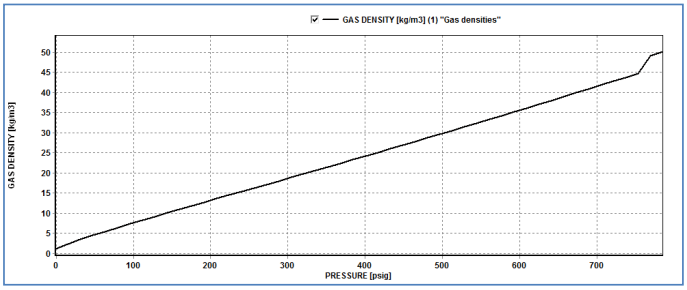

Figure 7-17: Gas Density (Kg/m3) – Temperature @ (100°F)

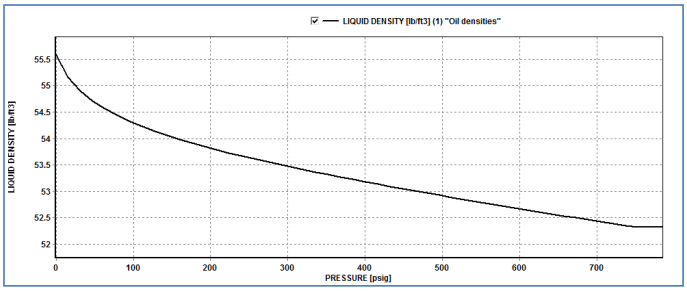

Figure 7-18: Oil Density (Kg/m3) – Temperature @ (100°F)

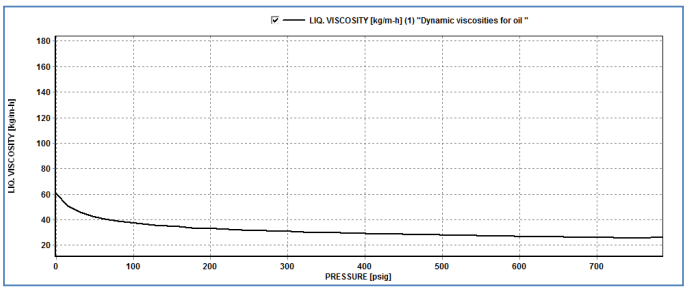

Figure 7-19: Oil Viscosity (Kg/m-h) – Temperature @ (100°F)

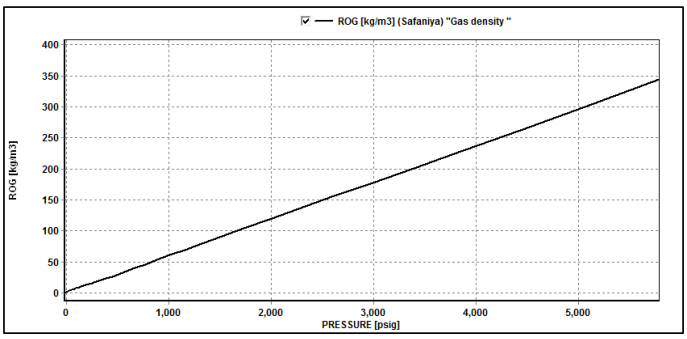

Figure 7-20: Gas Density (Kg/m3) – Temperature @ (100°F)

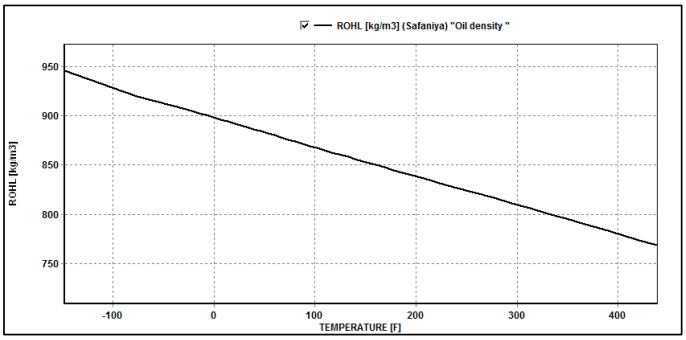

Figure 7-21: Oil Density (Kg/m3) – Temperature @ (100°F)

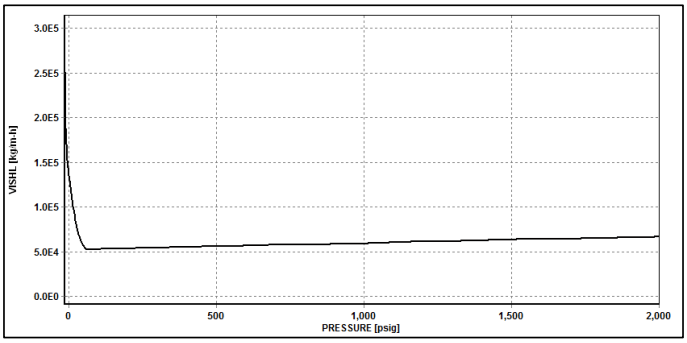

Figure 7-22: Oil Viscosity (Kg/m-h) – Temperature @ (100°F)

7.6. Gamma Calibration

The calibration of the gamma meters was carried out prior to the field measurement using a 42 inch pipeline spool. The wall thickness of this calibration spool was 22 mm compared to 25.4 mm of the measured pipeline. This provided a challenge for the field measurement team to correct for the difference in wall thickness. A detailed analysis was carried out to achieve this by correcting for the additional steel density encountered in the calibration spool.

7.7. Field-C – Holdup Field Measurements

The field measurement was carried out over three days, November 13, 14 and 17, 2012. The two gammas where located approximately 1.0 Km upstream of the separator for TL-09 and about 6.0 Km upstream of the separator for TL-10. The estimated pressure and temperature of the TL-09 (AM) fluid at the measurement location were 105 psig and 100°F respectively, while they were 82 psig and 100°F for TL-10 (AH) fluid.

The measurement was carried out using two gamma sources, Cobalt 60. The distance between the two gammas was (27.4) meter for TL-09 at low flow rate, (22) meter for TL-10 and (21) meter for TL-09 at normal flow rate. The pipe inclination was measured at zero degrees at both pipelines.

The measurement was made with different angles ranging from 90 to 45 degrees around the pipeline. However, the focus of the measurement was more on the 90 degrees vertical position which provides a direct representation of the holdup in the pipeline. The gamma measurement was conducted on the above ground section of the pipeline where a sectionalizing valve is installed on the trunkline just as it comes on the onshore side, see Figure 7-23 and Figure 7-24.

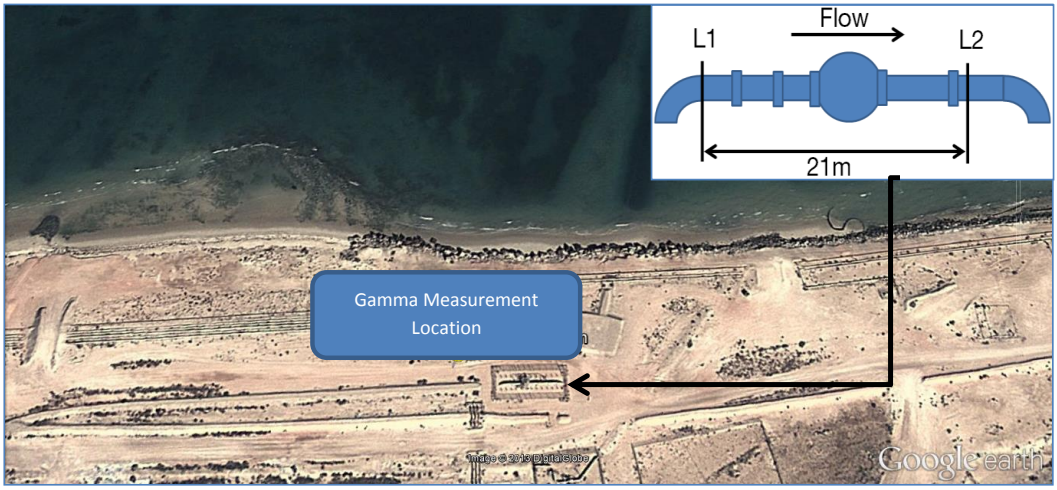

Figure 7-23: TL-09 Gamma Measurement Location at the onshore MOV Site

Figure 7-24: TL-10 Gamma Measurement Location at the onshore MOV Site

7.7.1. Field-C Holdup Measurements – TL-09 Low Flow Rate

The holdup data was calculated based on the following oil, gas and water densities and average water cut.

Table 7-4: TL-09 Holdup Calculation Parameters

Holdup Calculation Parameters		
Oil Density	0.8580	gr/cc
Gas Density	0.0065	gr/cc
Water Density	1.130	gr/cc
Water-cut (%)	16.2%	
Liquid Density	0.9021	gr/cc

Examination of the holdup data shown in Figure 7-25, Figure 7-26 and Figure 7-27, indicates a very high holdup at gamma-1 position compared to gamma-2 position, which sometimes exceed (1.0) due to a

higher local water cut compared to the average water cut in the pipe. This is most probably attributed to the location of the gamma-1 which was positioned directly after upward pipe inclination. This pipe arrangement causes a high concentration of liquid in this location due to the local slug initiation at the bottom of the pipe. These small slugs are quickly converted to small waves at gamma-2 position as shown in the liquid holdup figures. The frequency of those small slugs ranges between (10) to (20) seconds, with holdup values that range mostly between (0.1) and (1.0) at gamma-1 and (0.1) and (0.6) at gamma-2.

The few times that the water cut exceeded the (1.0) value at gamma-1 position indicates that the local water cut at this position was higher than the average water cut estimated for the whole pipeline.

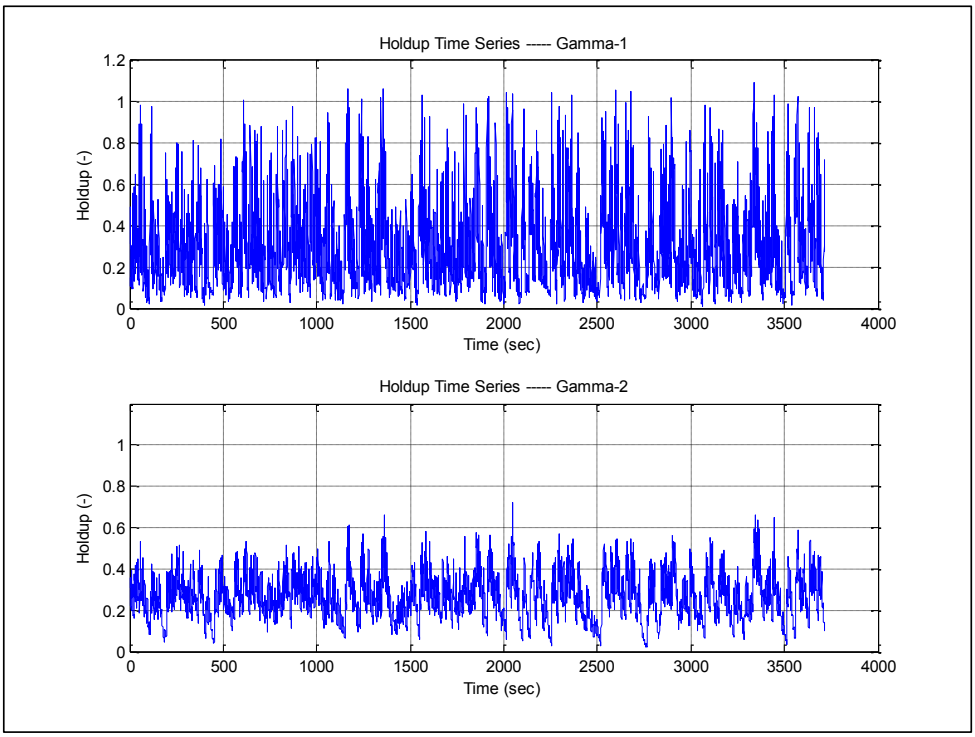

Figure 7-25: TL-09 Holdup Time Series with 16.2% Water Cut at Two Positions – Low Flow Rate (65 min)

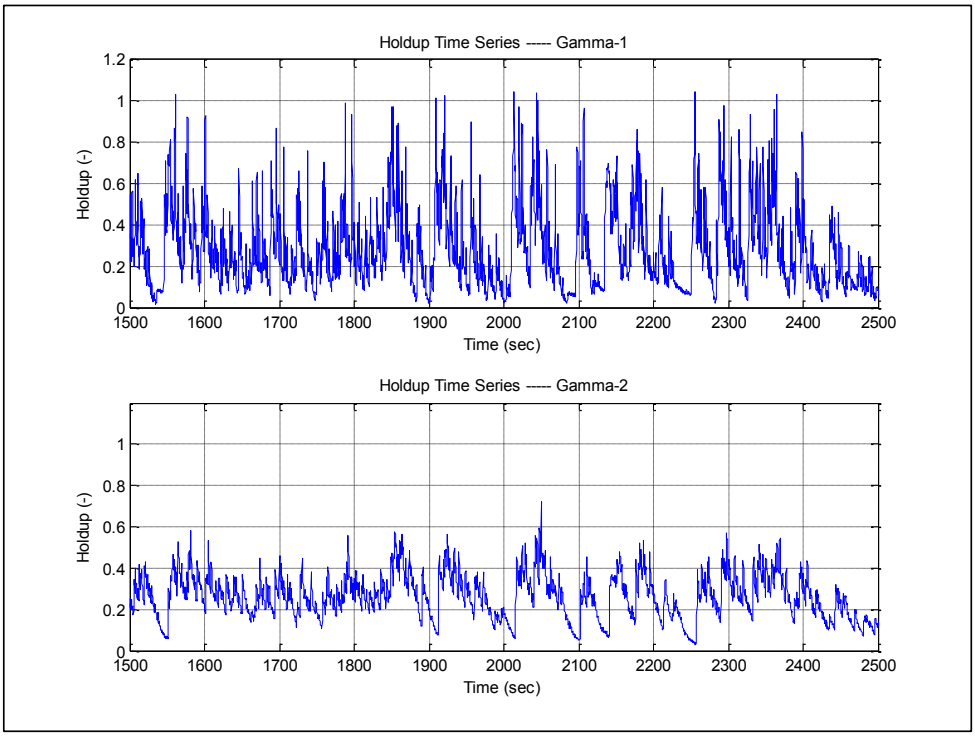

Figure 7-26: TL-09 Holdup Time Series with 16.2% Water Cut at Two Positions – Low Flow Rate (16 min)

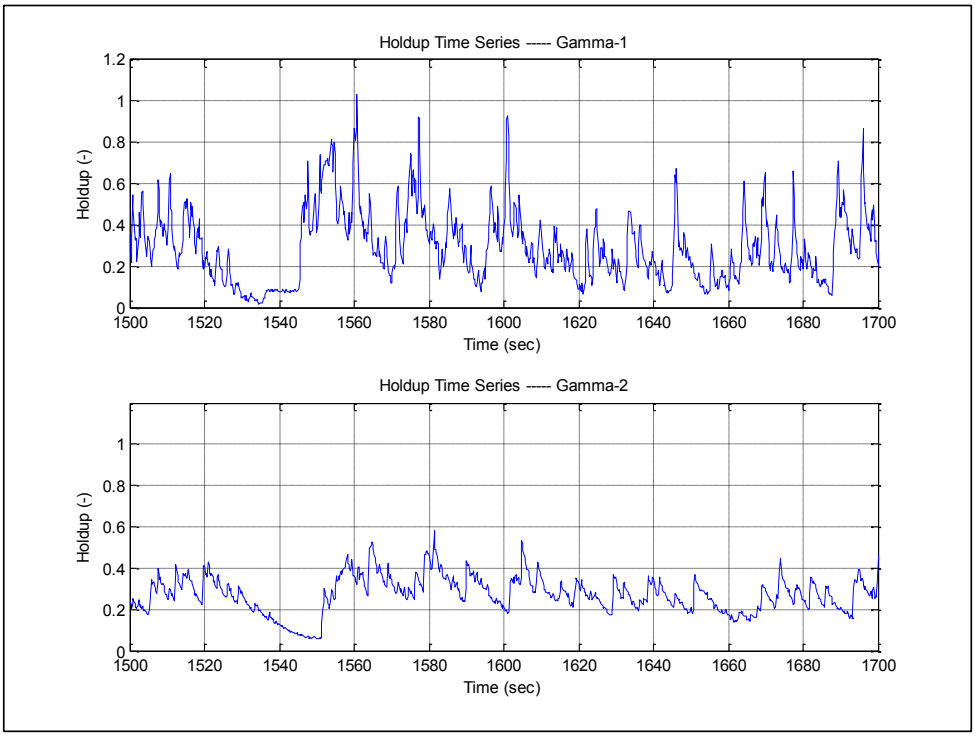

Figure 7-27: TL-09 Holdup Time Series with 16.2% Water Cut at Two Positions – Low Flow Rate (200 Seconds)

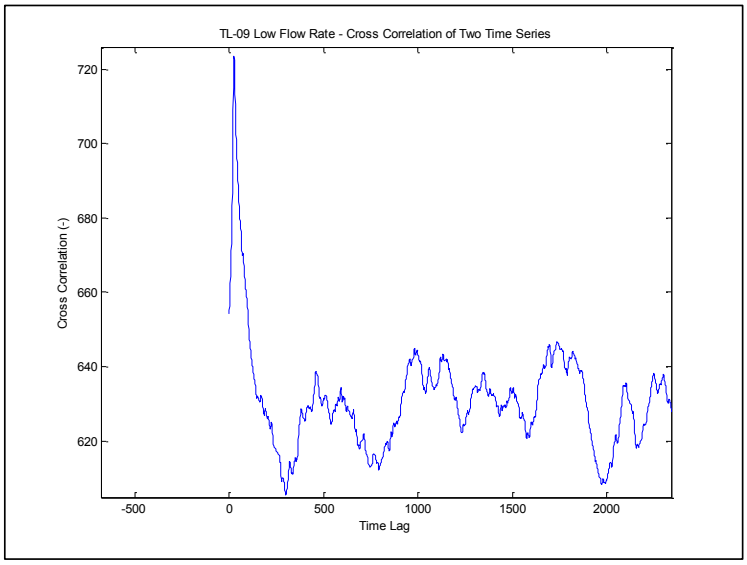

Figure 7-28: TL-09 Cross Correlation of Two Time Series – Low Flow Rate

Cross correlation of the two time series, results in a time shift of (5.4) seconds as shown in Figure 7-28. Using the distance between the gammas of (27.4) meter, one would obtain a velocity of 5.07 m/sec.

7.7.2. Field-C Holdup Measurements – TL-10 Normal Flow Rate

The holdup data was calculated based on the following oil, gas and water densities and average water cut.

Table 7-5: Holdup Calculation Parameters

Holdup Calculation Parameters		
Oil Density	0.8720	gr/cc
Gas Density	0.0092	gr/cc
Water Density	1.1300	gr/cc
Water-cut (%)	1.43%	
Liquid Density	0.8738	gr/cc

Analyzing the holdup time series shown in Figure 7-29, Figure 7-30 and Figure 7-31, indicates a stratified wavy behavior which was anticipated due to the relatively low flow rate. The holdup at gamma-1 position fluctuates more frequently due to its location just downstream of the upward inclined pipe. The holdup at gamma-1 position fluctuates between (0.15) and (0.5) while at gamma-2 position, it fluctuates between (0.2) and (0.5). There also appears to be a large oscillation frequency of approximately (200) seconds in addition to the 10 to 20 seconds frequency which exists at the small wave scale.

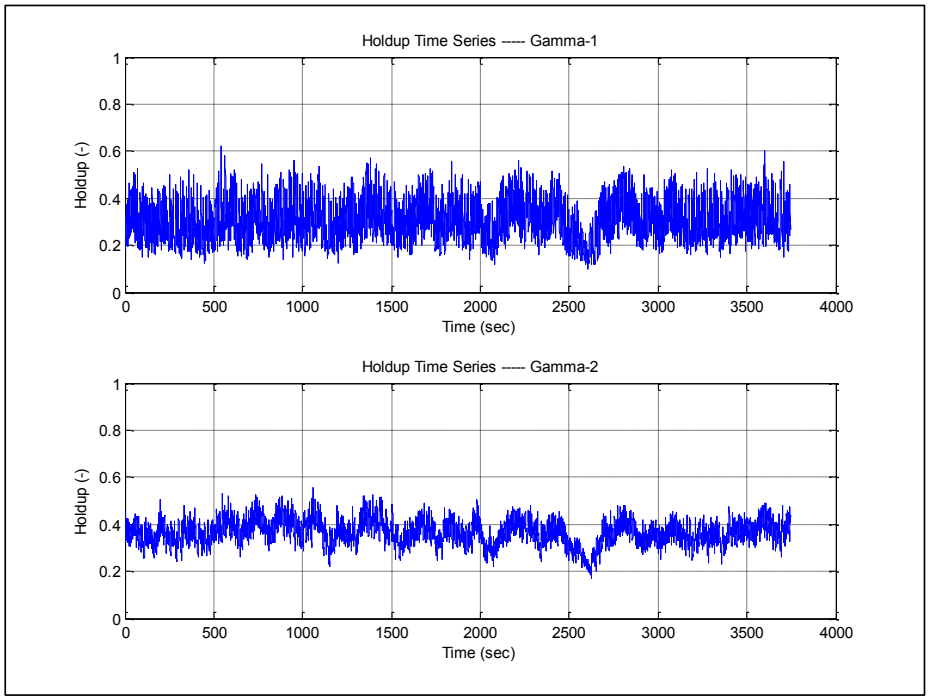

Figure 7-29: TL-10 Holdup Time Series with 1.43% Water Cut at Two Positions – Normal Flow Rate (65 min)

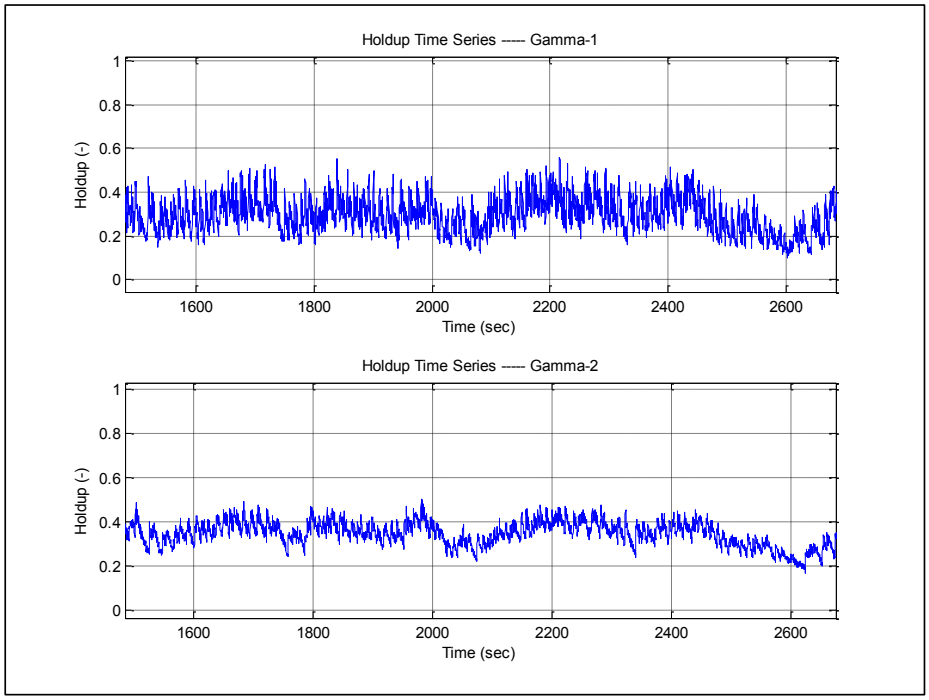

Figure 7-30: TL-10 Holdup Time Series with 1.43% Water Cut at Two Positions – Normal Flow Rate (17 min)

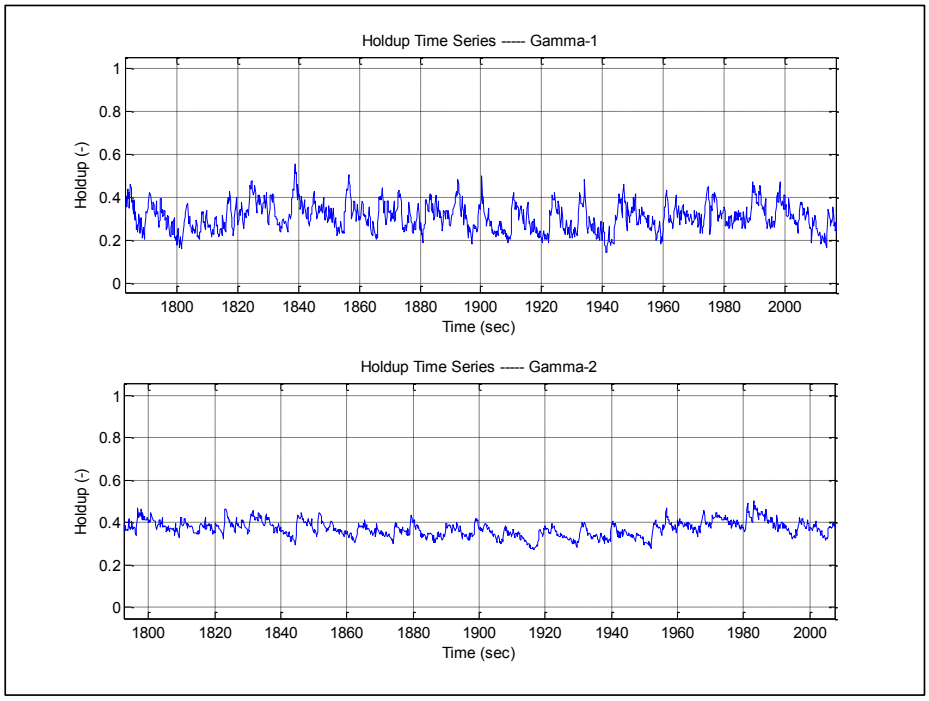

Figure 7-31: TL-10 Holdup Time Series with 1.43% Water Cut at Two Positions – Normal Flow Rate (200 Seconds)

Figure 7-32: TL-10 Cross Correlation of Two Time Series – Normal Flow Rate

Cross-correlating the two gamma series one can observe a maximum frequency of 40 points, each point is equal to a time step of 0.2 seconds, which gives a total time shift of 8 seconds. Using the already measured

distance between the two gammas of 22 meter, one can calculate the velocity of the slugs/waves which turns out to be 2.75 m/sec.

7.7.3. Field-C Holdup Measurements – TL-09 Normal Flow Rate

The holdup data was also calculated based on the following oil, gas and water densities and average water cut.

Table 7-6: Holdup Calculation Parameters

Holdup Calculation Parameters		
Oil Density	0.8580	gr/cc
Gas Density	0.0065	gr/cc
Water Density	1.130	gr/cc
Water-cut (%)	15%	
Liquid Density	0.9042	gr/cc

Examination of the holdup data shown in Figure 7-33, Figure 7-34, Figure 7-35 and Figure 7-36, indicates a very high holdup at gamma-1 position compared to gamma-2 position, which sometimes exceed (1.0) due to a higher local water cut compared to the average water cut in the pipe. This is most probably attributed to the location of the gamma-1 which was positioned directly after upward pipe inclination. This pipe arrangement causes a high concentration of liquid in this location due to the local slug initiation at the bottom of the pipe. These small slugs are quickly converted to small waves at gamma-2 position as shown in the liquid holdup figures. The frequency of those small slugs ranges between (10) to (20) seconds, with holdup values that range between (0.1) and (1.0) at gamma-1 and (0.1) and (0.7) at gamma-2. There is also an overlaying structure of oscillations with frequency of approximately (100) seconds which is shown clearly in Figure 7-35.

Finally, there is a macro level of oscillations that can be vaguely extracted from the time series in gamma-2 position. This macro level of oscillations shown in Figure 7-33 indicates a slugging frequency of approximately (1,000) seconds, equal to (16.6) minutes, which coincide with slugging frequency noted in the pressure readings depicted in Figure 7-12 for TP-17

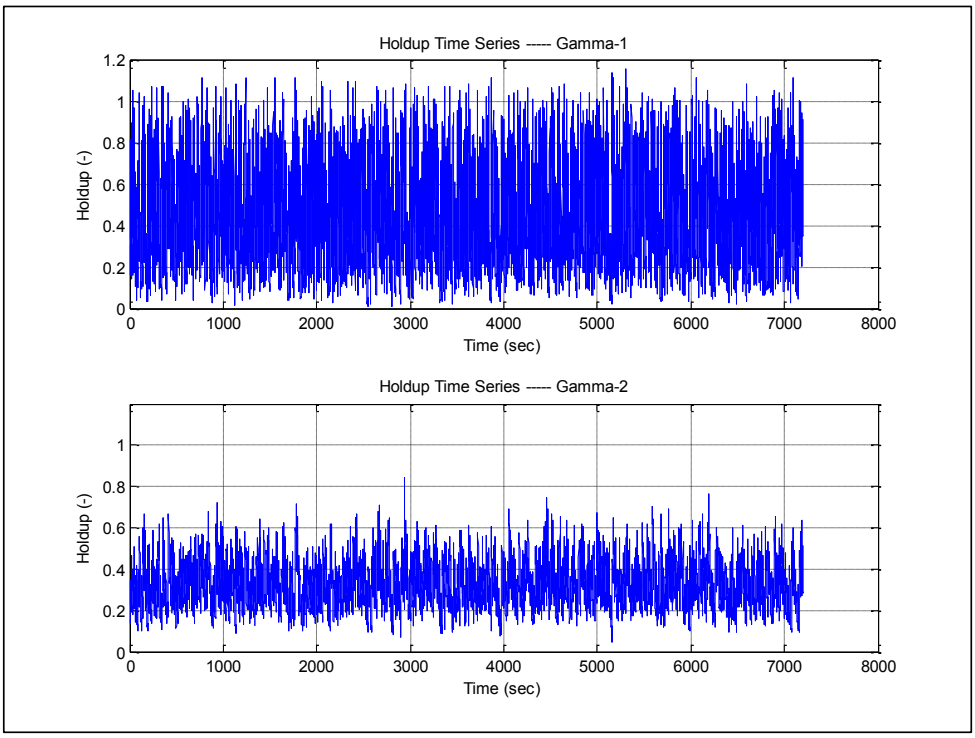

Figure 7-33: TL-09 Holdup Time Series with 15% Water Cut at Two Positions – Normal Flow Rate (120 min)

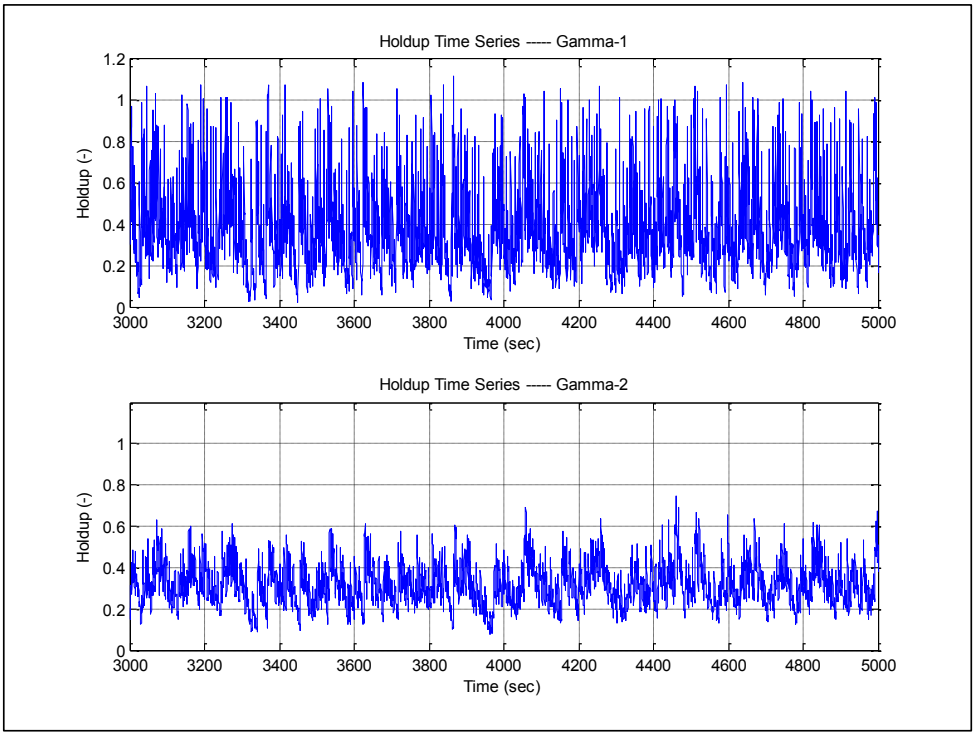

Figure 7-34: TL-09 Holdup Time Series with 15% Water Cut at Two Positions – Normal Flow Rate (33 min)

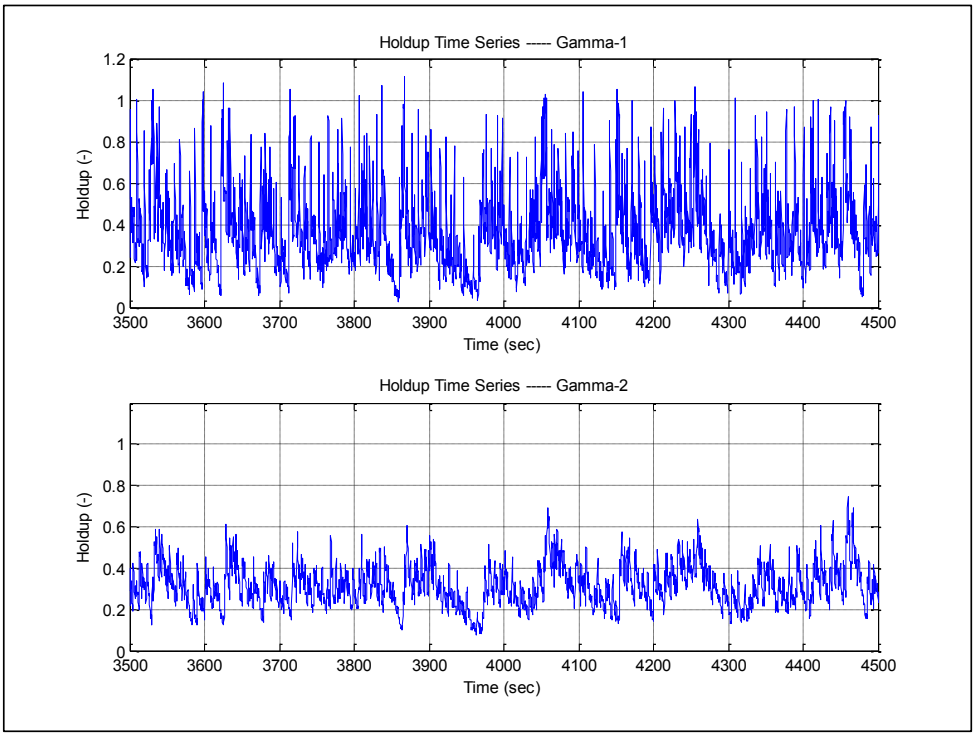

Figure 7-35: TL-09 Holdup Time Series with 15% Water Cut at Two Positions – Normal Flow Rate (16 min)

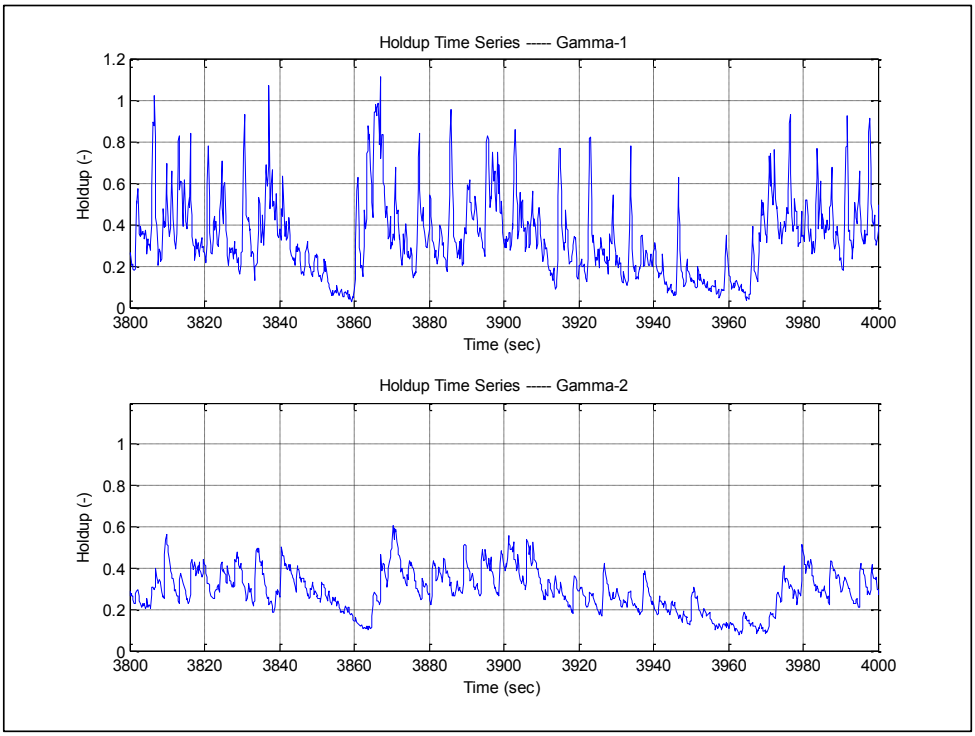

Figure 7-36: TL-09 Holdup Time Series with 15% Water Cut at Two Positions – Normal Flow Rate (200 seconds)

Cross correlation of the two time series, results in a time shift of (4.4) seconds as shown in Figure 7-37. Using the distance between the gammas of (21.0) meter, one would obtain a velocity of 4.77 m/sec.

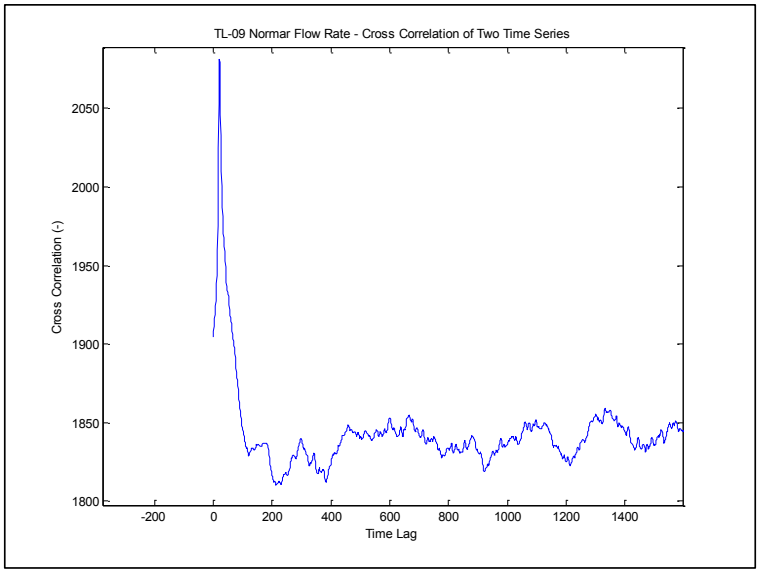

Figure 7-37: TL-09 Cross Correlation of Two Time Series – Normal Flow Rate

7.8. TL-09 & TL-10 Pipelines OLGA Simulation

Detailed simulation analysis was carried out using OLGA-7.2 for TL-09 and TL10 pipelines. The simulation results indicate a good agreement with the pressure and holdup results for the cases without slug tracking. The simulation was carried out with a coarse grid, (50) meters and (73) meters average section lengths for TL-09 and Tl-10 respectively. The comparison was carried out against the pipelines inlet pressure and the holdup measurements at the end of the pipeline.

The pressure comparison for TL-09 pipeline shown in Figure 7-38 and Figure 7-39 depicts OLGA pressure predictions with and without slug tracking for both low and normal flow rates for TL-09. The pressure predictions, without slug tracking, show accurate pressure results but without the (30) psi fluctuations observed in the measured data. However, the pressure predictions with slug tracking show an over predictions of almost (60) psi with a fluctuation of approximately (10) psi. The same kind of behavior is noticed for both the normal and reduced flow rates. The average holdup OLGA predictions for TL-09 pipeline showed good predictions for the non-slug tracking case. The holdup predictions with slug tracking show small hydrodynamic slugs with frequencies that range between (2 to 5) minutes and holdup that reaches (0.8). These holdup predictions are higher and less frequent than the field measurement stratified-wavy flow behavior.

For TL-10 pipeline, the OLGA pressure and holdup results are shown in Figure 7-42 and Figure 7-43. The pressure OLGA predictions indicate good agreement for both slug tracking and non-slug tracking cases with slight over-prediction for slug tracking case and slight under-prediction for the non-slug tracking case. The holdup predictions show stratified-wavy flow for non-slug tracking case with approximately (20) minutes frequency while the slug tracking case shows small hydrodynamic slugs with (5 to 10) minutes frequency with holdup values that reaches 1.0 in certain cases.

The extremely large slugs noticed in earlier simulations were not observed in these simulations which could be due to the lower flow rates encountered during the field measurements.

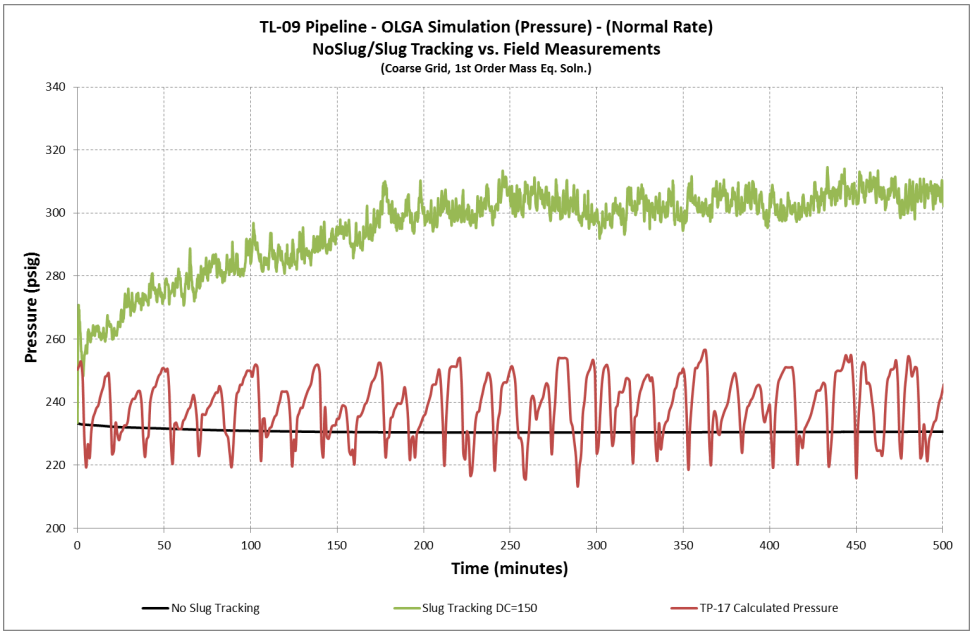

Figure 7-38: TL-09 Pipeline – OLGA Simulation Results (Coarse Grid) (Pressure) – (Normal Rate)

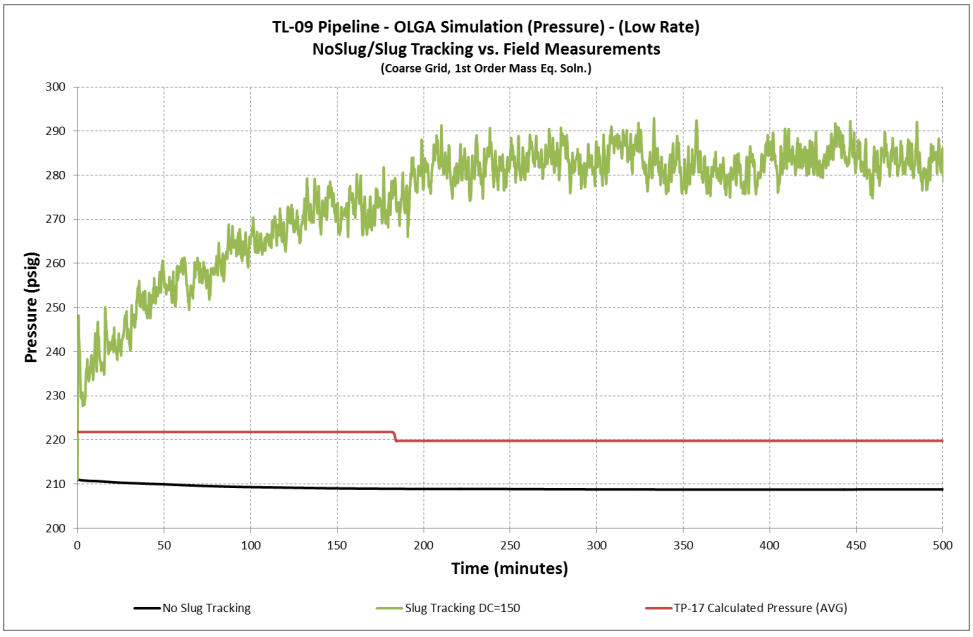

Figure 7-39: TL-09 Pipeline – OLGA Simulation Results (Coarse Grid) (Pressure) – (Low Rate)

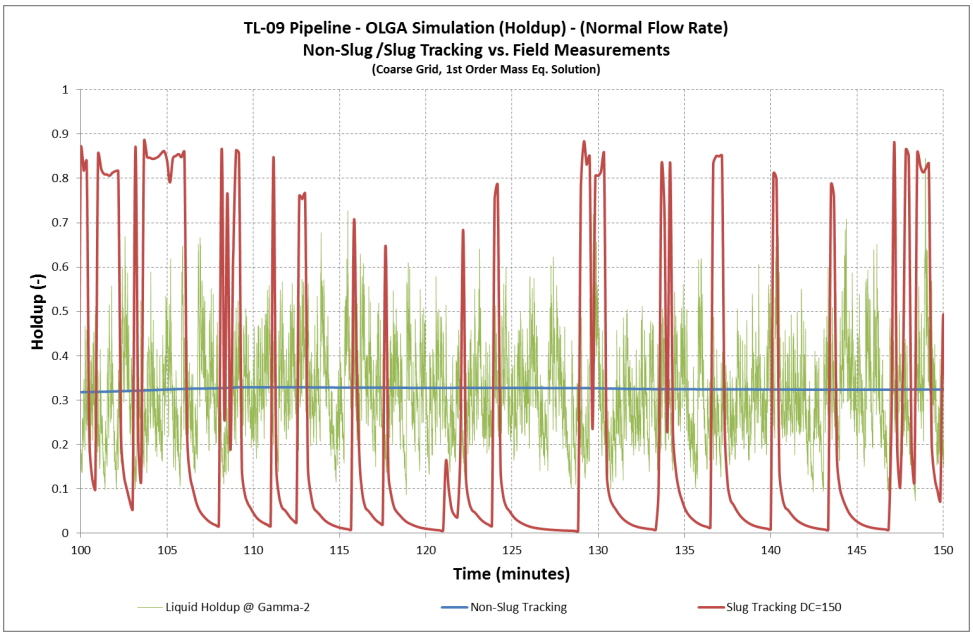

Figure 7-40: TL-09 Pipeline – OLGA Simulation Results (Coarse Grid) (Holdup) – (Normal Rate)

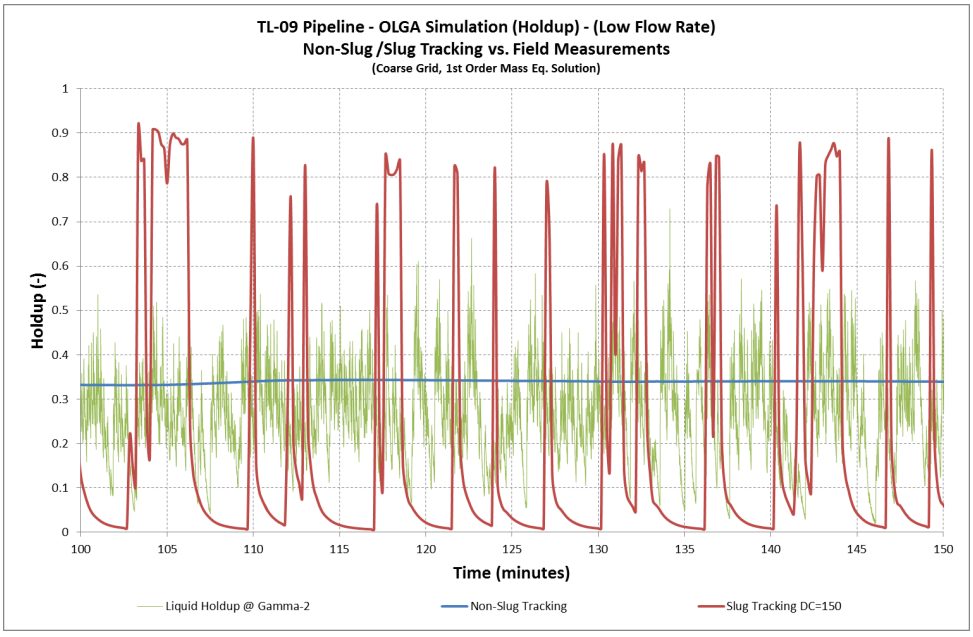

Figure 7-41: TL-09 Pipeline – OLGA Simulation Results (Coarse Grid) (Holdup) – (Low Rate)

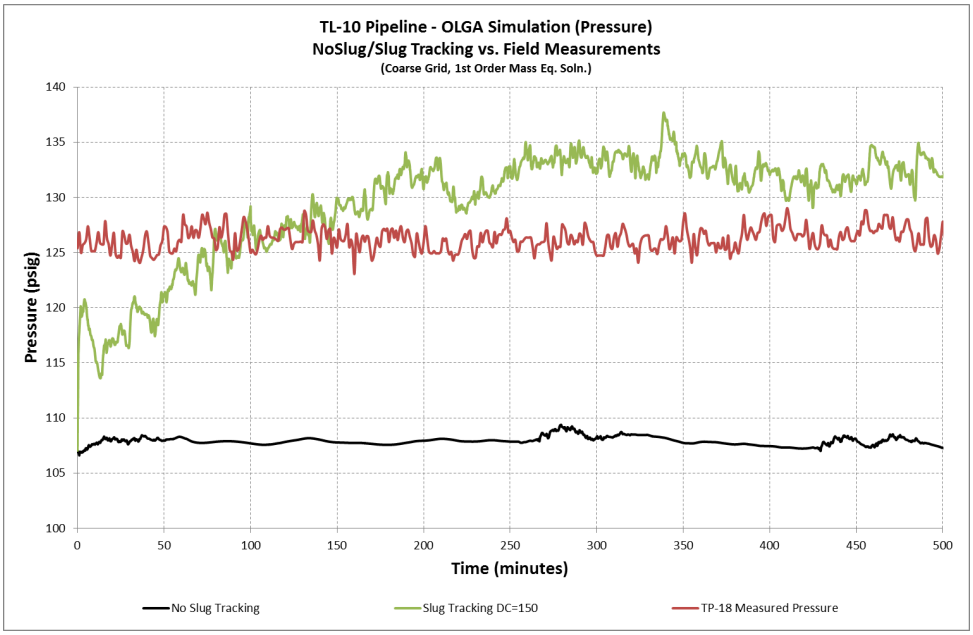

Figure 7-42: TL-10 Pipeline – OLGA Simulation Results (Coarse Grid) (Pressure) – (Normal Rate)

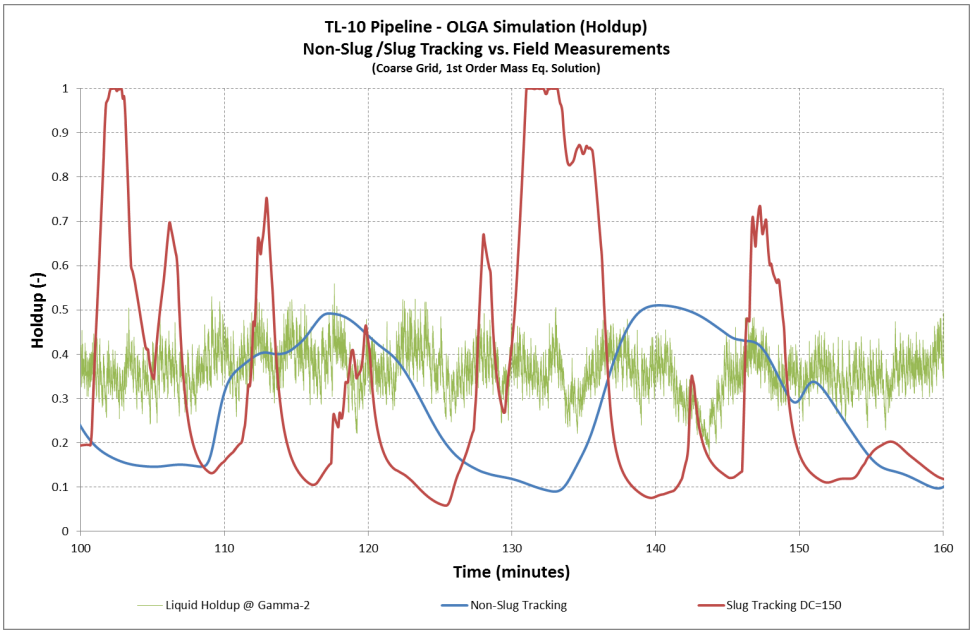

Figure 7-43: TL-10 Pipeline – OLGA Simulation Results (Coarse Grid) (Holdup) – (Normal Rate)

7.9. TL-09 & TL-10 Pipelines LedaFlow Simulation

Detailed simulation analysis was carried out using LedaFlow version (1.4.242.619), for TL-09 and TL10 pipelines. The simulation results indicate a good agreement with the pressure and holdup results for the cases without slug capturing. The simulation was carried out with a coarse grid, (50) meters and (73) meters average section lengths for TL-09 and Tl-10 respectively. The comparison was carried out against the pipelines inlet pressure and the holdup measurements at the end of the pipeline.

The pressure comparison for TL-09 pipeline shown in Figure 7-44 and Figure 7-45 depicts LedaFlow pressure predictions with and without slug capturing for both low and normal flow rates for TL-09. The pressure predictions, without slug capturing, show accurate pressure results for the normal flow rate but without the (30) psi fluctuations observed in the measured data. However, the pressure predictions with slug capturing show an under predictions of almost (40) psi for both normal and low flow rates. The average holdup LedaFlow predictions for TL-09 pipeline showed good predictions, for the non-slug capturing case with lower frequencies than the ones observed in field measurements as shown in Figure 7-46 and Figure 7-47.

For TL-10 pipeline, the LedaFlow pressure and holdup results are shown in Figure 7-48 and Figure 7-49. The pressure LedaFlow predictions indicate an under prediction for both slug capturing and non-slug capturing cases with slightly better results for the non-slug capturing case.

A grid dependency study was carried out to examine the impact of different grid sizes on slug capturing in LedaFlow. The pressure results shown in Figure 7-50, Figure 7-51 and Figure 7-52 indicate the positive impact of finer mesh sizes on slug capturing scheme as expected. The results significantly improved for both pipelines from the coarse grid case with (50*D) to (20*D) and finally to (10*D).

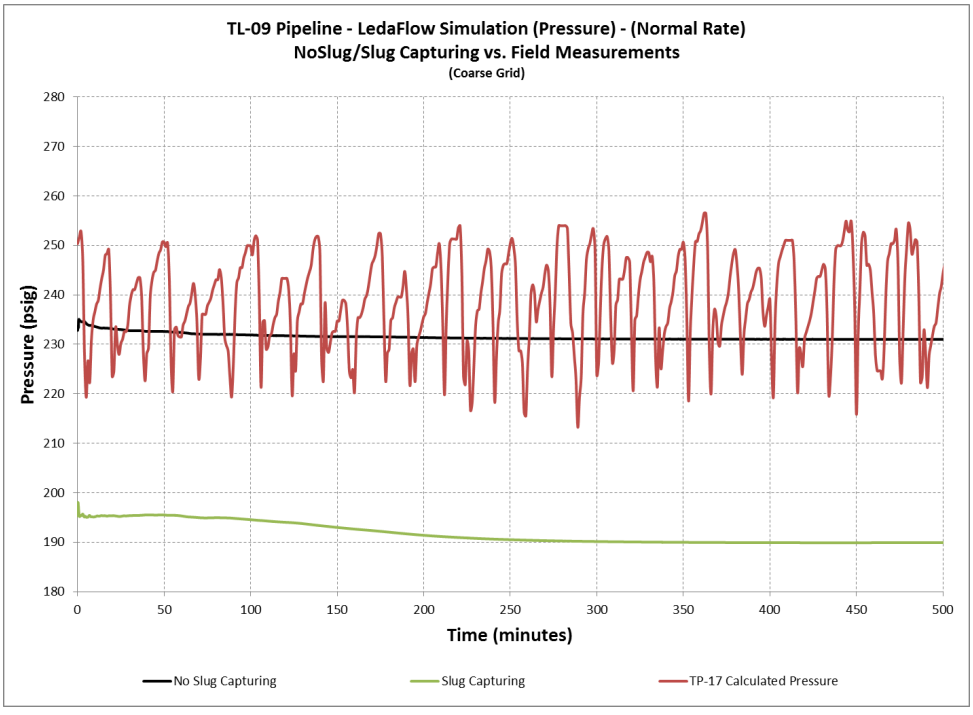

Figure 7-44: TL-09 Pipeline – LedaFlow Simulation Results (Coarse Grid) (Pressure) – (Normal Rate)

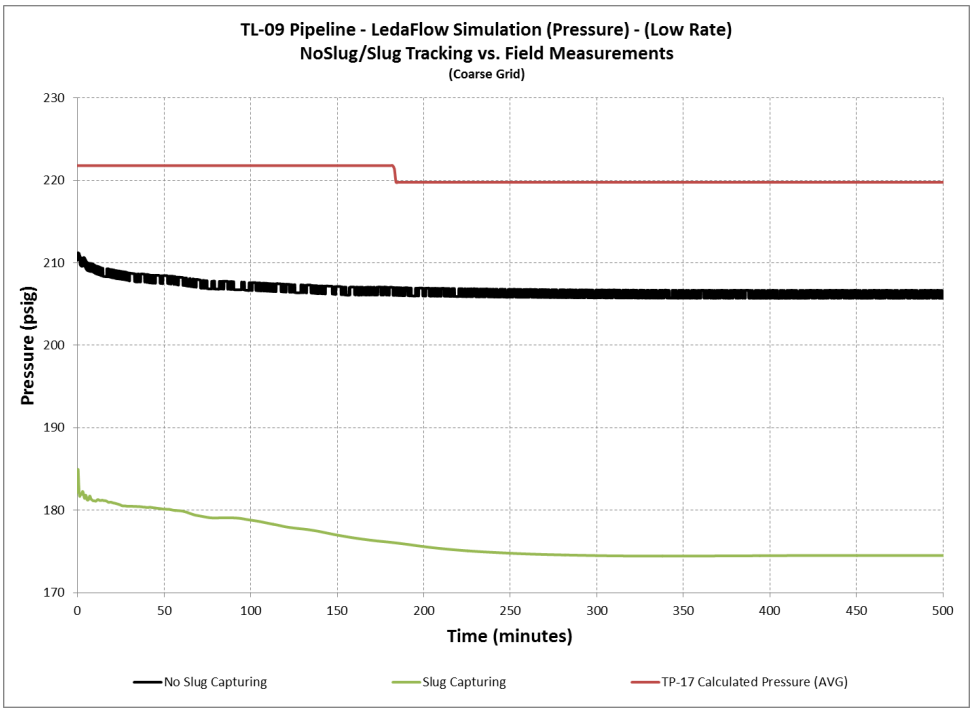

Figure 7-45: TL-09 Pipeline – LedaFlow Simulation Results (Coarse Grid) (Pressure) – (Low Rate)

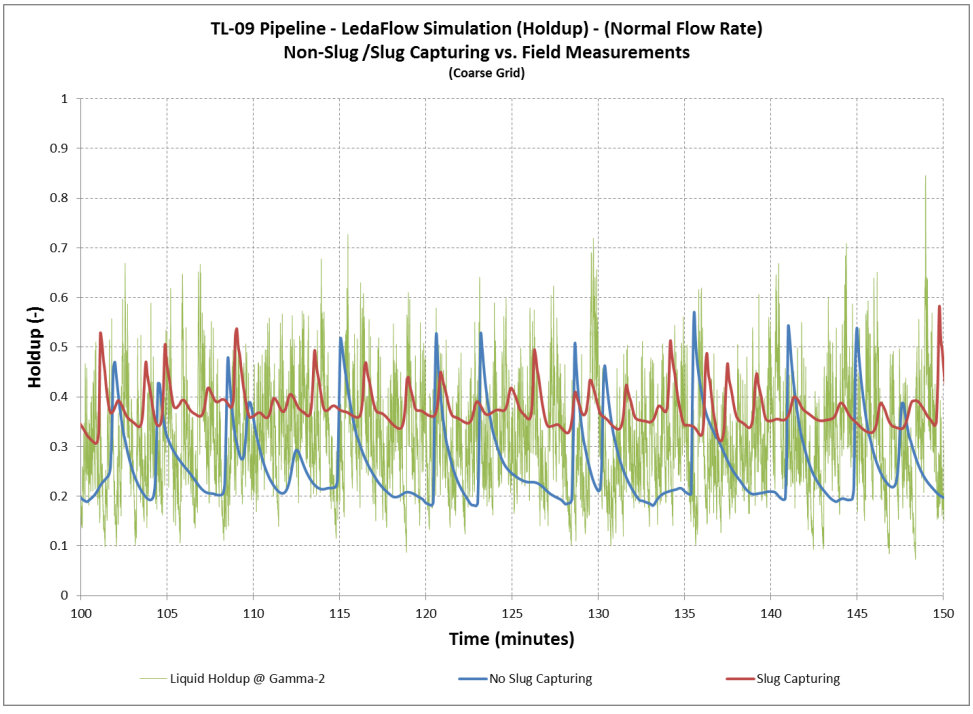

Figure 7-46: TL-09 Pipeline – LedaFlow Simulation Results (Coarse Grid) (Holdup) – (Normal Rate)

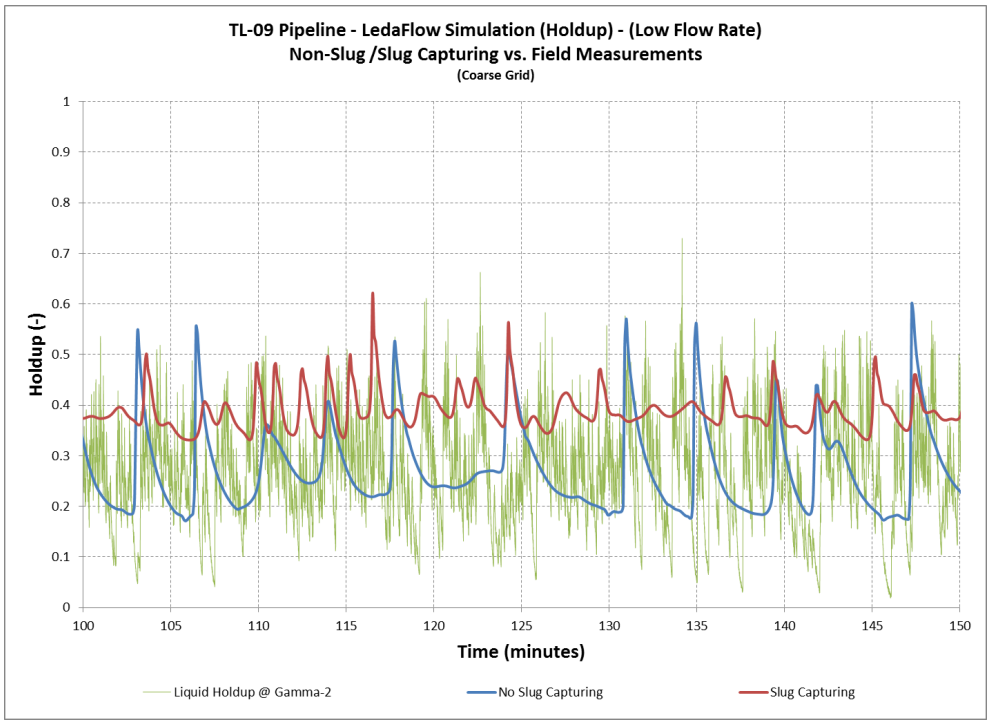

Figure 7-47: TL-09 Pipeline – LedaFlow Simulation Results (Coarse Grid) (Holdup) – (Low Rate)

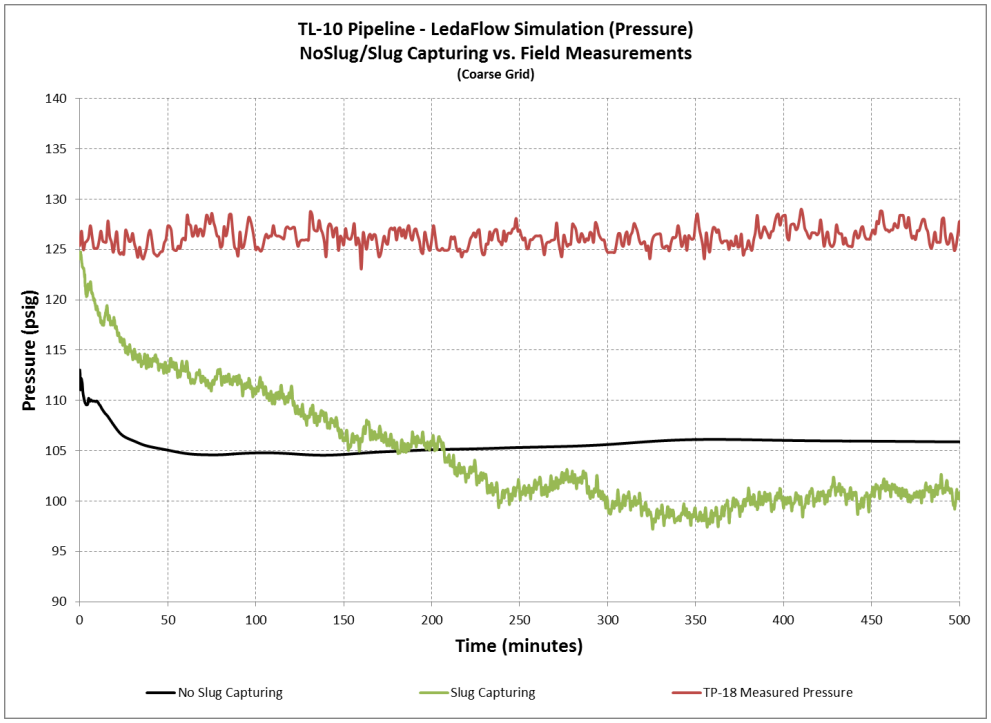

Figure 7-48: TL-10 Pipeline – LedaFlow Simulation Results (Coarse Grid) (Pressure) – (Normal Rate)

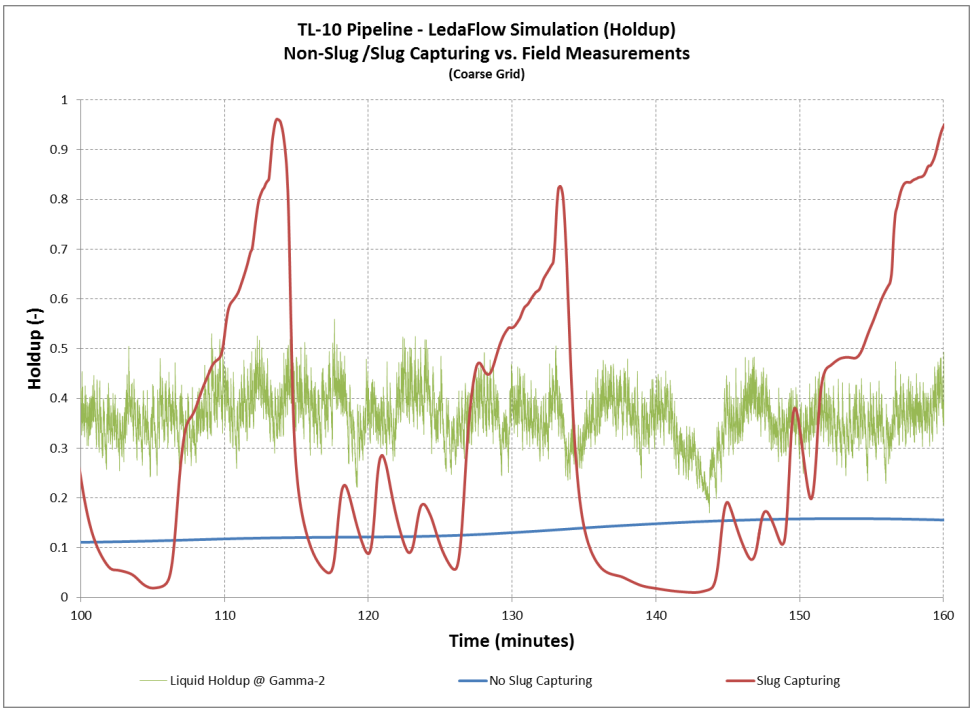

Figure 7-49: TL-10 Pipeline – LedaFlow Simulation Results (Coarse Grid) (Holdup) – (Normal Rate)

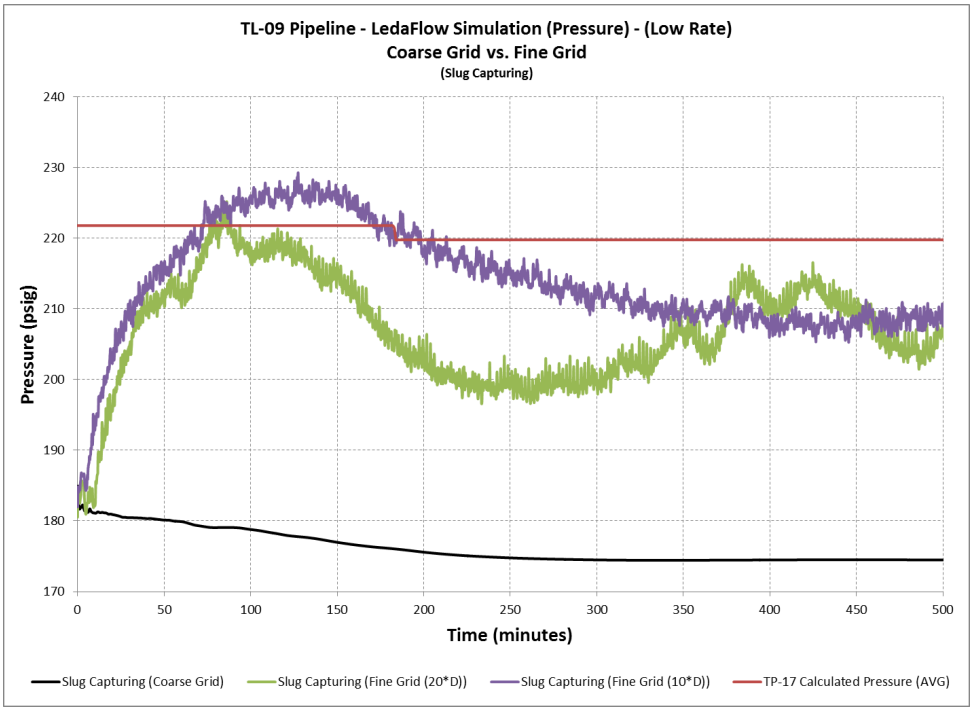

Figure 7-50: TL-09 Pipeline – LedaFlow Simulation Results (Coarse vs. Fine Grid) (Pressure) – (Low Rate)

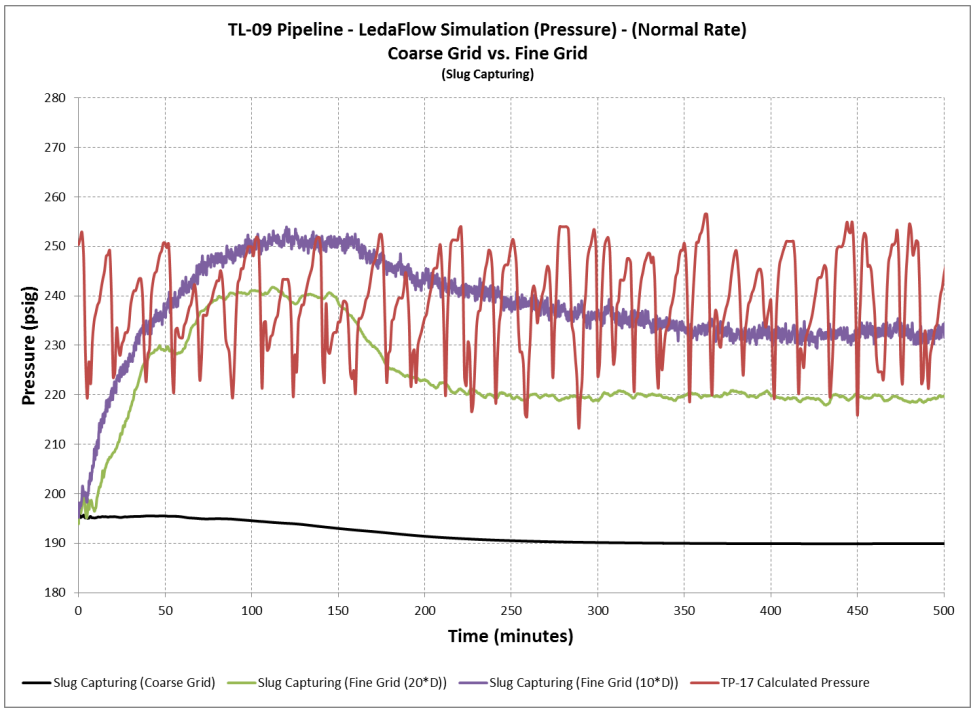

Figure 7-51: TL-09 Pipeline – LedaFlow Simulation Results (Coarse vs. Fine Grid) (Pressure) – (Normal Rate)

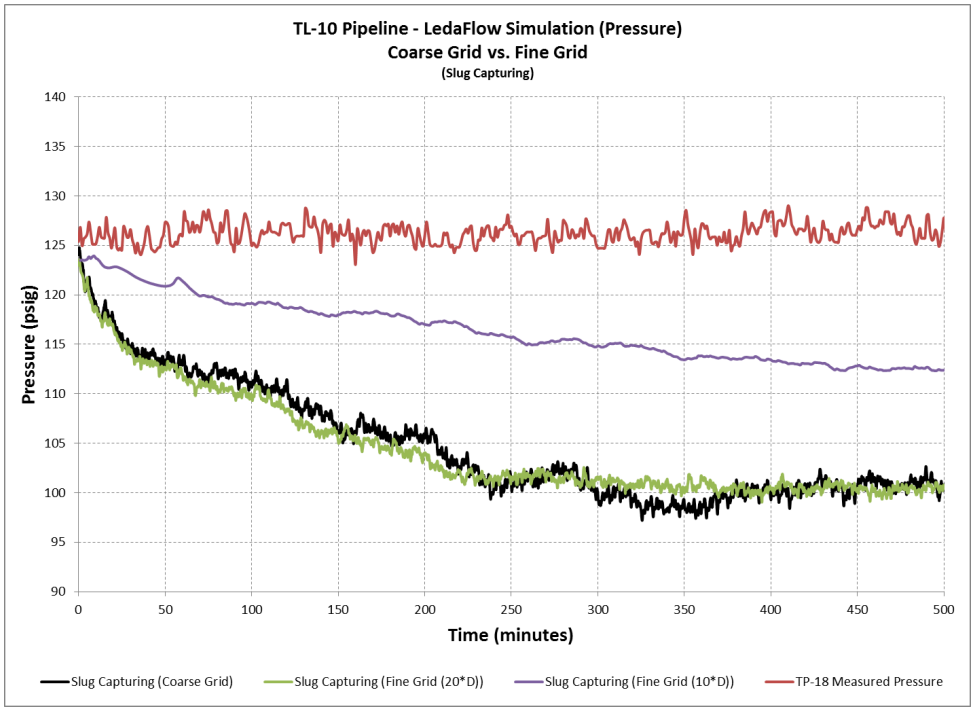

Figure 7-52: TL-10 Pipeline – LedaFlow Simulation Results (Coarse vs. Fine Grid) (Pressure) – (Normal Rate)

This page was intentionally left blank

8. FIELD-D – HOLDUP & PRESSURE MEASUREMENTS

Field-D holdup and pressure measurements were carried out on January 26-27, 2013. Additional measurement was also conducted on March 18, 2013 to verify results from the previous measurement. They were carried out on a 42 inch offshore pipeline, TL-AB01 connecting a main Tie-in Platform (TP-2) with an onshore Gas Oil and Separation Plant (GOSP). The holdup measurement was carried out using two gamma sources and detectors applied at various angles around the pipeline on the onshore side of the pipeline.

The motivation behind this measurement was the pressure discrepancy experienced with OLGA predictions compared to field pressure measurements which was an over prediction in the order of 10% to 50% depending on the flow rates and boundary conditions used in simulation.

8.1. Field-D Description

At the offshore side of Field-D, the oil is collected from various offshore production platforms into a main offshore Tie-in Platform (TP-2). The main TP-2 is then connected to an onshore crude oil processing facilities through large diameter, 42 inch, multiphase pipeline, which is approximately 60 Km long, as shown in Figure 8-2.

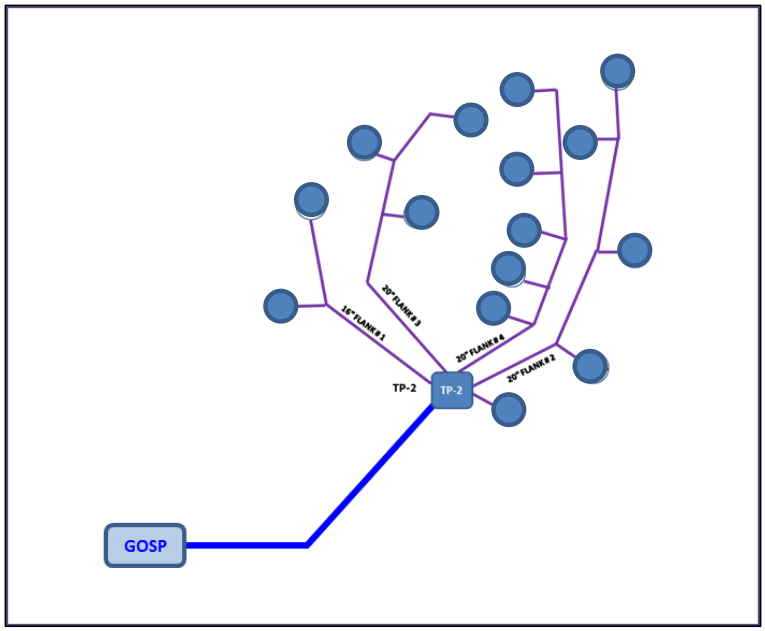

Figure 8-1: Field-D Overall Schematic

8.2. Flow Rates

The flow rate was obtained from the historical daily production rates from each well and compared against the total production received at the onshore GOSP facility and ESP data at each well. The oil flow rate was estimated by operations on June 26 at 285,000 BBL/Day at standard conditions with a water cut of 16.4%. The average superficial gas and liquid velocities as calculated by OLGA was (0.4) m/sec and (0.8) m/sec respectively.

8.3. Pipeline Details

TL-AB01 pipeline has an outside diameter of 42 inch with a wall thickness of 1.0 inch. The pipeline extends for approximately 60 Km from the offshore tie-in platform, TP-2, to the onshore GOSP facilities. The terrain can be described as being highly undulating with an overall upward slope as shown in Figure 8-2. The area where the holdup field measurements were carried out was an above ground area where a sectionalizing valve is installed at the beach side.

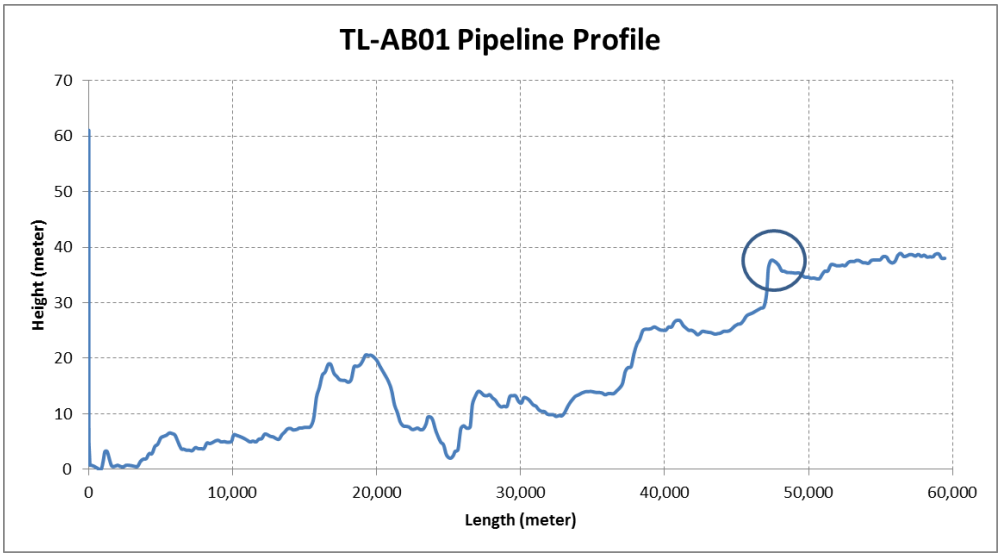

Figure 8-2: TL-AB01 Pipeline Profile

8.4. Inlet and Outlet Pressure

The GOSP separator pressure was set at 64 psig as shown in Figure 8-3. The pressure at the inlet of the GOSP was recorded at an average of 80 psig as shown in Figure 8-4. The pressure at the field measurement location was visually recorded at 128 psig during the measurement, while the pressure at TP-2 was recorded and shows an average pressure of 173 psig as shown in Figure 8-5.

The pressure was logged at the GOSP separator and inlet every (5) seconds while on the offshore side the logging was made every (1) minute.

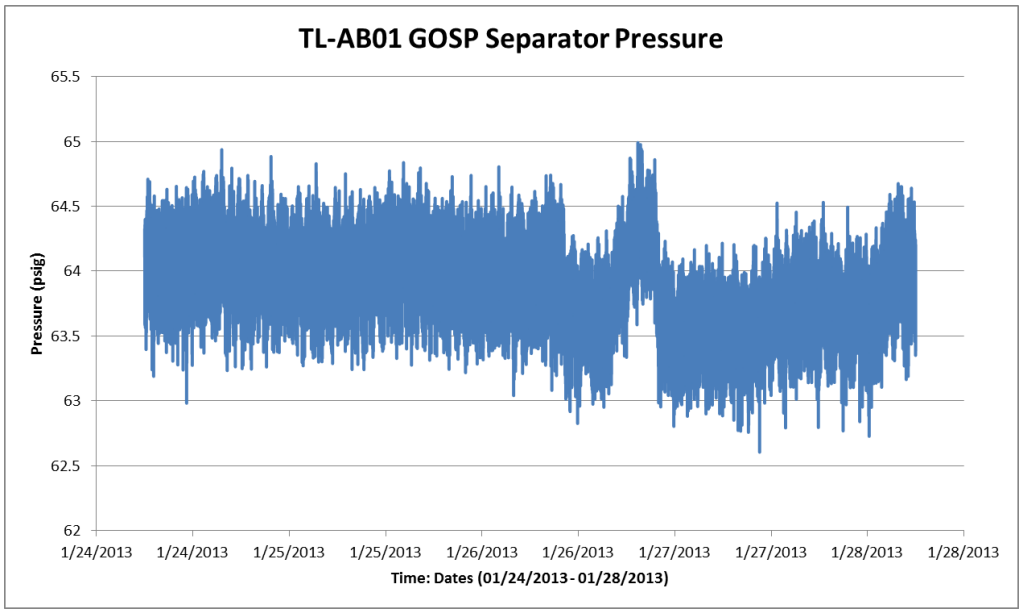

Figure 8-3: TL-AB01 GOSP Separator Pressure Readings on January 26-28, 2013

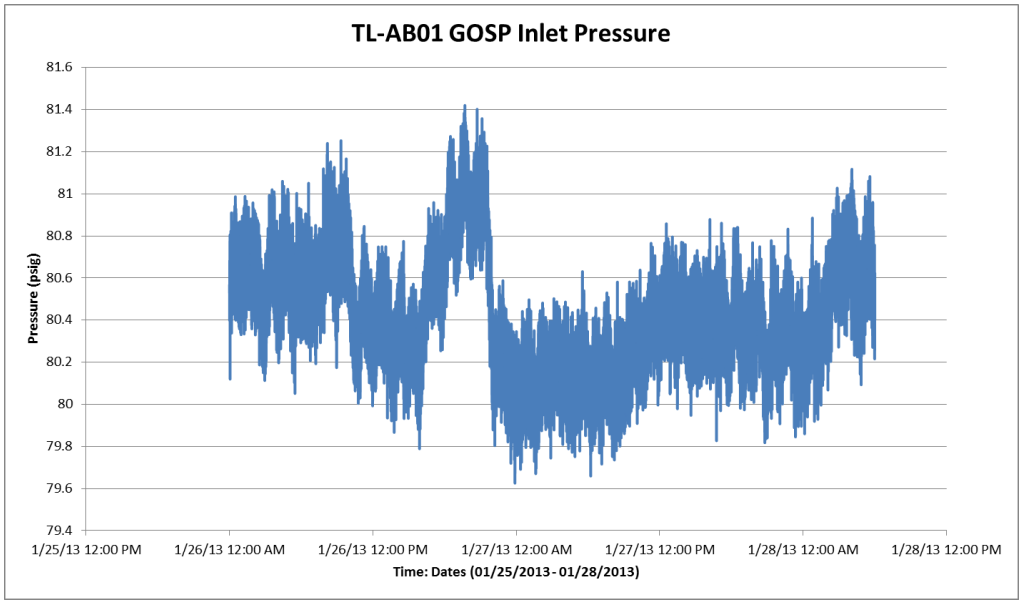

Figure 8-4: TL-AB01 GOSP Inlet Pressure Readings on January 26-28, 2013

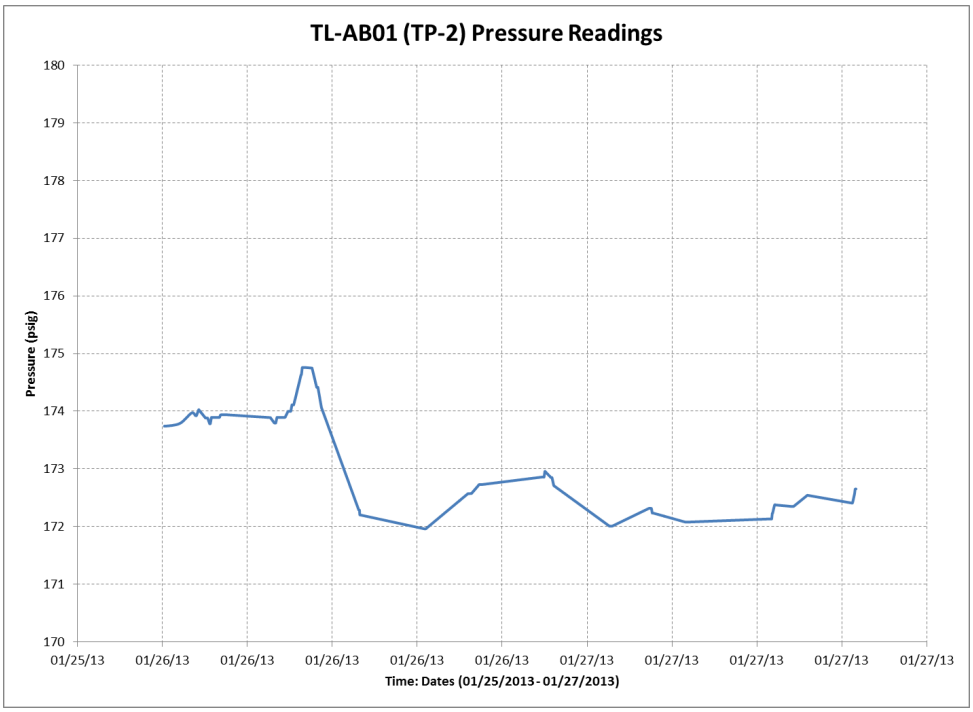

Figure 8-5: TP-2 Pressure Reading on January 26-27, 2013 – (Pressure Log at (1) minute frequency)

8.5. Field-D Fluid Properties

Field-D contains crude oil that can be characterized as Arab Medium (AM). The gas-oil ratio (GOR) in scf/stb for fluid is 84 and the API at 60°F is 28.2.

The phase envelope of TL-AB01 (AM) is shown in Figure 8-6, which indicates that the pipeline system is clearly in the two phase region.

The gas and liquid densities variations with pressure for both fluids are shown in Figure 8-7 and Figure 8-8. These figures were plotted for the (AM) fluids using OLGA at a temperature of 75°F. The oil viscosity was also plot at the same temperature which shows the variation with pressure from 0 to 500 psig as shown in Figure 8-9.

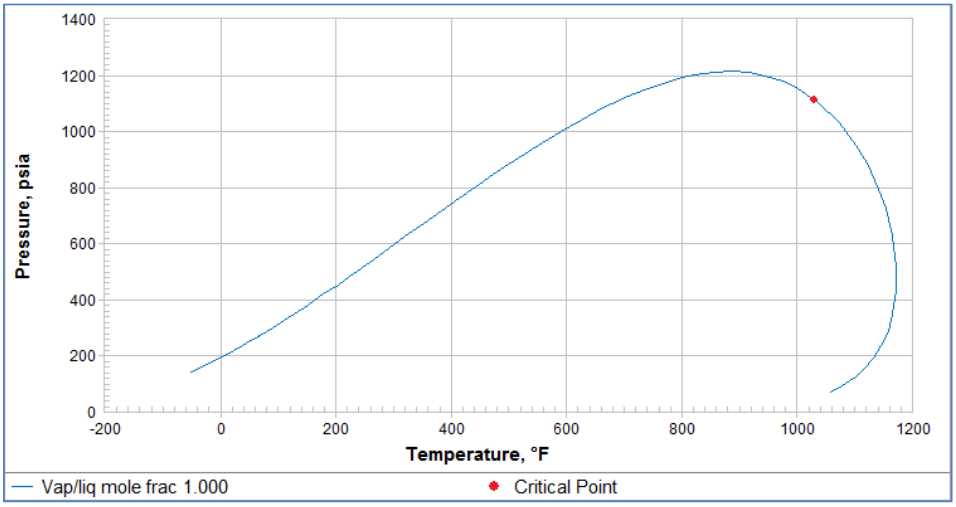

Figure 8-6: TL-AB01 (AM) Phase Envelope

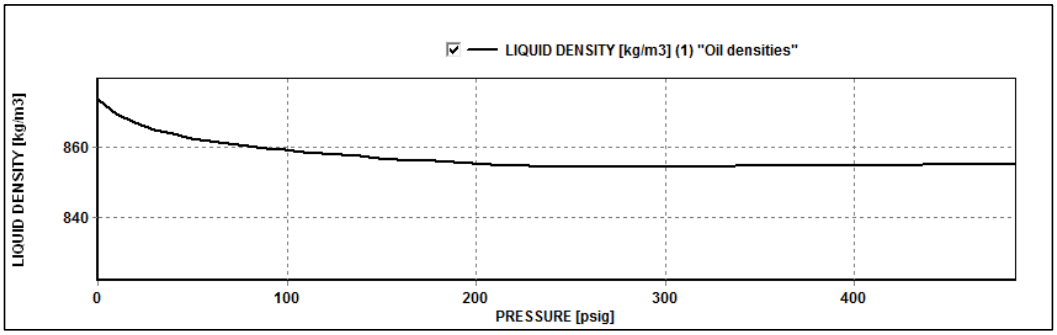

Figure 8-7: Oil Density (Kg/m3) – Temperature @ (75°F)

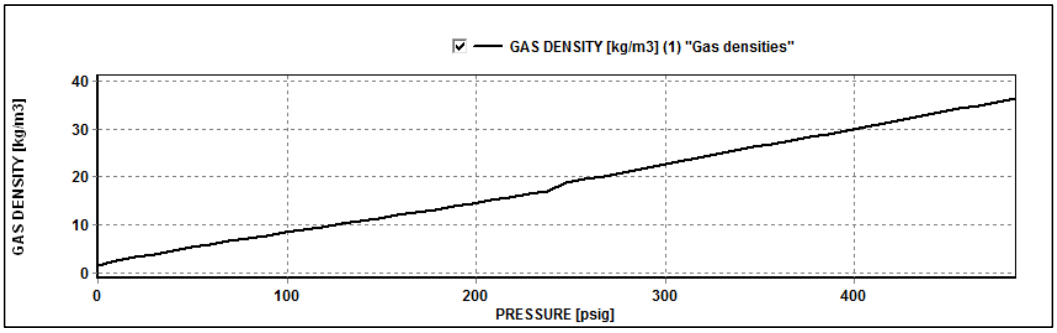

Figure 8-8: Gas Density (Kg/m3) – Temperature @ (175°F)

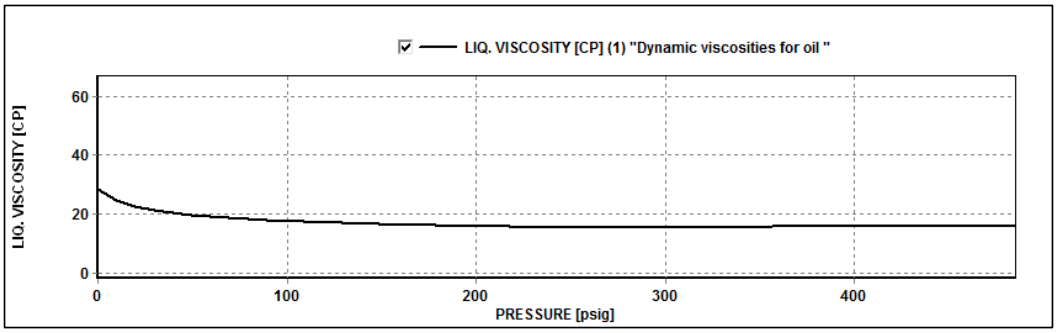

Figure 8-9: Oil Viscosity (Kg/m-h) – Temperature @ (75°F)

8.6. Gamma Calibration

The calibration of the gamma meters was carried out prior to the field measurement using a 42 inch pipeline spool. The wall thickness of this calibration spool was 22 mm compared to 25.4 mm of the measured pipeline. This provided a challenge for the field measurement team to correct for the difference in wall thickness. A detailed analysis was carried out to achieve this by correcting for the additional steel density encountered in the calibration spool.

8.7. Field-D – Holdup Field Measurements

The field measurements were carried out in Field-D on January 26-27, 2013. Measurements were carried out in three areas on the 42" Trunkline. They were all on the onshore side near the beach and upstream of the GOSP. The first location is at the beach with a steep uphill flow (Area-1) upstream of a main Valve area, and the next location is at the flat Valve area (Area-3) about 300 m from the beach. The last location is about 100 m downstream of the Valve (Area-2) with downhill flow. The schematic in Figure 8-10 displays the geometry and the measurement locations.

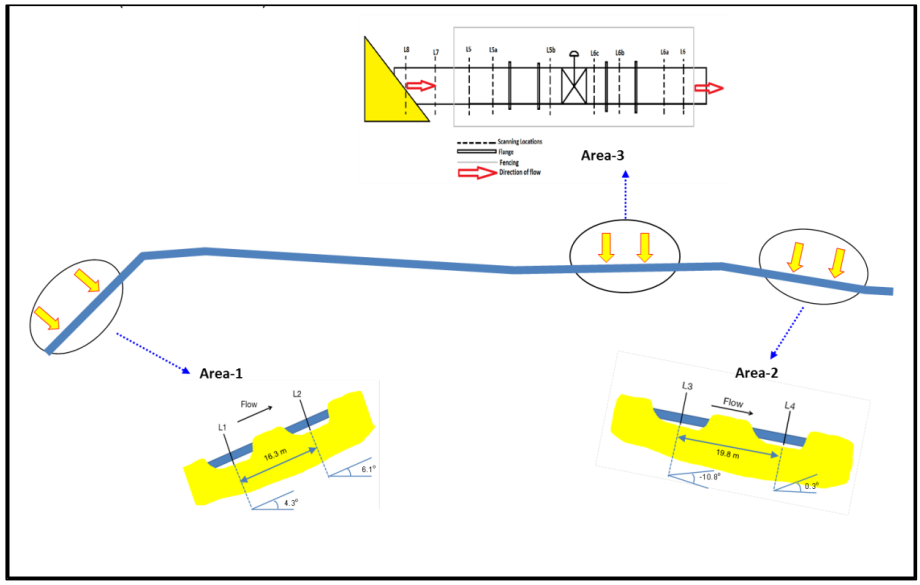

Figure 8-10: TL-AB01 Measurement Locations – Onshore Side

8.7.1. Field-D Holdup Measurements – Area-1

Holdup measurements were carried out at Area-1, in the steep uphill section of the pipeline at the beach, upstream of the main Valve area. The pipeline angle at that location ranges from (+4.3) degrees at gamma-1 to (+6.1) degrees at gamma-2.

The holdup data was calculated based on the following oil, gas and water densities and average water cut.

Table 8-1: TL-AB01 Holdup Calculation Parameters

Holdup Calculation Parameters		
Oil Density	0.8598	gr/cc
Gas Density	0.0102	gr/cc
Water Density	1.1630	gr/cc
Water-cut (%)	0.163	
Liquid Density	0.9092	gr/cc

By examination of the holdup time series at Area-1, shown in Figure 8-11, Figure 8-12 and Figure 8-13, one would notice a very high holdup, which sometimes exceeds unity, (1.0). This is mainly due to the local water holdup which normally exceeds the average water holdup in upwardly inclined pipes. Despite this uncertainty in the data, the overall flow behavior is still clear with no slugs or large roll waves.

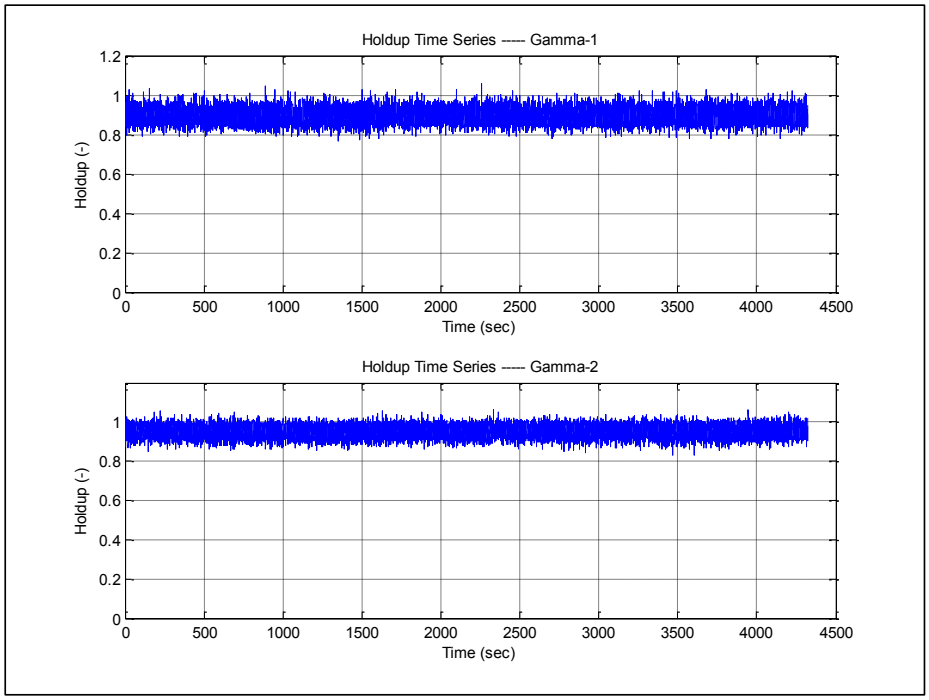

Figure 8-11: TL-AB01 Holdup Time Series with 16.3% Water Cut at Two Positions – (75 min) – Area-1

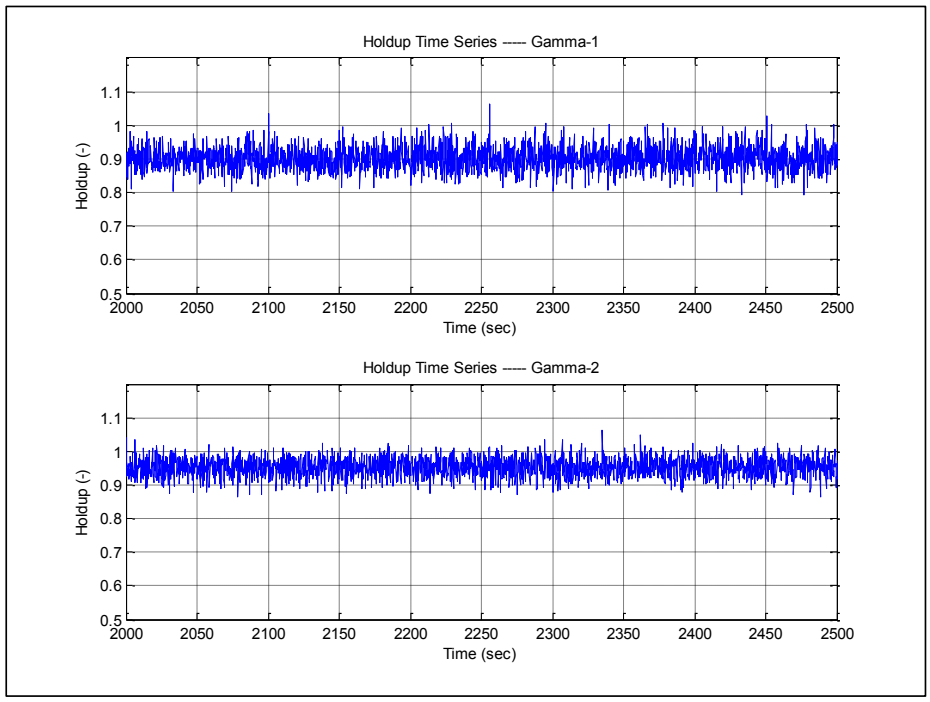

Figure 8-12: TL-AB01 Holdup Time Series with 16.3% Water Cut at Two Positions – (500 Seconds) – Area-1

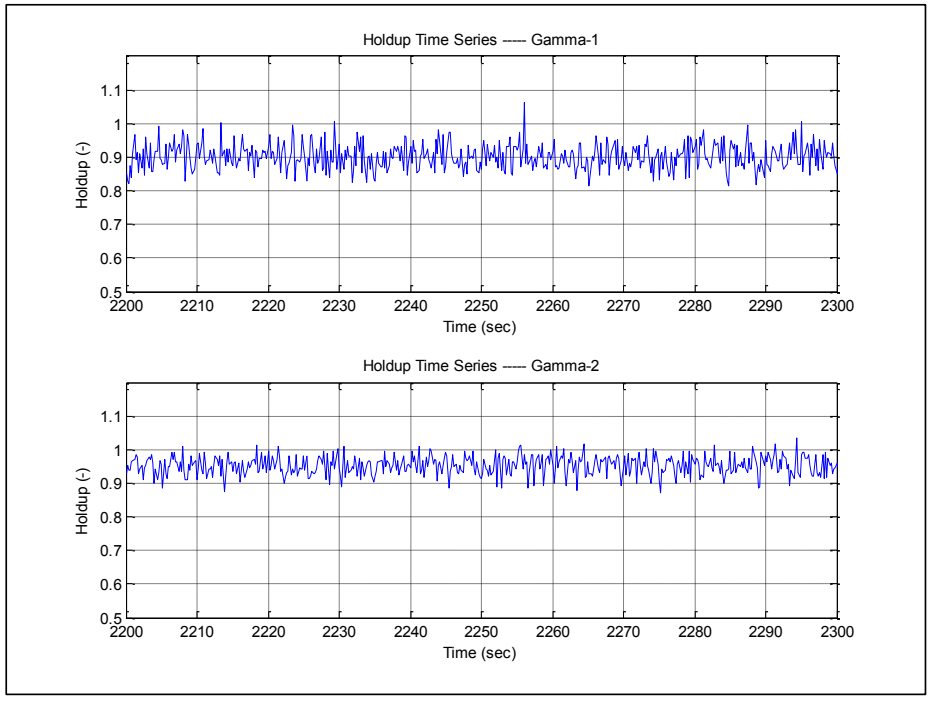

Figure 8-13: TL-AB01 Holdup Time Series with 16.3% Water Cut at Two Positions – (100 Seconds) – Area-1

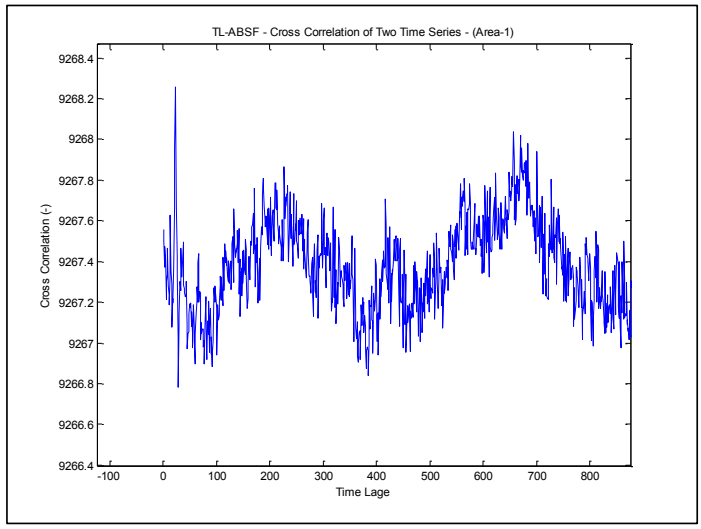

Figure 8-14: TL-AB01 Cross Correlation of Two Time Series – Area-1

Cross correlation of the two time series, results in a time shift of (4.8) seconds as shown in Figure 8-14. Using the distance between the gammas of (16.3) meter, one would obtain a velocity of 3.4 m/sec.

8.7.2. Field-D Holdup Measurements – Area-2

Holdup measurements were carried out at Area-2, in the steep downhill section downstream of the main Valve area. The pipeline angle at that location ranges from (-10.8) degrees at gamma-1 to (-10.5) degrees at gamma-2. Analyzing the holdup data, in Figure 8-15, Figure 8-16 one can notice a smooth stratified flow in the down-sloped pipe with holdup values at (0.2) at gamma-1 and (0.3) at gamma-2.

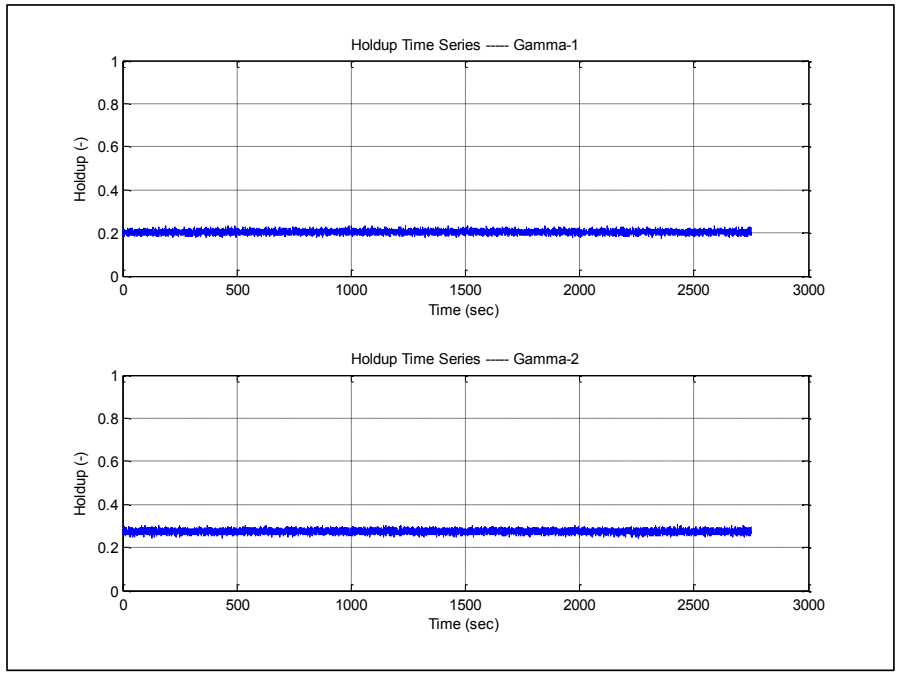

Figure 8-15: TL-AB01 Holdup Time Series with 16.3% Water Cut at Two Positions – (45 min) – Area-2

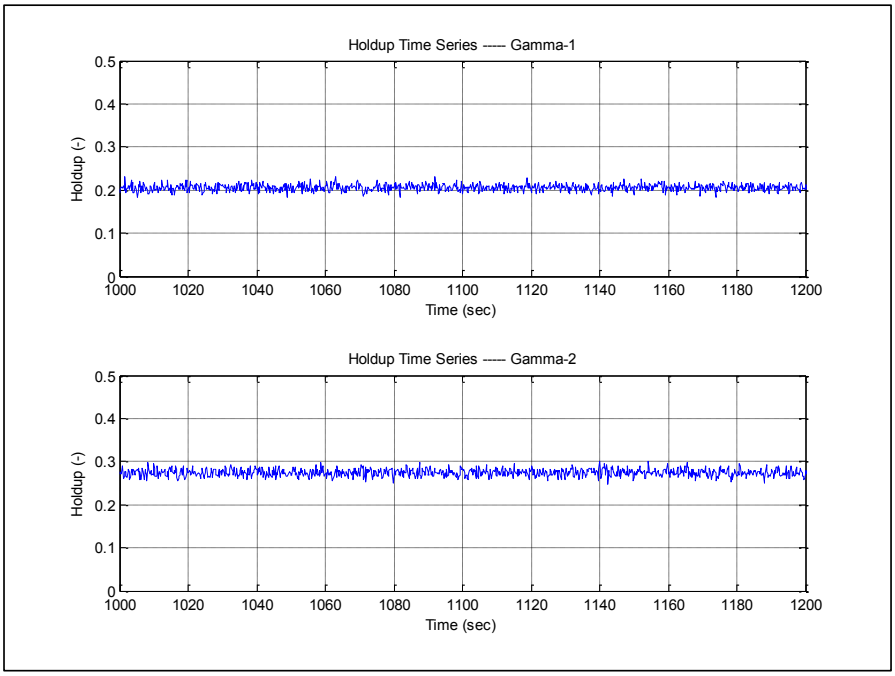

Figure 8-16: TL-AB01 Holdup Time Series with 16.3% Water Cut at Two Positions – (200 Seconds) – Area-2

8.7.3. Field-D Holdup Measurements – Area-3

Holdup measurements were carried out at Area-3, in the main valve area where the pipe extends for approximately 30 meters in a horizontal section. Analyzing the holdup data, in Figure 8-17 and Figure 8-18 one can notice a smooth stratified flow in the horizontal pipe section with holdup values at (0.6) at gamma-1 and (0.4) at gamma-2. The relatively large difference between the two holdup values is attributed to the large down-slope angle downstream of this horizontal section which pulls the liquid downward and causes the holdup to decrease quickly at gamma-2 position.

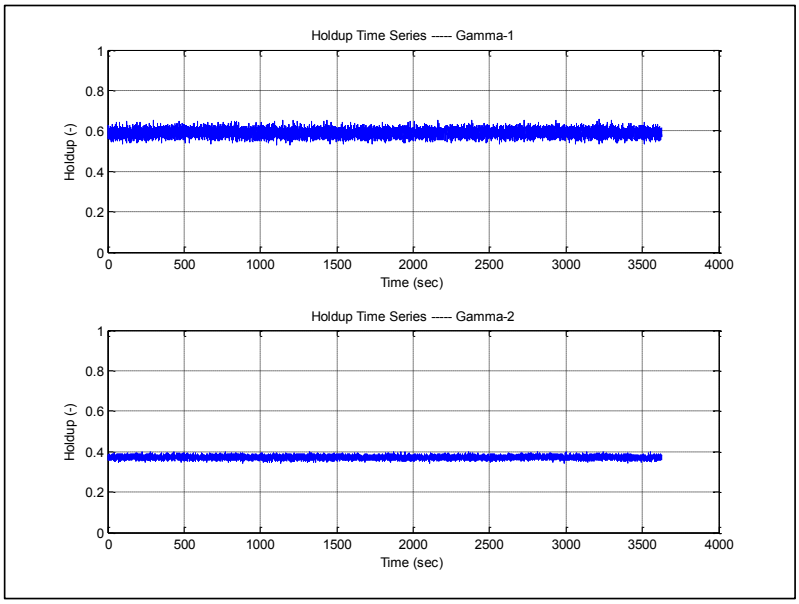

Figure 8-17: TL-AB01 Holdup Time Series with 16.3% Water Cut at Two Positions – (60 min) – Area-3

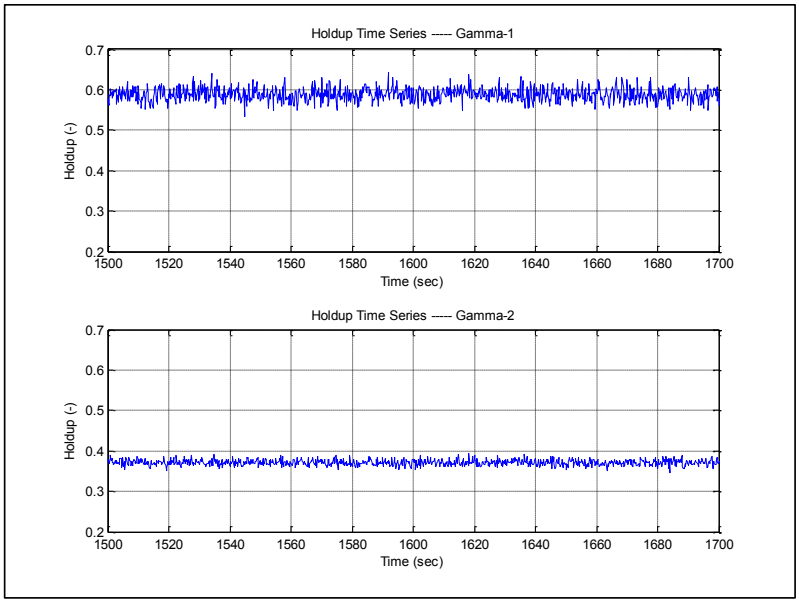

Figure 8-18: TL-AB01 Holdup Time Series with 16.3% Water Cut at Two Positions – (200 Seconds) – Area-3

8.8. TL-AB01 Pipelines OLGA Simulation

Detailed transient simulation analysis was carried out using OLGA 7.2 multiphase simulation package. The analysis was carried out using a coarse grid, with an average section length of 95 meters, and 1st order mass equation solver. The simulation was carried out with and without OLGA slug tracking option. The pressure comparison was carried out against the pressure readings at the inlet of the pipeline on the main offshore tie-in platform. On the other hand, the holdup comparisons were carried out against the holdup measurements at the (3) locations on the onshore side.

The pressure results show a very good agreement for the case without slug tracking. However, with slug tracking option enabled, and with a delay constant, DC=150, the pressure results show an over prediction of almost 40%, as shown in Figure 8-19.

The holdup results were similar as the pressure results in terms of accuracy as shown in Figure 8-20, Figure 8-21 and Figure 8-22. The slug tracking case shows large slugs with holdup reaching (1.0) at various locations. These slugs, which were not observed in field measurements, causes the over prediction of pressure at the inlet of the pipeline.

A careful examination of the fluid properties indicates that the fluid has a very low gas oil ratio (GOR = 84 scf/stb), which results in a very low gas flow rate. Thus the compressibility force in the pipeline system should be very low and very little slugs should be created in the system. This was evident in the holdup measurement carried out at the end of the pipeline, where most of the gas would have expanded from the liquid oil. At that position and despite the steep upward inclination angle, the system did not show any slugging behavior and the flow regime experienced was stratified wavy flow.

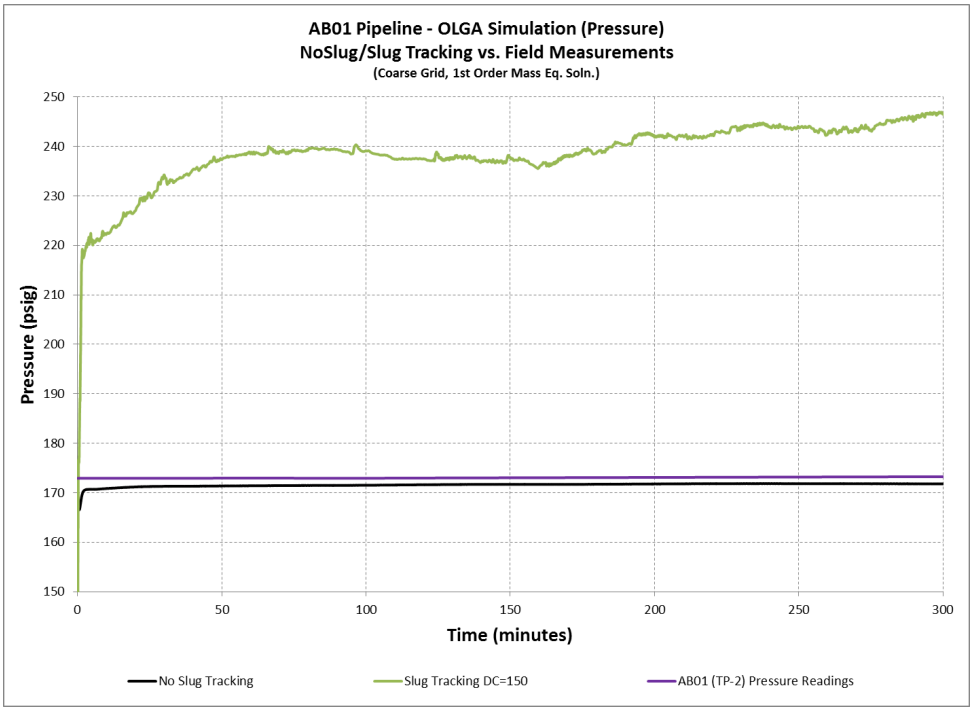

Figure 8-19: AB01 Pipeline – OLGA Simulation Results (Pressure) – (Pipe Inlet)

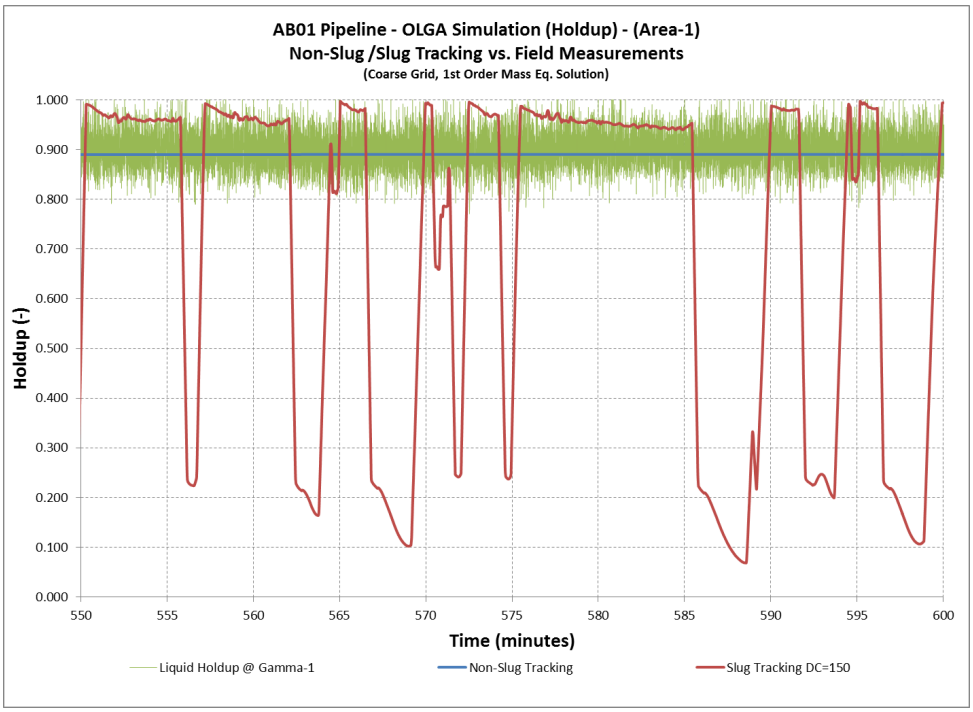

Figure 8-20: AB01 Pipeline – OLGA Simulation Results (Holdup) – (Area-1)

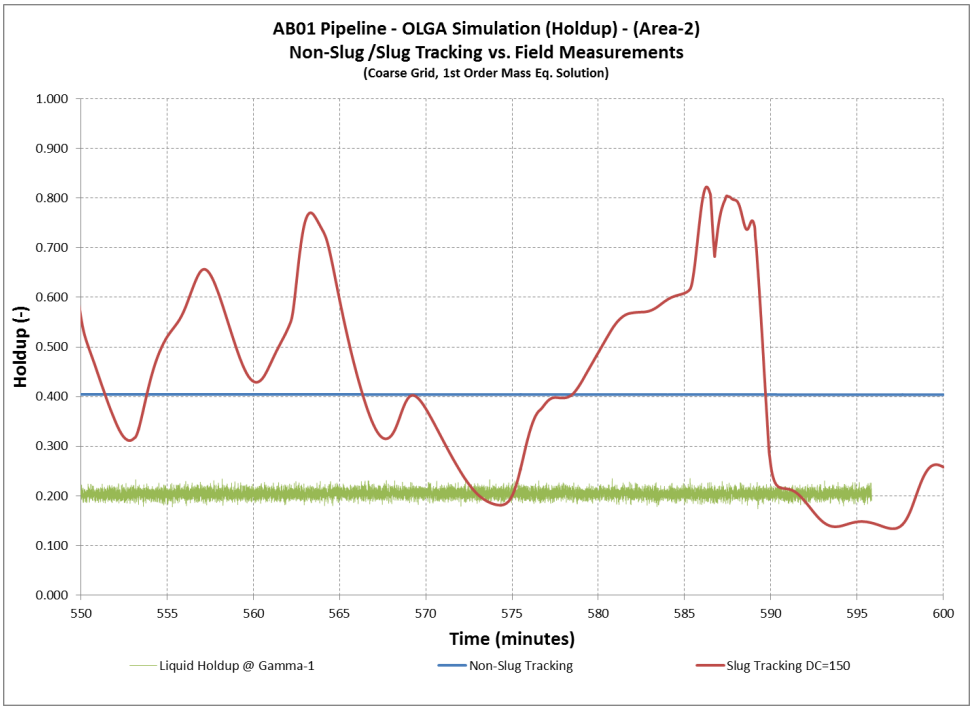

Figure 8-21: AB01 Pipeline – OLGA Simulation Results (Holdup) – (Area-2)

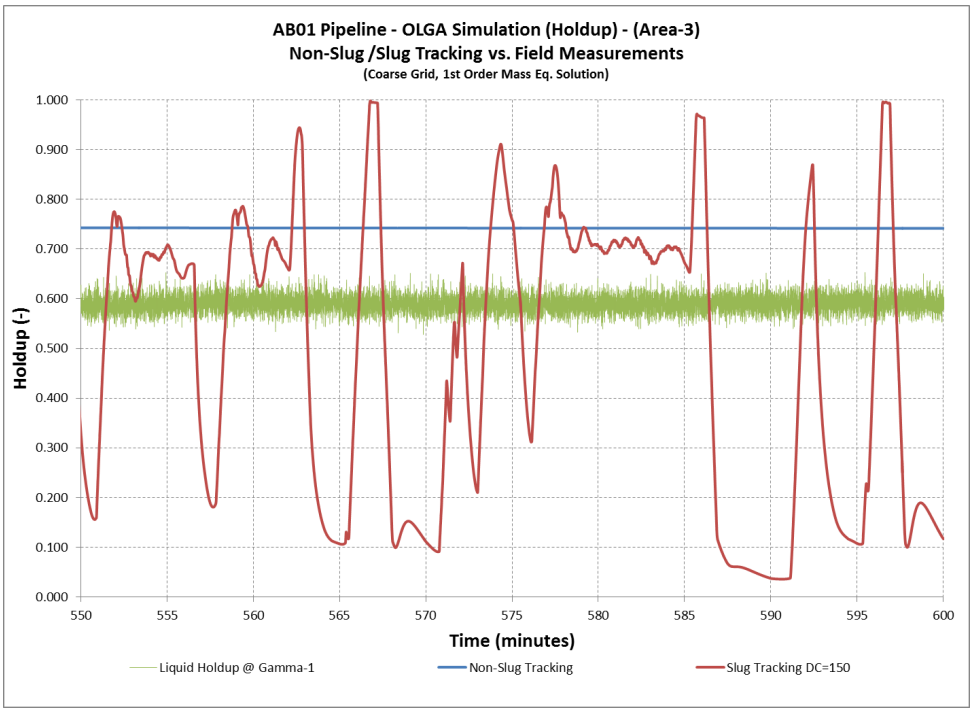

Figure 8-22: AB01 Pipeline – OLGA Simulation Results (Holdup) – (Area-3)

8.9. TL-AB01 Pipelines LedaFlow Simulation

Detailed transient simulation analysis was carried out using LedaFlow version (1.4.242.619), multiphase simulation package. The analysis was carried out using a coarse grid, with an average section length of 95 meters. The simulation was carried out with and without LedaFlow slug capturing option. The pressure comparison was carried out against the pressure readings at the inlet of the pipeline on the main offshore tie-in platform. On the other hand, the holdup comparisons were carried out against the holdup measurements at the (3) locations on the onshore side.

The pressure results show an over prediction without slug capturing and a slight under prediction with slug capturing as shown in Figure 8-23.

The holdup results shown in Figure 8-24, Figure 8-25 and Figure 8-26 indicate a good agreement at the uphill section (Area-1), while the results were over predicted for Area-2 and Area-3.

The fine grid analysis shown in Figure 8-27 indicates a reasonable improvement using the fine grid cases of (20*D) and (10*D). These results proved to be the best LedaFlow cases simulated for AB01 pipeline.

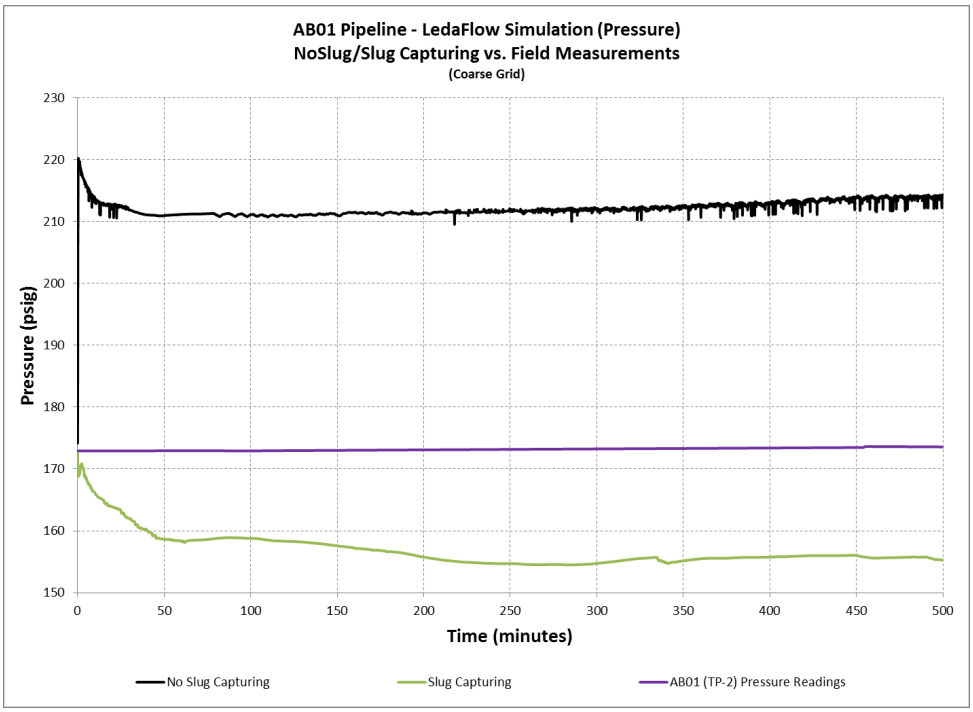

Figure 8-23: AB01 Pipeline – LedaFlow Simulation Results (Pressure) – (Pipe Inlet)

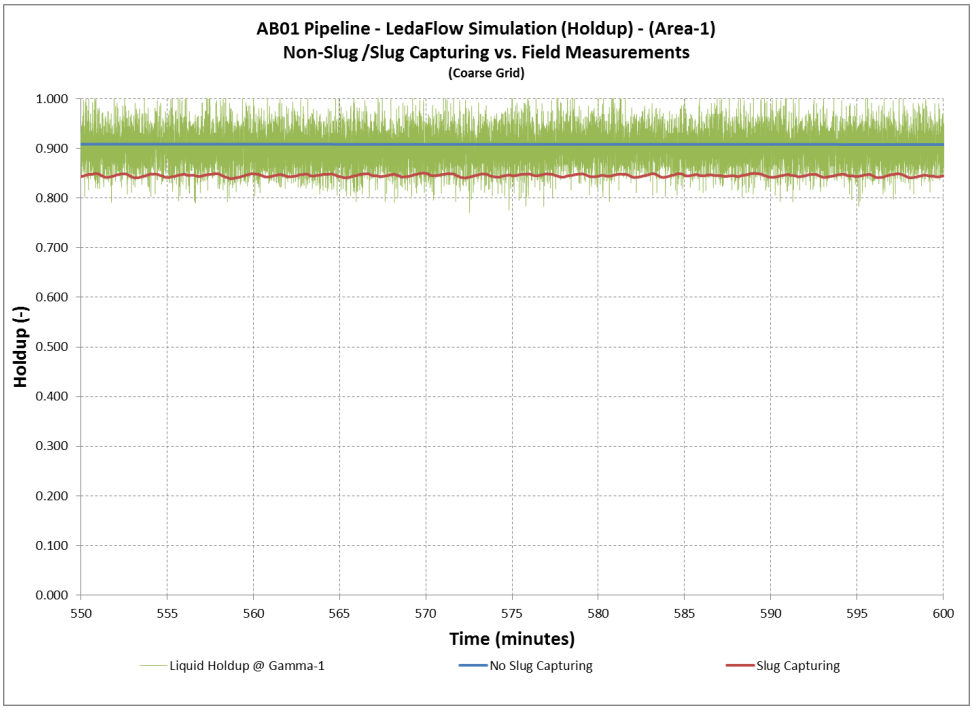

Figure 8-24: AB01 Pipeline – LedaFlow Simulation Results (Holdup) – (Area-1)

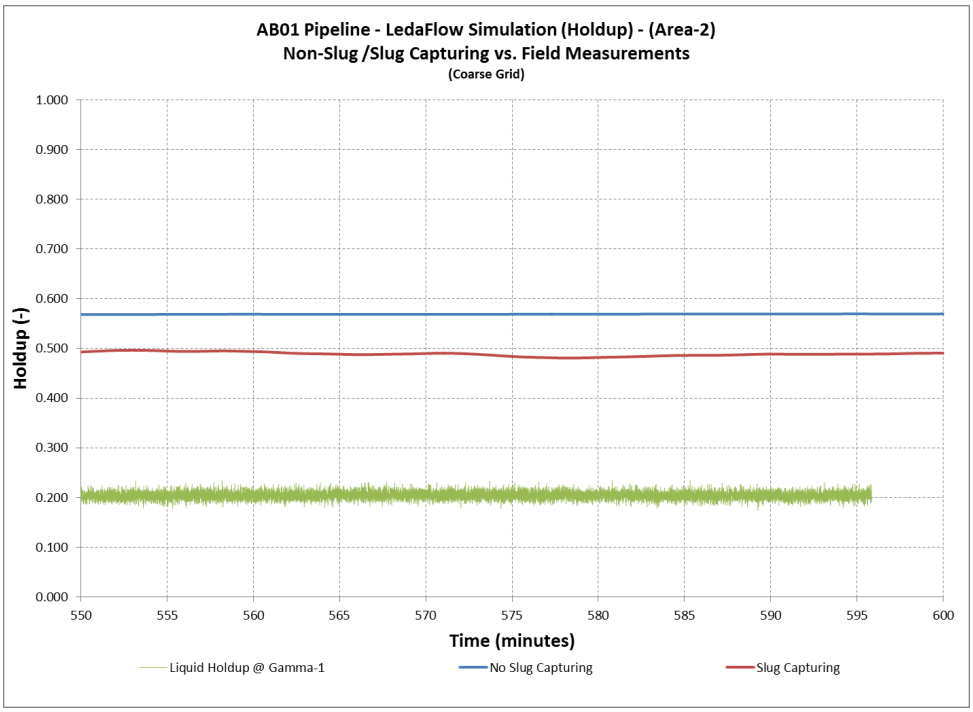

Figure 8-25: AB01 Pipeline – LedaFlow Simulation Results (Holdup) – (Area-2)

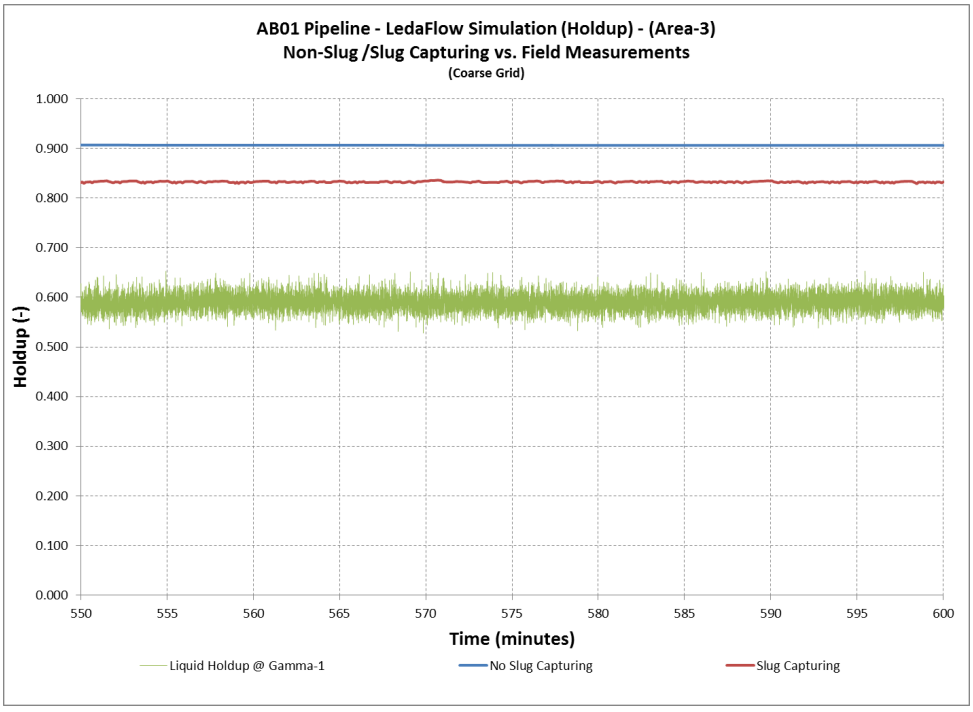

Figure 8-26: AB01 Pipeline – LedaFlow Simulation Results (Holdup) – (Area-3)

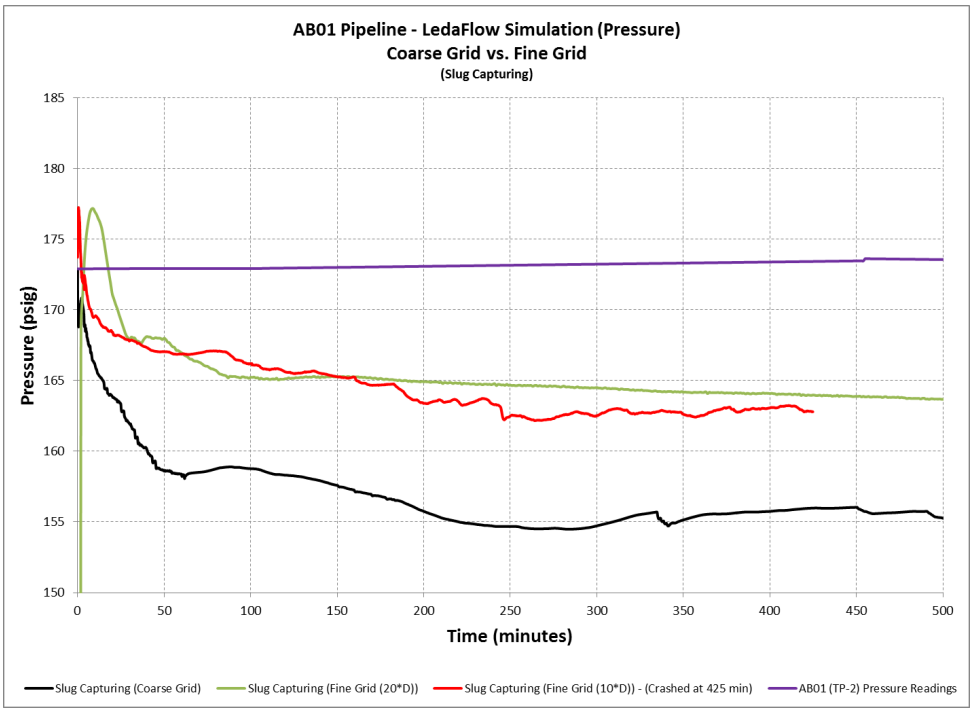

Figure 8-27: AB01 Pipeline – LedaFlow Simulation Results (Pressure) – (Pipe Inlet) – (Coarse vs. Fine Grid)

This page was intentionally left blank

9. FIELD-E – HOLDUP & PRESSURE MEASUREMENTS

Field-E holdup and pressure measurements were carried out on November 25-26, 2012. They were carried out on a 24 inch onshore pipeline, TL-12 connecting oil wells to a central processing facility where a gas oil separation is carried out. The holdup measurement was carried out using two gamma sources and detectors applied at various angles at various locations along the pipeline.

Figure 9-1: Field-D TL-12 Onshore Pipeline

The motivation behind this measurement was the pressure discrepancy experienced with OLGA predictions compared to field measurements for similar pipelines in the area which resulted in major difficulties for meeting the production targets for this oil and gas field. The OLGA pressure predictions were over 50% below the field observations.

9.1. Field-E Description

At Field-E, the oil is collected from various onshore wells into a main trunkline which connects it to the central processing facilities. The central processing facilities handle the production coming from various trunklines coming from different parts of the oil and gas field. The field oil wells were driven by electrical submersible pumps (ESP).

9.2. Flow Rates

The flow rates data were obtained from two sources. The first source is wells individual production rate collected from the online multiphase flow meters (MPFM). The second source of flow rate information is the ESP's production curves which provides the flow rate based on the intake pressure. This data was averaged over the whole month of production based on the number of days each ESP was operating. Comparing the two sets of data the MPFM data indicates a total liquid rate of 104,000 BBL/Day, while the ESP data suggests a total liquid rate of 109,000 BBL/Day.

After several discussions with operations, the decision was made to assume an average flow rate of 105,000 BBL/Day based on specific preferences of MPFM data over ESP data in certain oil wells and vice versa. As a result, the oil flow rate was approximately 90,000 BBL/Day with an average water cut of 14.3%. A total of (17) oil wells were connected to the pipeline all the way from first kilometer to kilometer (43). Each well was simulated individually along with the associated flow rate as shown in Table 9-1.

The superficial gas and liquid velocities ranges from 0.15 m/sec and 0.14 m/sec at the beginning of the pipeline to 10 m/sec and 0.75 m/sec at the end of the pipeline, respectively

Table 9-1: TL-12 Individual Well Flow Rates

Well number:	**Oil Flow Rate**	**Water Flow Rate**	**Water Cut**	**Well Tie-in Location from Remote Header (R.H.)**
	(BBL/D)	(BBL/D)	(%)	(km)
WELL-572	4750	900	15.9	0.00
WELL-573	7020	1440	17.0	0.00
WELL-571 (Press. Rec.)*	4650	760	14.0	11.32
WELL-591	5300	860	14.0	15.16
WELL-516	6870	850	11.0	19.63
WELL-542	5330	1020	16.1	20.42
WELL-545	6790	1010	12.9	20.42
WELL-522	6880	940	12.0	21.14
WELL-514	6570	980	13.0	22.64
WELL-513	4650	630	11.9	23.56
WELL-444	2680	330	11.0	31.26
WELL-028	4810	720	13.0	34.78
WELL-404	5000	1020	16.9	36.74
WELL-318 (Press. Rec.)*	5760	940	14.0	37.92
WELL-332	4260	870	17.0	39.63
WELL-399 (Press. Rec.)*	3360	690	17.0	41.98
WELL-233	5280	1080	17.0	43.37
Total	**105,000**		**14.3%**	55.09

*Press. Rec.: Pressure measurements were obtained at these locations using online pressure recorder

9.3. Pipeline Details

TL-12 pipeline has an outside diameter of 24 inch with a wall thickness of 12.7 mm. The pipeline extends for approximately 55 Km from the remote header all the way to the GOSP facilities. The terrain can be described as being highly undulating as shown in Figure 9-2. The two areas where the holdup field measurements were carried out were as shown in the figure with the first one being close to the remote header while the last one being close to the GOSP facilities.

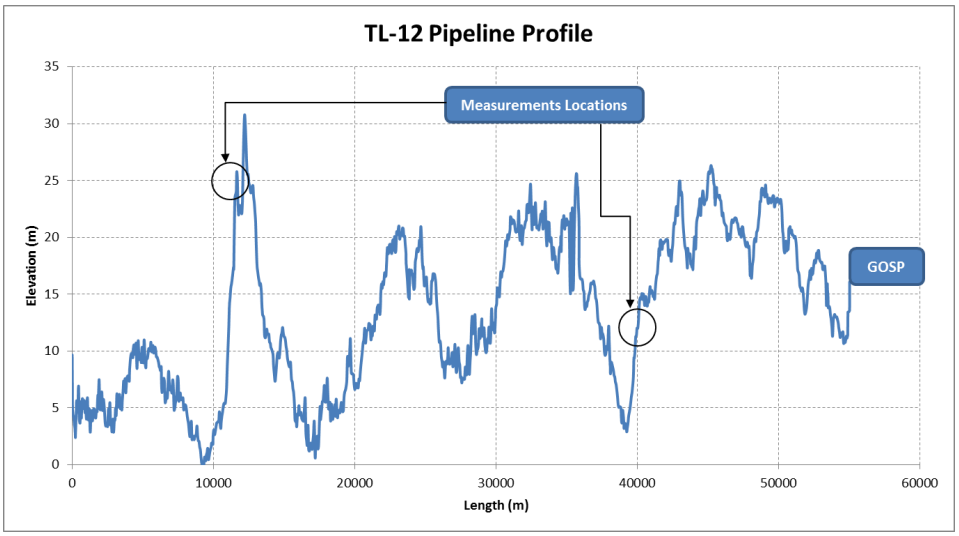

Figure 9-2: TL-12 Pipeline Profile

9.4. Inlet and Outlet Pressure

The GOSP separator pressure was set at 50 psig. In addition during the holdup measurement period, the pressure at three points along the pipeline was recorded using a pressure logging device. These locations were at Well-571 at (11.32) Km, Well-318 at (37.92) km and Well-399 at (41.98) Km from the pipeline inlet. The pressure logs for these measurements are shown in Figure 9-3, Figure 9-4, Figure 9-5, Figure 9-6 and Figure 9-7. Zooming into the pressure recording of Well-399, one could observe a small hydrodynamic cycle with a frequency of (20 to 30) seconds with a (2) psi amplitude, as shown in Figure 9-7. We could also notice a macro scale cyclic behavior in Figure 9-3, which repeats itself every (80 to 100) minutes with an amplitude of (2) psi. The pressure log of Well-318, shown in Figure 9-5 also indicates two scales of hydrodynamic slugs with a large scale that repeats every (5) minutes with an amplitude of (5) psi and a smaller scale fluctuations that repeats every (30) seconds with an amplitude of (2) psi.

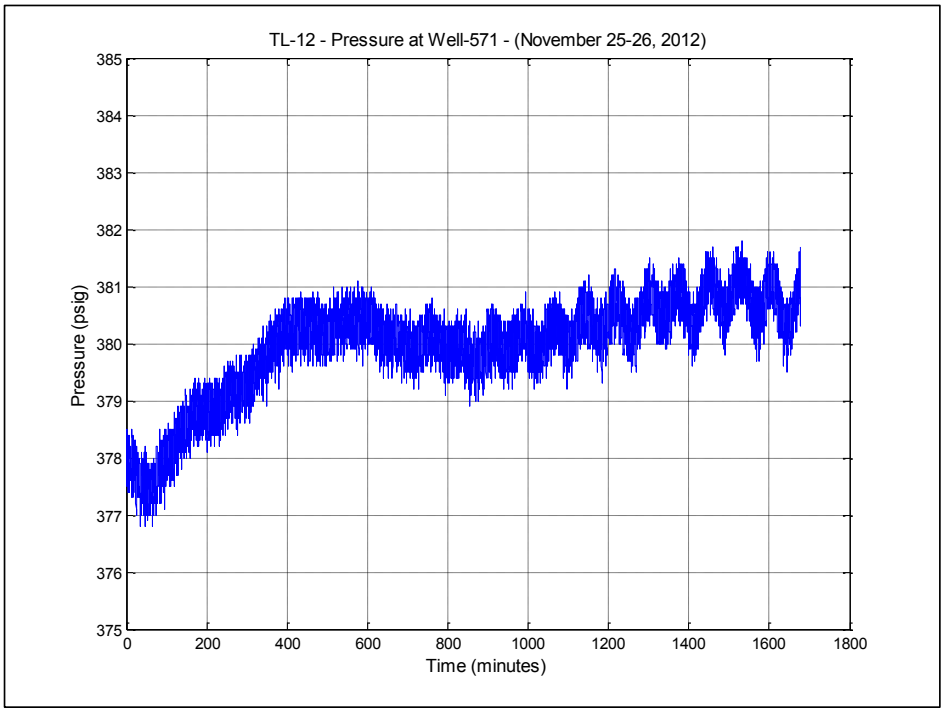

Figure 9-3: Pressure Log at Well-571 – (11.32 Km from Pipe Inlet) – (November 25-26, 2012)

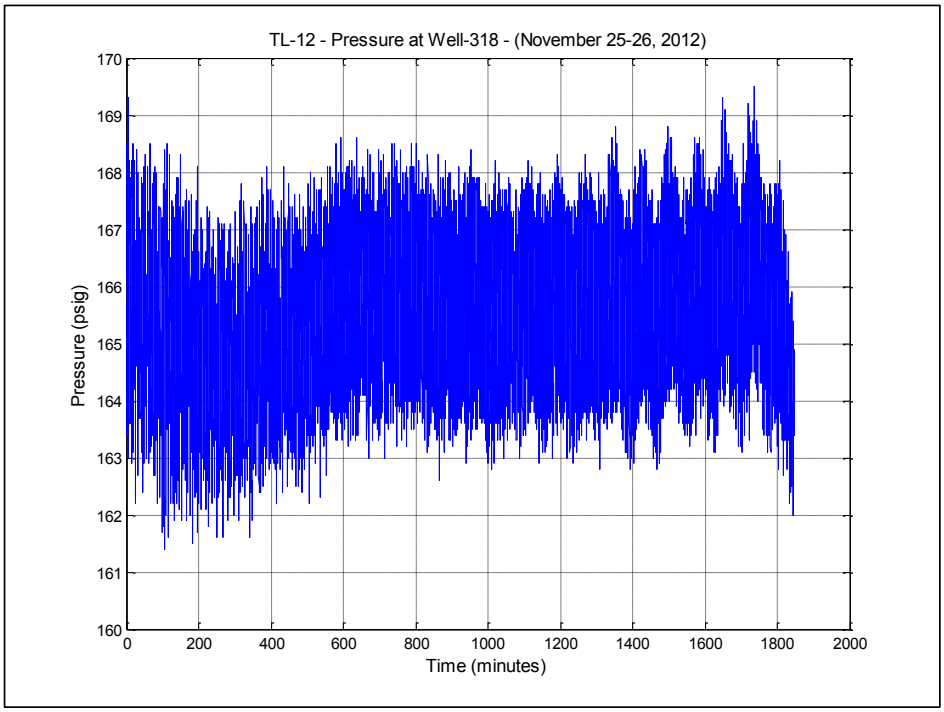

Figure 9-4: Pressure Log at Well-318 – (37.92 Km from Pipe Inlet) – (November 25-26, 2012)

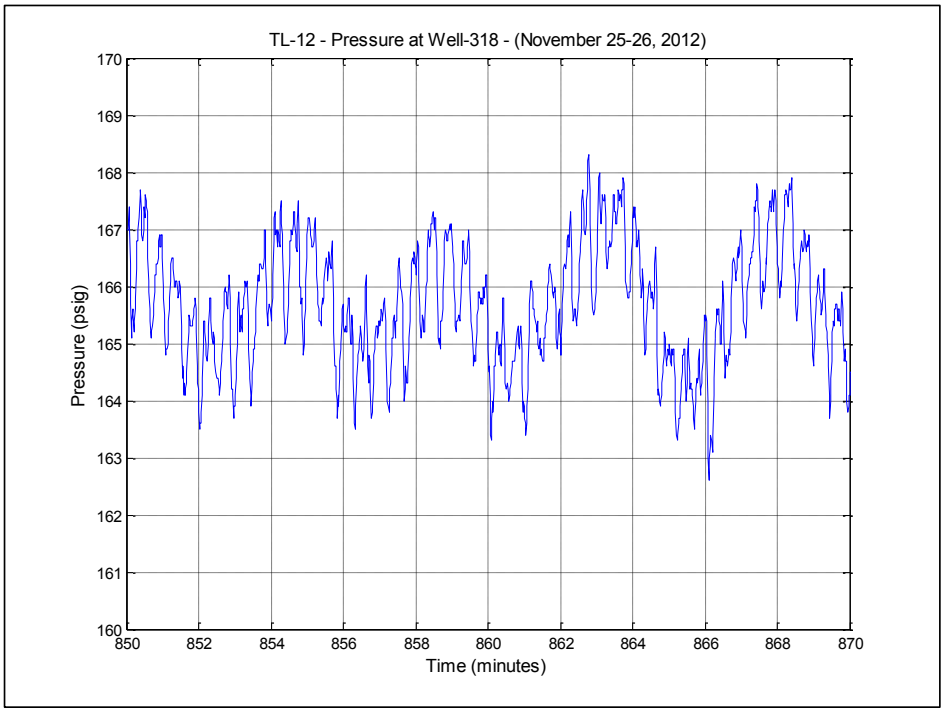

Figure 9-5: Pressure Log at Well-318 – (37.92 Km from Pipe Inlet) – (November 25-26, 2012) – (20 minutes)

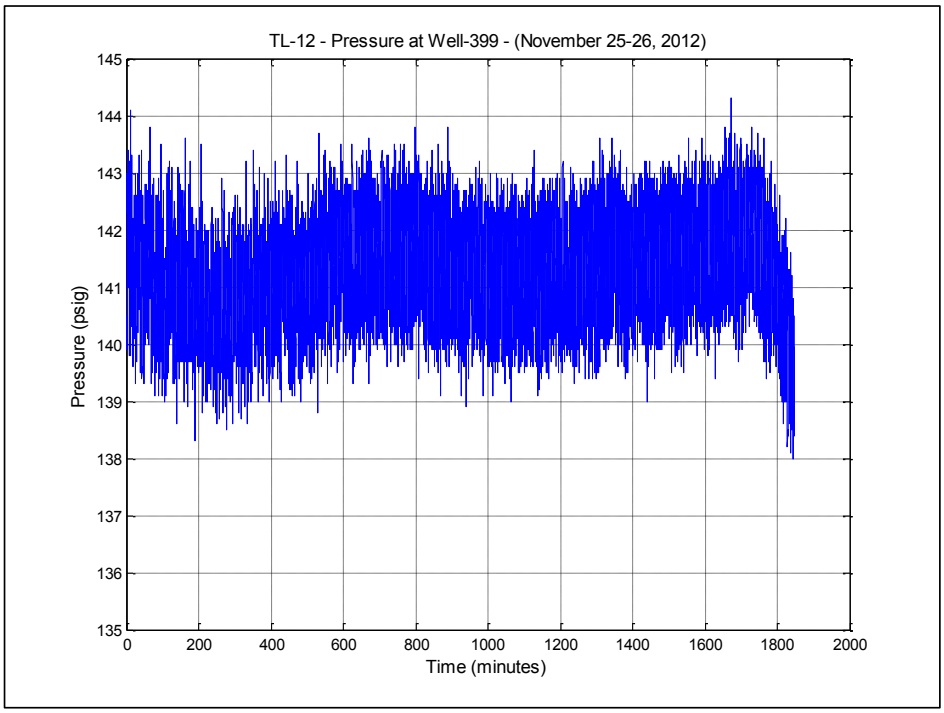

Figure 9-6: Pressure Log at Well-399 – (41.98 Km from Pipe Inlet) – (November 25-26, 2012)

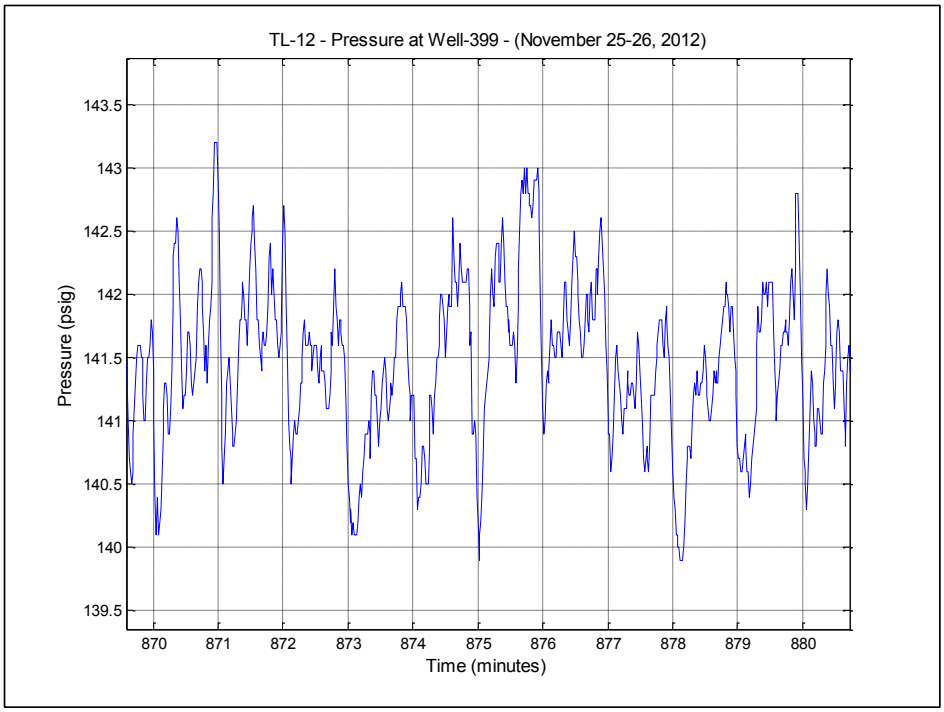

Figure 9-7: Pressure Log at Well-399 – (41.98 Km from Pipe Inlet) – (November 25-26, 2012) – (10 minutes)

9.5. Field-D Fluid Properties

Field-D contains crude oil that can be characterized as Arab Light (AL). The gas-oil ratio of the fluid is 341 scf/stb and the API at 60°F 32.4. The phase envelope of TL-12 (AL) is shown in Figure 9-8, which indicates that the pipeline system is clearly in the two phase region. The gas and liquid densities variations with pressure for TL-12 (AL) are shown in Figure 9-9 and Figure 9-10. These figures were plotted for the (AL) fluid using OLGA at a temperature of 100°F. The oil viscosity was also plot at the same temperature which shows the variation with pressure from 0 to 700 psig as shown in Figure 9-11.

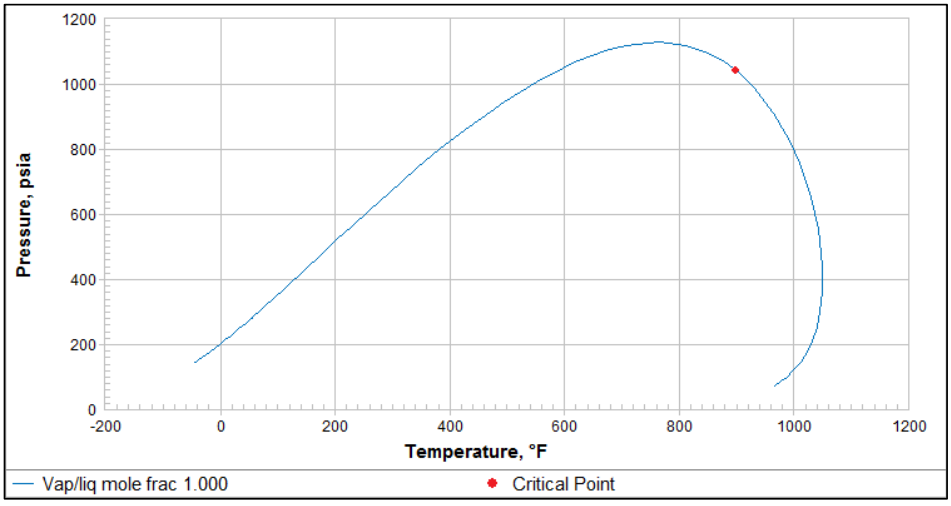

Figure 9-8: TL-12 (AL) Phase Envelope

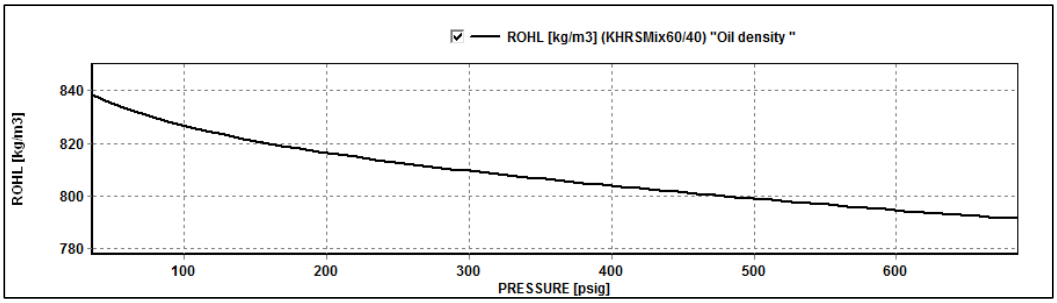

Figure 9-9: Oil Density (Kg/m3) – Temperature @ (100°F)

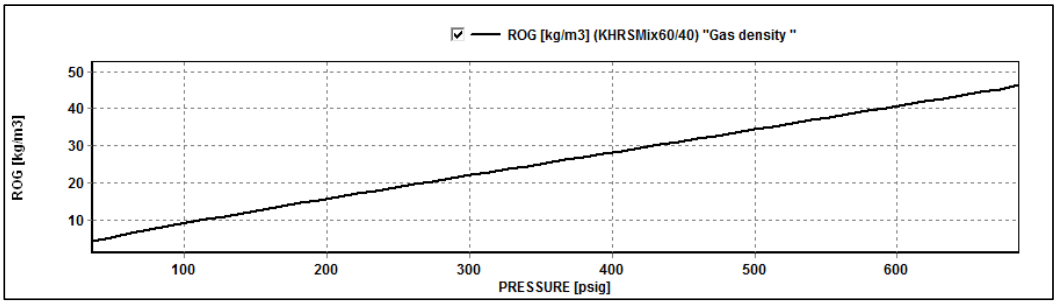

Figure 9-10: Gas Density (Kg/m3) – Temperature @ (100°F)

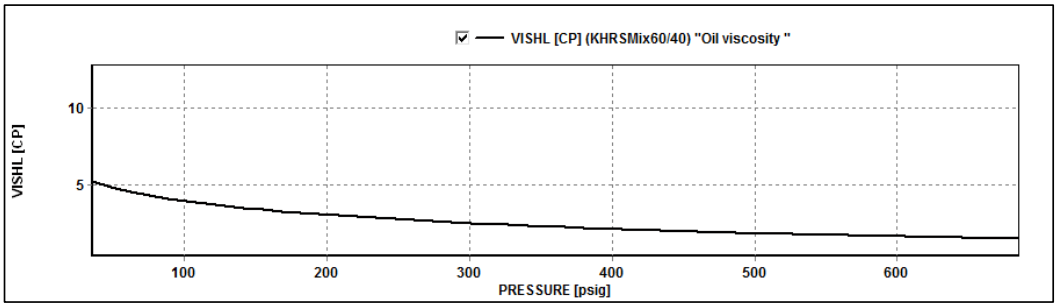

Figure 9-11: Oil Viscosity (Kg/m-h) – Temperature @ (100°F)

9.6. Gamma Calibration

The calibration of the gamma meters was carried out prior to the field measurement using a 24 inch pipeline spool. The wall thickness of this calibration spool was 15 mm compared to 12.7 mm of the measured pipeline. This provided a challenge for the field measurement team to correct for the difference in wall thickness. A detailed analysis was carried out to achieve this by correcting for the additional steel density encountered in the calibration spool.

9.7. Field-E – Holdup Field Measurements

The field measurements were carried out in Field-E on November 25-26, 2012. Measurements were carried out in two areas on the 24 inch Trunkline. The first area was close to the remote header location, Area-1, while the other one was closer to the GOSP facilities, Area-2, as shown in Figure 9-12.

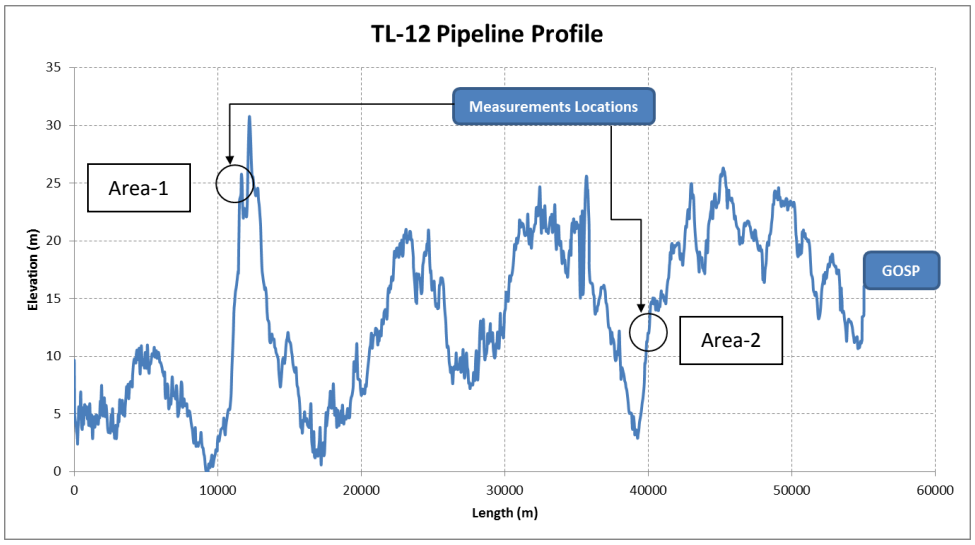

Figure 9-12: TL-12 Measurement Locations

9.7.1. Field-E Holdup Measurements – Area-1

Holdup measurements were carried out at Area-1, in the steep uphill section of the pipeline as shown in Figure 9-12. The pipeline angle at that location ranges from (+4.04) degrees at gamma-1 to (+4.95) degrees at gamma-2. Additional gamma measurement was conducted at location-3 with downward negative angle (-2.62) as shown in Figure **9-13**. The holdup data was calculated based on the oil, gas and water densities and average water cut shown in Table 9-2.

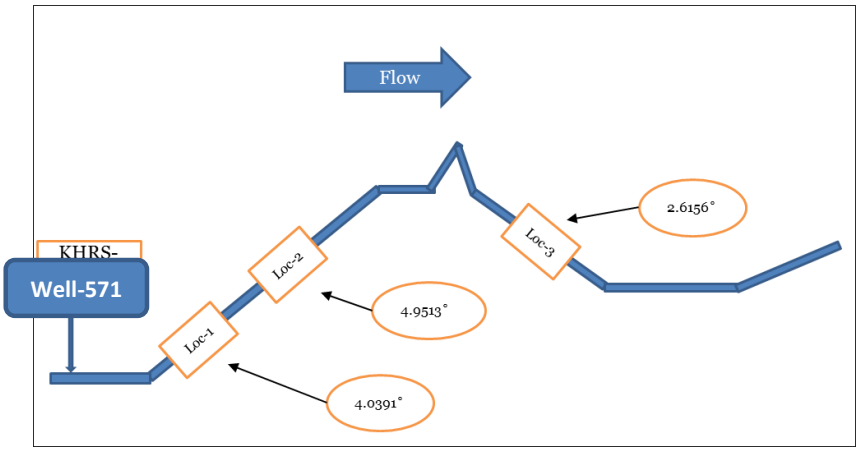

Figure 9-13: TL-12 Area-1 Gamma Locations and Angles

Table 9-2: TL-12 Holdup Calculation Parameters

Holdup Calculation Parameters		
Oil Density	0.7992	gr/cc
Gas Density	0.0272	gr/cc
Water Density	1.0430	gr/cc
Water-cut (%)	0.14	
Liquid Density	0.8333	gr/cc

The uphill holdup data shown in Figure 9-14, Figure 9-15 and Figure 9-16, indicate holdup that exceeds 1.0. This indicate a local water cut which is higher than the average water cut used to calculate the holdup values from the measured mixture density. This was expected as the flow rate in Area-1 is very low, 19,500 BBL/Day, compared to total liquid flow rate in pipeline, 105,000 BBL/Day. This was due to the fact that only three wells were connected to TL-12 main trunkline upstream of this point.

The combination of this low flow rate and the presence of water in the crude oil resulted in water settling at the low points of the pipeline, which causes the unreasonable holdup value of more than (1.0) that we observe in the holdup figures. These holdup measurement figures were calculated based on the average water cut estimated for the whole pipeline with all oil wells being connected to it.

The downhill holdup data shown in Figure 9-17, indicates very low holdup at 0.13 as expected in a downhill position accompanied with a very low flow rate.

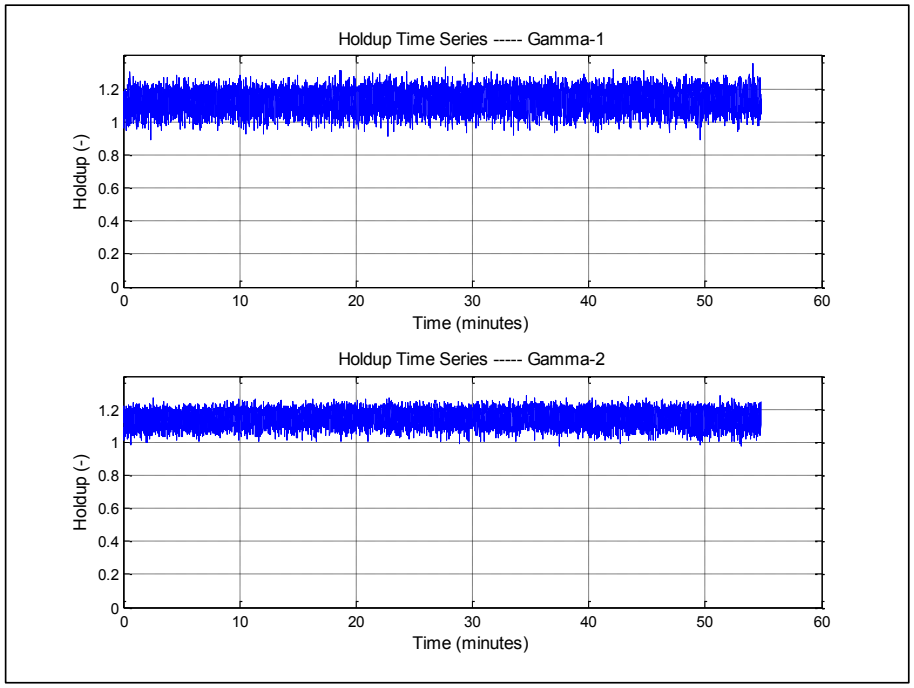

Figure 9-14: TL-12 Holdup Time Series with 14.3% Water Cut at Two Positions – (55 min) – Area-1 (Uphill)

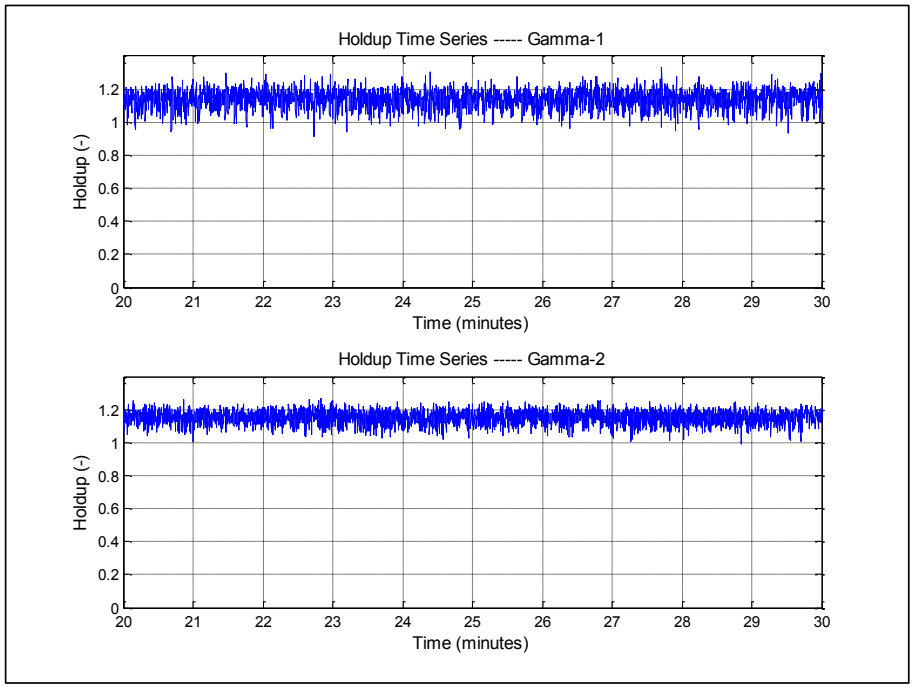

Figure 9-15: TL-12 Holdup Time Series with 14.3% Water Cut at Two Positions – (10 min) – Area-1 (Uphill)

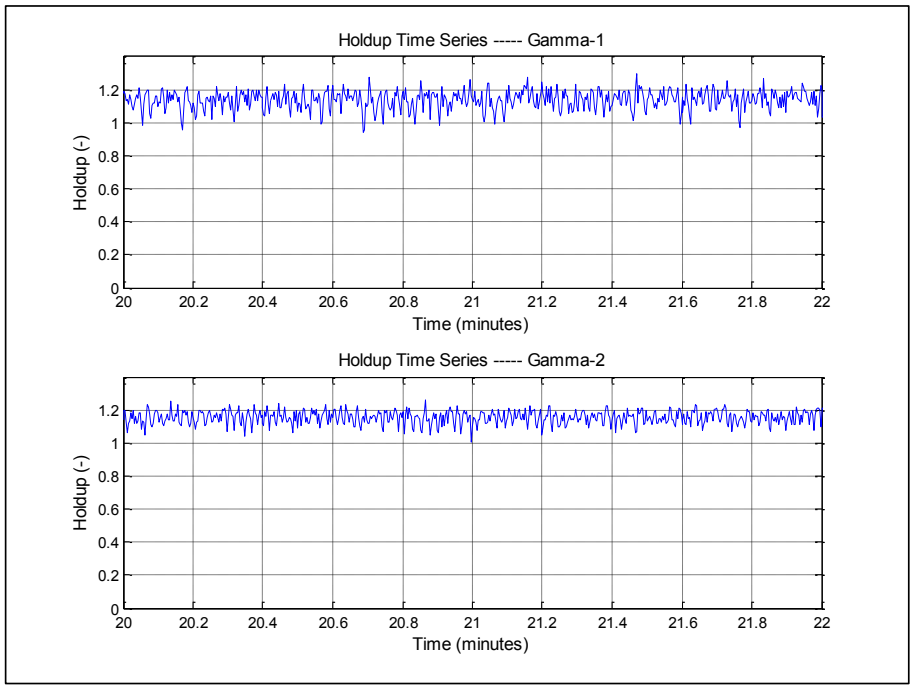

Figure 9-16: TL-12 Holdup Time Series with 14.3% Water Cut at Two Positions – (2 min) – Area-1 (Uphill)

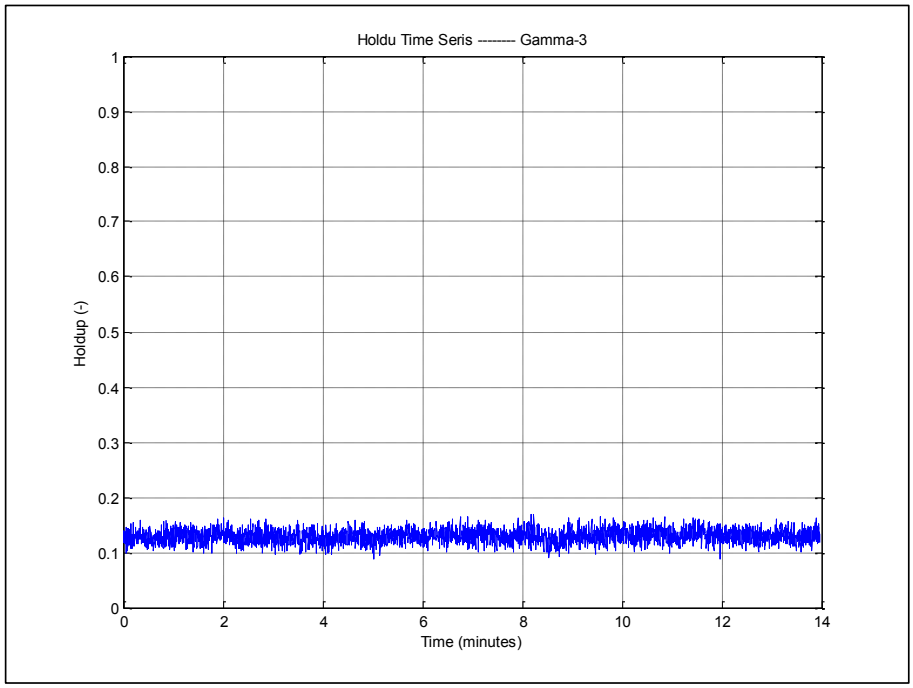

Figure 9-17: TL-12 Holdup Time Series with 14.3% Water Cut at Two Positions – (14 min) – Area-1 (Downhill)

9.7.2. Field-E Holdup Measurements – Area-2

Holdup measurements were carried out at Area-2, in the steep uphill section of the pipeline as shown in Figure 9-12. The pipeline angle at that location ranges from (+1.48) degrees at gamma-1 to (+0.79) degrees at gamma-2, as shown in Figure 9-18.

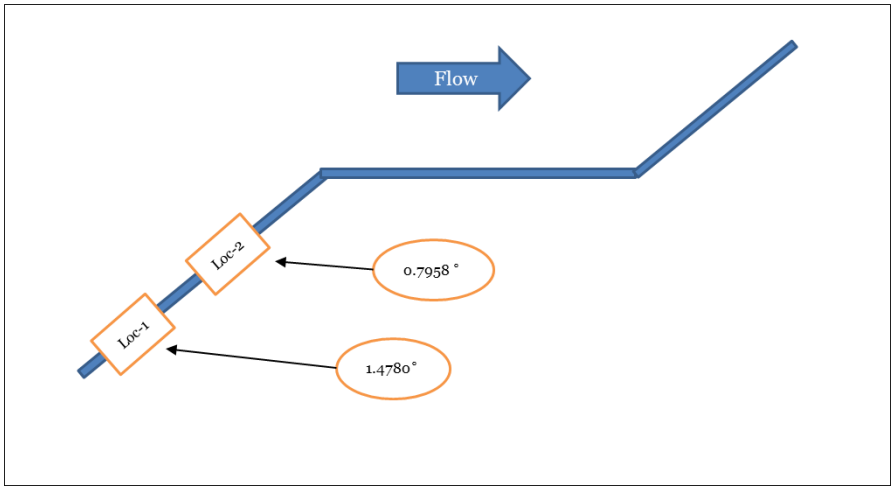

Figure 9-18: TL-12 Area-2 Gamma Locations and Angles

The holdup data measurement at locations (1) and (2) is shown in Figure 9-19, Figure 9-20, Figure 9-21 and Figure 9-22. The data indicates two scales of slugging behavior. The first one is a macro scale where a

group of small slugs gather together in (2) minutes clusters, followed by a group of slightly larger slugs in a (4) minutes cluster.

The small slugs cluster have a very high frequency of (5) seconds between slugs. They have a higher liquid film of approximately (0.5) and this cycle repeats itself every (4) minutes. The slightly larger slugs have a lower frequency of (10) seconds between slugs and a higher liquid film of approximately (0.3). The slug peaks were consistent for both types of slugs at a holdup of approximately (0.82).

The cross correlation of the two time series, shown in Figure 9-23, resulted in a time shift of (9) seconds and using the distance between the two gammas of (32.15) meters, one can obtain a velocity of (3.57) m/sec.

Conducting a detailed statistical analysis of approximately (480) slugs during the (80) minutes period shows a slugging frequency which ranges mostly between (5) and (20) seconds as shown in Figure 9-24. Also, a simple calculation of the frequency using the total number of slugs recorded in (80) minutes period, shows a frequency of (10) seconds between slugs which is in agreement with slug frequency statistical analysis.

Slug statistical analysis also calculates the slug front and tail velocities in addition to the slug lengths as shown in Figure 9-25, Figure 9-26, Figure 9-27, Figure 9-28, Figure 9-29 and Figure 9-30. The average front velocity was calculated at 3.94 m/sec while the average tail velocity was calculated at 3.87 m/sec. This indicates a growing slug behavior as the front velocity scoops more liquid from the liquid film into the slug body. The average slug length was about (15) meters which is equivalent to approximately (25*Dia.).

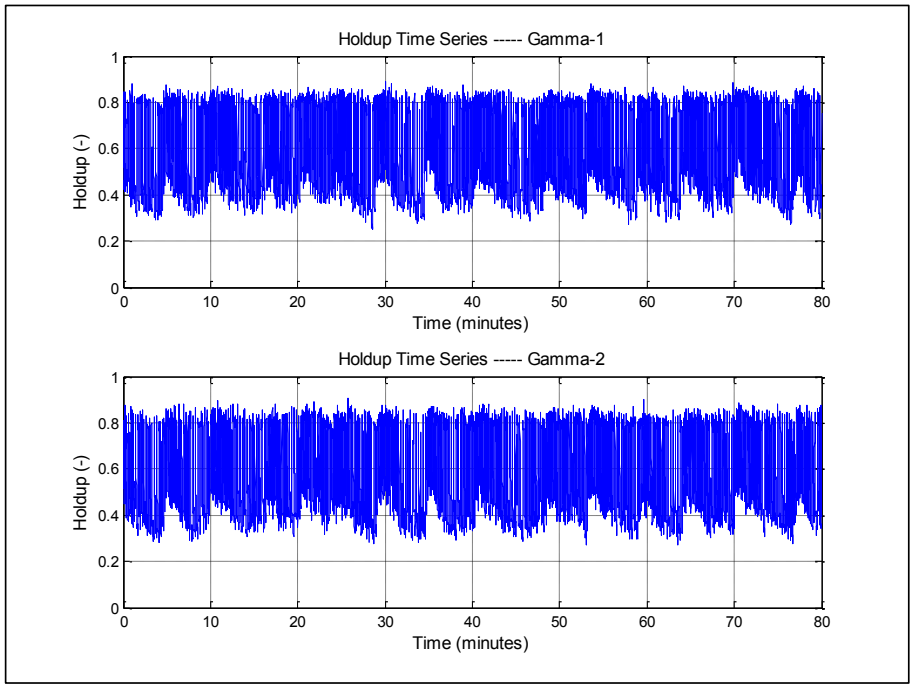

Figure 9-19: TL-12 Holdup Time Series with 14.3% Water Cut at Two Positions – (80 min) – Area-2

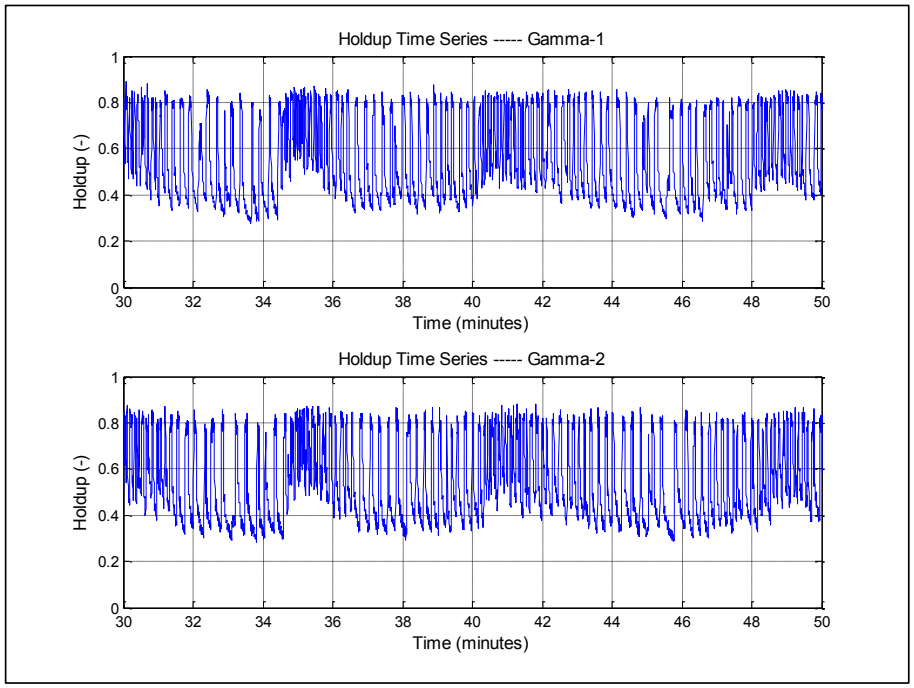

Figure 9-20: TL-12 Holdup Time Series with 14.3% Water Cut at Two Positions – (20 min) – Area-2

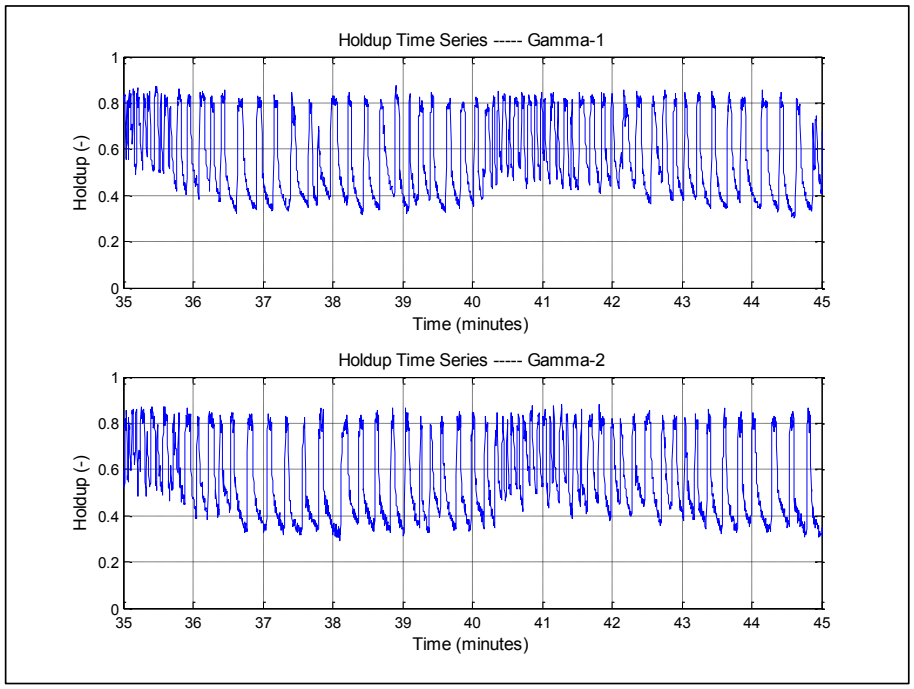

Figure 9-21: TL-12 Holdup Time Series with 14.3% Water Cut at Two Positions – (10 min) – Area-2

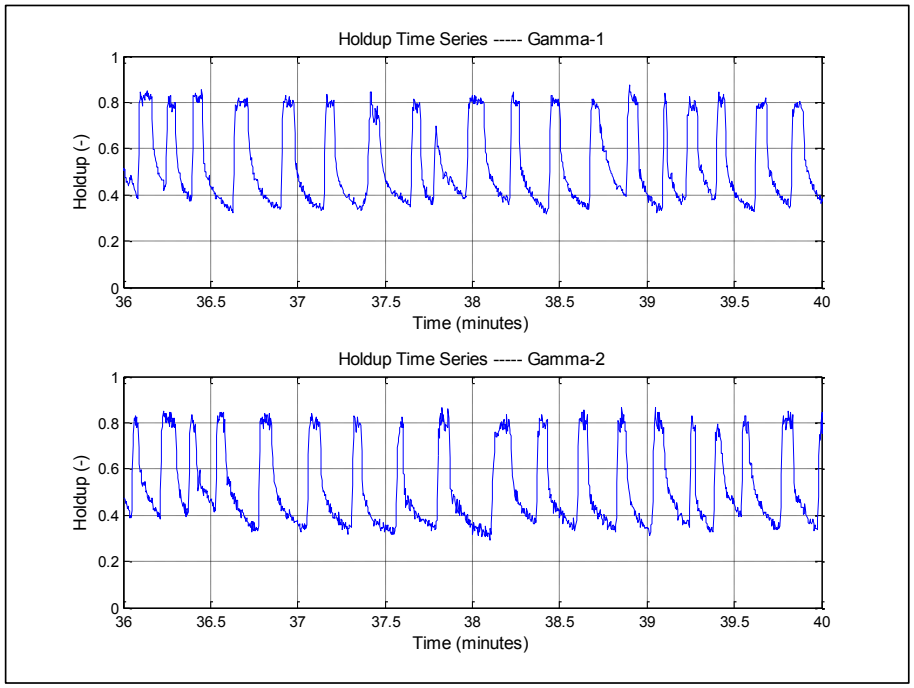

Figure 9-22: TL-12 Holdup Time Series with 14.3% Water Cut at Two Positions – (4 min) – Area-2

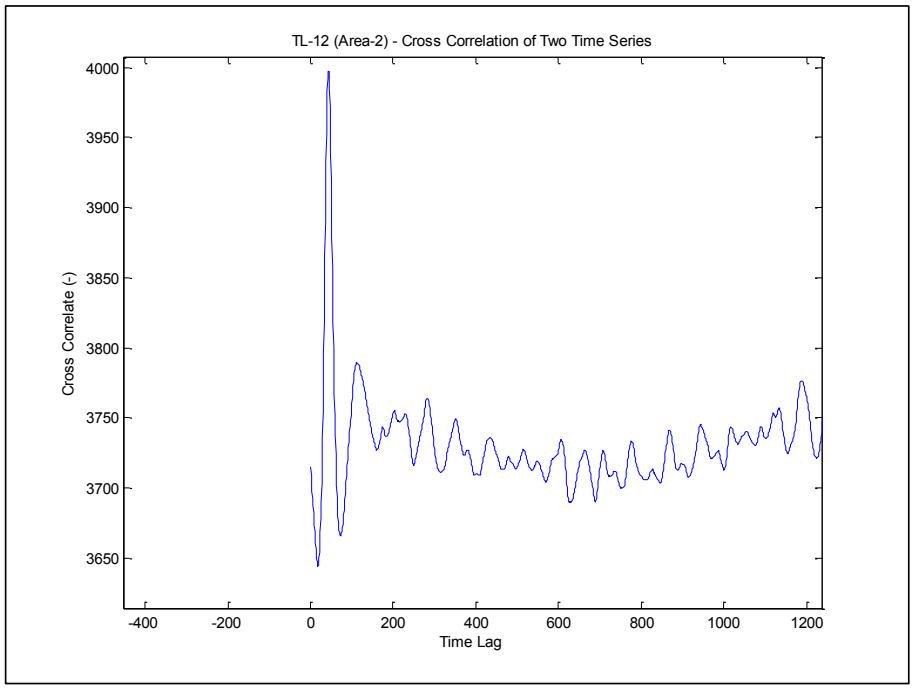

Figure 9-23: TL-12 Cross Correlation of Two Time Series – Area-2

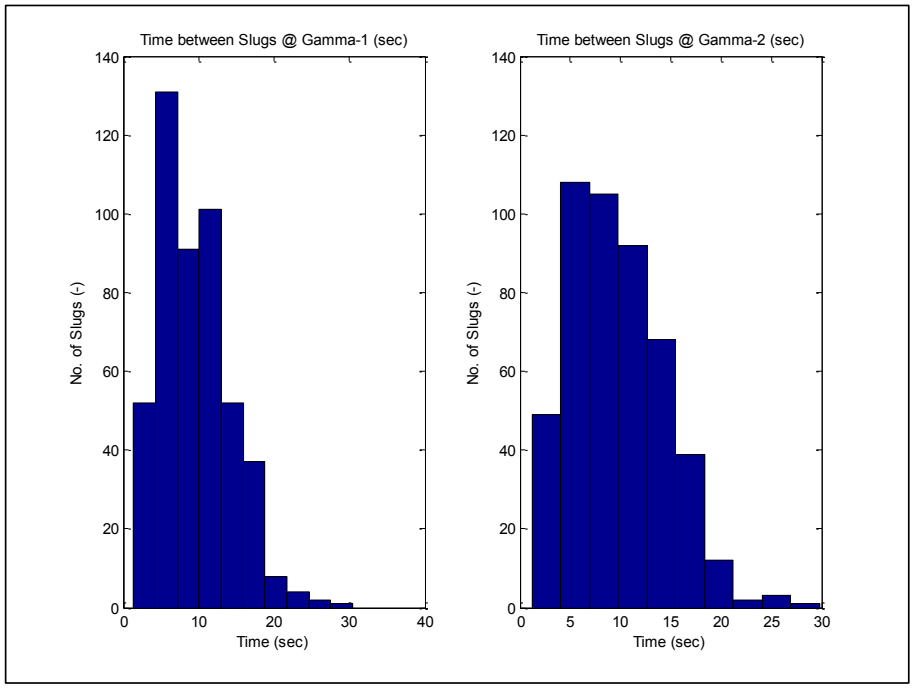

Figure 9-24: TL-12 Distribution of Slug Frequency – Area-2

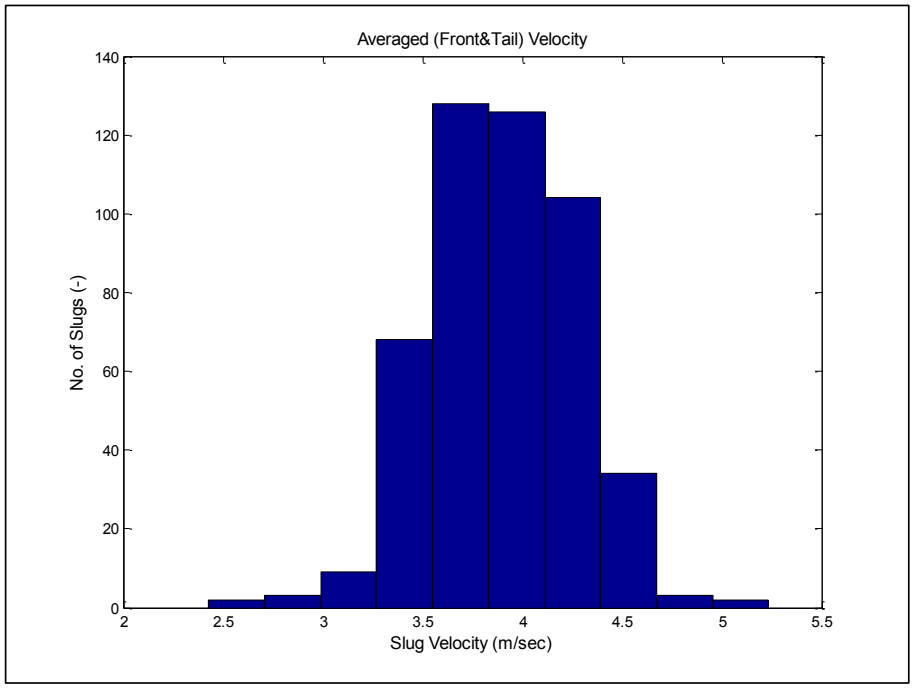

Figure 9-25: TL-12 Distribution of Average (Front & Tail) Slug Velocity – Area-2

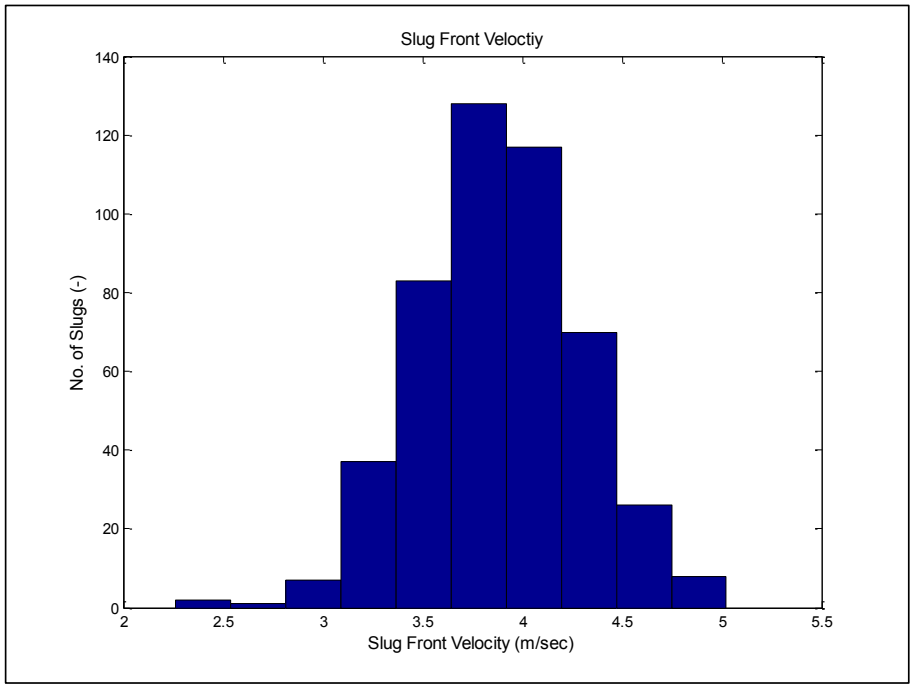

Figure 9-26: TL-12 Distribution of Front Slug Velocity – Area-2

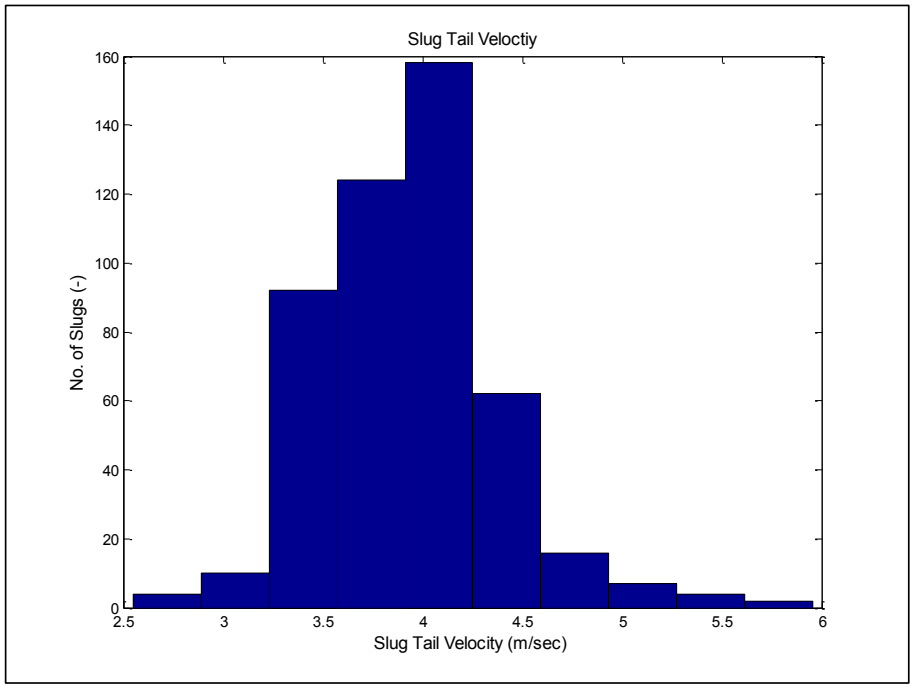

Figure 9-27: TL-12 Distribution of Tail Slug Velocity – Area-2

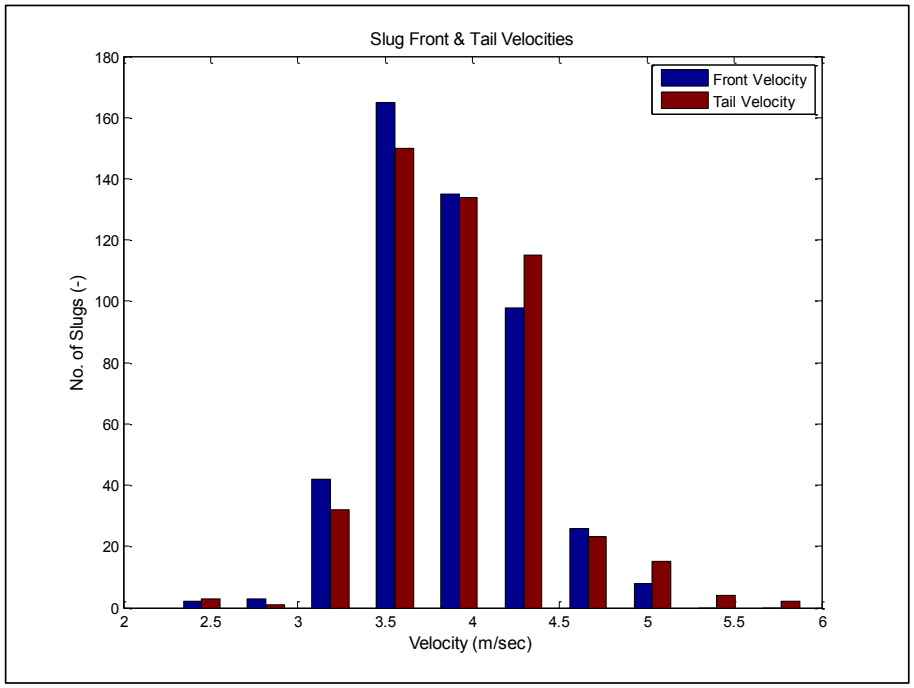

Figure 9-28: TL-12 Distribution of Front and Tail Slug Velocity – Area-2

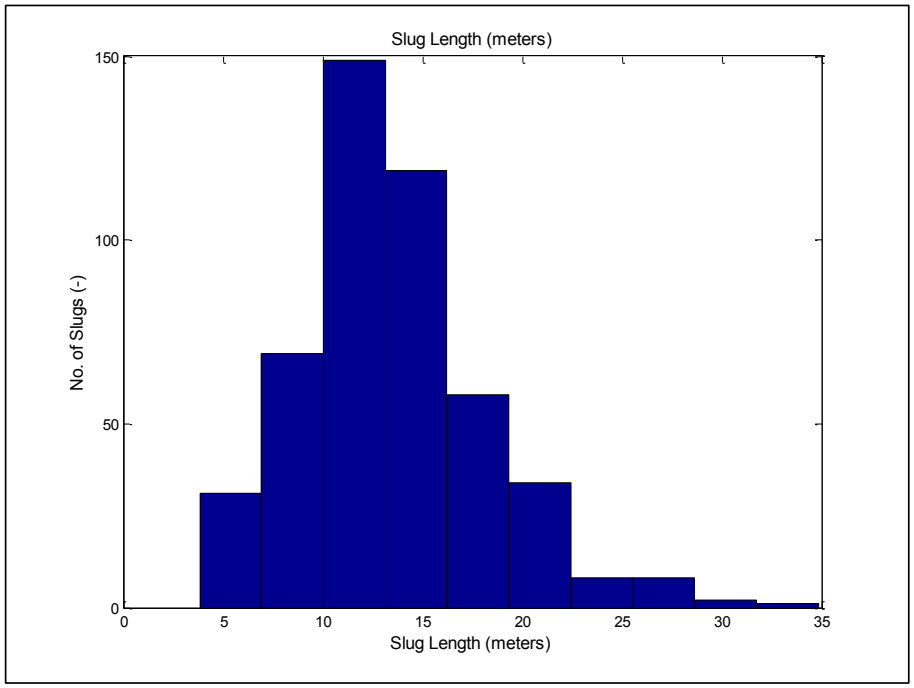

Figure 9-29: TL-12 Distribution of Slug Length (m) – Area-2

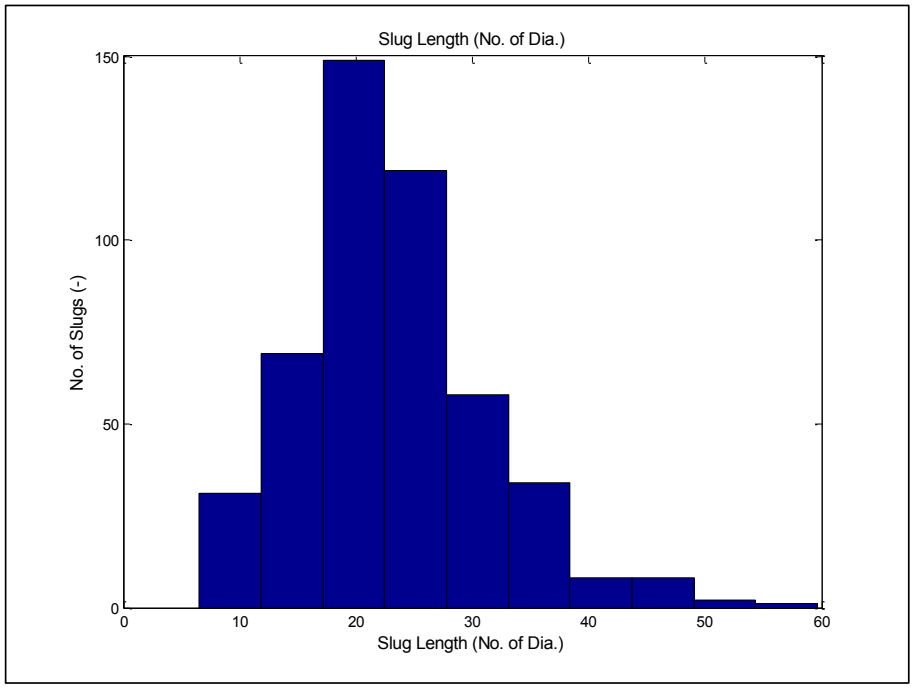

Figure 9-30: TL-12 Distribution of Slug Length (No. of Dia.) – Area-2

9.8. TL-12 Pipelines OLGA Simulation

Detailed simulation analysis was carried out for TL-12 pipeline using OLGA 7.2 commercial transient simulation package. The simulation was carried out with a coarse grid, (63.7) meters average section length, specified heat transfer coefficient of (0.35) Btu/(hr-ft2°F) and second order mass equation solver. A fine grid option was also utilized with an average section length of (9.75) meters. The comparison was carried out against the pipelines recorded pressure at the connection points with Wells (318, 199 and 571), and against the holdup measurements carried out at the two areas as explained before.

The pressure results shown in Figure 9-31, Figure 9-32 and Figure 9-33 indicate a good agreement with pressure predictions made by the non-slug tracking case for the pressure recording made at Well-318 and Well-399, which are close to the GOSP location. However, the case which provides the best results when compared against the pressure recordings made at Well-571 near the remote header at the inlet of the pipeline, was the slug tracking case with a delay constant of DC=50. One also can observe that OLGA took a very long time to reach the steady state solution with the slug tracking option with DC=50, approximately (250) minutes. The good agreement experienced at Well-571 could be a pure coincidence as OLGA development team advised earlier that with OLGA slug tracking module, the pressure drop is significantly over-predicted.

In order to investigate this, a slug tracking case with a coarse grid was simulated using a delay constant of DC=30, which is equivalent to a time delay of (4.9) seconds, was carried out. This time delay corresponds to the slugging frequency noted at Area-2. The OLGA pressure results shown in Figure 9-40, Figure 9-41 and Figure 9-42 indicate significant pressure over-prediction at the three wells Well-571, Well-399 and Well-318. This confirms that the earlier agreement experienced with slug tracking at a delay constant, DC=50, was a pure coincidence and does not reflect an accurate physical behavior with the current OLGA slug tracking module.

This indicates that with relatively high flow rate, approximately 100,000 BBL/Day, which is experienced towards the end of the pipeline, OLGA provides good predictions without slug tracking. However, with very low flow rates such as the one experienced at the beginning of the pipeline, approximately 14,000 BBL/Day at Well-571, OLGA fails to give good predictions. This could be due to the over-prediction trend that is experienced in OLGA slug tracking module.

The large discrepancy between OLGA pressure predictions and Well-571 pressure measurements could also be due to the uncertainties with the pipeline profile which is very important especially in low flow rates cases where static head is the dominant factor.

The OLGA holdup results which are depicted in Figure 9-34, Figure 9-35 and Figure 9-36 indicate similar results as the pressure ones. The holdup results at Area-1, with low flow rate, show a good agreement with the non-slug tracking case while the holdup results on Area-2, with higher flow rate, show a good agreement with the slug tracking case with a delay constant DC=150.

The fine grid, (10) meters section length, simulation, with slug tracking significantly over predict the pressure drop at the three wells locations with almost (100) psi as shown in Figure 9-37, Figure 9-38 and Figure 9-39.

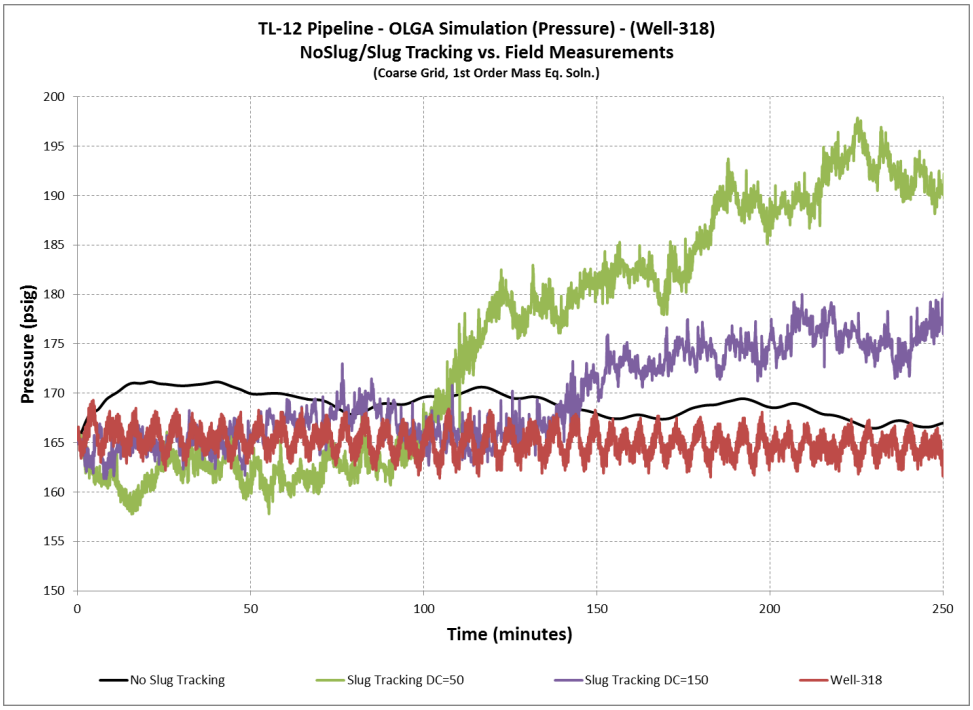

Figure 9-31: TL-12 Pipeline – OLGA Simulation Results (Pressure) – (Well-318)

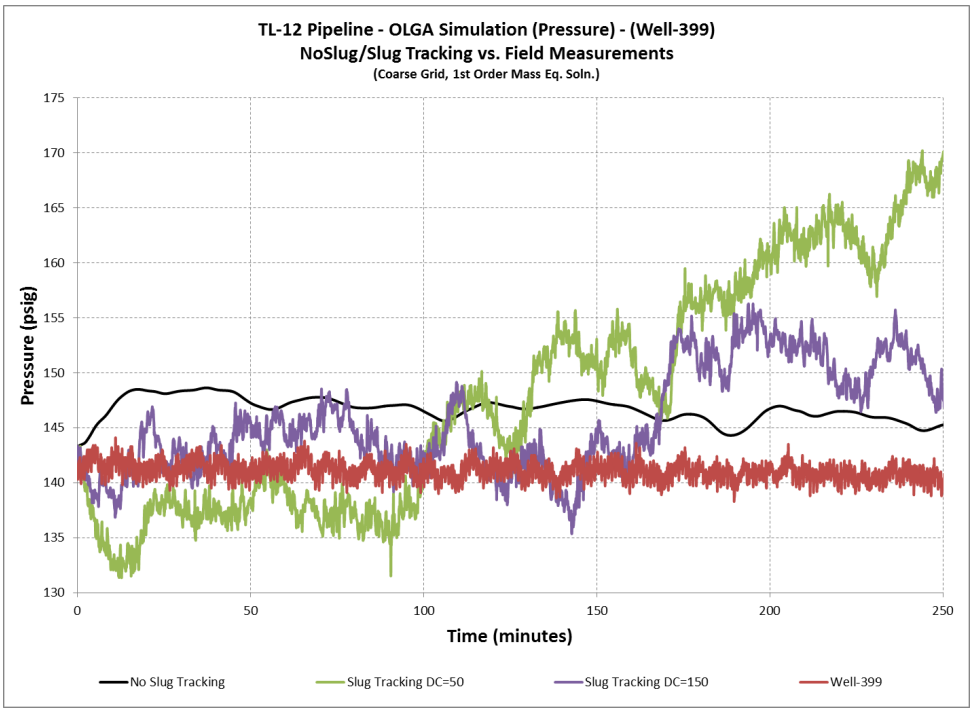

Figure 9-32: TL-12 Pipeline – OLGA Simulation Results (Pressure) – (Well-399)

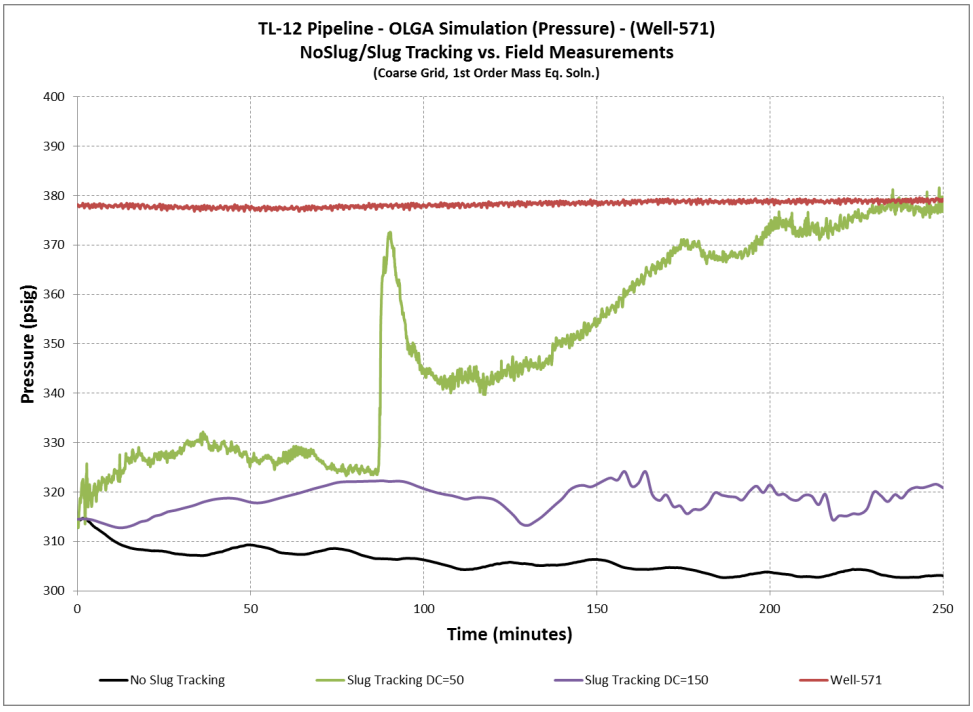

Figure 9-33: TL-12 Pipeline – OLGA Simulation Results (Pressure) – (Well-571)

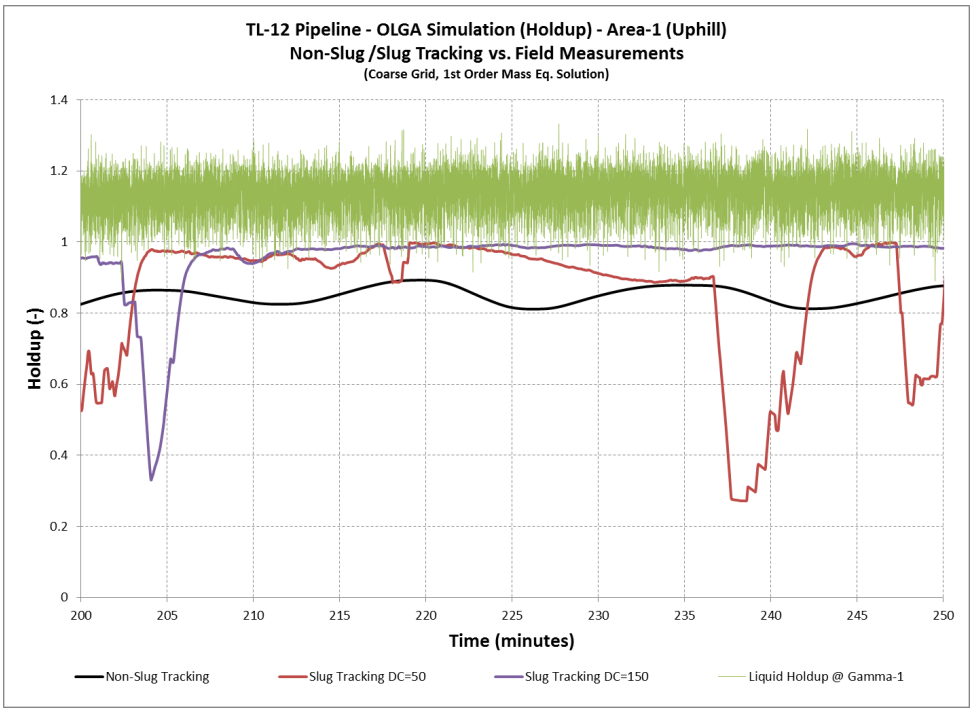

Figure 9-34: TL-12 Pipeline – OLGA Simulation Results (Holdup) – (Area-1) – (Uphill)

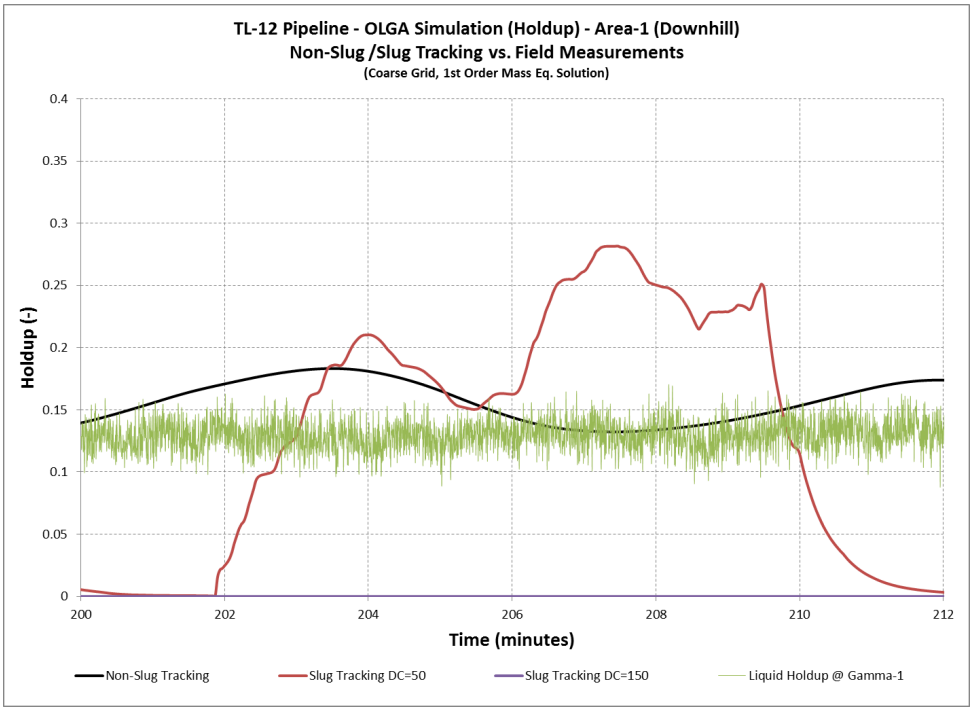

Figure 9-35: TL-12 Pipeline – OLGA Simulation Results (Holdup) – (Area-1) – (Downhill)

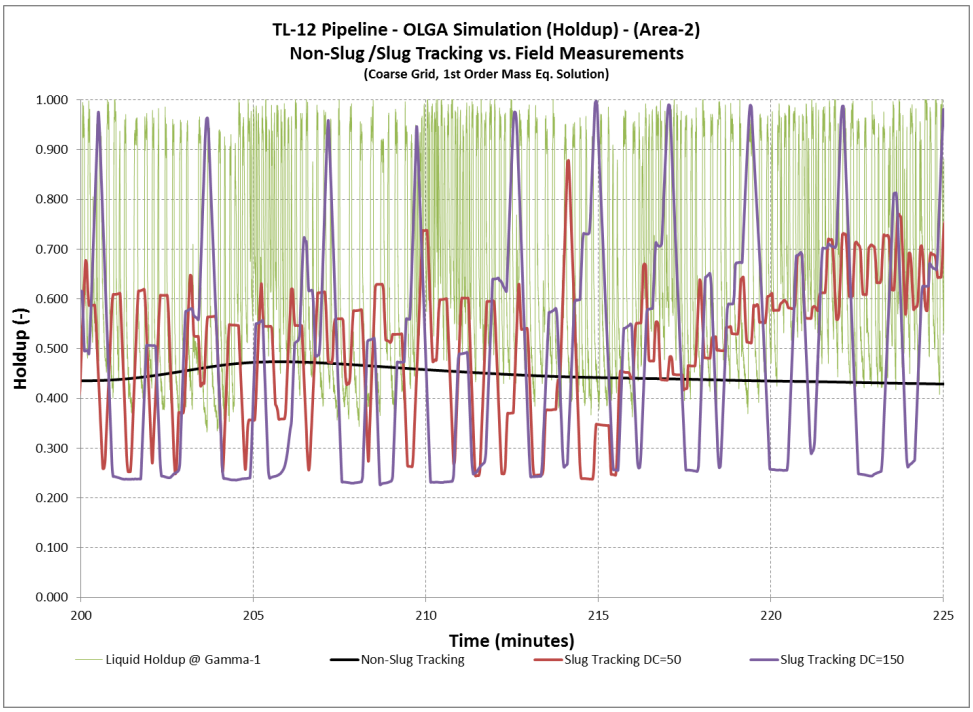

Figure 9-36: TL-12 Pipeline – OLGA Simulation Results (Holdup) – (Area-2)

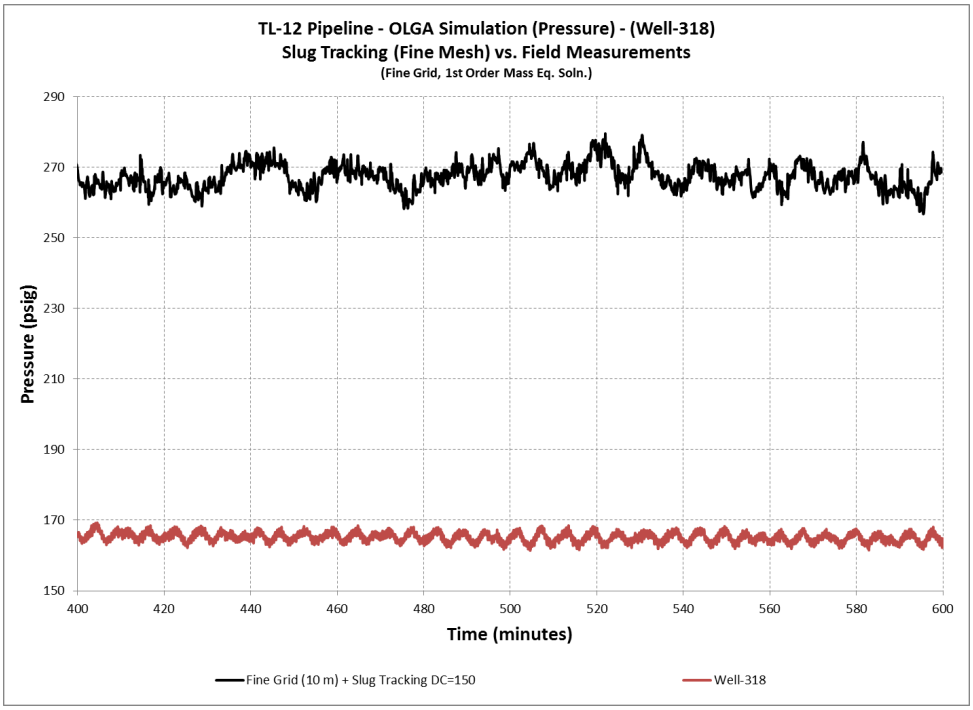

Figure 9-37: TL-12 Pipeline – OLGA Simulation Results (Fine Grid) (Pressure) – (Well-318)

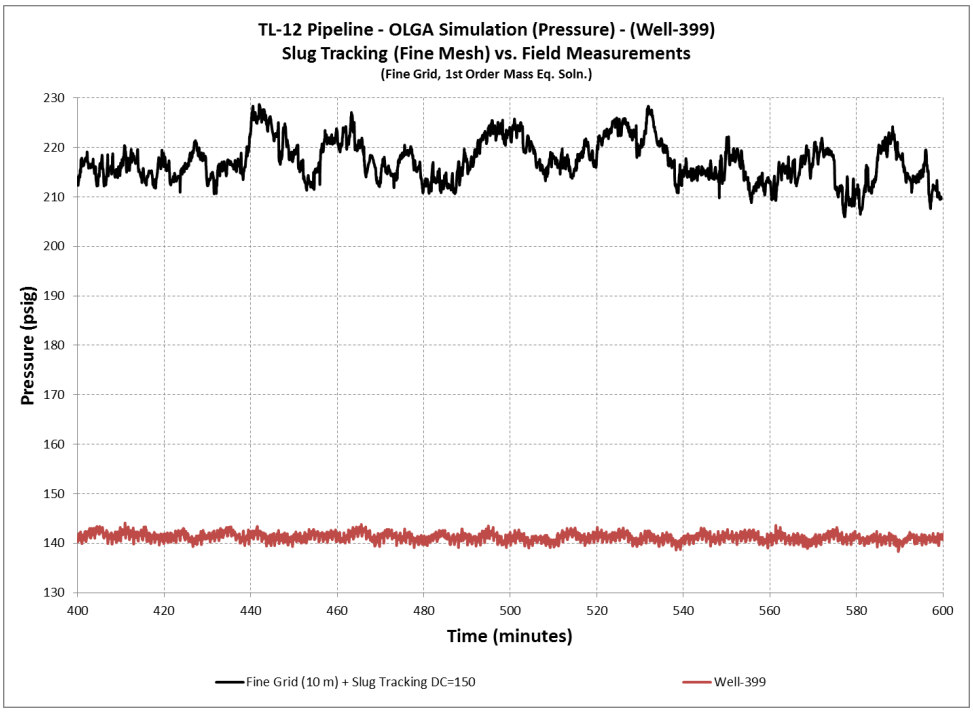

Figure 9-38: TL-12 Pipeline – OLGA Simulation Results (Fine Grid) (Pressure) – (Well-399)

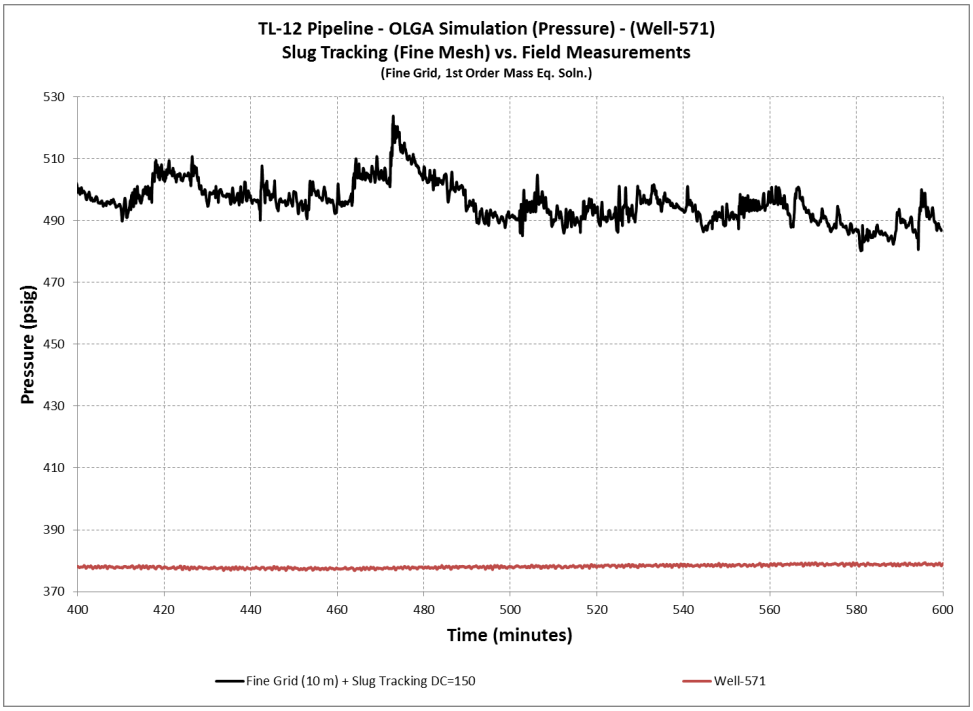

Figure 9-39: TL-12 Pipeline – OLGA Simulation Results (Fine Grid) (Pressure) – (Well-571)

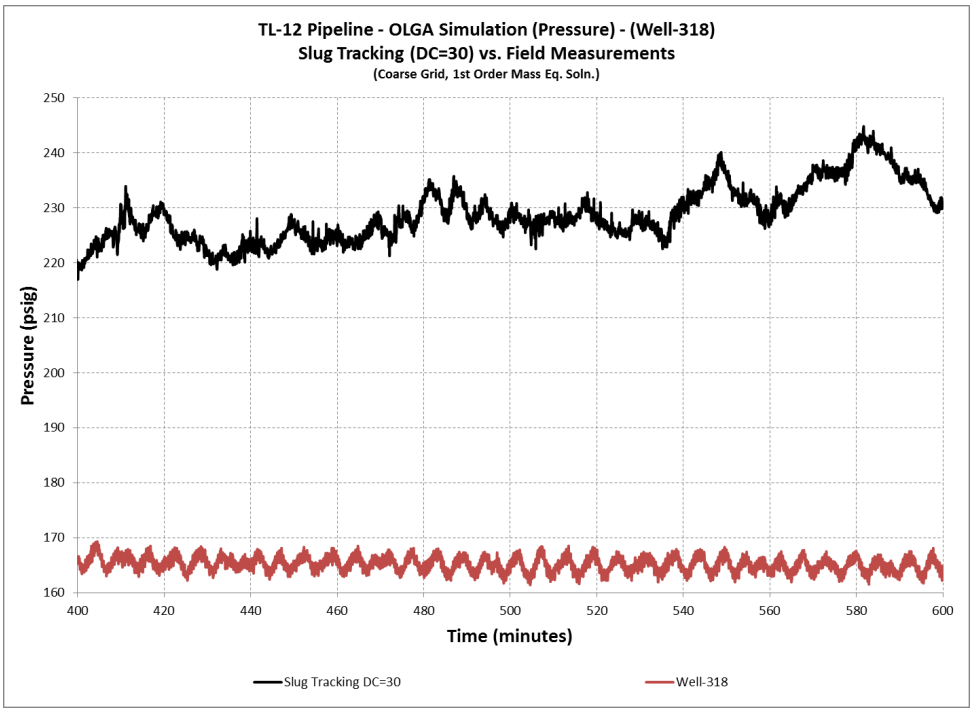

Figure 9-40: TL-12 Pipeline – OLGA Simulation Results (Slug Tracking DC=30) (Pressure) – (Well-318)

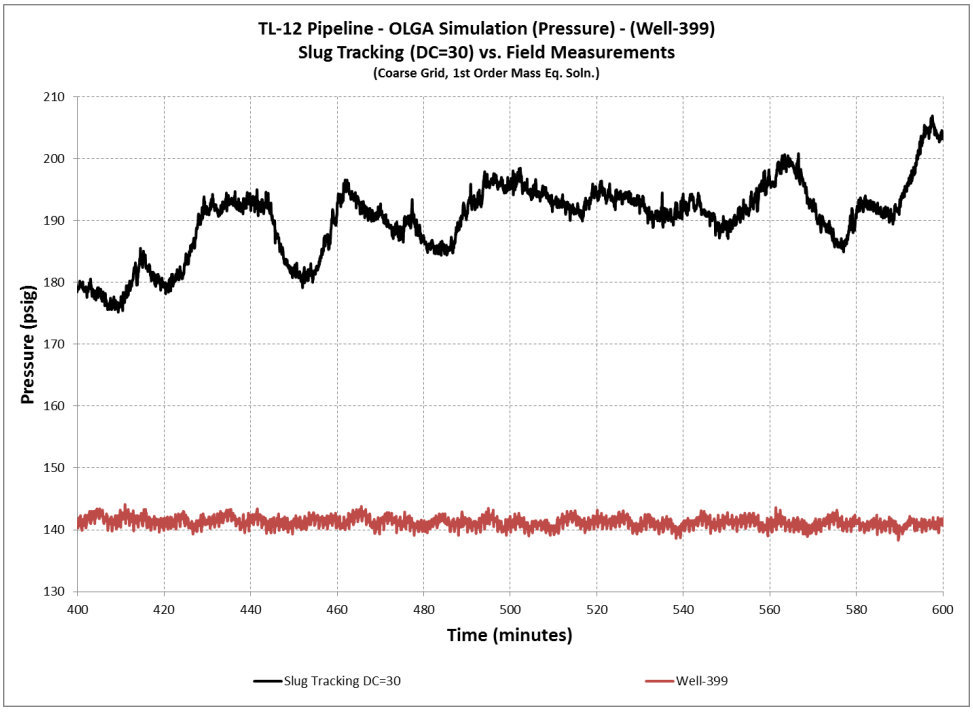

Figure 9-41: TL-12 Pipeline – OLGA Simulation Results (Slug Tracking DC=30) (Pressure) – (Well-399)

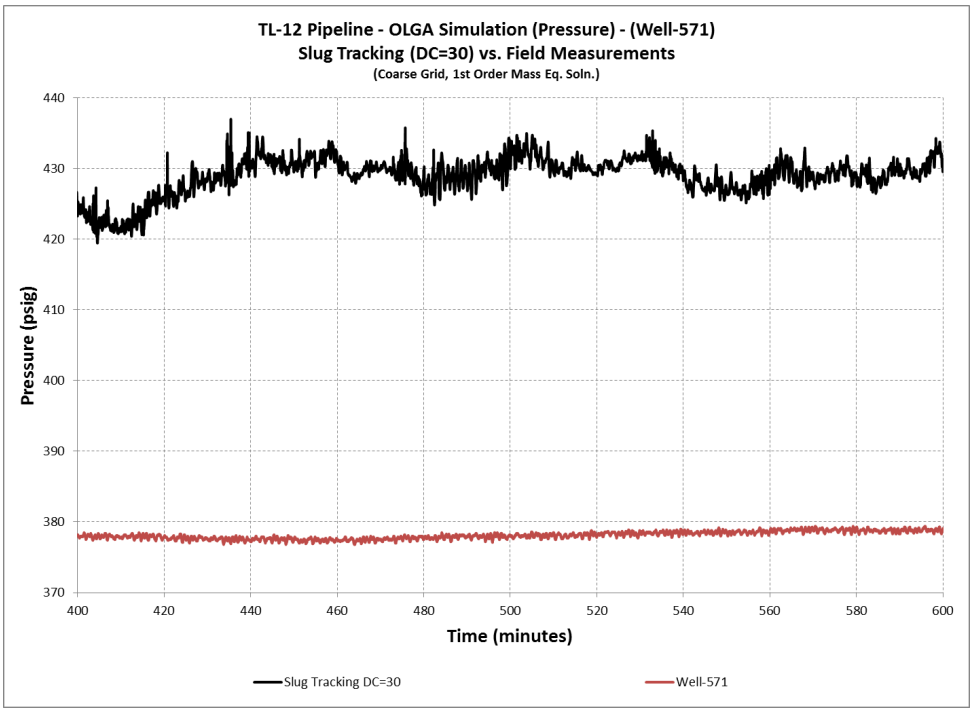

Figure 9-42: TL-12 Pipeline – OLGA Simulation Results (Slug Tracking DC=30) (Pressure) – (Well-571)

9.9. TL-12 Pipelines LedaFlow Simulation

Detailed simulation analysis was carried out for TL-12 pipeline using LedaFlow version (1.4.242.619), commercial transient simulation package. The simulation was carried out with a coarse grid, (63.7) meters average section length and specified heat transfer coefficient of (0.35) Btu/(hr-ft2°F). The comparison was carried out against the pipelines recorded pressure at the connection points with Wells (318, 199 and 571), and against the holdup measurements carried out at the two areas as explained before.

The pressure results shown in Figure 9-43, Figure 9-44 and Figure 9-45 indicate a good agreement with pressure predictions made by the slug capturing case for the pressure recording made at Well-318 and Well-399, which are close to the GOSP location. However, LedaFlow pressure results compared against recordings made at Well-571 near the remote header at the inlet of the pipeline, showed significant under prediction for both slug capturing and non-slug capturing cases.

The LedaFlow holdup results which are depicted in Figure 9-46, Figure 9-47 and Figure 9-48 indicate similar results as the pressure ones. The holdup results at Area-1, with low flow rate show a good agreement, while the holdup results on Area-2 with higher flow rate show a holdup under prediction.

The fine grid runs carried out with slug capturing shown in Figure 9-49, Figure 9-50 and Figure 9-51, indicate the expected improvements for Well-318 and Well-399. However, Well-571 results are still greatly under predicted even with fine grids of (30*D) and (15*D).

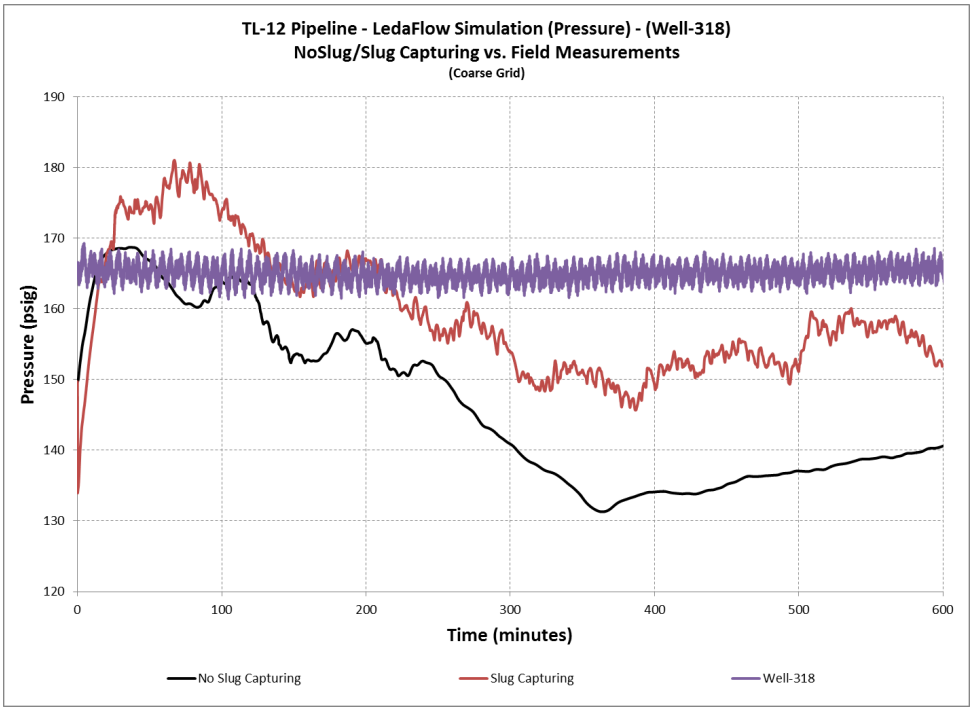

Figure 9-43: TL-12 Pipeline – LedaFlow Simulation Results (Pressure) – (Well-318)

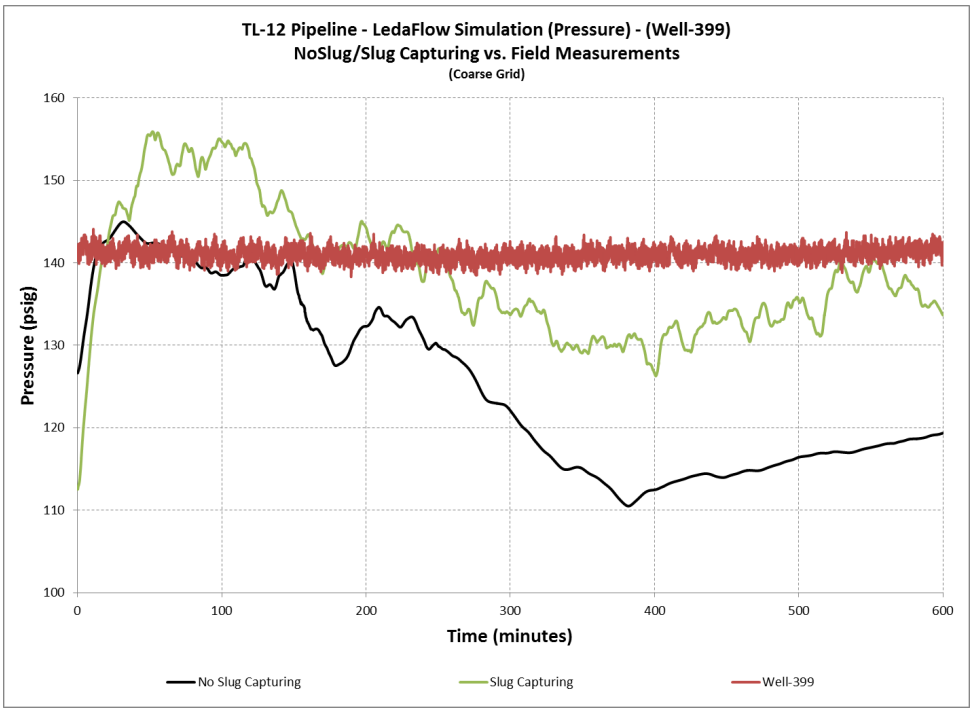

Figure 9-44: TL-12 Pipeline – LedaFlow Simulation Results (Pressure) – (Well-399)

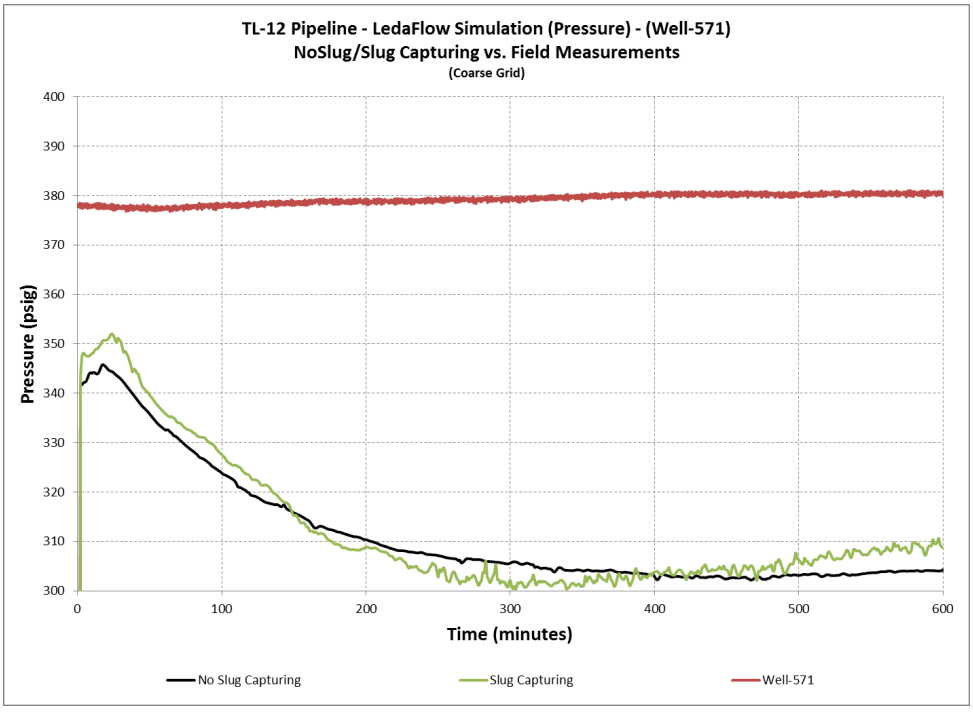

Figure 9-45: TL-12 Pipeline – LedaFlow Simulation Results (Pressure) – (Well-571)

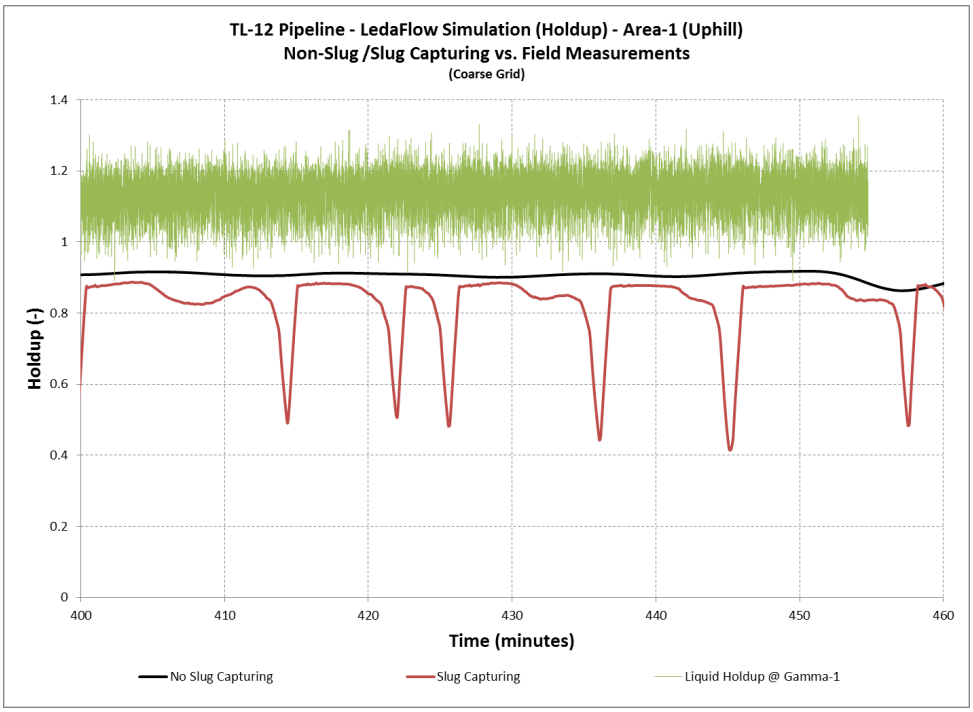

Figure 9-46: TL-12 Pipeline – LedaFlow Simulation Results (Holdup) – (Area-1) – (Uphill)

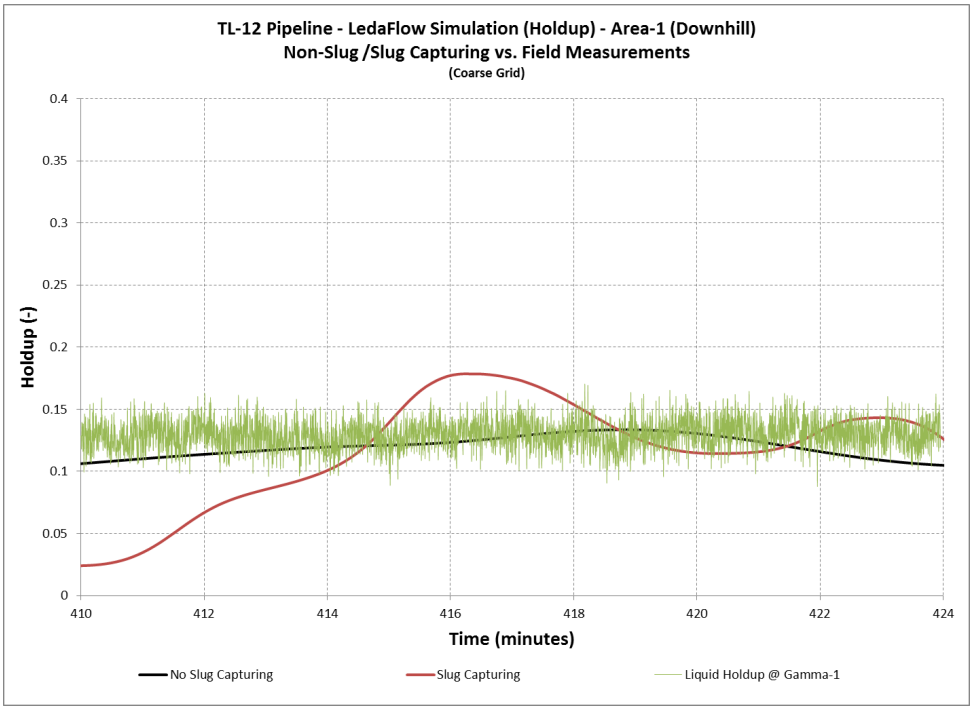

Figure 9-47: TL-12 Pipeline – LedaFlow Simulation Results (Holdup) – (Area-1) – (Downhill)

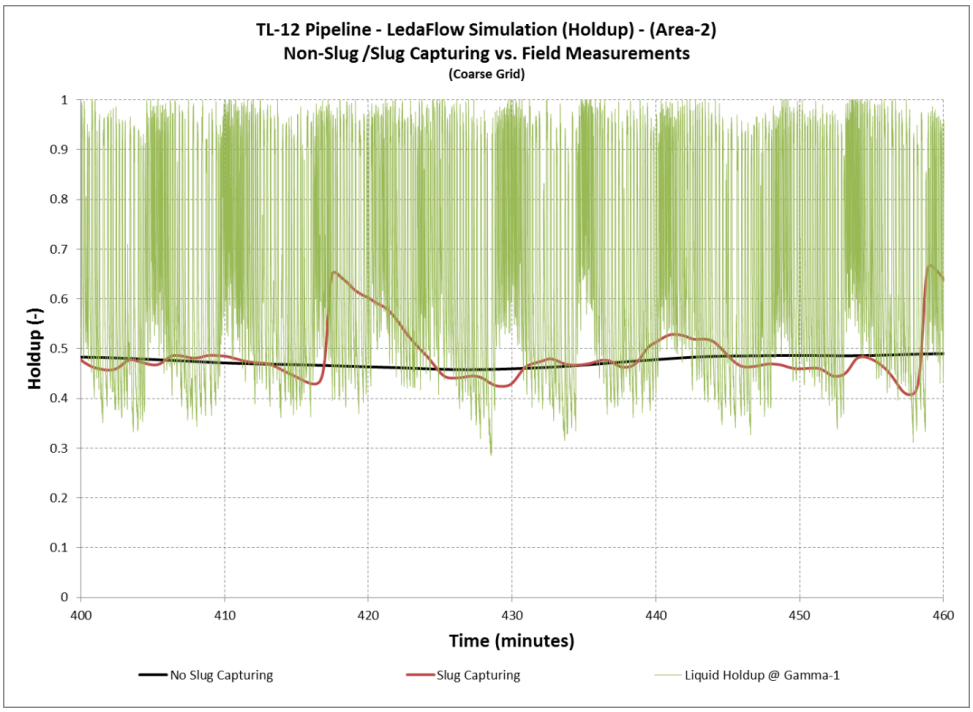

Figure 9-48: TL-12 Pipeline – LedaFlow Simulation Results (Holdup) – (Area-2)

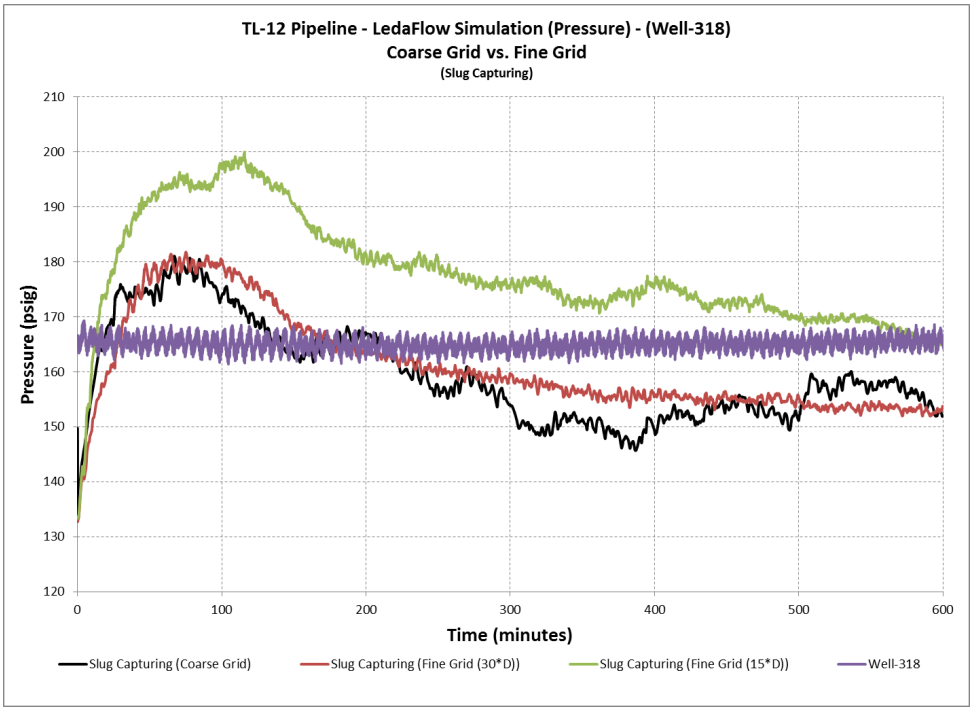

Figure 9-49: TL-12 Pipeline – LedaFlow Simulation Results (Pressure) – (Well-318) – (Coarse vs. Fine Grid)

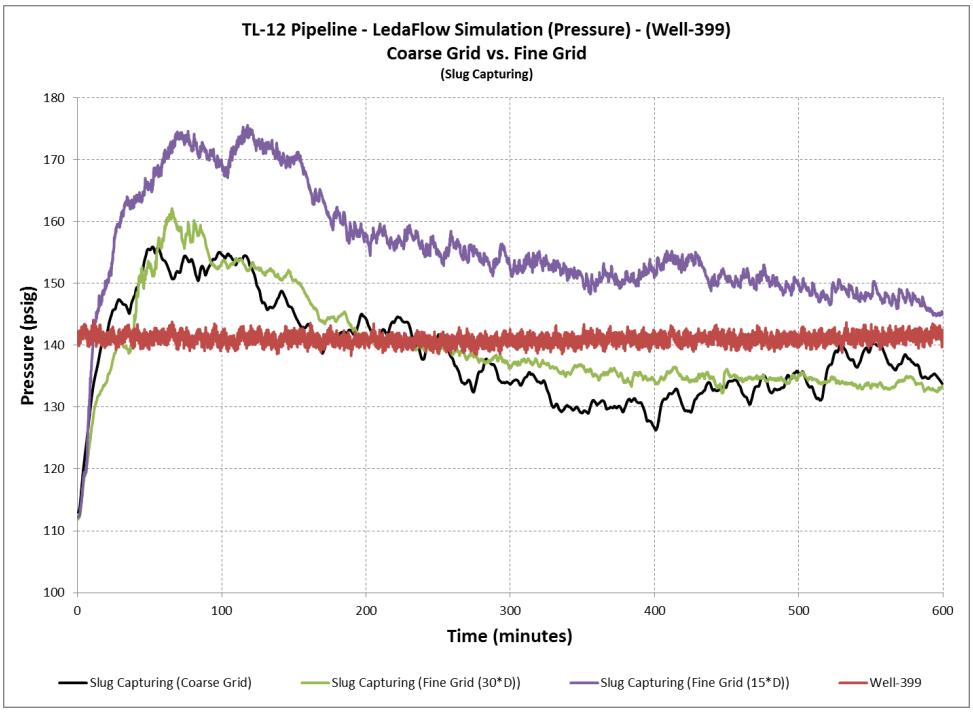

Figure 9-50: TL-12 Pipeline – LedaFlow Simulation Results (Pressure) – (Well-399) – (Coarse vs. Fine Grid)

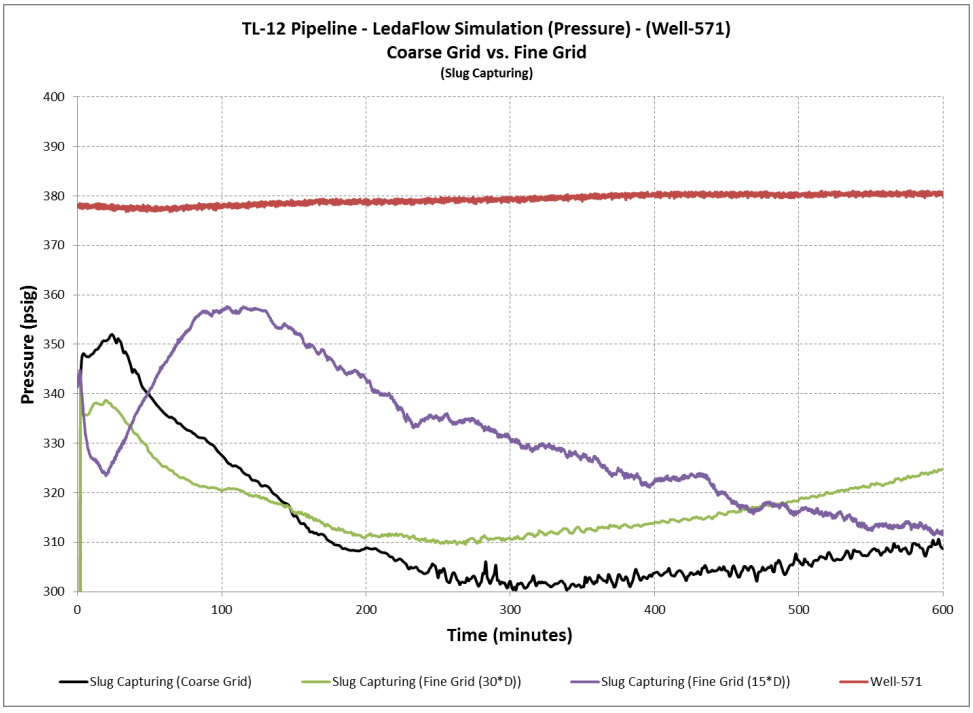

Figure 9-51: TL-12 Pipeline – LedaFlow Simulation Results (Pressure) – (Well-571) – (Coarse vs. Fine Grid)

This page was intentionally left blank

10. IMPACT OF CHOKED VALVES ON TERRAIN INDUCED SLUGS

During the simulation analysis of the large terrain slugs in Field-A, an observation was made which was related to the introduction of choked valves on slugging behavior. The simulation work conducted using both OLGA, slug tracking, and LedaFlow, slug capturing, indicates the amplification and/or generation of slugs due to the existence of choked valves. This phenomena which appears to be new in multiphase flow pipelines, was further investigated at NTNU multiphase flow laboratory. A set of experiments were conducted to examine the impact of choked valves on terrain-induced slugs and the results are discussed in this section. However, an introduction to the severe slugging phenomena and the methods to attenuate those slugs will be presented for a better understanding of the new phenomena.

10.1. Severe Slugging Phenomenon in Risers

Severe slugging phenomenon in risers has been investigated as early as 1973 by researchers such as Yocum (1973) and Schmidt et al. (1979). However, the first detailed mathematical model was described by Taitel (1986) which also described the four steps slugging cycle as follows: (1) liquid starts to accumulate at the bottom of the riser. (2) More liquid and gas enters the pipeline system causing more accumulation of liquid at the bottom of the riser and gas upstream of it. (3) The blocked gas gradually increases the pressure in the pipeline system until it reaches a level where it could blow the liquid out of the pipeline system. (4) A new cycle is started when liquid starts to accumulate again, see Figure 10-1.

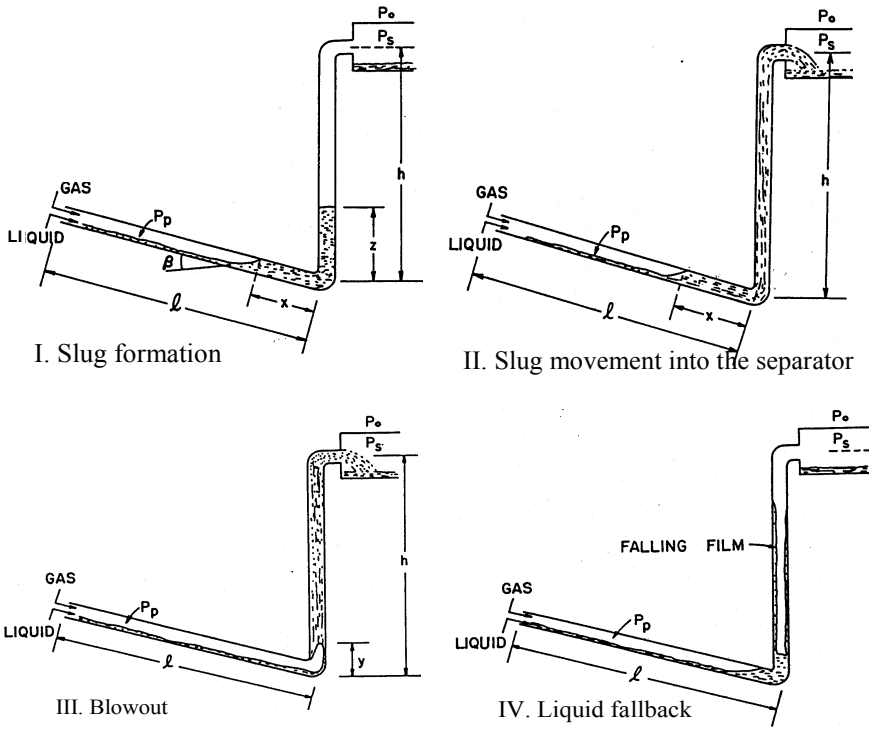

Figure 10-1: Riser Sever Slugging Cycle from Taitel (1986)

10.1.1. Mathematical Modelling of Severe Slugging in Risers

One of the earliest research that has been carried out on severe slugging was the work of Schmidt et al. (1979), where they have identified that the installation of a choke could eliminate slugging. Later, Boe (1981) established a stability criteria, which is a simple mathematical expression for the force balance acting on a layer of liquid at the bottom of the riser, which are the gas pressure in the pipeline leading to the riser bottom and the static head of the liquid in the riser. The force balance results in the following criterion:

$$U_{LS} \geq \frac{P_p}{\rho_l \, g \, \alpha \, L} \, U_{GS} \tag{10.1}$$

where, (P_p) is the pressure in the pipe leading to the riser bottom, $(U_{LS} \; and \; U_{GS})$ are the superficial liquid and gas velocities respectively, (ρ_l) is liquid density, (g) is gravitational constant, (α) is void fraction in the riser and (L) is the length of the pipe leading to the riser bottom.

Taitel (1986) further explored the phenomenon and came up with a more detailed model that includes choke and gas lift methods for slug elimination. This model will be briefly described in this section as it represents a very reasonable description of the physics entailed in severe slugging in risers.

Taitel riser severe-slug mathematical model can be obtained by assuming a small disturbance (y) at the bottom of riser as shown in Figure 10-2. The force balance per unit area acting on the liquid layer at the riser bottom can be described as follows:

$$\Delta F = \left[(P_s + \rho_l g h)\frac{\alpha l}{\alpha l + \alpha' y}\right] - [P_s + \rho_l g(h - y)] \tag{10.2}$$

The first term represents the gas compressibility force in the pipeline, while the second term represents counter balance force which consists of the separator pressure (P_s) and the liquid column in the riser with density (ρ_l) and height $(h - y)$. The gas holdup in the pipeline leading to the riser is denoted by (α) and the gas holdup of the small gas volume penetrating the riser is denoted by (α'). The value of (α') was found to be in the order of 0.5 to 0.75 as shown from experiments made by Jansen et al. (1996). The gas holdup (α) can be determined analytically using a stratified flow model and it usually has values that ranges between 0.8 and 1.0 as described by Taitel (1986).

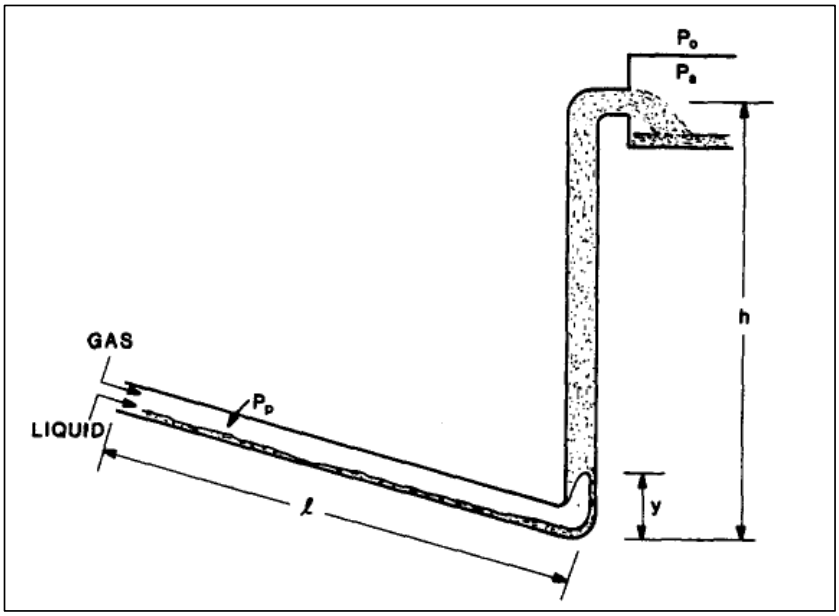

Figure 10-2: Pipeline riser configuration from Taitel (1986)

The analysis also ignores shear stresses due to low flow rates which are usually a characteristic of the slug flow, and it also assume isothermal expansion of gas which follows the ideal gas law. Taitel assumed that the liquid column in the riser will be blown out by the compressed gas only if (ΔF) increases with more gas penetration (y). Therefore, he concluded that the necessary condition for a stable flow in the pipeline-riser arrangement is:

$$\frac{\partial(\Delta F)}{\partial y} < 0 \quad at \quad (y = 0) \tag{10.3}$$

$$\frac{\partial(\Delta F)}{\partial y}(y = 0) = \left[\frac{(P_s + \rho_l g h)\,(\alpha l)(\alpha')}{(\alpha l)^2}\right] + (\rho_l g) \tag{10.4}$$

This leads to the famous Taitel stability criterion, with the introduction of atmospheric pressure (P_0):

$$\frac{P_s}{P_0} > \left[\frac{(\alpha/\alpha')\,l\, - h}{P_0\,/\,(\rho_l g)}\right] \tag{10.5}$$

This simple result indicates that the separator pressure has to be increased according to this formula in order to eliminate severe slugging. It also emphasizes the importance of length of the pipeline leading to the riser and the height of the riser. The longer the pipeline length the less stable the system is as it allows for a higher gas compressible force while the height of the riser provides a more stable system, Taitel (1986).

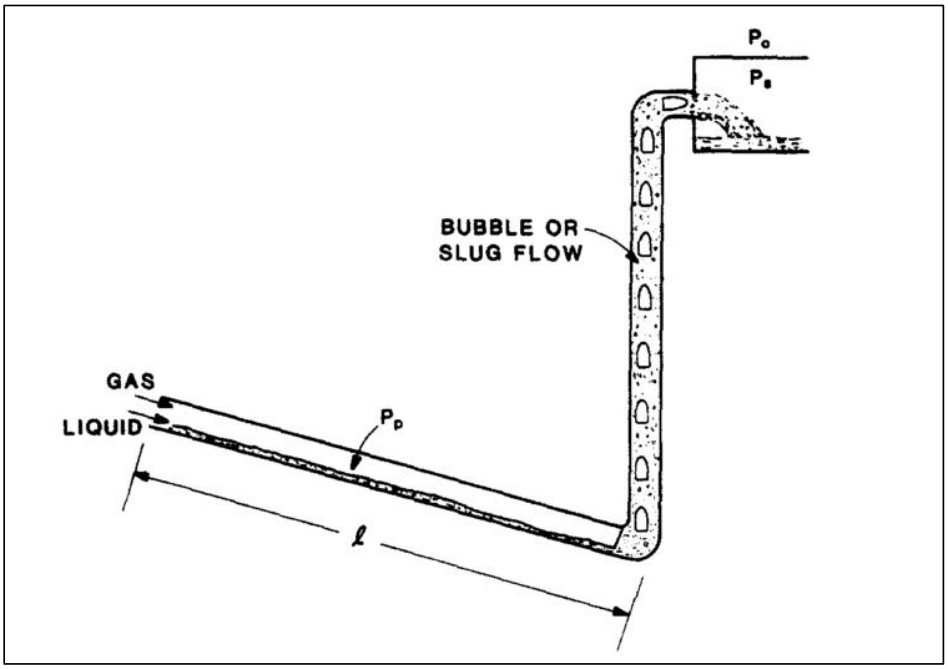

Figure 10-3: Riser Configuration – Steady State Operation from Taitel (1986)

The stability of a steady system where small bubbles or short slugs penetrate the riser as shown in Figure 10-3 can be easily incorporated by replacing the liquid density with a mixture density using the riser estimated holdup (Ø).

The introduction of a choke to the pipeline-riser system upstream of the separator, as shown in Figure 10-4, was also incorporated into the model by Taitel (1986) and was further developed and enhanced by Taitel et al. (1990) and Jansen et al. (1996). The analysis can be started by assuming that the pressure upstream of choke is given by:

$$P_b = P_s + CU_{ls}^2 \tag{10.6}$$

where, (P_b) stands for back pressure, (C) stands for choke coefficient and (U_{ls}^2) stands for the superficial liquid velocity in the riser. When the severe slugging cycle is about to be initiated and the gas pressure in the pipeline exceeds the hydrostatic pressure in the riser, and gas starts to intrude into the riser, the additional pressure is assumed to be equal to (Ky), where (K) is proportionality constant, Jansen et al. (1996).

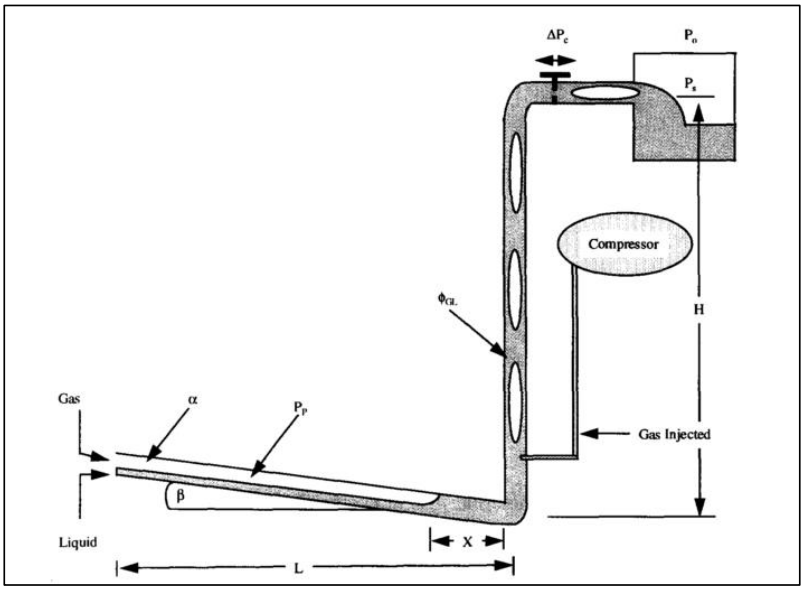

Figure 10-4: Pipeline-riser configuration with choking from Jansen et al. (1996)

Thus, one can write the choke upstream back pressure as:

$$P_b - P_s + CU_{ls}^2 = ky \tag{10.7}$$

Using the same analysis used above for the onset of severe slugging where, $\frac{\partial(\Delta F)}{\partial y} < 0 \quad at \quad (y = 0)$, one can obtain the following:

$$\Delta F = F_1 - F_2 = \left[\left(P_s + CU_{ls}^2 + \rho_l g h\right)\frac{\alpha l}{\alpha l + \alpha' y}\right] - \left[P_s + CU_{ls}^2 + Ky + \rho_l g(h - y)\right] \tag{10.8}$$

Using the condition of stability, one can obtain the following result:

$$\frac{P_s + CU_{ls}^2}{P_0} > \left[\frac{\left(\frac{\alpha l}{\alpha'}\right)\left(1 - \frac{K}{\rho_l g}\right) - h}{\frac{P_0}{(\rho_l g)}}\right] \tag{10.9}$$

This result states that if this criterion is satisfied, then no severe slugging will be initiated which leads to a stable flow in the riser, Jansen et al. (1996). It also coincides with the top of Boe (1981) criterion as shown in Figure 10-5.

The proportionality constant can be obtained by considering the force imbalance at the riser, which causes acceleration of gas and can be expressed by Newton's Law as follows:

$$A\,\Delta F = \frac{d(A(h - y)\,\rho_l\,U)}{dt} \tag{10.10}$$

where, (U) is total velocity of slug which is caused by the penetration of gas front at the bottom of riser. Plugging (U) for (U_{ls}) one obtains a relationship for the pressure drop across the choke with total velocity:

$$P_b = P_s + CU^2 \tag{10.11}$$

Manipulating equations (5.8, 5.9, 5.10 and 5.11), one can obtain the following result for small (y):

$$U^2 = U_{ls}^2 + \frac{2}{h} U_{ls}^2 y \tag{10.12}$$

Substituting equation (5.12) into (5.11) results in the following equation for (K):

$$K = \frac{2\,C\,U_{ls}^2}{h} \tag{10.13}$$

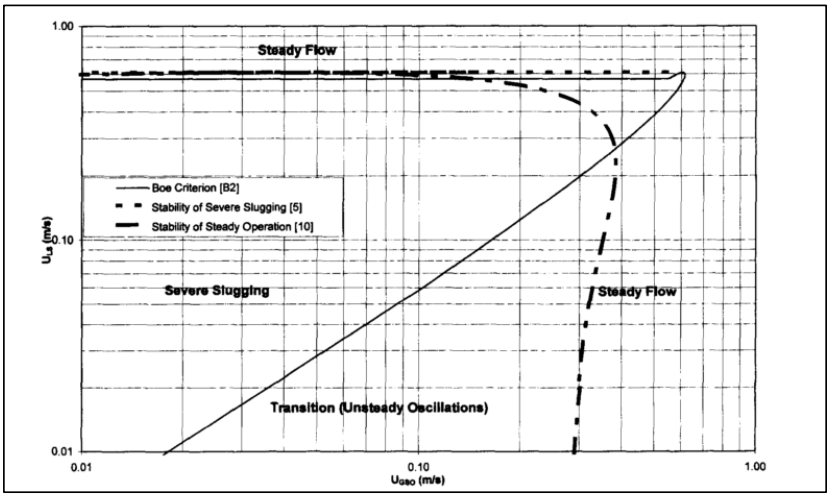

Figure 10-5: Severe slugging map from Jansen et al. (1996)

10.1.2. Attenuation of Severe Slugging in Risers

Severe Slug flow in oil and gas production fields is often operationally controlled using three fundamental approaches as described by Havre and Dalsmo (2002):

- Design Modifications
- Operational Modifications
- Control Methods

Design modifications refer to installation of various types of slug catchers, finger type or large separators, to properly handle the expected slug sizes and frequencies. Operational modifications, on the other hand, often relate to alteration of the production system operating pressure either upstream or downstream the pipeline system. Recently, advanced control methods, forward feed control and active feedback control methods, have been successfully implemented at many oil and gas pipeline installations around the world. This is usually carried out through the installation of a controlled choke at the end of the pipe, upstream of the slug catcher, to eliminate or tame slugs as described by many researchers over the last 35 years.

One of the first researchers to propose a feedback control approach to avoid riser slugging was Schmidt et al. (1979), which suggests an automatic control of a topside choke based on feedback from pressure upstream of the riser and flow measurement in the riser. Taitel (1986) few years later wrote that in a pipeline-riser arrangement, a steady operation can be achieved if the separator pressure is high enough to suppress the upstream gas expansion force. However, even under unstable steady state operation, where

slugs are normally expected, a proportional controlled choke that behaves under a specific algorithm can stabilize the flow. The control methods approach went through two phases. The first phase was the approach in which an automated choke setting is used to prevent slugs from occurring in the system, i.e.; operating outside the slug region. This required a large pressure drop across the choke and thus greatly limited the oil and gas production. An example of such application is the work by Courbot (1996) in his application of a control system approach on a topside choke at Dunbar pipeline presented the first known industrial application of slug taming using the theory established earlier by researchers such as Taitel and Schmidt. The application, although not optimized, proved to the industrial sector the effectiveness of such methods and paved the road for future industrial and academic research collaboration in this area. Henriot et al. (1999) revisited the Dunbar pipeline case and offered an optimized choke pressure drop through simulation work using TACITE multiphase simulation package.

The second phase was the approach that was first theoretically investigated by Taitel (1986), requires a much lower pressure drop but also needs a more sophisticated algorithms to control the choke as it will be operating within slug flow region. The first industrial application of this approach was implemented by Havre et al. (2000), who presented an anti-slug control system for the Hod-Valhall pipeline. An anti-slug controller, as defined by Storkaas (2005) in his PhD thesis, is a controller which stabilizes an unsteady slug flow while still operating within the slug flow regime boundary conditions. The implementation on the Hod-Valhall pipeline included both simulation and actual field work and proved to be very successful. Havre and Dalsmo (2002) later provided more details about the system introduced in their anti-slug controller. The interesting point was that the controller was capable of successfully taming the slug flow by constant micro movement of the choke openings at conditions where slug flow would have occurred without this micro movement as shown in Figure 10-6.

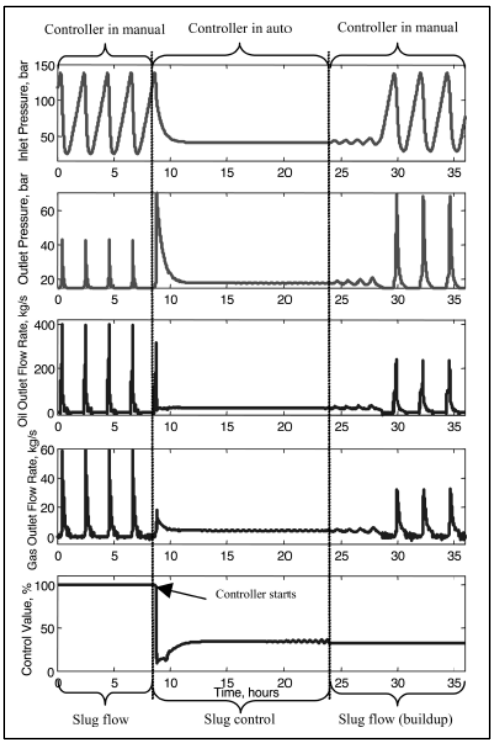

Figure 10-6: Anti-Slug controller applied to severe riser-induced slug flow from Havre and Dalsmo (2002)

Skofteland and Godhavn (2003) utilized a PID controller in their anti-slug system that was applied to Heidrun oil field and some experimental data from Sintef Multiphase Flow Laboratory at Tiller, Norway. More experimental work was also reported by Godhavn, Fard, et al. (2005) and Fard et al. (2006) along with extensive simulation work using OLGA multiphase flow simulation package. Godhavn, Strand, et al. (2005) provided yet another actual field application when they implemented their combined anti-slug controller with a predictive model to handle slugs at Tordis oil field.

Storkaas (2005) in his PhD thesis presented a simplified physical model. Algorithms that connect the choked valve opening to several topside measurements have been implemented with volumetric flow rate being considered in a secondary loop while pressure measurement is being used as the primary loop. Several other researchers have continued this path by implementing more sophisticated cascade algorithms such as Olsen (2006) and more recently Jahanshahi et al. (2012).

10.2. NTNU Multiphase Flow Lab Terrain-Induced Slugs Experiments

After noticing the occurrence of relatively large pressure fluctuations caused by slugs due to the introduction of chokes at the end of a hilly terrain pipeline, a set of experiments was planned and carried out at NTNU multiphase flow lab, shown in Figure 10-7.

Figure 10-7: NTNU Multiphase Flow Lab

The disappearance of those slugs were noticed when conducting simulation work using both OLGA and LedaFlow on 1999 field measurements such as G2NT2, see Figure 10-8. The objective of those experiments was to investigate this phenomenon and in general the impact of choked valve on terrain induced slugs.

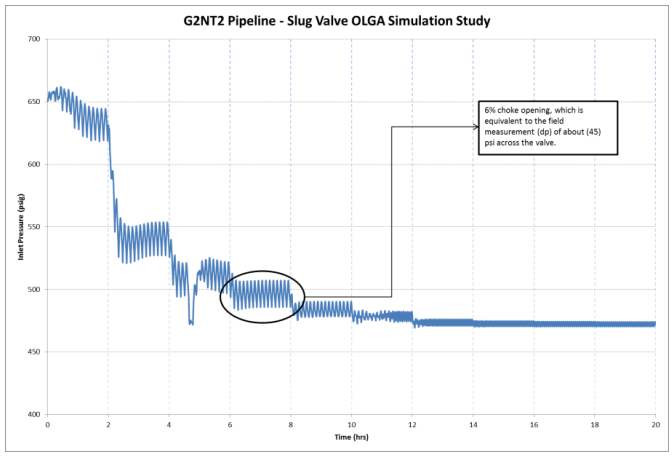

Figure 10-8: G2NT2 Pipeline OLGA Simulation with various choke openings

The lab experiments were conducted using air and water with various flow rates at atmospheric pressure conditions in a 60 mm diameter pipe. These lab experiments were conducted by connecting the air-water loop with a flexible pipe section that lies on the ground of the lab and then goes up back again and extends for a certain length, depending on the specific arrangement, and finally ends with a manual valve just before it connects to the atmospheric separator as shown in Figure 10-9. The opening of the manual valve was adjusted for every experiment and pressure and flow rates were logged to examine the impact of various valve openings on flow behavior.

Figure 10-9: NTNU Lab Experiments Arrangement

Several pipe arrangements were attempted as shown in Figure 10-11. The final pipe geometry which was assembled on May 23, 2014 was the longest one, approximately 100 meters, and the most successful one in terms of its ability to reproduce the phenomenon observed in the field measurements. The overall schematic of the lab experiment as shown in Figure 10-10.

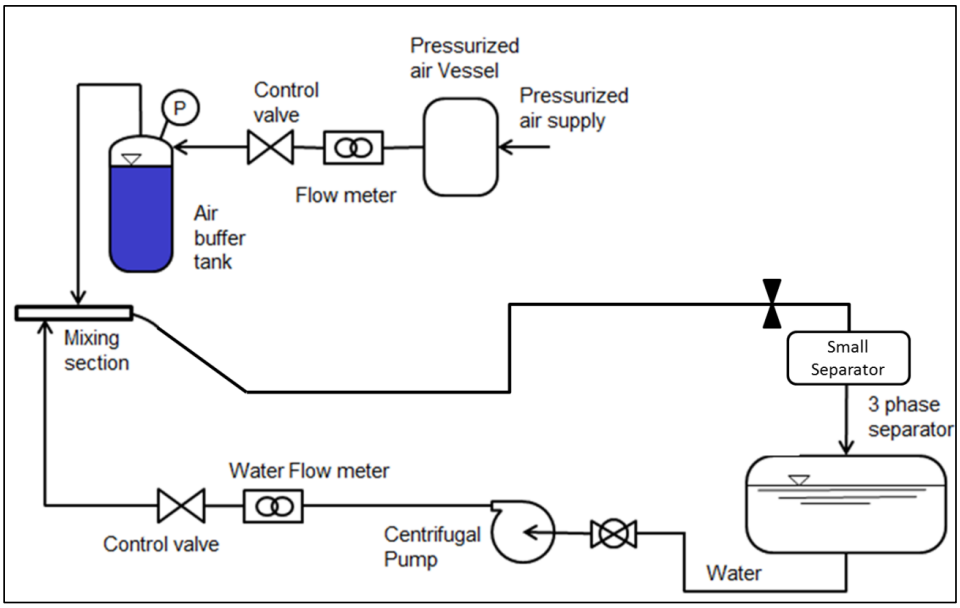

Figure 10-10: General Lab Experiments Schematic at NTNU Multiphase Flow Laboratory

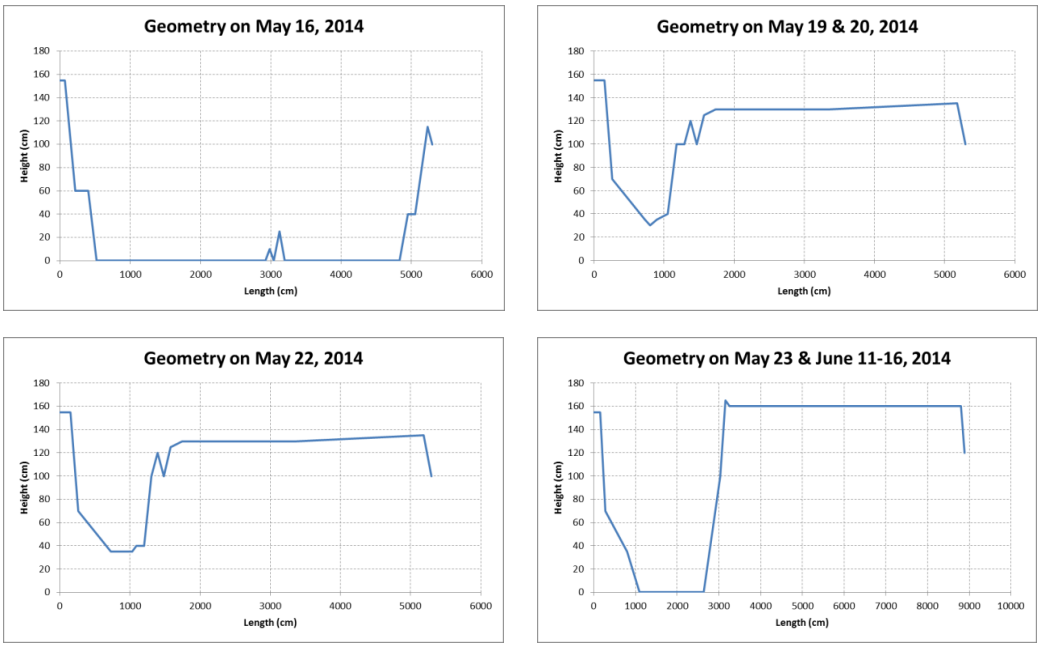

Figure 10-11: Pipe Geometry in Various NTNU Multiphase Lab Experiments

The qualitative and semi-quantitative data obtained from the experiments were supportive of the earlier findings, which is that slugs, if not completely prevented by additional pressure imposed by the choke, can accumulate at the choke opening and cause amplified pressure oscillations. This is especially true with very high pressure drop across the choke which is usually caused by very small choke opening. Extensive simulation work was also conducted to reproduce the lab experiments using OLGA and LedaFlow simulation packages.

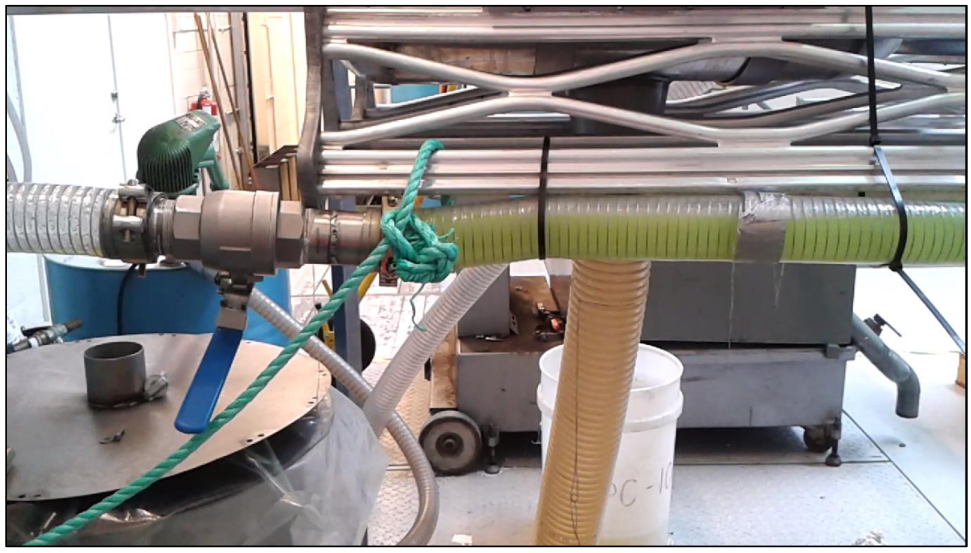

Figure 10-12: Accumulation of Liquid at the tight Valve Opening

10.3. Lab Experiments Results

Although a large number of experiments were conducted, only a few of them will be reported in this section, which reflects the most successful cases to reproduce the required phenomenon. A complete list of experiment results is available in Appendix-A. These experiments are associated with last pipe geometry, which was assembled on May 23, 2014 and used for the remaining period of experiments. The pressure logging frequency for all experiments was (1/100) milli-seconds.

10.3.1. May 25, 2014 – Experiment (02)

The experiment started with fully open valve for the first 20 minutes and then valve was gradually closed for the remaining 30 minutes of the experiment. The average flow rates recorded for this experiment were as follows:

Water flow rate (fully open valve) = 630 Kg/hr – USW = 0.064 m/sec
Air flow rate (fully open valve) = 3.1 Kg/hr – USG = 0.253 m/sec

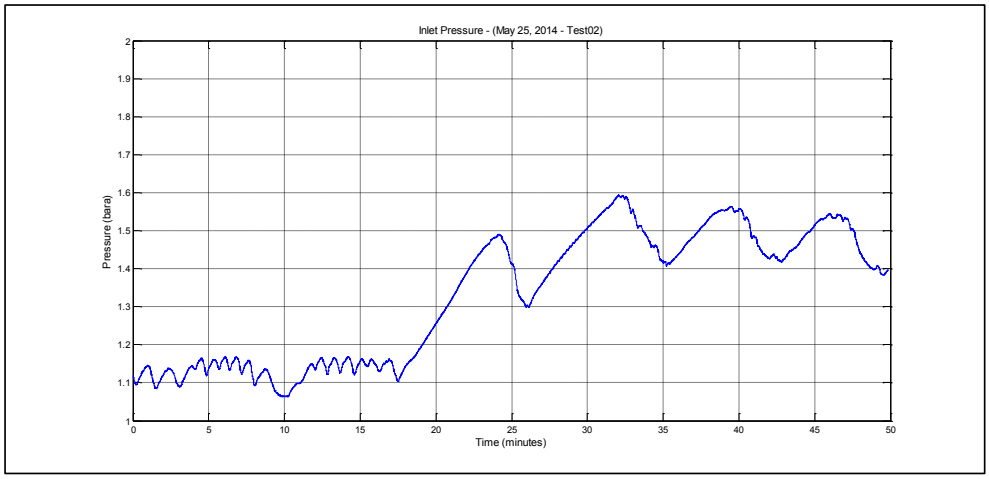

Figure 10-13: Inlet pressure log – May 25, 2014 Experiment-02

The inlet pressure log shown in Figure 10-13 indicates small scale slugs with fully open valve, where pressure oscillations were less than (0.1) bar in magnitude and approximately (1) minute in frequency. When the manual valve was choked, pressure fluctuation increased to approximately (0.2) bar in magnitude and a frequency of approximately (15) minutes.

This is mainly due to the accumulation of the initial small slugs at the tight valve opening which blocks the path for gas to penetrate and as such causes the pressure in the system to increase significantly and eventually creates even larger slugs, see Figure 10-12.

10.3.2. June 13, 2014 – Experiment (02)

Approximately (3) hours long experiment was carried out on June 13, 2014. A much higher air flow rate was used in this experiment (40.5) Kg/hr as opposed to only (3.1) Kg/hr in May 25, 2014 experiment. The experiment started with a fully open valve for about ten minutes and then the valve was tightly choked for almost (130) minutes. The valve was then fully open for (20) minutes and finally half choked for approximately (18) minutes. The average flow rates recorded for this experiment were as follows:

Water flow rate (fully open valve) = 630 Kg/hr – USW = 0.064 m/sec
Air flow rate (fully open valve) = 40.5 Kg/hr – USG = 3.321 m/sec

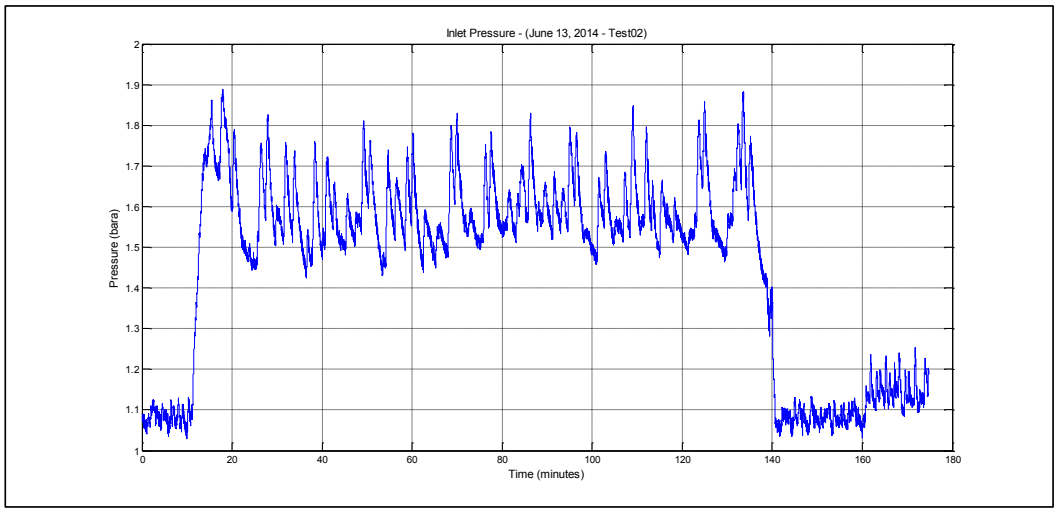

Figure 10-14: Inlet pressure log – June 13, 2014 Experiment-02

The higher air flow rate caused a higher frequency of fluctuations of approximately (1) minute with fully open valve. The amplitude of pressure fluctuation is around (0.05) bar. With tightly choked valve, the pressure fluctuation amplitude ranges between (0.2) and (0.3) bar, with approximately (5) minutes frequency. However, with half choked valve, the fluctuation frequency remained the same as fully open valve case at (1) minute with slightly higher amplitude of (0.1) bar, see Figure 10-14.

Here, we are also noticing the same phenomenon with a much higher air flow rate. The results in this experiment confirms the previous findings and emphasize the impact of very tight valve opening on the amplification of small slugs due to the accumulation of liquid at the valve opening.

10.3.3. June 13, 2014 – Experiment (03)

In this experiment a slightly higher air flow rate was used (60) Kg/hr. The experiment started with a fully open valve for about (15) minutes and then the valve was tightly choked for almost (50) minutes. The valve was then further choked for approximately (10) minutes and finally the valve was fully open for (10) minutes. The average flow rates recorded for this experiment were as follows:

Water flow rate (fully open valve) = 630 Kg/hr – USW = 0.064 m/sec
Air flow rate (fully open valve) = 59.5 Kg/hr – USG = 4.838 m/sec

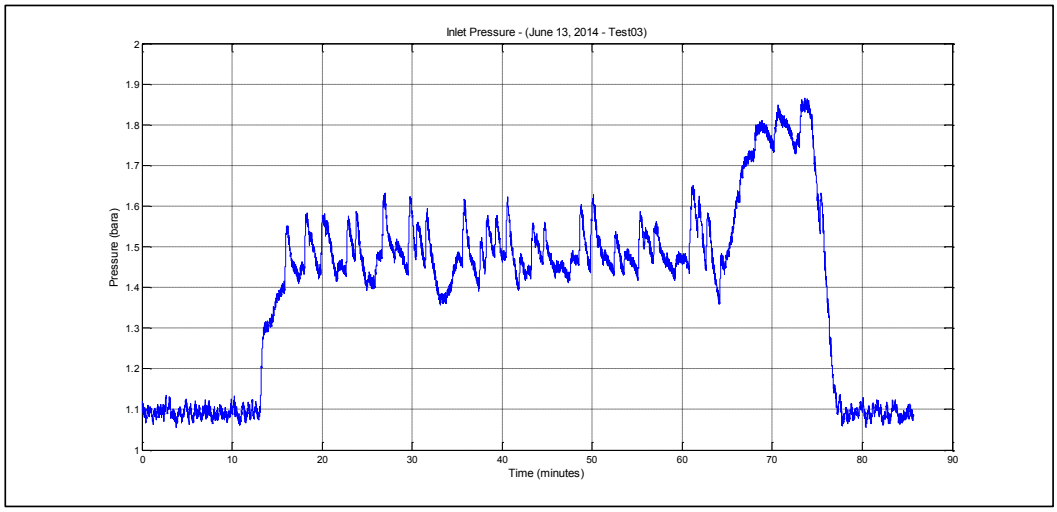

Figure 10-15: Inlet pressure log – June 13, 2014 Experiment-03

The higher air flow rate caused even a higher frequency of fluctuations of approximately (1/2) minute with fully open valve. The amplitude of pressure fluctuation is around (0.03) bar. With tightly choked valve, the pressure fluctuation amplitude ranges between (0.15) and (0.20) bar, with approximately (2) minutes frequency. Further choking of the manual valve caused the pressure to reach values close to the maximum allowable pressure in the system, which was set at 2.0 bara, and as such the measurement was stopped after just (10) minutes. However, the information obtained from those (10) minutes, shows the slugging is more well defined and slightly less frequent, with a frequency of (2) minutes and an amplitude of (0.1) bar, see Figure 10-15.

The same conclusion can be obtained from this experiment. It confirmed the behavior and showed that with further decrease of valve opening, liquid accumulation causes more pressure fluctuations and as such creates larger slugs in the pipeline system.

10.3.4. June 15, 2014 – Experiment (01)

In this experiment a very high water flow rate was used of approximately (1800) Kg/hr. The experiment started with a slightly choked valve for about (10) minutes and then the valve was further choked for almost (12) minutes. The valve was then tightly choked for approximately (12) minutes and finally the valve was fully open for about (10) minutes. The average flow rates recorded for this experiment were as follows:

Water flow rate (fully open valve) = 1800 Kg/hr – USW = 0.191 m/sec
Air flow rate (fully open valve) = 14 Kg/hr – USG = 1.159 m/sec

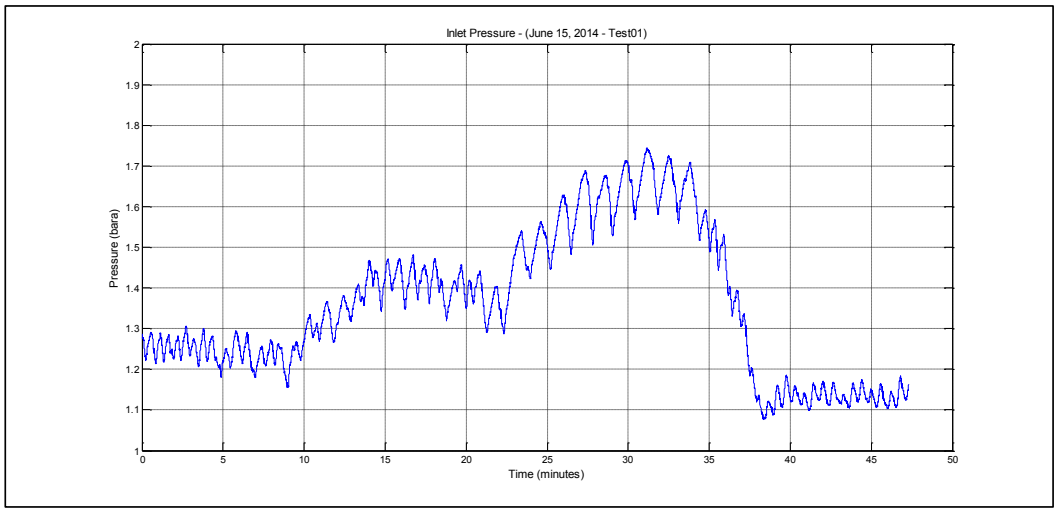

Figure 10-16: Inlet pressure log – June 15, 2014 Experiment-01

The higher water flow rate created a more well defined fluctuations with an amplitude of (0.06) bar and (1/2) minute frequency shown at the end of the plot in Figure 10-16. With almost half choked valve, shown at the beginning of the plot, one notices a slight increase in amplitude to (0.08) bar with the same frequency of (1/2) minute. Choking the valve even further seems to cause the slugs to merge, which results in a higher amplitude of (0.12) bar with a frequency of (1) minute. Finally, a tightly choked valve causes more slugs to merge and creates very well defined pressure oscillations with an amplitude of (0.18) bar and a frequency of (1.6) minutes.

The conclusion that can be obtained from this experiment is that even with a very high liquid flow rate which creates stable slugs with fully open valve, installing a choked valve at the end of the pipeline amplified those slugs and caused even a larger pressure oscillation in the system.

10.3.5. June 15, 2014 – Experiment (03)

In this experiment a very high water and air flow rates were used. The experiment started with a fully open valve for about (12) minutes and then the valve was further choked for almost (12) minutes. The valve was then tightly choked for approximately (12) minutes and finally the valve was fully open for about (8) minutes. The average flow rates recorded for this experiment were as follows:

Water flow rate (fully open valve) = 1800 Kg/hr – USW = 0.191 m/sec
Air flow rate (fully open valve) = 41 Kg/hr – USG = 3.362 m/sec

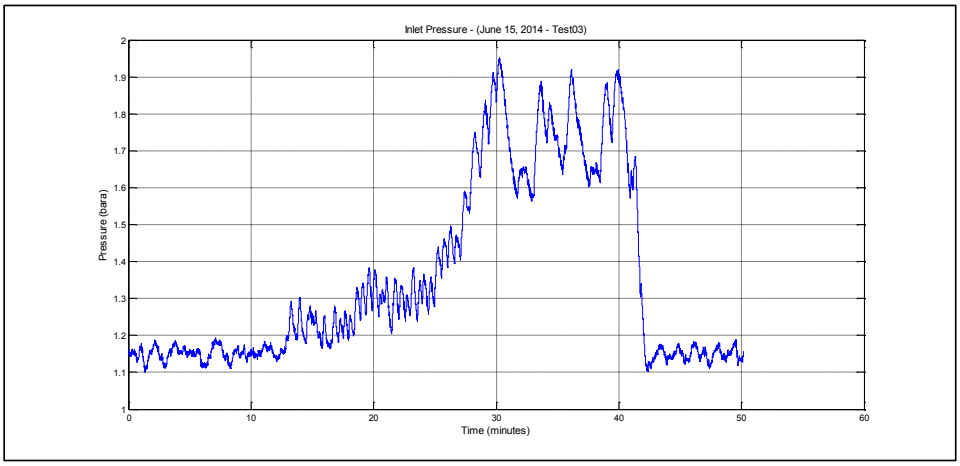

Figure 10-17: Inlet pressure log – June 15, 2014 Experiment-03

The higher water and air flow rates resulted in well-defined oscillations with fully opened valve. The amplitude of the oscillations was almost (0.08) bar with a frequency of almost (2) minutes. With a slightly more choked flow, the oscillations becomes slightly higher, (0.1) bar, with lower frequency of almost (1) minute. With tightly choked valve, the fluctuations are very clear and visible with an amplitude of approximately (0.3) bar and a (2) minutes frequency, see Figure 10-17.

This experiment provides yet another proof of the impact of choked valves on terrain-induced slug pipeline system when slugs are still created despite the introduction of the choked valves.

10.4. Simulation Modeling of Lab Experiments

The above (5) Lab experiments were simulated using OLGA and LedaFlow with different rates of success. The results are summarized below:

10.4.1. May 25, 2014 – Experiment (02) – Simulation

Several attempts were made to simulate this case using OLGA and LedaFlow without success. The case failed due to pressure exceeding the table values.

10.4.2. June 13, 2014 – Experiment (02) – Simulation

The case was successfully simulated with valve choked at 10%. OLGA simulation shows qualitatively the same behavior as the experiment results with slightly different slugging frequency. The amplitude to pressure fluctuation is also similar with approximately (0.2) bar for the lab experiment and (0.15) for the simulation. The difference in average pressure is about (0.8) bar but despite that difference the qualitative behavior is very similar and proves the choke induced slugs phenomena that was the motivation of these experiments. LedaFlow simulation results showed fixed pressure with choked valve at (2.4) bara.

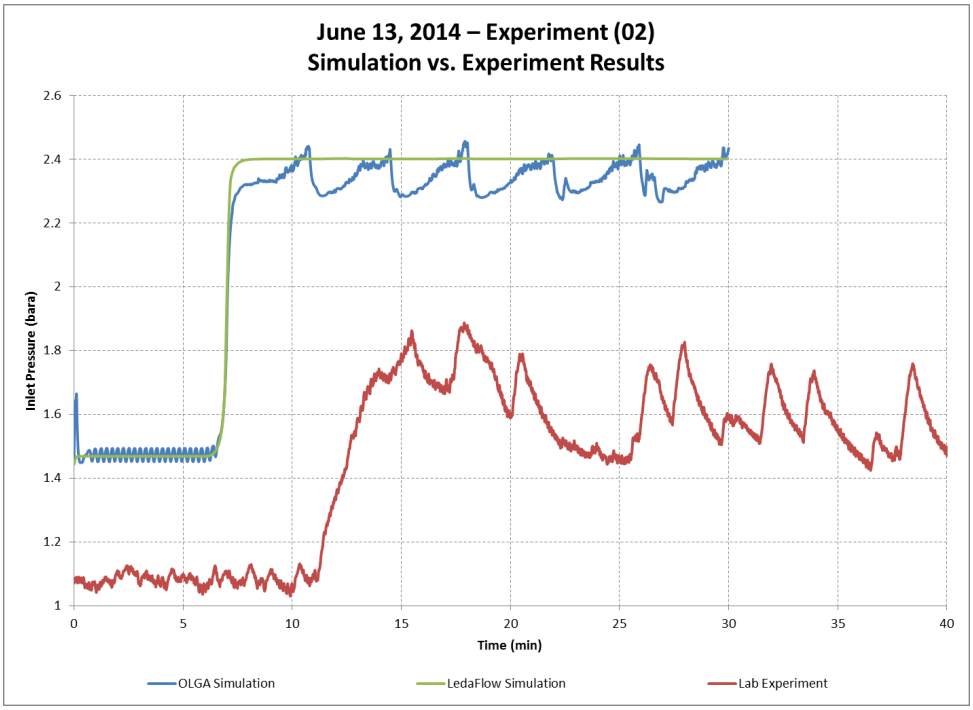

Figure 10-18: Simulation vs. Lab Experiments (June 13, 2014) – Experiment (02)

10.4.3. June 13, 2014 – Experiment (03) – Simulation

The case was successfully simulated with valve choked at 10%. OLGA simulation also showed good agreement with slugs frequency (3) minutes and amplitude of (0.2) bar. The difference in average pressure is about (1.0) bar. The results showed good agreement further proved the phenomena and confirm the behavior shown in the previous experiments simulation and results. LedaFlow showed fixed pressure with choked valve at (2.5) bara.

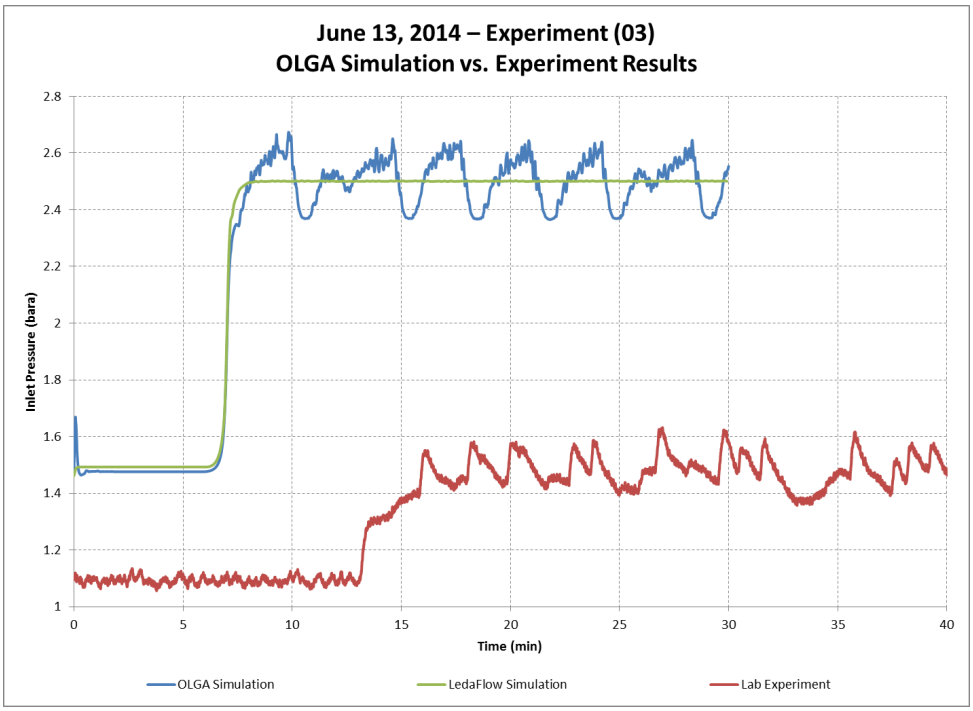

Figure 10-19: Simulation vs. Lab Experiments (June 13, 2014) – Experiment (03)

10.4.4. June 15, 2014 – Experiment (01) – Simulation

Several attempts were made to simulate this case using OLGA and LedaFlow without success. The case failed due to pressure exceeding the table values.

10.4.5. June 15, 2014 – Experiment (03) – Simulation

Several attempts were made to simulate this case using OLGA and LedaFlow without success. The case failed due to pressure exceeding the table values.

This page was intentionally left blank

11. FUTURE WORK

The focus of this work was on the collection and analysis of field measurements data. This should continue to be pursued in the future to document and analyze more field data which represents the true challenge for the multiphase flow simulation codes. The impact of scaling up the diameter coupled with a high pressure system could potentially lead to new challenges in the simulation of multiphase flow systems. An example of the positive impact this work had on multiphase flow simulation codes is the discovery of a major flaw in the OLGA slug tracking module.

Another challenge, which was visible in the simulation of the various cases, was the prediction of hydrodynamic slugs, which was shown to be a very difficult task for both slug tracking and slug capturing methods. None of the two approaches proved to be successful in simulating hydrodynamic slugs in a predictive manner.

Finally, more work should be carried out to investigate the new phenomenon which was discovered during the simulation of Field-A. The choked-valve induced slugs which was further confirmed by the lab experiments requires more research for correct mathematical modelling. More detailed experiments are also required in order to better understand the newly discovered behavior. More field measurements should also be carried out and is currently being planned at Saudi Aramco to investigate this with various flow rates and choke settings. New valve designs can be evaluated in order to minimize the liquid accumulation process when valves are choked.

This page was intentionally left blank

12. REFERENCES:

Abdul-Majeed, G. H. (2000). Liquid slug holdup in horizontal and slightly inclined two-phase slug flow. *Journal of Petroleum Science and Engineering, 27*(1), 27-32.

Al-Safran, E. (2009). Investigation and prediction of slug frequency in gas/liquid horizontal pipe flow. *Journal of Petroleum Science and Engineering, 69*(1-2), 143-155.

Al-Taweel, A. (2004). Saudi Aramco 1999 Data Comparison – Part 2. *Sacndpower, Norway*.

Alvarez, C., & Al-Awwami, M. (1999). *Wet Crude Transport Through a Complex Hilly Terrain Pipeline Network*.

Andreussi, P., Bendiksen, K., & Nydal, O. (1993). Void distribution in slug flow. *International journal of multiphase flow, 19*(5), 817-828.

Andreussi, P., Minervini, A., & Paglianti, A. (1993). Mechanistic model of slug flow in near-horizontal pipes. *AIChE journal, 39*(8), 1281-1291.

Andreussi, P., & Persen, L. (1987). Stratified gas-liquid flow in downwardly inclined pipes. *International journal of multiphase flow, 13*(4), 565-575.

Andreussi, P., Sangnes, E., Bonizzi, M., Nordsveen, M., Sletfjerding, E., & Berg Martiniussen, I. (2011). *Hydraulics Analysis of the Heidrun Offshore Field.* Paper presented at the 15th International Conference on Multiphase Production Technology.

Andritsos, N. (1986). *Effect of pipe diameter and liquid viscosity on horizontal stratified flow*: University of Illinois at Urbana-Champaign.

Andritsos, N., & Hanratty, T. (1987). Interfacial instabilities for horizontal gas-liquid flows in pipelines. *International journal of multiphase flow, 13*(5), 583-603.

Baker, O. (1954). Simultaneous flow of oil and gas. *Oil and Gas Journal, 53*, 583–603.

Barnea, D. (1987). A unified model for predicting flow-pattern transitions for the whole range of pipe inclinations. *International Journal of Multiphase Flow, 13*(1), 1–12.

Barnea, D., & Brauner, N. (1985). Holdup of the liquid slug in two phase intermittent flow. *International Journal of Multiphase Flow, 11*(1), 43-49.

Barnea, D., & Taitel, Y. (1989). Transient-formulation modes and stability of steady-state annular flow. *Chemical engineering science, 44*(2), 325-332.

Barnea, D., & Taitel, Y. (1993). Kelvin-Helmholtz stability criteria for stratified flow: viscous versus non-viscous (inviscid) approaches. *International journal of multiphase flow, 19*(4), 639-649.

Bendiksen, K. H. (1984). An experimental investigation of the motion of long bubbles in inclined tubes. *International Journal of Multiphase Flow, 10*(4), 467–483.

Bendiksen, K. H., & Espedal, M. (1992). Onset of slugging in horizontal gas-liquid pipe flow. *International journal of multiphase flow, 18*(2), 237-247.

Bendiksen, K. H., Espedal, M., & Malnes, D. (1988). *Phyiscal and Numerical Simulaiton of Dynamic Two-Phase Flow in Pipelines with Applicaitons to Existing Oil-Gas Field Lines*. Paper presented at the Conference on multiphase flow in industrial plants.

Bendiksen, K. H., Maines, D., Moe, R., & Nuland, S. (1991). The dynamic two-fluid model OLGA: Theory and application. *SPE production engineering, 6*(02), 171-180.

Bendiksen, K. H., Malnes, D., & Nydal, O. J. (1996). On the modelling of slug flow. *Chemical Engineering Communications, 141*(1), 71-102.

Benjamin, T. B. (1968). Gravity Currents and related phenomena. *Journal of Fluid Mechanics, 31*, 209-248.

Biberg, D. (1999). Liquid wall friction in two-phase turbulent gas laminar liquid stratified pipe flow. *The Canadian Journal of Chemical Engineering, 77*(6), 1073-1082.

Boe, A. (1981). Severe slugging characteristics. *Sel. Top. Two-Phase Flow, NTH, Trondheim, Norway*.

Bonizzi, M. (2003). *Transient one-dimensional modelling of multiphase slug flows.* Imperial College London (University of London).

Bratland, O. (2010). Pipe Flow 2, Multi-phase flow assurance, p. 41-93 [Electronic book]. *Availabl e: http://drbratland. com/PipeFlow2/index. html*.

Brill, J. P., Schmidt, Z., Coberly, W. A., Herring, J. D., & Moore, D. W. (1981). Analysis of two-phase tests in large-diameter flow lines in Prudhoe Bay field. *Society of Petroleum Engineers Journal, 21*(03), 363-378.

Cheremisinoff, N. P., & Davis, E. J. (1979). Stratified turbulent-turbulent gas-liquid flow. *AIChE journal, 25*(1), 48-56.

Cohen, L. S., & Hanratty, T. J. (1968). Effect of waves at a gas—liquid interface on a turbulent air flow. *Journal of Fluid Mechanics, 31*(03), 467-479.

Cook, M., & Behnia, M. (2000). Pressure drop calculation and modelling of inclined intermittent gas–liquid flow. *Chemical Engineering Science, 55*(20), 4699-4708.

Courbot, A. (1996). *Prevention of Severe Slugging in the Dunbar 16' Multiphase Pipeline*.

Danielson, T. J., Bansal, K. M., Djoric, B., Larrey, D., Johansen, S. T., De Leebeeck, A., & Kjolaas, J. (2012). *Simulation of slug flow in oil and gas pipelines using a new transient simulator.* Paper presented at the Offshore Technology Conference.

Danielson, T. J., Bansal, K. M., Hansen, R., & Leporcher, E. (2005). *LEDA: the next multiphase flow performance simulator.* Paper presented at the 12th International Conference on Multiphase Production Technology.

Dukler, A., & Fabre, J. (1994). GAS-LIQUID SLUG FLOW. *Multiphase science and technology, 8*(1-4).

Dukler, A. E., & Hubbard, M. G. (1975). A model for gas-liquid slug flow in horizontal and near horizontal tubes. *Industrial & Engineering Chemistry Fundamentals, 14*(4), 337-347.

Einstein, A. (1906). A new determination of molecular dimensions. *Ann. Phys, 19*(2), 289-306.

Espedal, M. (1998). An experimental investigation of stratified two-phase pipe flow at small inclinations. *Norwegian University of Science and Technology (NTNU), Department of Applied Mechanics, Thermo-and Fluid Dynamics*.

Espedal, M. (1999). Saudi Aramco 1999 Field Measurement Report. *Scandpower report no. 52.30.04/R1*.

Evans, R. D. (1955). *The atomic nucleus* (Vol. 582): McGraw-Hill New York.

Fabre, J. (2002). *Gas-liquid Slug Flow*. Paper presented at the Modelling and Control of Two-Phase Flow Phenomena.

Fabre, J., Grenier, P., & Gadoin, E. (1993). *Evolution of slug flow in long pipe*. Paper presented at the 6th International Conference in Multiphase Production.

Fabre, J., & Liné, A. (1992). Modeling of two-phase slug flow. *Annual Review of Fluid Mechanics, 24*(1), 21-46.

Falcone, G., F.Hewitt, G., & Alimonti, C. (2009). *Multiphase Flow Metering Handbook* (First Edition ed.). Great Britain: Elsevier.

Fan, Y., Clausen, R., Lockett, T., & Schutte, R. (2013). *Measurement and simulation of slug flow in a large diameter three-phase pipeline*. Paper presented at the 16th International Conference on Multiphase Production Technology.

Fard, M. P., Godhavn, J.-M., & Sagatun, S. I. (2006). Modeling of Severe Slug and Slug Control With OLGA.

Fuchs, P. (1997). *Kompendium - Fag 67173 Flerfase Rørstrømning (Compendium, Multiphase Pipe Flow, rev. 1997 Edition).* NTNU, Norwegian University of Science and Technology, Trondheim, Norway.

Godhavn, J.-M., Fard, M. P., & Fuchs, P. H. (2005). New slug control strategies, tuning rules and experimental results. *Journal of Process Control, 15*(5), 547-557.

Godhavn, J.-M., Strand, S., & Skofteland, G. (2005). *Increased oil production by advanced control of receiving facilities*. Paper presented at the IFAC world congress, Prague, Czech Republic.

Gomez, L., Shoham, O., & Taitel, Y. (2000). Prediction of slug liquid holdup: horizontal to upward vertical flow. *International Journal of Multiphase Flow, 26*(3), 517-521.

Gregory, G., Nicholson, M., & Aziz, K. (1978). Correlation of the liquid volume fraction in the slug for horizontal gas-liquid slug flow. *International Journal of Multiphase Flow, 4*(1), 33-39.

Gregory, G., & Scott, D. (1969). Correlation of liquid slug velocity and frequency in horizontal cocurrent gas-liquid slug flow. *AIChE Journal, 15*(6), 933-935.

Greskovich, E. J., Shrier, A. L. (1972). Slug frequency in horizontal gas-liquid slug flow Measurement and Instrumentation. *Ind. Eng. Chem. Proc. Design Dev, 11*(2), 317–318.

Hart, J., Hamersma, P., & Fortuin, J. (1989). Correlations predicting frictional pressure drop and liquid holdup during horizontal gas-liquid pipe flow with a small liquid holdup. *International Journal of Multiphase Flow, 15*(6), 947-964.

Havre, K., & Dalsmo, M. (2002). Active Feedback Control as a Solution to Severe Slugging. *Society of Petroleum Engineers*(SPE 79252).

Havre, K., Stornes, K., & Stray, H. (2000). Taming slug flow in pipelines. *ABB Review, December 2000*(No. 4), 55-63.

Henriot, V., Courbot, A., Heitzé, E., & Moyeux, L. (1999). Simulation of process to control severe slugging: Application to the Dunbar pipeline. *SPE Annual Technical Conference and Exhibition, SPE 56461*.

Hidy, G. M., & Plate, E. J. (1966). Wind action on water standing in a laboratory channel. *Journal of Fluid Mechanics, 26*(04), 651-687.

Hubbard;, M. (1965). *An analysis of horizontal gas-liquid slug flow. Ph.D. Thesis, .* University of Houston, Houston, Texas USA

Hurlburt, E., & Hanratty, T. (2002). Prediction of the transition from stratified to slug and plug flow for long pipes. *International journal of multiphase flow, 28*(5), 707-729.

Issa, R., & Kempf, M. (2003). Simulation of slug flow in horizontal and nearly horizontal pipes with the two-fluid model. *International journal of multiphase flow, 29*(1), 69-95.

Issa, R., & Woodburn, P. (1998). *Numerical prediction of instabilities and slug formation in horizontal two-phase flows.* Paper presented at the 3rd International Conference on Multiphase Flow, ICMF98, Lyon, France.

Jahanshahi, E., Skogestad, S., & Helgesen, A. H. (2012). *Controllability analysis of severe slugging in well-pipeline-riser systems.* Paper presented at the Proceedings of the 2012 IFAC Workshop on Automatic Control in Offshore Oil and Gas Production, Trondheim, Norway.

Jansen, F. E., Shoham, O., & Taitel, Y. (1996). The elimination of severe slugging—experiments and modeling. *International Journal of Multiphase Flow, 22*(6), 1055-1072.

Kawaji, M., Anoda, Y., Nakamura, H., & Tasaka, T. (1987). Phase and velocity distributions and holdup in high-pressure steam/water stratified flow in a large diameter horizontal pipe. *Int. J. Multiphase Flow, 13*(2), 145–159.

Kim, H., Lee, S., & Bankoff, S. (1985). Heat transfer and interfacial drag in countercurrent steam-water stratified flow. *International journal of multiphase flow, 11*(5), 593-606.

Kordyban, E. (1977). The transition to slug flow in the presence of large waves. *International Journal of Multiphase Flow, 3*(6), 603-607.

Kristiansen, O. (2004). *Experiments on the transition from stratified to slug flow in multiphase pipe flow.* NTNU - Norwegian University of Science and Technology, Trondheim, Norway.

Lin, P., & Hanratty, T. (1986). Prediction of the initiation of slugs with linear stability theory. *International journal of multiphase flow, 12*(1), 79-98.

Linehan, J. H. (1968). *INTERACTION OF TWO-DIMENSIONAL, STRATIFIED, TURBULENT AIR--WATER AND STEAM--WATER FLOWS*: Argonne National Lab., Ill.

Linga, H. (1991). *Measurements of Two Phase Flow Details - Non-Intrusive Methods Applied to Slug and Dispersed Flows.* NTNU, Trondheim, Norway.

Linga, H. (1997). *Modeling of Non-Ideal Effects of Gamma Densitometers*. Paper presented at the 4th World Conference on Experimental Heat Transfer, Fluid Mechanics and Thermodynamics.

Maher, K. (2006). Basic Physics of Nuclear Medicine Available from http://en.wikibooks.org/wiki/Basic_Physics_of_Nuclear_Medicine

Malnes, D. (1983). *Slug flow in vertical, horizontal and inclined pipes*: Institute for Energy Technology (IFE).

Mandhane, J., Gregory, G., & Aziz, K. (1974). A flow pattern map for gas—liquid flow in horizontal pipes. *International Journal of Multiphase Flow, 1*(4), 537-553.

McAlister, D. R. (2012). *Gamma Ray Attenuation Properties of Common Shielding Materials*. IL 60532, USA: PG Research Foundation, Inc. 1955 University Lane Lisle.

Milne-Thomson, L., & Rott, N. (1968). Theoretical hydrodynamics. *Journal of Applied Mechanics, 35*, 846.

Mishima, K., & Ishii, M. (1980). Theoretical prediction of onset of horizontal slug flow. *Journal of Fluids Engineering, 102*(4), 441-445.

Nicholson, M., Aziz, K., & Gregory, G. (1978). Intermittent two phase flow in horizontal pipes: predictive models. *The Canadian Journal of chemical engineering, 56*(6), 653-663.

Nicklin, D., Wilkes, J., & Davidson, J. (1962). Two-phase flow in vertical tubes. *Trans. Inst. Chem. Eng, 40*(1), 61-68.

Nydal, O., & Andreussi, P. (1991). Gas entrainment in a long liquid slug advancing in a near horizontal pipe. *International journal of multiphase flow, 17*(2), 179-189.

Nydal, O., & Banerjee, S. (1996). Dynamic slug tracking simulations for gas-liquid flow in pipelines. *Chemical Engineering Communications, 141*(1), 13-39.

Nydal, O., Pintus, S., & Andreussi, P. (1992). Statistical characterization of slug flow in horizontal pipes. *International Journal of Multiphase Flow, 18*(3), 439-453.

Olsen, H. (2006). *Anti-slug control and topside measurements for pipeline-riser system.* Unpublished Master Thesis, Norwegian University of Science and Technology, Trondheim, Norway.

Petrick, M., & Swanson, B. S. (1958). Radiation Attenuation Method of Measuring Density of a Two-Phase Fluid. *The Review of Scientific Instruments, 29*, 1079-1085.

Rasmussen, J. (2004). Saudi Aramco 1999 Data Comparison – Part 1. *Sacndpower, Norway*.

Rogero, E. C. (2009). *Experimental Investigation of Developing Plug and Slug Flows.* Universität München.

Russell, T., Etchells, A., Jensen, R., & Arruda, P. (1974). Pressure drop and holdup in stratified gas-liquid flow. *AIChE Journal, 20*(4), 664-669.

Schmidt, Z., Brill, J., & Beggs, H. (1979). Choking can eliminate severe pipeline slugging. *Oil & gas journal, 77*(46), 230-&.

Shea, R., Eidsmoen, H., Nordsveen, M., Rasmussen, J., Xu, Z., Nossen, J. (2004). *Slug frequency prediction method comparison.* Paper presented at the BHRG Multiphase Production Technology Proceedings, Banff, Canada.

Skofteland, G., & Godhavn, J. M. (2003). Suppression of Slugs in MultiphaseFlow Lines by Active Use of Topside Choke—Field Experience and ExperimentalResults, *Proc. of the 11thBHR GroupIntl. Conference on MultiphaseProduction, San Romeo, Italy*.

Storkaas, E. (2005). *Stabilizing control and controllability-Control solutions to avoid slug flow in pipeline-riser systems.* Norwegian University of Science and Technology, Trondheim, Norway.

Taitel, Y. (1986). Stability of severe slugging. *International journal of multiphase flow, 12*(2), 203-217.

Taitel, Y., & Barnea, D. (1990). Two Phase Slug Flow *Advances in Heat Transfer* (Vol. 20, pp. 83 - 132). San Diego, California: Academic Press Inc.

Taitel, Y., Bornea, D., & Dukler, A. (1980). Modelling flow pattern transitions for steady upward gas-liquid flow in vertical tubes. *AIChE Journal, 26*(3), 345-354.

Taitel, Y., & Dukler, A. E. (1976). A model for predicting flow regime transitions in horizontal and near horizontal gas-liquid flow. *AIChE Journal, 22*(1), 47-55.

Taitel, Y., & Dukler, A. E. (1977). A model for slug frequency during gas-liquid flow in horizontal and near horizontal pipes. *International Journal of Multiphase Flow, 3*(6), 585-596.

Taitel, Y., Vierkandt, S., Shoham, O., & Brill, J. P. (1990). Severe slugging in a riser system: experiments and modeling. *International journal of multiphase flow, 16*(1), 57-68.

Taylor, G. I. (1932). The viscosity of a fluid containing small drops of another fluid. *Proceedings of the Royal Society of London. Series A, 138*(834), 41-48.

Tomiyama, A. (1998). *Struggle with computational bubble dynamics*. Paper presented at the Third international conference on multi-phase flow (1998).

Wallis, G. B. (1969). One-dimensional two-phase flow.

Woods, B. D., & Hanratty, T. J. (1999). Influence of Froude number on physical processes determining frequency of slugging in horizontal gas–liquid flows. *International journal of multiphase flow, 25*(6), 1195-1223.

Yocum, B. T. (1973). *Offshore Riser Slug Flow Avoidance: Mathematical Models for Design and Optimization*. Paper presented at the SPE Europe Meeting.

Zabaras, G. (2000). Prediction of slug frequency for gas/liquid flows - SPE 65093. *SPE Journal, 5*(3).

Zheng, G., Brill, J. P., & Taitel, Y. (1994). Slug flow behavior in a hilly terrain pipeline. *International Journal of Multiphase Flow, 20*(1), 63-79.

This page was intentionally left blank

13. APPENDIX-A: Full List of Lab Experiments

This appendix contains the full list of all of the (37) lab experiments that was conducted to investigate the effect of choked valves on terrain-induced slugs. A set of four geometrical configurations were investigated shown in Figure **10-11**.

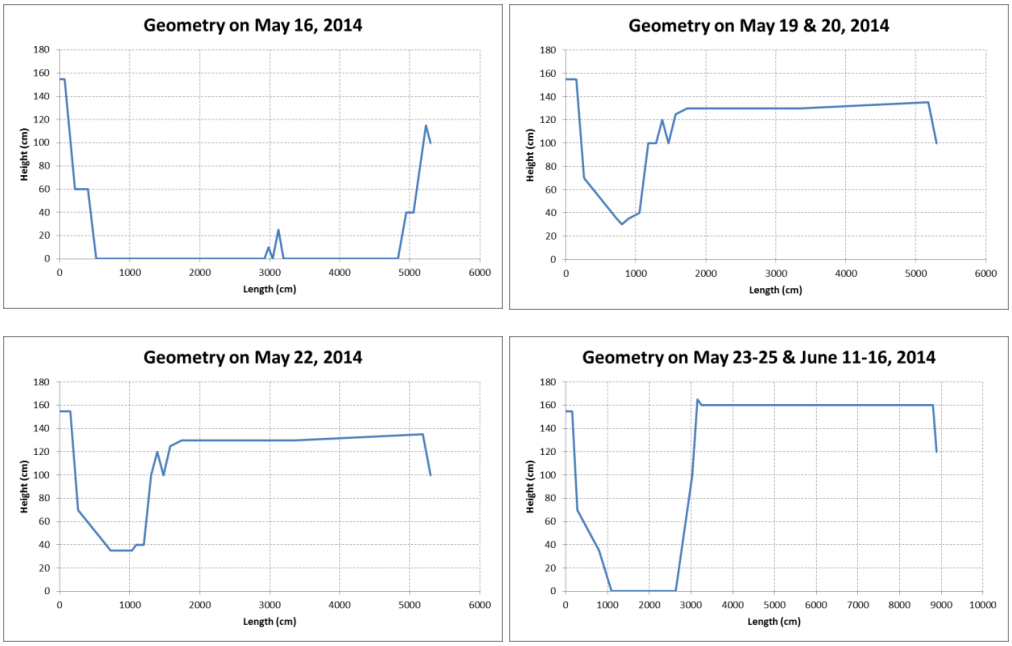

Figure 13-1: Pipe Geometry in Various NTNU Multiphase Lab Experiments

These experiments were conducted at NTNU multiphase flow laboratory between May and June, 2014. The objective of these experiments was to investigate the impact of valve choking on terrain-induced slugs and verify the simulation behavior noted when analyzing the field measurements in Field-A, where slugs amplified due to the existence of slug valves at the end of a highly terrain multiphase flow pipeline.

This phenomenon was counter-intuitive as valves are normally introduced to completely eliminate or at least reduce slugging phenomena in multiphase flow pipelines. The experiments were conducted using air and water, with a set of transparent fixed and flexible pipes which were 60 mm in diameter.

The air and water were mixed together in a mixing section before traveling through the 50 to 100 meter long pipe, depending on the pipe configuration. Air was drawn from the building air system and connected to an air tank which provided the required compressibility force in the pipeline system. The water was drawn from the bottom of a separator and was pumped into the pipe through a centrifugal pump.

The inlet pressure and air and water flow rates were logged for each experiment and the manual valve installed at the end of the pipe was manually opened and closed to examine its impact on flow behavior. A schematic of the general experiment setup is shown in Figure **10-10**.

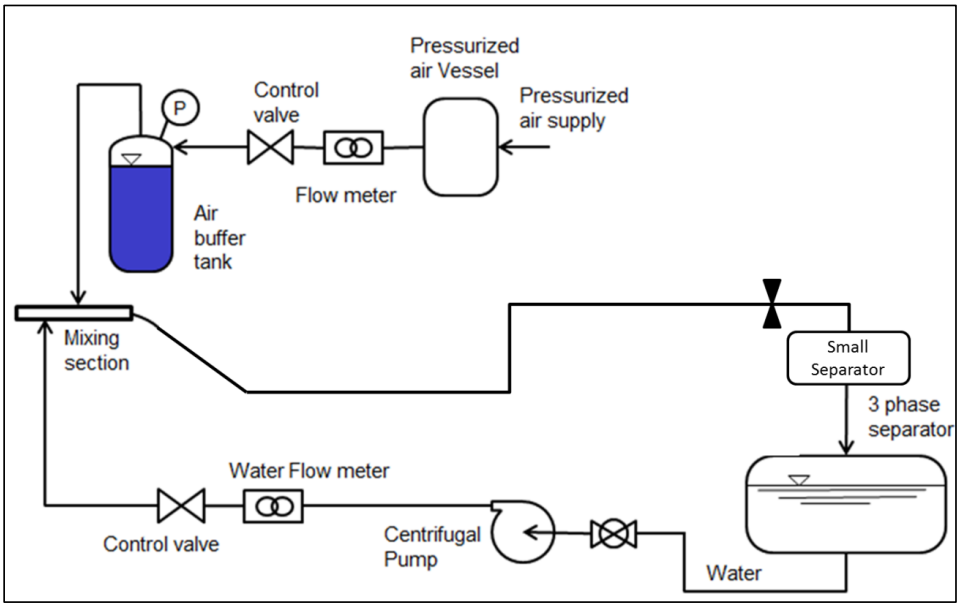

Figure 13-2: General Lab Experiments Schematic at NTNU Multiphase Flow Laboratory

The overall conclusion from these experiments was a further confirmation of the negative impact of choked valves on terrain-induced slugs, when slugs are created in the system. In other words, if the additional force exerted by the valve pressure drop is not sufficient to overcome the compressibility force and therefore eliminate the slugs, slugs are amplified by the presence of the choked valve in the pipeline system.

The amplification of the slugs occur due to the accumulation of liquid at the tight valve opening which results in a complete blockage which in turn compresses the gas upstream of the liquid and causes further enhancement of the pressure fluctuations and slug generation in the pipeline system.

Air and water flow rates were varied to investigate the various flow conditions and the table below shows the list of all the flow rate conditions examined during these experiments:

Table 13-1: NTNU Multiphase Flow Lab Experiments – Air and Water Flow Rates

Multiphase Flow Lab Experiments	Air Flow Rate (Kg/hr)	Air Flow Rate (USG) (m/sec)	Water Flow Rate (Kg/hr)	Water Flow Rate (USW) (m/sec)
May 16, 2014 – Experiment (01)	42.5	3.468	1,868	0.184
May 16, 2014 – Experiment (02)	42.5	3.468	1,868	0.184
May 19, 2014 – Experiment (01)	51.5	4.202	129	0.013
May 20, 2014 – Experiment (01)	24.7	2.015	1,257	0.124
May 20, 2014 – Experiment (02)	24.7	2.015	359	0.035
May 20, 2014 – Experiment (03)	78	6.364	1,689	0.166
May 20, 2014 – Experiment (04)	43.5	3.549	1,689	0.166
May 20, 2014 – Experiment (05)	8.2	0.669	1,689	0.166
May 22, 2014 – Experiment (01)	5	0.408	1,617	0.159
May 23, 2014 – Experiment (01)	29.8	2.431	1,257	0.124
May 23, 2014 – Experiment (02)	13.9	1.134	1,257	0.124
May 23, 2014 – Experiment (03)	13.9	1.134	1,257	0.124
May 24, 2014 – Experiment (01)	41	3.345	855	0.084
May 24, 2014 – Experiment (02)	18.7	1.526	1,958	0.193
May 25, 2014 – Experiment (01)	14.1	1.150	848	0.083
May 25, 2014 – Experiment (02)	3.1	0.253	647	0.064
May 25, 2014 – Experiment (03)	3.1	0.253	647	0.064
May 25, 2014 – Experiment (04)	3.1	0.253	1,617	0.159
May 25, 2014 – Experiment (05)	29.7	2.423	1,024	0.101
May 25, 2014 – Experiment (06)	53.8	4.390	1,024	0.101
June 11, 2014 – Experiment (01)	3.4	0.277	309	0.030
June 12, 2014 – Experiment (01)	3.2	0.261	503	0.050
June 12, 2014 – Experiment (02)	3.2	0.261	647	0.064
June 12, 2014 – Experiment (03)	7.2	0.587	647	0.064
June 12, 2014 – Experiment (04)	10.2	0.832	647	0.064
June 12, 2014 – Experiment (05)	19.3	1.575	647	0.064
June 13, 2014 – Experiment (01)	28.7	2.342	647	0.064
June 13, 2014 – Experiment (02)	40.7	3.321	647	0.064
June 13, 2014 – Experiment (03)	59.3	4.838	647	0.064
June 13, 2014 – Experiment (04)	14.2	1.159	1,940	0.191
June 15, 2014 – Experiment (01)	14.2	1.159	1,940	0.191
June 15, 2014 – Experiment (02)	30.1	2.456	1,940	0.191
June 15, 2014 – Experiment (03)	41.2	3.362	1,940	0.191
June 16, 2014 – Experiment (01)	40.7	3.321	1,028	0.101
June 16, 2014 – Experiment (02)	40.7	3.321	384	0.038
June 16, 2014 – Experiment (03)	29.7	2.423	384	0.038
June 16, 2014 – Experiment (04)	19.8	1.616	384	0.038

12.1 May 16, 2014 – Experiment (01)

The experiment started and ended with choked valve and half way through the experiment, the valve was slightly choked more as can be seen from the slight increase in fluctuation pressure at minute (22). The average flow rates recorded for this experiment were as follows:

Water flow rate (fully open valve) = 0.52 lit/sec
Air flow rate (fully open valve) = 42.5 Kg/hr

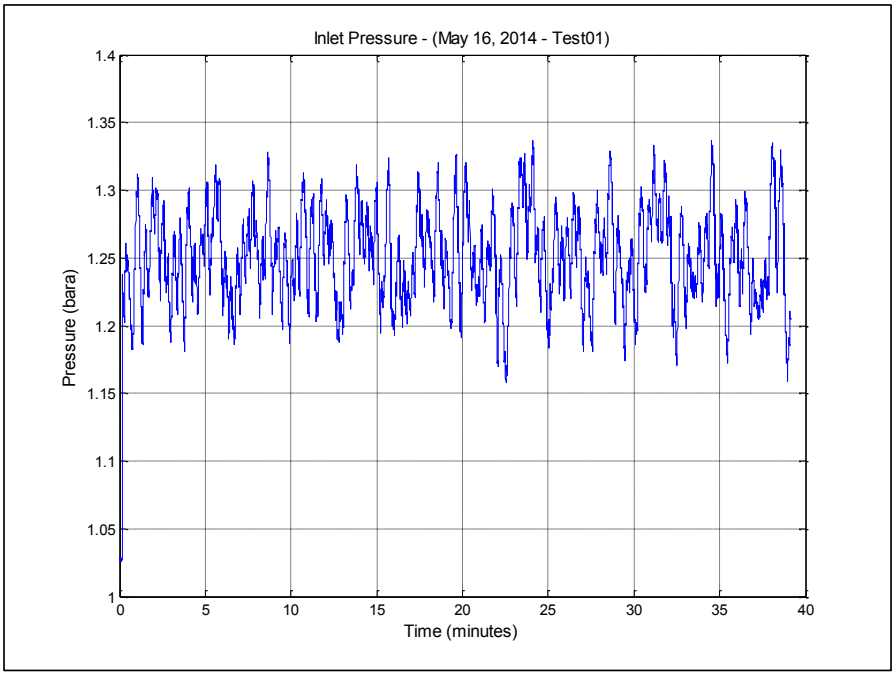

Figure 13-3: Inlet pressure log – May 16, 2014 Experiment-01

12.2 May 16, 2014 – Experiment (02)

The experiment started with a fully open valve for about (55) minutes and then the valve was tightly choked for almost (20) minutes. The valve was then fully open for (20) minutes. The average flow rates recorded for this experiment were as follows:

Water flow rate (fully open valve) = 0.52 lit/sec
Air flow rate (fully open valve) = 42.5 Kg/hr

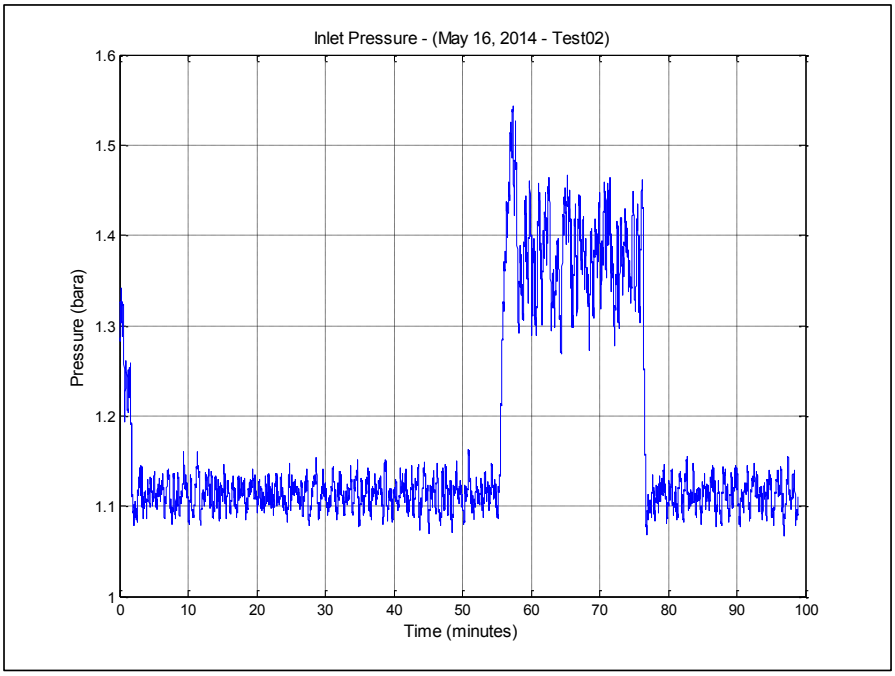

Figure 13-4: Inlet pressure log – May 16, 2014 Experiment-02

12.3 May 19, 2014 – Experiment (01)

The experiment started fully choked valve and half way through the experiment the valve was fully open. The average flow rates recorded for this experiment were as follows:

Water flow rate (fully open valve) = 0.036 lit/sec
Air flow rate (fully open valve) = 51.5 Kg/hr

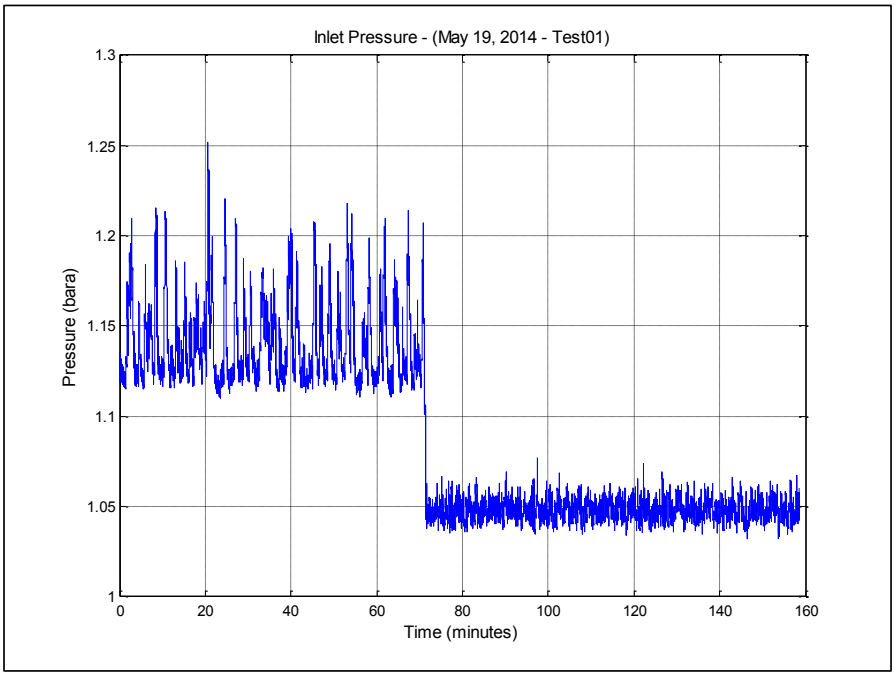

Figure 13-5: Inlet pressure log – May 19, 2014 Experiment-01

12.4 May 20, 2014 – Experiment (01)

The experiment started fully choked valve and half way through the experiment the valve was fully open. The average flow rates recorded for this experiment were as follows:

Water flow rate (fully open valve) = 0.35 lit/sec
Air flow rate (fully open valve) = 24.7 Kg/hr

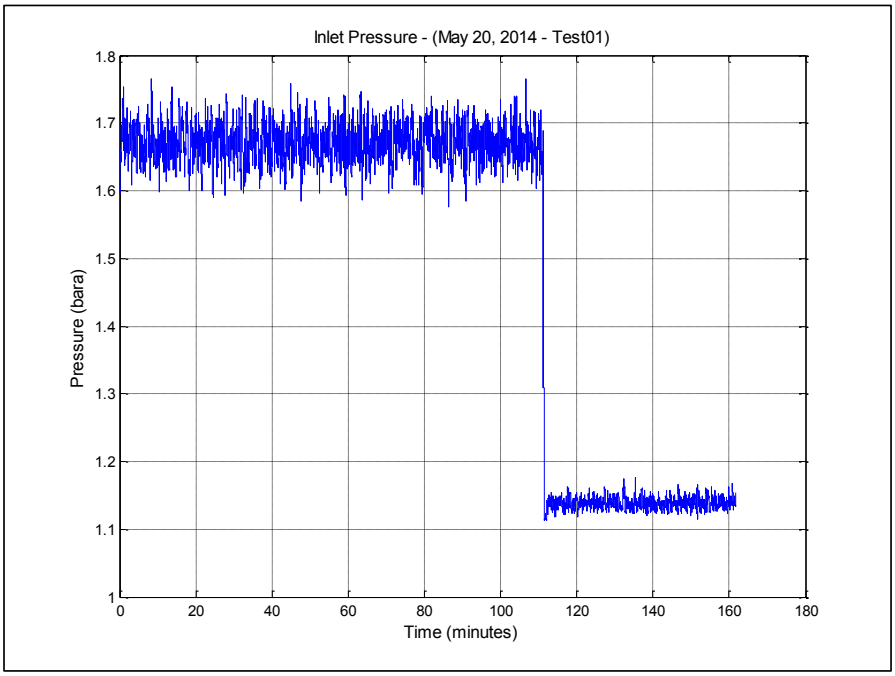

Figure 13-6: Inlet pressure log – May 20, 2014 Experiment-01

12.5 May 20, 2014 – Experiment (02)

The experiment started fully choked valve and half way through the experiment the valve was fully open. The average flow rates recorded for this experiment were as follows:

Water flow rate (fully open valve) = 0.1 lit/sec
Air flow rate (fully open valve) = 24.7 Kg/hr

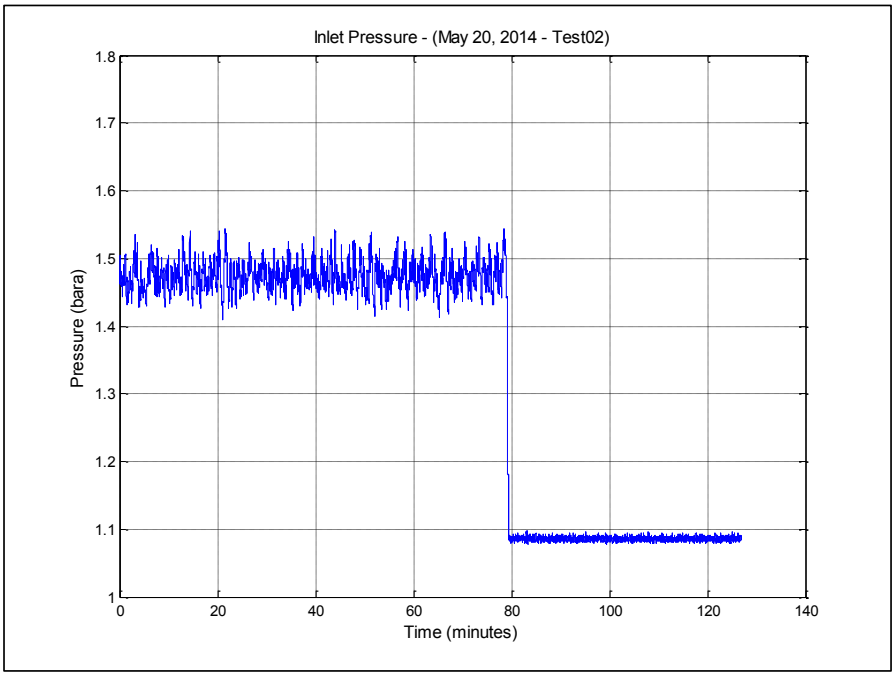

Figure 13-7: Inlet pressure log – May 20, 2014 Experiment-02

12.6 May 20, 2014 – Experiment (03)

The experiment started fully choked valve and half way through the experiment the valve was fully open. The average flow rates recorded for this experiment were as follows:

Water flow rate (fully open valve) = 0.47 lit/sec
Air flow rate (fully open valve) = 78 Kg/hr

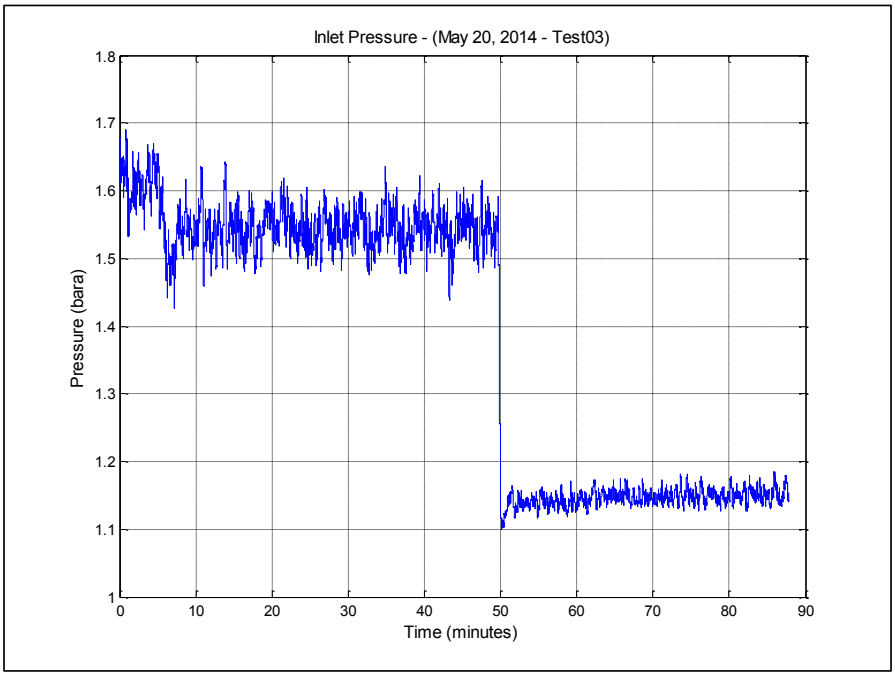

Figure 13-8: Inlet pressure log – May 20, 2014 Experiment-03

12.7 May 20, 2014 – Experiment (04)

The experiment started fully choked valve and half way through the experiment the valve was fully open. The average flow rates recorded for this experiment were as follows:

Water flow rate (fully open valve) = 0.47 lit/sec
Air flow rate (fully open valve) = 43.5 Kg/hr

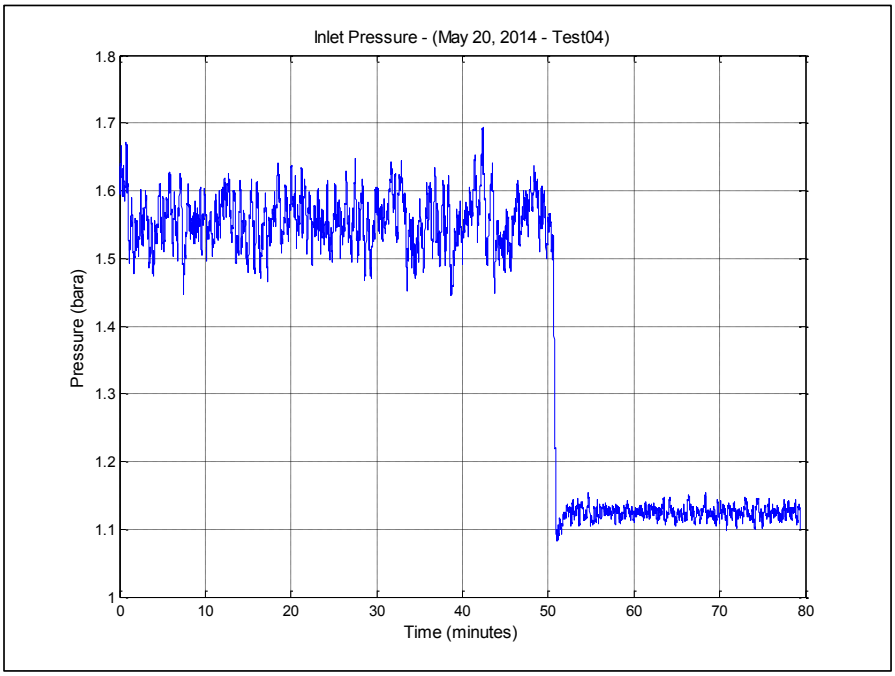

Figure 13-9: Inlet pressure log – May 20, 2014 Experiment-04

12.8 May 20, 2014 – Experiment (05)

The experiment started fully choked valve and half way through the experiment the valve was fully open. The average flow rates recorded for this experiment were as follows:

Water flow rate (fully open valve) = 0.47 lit/sec
Air flow rate (fully open valve) = 8.2 Kg/hr

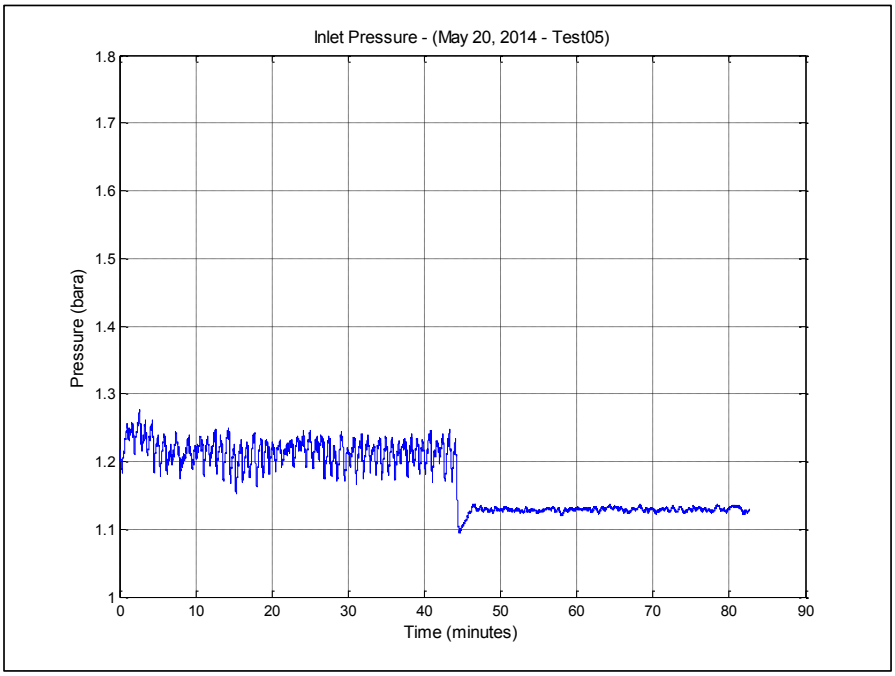

Figure 13-10: Inlet pressure log – May 20, 2014 Experiment-05

12.9 May 22, 2014 – Experiment (01)

The experiment started fully choked valve and half way through the experiment the valve was fully open. The average flow rates recorded for this experiment were as follows:

Water flow rate (fully open valve) = 0.45 lit/sec
Air flow rate (fully open valve) = 5.0 Kg/hr

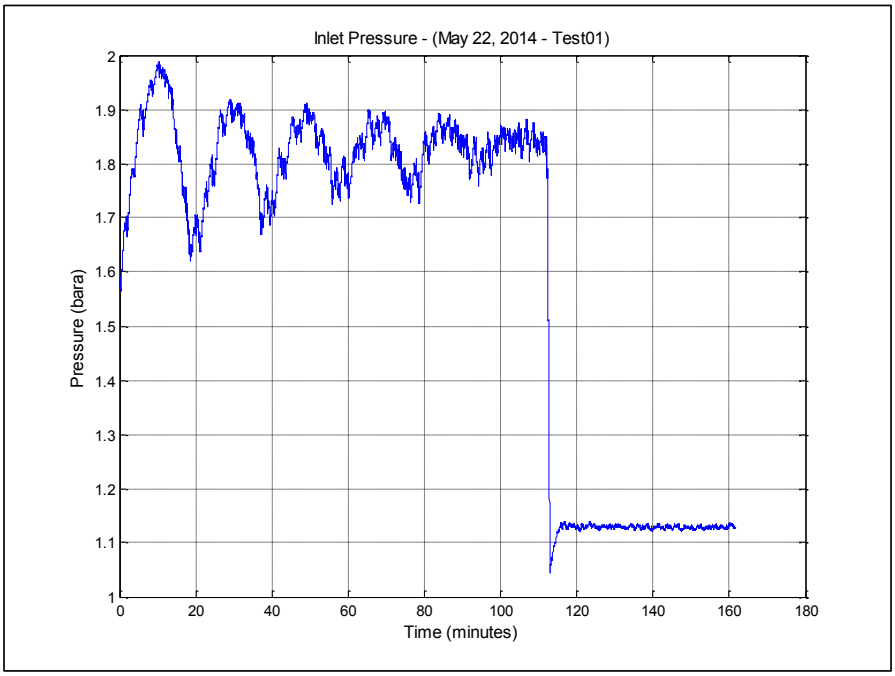

Figure 13-11: Inlet pressure log – May 22, 2014 Experiment-01

12.10 May 23, 2014 – Experiment (01)

The experiment started fully choked valve and half way through the experiment the valve was fully open. The average flow rates recorded for this experiment were as follows:

Water flow rate (fully open valve) = 0.35 lit/sec
Air flow rate (fully open valve) = 29.8 Kg/hr

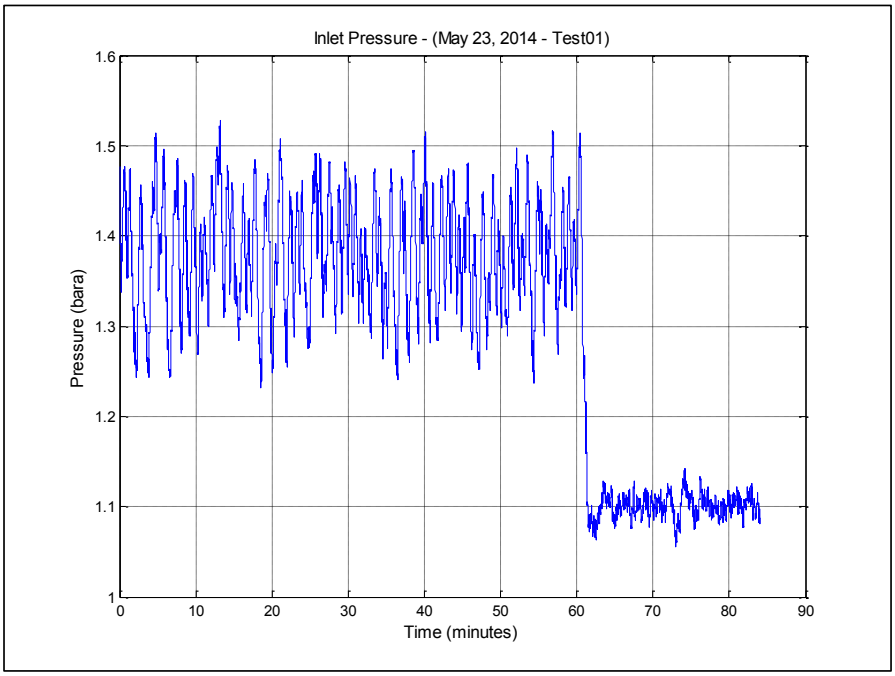

Figure 13-12: Inlet pressure log – May 23, 2014 Experiment-01

12.11 May 23, 2014 – Experiment (02)

The experiment started fully open valve and half way through the experiment the valve was fully choked for about (5) minutes. The valve was then slightly open for the remaining (20) minutes of the experiment. The average flow rates recorded for this experiment were as follows:

Water flow rate (fully open valve) = 0.35 lit/sec
Air flow rate (fully open valve) = 13.9 Kg/hr

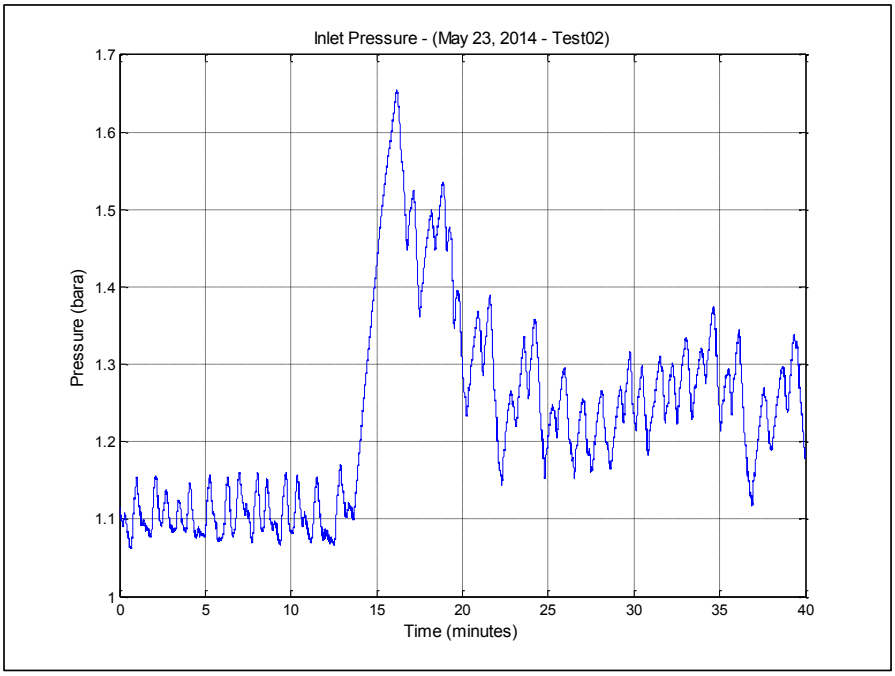

Figure 13-13: Inlet pressure log – May 23, 2014 Experiment-02

12.12 May 23, 2014 – Experiment (03)

The experiment started fully choked valve and half way through the experiment the valve was fully open. The average flow rates recorded for this experiment were as follows:

Water flow rate (fully open valve) = 0.35 lit/sec
Air flow rate (fully open valve) = 13.9 Kg/hr

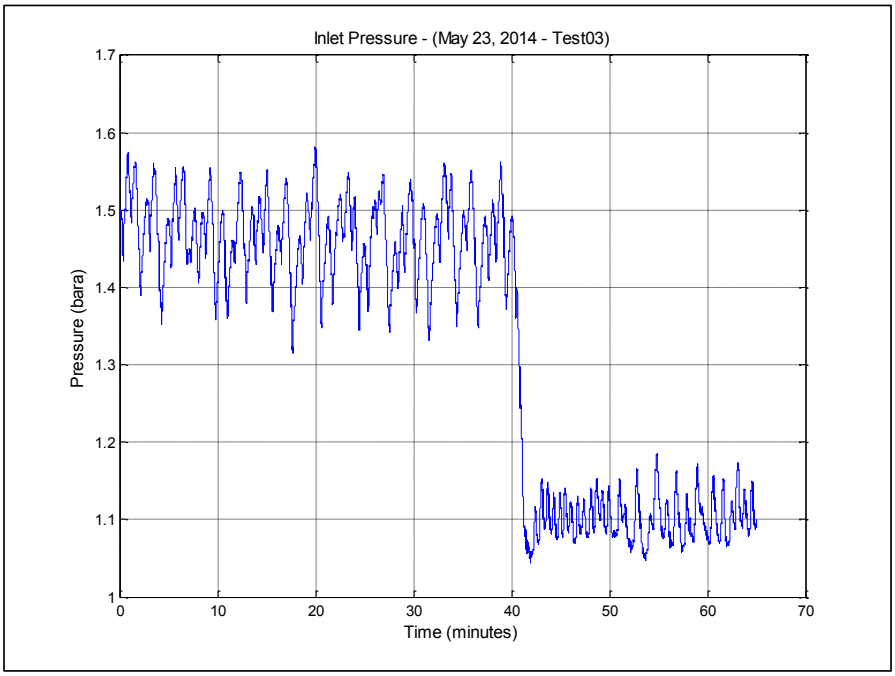

Figure 13-14: Inlet pressure log – May 23, 2014 Experiment-03

12.13 May 24, 2014 – Experiment (01)

The experiment started fully open valve and half way through the experiment the valve was fully choked, and then open and then half choked. Finally, the valve was fully open. The average flow rates recorded for this experiment were as follows:

Water flow rate (fully open valve) = 0.238 lit/sec
Air flow rate (fully open valve) = 41 Kg/hr

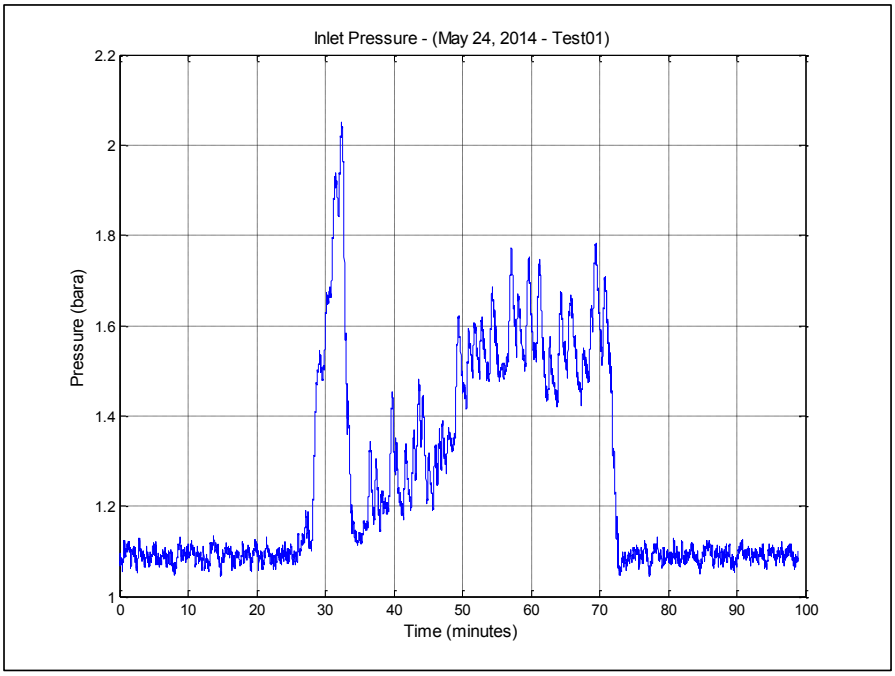

Figure 13-15: Inlet pressure log – May 24, 2014 Experiment-01

12.14 May 24, 2014 – Experiment (02)

The experiment started fully open valve for about (20) minutes and then the valve was fully choked. Finally, the valve was fully open. The average flow rates recorded for this experiment were as follows:

Water flow rate (fully open valve) = 0.545 lit/sec
Air flow rate (fully open valve) = 18.7 Kg/hr

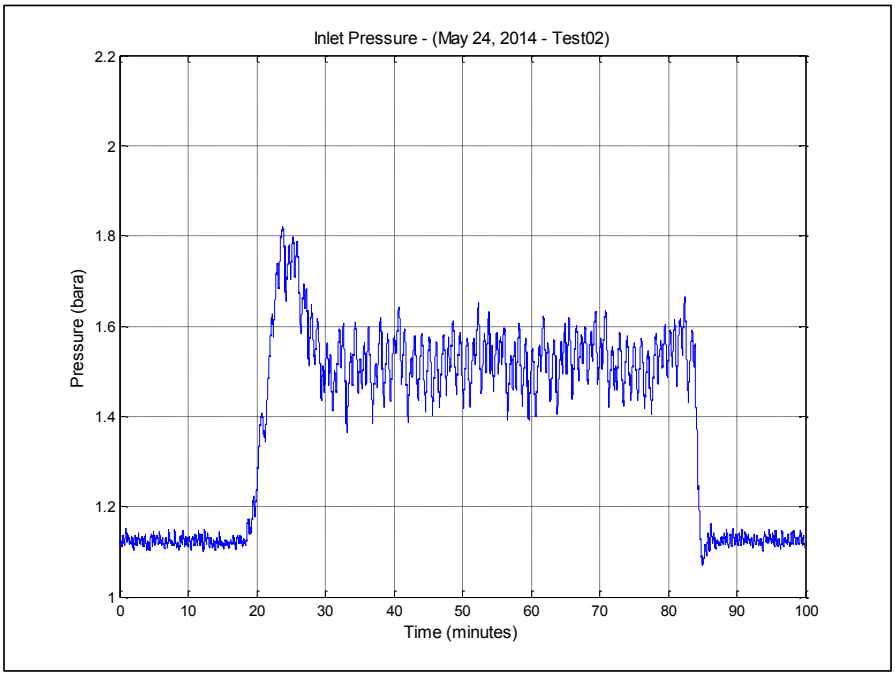

Figure 13-16: Inlet pressure log – May 24, 2014 Experiment-02

12.15 May 25, 2014 – Experiment (01)

The experiment started fully open valve for about (80) minutes and then the valve was fully choked. Finally, the valve was fully open. The average flow rates recorded for this experiment were as follows:

Water flow rate (fully open valve) = 0.236 lit/sec
Air flow rate (fully open valve) = 14.1 Kg/hr

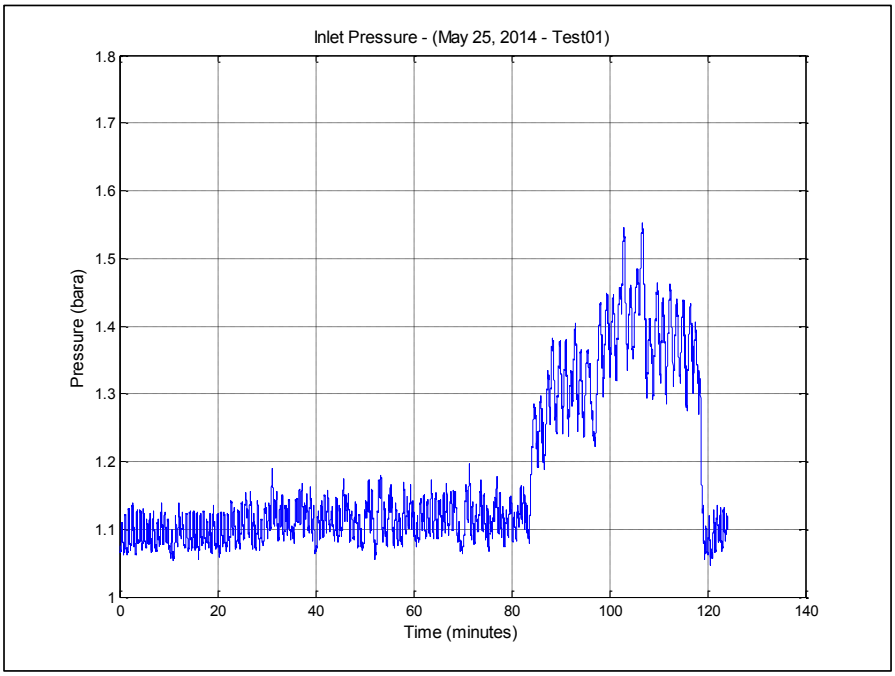

Figure 13-17: Inlet pressure log – May 25, 2014 Experiment-01

12.16 May 25, 2014 – Experiment (02)

The experiment started fully open valve for about (18) minutes and then the valve was fully choked. The average flow rates recorded for this experiment were as follows:

Water flow rate (fully open valve) = 0.18 lit/sec
Air flow rate (fully open valve) = 3.1 Kg/hr

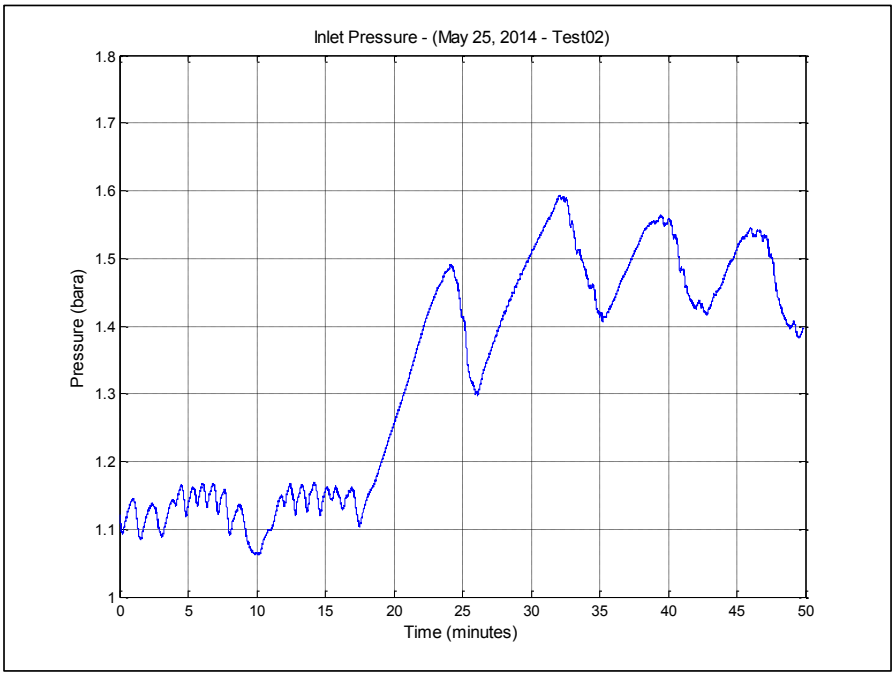

Figure 13-18: Inlet pressure log – May 25, 2014 Experiment-02

12.17 May 25, 2014 – Experiment (03)

The experiment started fully choked valve for about (5) minutes and then the valve was half choked for about (35) minutes and finally the valve was fully open. The average flow rates recorded for this experiment were as follows:

Water flow rate (fully open valve) = 0.18 lit/sec
Air flow rate (fully open valve) = 3.1 Kg/hr

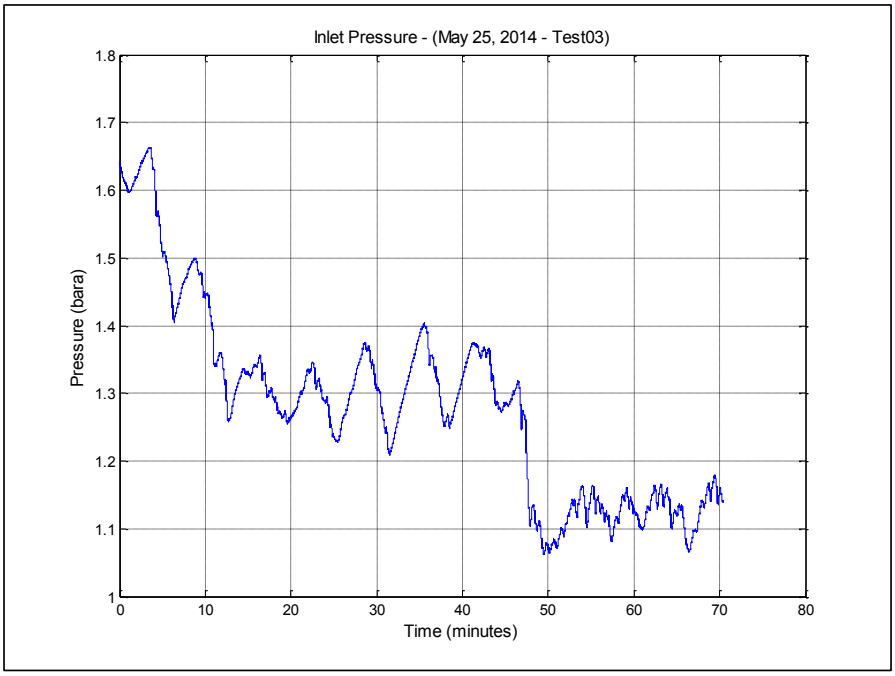

Figure 13-19: Inlet pressure log – May 25, 2014 Experiment-03

12.18 May 25, 2014 – Experiment (04)

The experiment started fully open valve for about (5) minutes and then the valve was half choked for about (20) minutes. The valve was then fully choked for about (10) minutes and then finally half choked for the remaining (15) minutes of the experiment. The average flow rates recorded for this experiment were as follows:

Water flow rate (fully open valve) = 0.45 lit/sec
Air flow rate (fully open valve) = 3.1 Kg/hr

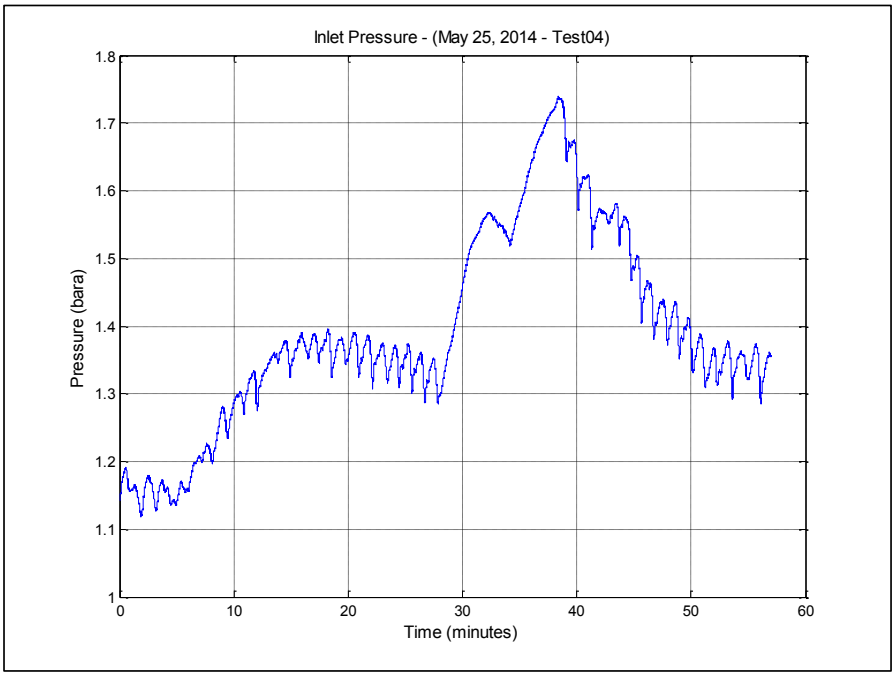

Figure 13-20: Inlet pressure log – May 25, 2014 Experiment-04

12.19 May 25, 2014 – Experiment (05)

The experiment started fully open valve for about (10) minutes and then the valve was fully choked for about (35) minutes. The valve was then fully open for about (15) minutes and then finally slightly choked for the remaining (25) minutes of the experiment. The average flow rates recorded for this experiment were as follows:

Water flow rate (fully open valve) = 0.285 lit/sec
Air flow rate (fully open valve) = 29.7 Kg/hr

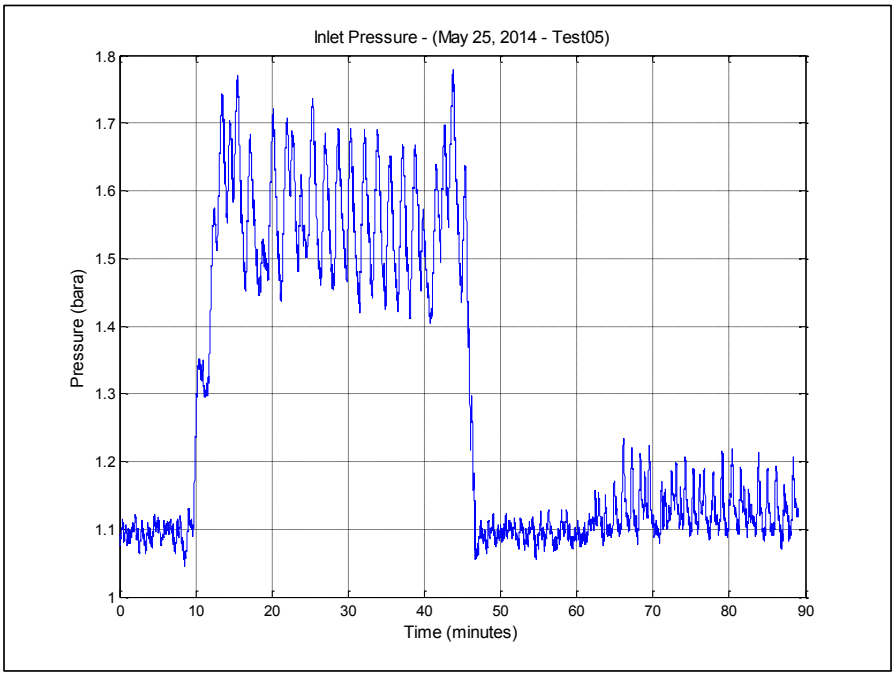

Figure 13-21: Inlet pressure log – May 25, 2014 Experiment-05

12.20 May 25, 2014 – Experiment (06)

The experiment started fully open valve for about (10) minutes and then the valve was fully choked for about (30) minutes. The valve was finally fully open for about (8) minutes. The average flow rates recorded for this experiment were as follows:

Water flow rate (fully open valve) = 0.285 lit/sec
Air flow rate (fully open valve) = 53.8 Kg/hr

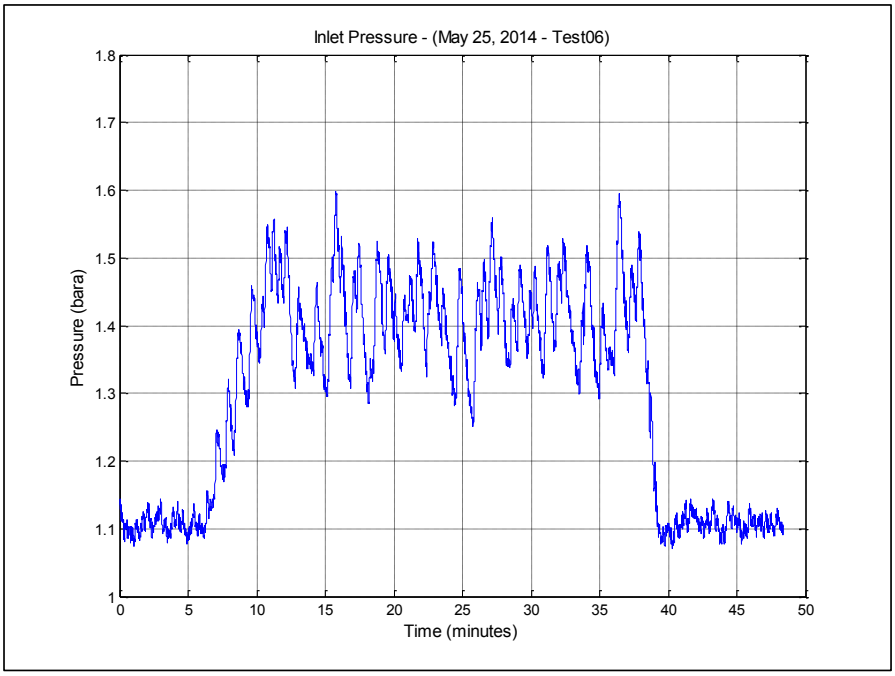

Figure 13-22: Inlet pressure log – May 25, 2014 Experiment-06

12.21 June 11, 2014 – Experiment (01)

The experiment started fully open valve for about (20) minutes and then the valve was fully choked for about (5) minutes. The valve was then half choked for (15) minutes. The valve was finally fully open for the remaining (20) minutes. The average flow rates recorded for this experiment were as follows:

Water flow rate (fully open valve) = 0.086 lit/sec
Air flow rate (fully open valve) = 3.4 Kg/hr

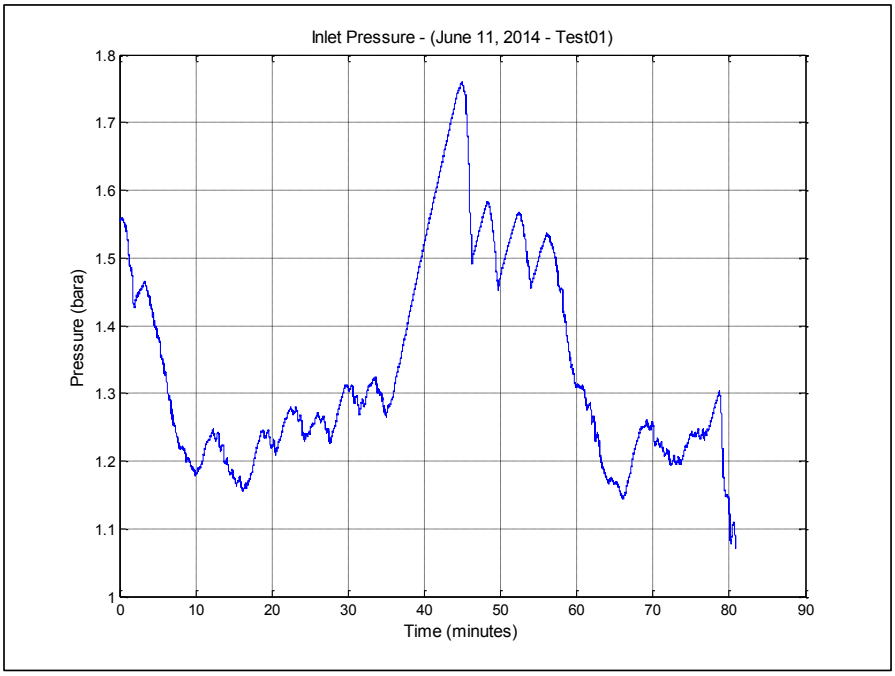

Figure 13-23: Inlet pressure log – June 11, 2014 Experiment-01

12.22 June 12, 2014 – Experiment (01)

The experiment started fully open valve for about (10) minutes and then the valve was fully choked for about (60) minutes. The valve was finally fully open for the remaining (40) minutes. The average flow rates recorded for this experiment were as follows:

Water flow rate (fully open valve) = 0.14 lit/sec
Air flow rate (fully open valve) = 3.2 Kg/hr

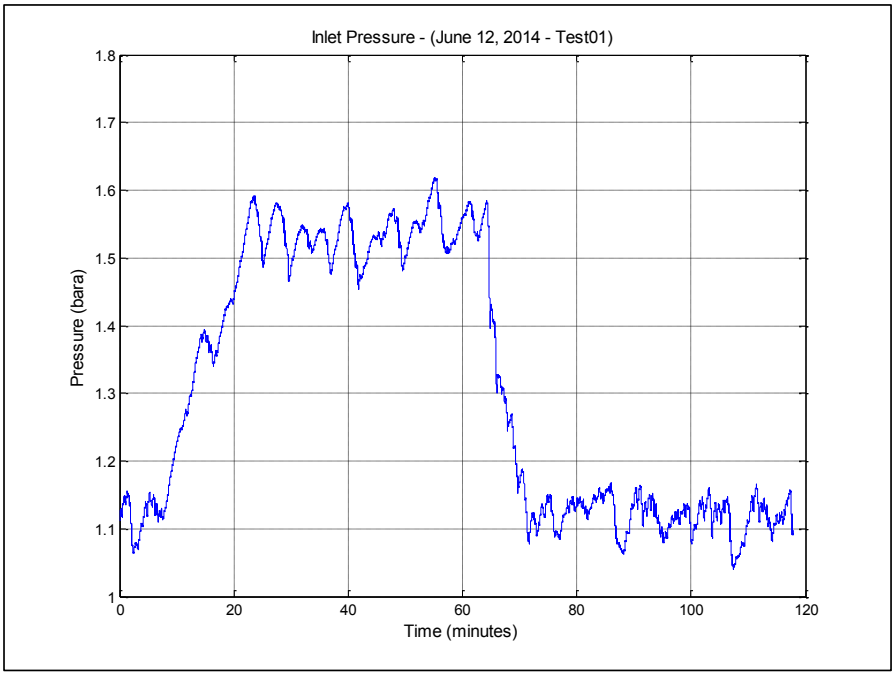

Figure 13-24: Inlet pressure log – June 12, 2014 Experiment-01

12.23 June 12, 2014 – Experiment (02)

The experiment started fully open valve for about (20) minutes and then the valve was fully choked for about (60) minutes. The valve was finally fully open for the remaining (30) minutes. The average flow rates recorded for this experiment were as follows:

Water flow rate (fully open valve) = 0.18 lit/sec
Air flow rate (fully open valve) = 3.2 Kg/hr

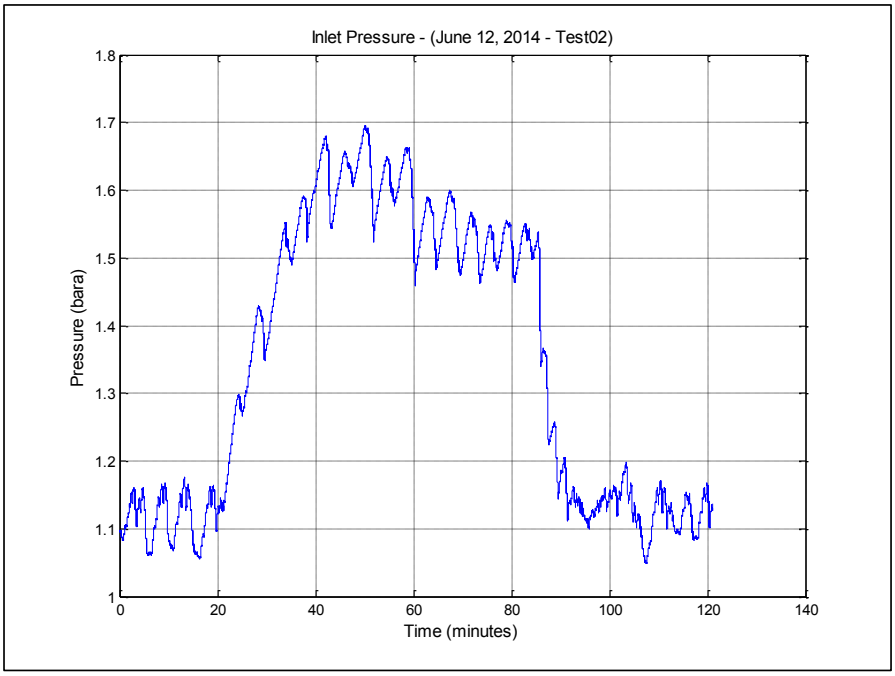

Figure 13-25: Inlet pressure log – June 12, 2014 Experiment-02

12.24 June 12, 2014 – Experiment (03)

The experiment started fully open valve for about (25) minutes and then the valve was fully choked for about (25) minutes. The valve was then slightly choked for about (20) minutes. The valve was finally fully open for the remaining (20) minutes. The average flow rates recorded for this experiment were as follows:

Water flow rate (fully open valve) = 0.18 lit/sec
Air flow rate (fully open valve) = 7.2 Kg/hr

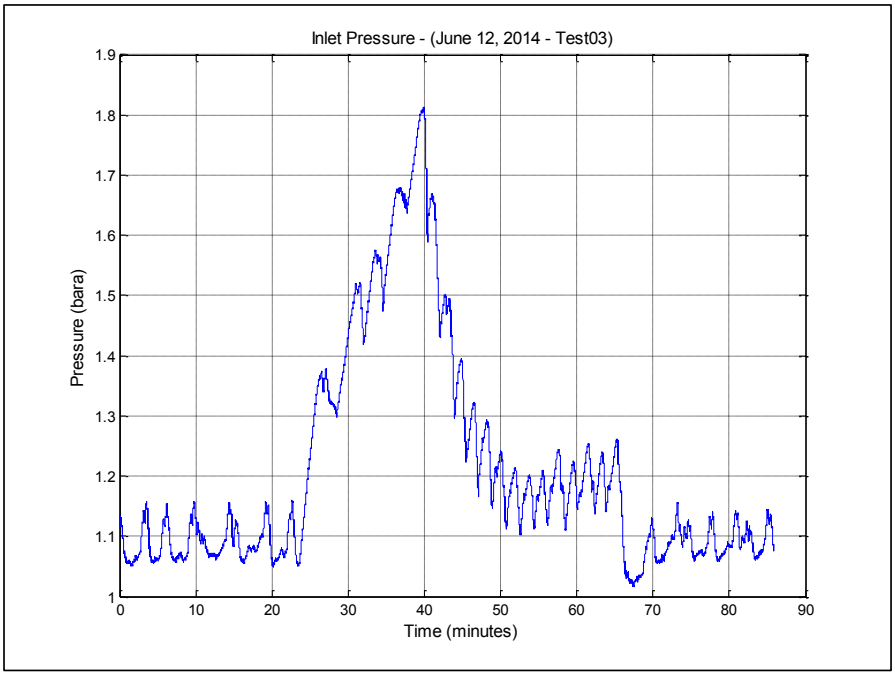

Figure 13-26: Inlet pressure log – June 12, 2014 Experiment-03

12.25 June 12, 2014 – Experiment (04)

The experiment started fully open valve for about (10) minutes and then the valve was fully choked for about (20) minutes. The valve was then slightly choked for about (20) minutes. The valve was finally fully open for the remaining (20) minutes. The average flow rates recorded for this experiment were as follows:

Water flow rate (fully open valve) = 0.18 lit/sec
Air flow rate (fully open valve) = 10.2 Kg/hr

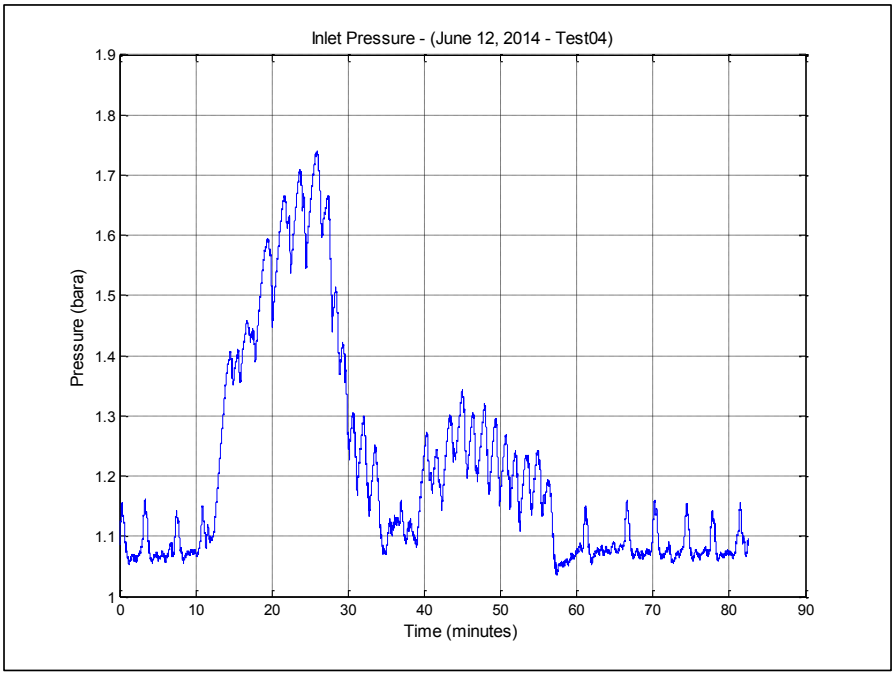

Figure 13-27: Inlet pressure log – June 12, 2014 Experiment-04

12.26 June 12, 2014 – Experiment (05)

The experiment started fully open valve for about (25) minutes and then the valve was fully choked for about (10) minutes. The valve was then half choked for about (20) minutes. The valve was finally fully open for the remaining (30) minutes. The average flow rates recorded for this experiment were as follows:

Water flow rate (fully open valve) = 0.18 lit/sec
Air flow rate (fully open valve) = 19.3 Kg/hr

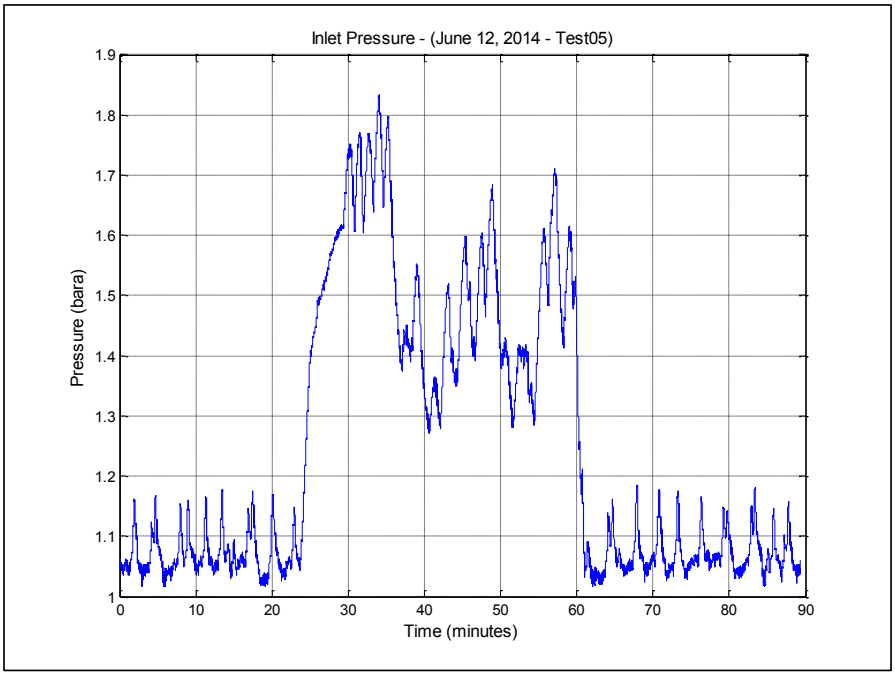

Figure 13-28: Inlet pressure log – June 12, 2014 Experiment-05

12.27 June 13, 2014 – Experiment (01)

The experiment started fully open valve for about (30) minutes and then the valve was fully choked for about (30) minutes. The valve was then half choked for about (20) minutes. The valve was finally fully open for the remaining (10) minutes. The average flow rates recorded for this experiment were as follows:

Water flow rate (fully open valve) = 0.18 lit/sec
Air flow rate (fully open valve) = 28.7 Kg/hr

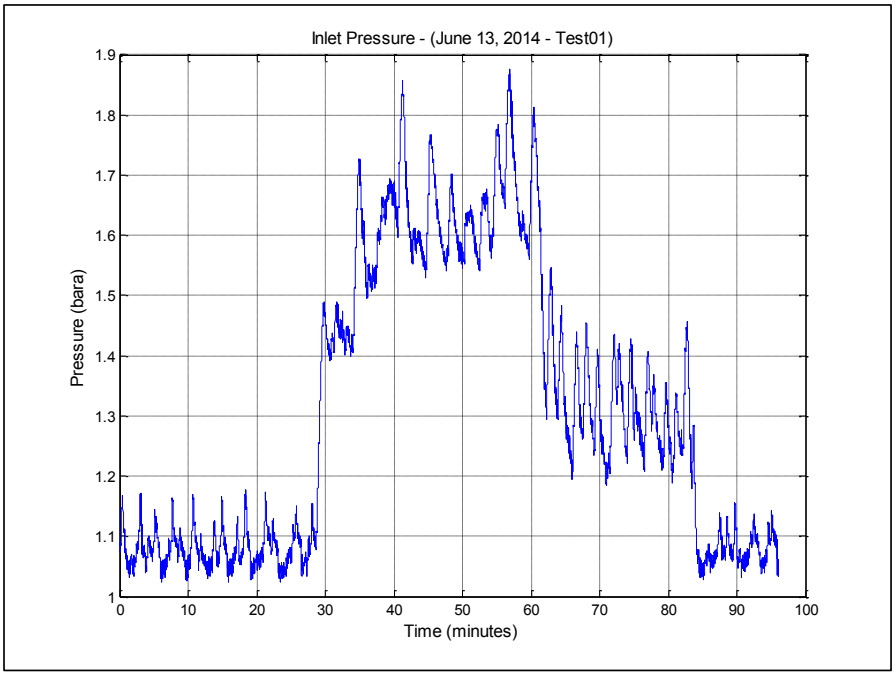

Figure 13-29: Inlet pressure log – June 13, 2014 Experiment-01

12.28 June 13, 2014 – Experiment (02)

The experiment started fully open valve for about (10) minutes and then the valve was fully choked for about (130) minutes. The valve was then fully open for about (20) minutes. The valve was finally slightly choked for the remaining (15) minutes. The average flow rates recorded for this experiment were as follows:

Water flow rate (fully open valve) = 0.18 lit/sec
Air flow rate (fully open valve) = 40.7 Kg/hr

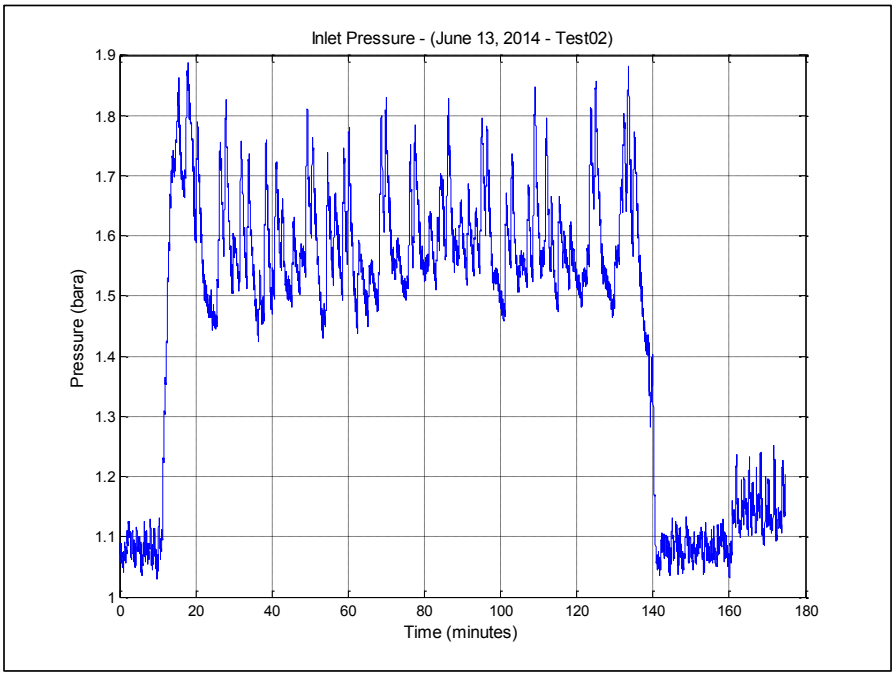

Figure 13-30: Inlet pressure log – June 13, 2014 Experiment-02

12.29 June 13, 2014 – Experiment (03)

The experiment started fully open valve for about (15) minutes and then the valve was half choked for about (50) minutes. The valve was then fully choked for about (10) minutes. The valve was then fully open for about (10) minutes. The average flow rates recorded for this experiment were as follows:

Water flow rate (fully open valve) = 0.18 lit/sec
Air flow rate (fully open valve) = 59.3 Kg/hr

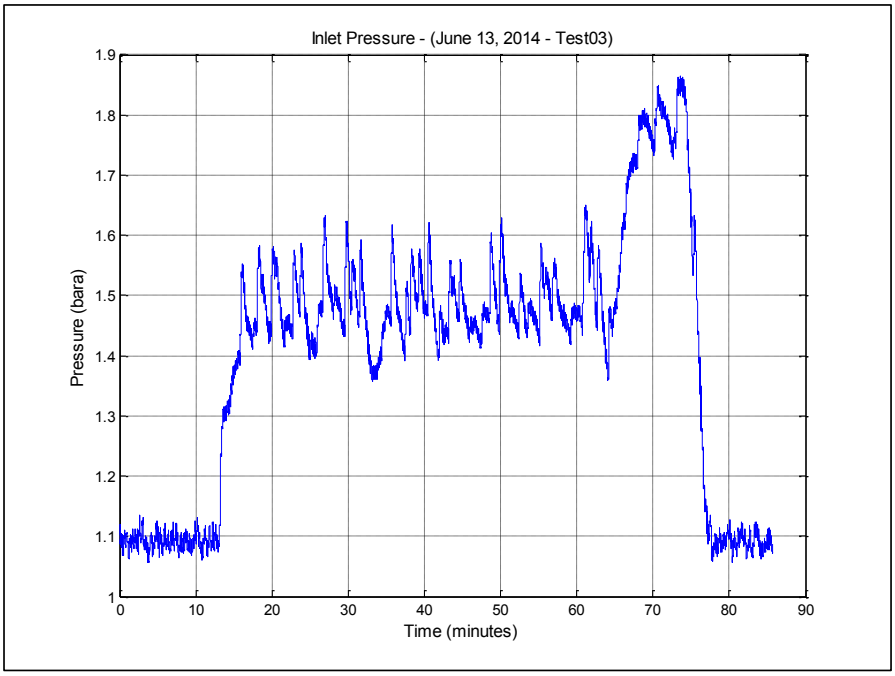

Figure 13-31: Inlet pressure log – June 13, 2014 Experiment-03

12.30 June 13, 2014 – Experiment (04)

The experiment started fully open valve for about (10) minutes and then the valve was fully choked for about (130) minutes. The valve was then fully open for about (20) minutes. The valve was finally slightly choked for the remaining (15) minutes. The average flow rates recorded for this experiment were as follows:

Water flow rate (fully open valve) = 0.54 lit/sec
Air flow rate (fully open valve) = 14.2 Kg/hr

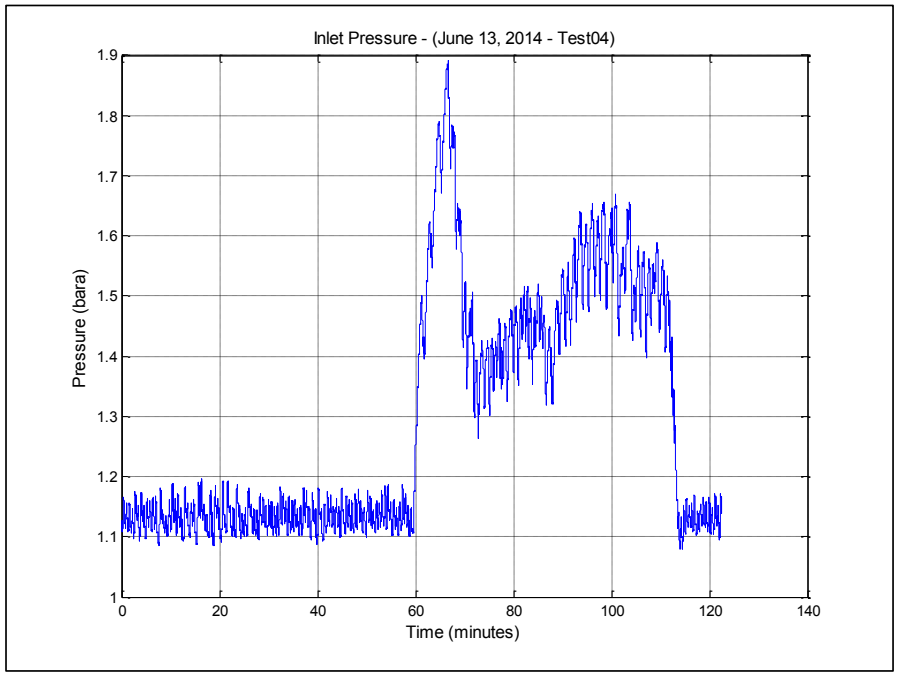

Figure 13-32: Inlet pressure log – June 13, 2014 Experiment-04

12.31 June 15, 2014 – Experiment (01)

The experiment started with slightly choked valve for about (10) minutes and then the valve was half choked for about (15) minutes. The valve was then fully open for about (15) minutes. The valve was finally fully open for the remaining (15) minutes. The average flow rates recorded for this experiment were as follows:

Water flow rate (fully open valve) = 0.54 lit/sec
Air flow rate (fully open valve) = 14.2 Kg/hr

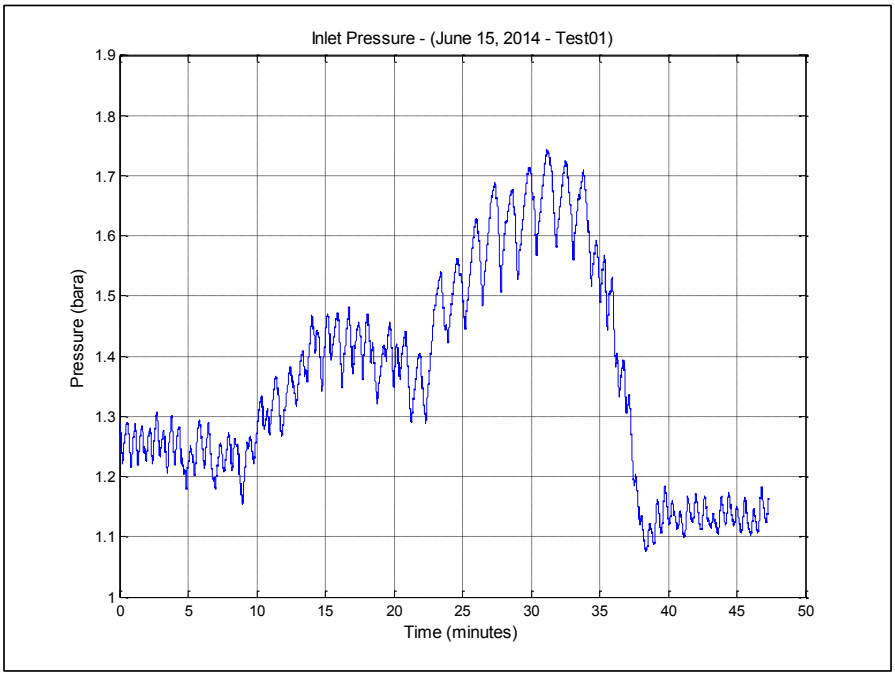

Figure 13-33: Inlet pressure log – June 15, 2014 Experiment-01

12.32 June 15, 2014 – Experiment (02)

The experiment started with fully open valve for about (10) minutes and then the valve was slightly choked for about (15) minutes. The valve was then half choked for about (15) minutes and then fully choked for (15) minutes. The valve was finally fully open for the remaining (5) minutes. The average flow rates recorded for this experiment were as follows:

Water flow rate (fully open valve) = 0.54 lit/sec
Air flow rate (fully open valve) = 30.1 Kg/hr

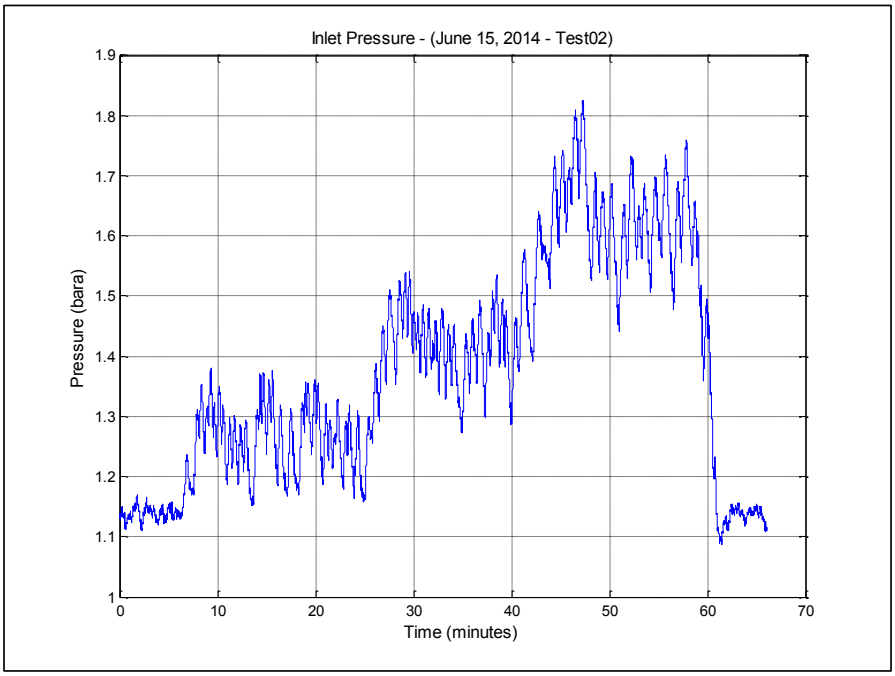

Figure 13-34: Inlet pressure log – June 15, 2014 Experiment-02

12.33 June 15, 2014 – Experiment (03)

The experiment started with fully open valve for about (15) minutes and then the valve was slightly choked for about (15) minutes. The valve was then fully choked for (10) minutes. The valve was finally fully open for the remaining (8) minutes. The average flow rates recorded for this experiment were as follows:

Water flow rate (fully open valve) = 0.54 lit/sec
Air flow rate (fully open valve) = 41.2 Kg/hr

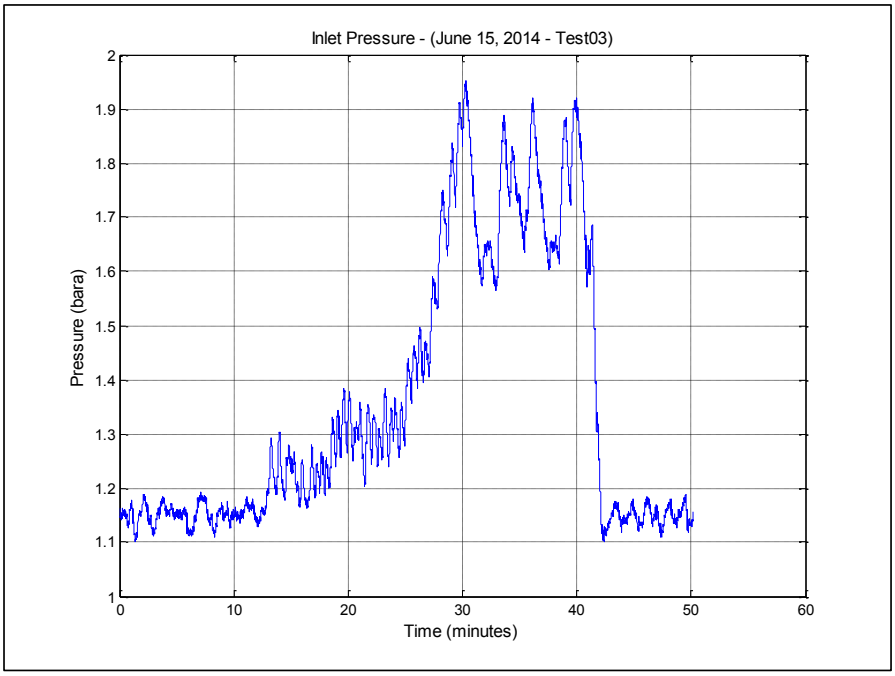

Figure 13-35: Inlet pressure log – June 15, 2014 Experiment-03

12.34 June 16, 2014 – Experiment (01)

The experiment started with fully open valve for about (5) minutes and then the valve was slightly choked for about (20) minutes. The valve was then half choked for about (35) minutes before the valve was fully choked for (10) minutes. The valve was finally fully open for the remaining (10) minutes. The average flow rates recorded for this experiment were as follows:

Water flow rate (fully open valve) = 0.286 lit/sec
Air flow rate (fully open valve) = 40.7 Kg/hr

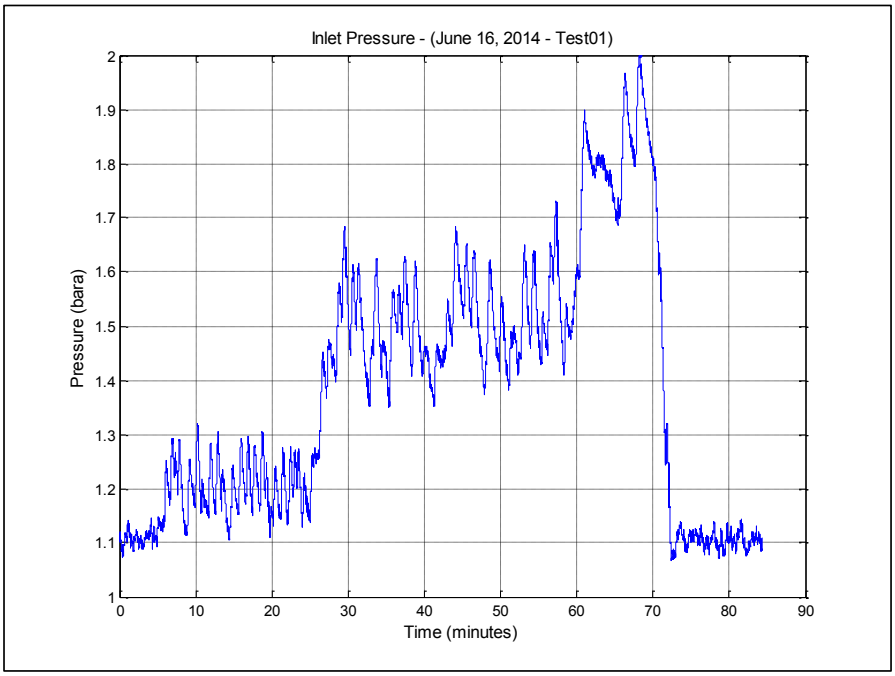

Figure 13-36: Inlet pressure log – June 16, 2014 Experiment-01

12.35 June 16, 2014 – Experiment (02)

The experiment started with fully open valve for about (5) minutes and then the valve was slightly choked for about (10) minutes. The valve was then half choked for about (40) minutes before the valve was fully choked for (50) minutes. The valve was finally fully open for the remaining (35) minutes. The average flow rates recorded for this experiment were as follows:

Water flow rate (fully open valve) = 0.107 lit/sec
Air flow rate (fully open valve) = 40.7 Kg/hr

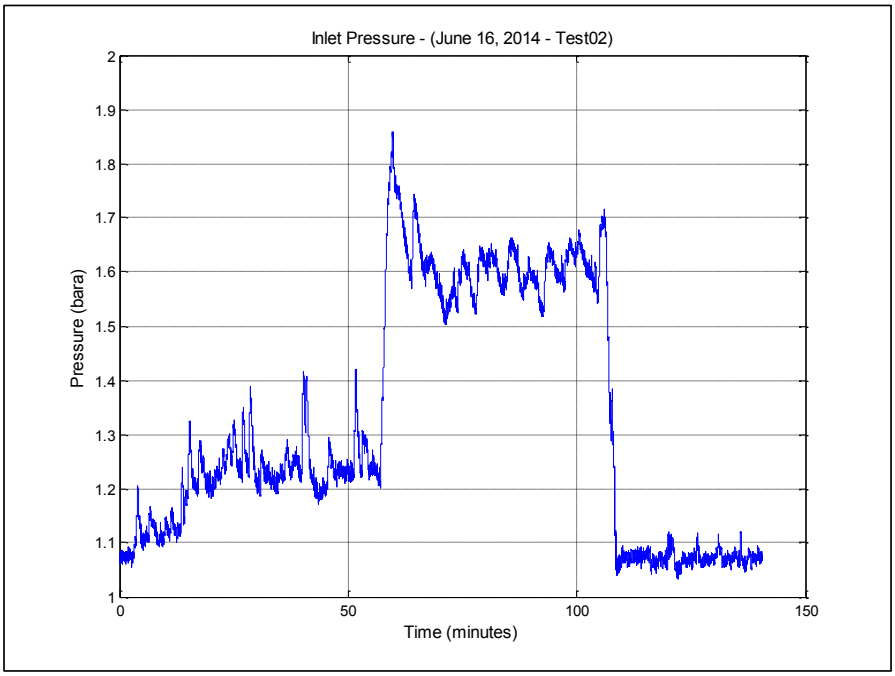

Figure 13-37: Inlet pressure log – June 16, 2014 Experiment-02

12.36 June 16, 2014 – Experiment (03)

The experiment started with fully open valve for about (30) minutes. The valve was then half choked for about (30) minutes before the valve was fully choked for (20) minutes. The valve was finally fully open for the remaining (5) minutes. The average flow rates recorded for this experiment were as follows:

Water flow rate (fully open valve) = 0.107 lit/sec
Air flow rate (fully open valve) = 29.7 Kg/hr

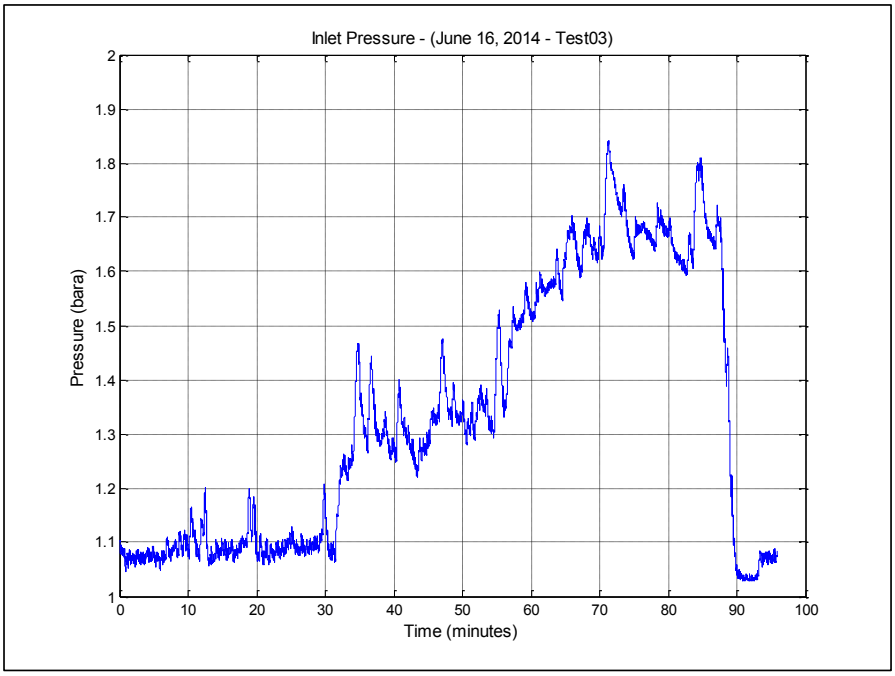

Figure 13-38: Inlet pressure log – June 16, 2014 Experiment-03

12.37 June 16, 2014 – Experiment (04)

The experiment started with fully open valve for about (30) minutes. The valve was then half choked for about (50) minutes. The valve was finally fully open for the remaining (3) minutes. The average flow rates recorded for this experiment were as follows:

Water flow rate (fully open valve) = 0.107 lit/sec
Air flow rate (fully open valve) = 19.8 Kg/hr

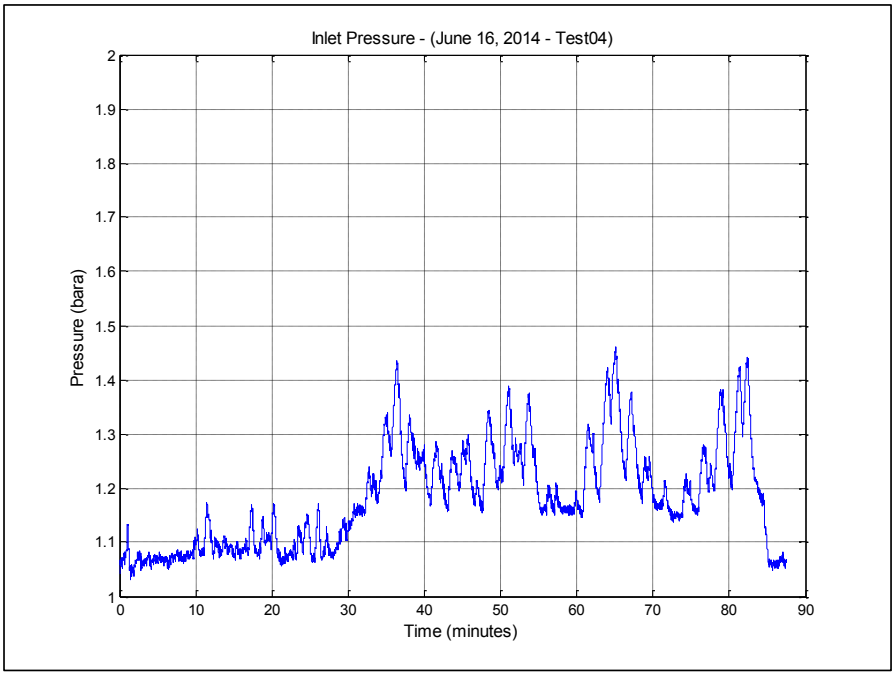

Figure 13-39: Inlet pressure log – June 16, 2014 Experiment-04

This page was intentionally left blank

14. APPENDIX-B: Gamma Measurements

Derivation of the Equations in Appendix of Harald Linga Paper – 1997, Linga (1997)				
Step-1	The general expression for the relation between the detector output signal (U) and the detected photon flux (N + M) is:	$U = U_0 + U_1(N + M)$	Where (U0) and (U1) are instrument constants. (N) and (M) are primary and secondary fluxes of photons.	Eq-(1)
Step-2	Now, we take (N), the primary flux fo photons, which is given by:	$N = N_0 \cdot e^{-\left\{\left(\mu_g \cdot \rho_g \cdot (1-H)\right)+\left(\mu_l \cdot \rho_l \cdot (H)\right)\right\} \cdot Z_0}$	Where (g & l) stands for gas and liquid and (H) is the holdup. (ρ) is density, (μ) is linear mass attenuation coefficient. (Z0) is effective beam length in pipe. And (N0) is the flux of primary photons if no attenuation occurs in the fluid.	Eq-(2)
Step-3	Now, we introduce the build-up factor (B)	$B = \frac{N}{N+M} = 1 + \frac{M}{N}$		Eq-(3)
Step-4	Now, we introduce the attenuation factor (K)	$K = e^{-\left\{\left(\mu_g \cdot \rho_g \cdot (1-H)\right)+\left(\mu_l \cdot \rho_l \cdot (H)\right)\right\} \cdot Z_0}$		Eq-(4)
Step-5	Now, the primary flux of photons (N) becomes:	$N = N_0 \cdot K$		Eq-(5)
Step-6	From Eq. (4)	$N + M = N \cdot B$		Eq-(6)
Step-7	By combining Eqs. (1) to (6), the detector output signal (U) can be written as:	$U = U_0 + U_1 \cdot N_0 \cdot B \cdot e^{-\left\{\left(\mu_g \cdot \rho_g \cdot (1-H)\right)+\left(\mu_l \cdot \rho_l \cdot (H)\right)\right\} \cdot Z_0}$		Eq-(7)
Step-8	Utilizing the attenuation factor (K) for a pipe filled with gas, H = 0	$U_g = U_0 + U_1 \cdot N_0 \cdot B_g \cdot K_g$	Here all the liquid terms in (Kg) disappears because H = 0	Eq-(8)

Step-9	Utilizing the attenuation factor (K) for a pipe filled with liquid	$U_l = U_0 + U_1 \cdot N_0 \cdot B_l \cdot K_l$	Here all the gas terms in (Kl) disappears because H = 1	Eq-(9)
Step-10	Subtracting Eqs. (8 & 9), the instrument constants in Eq. (1) can be determined as follows:	$U_1 \cdot N_0 = \dfrac{\frac{1}{B_g}(U_l - U_g)}{\frac{B_l}{B_g} \cdot K_l - K_g}$		Eq-(10)
Step-11	Substituting in Eq. (8) gives the other constant:	$U_0 = \dfrac{\frac{B_l}{B_g} \cdot K_l \cdot U_g - K_g \cdot U_l}{\frac{B_l}{B_g} \cdot K_l - K_g}$		Eq-(11)
Step-12	Defining the attenuation Ratio (R):	$R = \dfrac{K_g}{K_l}$		Eq-(12)
Step-13	Utilizing the definition of Kg & Kl plus the defining the the gas fraction (ε):	$K_g = e^{-\{(\mu_g \cdot \rho_g)\} \cdot Z_0}$ $\quad K_l = e^{-\{(\mu_l \cdot \rho_l)\} \cdot Z_0}$ $\quad \varepsilon = (1 - H)$		
Step-14	Now, we can express the attenuation factor (K) as:	$K = R^{\varepsilon} \cdot K_l \quad ; \quad K = \left(\frac{K_g}{K_l}\right)^{\varepsilon} \cdot K_l = (K_g)^{\varepsilon} \cdot (K_l)^{1-\varepsilon}$	This is done by simple manipulation of the powers.	Eq-(13)
Step-15	Now, by using Eqs. (10), (11), (12) & (13) and plugging back into Eq. (7):	$U = U_0 + U_1 \cdot N_0 \cdot B \cdot R^{\varepsilon} \cdot K_l$	Use Eq. (13) to replace (K)	
Step-16		$U = \dfrac{\frac{B_l}{B_g} \cdot K_l \cdot U_g - K_g \cdot U_l}{\frac{B_l}{B_g} \cdot K_l - K_g} + \dfrac{\frac{1}{B_g}(U_l - U_g)}{\frac{B_l}{B_g} \cdot K_l - K_g} \cdot B \cdot R^{\varepsilon} \cdot K_l$	Use Eq. (10 & 11) to replace (U0) & (U1 N0). Note that these two terms have the same denomenator	
Step-17		$U \cdot \left[\frac{B_l}{B_g} \cdot K_l - K_g\right] = \frac{B_l}{B_g} \cdot K_l \cdot U_g - K_g \cdot U_l + \frac{B}{B_g}(U_l - U_g) R^{\varepsilon} \cdot K_l$	Take the denomenator to the LHS	
Step-18		$\frac{U}{K_l} \cdot \left[\frac{B_l}{B_g} \cdot K_l - K_g\right] = \frac{B_l}{B_g} \cdot U_g - R \cdot U_l + \frac{B}{B_g}(U_l - U_g) \cdot R^{\varepsilon}$	Divide by (Kl) and Use (R) definition	

Step-19		$\frac{U}{K_l}\cdot\left[\frac{B_l}{B_g}\cdot K_l - K_g\right] = \frac{B_l}{B_g}\cdot(U_g - U_l) + (\frac{B_l}{B_g} - R)\cdot U_l + \frac{B}{B_g}(U_l - U_g)\cdot R^{\varepsilon}$	Add and subtract (Bl/Bg)/Ul on the RHS	
Step-20		$U\cdot\left[\frac{B_l}{B_g} - R\right] = \left[\frac{B_l}{B_g} - \frac{B}{B_g}R^{\varepsilon}\right]\cdot(U_g - U_l) + \left[\frac{B_l}{B_g} - R\right]\cdot U_l$	Now start manipulating the equations	
Step-21		$U = U_l + \frac{\left[\frac{B}{B_g}R^{\varepsilon} - \frac{B_l}{B_g}\right]}{\left[R - \frac{B_l}{B_g}\right]}\cdot(U_g - U_l)$	Continue manipulating until you get …	Eq-(14)
Step-22	Now, we need an expression for (R), so we start manipulating Eq. (11):	$U_0\cdot(\frac{B_l}{B_g}\cdot K_l - K_g) = \frac{B_l}{B_g}\cdot K_l\cdot U_g - K_g\cdot U_l$		
Step-23		$U_0\cdot(\frac{B_l}{B_g} - R) = \frac{B_l}{B_g}\cdot U_g - R\cdot U_l$	Now, we divide by (Kl):	
Step-24		$R = \frac{B_l}{B_g}\cdot\frac{(U_g - U_0)}{(U_l - U_0)}$	Now, we solve for (R):	Eq-(15)
Step-25	Now, we need to solve for (U) without (R) by substituting for it…	$U = U_l + \frac{\left[\frac{B}{B_g}R^{\varepsilon} - \frac{B_l}{B_g}\right]}{\left[\frac{B_l}{B_g}\cdot\frac{(U_g - U_0)}{(U_l - U_0)} - \frac{B_l}{B_g}\right]}\cdot(U_g - U_l)$	Now, we plug (R) back into Eq. (14):	
Step-26		$U = U_l + \frac{\left[\frac{B}{B_g}R^{\varepsilon} - \frac{B_l}{B_g}\right]}{\frac{B_l}{B_g}\cdot\left[\frac{(U_g - U_0)}{(U_l - U_0)} - 1\right]}\cdot(U_g - U_l)$	Now, manipulate the denominator by taking the common factor:	
Step-27		$U = U_l + \frac{\left[\frac{B}{B_g}R^{\varepsilon} - \frac{B_l}{B_g}\right]}{\frac{B_l}{B_g}\cdot\left[\frac{(U_g - U_l)}{(U_l - U_0)}\right]}\cdot(U_g - U_l)$	Continue, manipulating the denominator and then cancel out (Ug - Ul):	
Step-28		$U = U_l + \left[\frac{B}{B_g}R^{\varepsilon} - \frac{B_l}{B_g}\right]\frac{B_g}{B_l}\cdot(U_l - U_0)$	Now, we multiply (Bg/Bl) inside the brackets to get:	

Step-29		$U = U_l + \left[\frac{B}{B_l} R^{\varepsilon} - 1\right] \cdot (U_l - U_0)$	Now, we multiply (Bg/Bl) inside the brackets to get:	Eq --- (16)
Step-30	Now, we can easily solve for the gas (void) fraction (ε), to get:	$\varepsilon = \frac{\ln\left(\frac{B_l}{B} \cdot \frac{U - U_0}{U_l - U_0}\right)}{\ln\left(\frac{B_l}{B_g} \cdot \frac{U_g - U_0}{U_l - U_0}\right)}$	Now, we multiply (Bg/Bl) inside the brackets to get:	Eq --- (17)

This page was intentionally left blank

15. APPENDIX-C: OLGA & LedaFlow

A brief description of the governing equations and basic numerical approach for OLGA and LedaFlow is presented in this section.

15.1. OLGA Transient Multiphase Flow Code

OLGA was developed in the 1980's through a joint research project between IFE and SINTEF and was supported by a group of oil companies (Conoco Norway, Esso Norge, Mobil Exploration Norway, Norsk Hydro, Petro Canada, Saga Petroleum, Statoil and Texaco Exploration Norway). A first version of OLGA was developed in 1983 and was further developed until the first commercial version was released in 1988.

The development of OLGA code was made to fill in the gap left by the nuclear codes such as TRAC, RELAP and CATHARE which handle fast transients for relatively short pipelines in nuclear reactors. OLGA on the other hand was developed with the objective to simulate slow transients in oil and gas pipelines which are generally longer and requires time spans which can range from hours to several days, Bendiksen et al. (1988). OLGA applies two techniques to simulate slugs: a unit cell model approach which is the default approach with no considerations of the hydrodynamic slugs and a slug tracking approach which considers both terrain slug and hydrodynamic slugs and the interactions between them.

The governing equations described in this section are obtained from the famous Bendiksen et al. (1991) paper which describes the basic background behind OLGA multiphase flow model. The overall OLGA governing equations consists of separate mass conservation equations for gas, liquid bulk and liquid droplets as follows:

$$\frac{\partial}{\partial t}\left(V_g\rho_g\right) = -\frac{1}{A}\frac{\partial}{\partial z}\left(AV_g\rho_g v_g\right) + \psi_g + G_g \tag{15.1}$$

$$\frac{\partial}{\partial t}\left(V_l\rho_l\right) = -\frac{1}{A}\frac{\partial}{\partial z}\left(AV_l\rho_l v_l\right) + \psi_l\frac{V_l}{V_l+V_D} + \psi_e + \psi_d + G_l \tag{15.2}$$

$$\frac{\partial}{\partial t}\left(V_D\rho_l\right) = -\frac{1}{A}\frac{\partial}{\partial z}\left(AV_D\rho_l v_D\right) + \psi_l\frac{V_D}{V_l+V_D} + \psi_e - \psi_d + G_D \tag{15.3}$$

In the above equations, equations (14.1) to (14.3), (V_g, V_l, V_D) represents the volume fractions of gas, liquid and liquid droplets. (ρ, v, P) represents the density, velocity and pressure respectively. The mass transfer rate between phases is represented by (ψ_g), while the droplet entrainment and deposition rates are represented by (ψ_e, ψ_d). (G_f) represents the mass source of phase (f) and the subscripts (g, l, i, D) represents gas, liquid, interface and droplet respectively.

The conservation of momentum equations in OLGA for gas, droplet and liquid bulk are as follows:

$$\frac{\partial}{\partial t}\left(V_g\rho_g v_g\right) = -V_g\left(\frac{\partial P}{\partial z}\right) - \frac{1}{A}\frac{\partial}{\partial z}\left(AV_g\rho_g v_g^2\right) - \frac{\lambda_g}{2}\rho_g|v_g|v_g\frac{S_g}{4A} - \frac{\lambda_i}{2}\rho_g|v_r|v_r\frac{S_i}{4A} + V_g\rho_g g\cos(\alpha) + \psi_g v_a - F_D \tag{15.4}$$

$$\frac{\partial}{\partial t}\left(V_D\rho_l v_D\right) = -V_D\left(\frac{\partial P}{\partial z}\right) - \frac{1}{A}\frac{\partial}{\partial z}\left(AV_D\rho_l v_D^2\right) + V_D\rho_l g\cos(\alpha) - \psi_g\frac{V_D}{V_l+V_D}v_a + \psi_e v_i - \psi_d v_D + F_D \tag{15.5}$$

$$\begin{aligned}\frac{\partial}{\partial t}\left(V_l\rho_l v_l\right) = {} & -V_l\left(\frac{\partial P}{\partial z}\right) - \frac{1}{A}\frac{\partial}{\partial z}\left(AV_l\rho_l v_l^2\right) - \frac{\lambda_l}{2}\rho_l|v_l|v_l\frac{S_l}{4A} - \frac{\lambda_i}{2}\rho_g|v_r|v_r\frac{S_i}{4A} + V_l\rho_l g\cos(\alpha) \\ & + \psi_g\frac{V_l}{V_l+V_D}v_a - \psi_e v_i + \psi_d v_D - V_l d\left(\rho_l-\rho_g\right)g\frac{\partial V_l}{\partial z}\sin(\alpha)\end{aligned} \tag{15.6}$$

In equations (14.4) to (14.6) pipe inclination with the vertical is represented by (α) and the wetted parameters of gas, liquid and interface are represented by (S_g, S_l, S_i).

Before discretizing the governing equations, OLGA utilizes the conservation of mass equations to create a new equations called the pressure equation. The pressure equation is solved simultaneously with the momentum equation to obtain the pressure and phase velocities. This allows for stepwise time integration.

The pressure equation is obtained by expanding the density with respect to temperature, pressure and composition:

$$\rho_f = \rho_f(P, T, R_S) \tag{15.7}$$

$$R_S = \frac{m_g}{m_g + m_l + m_D} \tag{15.8}$$

Expansion of the gas mass conservation equation (14.1), the left side can be written as:

$$\frac{\partial V_g \rho_g}{\partial t} = \rho_g \frac{\partial V_g}{\partial t} + V_g \frac{\partial \rho_g}{\partial t} \tag{15.9}$$

$$\frac{\partial V_g \rho_g}{\partial t} = \rho_g \frac{\partial V_g}{\partial t} + V_g \left[\left(\frac{\partial \rho_g}{\partial P} \right)_{T,R_s} \frac{\partial P}{\partial t} + \left(\frac{\partial \rho_g}{\partial T} \right)_{P,R_s} \frac{\partial T}{\partial t} + \left(\frac{\partial \rho_g}{\partial R_s} \right)_{T,P} \frac{\partial R_s}{\partial t} \right] \tag{15.10}$$

The last two terms in equation (14.10) can be neglected for slow temperature transients. Using this result and adding all the three mass conservation equation yields the new pressure equation, which is represented in terms of pressure and phase velocities as follows:

$$\left[\frac{V_g}{\rho_g} \left(\frac{\partial \rho_g}{\partial P} \right)_{T,R_s} + \frac{1 - V_g}{\rho_l} \left(\frac{\partial \rho_l}{\partial P} \right)_{T,R_s} \right] \frac{\partial P}{\partial t} = -\frac{1}{A\rho_g} \frac{\partial \left(AV_g \rho_g v_g \right)}{\partial z} - \frac{1}{A\rho_l} \frac{\partial (AV_l \rho_l v_l)}{\partial z} - \frac{1}{A\rho_l} \frac{\partial (AV_D \rho_l v_D)}{\partial z} + \psi_g \left(\frac{1}{\rho_g} - \frac{1}{\rho_l} \right) + \left(\frac{G_g}{\rho_g} \right) + \left(\frac{G_l}{\rho_l} \right) + \left(\frac{G_D}{\rho_l} \right) \tag{15.11}$$

Finally, a mixture energy conservation equation is applied to solve for the pipeline's heat transfer and temperature calculations required for other parameters, which will not be discussed in this section.

The formulation presented in the above equations yields a set of coupled first order non-linear partial differential equations with complex coefficients, which creates great challenges in solving them numerically. Various approaches have applied by different multiphase flow codes which include, method of characteristics, finite difference, and finite element methods. In addition, the question of utilizing explicit versus implicit time integration methods is a fundamental one which requires a great attention in selecting the appropriate numerical method. OLGA utilizes a finite difference, implicit integration approach which enables it to carry out long, stable and slow transient multiphase flow simulation successfully without being limited by the CFL criterion which restricts the explicit integration methods, Bendiksen et al. (1988).

OLGA applies a step-wise scheme to solve for the various flow rate parameters as follows: first step, the two momentum equation and pressure equation are solved to obtain the pressure and phase velocities.

Second step, the mass conservation equations are applied and in the third step the energy equation is solved.

This approach proved to be very successful in OLGA however, it has a drawback as it yields an over-determined system where the mass conservation equations are utilized twice: in the pressure equation in step on and in the mass conservation equation in step two. Thus, the specific masses (m_f^{n+1}) and densities (ρ_f^{n+1}) solved in the two steps may not yield the correct volume phase fractions (V_f^{n+1}), which requires an additional volume error correction term (Δ^{n+1}) to satisfy the unity of the total volume fractions as follows:

$$V_f^{n+1} = \frac{m_f^{n+1}}{\rho_f^{n+1}} \tag{15.12}$$

$$V_g^{n+1} + V_l^{n+1} + V_D^{n+1} + \Delta^{n+1} = 1 \tag{15.13}$$

Ideally, one would like to have ($\Delta^{n+1} = 0$), but due to the over-determination of the system of equations, this does not happen. Therefore, the volume error term is required to be as minimum as possible to produce a successful run in OLGA, Bendiksen et al. (1988).

Finally, one has to bear in mind that OLGA is continuous development and all of the above basic assumptions might have been slightly modified throughout the years.

15.2. LedaFlow Transient Multiphase Flow Code

LedaFlow is a relatively new 1-D transient multiphase flow simulator which solves mass, momentum and energy conservation equations for each field (continuous, bubble and droplet). It applies a three-fluid-nine-field modeling concept to simulate the hydrodynamics and thermodynamics of multiphase flow in oil and gas pipelines. The three fluids being: oil, gas and water, while the nine fields represent the continuous, bubble and droplet of each fluid. In LedaFlow, the momentum and energy equations are solved for each fluid while the mass equation is solved for each of the nine fields. This yields a set of fifteen conservation equation that is solved using the (Semi-Implicit, Pressure Linked Equations) SIMPLE numerical method approach with staggered grid. An iteration scheme is applied to force a conservation of mass on the pressure-correction equation. Based on LedaFlow literature, a satisfactory convergence is normally reached with one to two iterations, Thomas J Danielson et al. (2005).

LedaFlow simulate slugs using two approaches: the unit cell model and slug capturing technique. Similar to OLGA approach, when slug capturing scheme is enabled the unit cell model suppressed and only slug capturing calculations are carried out. Slug capturing generally requires small mesh sizes but no specific guidelines are provided in LedaFlow documents, Thomas John Danielson et al. (2012).

The standard mass and momentum conservation equations are similar to the ones described in OLGA section before. However, closure models are certainly different and represents the data utilized to tune the LedaFlow models.